

NASA TM X-58168
JSC-09930

PROCEEDINGS OF THE



**NASA Earth Resources
Survey Symposium**

HOUSTON, TEXAS
JUNE 1975

N76-17588
THRU
N76-17612
Un: la
14344

**FIRST COMPREHENSIVE SYMPOSIUM
ON THE PRACTICAL APPLICATION
OF EARTH RESOURCES SURVEY DATA**

HC \$7.25

NASA EARTH

(NASA-TM-X-58168-VOL-1-D)

RESOURCES SURVEY SYMPOSIUM. VOLUME 1-D:

WATER RESOURCES First Comprehensive

Symposium on the Practical Application of

Earth Resources Survey Data (NASA) 527 p HC G3/43

**ORIGINAL CONTAINS
COLOR ILLUSTRATIONS**

Original photography may be purchased from:
EROS Data Center
10th and Dakota Avenue
Sioux Falls, SD 57198

VOLUME I-D

TECHNICAL SESSION PRESENTATIONS

WATER RESOURCES

**"Made available under NASA sponsorship
in the interest of early and wide dis-
semination of Earth Resources Survey
Program information and without liability
for any use made thereof."**



National Aeronautics and Space Administration
LYNDON B. JOHNSON SPACE CENTER

NASA TM X-58168

NASA  Earth Resources Survey Symposium

VOLUME I-D

TECHNICAL SESSION PRESENTATIONS

Water Resources

PREFACE

The first comprehensive symposium on the practical application of Earth resources survey data was sponsored by the NASA Headquarters Office of Applications from June 9 to 12, 1975, in Houston, Texas. The Lyndon B. Johnson Space Center acted as host.

This symposium combined the utilization and results of data from NASA programs involving LANDSAT, the Skylab Earth resources experiment package, and aircraft, as well as from other data acquisition programs.

The primary emphasis was on the practical applications of Earth resources survey technology of interest to a large number of potential users. Also featured were scientific and technological exploration and research investigations with potential promising applications.

The opening day plenary session was devoted to papers of general interest and an overview. The following 2-1/2 days were devoted to concurrent discipline-oriented technical sessions and to three special sessions covering State and Local Users, Coastal Zone Management, and User Services. These special sessions were structured to provide governmental and private organizations with a comprehensive picture of various applications in the management and implementation of remote-sensing data use in their own programs. The concluding day was a summary with selected state, international, and technical session papers, summaries of significant results from special and technical sessions, and an overview of federal agency and international activities and planning.

Volumes I-A, I-B, I-C, and I-D contain the technical papers presented during the concurrent sessions. Volume II contains the opening day plenary session, special sessions, and the concluding day summary session. Volume III contains a summary of each session by the chairman and session personnel and provides an overview of the significant applications that have been developed from the use of remote-sensing data. Volume III also includes the conclusions and needs identified during the individual sessions and workshops.

Opinions and recommendations expressed in these reports are those of the session members and do not necessarily reflect the official position of NASA.

Olav Smistad
Symposium Coordinator

NASA  **Earth Resources Survey Symposium**

PROGRAM COMMITTEE

Charles W. Mathews, NASA, Chairman
Joseph Carlson, Public Technology, Inc.
Dr. John DeNoyer, U.S. Geological Survey
Dr. M. Frank Hersman, National Science Foundation
Daniel J. Fink, AIAA, Space Applications Board
(NRC)
Harold Finger, General Electric Co.
Dr. Stanley Freden, NASA
Willis Hawkins, Lockheed Aircraft Corp.
Russell R. Schweickart, NASA
Pitt Thome, NASA

SYMPOSIUM COORDINATORS

JOHNSON SPACE CENTER

Olav Smistad
Edward O. Zeitler
Earth Resources Program Office

OFFICE OF APPLICATIONS

Dan Richard, User Affairs

ADMINISTRATIVE SUPPORT

Industrial Economics Research Division
Texas A. & M. University

PRECEDING PAGE BLANK NOT FILMED

SESSION LEADERS

AGRICULTURE

(Includes Agriculture, Forestry, Range Resource Inventory and Management)

Richard Baldwin, Chairman

Cargill, Inc., Minneapolis, Minn.

James Murphy

U.S. Department of Agriculture, Agricultural Stabilization and Conservation Service, Houston, Tex.

Ryborn Kirby

NASA Lyndon B. Johnson Space Center, Houston, Tex.

Kenneth Suit

NASA Lyndon B. Johnson Space Center, Houston, Tex.

ENVIRONMENT

(Environmental Surveys and Applications)

Kessler Cannon and Ronald Myles, Chairmen

Department of Environmental Quality, State of Oregon, Portland, Oreg.

Dr. Ralph Shay

Oregon State University, Corvallis, Oreg.

Dr. Lawrence Greenwood

NASA Langley Research Center, Hampton, Va.

Howard Curfman

NASA Langley Research Center, Hampton, Va.

GEOLOGY

(Includes Geological Structure, Landform Surveys, Energy and Extractive Resources)

Dr. Floyd Sabins, Chairman

Chevron Oil Field Research Co., La Habra, Calif.

Dr. Larry Rowan

U.S. Department of the Interior, U.S. Geological Survey, Reston, Va.

Dr. Nicholas Short

NASA Goddard Space Flight Center, Greenbelt, Md.

Robert Stewart

NASA Lyndon B. Johnson Space Center, Houston, Tex.

INFORMATION

(Information Systems and Services)

USER SERVICES

Dr. David Landgrebe, Chairman

Purdue University/Laboratory for Applications of Remote Sensing, West Lafayette, Ind.

Terry Phillips

Purdue University/Laboratory for Applications of Remote Sensing, West Lafayette, Ind.

Timothy White

NASA Lyndon B. Johnson Space Center, Houston, Tex.

Gerald Kenney

NASA Lyndon B. Johnson Space Center, Houston, Tex.

LAND USE

(Includes Regional Planning)

STATE/LOCAL

Charles Parrish, III, Chairman

Department of Natural Resources, State of Georgia, Atlanta, Ga.

Charles Meyers

U.S. Department of Interior, Office of Land Use and Water Planning, Washington, D.C.

Dr. Armond Joyce

NASA Lyndon B. Johnson Space Center, Earth Resources Laboratory, Bay St. Louis, Miss.

Robin Rowley

NASA Lyndon B. Johnson Space Center, Houston, Tex.

MARINE RESOURCES

(Includes Marine Resources, Ocean Surveys)

COASTAL ZONE MANAGEMENT

Senator A. R. (Babe) Schwartz, Chairman

Texas State Senator, Galveston, Tex.

John Sherman, III

National Oceanic and Atmospheric Administration, National Environmental Satellite Service - SPOC Group, Washington, D.C.

E. Lee Tilton, III

NASA Lyndon B. Johnson Space Center, Earth Resources Laboratory, Bay St. Louis, Miss.

William Stephenson

NASA Lyndon B. Johnson Space Center, Houston, Tex.

WATER RESOURCES

(Water Resources Management)

Dr. Daryl Simons, Chairman

Colorado State University, Fort Collins, Colo.

John Teerink

Bookman Edmonston, Inc., Sacramento, Calif.

Dr. Vincent Salomonson

NASA Goddard Space Flight Center, Greenbelt, Md.

Raymond Clemence

NASA Lyndon B. Johnson Space Center, Houston, Tex.

CONTENTS

Paper number		Page
VOLUME I-A		
Agriculture		
A-1	ESTIMATING VEGETATIVE BIOMASS FROM LANDSAT-1 IMAGERY FOR RANGE MANAGEMENT Paul M. Seevers, James V. Drew, and Marvin P. Carlson	1
A-2	DISCRIMINATING COASTAL RANGELAND PRODUCTION AND IMPROVEMENTS WITH COMPUTER-AIDED TECHNIQUES C. A. Reeves and D. P. Faulkner	9
A-3	USEFULNESS OF LANDSAT DATA FOR MONITORING PLANT DEVELOPMENT AND RANGE CONDITIONS IN CALIFORNIA'S ANNUAL GRASSLAND David M. Carneggie, Stephen D. DeGloria, and Robert N. Colwell	19
A-4	MONITORING VEGETATION CONDITIONS FROM LANDSAT FOR USE IN RANGE MANAGEMENT R. H. Haas, D. W. Deering, J. W. Rouse, Jr., and J. A. Schell	43
A-5	UTILIZATION OF LANDSAT IMAGERY FOR MAPPING VEGETATION ON THE MILLIONTH SCALE Donald L. Williams and Jerry C. Comer	53
A-6	LANDSAT-1 DATA, ITS USE IN A SOIL SURVEY PROGRAM F. C. Westin and C. J. Frazee	67
A-7	DELINEATION OF THE BOUNDARIES OF A BURIED PRE-GLACIAL VALLEY WITH LANDSAT-1 DATA J. B. Peterson, F. E. Goodrick, and W. N. Melhorn	97
A-8	ARE CLEAR-CUT AREAS ESTIMATED FROM LANDSAT IMAGERY RELIABLE? Y. Jim Lee	105
A-9	APPLICATIONS OF LANDSAT IMAGERY IN MONITORING THE FOREST OF THAILAND Boochana Klankamsorn and staff	Unavailable
A-10	OPERATIONAL CONSIDERATIONS FOR THE APPLICATION OF REMOTELY SENSED FOREST DATA FROM LANDSAT OR OTHER AIRBORNE PLATFORMS G. Robinson Barker and Terrance P. Fethe	115
A-11	TIMBER TYPE SEPARABILITY IN SOUTHEASTERN UNITED STATES ON LANDSAT-1 MSS DATA E. P. Kan and R. D. Dillman	135
A-12	MAPPING OF THE WILDLAND FUEL CHARACTERISTICS OF THE SANTA MONICA MOUNTAINS OF SOUTHERN CALIFORNIA J. D. Nichols	159
A-13	COMPUTER ANALYSIS AND MAPPING OF GYPSY MOTH DEFOLIATION LEVELS IN PENNSYLVANIA USING LANDSAT-1 DIGITAL DATA Darrel L. Williams	167
A-14	COMPUTER IMPLEMENTED CLASSIFICATION OF VEGETATION USING AIRCRAFT ACQUIRED MULTI-SPECTRAL SCANNER DATA William G. Cibula	183
A-15	THE USE OF SKYLAB DATA TO STUDY THE EARLY DETECTION OF INSECT INFESTATIONS AND DENSITY AND DISTRIBUTION OF HOST PLANTS W. G. Hart, S. J. Ingle, and M. R. Davis	203

Paper number		Page
A-16	AGRICULTURAL INVENTORY CAPABILITIES OF MACHINE PROCESSED LANDSAT DIGITAL DATA David L. Dietrich, Ronald E. Fries, and Dwight D. Egbert	221
A-17	AGRICULTURAL APPLICATIONS OF REMOTE SENSING – A TRUE LIFE ADVENTURE Earle S. Schaller	233
A-18	PRACTICAL APPLICATION OF REMOTE SENSING IN AGRICULTURE Richard A. Phelps	239
A-19	NEED FOR REMOTE SENSING IN AGRICULTURE Hosea S. Harkness	243
Environment		
E-1	WILDLIFE MANAGEMENT BY HABITAT UNITS – A PRELIMINARY PLAN OF ACTION Carl D. Frentress and Roy G. Frye	245
E-2	AN OVERVIEW OF THE DEVELOPMENT OF REMOTE SENSING TECHNIQUES FOR THE SCREWORM ERADICATION PROGRAM Charles M. Barnes and Frank C. Forsberg	263
E-3	THE RATIONALE FOR ATTEMPTING TO DEFINE SALT MARSH MOSQUITO-BREEDING AREAS IN GALVESTON COUNTY BY REMOTE SENSING THE ASSOCIATED VEGETATION Gerald K. Arp	289
E-4	PREDICTION OF HEALTH LEVELS BY REMOTE SENSING Marjorie Rush and Sally Vernon	301
E-5	MAPPING AND CLASSIFICATION OF STRIP MINES AND ACID MINE DRAINAGE THROUGH DIGITAL ANALYSIS OF LANDSAT-1 MULTISPECTRAL SCANNER DATA S. S. Alexander, D. Baumgardt, and J. Dein	Unavailable
E-6	APPLICATION OF EREP, LANDSAT, AND AIRCRAFT IMAGE DATA TO ENVIRONMENTAL PROBLEMS RELATED TO COAL MINING Roger V. Amato, Orville R. Russell, Kenneth R. Martin, and Charles E. Wier	309
E-7	LANDSAT INVENTORY OF SURFACE-MINED AREAS USING EXTENDIBLE DIGITAL TECHNIQUES Arthur T. Anderson, Dorothy T. Schultz, and Ned Buchman	329
E-8	REMOTELY-SENSED DATA USED TO DELINEATE LAND-WATER COVER IN COAL MINING REGIONS IN EASTERN TENNESSEE A. E. Coker, A. L. Higer, S. Sauer, and R. H. Rogers	Unavailable
E-9	QUANTITATIVE WATER QUALITY WITH LANDSAT AND SKYLAB Harold L. Yarger and James R. McCauley	347
E-10	LANDSAT-1 DATA AS IT HAS BEEN APPLIED FOR LAND USE AND WATER QUALITY DATA BY THE VIRGINIA STATE WATER CONTROL BOARD Peter L. Trexler and John L. Barker	371
E-11	THE LANDSAT-1 MULTISPECTRAL SCANNER AS A TOOL IN THE CLASSIFICATION OF INLAND LAKES D. H. P. Boland and Richard J. Blackwell	419
E-12	TROPHIC STATUS OF INLAND LAKES FROM LANDSAT Lawrence T. Fisher and Frank L. Scarpace	443
E-13	THE USE OF LANDSAT-1 IMAGERY FOR WATER QUALITY STUDIES IN SOUTHERN SCANDINAVIA Ulf Hellden	451

Paper number		Page
E-14	COMPARATIVE UTILITY OF LANDSAT-1 AND SKYLAB DATA FOR COASTAL WETLAND MAPPING AND ECOLOGICAL STUDIES Richard Anderson, Linda Alsid, and Virginia Carter	469
E-15	AUTOMATIC CATEGORIZATION OF LAND-WATER COVER TYPES OF THE GREEN SWAMP, FLORIDA, USING SKYLAB MULTISPECTRAL SCANNER (S-192) DATA A. E. Coker, A. L. Higer, R. H. Rogers, N. J. Shah, L. Reed, and S. Walker	479
E-16	A COMPARATIVE INTERREGIONAL ANALYSIS OF SELECTED DATA FROM LANDSAT-1 AND EREP FOR THE INVENTORY AND MONITORING OF NATURAL ECOSYSTEMS Charles E. Poulton	507
E-17	REMOTE SENSING APPLICATIONS IN KANSAS B. G. Barr, Jerry C. Coiner, and Donald L. Williams	569
E-18	REMOTE SENSING APPLICATIONS IN THE INVENTORY AND ANALYSIS OF ENVIRONMENTAL PROBLEMS Gordon E. Howard, Jr., and C. Al Waters, Jr.	585

VOLUME I-B

Geology

G-1	SLAR RECONNAISSANCE, MIMIKA-EILANDEN BASIN, SOUTHERN TROUGH OF IRIAN JAYA R. S. Wing and J. C. Mueller	599
G-2	LANDSAT IMAGE STUDIES AS APPLIED TO PETROLEUM EXPLORATION IN KENYA John B. Miller	605
G-3	DETECTABILITY OF GEOTHERMAL AREAS USING SKYLAB X-5 DATA Barry S. Siegal, Anne B. Kahle, Alexander F. H. Goetz, Alan R. Gillespie, and Michael J. Abrams	625
G-4	GEOLOGIC AND RELATED APPLICATIONS OF REMOTE SENSING IN GEORGIA Sam M. Pickering, Jr.	Unavailable
G-5	THE ANATOMY OF AN ANOMALY Nicholas M. Short and Ronald W. Marrs	641
G-6	USE OF SPECTRAL REFLECTANCE MEASUREMENTS OF ALTERED AND UNALTERED ROCKS IN SOUTH-CENTRAL NEVADA AS A BASIS FOR ENHANCEMENT OF LANDSAT IMAGES Lawrence C. Rowan, Alexander F. H. Goetz, and Roger P. Ashley	Unavailable
G-7	APPLICATION OF SKYLAB IMAGERY TO RESOURCE EXPLORATION IN THE DEATH VALLEY REGION Ira C. Bechtold, John T. Reynolds, and C. Gregory Wagner	665
G-8	A GEOLOGICAL INVESTIGATION OF SOUTHEASTERN ARIZONA USING LANDSAT IMAGERY AND GEO-PHYSICAL DATA Richard F. Pascucci	Unavailable
G-9	SUMMARY OF SPACE IMAGERY STUDIES IN UTAH AND NEVADA Mead LeRoy Jensen and Philip Laylander	673
G-10	GEOLOGIC SIGNIFICANCE OF FEATURES OBSERVED IN COLORADO FROM ORBITAL ALTITUDES Don L. Sawatzky, Gary Prost, Keenan Lee, and D. H. Knepper	713
G-11	THE APPLICATION OF RADAR IMAGERY TO SPECIFIC PROBLEMS OF INTERIOR ALASKA P. Jan Cannon	761

Paper number		Page
G-12	LANDSAT IMAGERY ANALYSIS AN AID FOR PREDICTING LANDSLIDE-PRONE AREAS FOR HIGHWAY CONSTRUCTION Harold C. MacDonald and Robert S. Grubbs	769
G-13	ACTIVE AND INACTIVE FAULTS IN SOUTHERN CALIFORNIA VIEWED FROM SKYLAB P. M. Merifield and D. L. Lamar	779
G-14	THE UTILIZATION OF LANDSAT IMAGERY IN NUCLEAR POWER PLANT SITING A. J. Eggenberger, D. Rowlands, and P. C. Rizzo	799
G-15	SMALL-SCALE IMAGERY: A USEFUL TOOL FOR MAPPING GEOLOGICAL FEATURES IN THE TEXAS GULF COASTAL PLAIN David L. Amsbury, Uel S. Clanton, and Von R. Frierson	833
G-16	APPLICATION OF SKYLAB IMAGERY TO SOME GEOLOGICAL AND ENVIRONMENTAL PROBLEMS IN ITALY R. Cassinis, G. M. Lechi, and A. M. Tonelli	851
G-17	SKYLAB PHOTOGRAPHY APPLIED TO GEOLOGIC MAPPING IN NORTHWESTERN CENTRAL AMERICA W. I. Rose, Jr., D. J. Johnson, G. A. Hahn, and G. W. Johns	869
G-18	IDENTIFICATION AND CORRELATION OF PRECAMBRIAN AND PHANEROZOIC ORTHOGONAL FAULT AND LINEAMENT SYSTEMS IN CENTRAL AND NORTHERN ARIZONA Donald P. Elston and William D. Dipaolo	Unavailable
G-19	QUANTIFICATION OF GEOLOGIC LINEAMENTS BY MANUAL AND MACHINE PROCESSING TECHNIQUES Melvin H. Podwysocki, Johannes G. Moik, and Walter C. Shoup	885
G-20	CREATING A SYSTEM FOR THE GEOLOGICAL EXPLOITATION OF SATELLITE IMAGES: AUTOMATIC MAPPING AND GEOPHYSICAL DATA COMPARISON S. Braconne, M. Cavalier, M. Dubesset, J. Guillemot, and M. Guy	905
G-21	APPLICATION OF SATELLITE PHOTOGRAPHIC AND MSS DATA TO SELECTED GEOLOGIC AND NATURAL RESOURCE PROBLEMS IN PENNSYLVANIA W. S. Kowalik, D. P. Gold, and M. Dennis Krohn	933
G-22	GEOLOGICAL MAPPING IN NORTHWESTERN SAUDI ARABIA USING LANDSAT MULTISPECTRAL TECHNIQUES H. W. Blodget, G. F. Brown, and J. G. Moik	971
G-23	NEAR-INFRARED REFLECTANCE ANOMALIES OF ANDESITE AND BASALT IN SOUTHERN CALIFORNIA AND NEVADA Howard A. Pohn	Unavailable
G-24	ENHANCEMENT OF LANDSAT IMAGERY BY COMBINATION OF MULTISPECTRAL CLASSIFICATION AND PRINCIPAL COMPONENT ANALYSIS A. Fontanel, C. Blanchet, and C. Lallemand	991
G-25	REMOTE SENSING FRACTURE STUDY WESTERN VIRGINIA AND SOUTHEASTERN KENTUCKY Gordon L. Owens and William M. Ryan	Unavailable
G-26	A SEARCH FOR SULFIDE-BEARING AREAS USING LANDSAT-1 DATA AND DIGITAL IMAGE-PROCESSING TECHNIQUES R. G. Schmidt, B. B. Clark, and R. Bernstein	1013
G-27	REGIONAL INVENTORIES AND MAPPING OF LAND RESOURCES AND ENVIRONMENTAL GEOLOGY USING REMOTELY SENSED DATA E. G. Wermund, L. F. Brown, Jr., and W. L. Fisher	1029

Paper number		Page
G-28	MINERAL TARGET AREAS IN NEVADA FROM GEOLOGICAL ANALYSIS OF LANDSAT-1 IMAGERY Monem Abdel-Gawad and Linda Tubbesing	1059
G-29	ATTEMPT AT CORRELATING ITALIAN LONG LINEAMENTS FROM LANDSAT-1 SATELLITE IMAGES WITH SOME GEOLOGICAL PHENOMENA POSSIBLE USE IN GEOTHERMAL ENERGY RESEARCH Enrico Barbicr and Mario Fanelli	1079
Information Systems and Services		
I-1	LAYERED CLASSIFICATION TECHNIQUES FOR REMOTE SENSING APPLICATIONS P. H. Swain, C. L. Wu, D. A. Landgrebe, and H. Hauska	1087
I-2	THE MIXTURE PROBLEM IN COMPUTER MAPPING OF TERRAIN: IMPROVED TECHNIQUES FOR ESTABLISHING SPECTRAL SIGNATURES, ATMOSPHERIC PATH RADIANCE, AND TRANSMITTANCE Harry W. Smedes, Roland L. Hulstrom, and K. Jon Ransow	1099
I-3	SECOND GENERATION DIGITAL TECHNIQUES FOR PROCESSING LANDSAT MSS DATA S. S. Rifman, K. W. Simon, and R. H. Caron	1161
I-4	THE SKYLAB CONCENTRATED ATMOSPHERIC RADIATION PROJECT Peter M. Kuhn, Victor S. Whitehead, and William E. Marlatt	1177
I-5	MARKING LANDSAT IMAGES WITH SMALL MIRROR REFLECTORS William E. Evans	1185
I-6	REMOTE SENSING A VALUABLE TOOL IN THE FOREST SERVICE DECISIONMAKING PROCESS Fleet L. Stanton	1197
I-7	SPACE TECHNOLOGY PUTTING IT IN THE EDUCATIONAL PERSPECTIVE Donna B. Hankins	1221
I-8	GROUND ZERO AND UP NEBRASKA'S RESOURCES AND LAND USE Donald M. Edwards and Roger Macklem	1225
I-9	AN UNSUPERVISED CLASSIFICATION OF MULTISPECTRAL SCANNER DATA USING CORRESPONDENCE ANALYSIS (CLAMS) J-M. Monget and P. Roux	1237
I-10	ADVANCES IN AUTOMATIC EXTRACTION OF EARTH RESOURCES INFORMATION FROM MULTISPECTRAL SCANNER DATA Jon D. Erickson	1245
I-11	IMAGE 100 - THE INTERACTIVE MULTISPECTRAL IMAGE PROCESSING SYSTEM Earle S. Schaller and Robert W. Towles	1275
I-12	GEOLOGIC ANALYSES OF LANDSAT-1 MULTISPECTRAL IMAGERY OF A POSSIBLE POWER PLANT SITE: EMPLOYING DIGITAL AND ANALOG IMAGE PROCESSING Jon R. Lovegreen, William J. Prosser, and Richard A. Millet	1293
I-13	THE SCREWORM ERADICATION DATA SYSTEM (SEDS) Matthew J. Quinn	1309
I-14	LANDSAT ACTIVITIES IN THE REPUBLIC OF ZAIRE Sendwe K. Ilunga	1313
I-15	REMOTE SENSING AS AN INNOVATION: HOW CAN WE IMPROVE ON ITS RATE OF ADOPTION? Buzz Sellman	1317

Paper number		Page
I-16	M-DAS – SYSTEM FOR MULTISPECTRAL DATA ANALYSIS Robert H. Johnson	1323
I-17	ERIPS – EARTH RESOURCE INTERACTIVE PROCESSING SYSTEM Matthew J. Quinn	1351
I-18	LOW-COST DATA ANALYSIS SYSTEMS FOR PROCESSING MULTISPECTRAL SCANNER DATA Sidney L. Whitley	1355
I-19	THE INTEGRATION OF MANUAL AND AUTOMATIC IMAGE ANALYSIS TECHNIQUES WITH SUPPORTING GROUND DATA IN A MULTISTAGE SAMPLING FRAMEWORK FOR TIMBER RESOURCE INVENTORIES: THREE EXAMPLES Michael J. Gialdini, Stephen Titus, James Nichols, and Randall W. Thomas	1377
I-20	DESIGN CRITERIA FOR A MULTIPLE INPUT LAND USE SYSTEM Frederic C. Billingsley and Nevin A. Bryant	1389
I-21	USER SERVICES AVAILABLE FROM USDA'S AERIAL PHOTOGRAPHY FIELD OFFICE Ronald A. Dickson	1397
I-22	THE TEXAS REMOTE SENSING TRAINING PROJECT John B. Wells	1403
I-23	INTERACTIVE DIGITAL IMAGE MANIPULATION SYSTEM (IDIMS) Janice Henze and R. DeZur	Unavailable
I-24	IMAGE ANIMATION FOR THEME ENHANCEMENT AND CHANGE DETECTION William E. Evans	1437
I-25	THE TOTAL EARTH RESOURCES SYSTEM OF THE 1980's: A VIEW OF THE FUTURE Charles E. Cheeseman and David W. Keller	1451
I-26	EARTH RESOURCES SURVEY AND THE SPACE SHUTTLE W. Kent Stow and Roman Andryczyk	1473
I-27	SENSOR EQUIPMENT OF THE GERMAN EARTH SCIENTIFIC AIRPLANE PROGRAM Peter Seige	1483

VOLUME I-C

Land Use

L-1	THE SOUTH DAKOTA COOPERATIVE LAND USE EFFORT. A STATE LEVEL REMOTE SENSING DEMONSTRATION PROJECT Paul A. Tessar, Dennis R. Hood, and William J. Todd	1499
L-2	AN EXAMINATION OF THE POTENTIAL APPLICATIONS OF AUTOMATIC CLASSIFICATION AND TECHNIQUES TO GEORGIA MANAGEMENT PROBLEMS Bruce Q. Rado	1525
L-3	OHIO'S STATEWIDE LAND USE INVENTORY: AN OPERATIONAL APPROACH FOR APPLYING LANDSAT DATA TO STATE, REGIONAL, AND LOCAL PLANNING PROBLEMS Paul E. Baldrige, Paul H. Goesling, Frank Leone, Charles Minshall, Robert H. Rodgers, and Carl L. Wilhelm	1541
L-4	ARIZONA LAND USE EXPERIMENT Carl C. Winikka and Herbert H. Schumann	1553

Paper number		Page
L-5	THE DESIGN, IMPLEMENTATION, AND USE OF A STATEWIDE LAND USE INVENTORY: THE NEW YORK EXPERIENCE Ernest E. Hardy	1573
L-6	ALASKAN RESOURCES, CURRENT DEVELOPMENT, TRADITIONAL CULTURE VALUES AND THE ROLE OF LANDSAT DATA IN CURRENT AND FUTURE LAND USE MANAGEMENT PLANNING Arthur LaPerriere	1603
L-7	THE NATIONAL LAND USE DATA PROGRAM OF THE U.S. GEOLOGICAL SURVEY James R. Anderson and Richard E. Witmer	1609
L-8	CASES IN THE RELATION OF RESEARCH ON REMOTE SENSING TO DECISIONMAKERS IN A STATE AGENCY James W. Jondrow	1617
L-9	COORDINATING APPLICATIONS OF REMOTE SENSING AT THE STATE LEVEL Marvin P. Carlson and James Barr	Unavailable
L-10	THE DEVELOPMENT OF A LAND USE INVENTORY FOR REGIONAL PLANNING USING SATELLITE IMAGERY A. H. Hessling and Timothy G. Mara	1631
L-11	LUMIS - A LAND USE MANAGEMENT INFORMATION SYSTEM FOR URBAN PLANNING Charles K. Paul	1637
L-12	THREE U.S. URBAN AREAS ANALYZED FROM AIRCRAFT, LANDSAT, AND SKYLAB SENSORS James R. Wray	Unavailable
L-13	SATELLITE INFORMATION ON ORLANDO, FLORIDA John W. Hannah, Garland L. Thomas, and Fernando Esparza	1665
L-14	LAND USE AND ENVIRONMENTAL ASSESMENT IN THE CENTRAL ATLANTIC REGION Robert H. Alexander, Katherine Fitzpatrick, Harry F. Lins, Jr., and Herbert K. McGinty III	1683
L-15	REMOTE SENSING IMPACT ON CORRIDOR SELECTION AND PLACEMENT F. J. Thomson and A. N. Sellman	1729
L-16	IMPROVED RESOURCE USE DECISIONS AND ACTIONS THROUGH REMOTE SENSING R. Hill-Rowley, M. Boylan, W. Enslin, and R. Vlasin	1747
L-17	DEVELOPMENT OF USER APPLICATIONS FOR EARTH RESOURCES SURVEY DATA IN URBAN AND REGIONAL PLANNING IN THE PUGET SOUND AREA Frank V. Westerlund	1769
L-18	APPLICATION OF SATELLITE REMOTE-SENSING DATA TO LAND SELECTION AND MANAGEMENT W. J. Stringer, J. M. Miller, A. E. Belon, L. H. Shapiro, and J. H. Anderson	1785
L-19	THREE EXAMPLES OF APPLIED REMOTE SENSING OF VEGETATION J. W. Rouse, Jr., A. R. Benton, Jr., R. W. Toler, and R. H. Haas	1797
L-20	INTERACTIVE MULTI-SPECTRAL ANALYSIS OF MORE THAN ONE SONRAI VILLAGE IN NIGER, WEST AFRICA Priscilla Reining and Dwight Egbert	1811
L-21	USE OF LANDSAT-1 IMAGERY FOR BROAD LAND USE PLANNING IN THE NORTHERN PART OF THAILAND Manu Omakupt	Unav lable

Paper number		Page
L-22	PRESENT AND POTENTIAL LAND USE MAPPING IN MEXICO Hector Garduño, Ricardo García Lagos, and Fernando García Simo	1823
L-23	LAND USE CLASSIFICATION IN BOLIVIA Carlos E. Brockman and William G. Brooner	1841
L-24	THE BRAZILIAN REMOTE SENSING PROGRAM R. A. Novaes and F. de Mendonca	Unavailable
L-25	APPLICATION OF LANDSAT AND SKYLAB DATA FOR LAND USE MAPPING IN ITALY J. Bodechtel, J. Nithack, G. DiBernardo, K. Hiller, F. Jaskolla, and A. Smolka	1863
Marine		
M-1	THE SIGNIFICANCE OF THE SKYLAB ALTIMETER EXPERIMENT - RESULTS AND POTENTIAL APPLICATIONS A. George Mourad, S. Gopalapillai, and M. Kuhner	1887
M-2	A COMPARISON OF SKYLAB S-193 AND AIRCRAFT VIEWS OF SURFACE ROUGHNESS AND A LOOK TOWARD SEASAT Duncan Ross	1911
M-3	SKYLAB S-193 RADSCAT MICROWAVE MEASUREMENTS OF SEA SURFACE WINDS R. K. Moore, A. K. Fung, J. Young, J. Claassen, H. Chan, M. Afarani, W. J. Pierson, V. J. Cardone, J. Hayes, W. Spring, C. Greenwood, and R. Salfi	1937
M-4	A PROCEDURE FOR ESTIMATION OF SEA-SURFACE TEMPERATURE FROM REMOTE MEASUREMENTS IN THE 10-13 μm SPECTRAL REGION David C. Anding	1953
M-5	SURFACE CIRCULATION IN THE GREAT LAKES AS OBSERVED BY LANDSAT-1 AUGUST 1972 TO DECEMBER 1973: SOUTHERN LAKE MICHIGAN Harry G. Stumpf and Alan E. Strong	1973
M-6	OCEAN COLOR IMAGERY COASTAL ZONE COLOR SCANNER Warren A. Hovis	1989
M-7	SKYLAB INVESTIGATION OF THE UPWELLING OFF THE NORTHWEST COAST OF AFRICA Karl-Heinz Szekiela, Dennis J. Suszkowski, and Paul S. Tabor	2005
M-8	THE FEASIBILITY OF UTILIZING REMOTELY SENSED DATA TO ASSESS AND MONITOR OCEANIC GAMEFISH Kenneth J. Savastano and Thomas D. Leming	2023
M-9	LANDSAT DIGITAL DATA PROCESSING - A NEAR REAL-TIME APPLICATION John Barker, Charles Bohn, Locke Stuart, and John Hill	2063
M-10	NEARSHORE COASTAL MAPPING Fabian C. Polyn, and David R. Lyzenga	2075
M-11	QUANTITATIVE SUSPENDED SEDIMENT MAPPING USING AIRCRAFT REMOTELY SENSED MULTISPECTRAL DATA Robert W. Johnson	2087
M-12	REMOTE SENSING OF SALINITY Gary C. Thomann	2099

Paper number		Page
M-13	AUTOMATIC INTERFACE MEASUREMENT AND ANALYSIS Kenneth H. Faller	2127
M-14	THE MAPPING OF MARSH VEGETATION USING AIRCRAFT MULTISPECTRAL SCANNER DATA M. Kristine Butera	2147

VOLUME I-D

Water

W-1	THE USE OF SKYI AB AND LANDSAT IN A GEOHYDROLOGICAL STUDY OF THE PALEOZOIC SECTION, WEST-CENTRAL BIGHORN MOUNTAINS, WYOMING Barbara J. Tomes	2167
W-2	HYDROGEOLOGICAL INVESTIGATIONS IN THE PAMPA OF ARGENTINA Wolfgang Kruck and Wilfried Kantor	2183
W-3	HYDRO-MORPHOLOGICAL EVALUATION OF FALSE COLOR COMPOSITE MADE FROM MULTISPECTRAL IMAGERY FOR AREA BETWEEN THE GANGES AND JUMNA RIVERS, INDIA S. K. Sharma and S. C. Sharma	Unavailable
W-4	URBAN LAND USE REMOTE SENSING OF GROUNDBASIN PERMEABILITY Larry R. Tinney, John R. Jensen, and John E. Estes	2199
W-5	MICROWAVE REMOTE SENSING OF SOIL MOISTURE Fawwaz T. Ulaby, Percy P. Batlivala, Josef Cihlar, and Thomas Schmugge	2207
W-6	SOIL MOISTURE DETECTION FROM SKYLAB Joe R. Eagleman and Wen C. Lin	2233
W-7	THE CORRELATION OF SKYLAB L-BAND BRIGHTNESS TEMPERATURE WITH ANTECEDENT PRECIPITATION Marshall J. McFarland	2243
W-8	FLOOD HAZARD STUDIES IN CENTRAL TEXAS USING ORBITAL AND SUBORBITAL REMOTE SENSING IMAGERY Victor R. Baker, Robert K. Holz, and Peter C. Patton	2253
W-9	AN INUNDATION STUDY OF THE LOWER MAGDALENA-CAUCA RIVER BASIN Eduard van Es, Hernán Gómez, and Robert Soeters	2295
W-10	REMOTE SENSING OF MISSISSIPPI RIVER CHARACTERISTICS J. F. Ruff, M. M. Skinner, B. R. Winkley, D. B. Simons, and D. E. Dorratcague	2299
W-11	APPLICATION OF THERMAL SCANNING TO THE STUDY OF TRANSVERSE MIXING IN RIVERS J. Wayland Eheart	2317
W-12	UTILIZATION OF LANDSAT DATA FOR WATER QUALITY SURVEYS IN THE CHOPTANK RIVER James M. Johnson, Philip Cressy, and William C. Dallam	2325
W-13	HYDROLOGIC LAND USE CLASSIFICATION OF THE PATUXENT RIVER WATERSHED USING REMOTELY SENSED DATA William C. Dallam, Albert Rango, and Lurie Shima	2351
W-14	LAND USE CLASSIFICATION FOR HYDROLOGIC MODELS USING INTERACTIVE MACHINE CLASSIFICATION OF LANDSAT DATA Thomas J. Jackson, Robert M. Ragan, and Richard M. McCuen	2365

Paper number		Page
W-15	REMOTE SENSING TECHNIQUES FOR PREDICTION OF WATERSHED RUNOFF Bruce J. Blanchard	2379
W-16	WATER-MANAGEMENT MODEL IN FLORIDA FROM LANDSAT-1 DATA A. L. Higer, E. H. Cordes, A. E. Coker, and R. H. Rogers	2407
W-17	THE USE OF LANDSAT DCS AND IMAGERY IN RESERVOIR MANAGEMENT AND OPERATION Saul Cooper, Paul Bock, Joseph Horowitz, and Dennis Foran	2443
W-18	THE APPLICATION OF REMOTE SENSING TECHNOLOGY TO THE INVENTORY OF PLAYA LAKES IN THE HIGH PLAINS OF TEXAS A. Wayne Wyatt, Michael L. Ellis, and Ann E. Bell	2523
W-19	REMOTE SENSING APPLICATIONS IN WATER RESOURCES MANAGEMENT BY THE CALIFORNIA DEPARTMENT OF WATER RESOURCES Barry Brown	2531
W-20	A COMPARATIVE STUDY OF MULTISPECTRAL SATELLITE DATA (SKYLAB, LANDSAT) FOR EUROPEAN APPLICATIONS J. Bodechtel, R. Dittel, and R. Haydn	Unavailable
W-21	EVALUATION OF THERMAL X/5 DETECTOR SKYLAB S-192 DATA FOR ESTIMATING EVAPOTRANSPIRATION AND THERMAL PROPERTIES OF SOILS FOR IRRIGATION MANAGEMENT D. G. Moore, M. L. Horton, M. J. Russell, and V. I. Myers	2561
W-22	REMOTE SENSING INPUTS TO WATER DEMAND MODELING John R. Jensen, Larry R. Tinney, and Michael Rector	2585
W-23	AREAL EXTENT OF SNOW ESTIMATION IN THE NORTHERN SIERRA NEVADA MOUNTAINS USING LANDSAT-1 IMAGERY Edwin F. Katibah	2621
W-24	SNOW SURVEY FROM SPACE, WITH EMPHASIS ON THE RESULTS OF THE ANALYSIS OF SKYLAB EREP S-192 MULTISPECTRAL SCANNER DATA James C. Barnes and Michael D. Smallwood	2643
W-25	FACTORS AFFECTING SNOW ASSESSMENT FROM LANDSAT DATA David F. McGinnis, Jr., Michael C. McMillan, and Donald R. Wiesnet	2661
W-26	OPERATIONAL WATER MANAGEMENT APPLICATIONS OF SNOWCOVERED AREA OBSERVATIONS Albert Rango, Vincent V. Salomonson, and James L. Foster	2669

THE USE OF SKYLAB AND LANDSAT IN A GEOHYDROLOGICAL
STUDY OF THE PALEOZOIC SECTION, WEST-CENTRAL
BIGHORN MOUNTAINS, WYOMING.

W-1

By Barbara J. Tomes, Department of Geology, University of
Wyoming, Laramie, Wyoming 82071

N76-17589

ABSTRACT

Sites of geologic structures were identified using Skylab and LANDSAT imagery, and their relationships to groundwater recharge and discharge were studied. The study area lies along the western slope of the Bighorn Mountains. Runoff flowing from the Precambrian core of the Bighorn Mountains sinks as it flows over outcrops of the Bighorn dolomite. A comparison of photo-geologic maps prepared from Skylab and LANDSAT imagery and a geologic map compiled by Darton (1906) illustrates that photomapping, by itself, cannot supply adequate detail but can supplement reconnaissance mapping. Lineation maps were compiled from LANDSAT and Skylab images and compared to similar maps compiled by other investigators. Many of the lineations are expressions of tectonic activity that affect fractures, and consequently, groundwater recharge. Hydrologic features, in the form of sinks and springs, on four creeks in the study area were located on the lineation maps and their relationships to the lineations were observed. A direct correlation exists between mapped lineations and the hydrologic features. A comparison of the interpretations of other investigators, made independent of the geohydrological study, also show a direct correlation. This observation indicates direction of movement and the quantity of groundwater recharge and discharge, expressed as fracture concentration, may be estimated by comparing lineation maps to drainage and geologic maps in areas where groundwater movement is fracture controlled.

INTRODUCTION

Satellite imagery was used as an aid in the identification of sites of groundwater recharge and discharge to the Bighorn Basin of northern Wyoming. The study area lies along the western slope of the Bighorn Mountains between Shell Canyon and the Tensleep fault encompassing approximately 700 square miles (Figures 1, 2a, and 2b). In this region, the Paleozoic rocks that comprise the aquifer are impermeable unless fractured. Groundwater itself cannot be detected from satellite imagery but geologic structures controlling recharge are readily observed. LANDSAT imagery, and Skylab and high-altitude aerial photography have proven valuable in defining the structural framework of the region.

Paleozoic rocks cropping out in the study area include the Pennsylvanian Tensleep and Amsden formations, Mississippian Madison limestone, Ordovician Bighorn dolomite, and Cambrian Gros Ventre, Gallatin, and Flathead formations. Figure 3 illustrates a schematic stratigraphic section of the study area. Runoff flows from the Precambrian core of the Bighorn Mountains across the Paleozoic section and into the Bighorn Basin. Water normally carried in surface streams often sinks as it flows over the outcrops of the Bighorn dolomite, the first Paleozoic carbonate encountered in the downstream direction. Down-gradient, but up-section, a portion of the water lost to sinks reappears in springs. Known sinks and springs are located on Figures 4a and 4b. All the upstream sinks are found in the Bighorn dolomite. Springs downstream are usually found in the Madison limestone. In two cases the water sinks and rises twice in a single drainage.

On the four particular creeks in the study area, the upper sinks are associated with cavern systems ranging from a few hundred feet to almost one mile of known passage. The significance of the sinks, springs, and photo linear elements detected on spacecraft imagery may best be exemplified by F-Bar Cave on Medicine Lodge Creek, which developed as Medicine Lodge Creek eroded into the Bighorn dolomite. The occurrence of slickensides of the walls of the cave demonstrates structural control of the passages. A large volume of water flows into the cavern and follows passages developed along fractures. One quarter mile downstream from the sinks, water rises in the bed of Medicine Lodge Creek from springs probably controlled by bedding planes, fractures, or both.

PREVIOUS WORK

Darton (1906) compiled the only published geological map of the entire area. Wilson (1938) studied a one-to-five mile wide strip along the Tensleep fault, Lowry (1962) wrote a USGS open file report on groundwater in the vicinity of the town of Tensleep, Wyoming, Mackin (1947) and Fanshawe (1971) described the structural evolution of the Bighorn Basin, and Hoppin and Palmquist (1965) and Hoppin, Palmquist, and Williams (1965) defined tectonic controls in the Bighorn Mountains. Blackstone (1973), Hoppin (1973), and Hoppin and Jennings, (1971) studied the structural geology in north-central Bighorn Mountains and used satellite imagery in their work.

METHODOLOGY

Several types of imagery are available for this area; LANDSAT (1:3,000,000), Skylab S-190A (1:2,800,000), Skylab S-190B (1:850,000), and aircraft (various scales). Although the study involved all three types of imagery, only applications of LANDSAT and Skylab imagery will be summarized here. Prior to interpreting the imagery, the writer spent several weeks mapping the geologic and hydrologic features in parts of the study area during the summer and fall of 1974. As a result, many of the interpretations reflect experience gained from the field studies.

The LANDSAT and Skylab images examined are described in Table I.

LANDSAT

<u>Date</u>	<u>Image Number</u>	<u>Ground Condition</u>	<u>Image Quality</u>
5 Aug 72	1013-17291	no snow cover	excellent
7 Sep 73	1409-17285	10% snow cover	excellent
16 Oct 72	1785-17294	no snow cover	excellent
21 Nov 72	1121-17301	40% snow cover	excellent

Table I. (cont.)

<u>Date</u>	<u>Image Number</u>	<u>Ground Condition</u>	<u>Image Quality</u>
1 Feb 73	1193-17301	90% snow cover	excellent
14 Feb 74	1571-17252	60% snow cover	excellent
19 Feb 73	1211-17302	total snow cover	excellent

Skylab

<u>Date</u>	<u>Track Number</u>	<u>Pass Number</u>	<u>Image Number</u>	<u>Image Quality</u>
13 Jun 73	5	10	S-190A Frames 227-229	10% cloud cover
			S-190B Frames 146-147	10% cloud cover

Table I.

All available LANDSAT imagery for spring and early summer of 1972 and 1973 were cloud covered. The June 1974 images were cloud-free but were not available for this study.

Photogeological maps of the area were compiled first using LANDSAT (Figure 5a) and Skylab (Figure 5b). A comparison of the remote sensing maps and the geological map prepared by Darton (1906, Figure 5a) illustrates a similarity but the imagery revealed that Darton's map is geographically imperfect. For example, streams were misplaced and the aerial extent of outcrops was distorted. A Skylab image superimposed on Darton's map is used to refine the geologic mapping (Figure 6b). Streams were correctly placed and the geology was adjusted. Much detail, however, was not discernible. One problem encountered was the two completely different grid locations.

Photolinear maps of the study area have been prepared by Blackstone (1973, Figure 7a), Hoppin (1973), Hoppin and Jennings (1971, Figure 7b), and Earle (unpublished, Figure 7c). Each map is somewhat different and reflect different interpretations. Two photolinear maps were compiled by the author for this report using LANDSAT (Figure 3a) and Skylab (Figure 8b). Hoppin (1974), described the problems of terminology regarding lineaments and linears detectable on spacecraft imagery. He defines linears as "single rectilinear elements, commonly, but not necessarily, of structural origin. Lineaments are "rectilinear lines or zones of structural discordance of regional extent." For purposes of this report, lineaments have not been used because of the broad scale relationships they imply. Instead, "major" and "minor" linears are delineated although some "major" linears may in fact be lineaments. Care was taken to eliminate cultural-related linears such as tree lines, clear cutting, and fence lines. Figure 8a is a representation of "major" linears or very broad scale features easily detected at a glance. Figure 7b illustrates "minor" linears or features which are much more subtle to detect, but reflect definite linear continuity. These maps were prepared from various interpretations compiled at different times from the different images described in Table I.

RESULTS

A direct correlation may exist between geohydrological features and linears. Many of the linears are expressions of tectonic features that affect the geohydrological system in the area. Linears appear to correlate with fractures which control the flow of water. A comparison of the hydrological features and linears (Figures 9a, 9b, and 9c) yields the following results in each of the four drainages in the study area:

Trapper Creek - The cave behind the sinks has not been explored due to a log jam but examination of springs downstream that rise from the Devonian rocks on the north face of Trapper Canyon suggests that the spring water is not the same water flowing into the sink. The sink occurs at the intersection of a major and minor linear (Figure 9b). The minor east-west linear appears to line up with a line of mountain crests in the Precambrian core to the east. This alignment suggests that the minor linear may be a major structural element. In that case, the sinks would occur at the intersection of two major linears.

Dry Medicine Lodge Creek - One of the major cave systems known in the Bighorn Mountains occurs at the intersection of several linears. Within the cave is a network of passages along joints, fractures and faults, many of which contain flowing water. The water does not reappear in any large sinks downstream and is assumed to be recharging the Paleozoic aquifer. A few miles downstream from the cavern, the position of the springs and sinks have migrated upstream during the summer and are presumed related to isolated water table conditions and not major linear elements. The springs furthest downstream issue from fractures in the Madison Limestone.

Medicine Lodge Creek - Located at the sinks of Medicine Lodge Creek is P-Bar Cave, a fracture controlled cave situated at the intersection of two major linears. A large amount of water enters the cave and springs rise from the creek bed a few hundred feet below the cave. Dye-tests conducted by the author prove that this water is the same as that entering the cave. A number of minor linears photomapped in the vicinity of the cave have an orientation parallel to the apparent orientation of passages within the cave.

Canyon Creek - The sinks and springs of Canyon Creek are each associated with major linears. Dye tests conducted by the author revealed that the sinks and springs are directly connected and no groundwater recharge is occurring at this location. The upstream sinks and springs are both sites of open passable caves although open passage between the two does not exist. The downstream sinks and springs are not associated with caverns and they are clogged with debris.

CONCLUSIONS

The value of satellite imagery in the geohydrological application in this study results because the images aid the investigator in locating structural features that may influence groundwater flow. Results of this study suggest that the hydrologic features are partially controlled by large-scale structural features detectable on satellite imagery. A direct correlation exists between mapped linears and the hydrologic features observed but because of the field research prior to the image interpretations, the author's interpretation may be biased. A comparison of the interpretations of other investigators, made independently of the geohydrological study, also shows a direct correlation between the location of sinks and springs with linear or linear intersections. This observation indicates direction of movement and the quantity of groundwater recharge may be expressed as a function of fracture concentration, taken from photolinear maps that are compared with drainage and geological maps in an area where groundwater movement is fracture controlled. The right compilation of fractures, geology, and water drainage could result in a location of groundwater recharge and discharge sites. If one could assume similar relationships between structure and groundwater movement in other areas (such as on the east flank of the Bighorn Mountains) application of satellite data would be straightforward.

Unfortunately, the hydrological systems in most areas are extremely complex and analyses require both remote sensing study and extensive field research.

The program of continuous LANDSAT coverage was particularly useful because it provided a capability to study imagery acquired during a number of weather and seasonal conditions. The disadvantage of LANDSAT imagery is its limited resolution. Definition of lithologic contacts is extremely difficult. The Skylab photography was far superior in resolution but cloud cover and shadows obscured part of the area. The discontinuity resulting from the cloud cover is a major disadvantage when using the photography in a reconnaissance study. The cloud-free portion of the Skylab photography is excellent for geologic mapping, particularly when utilizing the capability to view Skylab photography in stereo, but some units such as the Madison Limestone and Bighorn dolomite were difficult or impossible to differentiate.

SELECTED REFERENCES

- Blackstone, D. L., Jr., 1973, Analysis of linear photo elements, Bighorn-Pryor Mountains, Montana and Wyoming; Special Report, ERTS Contract NAS 5-21799.
- Darton, N. H., 1906, Geology of the Bighorn Mountains; USGS Prof. Paper 51, 129 p.
- Earle, Jan, 1974, Map of photo-linear elements interpreted from ERTS-1 winter imagery; unpublished.
- Fanshawe, John R., 1971, Structural evolution of the Bighorn Basin; 23rd Ann. Field Conf., Wyoming Geological Association Guidebook, pp. 35-37.
- Hoppin, Richard A., 1973, Utilizing ERTS-1 imagery for tectonic analysis through study of the Bighorn Mountains region; Progress Report, ERTS Contract NAS 5-21852, microfilm E73-10420.
- _____, 1974, Lineaments: Their role in tectonics of central Rocky Mountains; AAPG Bull, V. 58, no. 11, pp. 2260-2273.
- Hoppin, R. A., and Jennings, T. V., 1971, Cenozoic tectonic elements, Bighorn Mountains region, Wyoming and Montana; 23rd Ann. Field Conf., Wyoming Geological Association Guidebook, pp. 39-47.
- Hoppin, R. A., and Palmquist, John C., 1965, Basement influence on later deformation; the problem techniques of investigation and examples from the Bighorn Mountains of Wyoming; AAPG Bull., V. 49, no. 7, pp. 993-1003.
- Lowry, Marlin E., 1962, Development of groundwater in the vicinity of Tensleep, Wyoming; USGS open file report.
- Thom, W. T., Jr., 1947, Structural features of the Bighorn Basin Rim; 2nd Ann. Field Conf., Wyoming Geological Association Guidebook, pp. 173-177.
- Wilson, Charles W., 1938, The Tensleep Fault, Johnson and Washakie counties, Wyoming; Jour. of Geol., V. 48, no. 6, pp. 868-881.

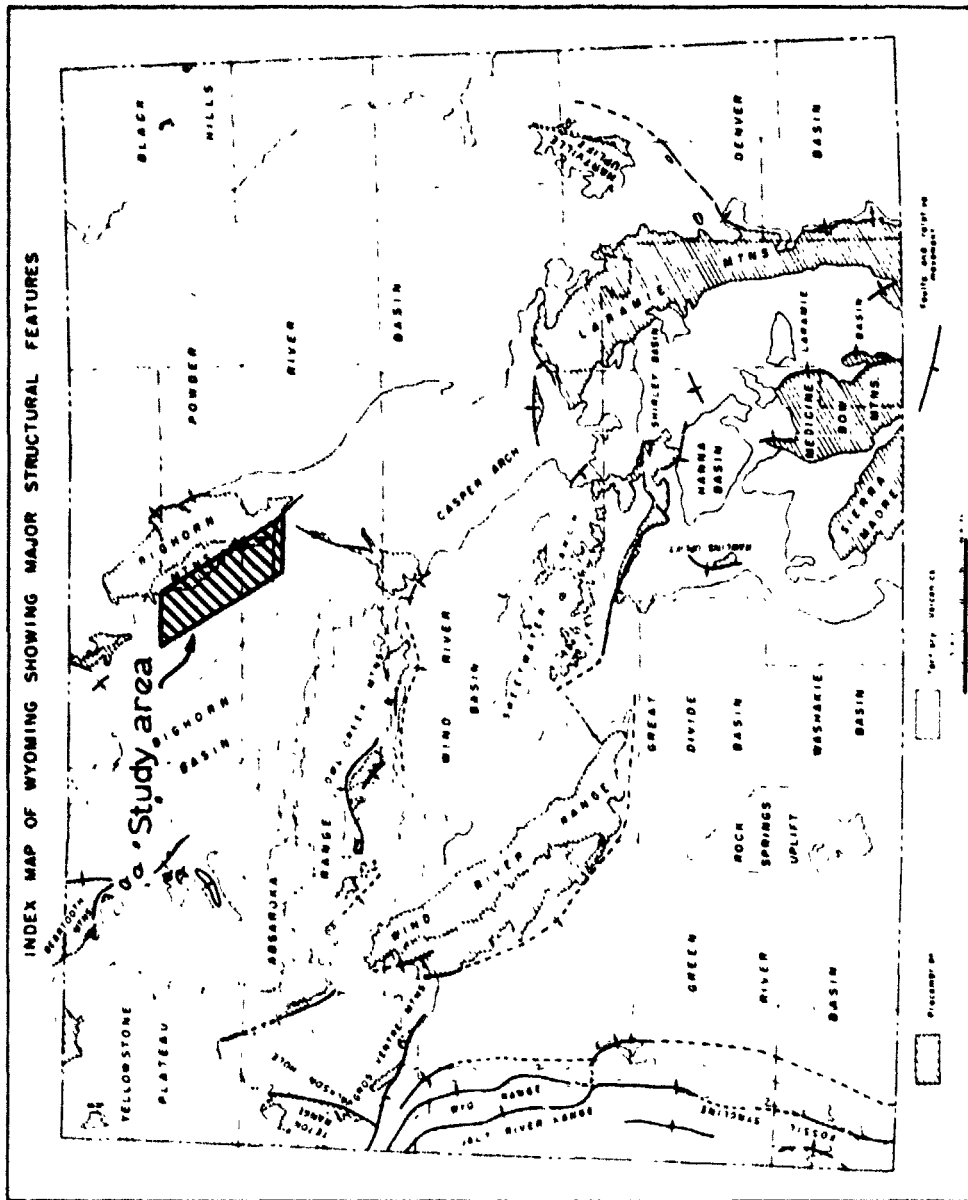


Figure 1 Index Map showing Study Area

**REPRODUCIBILITY OF THE
GENERAL EDGE IS FOUR**

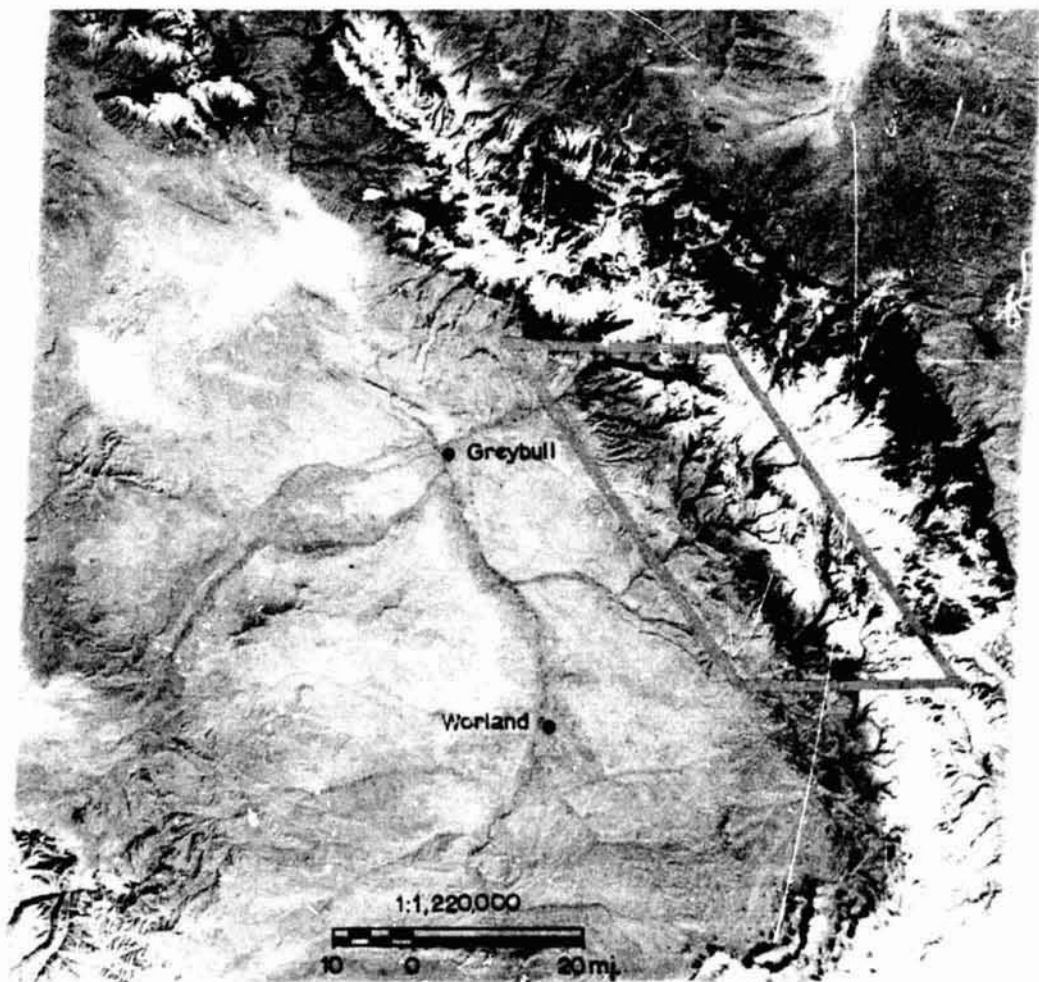
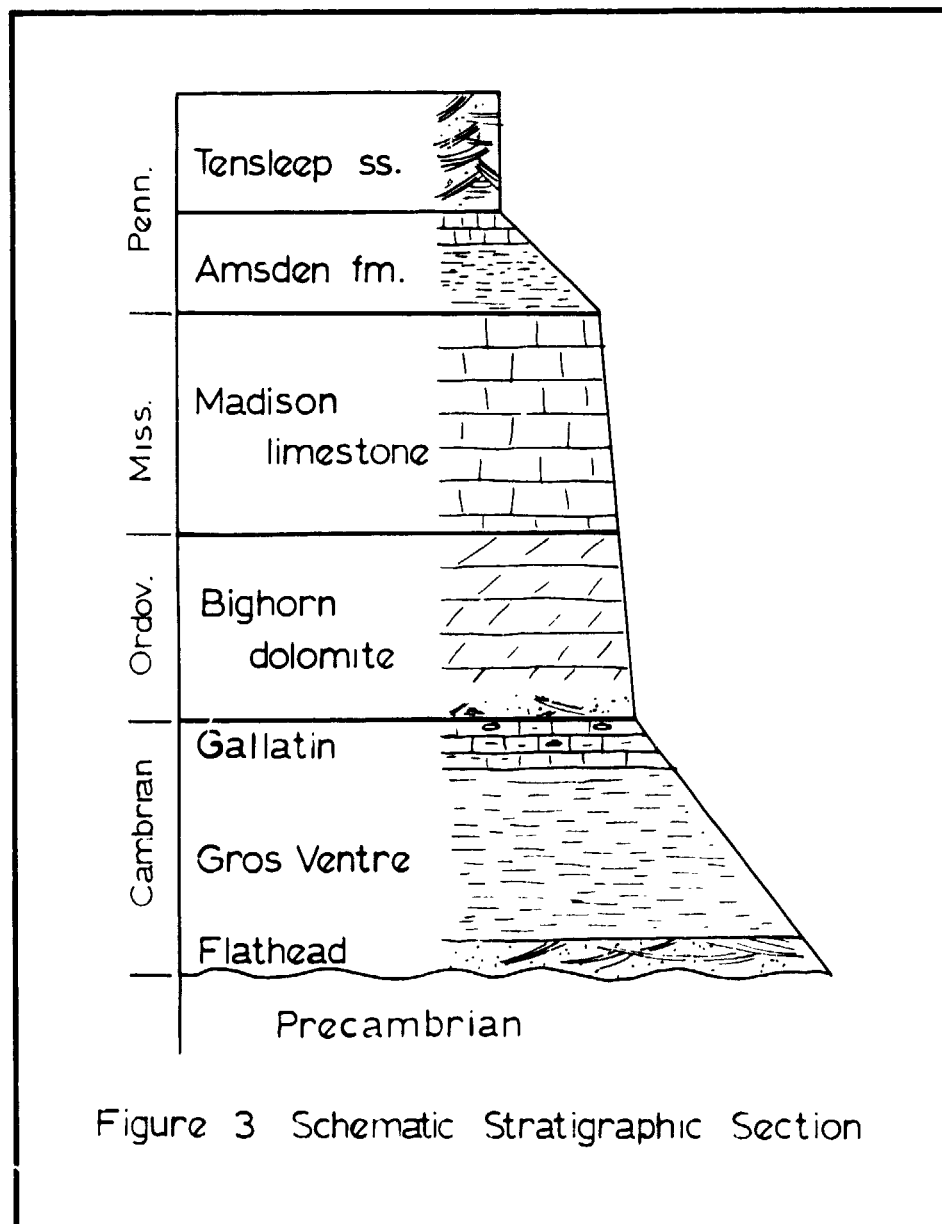


Figure 2a. LANDSAT image 1121-17301-5, 21 November, 1972, showing Bighorn Basin and Bighorn Mountains. Study area is outlined.



Figure 2b. Skylab II, track 5, pass 10 photograph, frame 228, June 13, 1973, showing Bighorn Basin and Bighorn Mountains. Study area is outlined.



REPRODUCIBILITY OF THE
ORIGINAL PAGE IS POOR

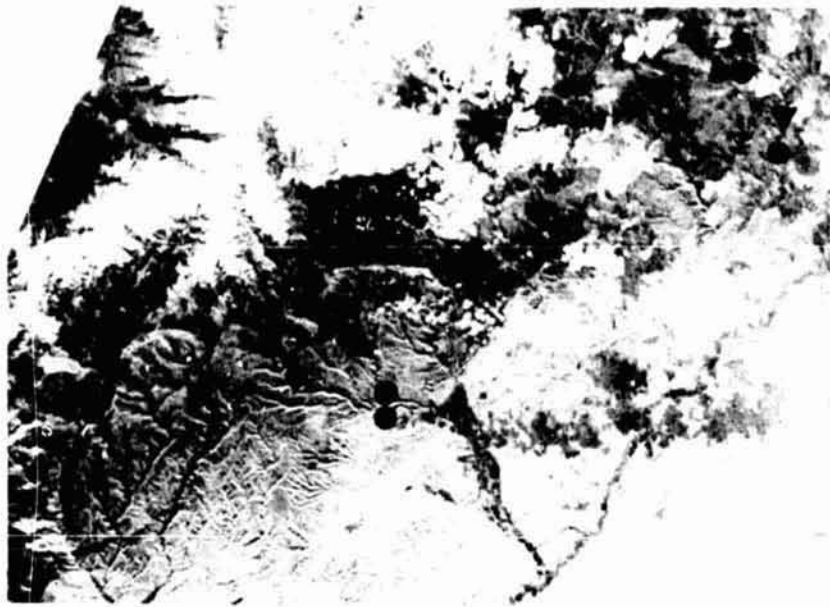


Figure 4b. Skylab

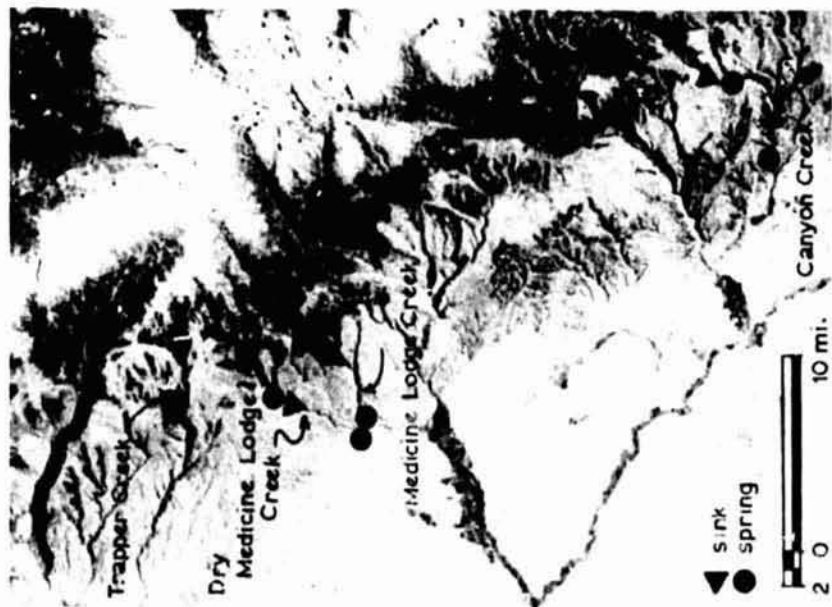


Figure 4a. LANDSAT

LANDSAT-1 image 1409-17285-5 and Skylab II track 5 pass 10 S190-B photograph showing location of known sinks and springs on four creeks in the study area.

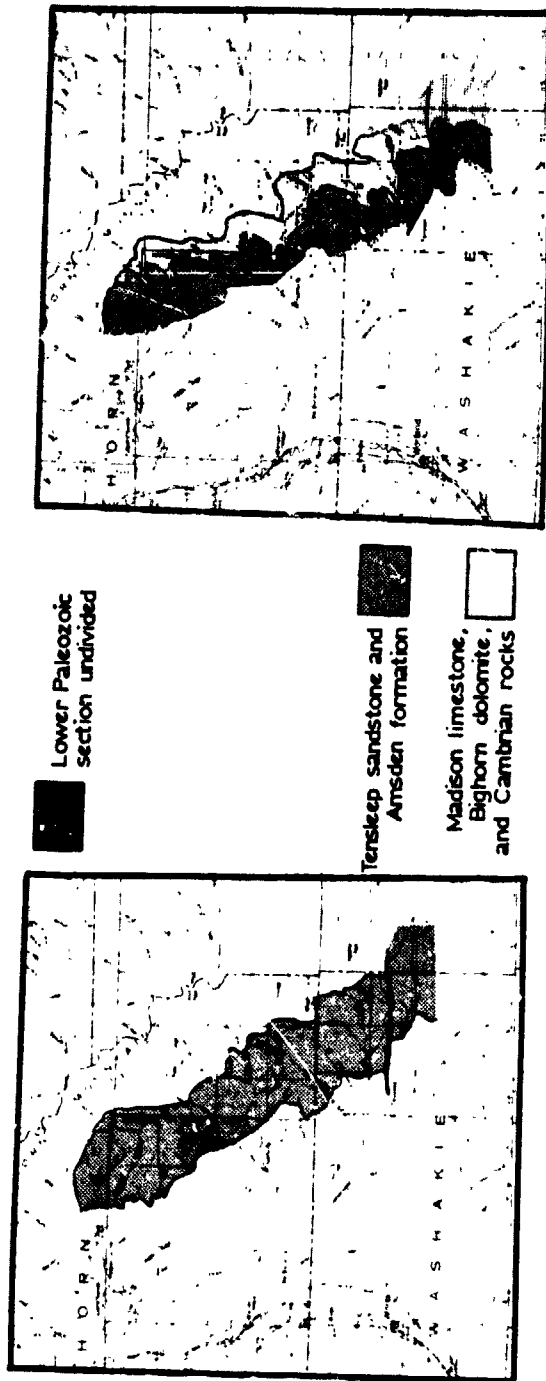
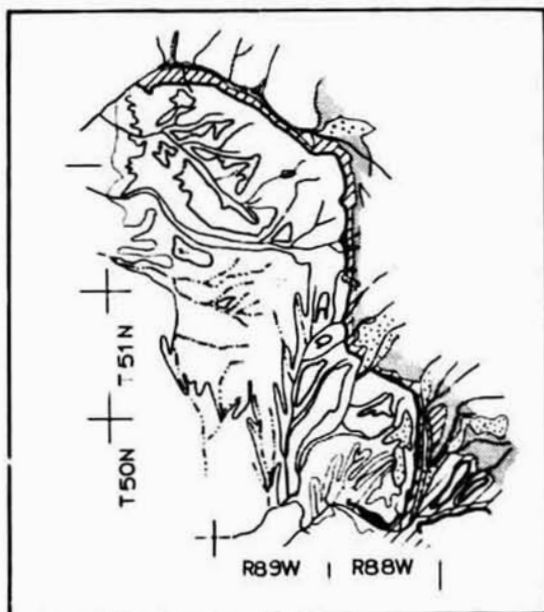


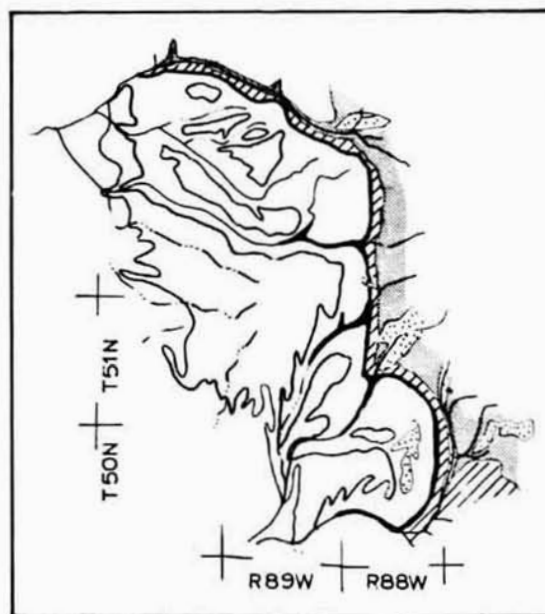
Figure 5a.

Geology of study areas as interpreted from LANDSAT (a) and Skylab (b).

Figure 5b.



6a.

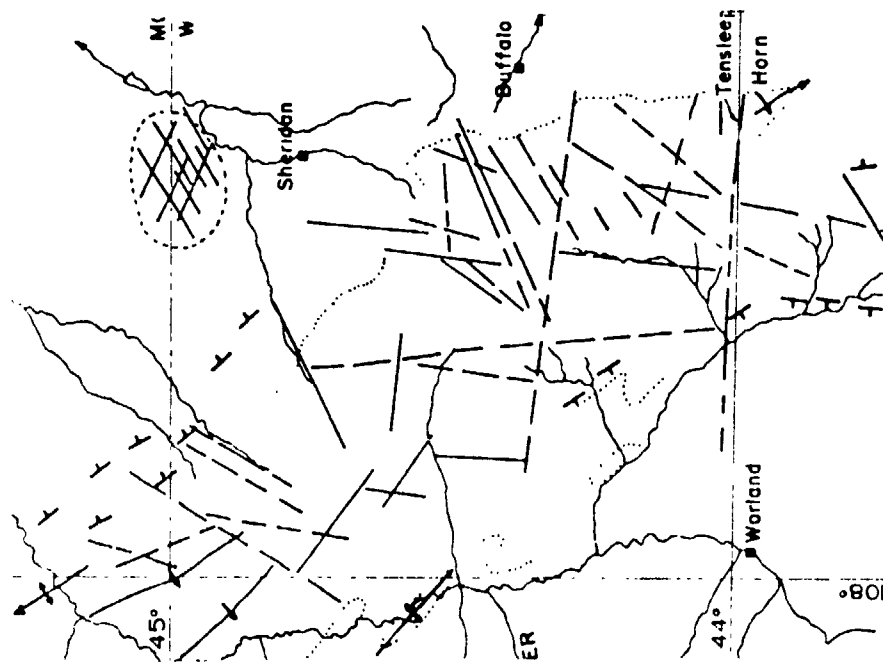


6b.

Figure 6a. Geological map compiled by Darton (1906).

Figure 6b. Darton's geological map geographically corrected using Skylab photography.

-  Tertiary sediments
-  Pennsylvanian Tensleep sandstone
-  Mississippian Madison limestone
-  Ordovician Bighorn dolomite
-  Cambrian formations undivided
-  Precambrian rocks



(Blackstone, 1973)
7a.



(Hoppin, 1973)
7b.



Photolinear maps of the Highhorn Mountains, compiled by Blackstone (1973) and Hoppin (1973).

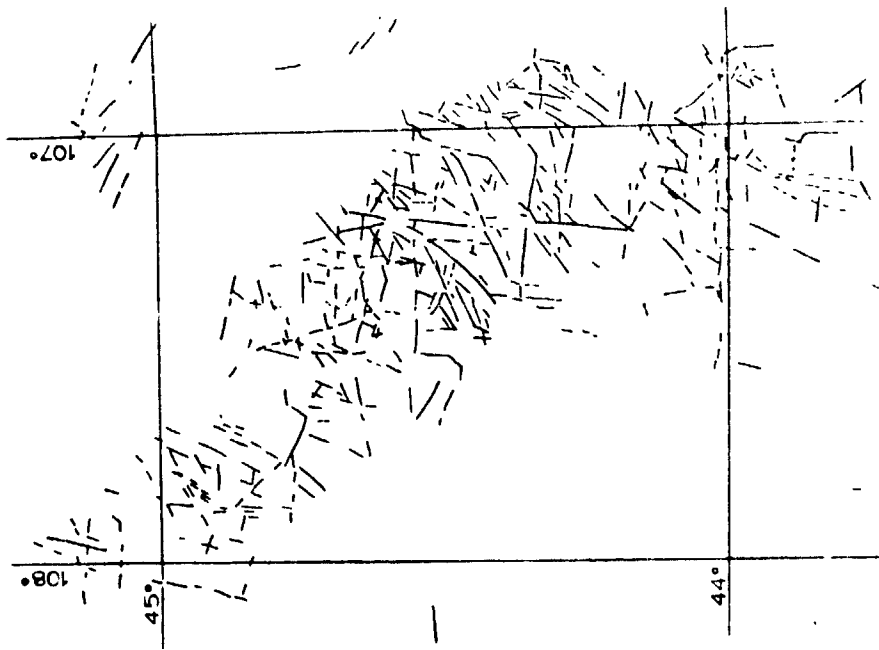
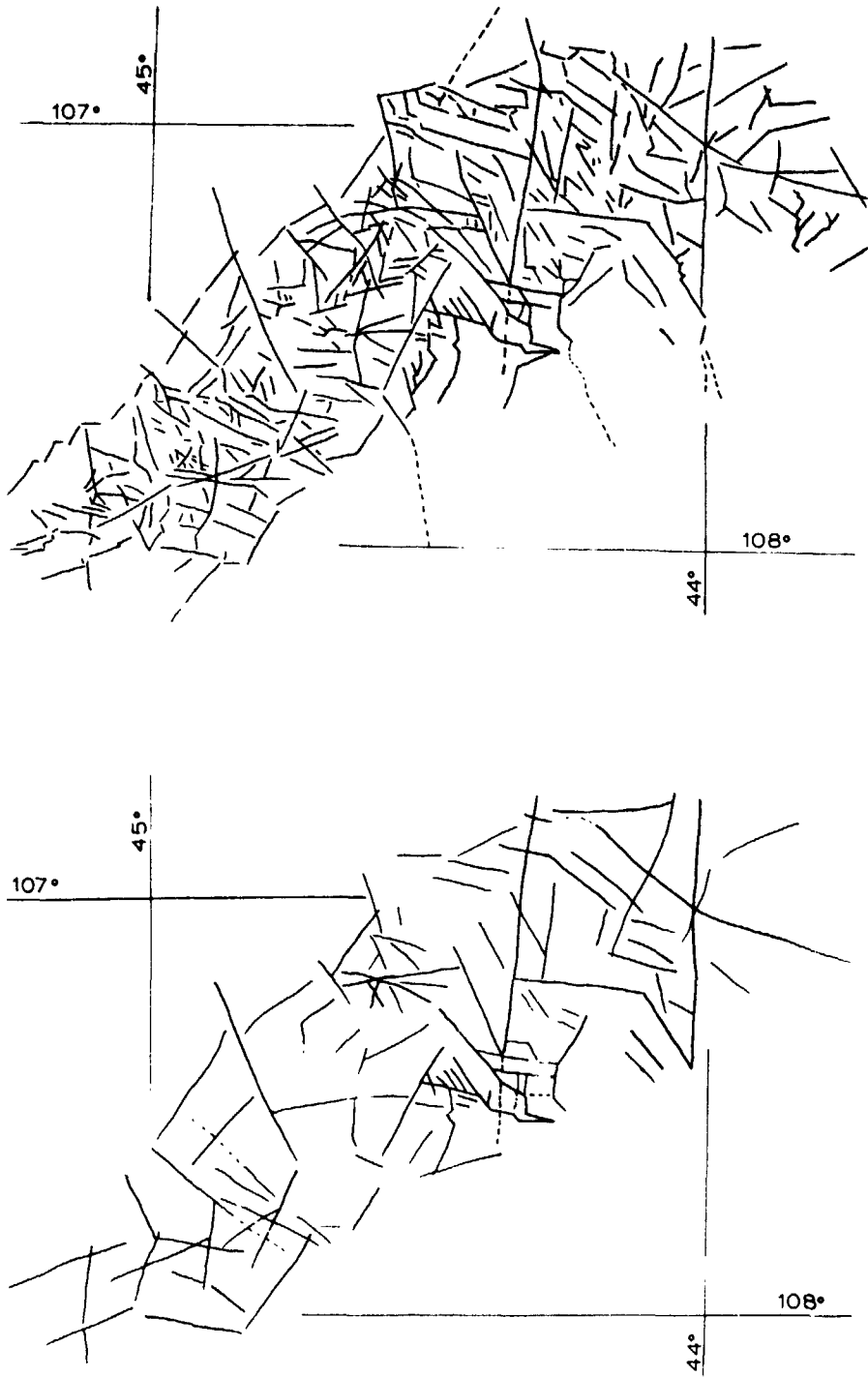
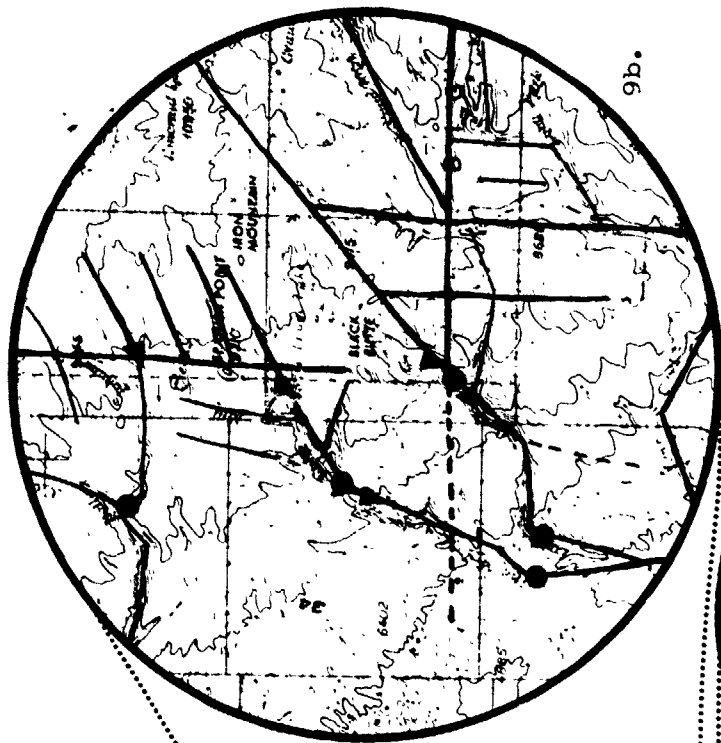


Figure 7c. Photolinear of Bighorn Mountains compiled by Earle, (1974).

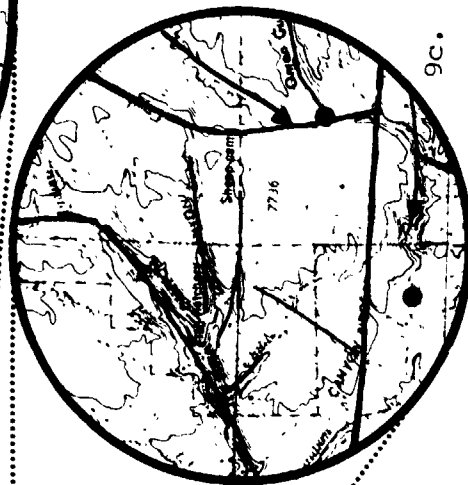
Earle, (1974)
7c.



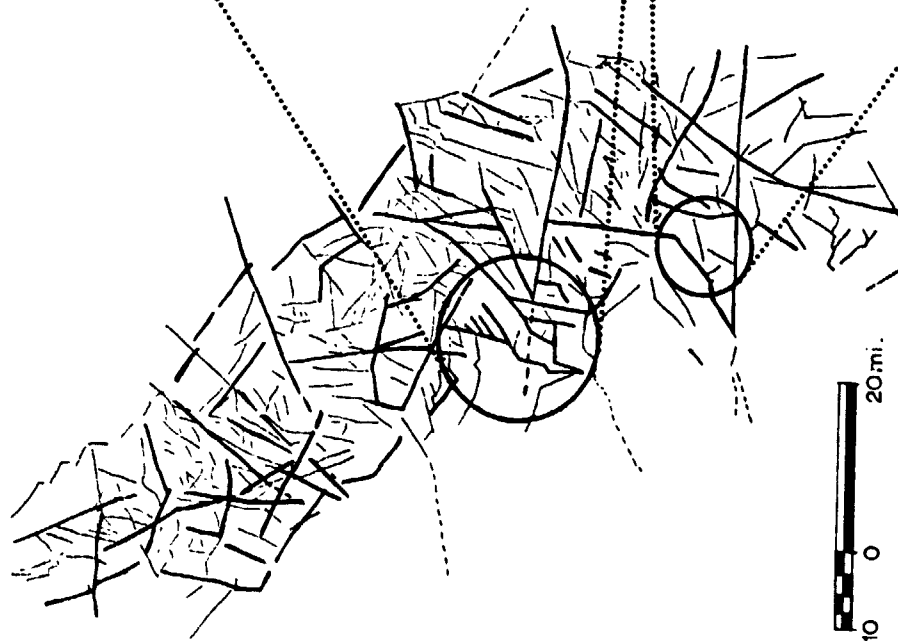
Figures 8a and 8b. Photolinear maps of the Bighorn Mountains.



9b.



9c.



9a.

Figure 9a. Major and Minor linears of the Bighorn Mountains.
 Figure 9b,9c. Details (1:250,000) of the major and minor linears in the vicinity of the four creeks studied.

HYDROGEOLOGICAL INVESTIGATIONS IN THE PAMPA OF ARGENTINA W-2

By Wolfgang KRUCK and Wilfried KANTOR,
Bundesanstalt für Geowissenschaften und Rohstoffe, Hannover, Germany

N76-17590

ABSTRACT

In large areas of the Argentinian Pampa the salinization of ground water creates water supply difficulties.

Investigations of satellite imagery (Landsat-1 and Skylab) which were based on an extensive ground survey revealed that differences in the vegetation cover are closely related to depth and salinity of ground water.

Narrow elongated depressions called "bajos" are often the only indication of fresh ground water. They can be easily detected on the imagery.

Due to their high resolution Skylab photos even allow a quantitative estimation of fresh ground water situated below the bajos. In general however Landsat-1 imagery sufficed for evaluation.

In the area of the Rio Tercero a fossil drainage pattern discovered and in Corrientes province, soil types could be discriminated and compared to the SOIL MAP OF THE WORLD.

The use of satellite imagery in the future will reduce the number of observation points for hydrogeological reconnaissance mapping by up to 75 % in areas with similar hydrogeological conditions.

INTRODUCTION

The lack of fresh ground water for consumption by humans and livestock in the Argentinian Pampa led to an intensive hydrogeological investigation in an area of about 50,000 km² situated between the Sierra de Córdoba in the West and the Rio Paraná in the East (Fig. 1).

The ground survey was carried out by the Institute of Geoscience and Natural Resources of Germany, in cooperation with Argentinian Organizations, Minería y Geología and Subsecretaría de Recursos Hídricos.

In the scope of a NASA project (SR No. 330) the value of Landsat-1 and Skylab data was to be put to the test with regard to the hydrogeological problems.

Initially Landsat-1 imagery covering the whole project area was used for the investigation. The results have been represented in a final NASA report.

Skylab photos available later covered only half the project area but included additional areas in the Northeast and Southwest. From the Skylab photography use was made mainly of IR color photos as these represented contrasts most clearly.

GEOLOGICAL AND HYDROGEOLOGICAL CONDITIONS OF THE PAMPA

In the project area the water level of an upper ground water body, developed in quaternary loess sediments, is situated between 0-20 m below the surface. The ground survey revealed a relationship between morphology, depth to ground water and salinity of ground water. This relationship is reflected by a number of features and units at the earth's surface and can therefore be observed on Landsat-1 and Skylab imagery.

Areas with saline and fresh ground water due to different depths
to ground water

The area under investigation is generally characterized by the relatively high salt content of the near - surface ground water. However the salt content of the ground water differs considerably from place to place.

Regions with a ground water table of less than about 5-7 m appear light blue in Skylab IR color photos (Fig. 2). High evapotranspiration in the loess sediments results in increased soil and ground water salinity which leads to unfavourable conditions for certain plant species. These areas are favoured predominantly by halophytes.

The best growth conditions prevail in regions where the ground water levels are situated below the area of influence of evapotranspiration (approx. 10 m or deeper).

In Skylab IR color photos these areas are mainly reddish colored, indicating that they are densely covered by vegetation with a high chlorophyll content.

Generally ground water mineralization increases with decreasing depth to ground water. It can be assumed that the effect of evaporation acts to a depth of about 3 m. Transpiration by plants increases the potential pump lift by 2 to 7 m.

"Bajos"

Bajo is the Argentinian term used to describe elongated flat depressions without surface drainage. In satellite imagery they appear as sharply defined strips. They run more or less straight in a ENE-WSW direction, are usually between 100-200 m wide and are spaced at relatively even distances of approx. 2 km, as can be seen in satellite imagery (Fig. 2 b and Fig. 3).

The constant pattern of the bajos throughout the Pampa region suggests a tectonic origin, probably due to fractures in the deep underlying crystalline bedrock.

After heavy rainfall water collects in the bajos. It is here that more water infiltrates than in the vicinity. As a result fresh water lenses are formed, under the bajos, in the saline ground water body, thereby offering water supply possibilities for rural needs (Fig. 4).

Geophysical research and pumping tests revealed that for the calculation of fresh water reserves (salt content lower than 1 g/l), a medium thickness of 20 m can be assumed. The volume of the fresh water impregnated sediment

therefore can be calculated from space by using the formula:

$$V = W \times L \times T$$

=====

V = Volume of the fresh water saturated sediment

W = Width of the bajo

L = Length of the bajo

T = Known medium thickness of the fresh water saturated sediment

About 10 % of the Volume (V) is assumed to be the total quantity of extractable fresh ground water.

As an example, the fresh water content in the boxed section of Fig. 3 should be calculated:

$$V = 400 \text{ m} \times 3000 \text{ m} \times 20 \text{ m}$$

$$V = 24,000,000 \text{ m}^3$$

Extractable fresh ground water in this bajo section is therefore 10 % from
 $24,000,000 \text{ m}^3 = 2,400,000 \text{ m}^3$.

=====

ANCIENT RIVER BEDS OF THE RIO TERCERO

In the Southwest of the project area and adjacent to the South a net-like pattern of light grey to light blue stripes can be observed on the Skylab IR color photo (Fig. 5). These parts of the area are only sparsely developed agriculturally. The soil probably consists of fluvial sand deposited in ancient beds of the Rio Tercero. It can be assumed that due to the strong percolation into the sandy soil there is insufficient soil moisture for abundant vegetation.

Bajos were frequently adapted by the drainage system of the Rio Tercero. For the origin of the pattern the following theories are thought to be reasonable:

- The Rio Tercero formerly entered the Arroyo de las Tortugas in the East (Fig. 5). In the course of time the Rio displaced its river bed further to the West, probably induced by tectonic movements, temporarily draining even to the West of the current river bed.
- The Rio Tercero had a net-like pattern during an earlier wetter climate.

STUDY OF SOIL AND VEGETATION

Pedological units were delineated on an IR color photo showing about 13,000 km² of Corrientes province, Northern Argentina (Fig. 6). No ground truth has been carried out in this region. The investigation was possible only by comparison of different colored and textured units on the photo with the pedological units on the SOIL MAP OF THE WORLD (FAO, UNESCO 1971), as well as by analogic conclusions from the project area further in the Southwest.

The soil types delineated on the SOIL MAP OF THE WORLD (1 : 5,000,000) can be correlated with units on the photo. Locally, due to its larger scale, the image allows a further differentiation, e.g.: East and West of the Rio Paraná where exclusively mollic planosols are delineated on the map. In the Western area where a number of open waters and more intensive vegetation can be observed, the distribution of hydromorphic soils is taken into account.

The sediments in the investigated area are of fluvial and aeolian origin. The soil moisture is influenced by the river floods and depth to ground water. A clue to estimating depth to water is the distribution and accumulation of open waters assuming that the sediments are permeable.

Different intensity and chlorophyll content of vegetation is imaged by different red tones on the photo. This is an important criterion for soil type identification as the predominant natural vegetation in this region reflects the genuine connection between vegetation, soil and climate.

Soil types in the investigated area

The pedological symbols and the description of soils, vegetation and lithological units were drawn from the SOIL MAP OF THE WORLD.

The predomination of sand or clay in a soil type, which could be detected on the image, has been marked as index s (= sand) or c (= clay) over the soil symbol.

- Wm_c - = Mollic planosols (predominantly clayish)

Image characteristic: (I.C.) Predominantly pale pink tones, insignificant textured areas. Regular soil conditions. No agriculture.

Deep eroded river beds, refer to deep ground water table. Green-blue and blue patches in the drainage area of the rivers, show areas with high soil moisture and some open waters, near surface ground water.

Description taken from
SOIL MAP OF THE WORLD
- (SMW):

Xerophytic deciduous forest, wet palm
savanna. Paraná alluvium and
Pampean formation.

- Wm_s - = Mollic planosols (predominantly sandy)

I.C.: Predominantly pink to white tones; mixed texture;
in the North, blue colored areas.
Natural vegetation and agriculture (field pattern
observable). Few open waters indicate a relatively
deep ground water table. To the North reduction
of depth to ground water.

S.M.W.: Xerophytic deciduous forest, wet palm savanna;
Paraná alluvium.

- Je - = Eutric fluvisols

I.C.: Predominantly dark-blue to grey-blue areas with
some pink strips indicate flooded areas with
locally dense swamp vegetation.

S.M.W.: Wet palm savanna, swamps and meadows.
Alluvium of the valleys and depressions with
internal drainage.

- We_c - = Eutric planosols (predominantly clayish)

I.C.: Predominantly blue-green areas with a few pink
patches. Isolated field pattern. These areas
are less moist than the - Je - areas, to which
they are adjacent in the South. It can be assumed
that the Rio Corrientes has a steeper slope in the
- We_c - area.

S.M.W.: Xerophytic deciduous forest palm savanna;
Alluvium.

- We_s - = Eutric planosols (predominantly sandy)

I.C.: Predominantly light grey to whitish and pink. A
great number of open waters directed North to
South (probably initiated by the wind). Near
surface ground water. Agriculture dominates.

S.M.W.: Xerophytic deciduous forest, palm savanna;
Alluvium.

- Gm - = Gleysoils

I. C. : Predominantly red-brown purpur with striey texture, e. g. : on the riverside meadows of the Rio Paraná.
Probably vegetation of hydrophile plants.

S. M. W. : On the SOIL MAP this soil type is not delineated in the investigated area. Probably because of its small distribution it is connected to mollic planosols.

The resolution of the Skylab photo also allows large scale pedological differentiation due to the individual soil textures and colors.

The satellite image is an important tool for the preparation of pedological mapping and the determination of key areas in regions with natural conditions of vegetation. Its application allows a considerable reduction of field costs as ground conditions can be estimated and a preselection of the equipment is possible.

BENEFITS OF LANDSAT-1 AND SKYLAB DATA APPLICATION

About 20 available wells per 100 km² are needed for conventional reconnaissance mapping of depth to water and salinity in the Pampa.

Large scale mapping for water supply purposes was carried out using about 80 wells per 100 km².

With the aid of Landsat-1 and Skylab imagery the number of observation points for reconnaissance mapping can be reduced by up to 50 % and for large scale mapping up to 75 %. This equates to a reduction of field costs from \$600 to \$300 (rec. mapping) or respectively, from \$2,400 to \$600 per 100 km² (large scale mapping).

In general Landsat-1 imagery sufficed for these evaluations. Only in cases where higher resolution is needed, e. g. : calculation of bajos fresh water reserves, do Skylab photos allow a more precise determination.

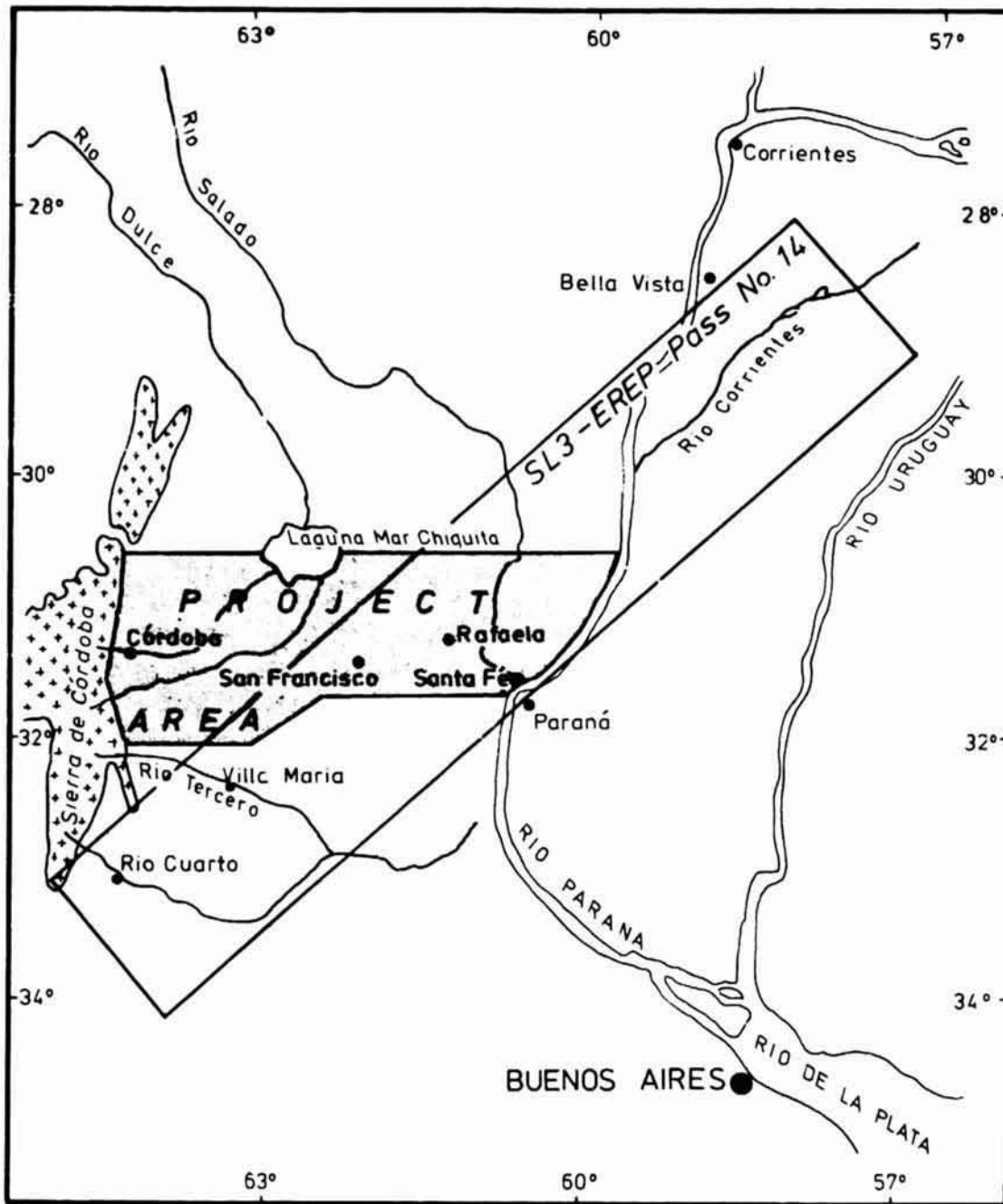
CONCLUSIONS

Satellite imagery in combination with ground investigations allows the identification and delineation of the near surface ground water (depth to ground water, salinity). The degree of precision achieved is greater than that obtainable by conventional ground survey methods alone.

In future it will be possible to produce hydrogeological maps, cheaply and more quickly, of areas with similar climatological and hydrogeological conditions.

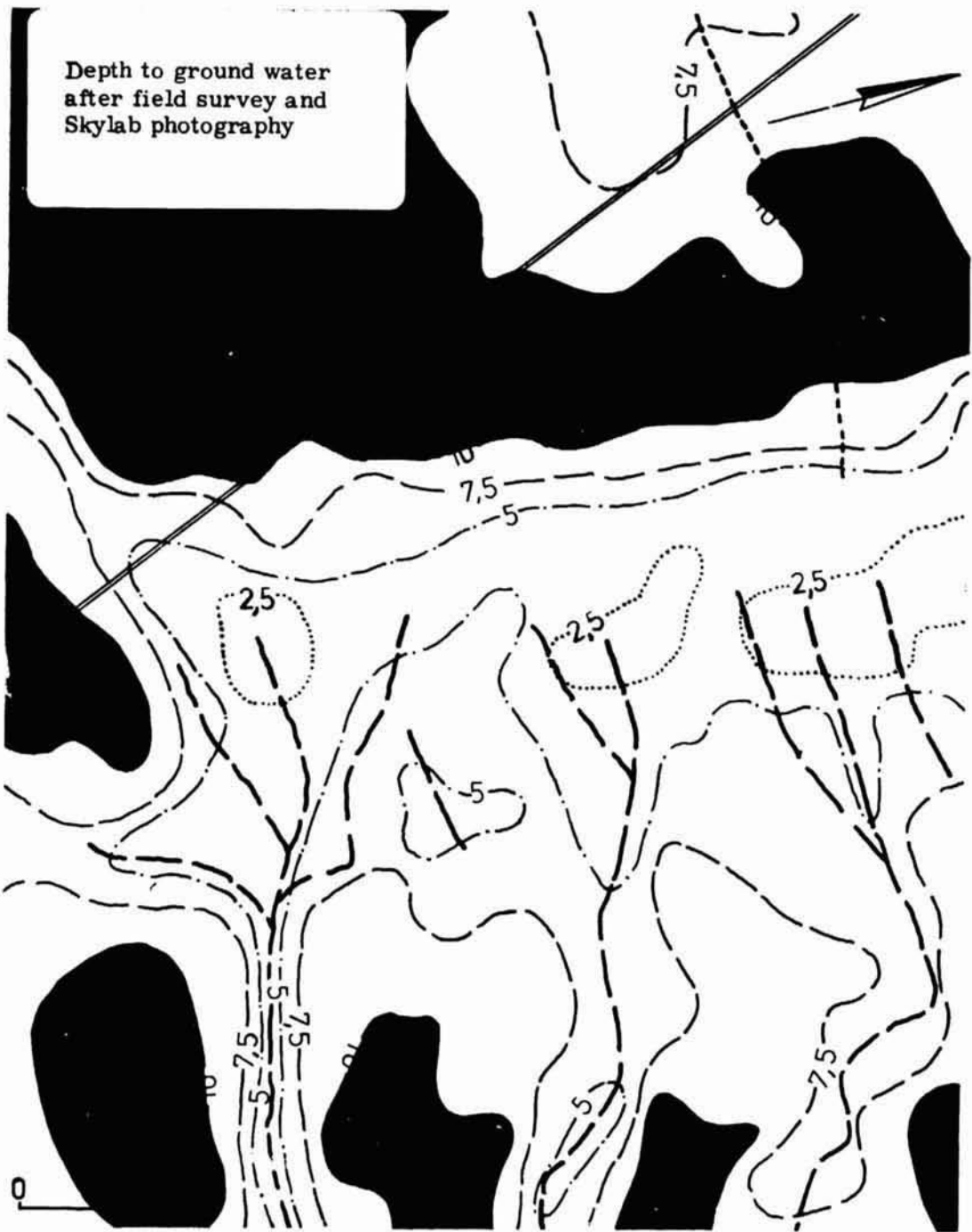
References

- Bundesanstalt für Bodenforschung, unpublished report of the "Deutsche Hydrogeologische Mission in Argentinien (DHGM)": Recursos de agua y su aprovechamiento en la llanura pampeana y en la valle del Conlara. Tomo 2, llanura pampeana, - Hydrogeologia - Bundesanstalt für Bodenforschung, Hannover 1973.
- RANGO, A. & ANDERSON, A.T., 1973: ERTS-1 Flood hazard Studies in the Mississippi River Basin, Goddard Space Flight Center, Greenbelt, Maryland, 1 - 39.
- KRUCK, W., 1974: Hydrogeologic Evaluation of ERTS & EREP Data for the Pampa of Argentina. - Proceedings COSPAR Workshop on space applications of direct interest to developing countries. Vol. II; pp. 134-140; INPE São José dos Campos, São Paulo, Brazil.



Outline map of the project area and EREP-pass coverage

Fig. 1



- | | | | |
|---|---|--|--------------|
| 5 | Isolines of depth to ground water in meters | | Road |
| | Depth to ground water more than 10 m | | Bajo |
| | Depth to ground water less than 2,5 m | | Water course |

Fig. 2a

REPRODUCIBILITY OF THE
ORIGINAL PAGE IS POOR



SL 3 - 34 - 163

Fig. 2 b

Intensity of vegetation indicating depth to ground water

REPRODUCIBILITY OF THE
ORIGINAL PAGE IS POOR

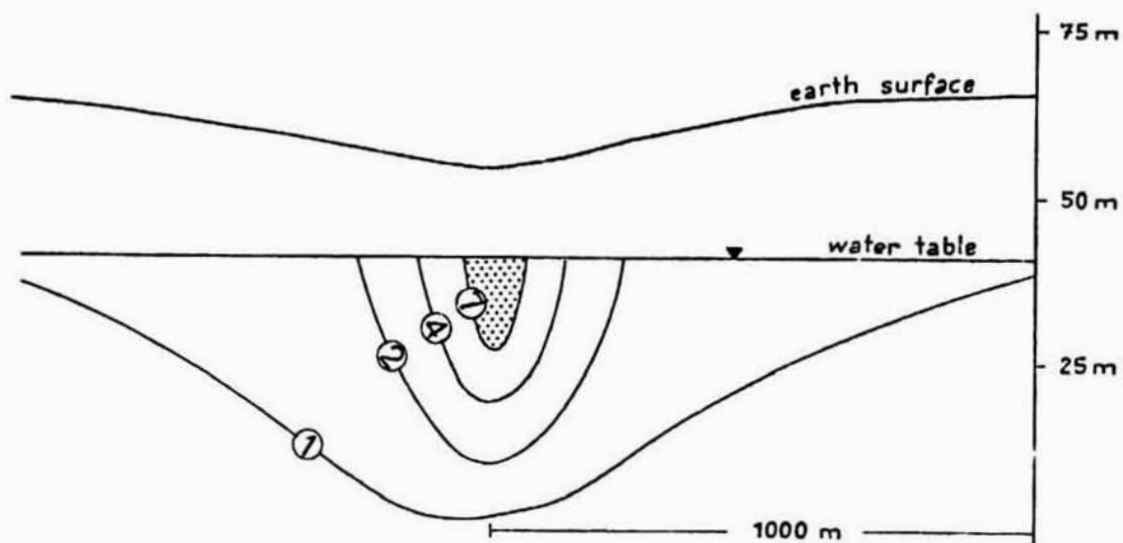
Enlargement of an area with "bajos" (b)



Boxed bajo section used to demonstrate estimation of fresh
ground water reserves (see text)
Photograph Earth Terrain Camera

Fig. 3

SIMPLIFIED CROSS SECTION OF A "BAJO"
 (with the aid of geo-electrical profiles)



Ohm · m	salt content g/l
7	~ 1
4	~ 1,8
2	~ 3,5
1	~ 7



Isolines of apparent resistivity (Ohm · m)



Fresh ground water (7 Ohm · m)

Fig. 4

REPRODUCIBILITY OF THE
ORIGINAL PAGE IS POOR

Ancient drainage pattern and current course of the Rio Tercero



0 25 km

Fig. 5

Soil units in the Province of Corrientes



We _s	Eutric planosols, sandy	(SI. 3 - 34 - 165)
We _c	Eutric planosols, clayey	
Wm _s	Mollie planosols, sandy	
Wm	Mollie planosols, clayey	
Je	Eutric fluvisols	
Gm	Gleysols	

Fig. 6

By Larry R. Tinney, John R. Jensen, and John E. Estes
Geography Remote Sensing Unit, University of California, Santa Barbara, California

ABSTRACT

N76-17591

A remote sensing analysis of the amount and type of permeable and impermeable surfaces overlying an urban recharge basin is discussed. An effective methodology for accurately generating this data as input to a safe yield study is detailed and compared to more conventional alternative approaches. The amount of area inventoried, approximately 10 sq. miles, should provide a reliable base against which automatic pattern recognition algorithms, currently under investigation for this task, can be evaluated. If successful, such approaches can significantly reduce the time and effort involved in obtaining permeability data, an important aspect of urban hydrology dynamics.

INTRODUCTION

The Geography Remote Sensing Unit (GRSU), University of California, Santa Barbara, in cooperation with the Santa Barbara County Office of Environmental Quality, is currently involved in an effort to determine both the type and amount of permeable surfaces overlying a predominantly urban groundwater recharge basin. The areal extent of this groundwater basin (see Figure 1) is approximately 10 sq. miles. This basin provides an estimated 20% of the water currently used by the Goleta County Water District. Goleta County Water District supplies water to an unincorporated urban and rural population that has increased nearly 700% during the last twenty years and is currently estimated at 72,000. This dramatic population increase, coupled with limited local water supplies, has resulted in the implementation of a building moratorium which has been in effect for the past two years. Of crucial concern to any litigation concerning this moratorium in particular, and to water district management in general, is the safe or sustained yield of the Goleta water basin. The safe yield of a groundwater basin is directly dependent upon the type, amount, and spatial distribution of permeable surfaces overlying the recharge portion of the basin.

Two previous studies detailing the geology and safe yield of the Goleta groundwater basin are considered outdated (Upson, 1951, and Evenson, 1962). This relative obsolescence is in part due to the effects of increasing urbanization which commonly changes a basin's peak flow characteristics, increases total runoff, and often adversely affects groundwater quality. Figure 2 graphically illustrates an example of the general increase in the number of overbank flows, a factor related to both peak flow and total runoff, that might be expected with increasing urbanization.

* "Long-term sustained yield in a rate of withdrawal equal to the sum of changes in recharge and discharge that take place as a result of withdrawals and lowering of water levels by pumping" (Water Resources Council, 1973).

PRECEDING PAGE BLANK NOT FILMED

Table I shows the dramatic increase in sediment yield commonly found as one goes from rural to urban landscapes (from Leopold, 1968).

The research presented in this paper was conducted by GRSU personnel as part of a study by the Santa Barbara County Office of Environmental Quality to revise previous estimates of the Goleta Basin's safe yield. The initial stage of our research involved the detailed delineation of permeable and impermeable surfaces on low altitude conventional black and white photography. Impermeable surfaces were broadly defined to include roads, parking lots, etc., while permeable surfaces were more specifically categorized as to their type. This information was manually transferred to overlays and automatically mensurated by a video image analyzer capable of density slicing and digital planimetry. Accuracies and costs associated with this technique have been documented and compared to more conventional approaches.

Data generated during this initial research phase is currently being used to provide reliable training samples for a pattern recognition analysis of high altitude color infrared photography. The spectral signatures of these samples are providing the statistics by which the remaining portion of the study area will be automatically classified. Previous automatic classifications of impervious surfaces have been hampered by a lack of reliable data against which the classifier results can be compared. The extent of this study area and amount of photointerpreted data available to this study are such that a more reliable assessment of classification accuracies can be achieved. Preliminary analysis of the results of our pattern recognition research, discussed later, are considered encouraging.

PROJECT METHODOLOGY

Trained image interpreters were employed to classify and categorize data present on the black and white imagery. The interpreters were asked to classify the various land uses into four categories. These categories were:

1. Non-permeable surfaces: generally defined to include roads, roofs, parking lots, and other impervious surfaces.
2. Permeable surfaces: specifically defined as either
 - 2A. Lawns,
 - 2B. Irrigated agriculture and open space,
 - 2C. Native vegetation.

These initial interpretations were accomplished from low altitude conventional black and white photography flown in June 1974 and printed at a nominal scale of 1:7,200. Acetate overlays were placed directly upon the photographs and three classes color coded by the image interpreters. Owing to the suburban nature of the Goleta environment, the most detailed category was lawns; this category was left clear. The overlays were then subdivided into 3 inch square cells suitable for analysis by the video image analyzer.

The color coded overlays were then density sliced by the video image analyzer to take advantage of this system's electronic planimetry capability. By the selective use of color filters placed between the video camera and the color coded overlays a potentially large number of classes can be distinguished by their tonal density values alone. Such a procedure, especially when combined with a pattern recognition algorithm, may also provide the basis for thematic map encoding, as discussed by many land use information system proposals. The procedures developed and utilized in connection with this project proved highly efficient, requiring less than one day of labor to extract all four class area estimates, on a grid basis for the entire ten square mile study region.

Figure 3 illustrates a two-class example, as interpreted from the low altitude photography, including 1) the original photography, 2) the photo interpreted overlay of the scene, and 3) the corresponding video enhancement and planimeter values. Table II summarizes the results of this analysis for the entire Goleta recharge basin.

ANALYSIS OF ALTERNATIVES

In addition to the techniques discussed above, various alternative methodologies were available for supplying the information required for the Goleta Basin safe yield study. Extensive field investigations were definitely prohibitive due to both time and monetary constraints. Sampling techniques used in conjunction with aerial photography were also not deemed appropriate as the spatial dimension of the data was to be retained for our automatic pattern recognition studies and possible "updates" of the safe yield in the future.

The most viable alternative available at the inception of the project was considered to be direct visual estimation from the photography. An analysis of the accuracies obtained using such a procedure are detailed in Table III and compared to the actual project methodology involving image interpretation and video planimetry of color coded overlays. It should be emphasized here that when monetary, accuracy, and time constraints are such that the more detailed analysis is not feasible, this option could be considered a viable alternative.

Another somewhat less optimal alternative is visual estimation from the color coded overlays. This results in improved accuracies, also detailed in Table III, when compared to visual estimates made directly from the photographs. This technique, however, still involves the major project expense of interpreter overlay compilation. Once the overlays have been generated the video enhancement and planimetry costs are negligible (less than 8 hours labor for the study region), provided the analyzing equipment is available. The alternative of manually planimetrying each class was found infeasible at the original imagery scale due to the intricate nature of the class distributions. Indeed, this intricacy presented an obstacle to evaluating the relative accuracies of the various procedures by necessitating the photographic enlargement of selected scenes to scales more easily planimetryed.

The most automated technique examined, which is still under investigation, involves the application of a pattern recognition algorithm to a digitized representation of color infrared photography. A maximum likelihood algorithm trained on samples of the four classes has been used to classify a small portion of a NASA high altitude color infrared photograph. When the lawn, irrigated agriculture, and open space in this study area were aggregated to one permeability class, a mean classification accuracy of 75% was achieved. The major assignment to permeable classes appears to be based primarily upon the high reflectance of vegetation in the infrared spectral region. These results are considered encouraging, though preliminary in nature as less than 5% of the study area was analyzed.

Present research is being directed towards expanding these preliminary results and assessing the nature and extent of the major variables affecting both accuracy and the transferability of this methodology to other regions.

CONCLUSIONS

This research has documented an effective methodology to accurately generate quantitative urban groundbasin data useful for determining safe yield values. The extensive amount of accurate data generated by this project from low altitude photography has provided a reliable basis against which automatic techniques, based upon high altitude color infrared photography, can be evaluated. The methodology utilized for this project takes advantage of an image interpreter's ability to precisely delineate permeable from impermeable surfaces in complex urban environments, and a video image analyzer's ability to accurately and rapidly extract quantitative area estimates for assigned classes. Analysis of our results by the cooperating user agency, the Santa Barbara County Office of Environmental Quality, has just begun. As close user-researcher contact has been maintained throughout this study a favorable user response is anticipated. If successful, approaches such as those discussed herein will significantly reduce the time and effort involved in generating permeability data, an important aspect in determining urban hydrology dynamics.

REFERENCES

- Evenson, R. E., Wilson, H. D. Jr., and Muir K. S., "Yield of the Carpinteria and Goleta Ground-Water Basins, Santa Barbara County, California," 1941 to 1958: U.S. Geological Survey Open File Report 112, 1962.
- Leopold, L. B., "Hydrology for Urban Land Planning - A Guidebook on the Hydrologic Effects of Urban Land Use" U.S. Geologic Survey Circular 554, 1968, 18pp.
- Upton, J. E., "Geology and Ground-Water Resources of the Southern Coastal Basins of Santa Barbara County, California, with a Section on Resources by H. G. Thomasson, Jr." U.S. Geological Survey Water Supply Paper 1108, 1951, 144pp.
- Water Resources Council, "Essentials of Ground-Water Hydrology Pertinent to Water Resources Planning, Washington D.C., August 1973, 48pp.

TABLE I

	Drainage Area (sq. mi.)	Sediment	
		Tons Per Year	Tons Per Year Per sq. mi.
RURAL (Watts Branch in Rockville, Md.)	3.7	1,910	516
URBAN (Little Falls Branch near Bethesda, Md.)	4.1	9,530	3,220

TABLE IIA
GOLETA RECHARGE BASIN: ACREAGES

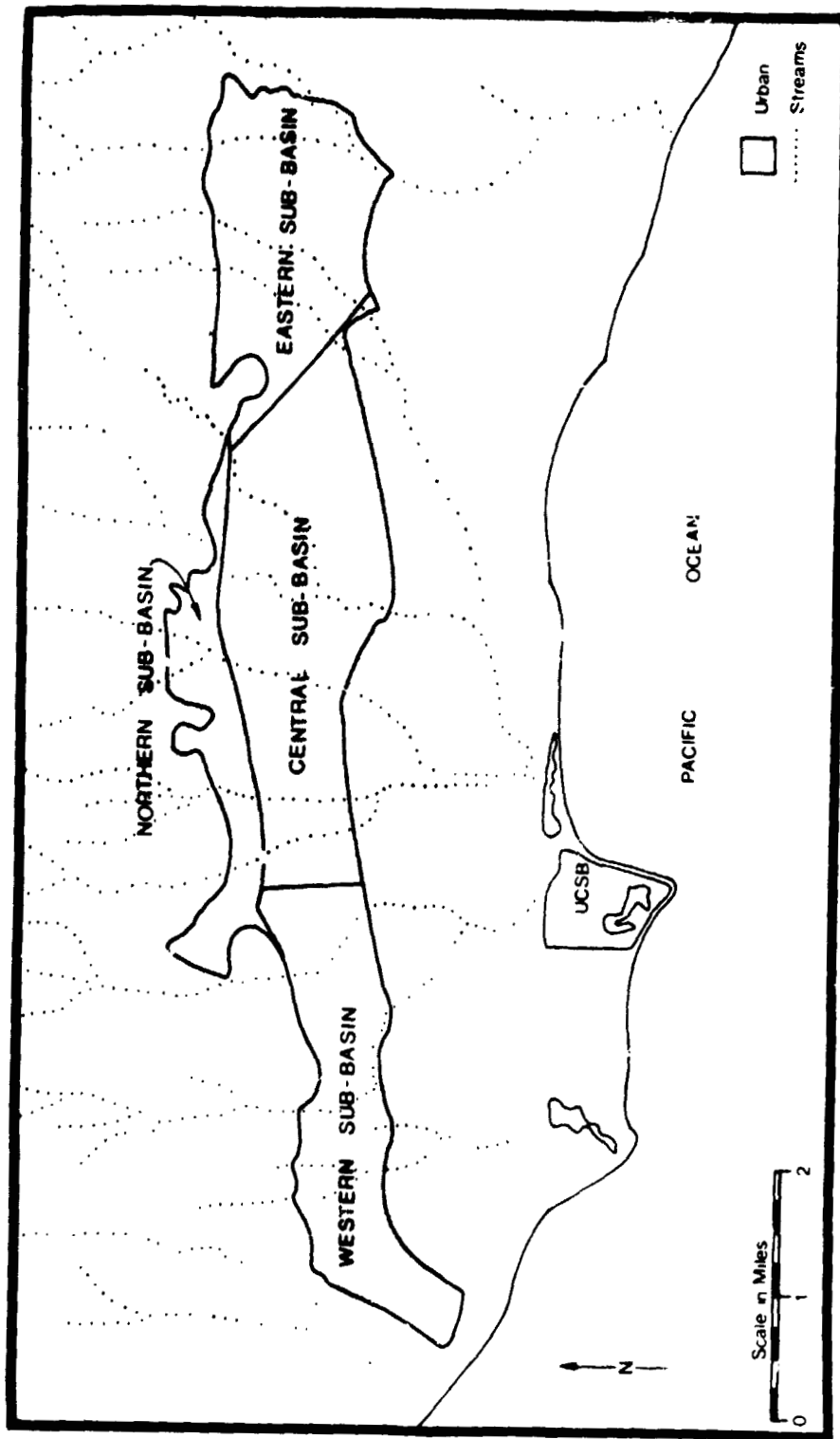
Class	Sub-Basins				Total
	Western	Central	Northern	Eastern	
1 Impermeable	357	1,134	209	695	2,394
2A Lawns	204	622	164	450	1,440
2B Irrigated Agriculture & Open Space	135	234	112	76	557
2C Natural Vegetation	648	594	203	399	1,845

TABLE IIB
GOLETA RECHARGE BASIN: PERCENTAGES

Class	Sub-Basins				Total
	Western	Central	Northern	Eastern	
1 Impermeable	27	44	30	43	38
2A Lawns	15	24	24	28	23
2B Irrigated Agriculture & Open Space	10	9	16	5	9
2C Natural Vegetation	48	23	30	24	30

TABLE III

	Visual Estimation from Photographs	Visual Estimations from Image Inter- preted Overlays	Video Plani- metering of Overlays Inter- preted
Mean Absolute Accuracies of Permeable versus Non-Permeable Area Measurements	85.8%	95.4%	98.5%



Geography Remote Sensing Unit, University of California at Santa Barbara

Figure 1. Goleta, California, Recharge Basin, by Sub-Basins. Pattern delineates general urban areas.

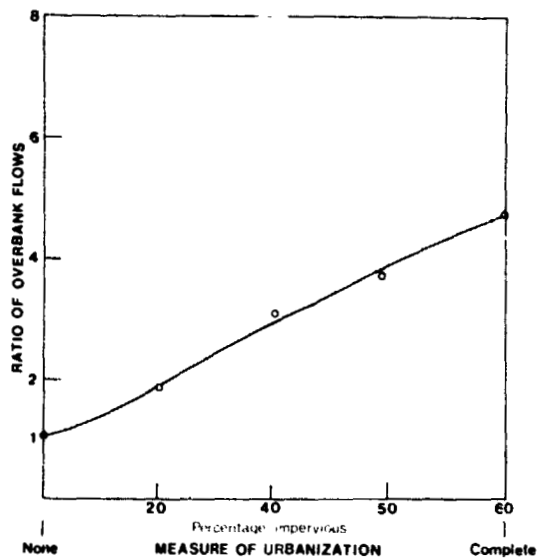


Figure 2. Graphic example of the general increase in the number of overbank flows associated with increasing urbanization (from Leopold, 1968).

WATER BASIN PERMEABILITY STUDY

1972 BLACK AND WHITE
AERIAL PHOTOGRAPH



Courtesy of Pacific Western Aerial Surveys
Santa Barbara, California

PHOTO INTERPRETATION



☐ Permeable
■ Impermeable

VIDEO ENHANCEMENT AND
ELECTRONIC PLANIMETERING



■ Permeable : 2.0 Acres = 46 %
☐ Impermeable : 2.4 Acres = 54 %

Geography Remote Sensing Unit, University of California at Santa Barbara

Figure 3. Permeability Study Methodology.

Fawwaz T. Ulaby, Percy P. Batlivala and Josef Cihlar,
University of Kansas, Lawrence, Kansas 66045, and
Thomas Schmugge, NASA Goddard Space Flight Center,
Greenbelt, Maryland 20771

ABSTRACT

N76-17592

Plant growth, partitioning of rainfall into surface runoff and infiltration components, and evaporation loss to the atmosphere, among other processes, all depend on the amount of water present in the soil. This paper examines the potential application of microwave remote sensing devices in estimating soil moisture content over extended areas. Experimental measurements involving both active and passive microwave sensors acquired from a variety of platforms are presented.

INTRODUCTION

Soil water plays a fundamental role in mass and energy exchange processes near the earth's surface. Its importance has long been recognized and is topical in such disciplines as meteorology, climatology, plant physiology, geomorphology, and others. More recently, soil moisture has been used as an input parameter in various models to permit a better management of the human environment. For example, models of watershed performance, river forecasting and crop inventory and yields require knowledge of soil moisture as a function of time and location.

The spatial variability of soils and terrain characteristics influencing the amount of water retained in the soil makes remote sensing a unique tool for soil moisture determination over large areas, within a short time, and at a reasonable cost. Several regions of the electromagnetic spectrum are sensitive to the presence of water in the soil. Microwave frequencies have the added advantages of depth of penetration and independence of the time of day and most weather conditions.

The backscattering and emission behavior of an extended target, such as a soil medium, is characterized in terms of the target's scattering coefficient σ° and emissivity ϵ . Thus, σ° and ϵ represent the link between the target properties and the scatterometer and radiometer responses. For a given set of sensor parameters (wavelength, polarization and incidence angle relative to nadir), σ° and ϵ of bare soil are functions of the soil surface roughness (and subsurface if significant penetration is occurring) and dielectric properties. The dielectric properties are in turn strongly influenced by the soil water content as is illustrated in Figure 1 where the real (k_1) and imaginary (k_2) parts of the relative dielectric constant of three soil types are shown as a function of water content at 1.3 GHz [1]. The curves shown represent averages of experimental measurements reported by several investigators. The separation in the curves of k_1 and k_2 due to soil type appear to be associated with the proportion of clay particles in the soil. This separation has been found to be more pronounced at frequencies below 1.3 GHz [2] but is practically absent above 4.0 GHz [1].

From a theoretical point of view, the effect of soil moisture content on σ° and ϵ can be demonstrated by considering the single case of a homogeneous medium with a perfectly smooth surface. Under these conditions σ° is directly proportional to the soil power reflection coefficient ρ and $\epsilon = 1 - \rho$. Figure 2 presents the dependence of ρ (and ϵ) on moisture content at normal incidence for three microwave frequencies and three soil types [1]. Among the three variables considered in Figure 2, it is clearly evident that moisture content is the most influential.

Under natural conditions, several interference effects are introduced which complicate the task of recovering soil moisture information from the microwave measurements. First, most soil surfaces are not perfectly smooth at microwave frequencies. Consequently σ° and ϵ are affected by both the dielectric properties and the geometrical configuration of the scattering (and emitting) elements present within the resolution cell. Secondly, vegetation cover can modify the sensor response to soil moisture variations by attenuating the soil scattering and emission components and by adding contributions of its own. The masking effect caused by the vegetation depends on the geometry and biomass of the vegetation canopy and the sensor parameters used. Since vegetation is a lossy dielectric, its attenuation increases with frequency and plant moisture content. Thirdly, soil moisture usually varies with depth, thus precluding derivation of a unique soil water content profile from a single microwave measurement.

To counter the interfering effects of roughness and vegetation cover and to incorporate the variability of the soil moisture profile, the investigator has basically four parameters at his disposal. Three of these are system parameters, namely frequency, incidence angle, and polarization. The fourth variable is the type of microwave sensor used: active or passive. Due to the characteristics of illumination, the two types of sensors also differ in their response to the interfering effects. Consequently, the problem in developing a technique for microwave remote sensing of soil moisture can be defined as identifying such sensor/frequency/incidence angle/polarization combination(s) at which the sensitivity to soil moisture is maximized while the effect of interfering parameters is at a minimum.

The remainder of this paper is divided into two major sections, one covering active microwave measurements while the other covering passive microwave measurements of soil moisture. Due to space limitations, no detailed description of the systems used to acquire the reported data will be included.

ACTIVE MICROWAVE RESPONSE TO SOIL MOISTURE

Only results of experimental measurements acquired by ground-based and airborne scatterometers to determine the backscattering coefficient (σ^0) response to soil moisture will be presented in this section; measurements from a satellite platform were acquired by Skylab and will be reported in this symposium by Eagleman and Lin [3]. The ground-based experiments employed the University of Kansas truck-mounted Microwave Active Spectrometer (MAS) systems which covered the frequency range 2-18 GHz [4-6] while the airborne data was acquired by the NASA/JSC 13.3 GHz scatterometer [7].

Figure 3 shows the measured scattering coefficient σ^0 of a bare field as a function of gravimetric moisture content at 4.7 GHz for HH and VV polarizations for several angles of incidence [8]. The field surface, having a r.m.s. height of 2.5 cm, is described as slightly rough in terms of the wavelength (6.4 cm). The moisture content is an effective value calculated on the basis of the soil moisture and bulk density profiles within the skin depth [8]. The data shown in Figure 3 indicates a fairly linear response to the effective moisture content at all incidence angles. The only major deviation is the data set at the highest moisture content which exhibits a higher response at nadir and 10° and lower response at the higher incidence angles. The cause of this deviation is attributed to change in surface roughness induced by heavy rainfall shortly before recording this particular data set. From Figure 3 it is also apparent that the response to moisture change is highest at nadir.

As a quantitative measure of the scattering coefficient response to soil moisture, the moisture sensitivity S_V was defined as the change in σ^0 caused by 0.01 g/cm^3 change in the effective moisture content (slope of the linear regression lines shown in Figure 3). Figure 4 shows S_V as a function of incidence angle at three microwave frequencies and two polarizations. In general, a) S_V decreases rapidly between nadir and 20° and then levels off past 30° or 40° , b) this angular dependence appears more pronounced at 7.1 GHz compared to 4.7 GHz, and c) HH polarization exhibits better sensitivity than VV polarization at the same frequency and incidence angle.

Based on the above results for a bare field having a slightly rough surface in terms of the wavelength, the potential of radar as a soil moisture sensor looks very promising. As surface roughness is varied, however, the absolute magnitude of σ^0 as well as its slope (S_V) may also vary [9, 10]. The effect of roughness is illustrated in Figures 5 and 6 at 2.75 GHz and 7.25 GHz, respectively, where the angular response of σ^0 is shown for three fields having approximately the same moisture content but considerably different surface roughnesses [10]. Consistent with theoretical expectations, at 2.75 GHz σ^0 of the smooth field appears extremely sensitive to incidence angle near nadir while at the other extreme, the rough field shows an almost Lambertian behavior. The medium rough field shows a response intermediate between the other two. In terms of the range of surface roughness commonly encountered in the natural environment, the smooth field is almost artificial. Keeping this in mind, if an incidence angle were to be specified at which the effect of roughness is minimal, the range around 5° might be appropriate.

As the microwave frequency is increased from 2.75 GHz (Figure 5) to 7.25 GHz (Figure 6), all fields appear relatively rougher, thereby changing the shapes of the curves which gives rise to an intersection point of the three curves around 18° . Between these two frequencies, measurements were also acquired at six other frequencies for the same angles of incidence. Analysis of the entire data indicates that there exists a correspondence between frequency and an "optimum" incidence angle (in

terms of minimum sensitivity to surface roughness) at which the correlation coefficient between σ° and moisture content is a maximum for the data from all three fields combined [10]. An example is shown in Figure 7 where σ° is plotted as a function of moisture content at 4.75 GHz, 10° incidence angle and VV polarization. Considering the wide range of surface roughness included in this analysis and the standard deviations associated with the measurements of σ° and soil moisture content, a correlation coefficient of 0.69 should be considered quite good.

Next, the effect of vegetation cover will be examined. In Figures 8a through 8d, the angular response of σ° at 5.9 GHz is shown for corn, milo, soybeans and alfalfa canopies, respectively [11]. Each figure contains two measured curves corresponding to very different soil moisture contents (in % by weight over the top 5 cm). All three row crops (corn, milo and soybeans) indicate substantial differences in σ° near nadir due to the corresponding differences in soil moisture. As incidence angle is increased away from nadir, however, the response to soil moisture variation appears to decrease which is attributed in part to the increase in effective vegetation biomass separating the sensor from the soil surfaces and in part to the decrease in the magnitude of the soil moisture sensitivity S_v (Figure 4). Alfalfa, on the other hand, shows an almost opposite trend. Based on the shape of the angular response curve of the low moisture case, it was suggested that alfalfa appears (electromagnetically) like a relatively smooth surface at 5.9 GHz [11]. Hence, with a large backscatter component of its own at nadir, the contribution of the attenuated (by the alfalfa) soil component is not large enough to show a difference in the return. As a "smooth" surface, σ° of alfalfa exhibits a fast decay with incidence angle, thereby contributing a smaller component to the backscattered return than the component contributed by the underlying wet soil at angles away from nadir. Due to this difference in behavior between alfalfa and the other crops, the correlation coefficient between σ° at 4.7 GHz and soil moisture, calculated using measured data from all four crops combined, was observed to be higher at 10° than at nadir [11] (Figure 9b). Linear regression lines at 10° and 30° are shown in Figure 10 for HH polarization. The calculated slope and correlation coefficient of regression lines similar to those of Figure 10 at 4.7 GHz and 7.1 GHz are plotted in Figure 9 as a function of incidence angle. Although the 4.7 GHz soil moisture response at 10° appears slightly lower than at nadir, the higher correlation coefficient at 10° together with the earlier observation (Figure 7) regarding the optimum frequency-incidence angle combination for minimizing the effect of soil surface roughness, suggest 10° incidence angle and 4.7 GHz as design parameters for large area soil moisture mapping with radar. It should be noted, however, that the analysis leading to this choice of sensor parameters is based on limited coverage in terms of types of vegetation canopies and soil surface structures (the effect of row patterns, e.g., has not yet been fully examined). Measurements acquired from fields covered with very dense continuous canopies approximately 1 meter tall indicate no response to soil moisture variations at frequencies above 2.75 GHz [12]. Hence if lower frequencies are to be used to penetrate such vegetation canopies, the above choice of incidence angle (10°) will have to be modified to a value closer to nadir.

During a flight by the NASA/JSC P3A aircraft over a test site near Garden City, Kansas, measurements were acquired by a 13.3 GHz scatterometer from several fields each of which was found (from aerial photography and field crew's reports) to contain sections into which irrigation water was flowing and sections ready for irrigation but not yet wetted [7]. For each of these fields, the effect of the irrigation on the radar return appeared to produce a difference of about 7 dB at angles within 40° from nadir. An example is given in Figure 11 [7] where the measured σ° curves for the irrigated and non-irrigated sections of a corn field are shown. Since all ground conditions, except for soil water content, were similar over the entire field, the differences in σ° can only be attributed to the effect of moisture.

The test site consisted of 706 fields, of which, on the basis of ground truth information, 687 were judged as dry and 19 were judged as wet. Some of the fields in the test site were bare ground while the majority were planted with corn, sorghum, alfalfa, sugar beets and wheat. Figure 12 shows the average σ° curves for each of these two sets as a function of incidence angle [7]. The results clearly demonstrate the capabilities of radar in separating dry terrain from wet terrain under a variety of vegetation covers.

To examine the moisture response in more detail, σ° is plotted in Figure 13 at three angles of incidence as a function of moisture content (measured with a surface neutron probe) for fields where the latter information was available. Although this set of seven fields includes both bare ground and a variety of crop types, σ° indicates an almost linear response to soil moisture at 10° with a slope of 0.185 dB per 1% moisture content change. At 20° a weaker response is observed up to about 30% moisture content, followed by a sudden increase (field #125) which may be related to the furrow

geometry relative to the scatterometer. In contrast, at 50° incidence angle, the soil moisture response appears to be dominated by the other characteristics of the fields.

PASSIVE MICROWAVE RESPONSE TO SOIL MOISTURE

To study the use of microwave radiometers for the remote sensing of soil moisture instruments in the wavelength range 0.8 to 21 cm (3.7 GHz to 1.4 GHz) were flown on board the NASA CV-990 over agricultural test sites around Phoenix, Arizona and in the Imperial Valley of Southern California. On the same day ground measurements of soil moisture were also made.

The 1.55 cm radiometer was a scanning instrument receiving horizontally polarized radiation from a swath whose width is approximately twice the A/C altitude. Figure 14 is an example of the results from this instrument for an East-West track over the Imperial Valley, starting over the Salton Sea and ending over the desert east of the agricultural area. Brightness temperatures for the sea, desert, and several agricultural fields with a range of moisture contents are indicated. The rectangular patterns of these fields is clearly evident. Figure 15 is a plot of the 21 cm and thermal IR brightness temperature for the same flight line. The brightness temperature for the water is 20°K lower at 21 cm than at the 1.55 cm wavelength. This factor plus the greater depth penetration at 21 produce the greater sensitivity to soil moisture at this wavelength.

Brightness temperatures for the individual fields were compared with ground measurements of soil moisture. Figure 16 gives the results for the 1.55 cm scanning radiometer and the average soil moisture in the top cm for the 3 flights in 1972 for light soils (sandy loam and loam) and heavy soil (clay loam). The range of brightness temperature is the same for both soil types and there is clearly a linear decrease of brightness temperature with soil moisture. The depression of the brightness temperature for a given moisture content is less for the heavy soils (greater field capacity) than for the light soils. The slope is less for the heavier soils because of the greater range of soil moisture that is possible for these soils. If the soil moisture is expressed as the percent of field capacity, this difference can be accounted for as shown in Figure 17. Visually the scatter in the data is somewhat smaller and the correlation coefficient for these data is greater than for the light and heavy soils separately.

Similar behavior is observed for the brightness temperatures obtained with the 21 cm radiometer, i.e. a linear response when plotted as a function of the soil moisture expressed as percent of field capacity in the top centimeter (Figure 18). When plotted versus the same quantity for the 2.5 cm layer there appears to be flat region out to about 50% of field capacity where the linear decrease begins (Figure 19). When the brightness temperatures are compared with the moisture in the 5 cm layer the flat region extends to higher moisture values. The behavior of the 21 cm results is qualitatively similar to those observed at 1.55 cm except that there was a greater range of brightness temperatures observed at 21 cm (about 100°K) than at 1.55 cm which is consistent with the larger dielectric constant for water at the longer wavelengths. Thus the 21 cm radiometers appear to be responding to the moisture in a layer 1 to 2 centimeters thick at the surface.

The Nimbus 5 satellite, launched on December 12, 1972, carries an Electrically Scanning Microwave Radiometer (ESMR) operating at a wavelength of 1.55 cm. A brightness temperature map of the U. S. is shown in Figure 20 for a 2 day period in January, 1973; two of the regions having lowered brightness were the lower Mississippi Valley and the Great Salt Desert southwest of the Great Salt Lake. Figure 21 is a brightness temperature contour map for the Mississippi Valley using data of 22 January 1973. This was following a period of heavy rain over the area. The region of lowered brightness temperature is the relatively flat land on either side of the river which corresponds to an outwash aquifer where unconsolidated sand and gravel deposits are capable of storing large amounts of ground water. This land would be essentially devoid of vegetation in January. The brightness temperature for the northern portion of the region, from Cairo, Illinois to Memphis on the west side of the river, were compared with the average daily rainfall taken from 28 stations in this area. The results are shown in Figure 22. In general low brightness temperatures were observed for the period immediately after a heavy rain, e.g. the sharp drop observed after 20 January. This was followed by a gradual warming trend as the area dried out.

A similar dependence of brightness temperature on rainfall was observed for the Great Salt Desert; a brightness temperature contour map for this area is shown in Figure 23 using data from 5 June 1973. It is observed that the region of lowered brightness temperatures corresponds to the salt desert. To obtain a time history of brightness temperature variations, similar maps were produced on about a weekly basis;

the minimum brightness temperatures observed over the desert are plotted versus time in Figure 24. For comparison the brightness temperatures of a reference point 60 km west of Wenclover were also plotted to indicate the type of seasonal variation that might be expected for the usual terrain outside the desert area. In general the brightness temperature for this location varies rather smoothly from a maximum of 280°K in July and August down to a minimum 240°K for January and February and appears to repeat from one year to the next. The minimum brightness temperature over the Great Salt Lake Desert followed a similar sort of seasonal variation with its maximum occurring in July and August. However, the minima were in November in response to the fall rains during both years. There is a significant difference in the level of the brightness temperature for the summers of 1973 and 1974. The minimum temperatures observed over the Great Salt Lake Desert in the summer of 1974 were 20°-30°K higher than those observed during the summer of 1973. The rainfall during the summer of 1974 was only 50% of normal while in 1973 it was slightly above normal. The average monthly rainfall for eight stations surrounding the basin is shown as bar graphs on the bottom of this figure and clearly indicates this difference in rainfall for the two summers. The response to the heavier fall rains of November, 1973 and October, 1974 is indicated and in particular the lowest brightness temperature was observed on 18 November 1973 when more than 1 cm of rain was recorded at the eight stations. The month with heaviest average rain (about 4 cm) was July, 1973, with the rain occurring during two brief periods 12-14 July and 19-21 July. This is reflected in the lowered brightness temperature for 14 and 20 July (214°K and 205°K respectively).

It appears in both situations that the radiometer may be responding to a combination of surface water resulting from recent rains and fluctuations in the level of water table. With regard to the latter the fluctuations in brightness temperature may be due to changes in the area over which the high water table has a surface manifestation.

CONCLUSIONS

Evaluation of the total available experimental data acquired by microwave sensors from ground-based, airborne and spaceborne platforms reveals that under the majority of surface cover conditions, microwave sensors are capable of detecting soil moisture variations. The accuracy associated with a quantitative determination of moisture content is, however, subject to the choice of sensor parameters (frequency, incidence angle and polarization) and to ground conditions (surface roughness, vegetation cover and soil temperature). Continued work towards an operational satellite soil moisture mapping system involves the establishment of optimum sensor (active and passive)/sensor parameter combination(s) and testing over a wide range of terrain characteristics.

REFERENCES

- [1]. Cihlar, J. and F. T. Ulaby, "Dielectric Properties of Soils as a Function of Moisture Content," RSL Technical Report 177-47, University of Kansas Center for Research, Inc., Lawrence, Kansas, November, 1974.
- [2]. Leschanskii, Yu. I., G. N. Lebedeva and V. D. Schumilin, ("Electrical Parameters of Sandy and Loamy Soils in the Range of Centimeter, Decimeter and Meter Wavelengths"). *Izvestiya Vysshich Uchebnich Zavedenii, Radiofizika*, vol. 14, no. 4, pp. 562-569, 1971.
- [3]. Eagleman, J. R. and W. Lin, "Soil Moisture Detection from Skylab," NASA Earth Resources Survey Symposium, Houston, Texas, 1975.
- [4]. Ulaby, F. T., "4-8 GHz Microwave Active and Passive Spectrometer (MAPS) Volume I: Radar Section," RSL Technical Report 177-34, University of Kansas Center for Research, Inc., Lawrence, Kansas, April, 1973.
- [5]. Bush, T. F. and F. T. Ulaby, "8-18 GHz Radar Spectrometer," RSL Technical Report 177-43, University of Kansas Center for Research, Inc., Lawrence, Kansas, September, 1973.
- [6]. Oberg, J. M. and F. T. Ulaby, "MAS2-8 Radar and Digital Control Unit," RSL Technical Report 177-37, University of Kansas Center for Research, Inc., Lawrence, Kansas, October, 1974.

- [7]. Dickey, F. M., C. King, J. C. Holtzman and R. K. Moore, "Moisture Dependency of Radar Backscatter from Irrigated and Non-Irrigated Fields at 400 MHz and 13.3 GHz," IEEE Trans. on Geoscience Electronics, vol. GE-12, no. 1, pp. 19-22, 1974.
- [8]. Ulaby, F. T., J. Cihlar and R. K. Moore, "Active Microwave Measurement of Soil Water Content," Remote Sensing of Environment, vol. 3, pp. 185-203, 1974.
- [9]. Ulaby, F. T., "Radar Measurement of Soil Moisture Content," IEEE Trans. on Antennas and Propagation, vol. AP-22, no. 2, pp. 257-265, March, 1974.
- [10]. Ulaby, F. T., P. P. Batlivala and J. Cihlar, "Effects of Roughness on the Radar Response to Soil Moisture of Bare Ground," RSL Technical Report 264-5, University of Kansas Center for Research, Inc., Lawrence, Kansas, May, 1975.
- [11]. Ulaby, F. T., "Radar Response to Vegetation," IEEE Trans. on Antennas and Propagation, vol. AP-23, no. 1, January, 1975.
- [12]. Ulaby, F. T. and P. P. Batlivala, "Measurement of Radar Backscatter from a Hybrid of Sorghum," RSL Technical Report 264-2, University of Kansas Center for Research, Inc., Lawrence, Kansas, May, 1975.

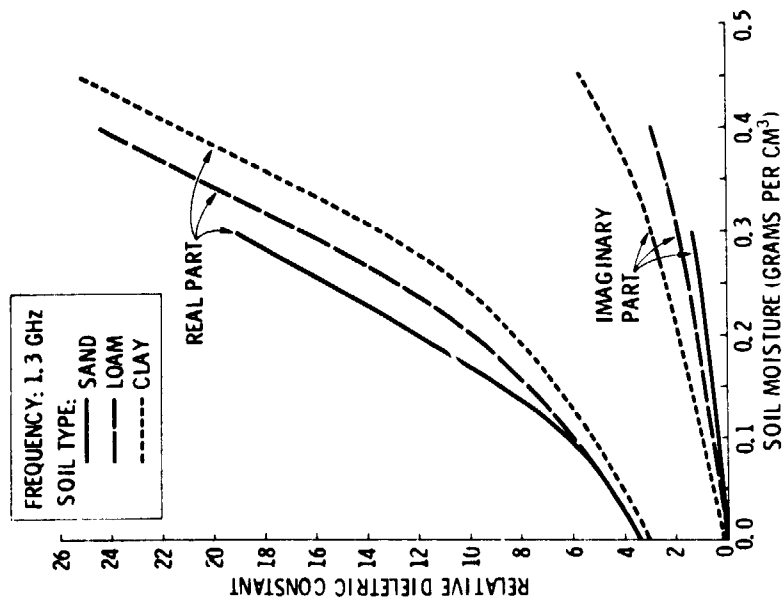


Figure 1. Representative dielectric constant values as a function of volumetric water content for sand, loam, and clay at 1.3 GHz.

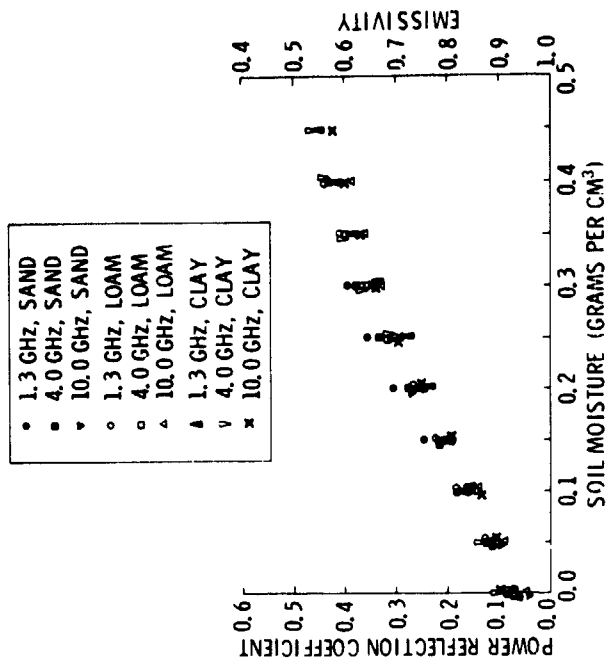


Figure 2. Power reflection coefficient and emissivity as a function of volumetric water content, frequency, and soil type.

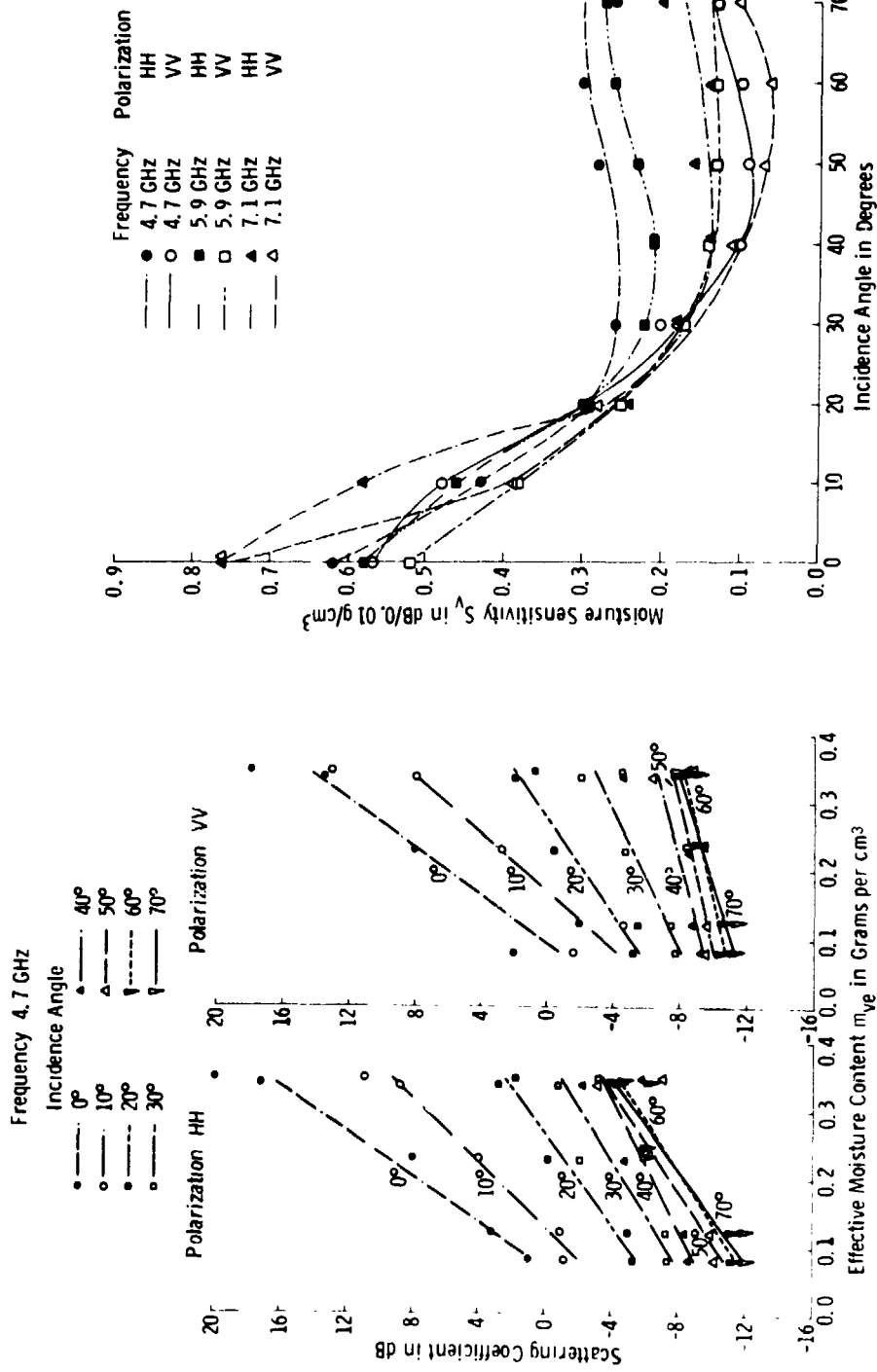


Figure 3. Scattering coefficient as a function of effective moisture content. Frequency is 4.7 GHz.

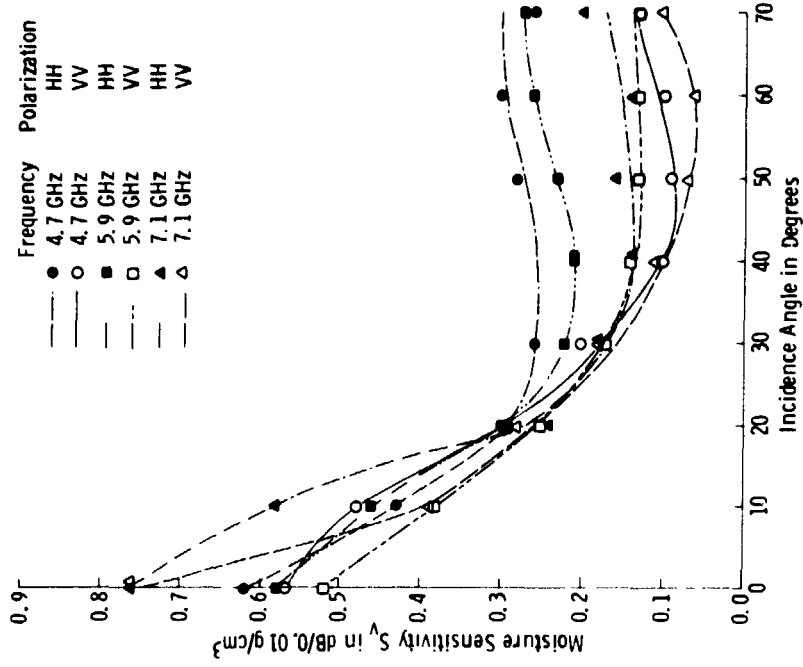


Figure 4. Moisture sensitivity S_v as a function of incidence angle.

Frequency: 2.75 GHz
Polarization: VV

RMS Height in cm	Soil Moisture in g/cm ³
0.88	0.351
2.6	0.327
4.3	0.306

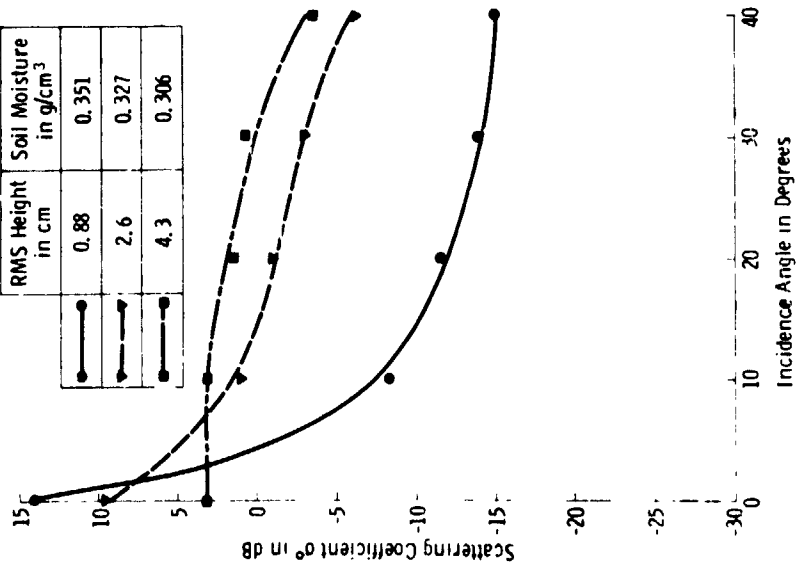


Figure 5. Angular response for three bare fields with similar soil moisture conditions but considerably different surface roughnesses.

Frequency: 7.25 GHz
Polarization: VV

RMS Height in cm	Soil Moisture in g/cm ³
0.88	0.233
2.6	0.344
4.3	0.352

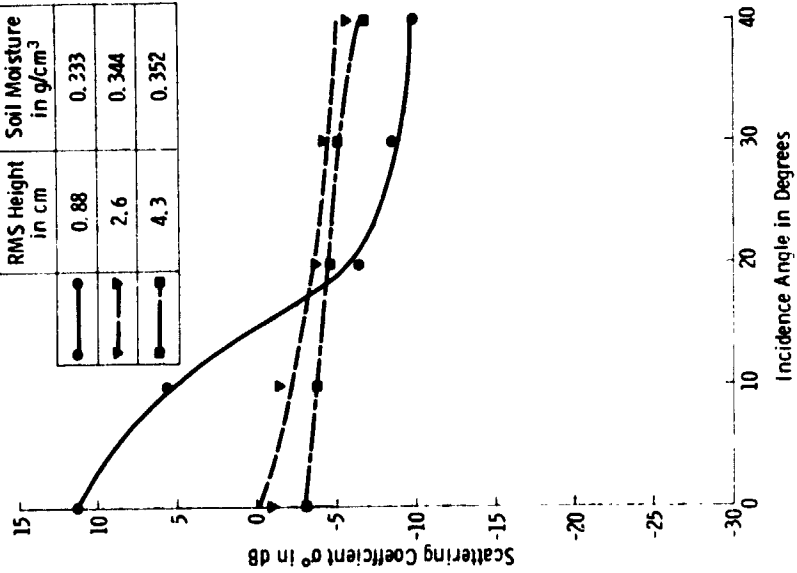


Figure 6. Angular response for three bare fields with similar soil moisture conditions but considerably different surface roughnesses.

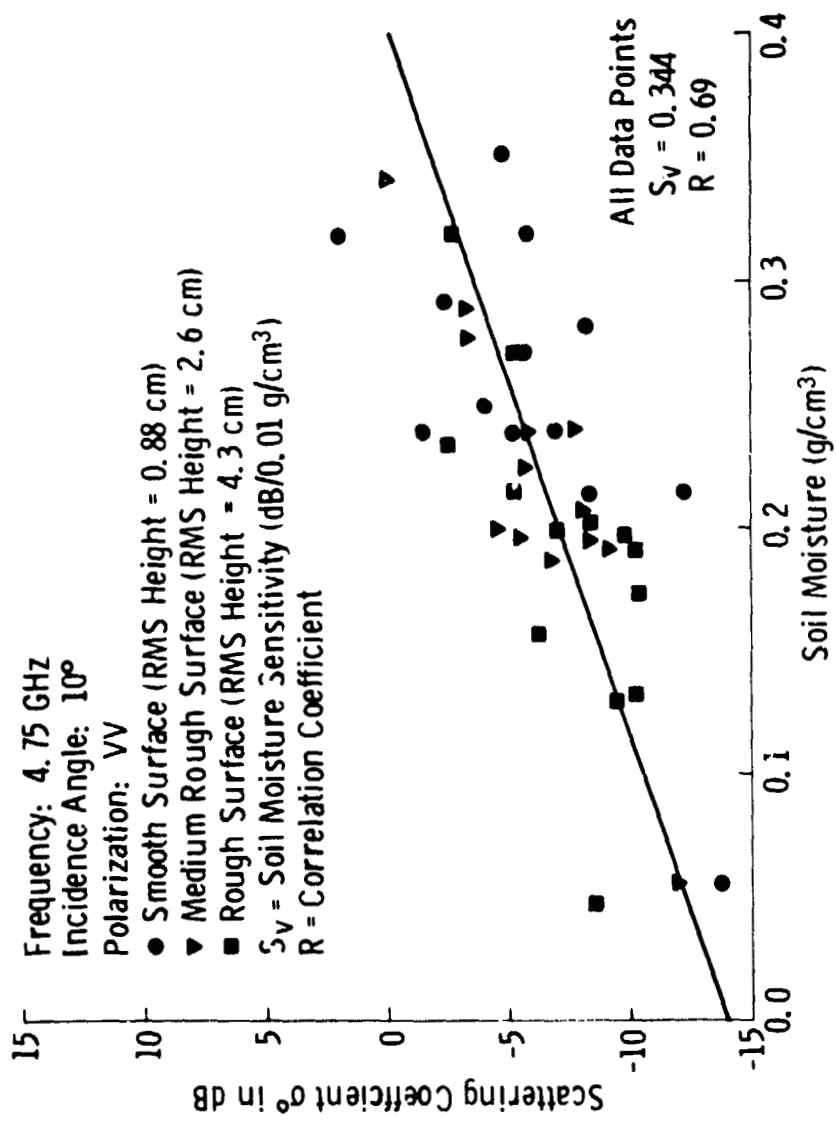


Figure 7. Scattering coefficient response as a function of soil moisture for three surface roughness profiles combined.

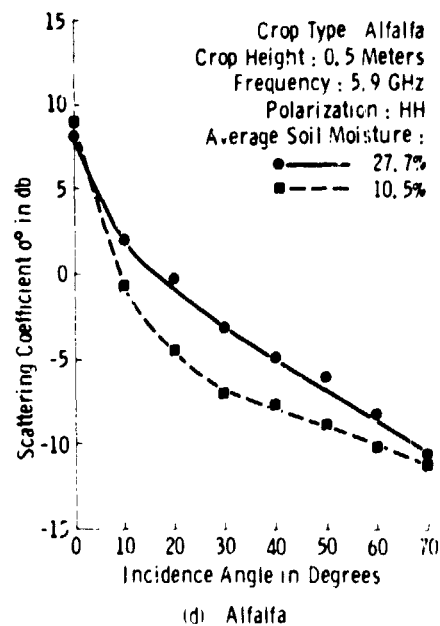
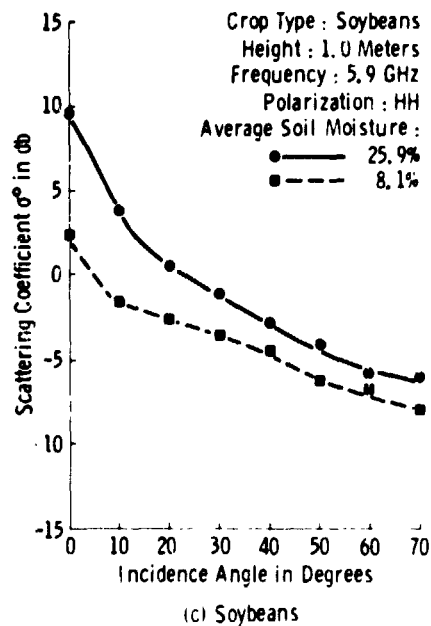
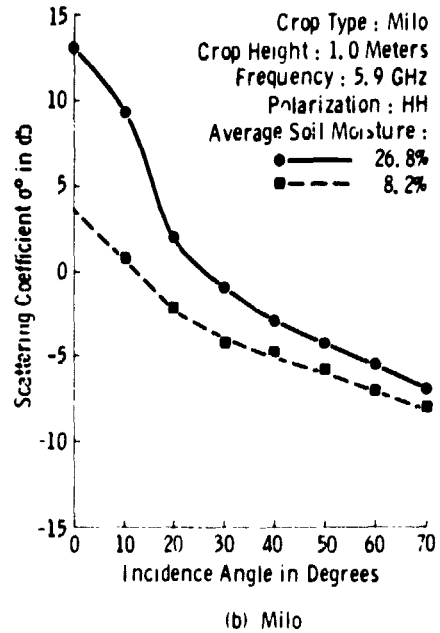
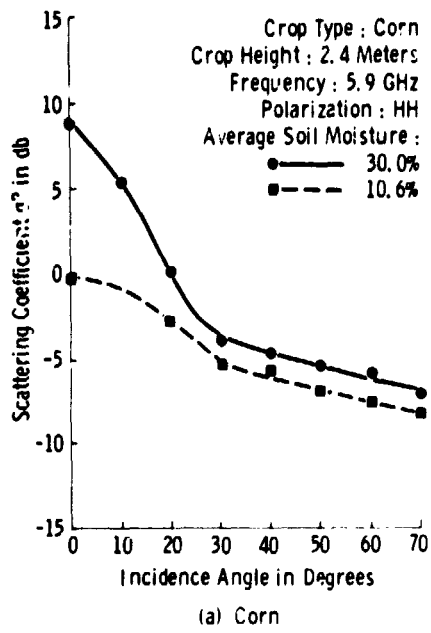


Figure 8. Scattering coefficient response at 5.9 GHz for low and high soil moisture conditions. Polarization is HH.

Designation	Polarization	Frequency
---○---	HH	4.7 GHz
---▲---	HH	7.1 GHz
---●---	VV	4.7 GHz
---△---	VV	7.1 GHz

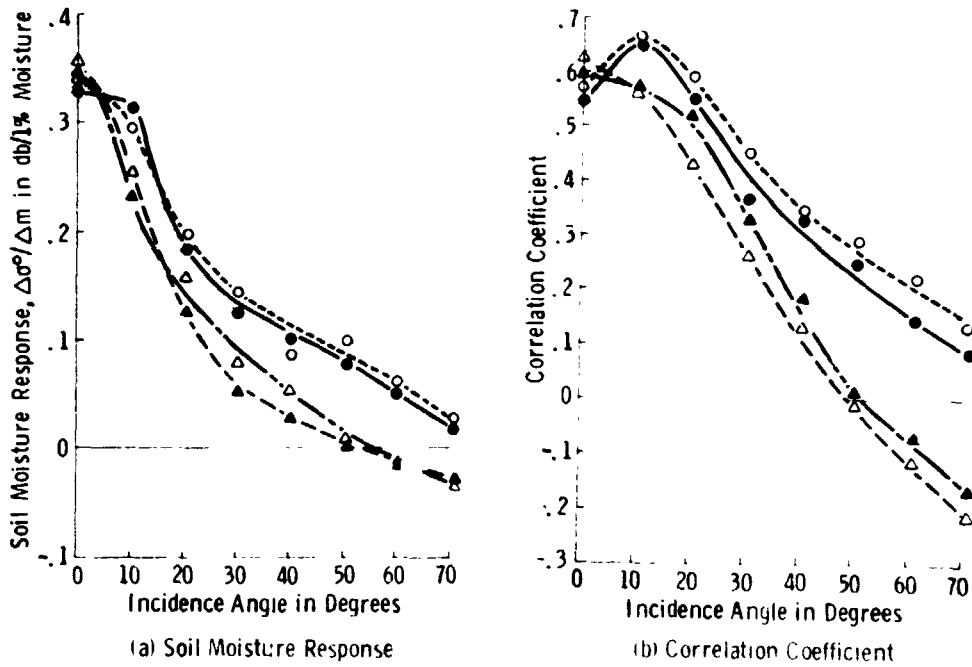


Figure 9 Variation of soil moisture response and corresponding correlation coefficient as a function of incidence angle for entire data set regardless of crop type. (a) Soil moisture response. (b) Corresponding correlation coefficient.

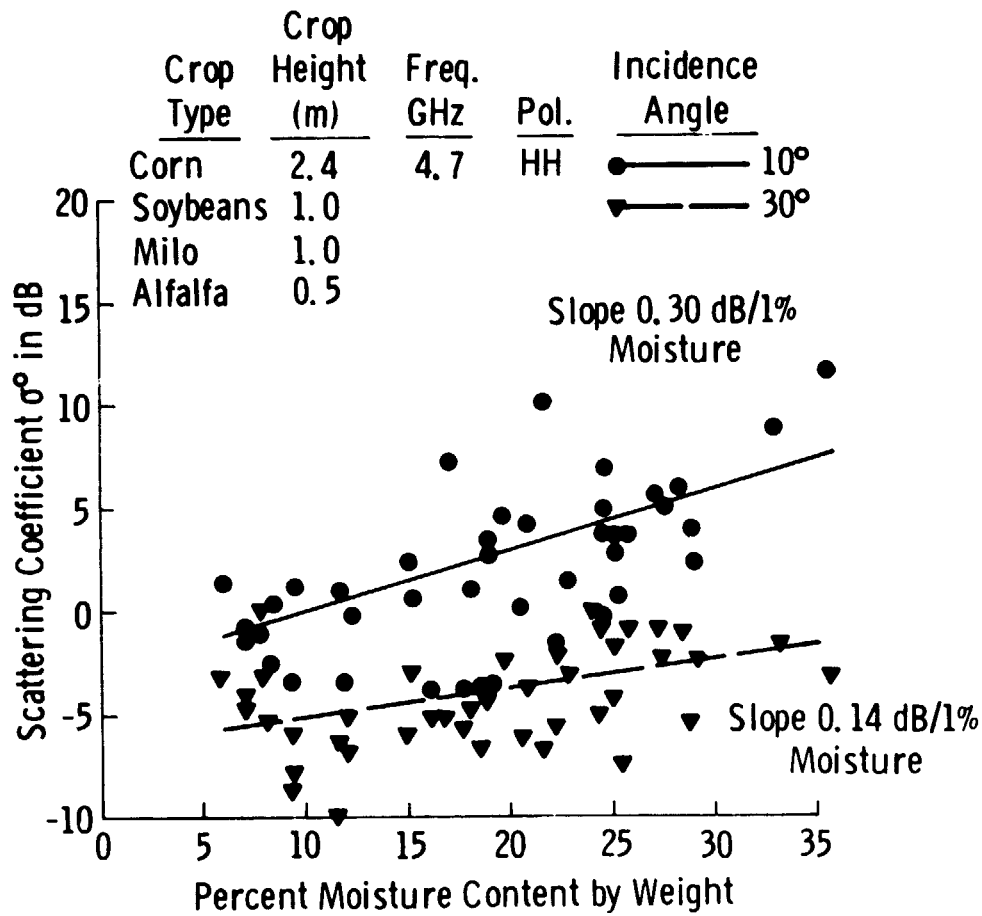
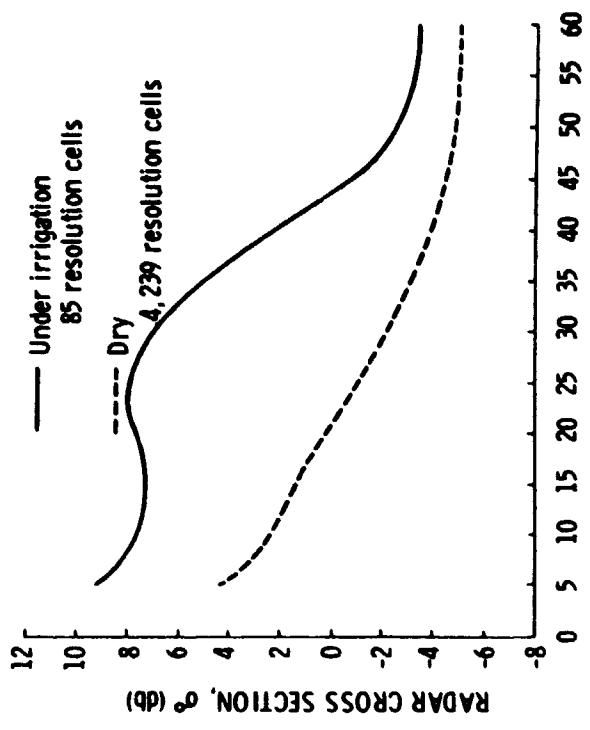


Figure 10 Scattering coefficient response as a function of soil moisture for entire data set regardless of crop type.

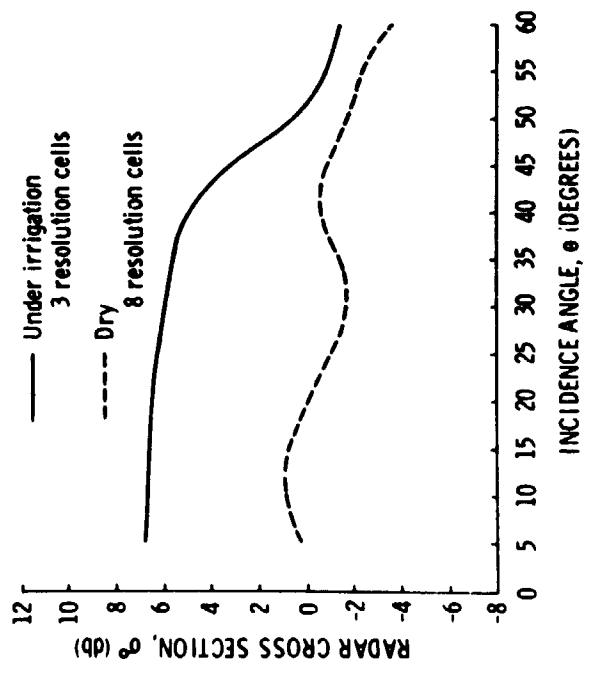
Mission 133
 13.3 GHz
 VV Polarization
 Site 76
 25 June 1970



INCIDENCE ANGLE, θ (DEGREES)

Figure 12. Average scattering coefficient as a function of incidence angle for irrigated and dry terrain.

Mission 133.
 13.3 GHz
 VV Polarization
 Field 222, Site 76
 26 June 1970



INCIDENCE ANGLE, θ (DEGREES)

Figure 11. Scattering coefficient as a function of incidence angle for irrigated and non-irrigated sections of a corn field.

Field	Soil Moisture
#30: Wheat: Stubble, Just Cut	15.7%
#37: Wheat: Ripe, 24" Tall	19.5%
#122: Bare: Cultivated	21.8%
#31: Bare: Cultivated; 10 % Stubble	23.9%
#14: Corn: 16" Tall	29.3%
#18B: Alfalfa: 10" Tall, Mixed Wheat	31.0%
#125: Sorghum: 4" Tall, 5% Emerged	37.5%

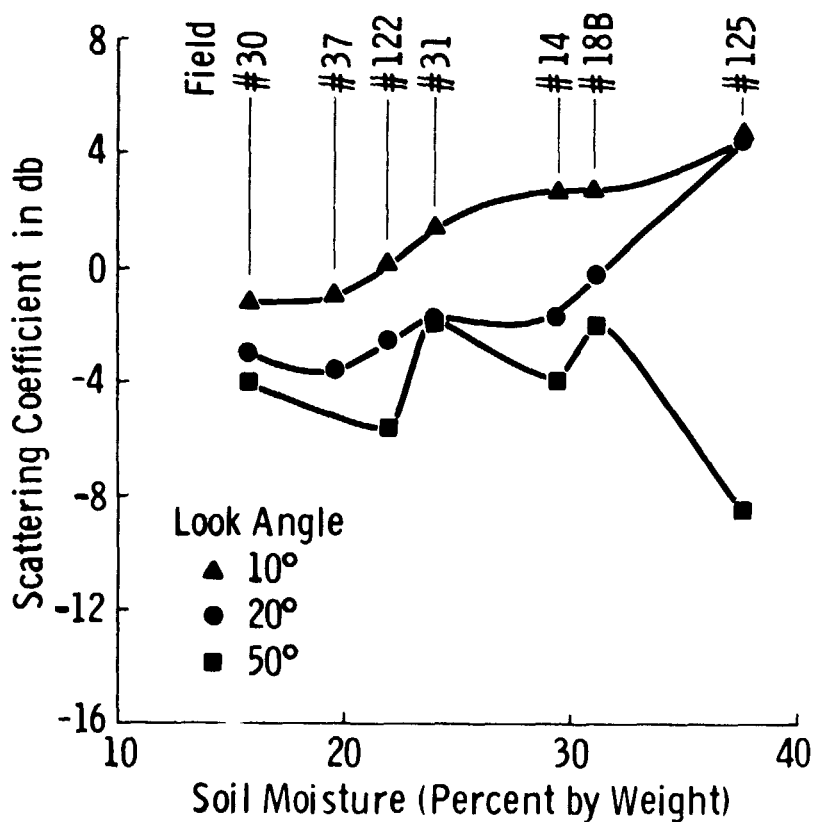


Figure 13. Scattering coefficient as a function of soil moisture content at 13.3 GHz, VV polarization. Garden City, Kansas.

1.55 CM MICROWAVE IMAGE OF THE IMPERIAL VALLEY

FEBRUARY 8, 1973

AIRCRAFT ALTITUDE = 0.6 Km ABOVE TERRAIN

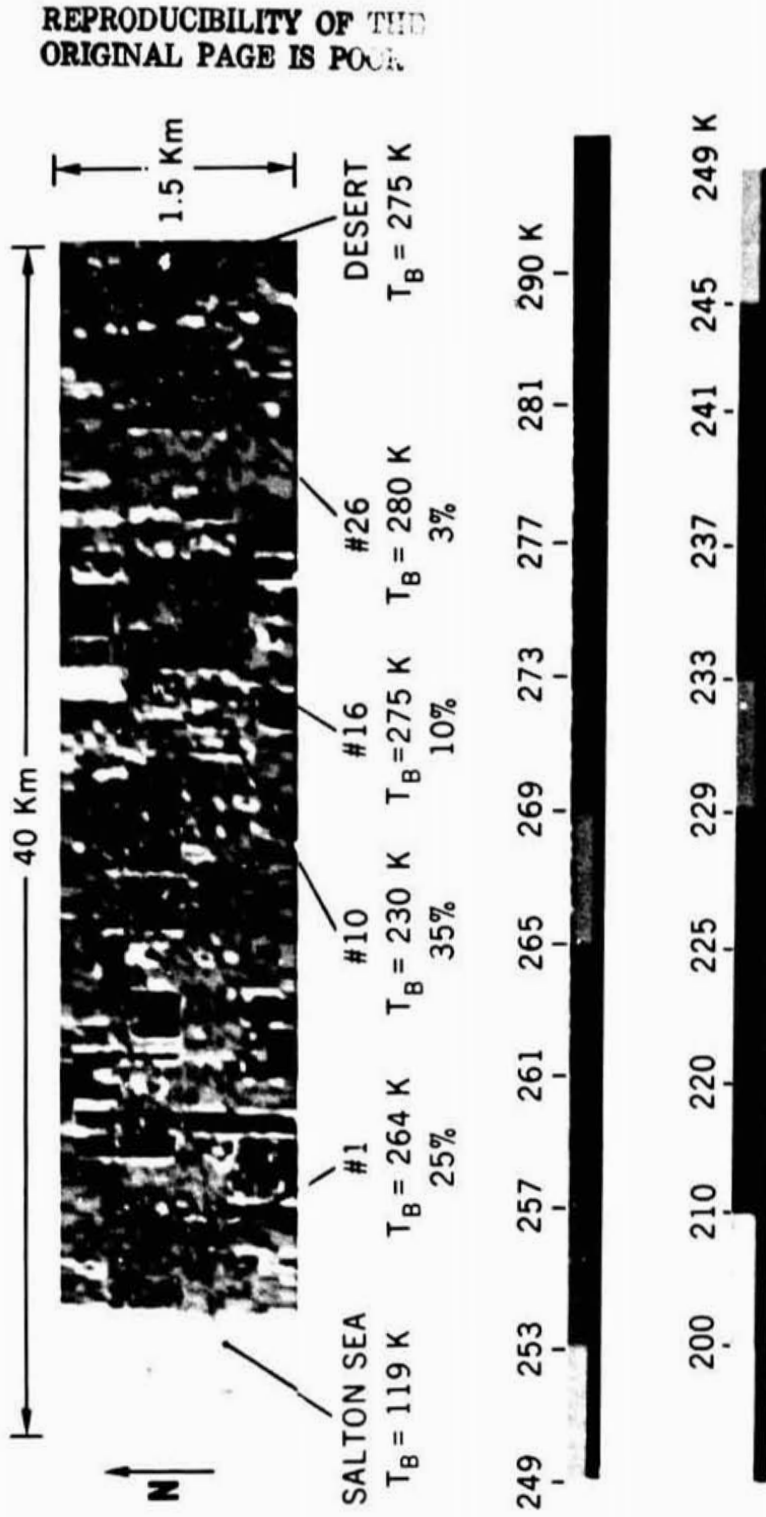


Figure 14.

**INFRARED (10-12 μm) AND 21 CM
BRIGHTNESS TEMPERATURES
OVER
IMPERIAL VALLEY, CALIFORNIA
AIRCRAFT ALTITUDE = 0.6 KM**

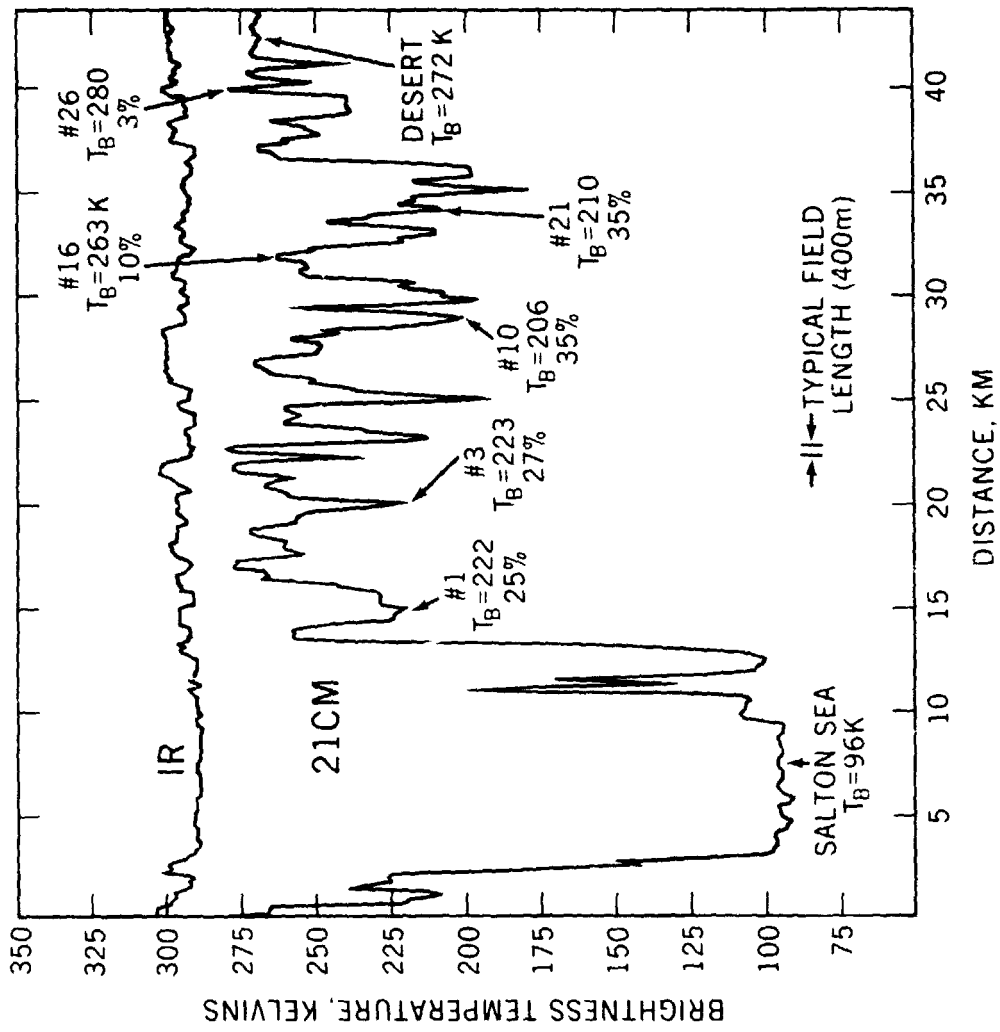


Figure 15.

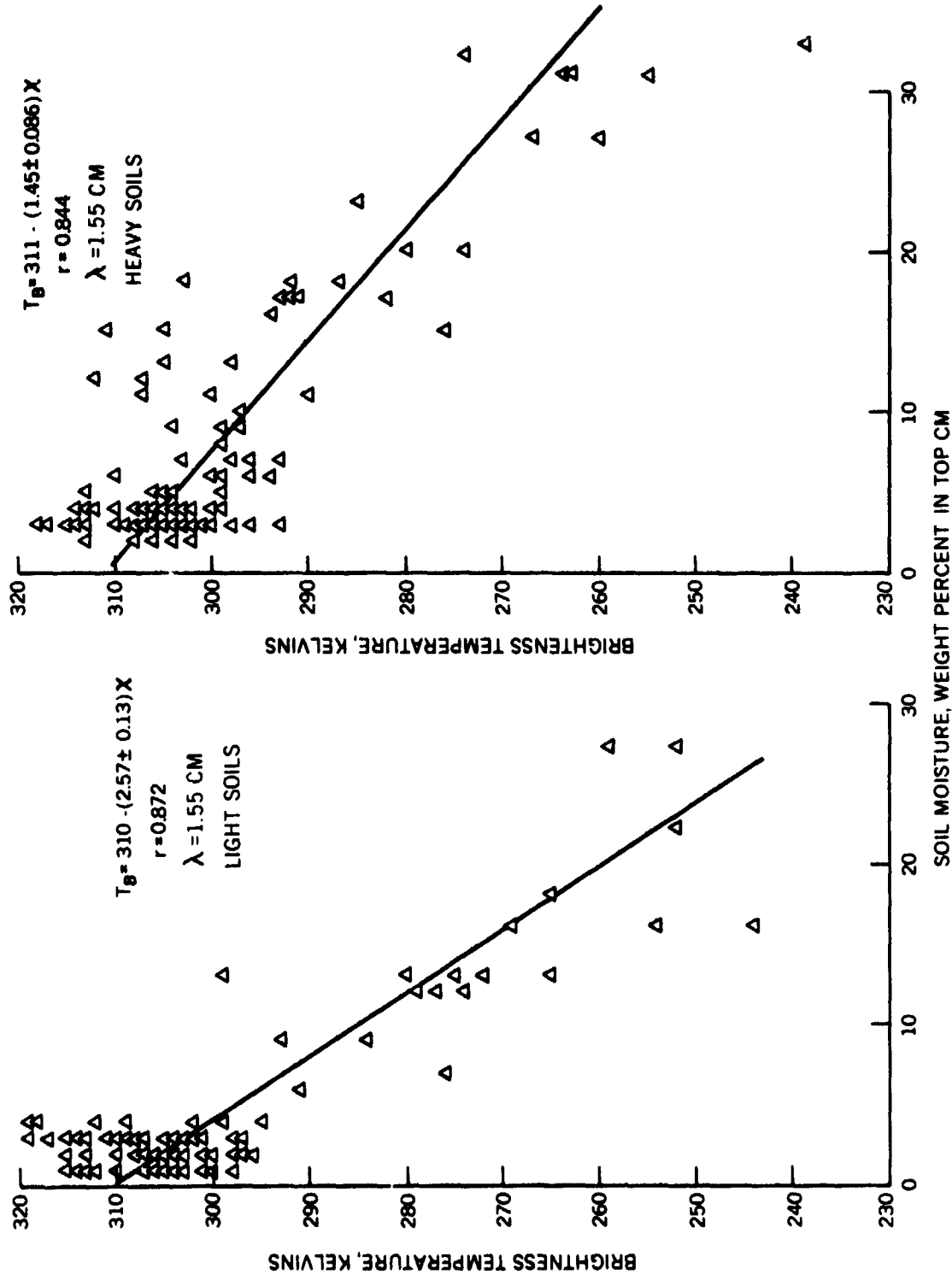


Figure 10. Plot of 1.55 cm brightness temperatures versus soil moisture for light soils (sandy loam and loam) and heavy soils (clay loam).

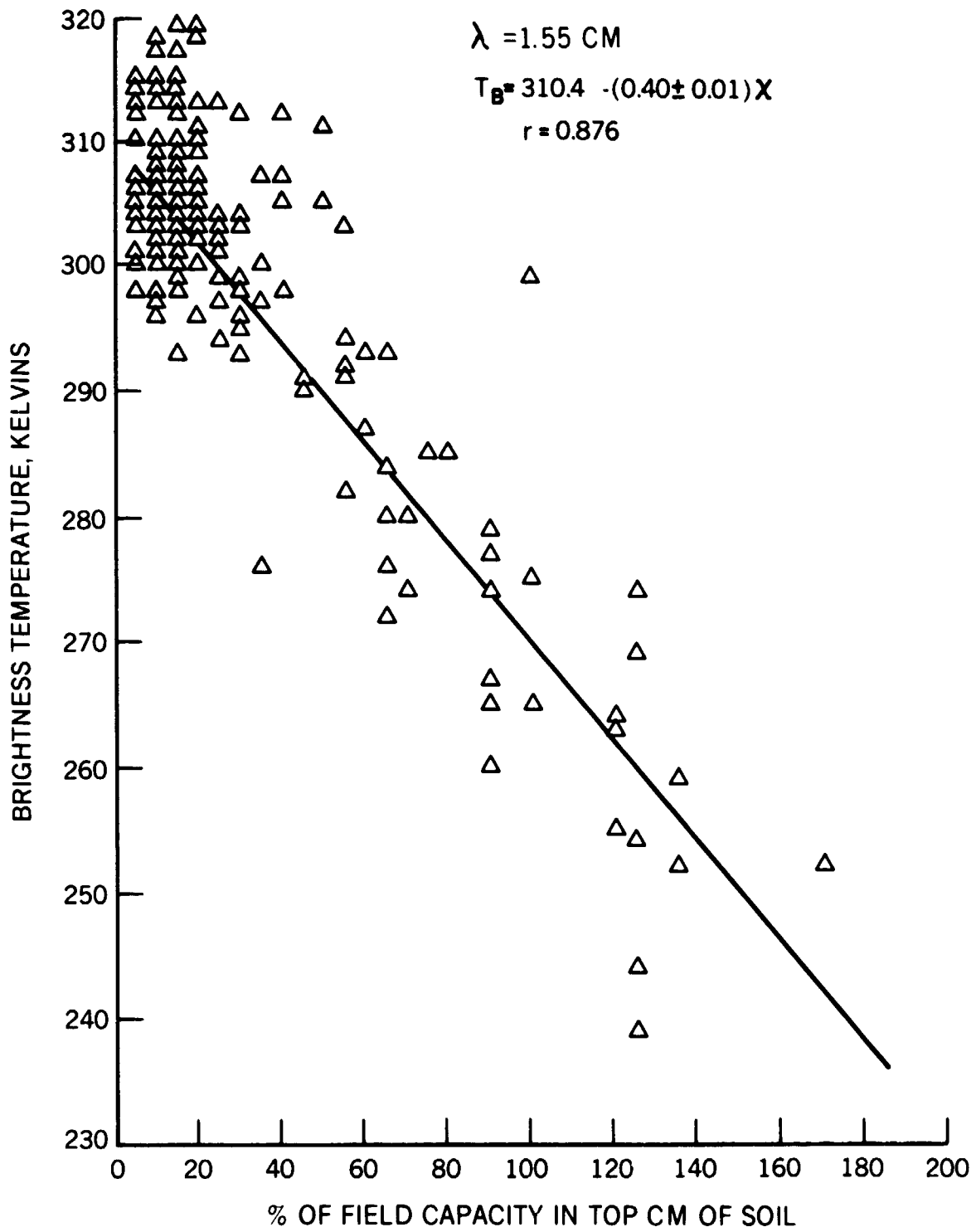


Figure 17. Plot of 1.55 cm brightness temperature versus soil moisture in top 1 cm expressed as a percent of field capacity.

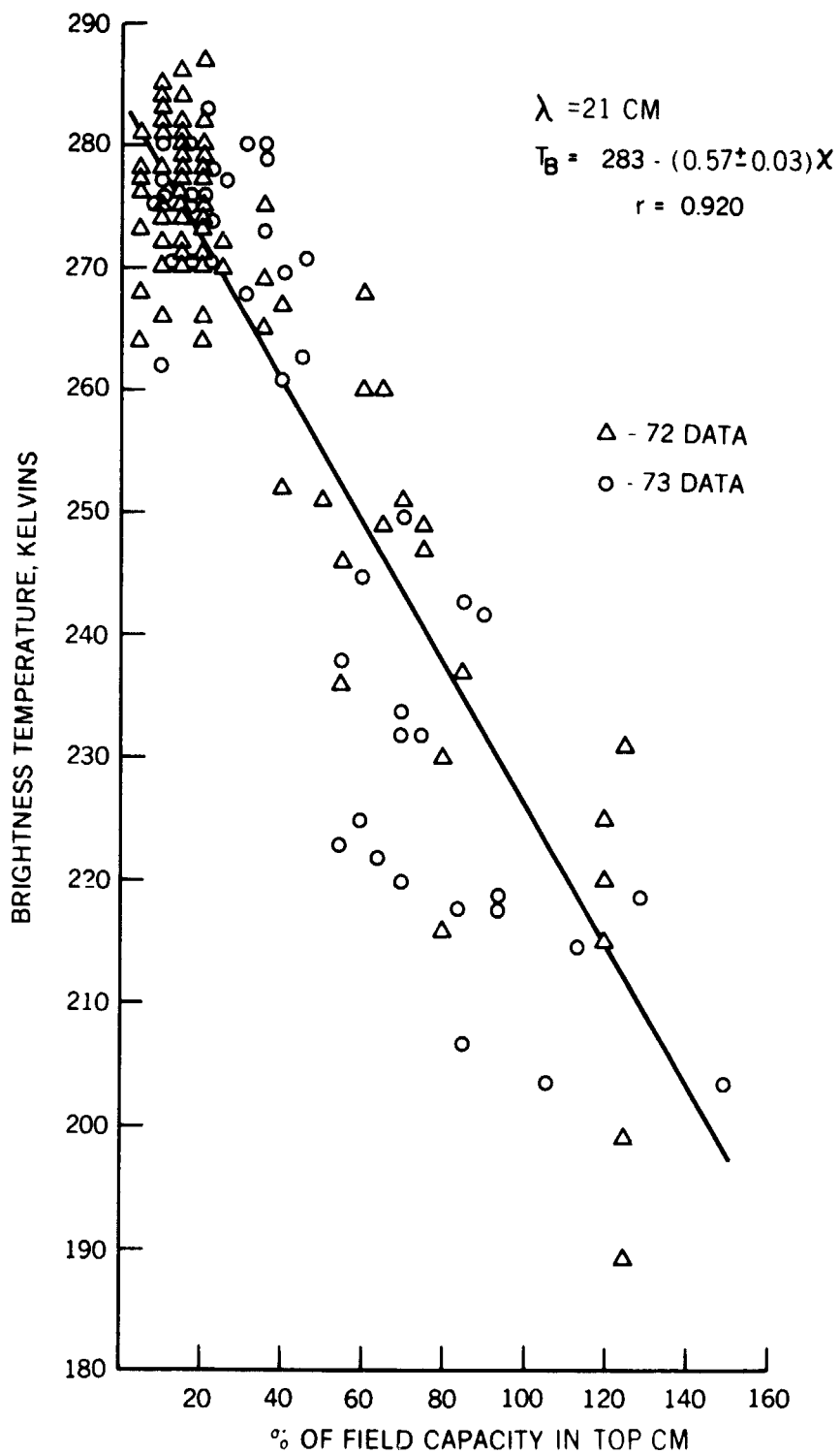


Figure 18. Plot of 21 cm brightness temperature versus soil moisture in top 1 cm expressed as a percent of field capacity.

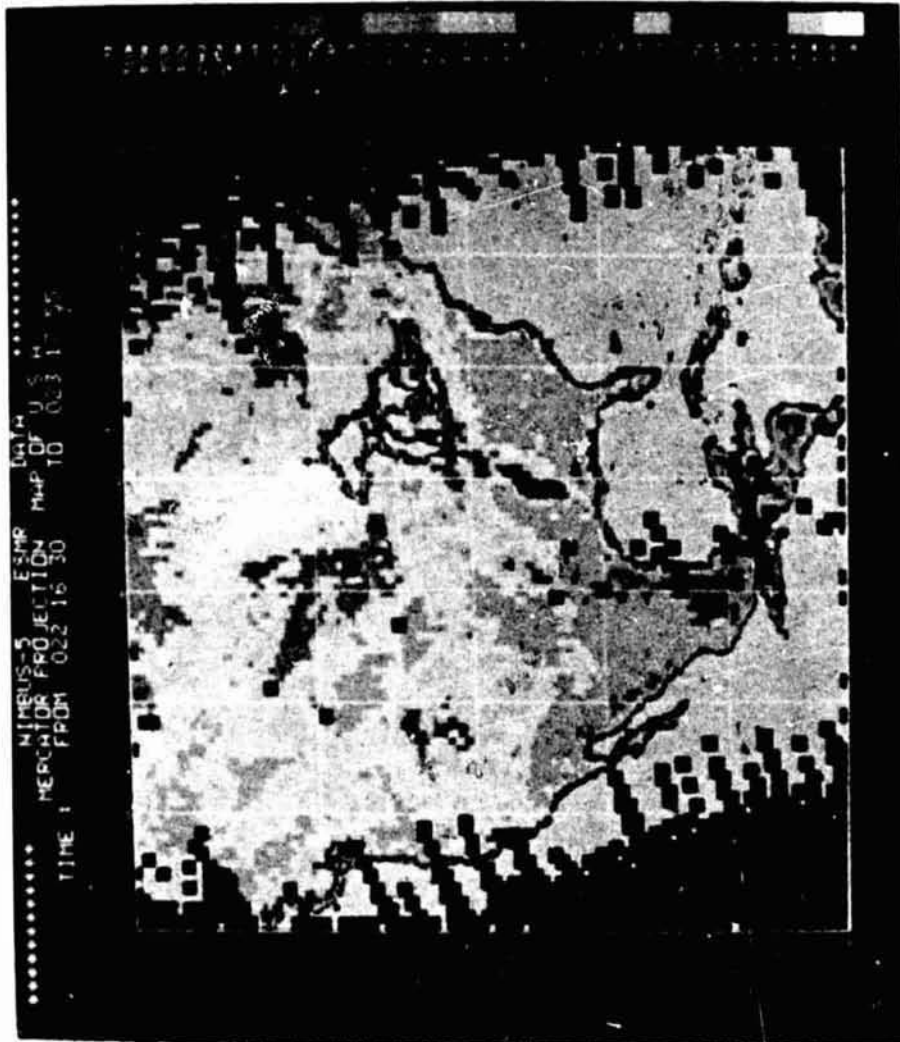


Figure 20.
NIMBUS 5 ELECTRICALLY SCANNING
MICROWAVE RADIOMETER
(19.35 GHz, 1.55cm)
BRIGHTNESS TEMPERATURE COMPOSITE.
JANUARY 22 AND 23, 1973

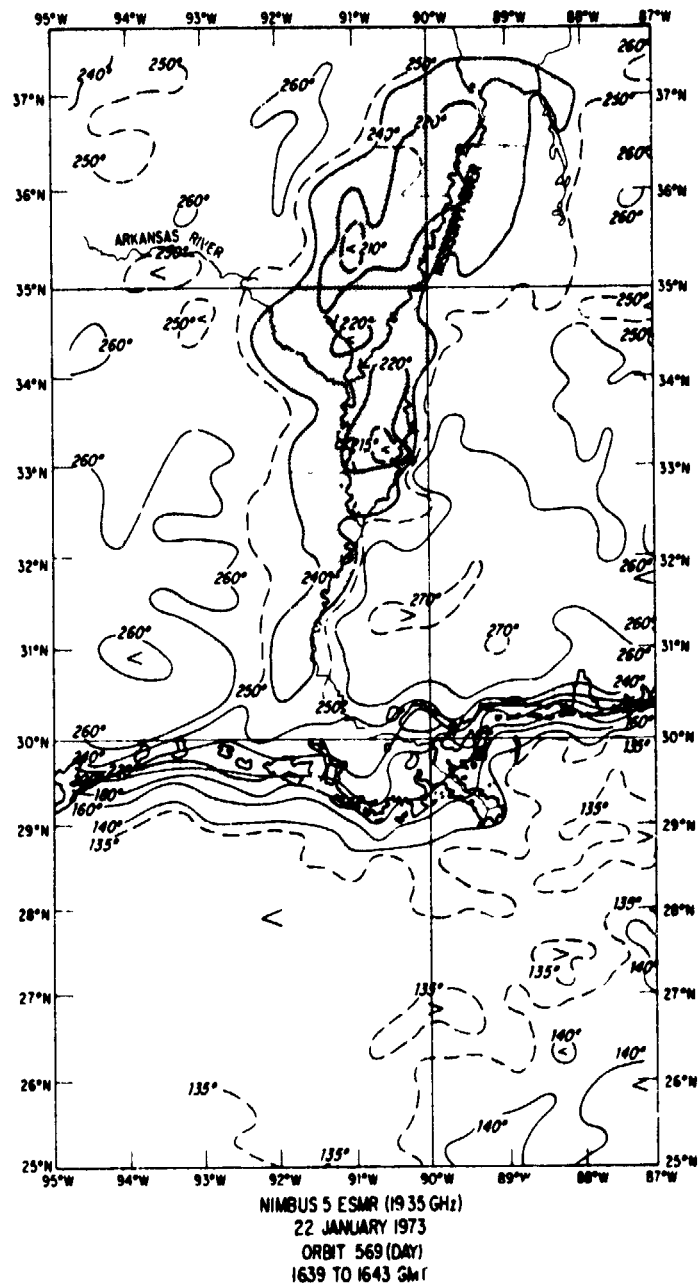


Figure 21. A brightness temperature contour map of the lower Mississippi Valley using the data of 22 January 1973. The contour interval is 10°K.

**COMPARISON ESMR BRIGHTNESS TEMPERATURE WITH AVERAGE RAINFALL
FOR NORTHERN TEST AREA**

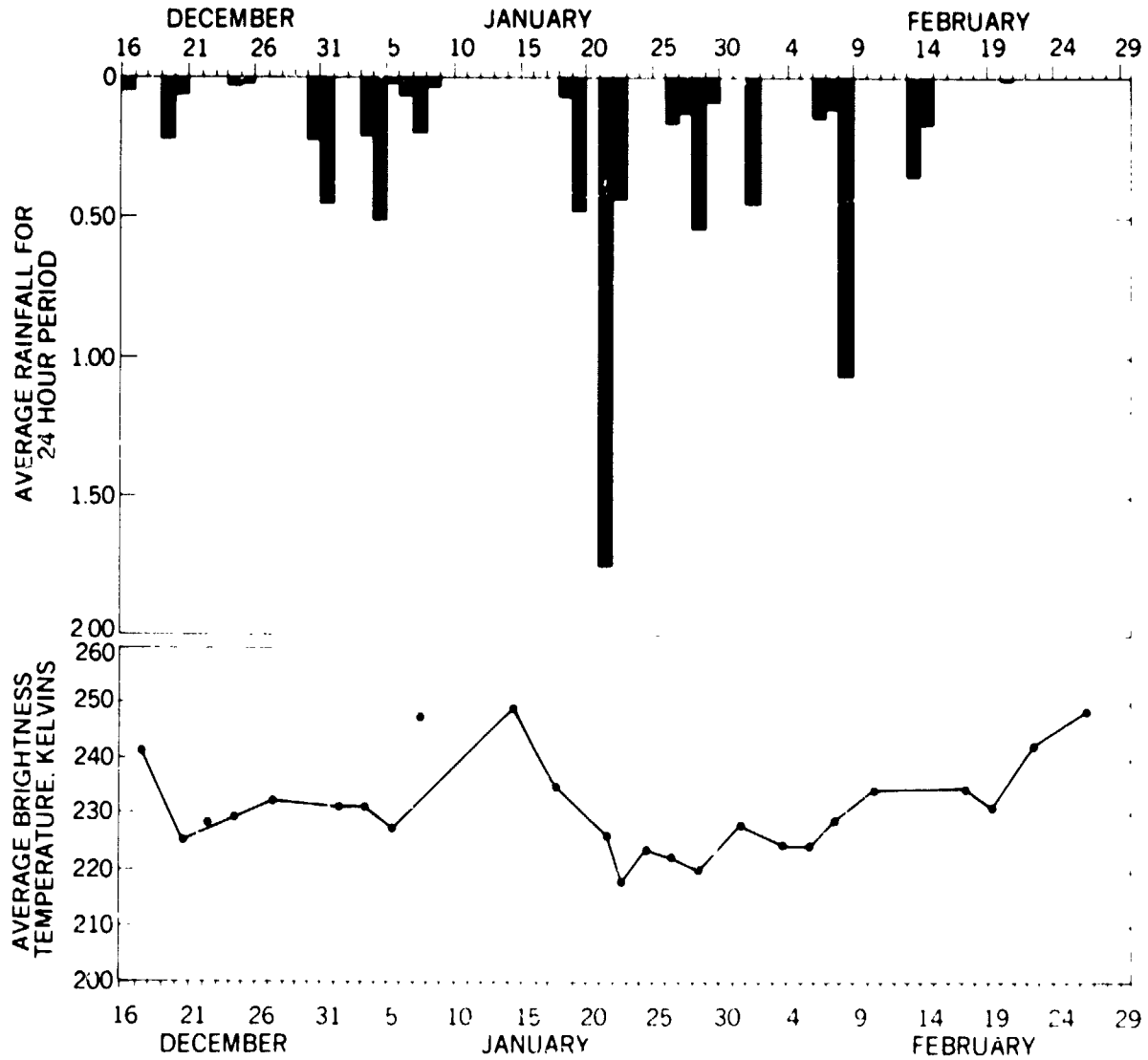


Figure 22.

ESMR BRIGHTNESS TEMPERATURE CONTOURS
GREAT SALT LAKE DESERT 6/5/73

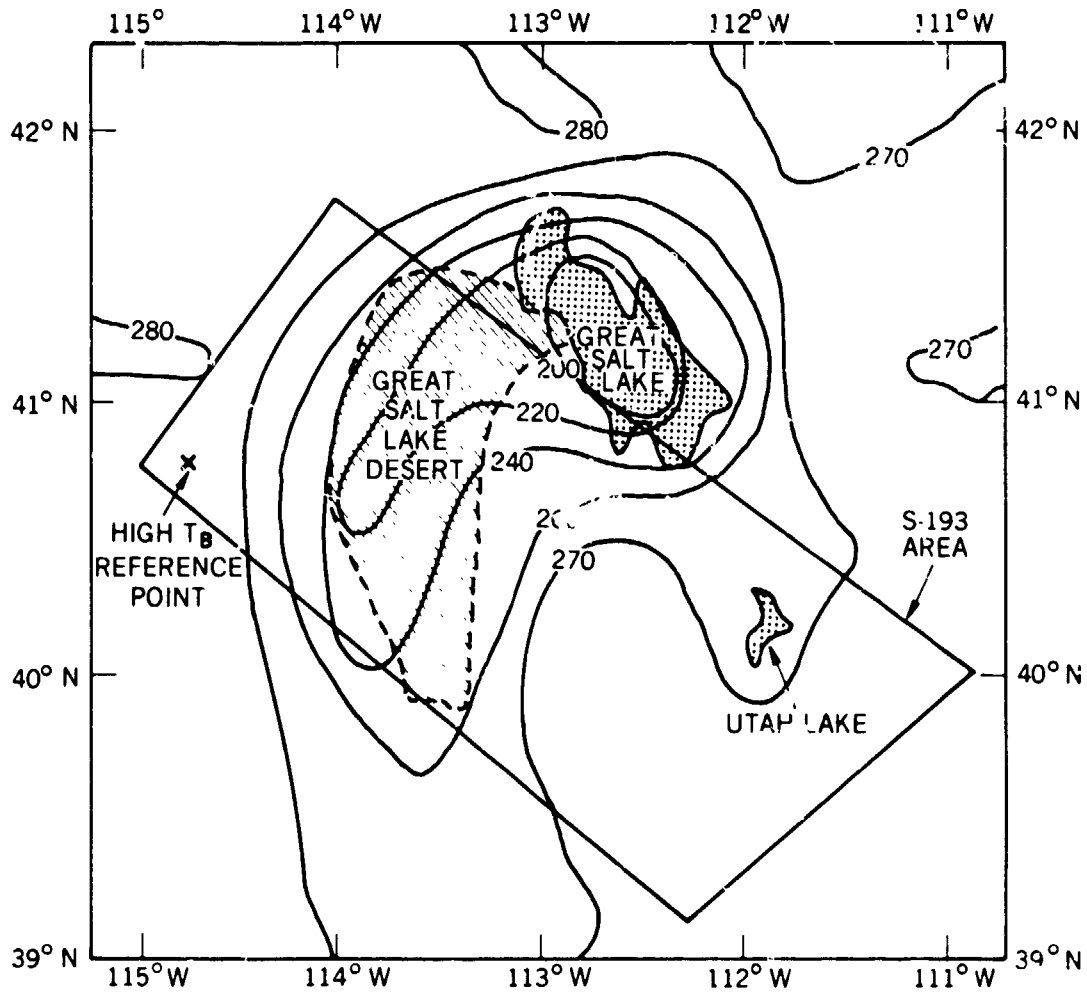


Figure 23.

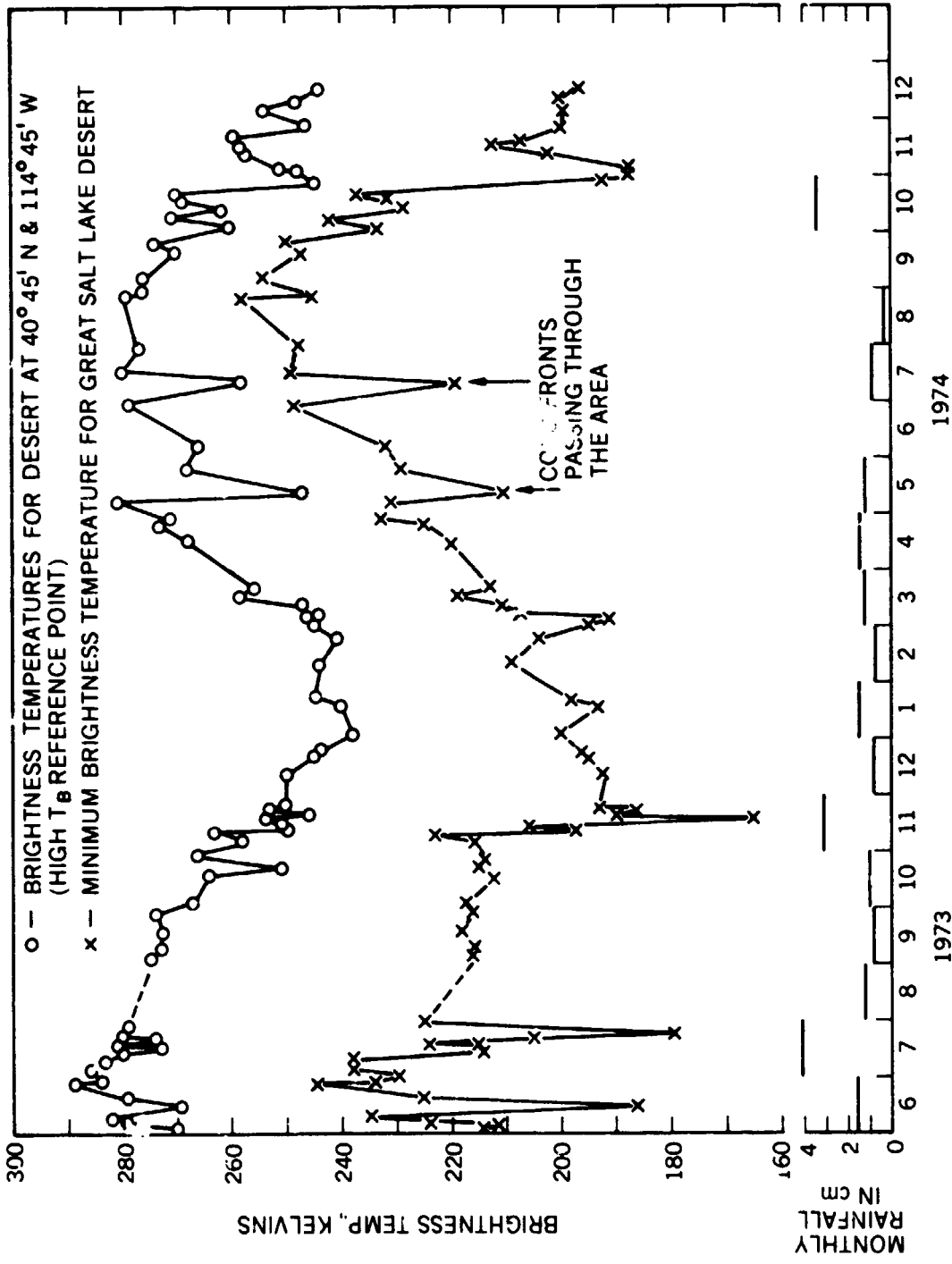


Figure 24. Temporal variations of the minimum recorded ESMR brightness temperature over the Great Salt Lake Desert (x) compared with the ESMR brightness temperature (o) of the reference point outside the desert (as indicated in Figure 23).

SOIL MOISTURE DETECTION FROM SKYLAB

W-6

By Joe. R. Eagleman and Wen C. Lin
University of Kansas, Lawrence, Kansas

ABSTRACT

N76-17598

An investigation was designed for the Skylab satellite to determine the feasibility of remote sensing of the soil moisture content of the surface from various microwave sensors. Skylab data for the experiment were collected during passes 5, 10, 16, and 38 across the two test sites selected in eastern Kansas and western Texas. Pass 38 covered both test sites giving five data sets for the analysis. As Skylab data were being taken the moisture content of the soil was sampled by ground crews for each 2.5 centimeter depth from the surface to 15 centimeters at interval of about six kilometers along two different routes along the test sites. This resulted in a total of 2250 soil moisture samples corresponding to different locations and six different depths. Skylab data were collected by passive microwave radiometers at wavelengths of 2.1 and 21 centimeters by the S193 and S194 microwave sensors. An active microwave system also collected scatterometer data at a wavelength of 2.1 centimeters. Aircraft underflights and a Nimbus-5 satellite provided additional data from microwave sensors corresponding to the Skylab passes. The analysis of microwave data have revealed that the longer wavelength L-Band passive radiometer gives the best correlation with soil moisture content of the upper 2.5 centimeter depth of soil. These correlations were quite good and were apparently influenced very little by other factors such as terrain, vegetation and cloud cover, with the only major disadvantage of the L-Band radiometer being the size of the resolution cell. The shorter wavelength radiometers were influenced more by cloud cover and vegetation, but do have the advantage of a smaller size of resolution cell. The relationship between the soil moisture content and the radiometric antenna temperature has been used to calculate soil moisture levels from satellite altitudes with several applications suggested by this capability.

INTRODUCTION

Soil moisture content is a continuously changing parameter of the earth's surface that is important in a variety of applications from agricultural to flood forecasting. Moisture measurements can be obtained directly but are time consuming and are indicative of only the spot which is sampled. Therefore, there is considerable interest in using promising remote sensing techniques for measuring the moisture content of large areas.

An investigation was designed for the Skylab satellite directed toward determining the feasibility of monitoring the soil moisture content by various microwave sensors. The investigation included collection of 2250 soil moisture samples at six different depths throughout two test sites while the Skylab microwave sensors were making measurements with passive radiometers at 2.1 and 21 centimeters (S193 and S194). An active system (S193) also collected scatterometer data at 2.1 centimeters.

SOIL MOISTURE MEASUREMENTS

The Skylab soil moisture experiment was conducted over two test sites in order to encounter the maximum differences in soil moisture content. These sites were located in western Texas and eastern Kansas. During the Skylab passes field data were collected for each 2.5 centimeters depth down to 15 centimeters at interval of approximately six kilometers along two routes through the test sites. This resulted in soil samples from 42 to 120 different locations for the four different Skylab passes with samples from six different depths at each location. After collection of the soil samples in tin containers they were taken to the laboratory where they were weighed and dried so that the percentage of moisture in the soil sample was determined

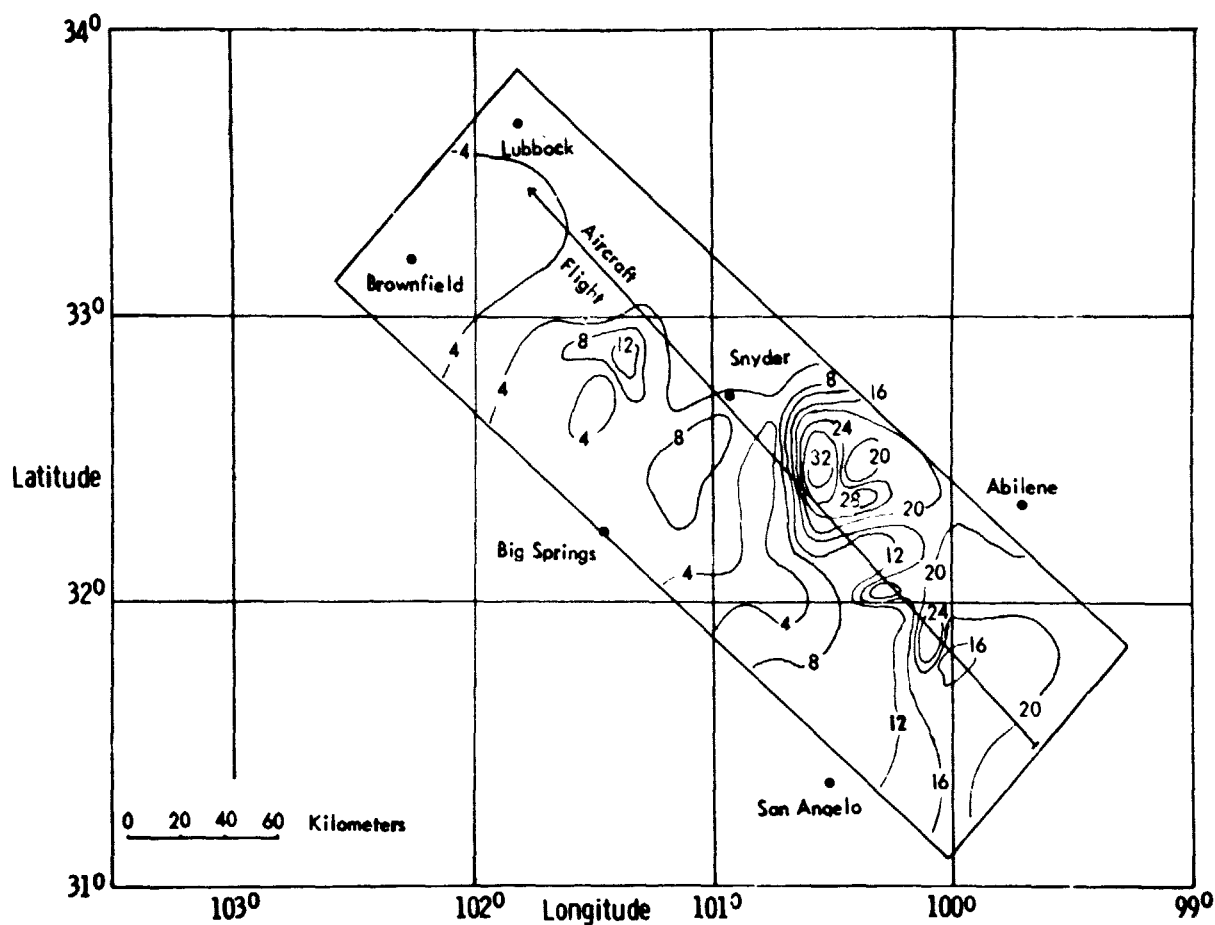


Figure 1. The distribution of Soil Moisture (percentage by weight) within the Texas test site on June 5, 1973.

on a weight basis. The sampling procedure required from one to three days for completion; therefore adjustments in soil moisture content were required because of evapotranspiration losses. The water balance technique for calculating soil moisture levels from climatic data was used to correct for changes in soil moisture content for those samples which did not correspond exactly to the time of the Skylab pass. The water balance calculations were also used to add to the ground truth information in those geographical areas where direct measurements of soil moisture content were not available. Soil moisture variations were calculated by the methods of Eagleman (1971) and Thornthwaite (1948). These methods have previously been shown to produce satisfactory estimates of soil moisture. The daily variation of soil moisture storage in the upper 15 centimeters of soil depth was computed for 61 stations on a daily basis from May 1 to September 13, 1973 in Texas and New Mexico and for 57 stations for May 22 to September 18, 1973 in Kansas. The moisture content of the upper 15 centimeter layer was partitioned into each of the separate 2.5 centimeter layers by using the measured moisture profile from sites where soil moisture data were available with the assumption that the moisture profile at the calculated sites was the same as that at the nearest measured site.

For some of the comparisons between soil moisture content and microwave data the distribution of moisture content over large areas was required (Figure 1). For these comparisons the technique of a weighted linear trend

surface which was based on distance for weight and a least squares solution for each grid intersection was used to obtain the distribution of soil moisture content over the entire test site. Figure 1 shows the variations in soil moisture content throughout the test site for the Skylab pass on June 5, 1973.

DATA FROM SKYLAB MICROWAVE SENSORS

Data were collected from Skylab with two different radiometers and a scatterometer. The S194 L-Band radiometer is a passive, non-imaging sensor operating with a 21 centimeter wavelength at a center frequency of 1.4 GHz. This radiometer utilizes a hard-mounted antenna with a 15° half-power beam width and a field of view centered about the nadir point. The size of the halfpower footprint corresponds to a circle with a 115 kilometer diameter. Absolute antenna temperatures were collected with the L-Band radiometer to an accuracy of one degree Kelvin. Data were also collected for the soil moisture experiment by the S193 microwave system in the cross track contiguous mode at zero degrees roll and 29.4° pitch forward. The S193 sensor collected data with a passive microwave sensor operating at a wavelength of 2.1 centimeters and a frequency of 13.9 GHz with the active microwave system collecting scatterometer data at a wavelength of 2.1 centimeters. In the cross track contiguous mode the S193 antenna sweeps in the roll plane both to the left and to the right of the sub-satellite point. Since the antenna excursions extended 11.4° to the left and right the difference in incidence angle from the centerline to the edge was only about two degrees for a forward pitch of 29.4° . The radiometer footprint size is about 17 x 21 kilometers, whereas the scatterometer footprint is about 13 x 16 kilometers. Aircraft underflight data were also collected with a microwave system comparable to the Skylab S193 instrument. The Skylab and aircraft data have also been supplemented with Nimbus-5 microwave data obtained at a wavelength of 1.55 centimeters. The Nimbus-5 footprint size ranged from 25 to 40 kilometers because of angle variations across the test site. Information from these various sensors has been analyzed for sensitivity to surface moisture conditions.

RELATIONSHIP BETWEEN SOIL MOISTURE AND MICROWAVE DATA

L-Band Radiometer

The S194 brightness temperature for every seven kilometers along the flight track was compared with average percentage of soil moisture content within a circular area of 115 kilometers diameter. Scattergrams for the three passes over the Texas site and two passes over the Kansas site are shown in Figure 2. Prior correlations with soil moisture at different depths as well as skin depth calculations showed that the soil moisture content of the upper 2.5 centimeters depth of soil was most likely to influence the L-Band radiometer. The correlation indices between the L-Band brightness temperature and the soil moisture content of the upper 2.5 centimeters depth of soil were quite high for all five passes across Texas and Kansas with a variation from -0.996 to -0.945 . The L-Band radiometer operating at a longer wavelength than the other microwave sensors should be less influenced by cloud cover and amount of vegetation on the surface and has given the highest correlations of any of the other microwave sensors.

For comparison and combination of data obtained during different Skylab passes the weighted antenna temperature was adjusted for differences in ground temperature which varied from about one degree centigrade to five degrees centigrade among the five sets of data. The surface temperature was estimated from air temperature data from weather stations throughout the test site. Although surface temperature is very sensitive in low moisture conditions with clear skies at midday the soil temperature below the surface is closer to the

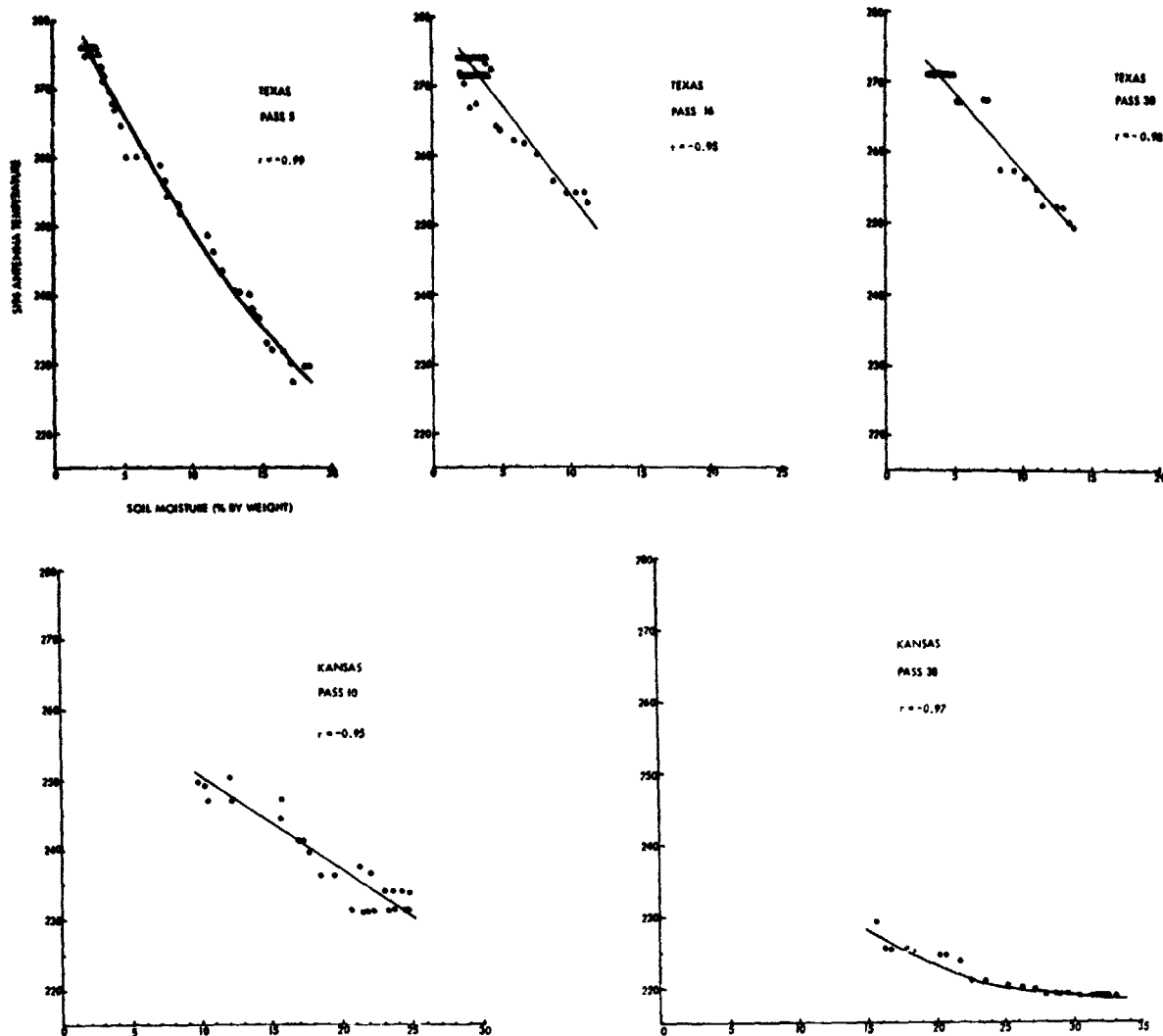


Figure 2. Relationships between S194 antenna temperature and soil moisture content for five Skylab passes across Kansas and Texas.

fluctuations of air temperature. Due to greater skin depth for the S194 radiometer the probable error of the estimated ground temperature is less for the S194 sensor than for other data.

The brightness temperature measured by a downward looking microwave radiometer is given by:

$$T_B = L (\epsilon T_g + T_{sc}) + T_u$$

where L is the atmospheric transmittance, ϵ is the target emissivity, T_g is the ground temperature, T_{sc} is the upward scattered radiation and T_u is the upward emission by the atmosphere. For a plane surface model, T_{sc} can be expressed in terms of the downward emitted radiation T_d and the surface reflectivity, $r = 1 - \epsilon$:

$$T_{sc} = (1 - \epsilon) T_d$$

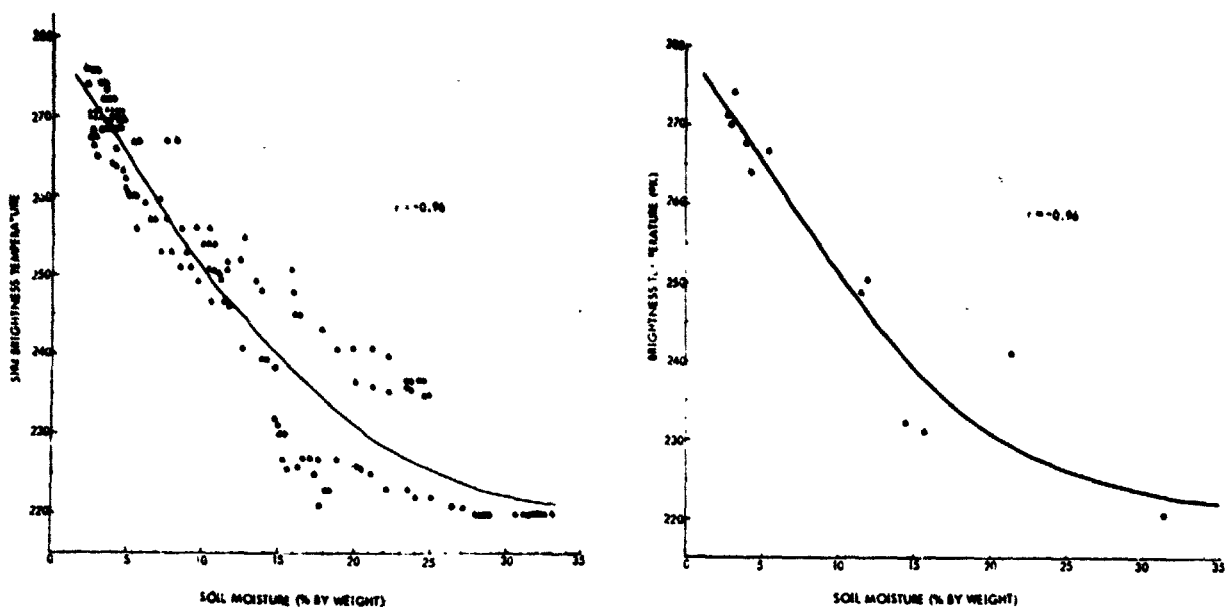


Figure 3. Composite relationship between S194 brightness temperature and soil moisture content for overlapping footprints (left) and independent footprints.

At 1.4 GHz (S194 frequency), L and T_u at nadir were calculated to be about 0.993 and 2°K, respectively (Eagleman and Ulaby, 1974). T_d includes downward emitted atmospheric radiation as well as galactic radiation and is estimated to be about 7°K. Attenuation by clouds in this frequency range is very small (Benoit, 1968) and hence can be neglected. Therefore, the adjusted brightness temperatures were obtained by:

$$T_{aw} = T_{ac} + 0.993 \times \epsilon(300 - T_g).$$

The five data sets were combined to form a composite relationship between the adjusted brightness temperature and moisture content of the upper 2.5 centimeter layer of soil as shown in Figure 3. The correlation index for the second degree curvilinear relationship is -0.96. For the halfpower footprint of 115 kilometers diameter, the footprint overlap from one S194 measurement point to the next was approximately 92 percent. Independent footprints based on the halfpower footprint of the S194 were also analyzed. There were three independent footprints for pass 5 and pass 16, two for pass 10 and four for pass 38. These twelve independent samples are also shown in Figure 3 with a resulting correlation index of -0.96 which is the same as that obtained for the overlapping footprints. A straight line correlation gave a decrease of 2°K per percent soil moisture in comparison to 2.2°K obtained by Schmugge et. al. (1974).

In order to make sure the correlations between the S194 microwave data and the soil moisture content do not develop because of a relationship to a third parameter, variations of antenna temperature and soil moisture content are shown in Figure 4 for two different passes which traveled across the same general terrain in Texas. On June 5, 1973 the soil moisture content was low in the northwest part of the Texas test site and high in the southeast. The antenna temperatures dropped from a high value in the northwest to a lower value in the southeast. On August 8, 1973 Skylab collected data over the same general area and the soil moisture content was reversed with low values

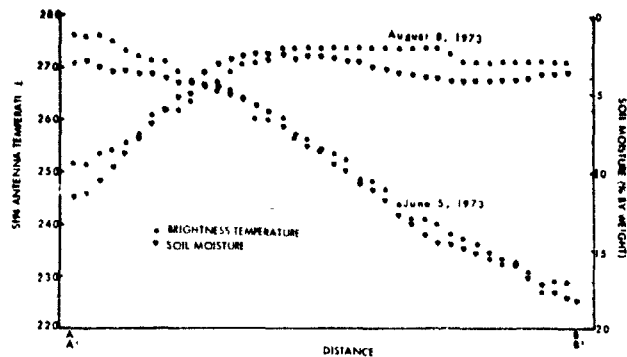
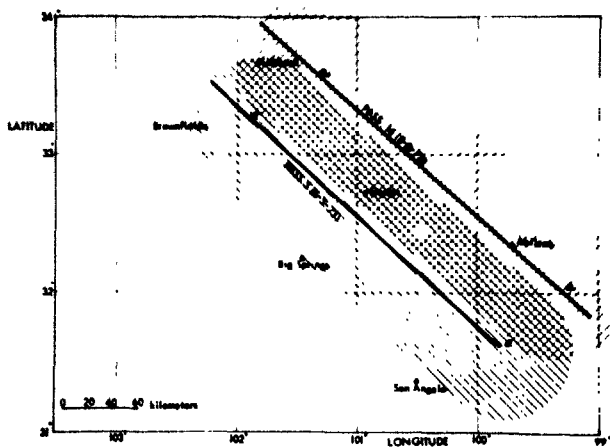


Figure 4. Soil moisture variations and S194 antenna temperature variations across the Texas site for two different Skylab passes.

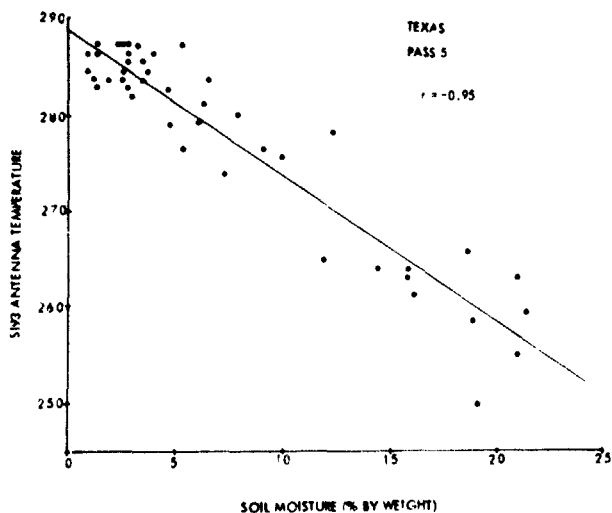


Figure 5. Relationship between S193 passive radiometric temperature and soil moisture content across the Texas test site on June 5, 1973.

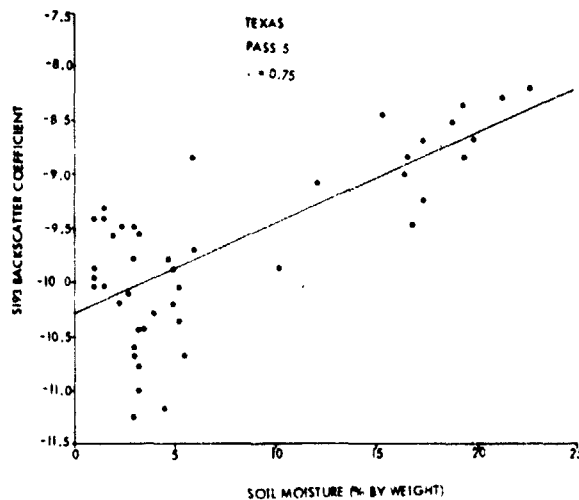


Figure 6. Relationship between the S193 scatter coefficient and soil moisture content across the Texas test site on June 5, 1973.

of moisture content in the southeast and higher values in the northwest. On this day the antenna temperature again responded to differences in soil moisture content rather than other variables such as differences in vegetation, cloud cover or soil texture. This provides convincing evidence that the correlations between the S194 microwave sensor and the moisture content of the upper 2.5 centimeters of soil are real and that the S194 passive radiometer may be a very useful instrument for measuring the soil moisture content from the vantage point of space.

S193 Passive and Active Microwave Sensors

Passive radiometer data from the S193 sensor operating at 2.1 centimeter wavelength were collected for pass 5 and pass 16 over the Texas test site. The location of the S193 footprints which were about 17 x 21 kilometers in size for the radiometer were plotted by computer and an overlay over the soil moisture content distribution map was made to determine the soil moisture content within each footprint. If individual footprints covered an urban area or large lake these data were not included in the analysis. The variations in S193 radiometric temperature and scatter coefficient with soil moisture content are shown in Figures 5 and 6 for pass 5. The correlation of the passive radiometer and soil moisture content in the upper 2.5 centimeters of soil is -0.92. The individual footprints of the S193 scatterometer were analyzed in a manner similar to the passive radiometer. The active microwave sensor footprint was slightly smaller with a size of about 13 x 16 kilometers. Variations in backscatter coefficients with soil moisture content produced a correlation coefficient of 0.52. Since there are slight variations in the incidence angle between the center and the edges of the test site which amount to about two degrees for the forward pitch mode at 29.4° the influence of angular variations was investigated by plotting data from these central four lines from the microwave sensor as a function of soil moisture content as shown in Figures 5 and 6. This improved the correlation coefficient for the passive radiometer from a value of -0.92 to -0.95 and for the scatterometer from 0.52 to 0.75. This shows that small variations in incidence angle are more important for the scatterometer coefficient than for the passive radiometer.

Nimbus Microwave Data

The Nimbus-5 satellite also collected data over the Texas test site on June 5, 1973 with the ESMR data obtained by a passive radiometer operating at 1.55 centimeter wavelength. The Nimbus data were collected while the satellite passed across New Mexico. The largest soil moisture variations on June 5 across the Texas site occurred from the northwest to the southeast. Since the satellite passed across New Mexico and the radiometer scanned across a distance of about 1900 kilometers, the angle varied across the Texas test site from 16.8° to 30.4°. This difference in angle further complicated the analysis of radiometer antenna temperature and soil moisture content. Since the incidence angle affects the relationship between antenna temperature and soil moisture content, a different analysis was performed for each incidence angle. There were differences in correlations for the different angles because of variations in the antenna temperature response for different angles. With these limited data, the best correlation was obtained for an incidence angle of 17.9° for which a correlation of -0.78 was obtained.

Aircraft Underflight Analysis

An Aircraft underflight on June 6, 1973 provided additional detailed information across the Texas test site. The data were collected with an NC-130B airplane flown at an altitude which varied from 2225 to 2743 meters above the surface. The ground speed of the aircraft averaged approximately 86 meters per second. Data were collected with an RC8 camera using color film and with a 2.1 centimeter wavelength passive radiometer and active scatterometer. The microwave system has a halfpower beam width of 1.8° and this beam was directed approximately 30° from nadir behind the aircraft. An elliptical footprint was obtained which varied from 79 x 92 meters in diameter at an altitude of 2225 meters to 98 x 116 meters at an altitude of 2743 meters. The time between the radiometer and the scatterometer was only 10 microseconds,

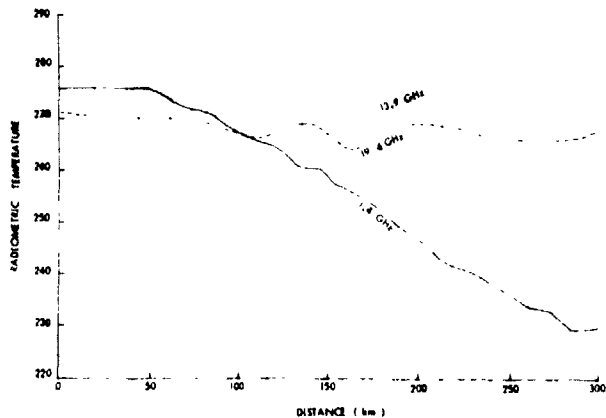


Figure 7. Variations in antenna temperature across the Texas test site on June 5, 1973 for three satellite passive radiometers.

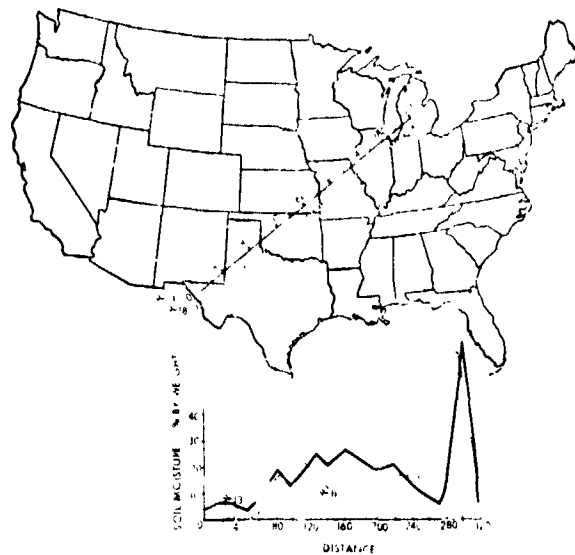


Figure 8. Soil moisture variations across the United States as calculated from Skylab L-Band radiometric temperature measurements on September 13 and 18, 1973.

giving a difference between the location of the radiometer and scatterometer footprint of only about one millimeter at the aircraft's velocity, which means that they were looking at the same terrain. The ground truth information was collected primarily for the satellite sensors so that the distance between samples was about six kilometers. This is very coarse data for the aircraft which is sensitive to areas about 92 meters across; however, it was possible to use the geographical distribution of soil moisture as shown in Figure 1 to obtain some indication of the response of the microwave sensors from the aircraft. The aircraft data were quite sensitive to terrain features. By simple geometry the location of the microwave footprint could be found in the aerial photographs. Using this procedure data points corresponding to only certain terrain features could be analyzed. Low correlations were obtained for vegetated surfaces such as range land. The best correlation (-0.73) was obtained for cultivated fields by averaging 50 data points. Correlations between the scatterometer data and the soil moisture content of the cultivated fields resulted in a lower coefficient of 0.27.

APPLICATIONS

Some of the difference in response of the different satellite sensors can be seen in Figure 7 which shows the variations in antenna temperature across the test site for the S194 passive radiometer (1.4 GHz) with a large footprint, the S193 radiometer (13.9 GHz) and the Nimbus radiometer (19.4 GHz). The L-Band radiometer is useful for sensing the moisture content of large areas while the minute detail can be provided by the radiometer data from aircraft; therefore, different applications are possible for these various sensors. The remote sensing of soil moisture with the small footprint from the aircraft sensors would be more useful in determining the moisture content of individual fields which has agricultural implications for irrigation scheduling and perhaps planting depth as well as time of planting. Information over a slightly larger area would be useful for flood forecasting

for individual river basins and other problems of similar scale. Drought occurrence over large areas or flood forecasting for very large water sheds might require data over large areas such as from the S194 sensor.

Since the best correlation between soil moisture content and microwave data was obtained for the L-Band radiometer onboard Skylab, this information has been used to estimate the soil moisture content across the United States. The regression equation with soil moisture as the dependent variable is:

$$SM = 253.03 - 1.4898 AT + 0.00210 AT^2$$

where SM is soil moisture content in percent by weight and AT is the S194 antenna brightness temperature. This equation with adjustments for differences in ground temperature was used to estimate the distribution of soil moisture across the United States along two different Skylab III tracks as shown in Figure 8. Since the equation used to calculate soil moisture is based on five different passes which collected data over various types of soil with various vegetation cover and soil moisture content, it can be assumed that variations in these parameters are not a serious problem in estimating soil moisture content using a wavelength of 21 centimeters. Since the correlation coefficient was quite good even though there were large variations in the surface characteristics, the potential for remote sensing of soil moisture appears to be quite good. The microwave sensor with longer wavelengths have the advantage of greater penetration and smaller interference from vegetation and cloud cover and the shorter wavelengths have the advantage of a smaller resolution cell for the same size antenna.

REFERENCES

- Benoit, Andre, 1968, "Signal Attenuation Due to Neutral Oxygen and Water Vapor, Rain and Clouds", The Microwave Journal, 11, 73-80.
- Eagleman, Joe R., 1971, "An Experimentally Derived Model for Actual Evapotranspiration", Agricultural Meteorology, 8, 385-394.
- Eagleman, Joe R., and F.T. Ulaby, 1974, "Remote Sensing of Soil Moisture by Skylab Radiometer and Scatterometer Sensors", Advances in the Astronautical Science, The Skylab Results, vol. 31, part 2, 681.
- Schmugge, T., P. Gloersen, T. Wilheit and F. Geiger, 1974, "Remote Sensing of Soil Moisture with Microwave Radiometers", Journal of Geophysical Research, 79, 317-323.
- Thorntwaite, C.W., 1948, "An Approach Toward a Rational Classification of Climate", Geographical Review, 38, 55-94.

THE CORRELATION OF SKYLAB L-BAND BRIGHTNESS TEMPERATURES
WITH ANTECEDENT PRECIPITATION

W-7

By Marshall J. McFarland, University of Oklahoma, Norman, Oklahoma

N76-17594

ABSTRACT

The S194 L-band radiometer flown on the Skylab mission measured terrestrial radiation at the microwave wavelength of 21.4 cm. The terrain emissivity at this wavelength is strongly dependent on the soil moisture content, which can be inferred from antecedent precipitation. For the Skylab data acquisition pass from the Oklahoma panhandle to southeastern Texas on 11 June 1973, the S194 brightness temperatures are highly correlated with antecedent precipitation from the preceding eleven day period, but very little correlation was apparent for the preceding five day period. The correlation coefficient between the averaged antecedent precipitation index values and the corresponding S194 brightness temperatures between 230 K and 270 K, the region of apparent response to soil moisture in the data, was -0.97. The equation of the linear least squares line fitted to the data was: $API (cm) = 31.99 - 0.114 T_B (K)$, where API is the antecedent precipitation index and T_B is the S194 brightness temperature.

INTRODUCTION

The accurate determination of the temporal and spatial distribution of soil moisture is of importance in several disciplines. The meteorologist is interested in the moisture content of the upper several centimeters of the soil due to the governing effects of soil moisture on the soil thermal properties, the evapotranspiration rates, and the resulting influence on the heat and moisture transport at the atmosphere-earth boundary. As an example, studies of the severe thunderstorm indicate that the inflow air source region is from the near surface layer of the atmosphere (Marwitz, 1972; Davies-Jones, 1974; and Sasaki, 1973). The addition of either heat or moisture to the inflow air adds energy to the storm. Beebe (1974) found that the tornado frequency maxima in the Texas panhandle was centered in the region of intense irrigation and attributed the maxima to the increased water vapor content of the lower atmosphere as a result of evapotranspiration from the irrigated fields. The hydrologist is interested in the soil moisture content because the soil moisture in the upper several centimeters largely determines the amount of precipitation which appears as surface runoff, the component responsible for flooding. The productivity of agricultural areas and rangeland is a function of the soil moisture available for plant growth. If the moisture content could be monitored, better usage of rangeland and improved crop yield estimates are possible.

Before the advent of remote sensing technology, accurate soil measurements were possible through such direct methods as neutron scattering probes, tensiometers, and oven drying and weighing. These methods all share common problems; they are time-consuming and representative of only very small areas. Measurements of soil moisture distribution over large areas, especially those with differing vegetative cover and soil type and those not readily accessible, are not possible by direct methods. Because of a pronounced need for soil moisture information, those hydrologists responsible for river stage forecasting and flood warnings have developed various parameters derived from precipitation measurements to quantify the soil moisture over the fairly large areas encompassed by river watersheds.

Based on the obvious but complex relationships between precipitation, evapotranspiration, surface and subsurface runoff, and soil moisture, the precipitation history over an area is commonly used to infer the soil moisture. From this, the amount of precipitation required to produce flooding given the inferred soil moisture content can be empirically determined. Many models for characterizing the precipitation history have been devised; one of the simplest in concept and computation is (Linsley, Kohler, and Paulhus, 1958):

$$API = \sum_{i=1}^n K^i P_i$$

2243

PRECEDING PAGE BLANK NOT FILLED

where API = antecedent precipitation index, and P_1 = daily precipitation for each day from n days previous to the current day. The parameter K which is less than unity characterizes the loss of moisture from the soil due to evapotranspiration and subsurface runoff. The values normally are empirically assigned in the range 0.85 to 0.95 as a function of soil type, slope, season, and vegetative cover. The value may either be constant or may vary as a function of time.

REMOTE SENSING OF SOIL MOISTURE

The remote sensing of soil moisture is possible through several physical properties of water and the water-soil mixtures. Water has a greater specific heat than soil, so for a given input of heat energy, the temperature of moist soil will be lower than that of dry soil. Similarly, after radiational cooling, the moist soil will have a higher temperature due to its thermal inertia. Thus remote sensing in the thermal infrared at two or more times during the day can be used to indirectly determine the amount of water present in the surface layer of soil (Blanchard, Greely, and Goettelman, 1974).

Another remote sensing technique is based on the darkening (decreased reflectance) of soil as it is progressively moistened, apparently as a result of the optical effects of surrounding the soil particles with free water. Within a narrow range of soil types and for bare earth, remote sensing in the optical to near infrared can be used to determine the soil moisture areal distribution.

Both of these techniques, although successful under controlled conditions, most notably bare ground, are completely overshadowed in scope and importance by remote sensing in the microwave portion of the spectrum. Water has the highest dielectric constant of naturally occurring abundant materials; soils have very low dielectric constants at microwave frequencies. When varying amounts of water are added to the soil, the resulting mixture will have a dielectric constant proportional to the relative amounts of water, soil, and air present (Poe, Edgerton, and Stogryn, 1971). However, if small amounts of water are added to completely dry soil, the water is tightly bound to the soil particles (with a structure resembling that of ice which has a low dielectric constant), and the dielectric constant of the mixture does not appreciably change (Schmugge, Gloerson, and Wilheit, 1972 and Schmugge, et.al., 1974). This low water content probably corresponds to hygroscopic water so is not available for evapotranspiration and plant growth. With a greater water content, the water appears as free water in the soil pore spaces and produces the dielectric constant changes predicted and observed in the soil-water-air mixture as the moisture content ranges from the wilting point to field capacity.

Since the emissivity in the microwave wavelengths of radiation is strongly influenced by the dielectric constant, remote sensing in the microwave frequencies has a significant potential in the determination of soil moisture.

MICROWAVE REMOTE SENSING OF SOIL MOISTURE

Although soil moisture has a pronounced influence on the microwave emission, the factors of soil type, surface roughness, and vegetative cover also affect the emissivity. The soil type and soil moisture determine the soil emissivity; the surface roughness and vegetative cover modify the emission from the underlying soil by scattering and surface emissions (Newton, Lee, Rouse, and Paris, 1974). The effects of surface roughness and vegetative cover are wavelength dependent. The effect of small scale variations of soil type and soil moisture is minimized in remote sensing from aircraft or earth satellite altitudes since the antenna receives radiation that is effectively integrated over a fairly large ground area, thus providing soil moisture information representative of large areas.

At longer wavelengths, the skin depth (the depth of the surface layer contributing to the total emitted microwave radiation) increases. Although some investigators have reported

skin depths in excess of the free space wavelength at L-band wavelengths (Poe and Edgerton, 1972), a general consensus of the skin depth is of the order of several centimeters under varying field conditions. The major significance is that remote sensing in L-band microwave can provide measurements of the sub-surface soil moisture content under varying conditions of soil type, surface roughness, and vegetative cover.

A further advantage of the longer wavelength is that atmosphere and weather phenomena including clouds and precipitation are essentially transparent to the emitted microwave radiation due to the small particle size in relation to the wavelength. At L-band wavelengths, remote sensing operation is not restricted by adverse weather conditions. At shorter microwave wavelengths, such as the one to ten centimeter range commonly used for weather radar, however, the larger cloud particles and precipitation particles are effective scatterers and absorbers of emitted microwave radiation.

For L-band wavelengths, the terrain apparent radiometric temperature (the brightness temperature) received at the antenna can be expressed as the product of the emissivity and the actual or thermometric temperature of the radiating terrain skin depth. The atmospheric emission and the surface reflection of sky radiation components of the brightness temperature are both very small (Allison, et.al., 1974 and Blanchard, 1974). Since the emissivities are less than one and absolute surface temperatures range from 270 K to 310 K, the brightness temperature is more sensitive to changes in emissivity than to normal changes in surface temperature. Again the averaging effect of the large footprint is advantageous.

The Skylab soil moisture experiment conducted by Dr. J. R. Eagleman of the University of Kansas has produced excellent results in the correlation of S194 brightness temperature and soil moisture (Eagleman, 1974, and Eagleman, et.al., 1974). For five data sets of tracks of 100 to 300 km length in Kansas and Texas, soil moisture measurements at six depths for six km intervals along the ground track centerline were correlated with the S194 brightness temperatures. The correlation coefficients of brightness temperature to soil moisture (percent water by weight) ranged from -0.808 to -0.984 for the uppermost 2.5 cm layer and -0.765 to -0.979 for the uppermost 7.5 cm layer for the five data sets (Eagleman, 1974).

Since the half-power footprint has a diameter in excess of 100 km, the 100 km to 300 km track lengths represent few independent measurements. Another greater problem lies in the representativeness of center-line soil moisture measurements at selected sites to the actual soil moisture within the footprint area, especially if the footprint area is not suited for conventional soil moisture sampling, or if evapotranspiration or precipitation occurs between the time-consuming sampling and the sensor pass time. However, in view of the good agreement between the data sets, these high correlations are indicative of the response of the S194 L-band radiometer to soil moisture.

SKYLAB S194 L-BAND RADIOMETER AND DATA ACQUISITION

The S194 L-band radiometer was one of six sensors known collectively as the Earth Resources Experiment Package (EREP) flown on the NASA Manned SKYLAB missions from May 1973 to February 1974. The L-band radiometer measured terrestrial surface brightness temperatures along the satellite ground track in the microwave radiation band centered at 21.4 cm wavelength (1.41 GHz). The footprint, or sensor instantaneous ground viewing area, at the half-power point (-3dB) is a circular area with a 115 km diameter area for the 15 degree viewing angle. A footprint size of approximately 280 km diameter accounted for 90 percent of the total energy received at the antenna. The spacecraft altitude was 439.24 km (237 nmi, with an altitude velocity of 7.65 km/sec. The S194 data acquisition rate was approximately three data points per second (one data point per 2.48 surface kilometers). In this study, every third data point, termed a measurement point, was used in the correlations. For the half-power footprint of 115 km diameter, the footprint overlap from one measurement point to the next was near 87 percent. The footprint overlap for each data point was near 95 percent. For the 930 km length of the ground track used in this study (Figure 1) there were eight independent sensor footprint areas at the half-power footprint size.

For a more detailed description of the S194 Radiometer and descriptions of the other EREP sensors, see the "Skylab EREP Investigator's Data Book" (NASA, 1972a) and the "Summary of Flight Performance of the Skylab Earth Resources Experiment Package (EREP)" (NASA, 1974). The S194 data used in the study was gathered in support of the severe storm environments (EPN-582) task of atmospheric investigations (NASA, 1972b).

The S194 brightness temperatures over the study area ranged from 229.8 K to 275.2 K. These values for an assumed emitting skin depth temperature of 298 K, the approximate air temperature along the ground track at the time of the data pass, would produce an emissivity range from .77 for very moist terrain and .92 for very dry terrain; both vegetated. Beyond the study area, the brightness temperatures decreased to 95 K over the Gulf of Mexico for an emissivity of .31 (water temperature assumed to be near 300 K from airborne PRT-5 thermal infrared readings).

The study area includes the loose sandy soils and sparse vegetative cover of the high plains of the Texas and Oklahoma panhandles to the tight clay soils and heavily vegetated terrain of eastern Texas. The weather conditions at the time of the pass at 1518 to 1520 GMT (1018 to 1020 CDT) varied from thin broken cirrus (not visible in the S190A color photography) over the Texas and Oklahoma panhandles to multi-layered overcast conditions from just south of the Red River to the Louisiana border. Precipitating moderate thunderstorms with an areal coverage of 30 percent were occurring from the Fort Worth area to near 160 km southeast along the ground track. Their rainfall amounts were generally light since the cells, as determined from GSW weather radar film, were three to five miles in diameter and were moving toward the north. The air temperatures along the track ranged from 294 K to 299 K.

CORRELATION OF S194 BRIGHTNESS TEMPERATURES AND API

Since soil moisture measurements were not available along the ground track, the soil moisture was parameterized by the antecedent precipitation index. The antecedent precipitation index (API) was calculated for each of the 180 precipitation reporting stations of the NOAA Climatological network along the ground track (NOAA, 1973a and 1973b). The ground track, the sensor viewing area (115 km diameter), and the location of the precipitation reporting stations are shown in Figure 2. Two sets of API were calculated for each station. One API set was calculated for the preceding eleven days (1-11 June) precipitation data and the other API set was calculated for the preceding five days. The set for eleven days was then plotted and contoured to investigate the continuity of the API values and possible influence of events not represented from centerline values. This pattern is shown in Figure 3.

The precipitation totals for the first eleven days of June 1973 ranged from zero in the Texas and Oklahoma panhandles to near 25 cm (10 inches) in the Dallas area. To eliminate the influence of very high daily point values of precipitation in the calculation of the API, the maximum daily rainfall for the API calculation was arbitrarily set at 5.08 cm (2.0 inches). The physical rationale for the assumption is that amounts in excess of 5.08 cm contribute to immediate runoff but probably do not contribute to increased soil moisture.

The arithmetic average of the API for the 115 km diameter footprint coincident with the position of the spacecraft for every third data point was then calculated for correlation with the S194 brightness temperatures. The value of the parameter K was set at 0.9 after trials within the range 0.85 to 0.95 showed the best correlation of API to S194 brightness temperatures at that value, although the correlations were good for all values in the range. The S194 brightness temperature at every third data point (one measurement point) and the footprint API are displayed in Figures 4a, 4b, and 5. Several features are noteworthy:

- 1) There is a pronounced correlation between the S194 brightness temperature and the eleven-day API averaged over the footprint.
- 2) There is very little correlation between the S194 brightness temperature and the five-day API. As evident in Figure 4b, there had been no precipitation over much of the ground track within the previous five days. If the S194 is used as the "ground truth" for the API accuracy as a soil moisture indicator, then the API must include precipitation data for a longer period than five days, the number of days used in the antecedent moisture

conditions (AMC) in the Soil Conservation Service Handbook of Hydrology (1972).

3) The correlation is best for values of the API above 1.75, which is consistent with theory for low moisture values. This relationship is especially evident from Figure 5.

4) The influence of surface water of precipitation and lakes is not readily apparent, possibly due to the small areal extent in comparison with the sensor footprint. The surface water of precipitation may contribute to the lowest S194 values, but this cannot be confirmed.

CONCLUSIONS

In at least one data set of API and S194 brightness temperatures, several significant points emerged. In addition to the known capability of L-band remote sensors to accurately detect soil moisture for small bare-ground areas, the L-band appears well-suited as a sensor for the spatial mapping of soil moisture over large inhomogeneous areas with respect to soil type, vegetative cover, terrain, and weather. Also the API even in a very simple form appears to be an accurate index of soil moisture but only when a precipitation history in excess of five days is included; the optimal precipitation history period may be as long as one month. As these study results are confirmed by independent data sets, the API may be refined as an accurate soil moisture indicator for meteorological and agricultural applications and L-band microwave radiometry may be used to develop and refine models of evapotranspiration and runoff.

ACKNOWLEDGMENTS

This research was conducted under SKYLAB Experiment Project Number 582, Severe Storm Environments by Dr. D. E. Pitts, Dr. Y. K. Sasaki, and Mr. J. T. Lee and under NASA contract NAS 9-13360 with Dr. Y. K. Sasaki of the University of Oklahoma. Dr. D. E. Pitts, Johnson Space Center, Houston, Texas, provided the SKYLAB data and Mr. J. T. Lee, National Severe Storms Laboratory (NOAA, ERL), Norman, Oklahoma, provided the radar and precipitation data. Dr. Y. K. Sasaki, Dr. D. E. Pitts, and Dr. Bruce Blanchard, Southern Plains Watershed Research Center (USDA-ARS), Chickasha, Oklahoma, provided invaluable assistance.

REFERENCES

- Allison, L. J., E. B. Rodgers, T. T. Wilheit, and R. Wexler, 1974: A Multi-Sensor Analysis of Nimbus 5 Data on 22 January 1973. Goddard Space Flight Center, Preprint X-910-74-20, 54 pp.
- Beebe, R. C., 1974: Large Scale Irrigation and Severe Storm Enhancement. Symposium on Atmospheric Diffusion and Air Pollution, American Meteorological Society, Boston, Mass., 392-395.
- Blanchard, B. J., 1974: Passive Microwave Measurement of Watershed Runoff Capability. Doctoral Dissertation, University of Oklahoma, 88 pp.
- Blanchard, M. B., R. Greely, and R. Goettelman, 1974: Use of Visible, Near-Infrared, and Thermal Infrared Remote Sensing to Study Soil Moisture. Ninth International Symposium on Remote Sensing of Environment, Environmental Research Institute of Michigan, Ann Arbor, 693-700.
- Davies-Jones, R. P., 1974: Discussion of Measurements Inside High-Speed Thunderstorm Updrafts. Journal of Applied Meteorology, 13, No. 6, 710-717.
- Eagleman, J. R., 1974: Moisture Detection from Skylab. Ninth International Symposium on Remote Sensing of Environment, Environmental Research Institute of Michigan, Ann Arbor, 701-705.
- Eagleman, J. R., E. C. Pogge, R. K. Moore, N. Hardy, W. Lin, and L. League, 1974: Detection of Moisture and Moisture Related Phenomena from Skylab. University of Kansas, Lawrence, 18 pp.

- Linsley, R. K., Jr., M. A. Kohler, and J. L. H. Paulhus, 1958: Hydrology for Engineers. McGraw-Hill, New York, 340 pp.
- Marwitz, J. D., 1972: The Structure and Motion of Severe Hailstorms. Part I: Supercell Storms. Journal of Applied Meteorology, 11, No. 1, 166-179.
- NASA, 1972a: Skylab EREP Investigator's Data Book. Principal Investigator Management Office, Johnson Space Center, Houston, Texas.
- NASA, 1972b: Appendix B - Mission Requirements: Earth Resources Requirements Skylab Missions SL-1/SL-2, SL-3, and SL-4. Skylab Program Offices, NASA Manned Spacecraft Center and Marshall Space Flight Center, December 1972.
- NASA, 1974: Summary of Flight Performance of the Skylab Earth Resources Experiment Package (EREP). NASA Johnson Space Center, Houston, Texas, 44 pp.
- Newton, R. W., S. L. Lee, J. W. Rouse Jr., and J. F. Paris, 1974: On the Feasibility of Remote Monitoring of Soil Moisture with Microwave Sensors. Ninth International Symposium on Remote Sensing of Environment, Environmental Research Institute of Michigan, Ann Arbor, Michigan, 725-738.
- NOAA, 1973a: Climatological Data - Oklahoma. Environmental Data Service, NOAA, Asheville, N. C., Vol. 82, No. 6, June 1973, 25 pp.
- NOAA, 1973b: Climatological Data - Texas. Environmental Data Service, NOAA, Asheville, N.C., Vol. 78, No. 6, June 1973, 49 pp.
- Poe, A., and A. T. Edgerton, 1972: Soil Moisture Mapping by Ground and Airborne Microwave Radiometry. 4th Annual Earth Resources Program Review, Vol. IV, pp. 93-1 to 93-23.
- Poe, A., A. Stogryn, and A. T. Edgerton, 1971: Determination of Soil Moisture Content Using Microwave Radiometry. Summary Report 1684R-2, Aerojet-General Corporation, El Monte, California, 18 pp.
- Sasaki, Y. K., 1973: Mechanism of Squall-Line Formation as Suggested from Variational Analysis of Hourly Surface Observations. Eighth Conference on Severe Local Storms, American Meteorological Society, Boston, Mass., 300-307.
- Schmugge, T., P. Gloerson, and T. Wilheit, 1972: Remote Sensing of Soil Moisture with Microwave Radiometers. Report No. X-652-72-305, Goddard Space Flight Center, Greenbelt, Maryland, 32 pp.
- Schmugge, T., P. Gloerson, T. Wilheit, and F. Geiger, 1974: Remote Sensing of Soil Moisture with Microwave Radiometers. Journal of Geophysical Research, 79, No. 2, 317-323.
- Soil Conservation Service, 1972: SCS National Engineering Handbook - Section 4 - Hydrology. U.S. Dept. of Agriculture, Soil Conservation Service, August, 1972.



Figure 1. Skylab ground track, 1518 - 1520 GMT, 11 June 1973.

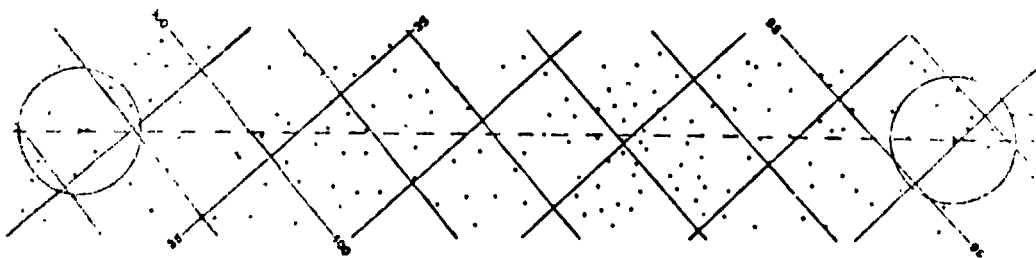


Figure 2. Location of the precipitation reporting stations used in the computation of antecedent precipitation. The approximate (due to map projection) sensor footprint area is shown as the circular areas at each end of the study area.

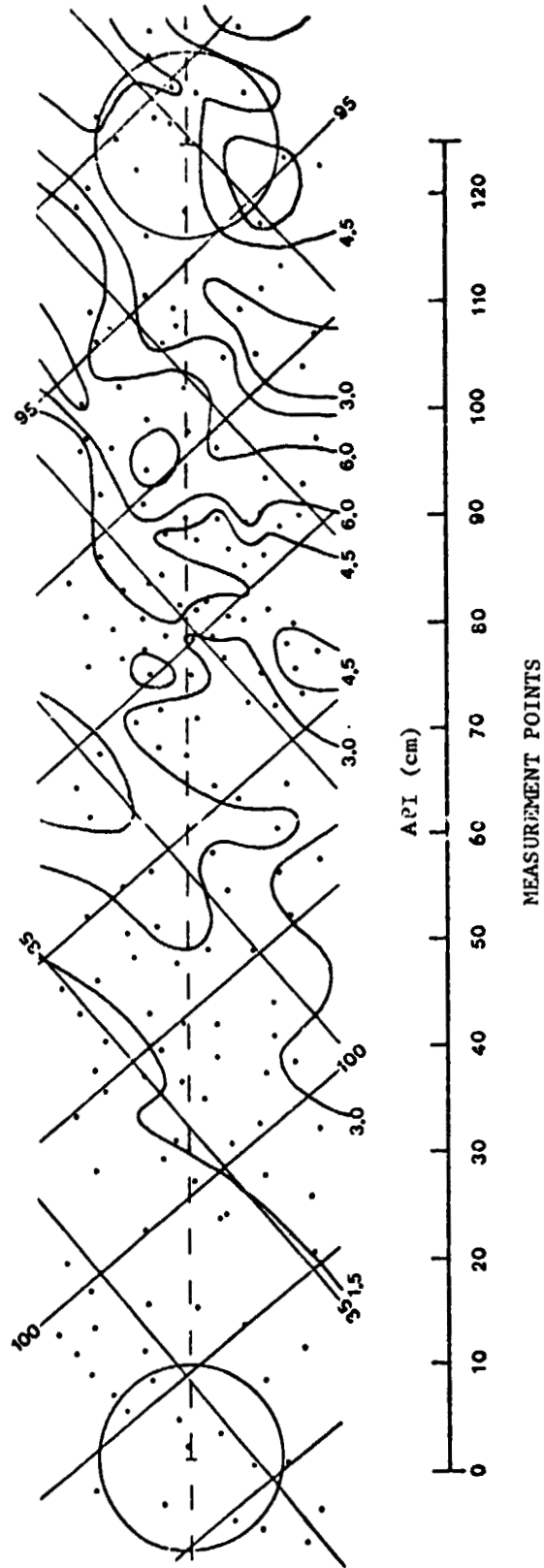


Figure 3. Contoured API values for the eleven day antecedent precipitation, 11 June 1973. The centerline API values are generally, but not always, representative of the API values averaged over the sensor footprint area.

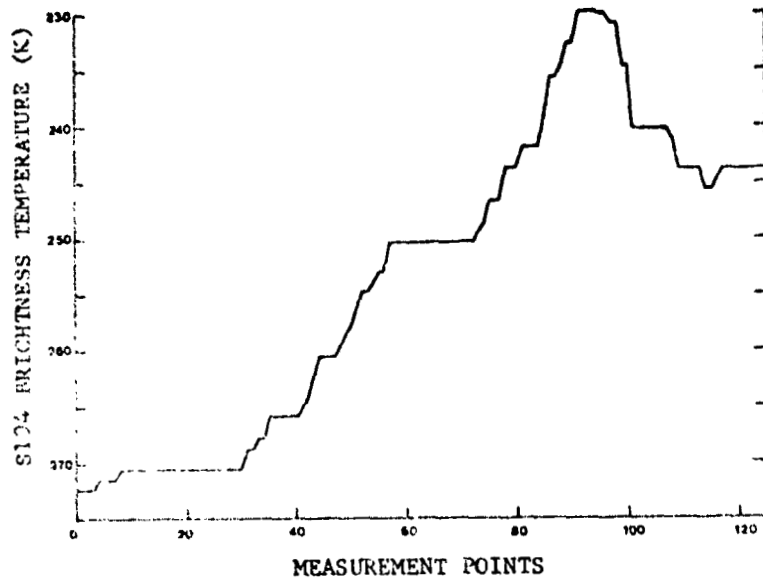


Figure 4a. S194 brightness temperature along the ground track.

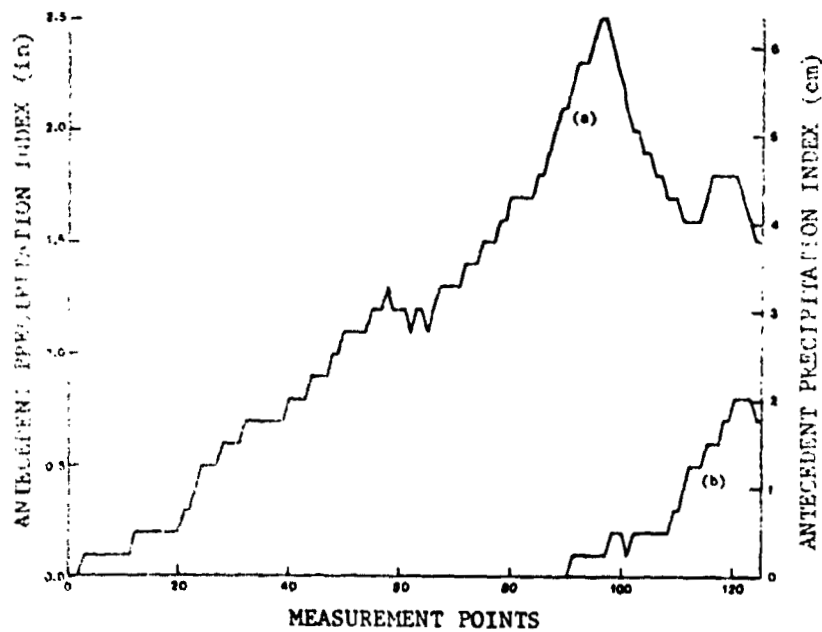


Figure 4b. Antecedent precipitation index (API) along the ground track. The eleven day API is (a); the five day API is (b).

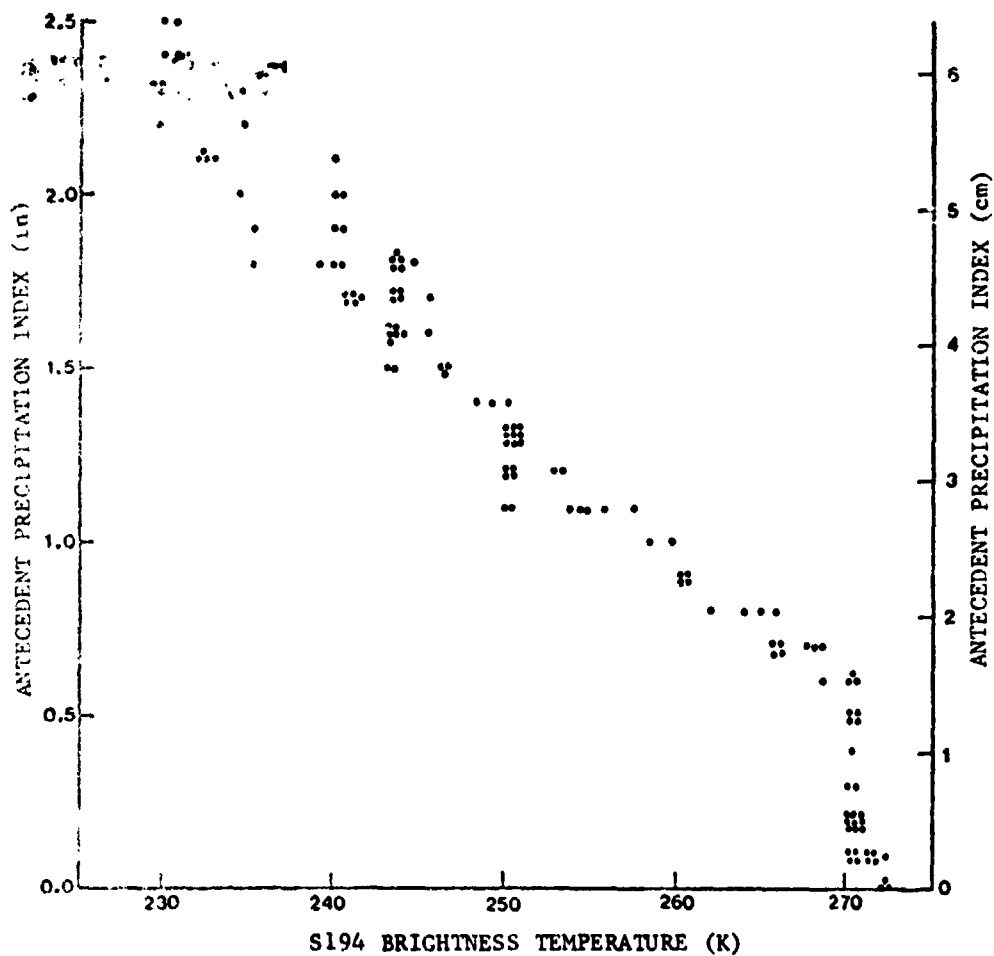


Figure 5.

Correlation of S194 brightness temperature to antecedent precipitation index (API). The lack of response of the brightness temperature at low API values, which correspond to low soil moisture, is consistent with theory. For the units in inches the linear least squares line fitted through the data points between 230 K and 270 K is: $API = 12.61 - 0.045 T_B$. For API in cm, the equation is: $API = 31.99 - 0.114 T_B$. The correlation coefficient for the brightness^B temperature range 230 to 270 K was -0.9715.

FLOOD HAZARD STUDIES IN CENTRAL TEXAS
USING ORBITAL AND SUBORBITAL REMOTE
SENSING IMAGERY

W-8

By Victor R. Baker, Department of Geological Sciences; Robert K. Holz, Department of Geography; and Peter C. Patton, Department of Geological Sciences, The University of Texas at Austin, Austin, Texas 78712

N76-17595

ABSTRACT

Central Texas is subject to infrequent, unusually intense rainstorms which cause extremely rapid runoff from drainage basins developed on the deeply dissected limestone and marl bedrock of the Edwards Plateau. One approach to flood hazard evaluation in this area is a parametric model relating flood hydrograph characteristics to quantitative geomorphic properties of the drainage basins. Our preliminary model uses multiple regression techniques to predict potential peak flood discharge from basin magnitude, drainage density, and ruggedness number. After mapping small catchment networks (4 to 20 km²) from remote sensing imagery, input data for the model are generated by network digitization and analysis by a computer-assisted routine of watershed analysis.

The study evaluated the network resolution capabilities of the following data formats: (1) large-scale (1:24,000) topographic maps, employing Strahler's "method of v's," (2) standard low altitude black and white aerial photography (1:13,000 and 1:20,000 scales), (3) N.A.S.A. - generated aerial infrared photography at scales ranging from 1:48,000 to 1:123,000, and (4) Skylab Earth Resources Experiment Package S-190A and S-190B sensors (1:750,000 and 1:500,000 respectively). Resolution, measured as the number of first order streams or as the total channel length identified in small drainage areas, is strongly dependent on basin relief. High-density basins on the Edwards Plateau were poorly depicted on orbital imagery. However, the orbital network definition of low relief basins on the inner Texas Coastal Plain is nearly as accurate as results from large-scale topographic maps.

The Skylab earth terrain camera (S-190B) and N.A.S.A. - generated aerial infrared type 2443 imagery at 1:48,000 scale were found to be useful for botanic, soils, and geomorphic flood hazard zonation. Studies of the Colorado River valley near Austin, Texas, easily distinguished infrequent (100 to 500 year recurrence interval), intermediate (10 - 30 year), and frequent (1 to 4 year) hazard zones. These mapping techniques are especially applicable to the rapid regional evaluation of flood hazards in areas that lack the time and money to generate more accurate engineering-hydraulic flood hazard maps.

INTRODUCTION

Flood hazard evaluation can be approached from two viewpoints. The "upstream" approach consists of evaluating the interaction of rainfall inputs and physiographic factors in producing flood responses on small watersheds.

The "downstream" approach maps flood hazard zones in the broad alluvial valleys which rivers develop after collecting the flow of numerous tributaries. In this study, we have attempted to apply remote sensing imagery to both aspects of the flood hazard evaluation problem.

Central Texas includes parts of two major physiographic provinces, the gently undulating Gulf Coastal Plain in the south and southeast, and the uplifted Edwards Plateau in the north and northwest. The plateau, which is underlain by interbedded, soft limestone, dolomite and marl, has been deeply eroded to produce locally steep slopes. The boundary between these two physiographic provinces is marked by a sharp change in elevation at the Balcones Fault Zone.¹ The precipitation falling on the plateau drains across the fault zone into the major rivers of the Gulf Coastal Plain, including the Guadalupe, Colorado, Brazos, and Trinity.

Central Texas is subject to irregular, but chronic flooding of sometimes extraordinary magnitude in the frequency range of 10 - 50 years.² The controlling factors in this pattern of flooding are climate and physiography. Mean annual precipitation along the Balcones Escarpment varies from 83 cm at Austin to 56 cm at Bracketville (Figure 1), in Kinney County, near the border with Mexico. Climatically the area is located in that zone where the middle-latitude, humid subtropical climate of the east grades into the middle-latitude steppe climate to the west. Humid air masses can penetrate the area at any time of the year, but a lack of triggering devices may lead to extended periods of dry conditions. In any one year the border between humid subtropical climate and middle-latitude steppe may shift completely across the region. As a result annual rainfall is highly variable, ranging from over 130 cm to less than 35 cm. Even in the dry and hot summers, tropical disturbances can bring very heavy rainfall and rapid runoff from high gradient plateau streams flowing on bedrock. Great variation in stream flow is characteristic seasonally and annually.

Air masses of marine tropical origin are responsible for the greatest flood-producing storms in Texas. These storms result from easterly waves which develop along the Intertropical Convergence Zone located over the Gulf of Mexico in summer. The air masses in these waves are warmed and they pick up great quantities of moisture during passage over thousands of kilometers of warm tropical seas.³ A typical storm occurred on September 9 - 10, 1952, when almost simultaneously over central Texas, a pressure surge from the northeast came into contact with an easterly wave trough. The warm moist tropical air of the trough was lifted over the combined barriers of the Balcones Escarpment and the steep pressure gradient from the northeast. Rainfall totals of 50 - 66 cm were recorded in a localized area over the upper Pedernales and Guadalupe Rivers, although generally heavy rains fell throughout the entire area.⁴ A particularly intense cell located between Storewall and Johnson City produced a peak flood stage at the Johnson City bridge on the Pedernales of 15 meters as recorded by local residents. The magnitudes of the stream discharge peaks resulting from such storms include many of the maxima contributed by a given area for drainage basins in the United States⁵ (Figure 2).

FLOOD RESPONSE OF SMALL DRAINAGE BASINS

The shape and dimensions of a flood hydrograph, the graph of storm runoff as a function of time, are controlled by many interrelated factors. These factors can be separated into two main categories: transient and permanent.⁶ Transient controls mainly represent climatic factors, and permanent controls are associated with physical characteristics of the drainage basin. Because virtually all of the controls are dependent in some way on one another, identifying and quantifying individual factors provide a major difficulty in establishing meaningful statistical relationships between various controls. The usual solution to this problem is selection of variables which are as physically independent as possible. The importance of quantitative geomorphology is obvious because the most easily obtained data is that which can be quantified from maps, aerial photographs, and other remote sensing imagery. In this study we attempted to assess the influence of a large number of hydrogeomorphic parameters on flood response.⁷ Computer generation of morphometric measures eased the data acquisition problem and allowed the comparison of data generated from various types of imagery (see Appendix).

Parametric models of flood response are frequently employed to predict flood response from the geomorphic properties of drainage basins.⁸ Such models identify variables that have significance in the processes that transform drainage basin input (high intensity rainfall) to output (flood hydrograph). A model for central Texas was formulated from morphometric data collected from 1:24,000 scale topographic maps of small drainage basins. The stream networks for these basins were quantified by performing a Horton analysis.⁹ Stream lengths were determined by the crenulation method¹⁰ and streams were ordered both by the Strahler¹¹ and Shreve¹² methods. The following variables were recorded for each basin: drainage area; Strahler order; Shreve magnitude (the number of first-order streams), number of streams of a given order, total stream length, basin length, relief, main stream length, and number of segments of all orders. From these variables additional measures of the drainage basin were calculated, as follows: drainage density, relief ratio, ruggedness number, and first-order channel frequency. Linear and areal measurements were performed automatically by the computer-assisted procedure described in the appendix.

The morphometric and the runoff data were entered into a correlation analysis and morphometric variables highly correlated with area were then eliminated to avoid autocorrelation (Table 1). Morphometric variables related to discharge, Shreve magnitude, drainage density, ruggedness number (relief times drainage density) and total relief were entered into a stepwise multiple regression analysis. The multiple regression technique allows for the selection of that variable which initially explains the most variability in the dependent variable, in this case, maximum peak discharge.

In descending order of importance, the additional variables are included in the regression until there is no significant increase in the variability explained. The resulting relationship was:

$$Q_{\max} = 5930.3 + 20.7 M - 616.1 Dd, \\ s$$

where

Q_{max} = maximum flood discharge of record (cubic feet per second),

M_s = Shreve magnitude of the basin, and

D_d = drainage density (miles/miles²).

In statistical terms, Shreve magnitude and drainage density explained 86 percent of the variability in maximum discharge. Comparison of the model to the input data is facilitated by comparing observed and computed maximum discharge for the study basins (Figure 3).

The above model was derived from morphometric data generated by a conventional analysis of large-scale topographic maps. Much of the world, however, lacks detailed topographic surveys. Many areas require hydrologic reconnaissance information that may only be available from high-altitude aerial or even orbital imagery. Can these data formats provide the necessary input data for flood response models? A major aim of this research was to seek answers to this question.

NETWORK AND CHANNEL RESOLUTION

The generally arduous nature of quantitative drainage network analysis has resulted in relatively few studies that compare network resolution on a variety of map and remote sensing imagery formats. In this study eight sources of graphic information (Table 1) were examined to determine their usefulness in delineating stream networks. These sources may be divided into three broad groups: topographic maps, suborbital imagery (aircraft), and imagery generated from space by Skylab. Many complex factors contributed to the degree of network resolution achieved from each imagery source. These factors are best illustrated by considering selected results from individual study basins.

Bee Creek is a small tributary of the Colorado River developed on deeply dissected marl and limestone bedrock near Austin, Texas. The relief ratio (ratio of basin relief to basin length) is 0.03. The basin is characterized by steep slopes, brushy vegetation, and thin, discontinuous soils. Orbital imagery of the basin revealed the considerable resolution capabilities of the Skylab EREP earth terrain camera over the EREP multispectral photographic camera (Figure 4). At least 44 first-order streams were identified with the terrain camera in the 8.2 km² basin. The S-190A multispectral image revealed only 14 first-order streams. The topographic map analysis (Figure 5), in contrast, shows the interpretive advantages of contour crenulation analysis and of large scale formats (1:24,000) for network interpretation. Resolution of various scales and types of imagery can be further quantified by the use of Horton's law of stream numbers (Figure 6).

A question arises in deeply dissected basins such as Bee Creek concerning the detail of the actual network and the significance of that detail for flood runoff. A precise stereoscopic interpretation of low altitude black and white aerial photographs revealed that numerous small gullies

develop on hillslopes in the Bee Creek basin as an adjunct to the continuous channel network (Figure 7). A detailed field study (Figure 8) showed that these gullies averaged 30 meters in length. This and other field studies suggest that all forms of imagery for drainage network mapping fail to adequately depict the high-density gully systems that may occur in high relief study basins. Most of the gullies studied in the field would result in an order of magnitude increase in first-order stream frequency for a given basin. However, the hydrologic significance of the gullies is probably much less than that of the continuous channel network. The gullies constitute a channel flow component of local hillslope hydrologic systems. Their high channel roughness and irregular gradients clearly distinguish them from the more efficient stream channel system that is accurately displayed on smaller scale imagery.

Dry Prong Deep Creek basin is developed on interbedded sandstone and shale units. It has a relief ratio of 0.021. As in the case of Bee Creek, topographic map and suborbital imagery (Figure 9) proved to be much more accurate for network resolution than did Skylab imagery (Figure 10). However, Wilbarger Creek, a coastal plain basin with a relief ratio of only 0.01 was quite accurately depicted by the earth terrain camera (Figure 11). This basin occurs in an agricultural area with thick soils developed on the relatively permeable Austin Chalk. Channels with their attendant land use changes extend at angles across the more regular tones, textures and patterns of the cultivated land. The angular trend of these linears frequently allows an interpreter to trace a stream channel to a bifurcation point which might go unnoticed, especially among lower stream orders. Wilbarger Creek's drainage density is only 2.1 km/km² in contrast to Bee Creek's density of 7.8 km/km². Bee Creek's more detailed pattern is partly obscured by tall, brushy vegetation and strong shadows that mask the photographic expression of the channels.

Although drainage network resolution appears to be controlled by a complex of factors, including scale, vegetation, land use, shadow tone, and texture, basin relief acts in an integrating fashion. For similar-sized drainage basins, Shreve magnitude (the total number of first-order streams) calculated from various imagery formats is a clear function of relief ratio (Figure 12). In general, the large-scale topographic maps gave the highest resolution of first-order streams, while the S-190A imagery provided the least. Furthermore, with increasing relief ratio the number of first-order streams "lost" in this sequence increases, as the decreasing slope of the individual lines demonstrates. Probably many of the first-order streams in regions of steep relief are actually the small gullies of hillslope systems that are easily obscured by vegetation and not enhanced by shadow effects.

Total channel length measured in a basin can also be used as a quantitative guide to resolution. A plot of this parameter against relief ratio (Figure 13), reveals greater losses in total channel length between topographic map and Skylab measurements of basins of high relief ratio than for basins of low relief ratio. Another guide to resolution is the demonstrated correlation between drainage density and the frequency of first-order streams.¹³ When this relationship is plotted for the topographic map and Skylab data (Figure 14), the slope of the relationship is preserved, although the data plots closer to the origin as resolution decreases. The fact that the slope of the line is preserved indicates that the decrease in drainage

density on the Skylab imagery is a result of the loss of first-order stream lengths, and not a result of the loss of higher order stream lengths.

These relationships suggest that the drainage network results obtained from Skylab imagery, in spite of the various external controls on resolution, conform proportionately to the topographic map base data. The results are encouraging, for it should be possible because of this proportionality, to generate additional relationships similar to the drainage density, channel frequency, Shreve magnitude-relief ratio relationship and thereby more accurately portray drainage basin characteristics from Skylab data.

The problem of interpreting relief from small-scale orbital imagery is a severe limitation on its hydrologic applications. However, it may be possible to develop correlations between planimetric variables and relief for local geomorphic provinces. In central Texas, for example, Shreve magnitude was found to be strongly correlated to ruggedness number, the dimensionless product of total basin relief and drainage density (Figure 15). The strong dependence on local relief of both the hydrologic responses of drainage basins and the resolution capabilities of various types of imagery dictates that hydrologic reconnaissance studies using planimetric small-scale remote sensing imagery can be accomplished only if the investigator performs careful calibrations of the types illustrated in Figures 12, 13, 14 and 15. If areas of considerable local relief (hill or mountain terrain) lack accurate topographic maps, small-scale stereo imagery can be used to generate maps of the type shown in Figure 7.

FLOOD PLAIN MAPPING STUDIES

The accelerating demand for flood hazard information makes imperative an evaluation of alternative techniques to standard engineering flood line and regional flood analyses.¹⁴ Different mapping techniques may be appropriate to different localities depending on the local hydrologic regime, the level at which planning is being performed, and the funds available to finance the study. A geomorphic approach to flood hazard mapping can be used effectively at the state-wide or regional scale to provide interim information prior to detailed hydrologic and hydraulic studies on a local basis. If included within an overall program of regional environmental geological mapping, morphological flood plain mapping can provide a relatively inexpensive by-product of a general program of environmental inventory based on the interpretation of remote sensing imagery.

The geomorphic approach to flood-hazard mapping advocated here should not be confused with physiographic correlation of specific topographic features with flood discharges of known frequency.¹⁵ It involves the more extensive investigation of morphology, sedimentology, distinctive erosional features,¹⁶ time sequences of channel abandonment, and the compilation of existing pedologic, botanic, and hydrologic information.¹⁷ A base map is developed by mapping typical geomorphic flood plain features¹⁸ and associated terraces from remote sensing imagery and from selected field studies. The available soils, vegetational, historical flood, and hydrologic-hydraulic information can then be superimposed on the geomorphically delineated flood plain. The skilled investigator will use each technique to check and balance the other.

As a test of the hydrogeomorphic method of flood plain mapping, a detailed study was initiated of the Colorado River valley between Austin and La Grange, Texas. The channel forms of the Colorado's valley were mapped from N.A.S.A. - generated high altitude color aerial infrared (type S0117) photographs (1:116,000 scale). The map (Figure 16) revealed crosscutting relationships for distinct assemblages of ancient channel patterns associated with multiple levels of the Colorado River flood plain. The imagery easily distinguished these channel forms from upland physiography and from modern active channels of the Colorado River.

Resolution of the Skylab S-190B sensor (earth terrain camera) was tested relative to aerial infrared imagery for geomorphic flood hazard mapping (Figure 17). The S-190B map was produced in only 15 minutes. The infrared map, in contrast, required 1 hour for interpretation. The Skylab imagery, although providing less detail, easily distinguished the high and low sinuosity forms recognized by the aircraft imagery as well as the alluvial valley marginal scarps. Man-made features (e.g., Bergstrom A.F.B.) were resolved with nearly equal precision by Skylab and by the aerial photography.

Comparison of the mapped paleochannel forms to historic and hydrologic regional flood lines (Figure 18) shows that the low sinuosity channels on the older terraces are flooded by extremely rare, high magnitude events (e.g., the 100-year flood).¹⁹ The distinctive modern bars and channels are flooded with much greater frequency, probably in the 1-4 year recurrence interval range. A zone of intermediate hazard occurs in abandoned high-sinuosity forms below a prominent terrace that is easily recognized on orbital imagery. An upper boundary to these flood hazard zones is provided by the scarps bordering the alluvial valley of the Colorado River. Water from the largest historic Colorado River flood reached this margin in 1935. S-190B imagery, therefore, provides a rapid tool for hydrogeomorphic flood hazard mapping. The basic flood hazard zones can be distinguished for central Texas river flood plains, but the precise location of the intermediate frequency hazard zone requires large-scale suborbital imagery for its interpretation.

In order to establish the precise ground truth for the above analysis, we used stereo pairs of conventional aerial black and white, panchromatic photography at 1:22,000 scale for extremely detailed mapping (Figure 19). Field studies and cross-valley profiles (Figure 20) revealed that the various paleochannel assemblages are associated with river terrace levels described as "younger nondissected terraces" in the old descriptive geomorphic literature.²⁰ Channel 6B is a channel cut in bedrock (Figure 20). Channels 6, 6A, and 6B all occur at the same topographic level, but are composed of alluvium that exhibits at least three distinct channel patterns. Channel 7 includes a complex of highly dissected valley margin surfaces, named the Capitol and Asylum Terraces by the early workers.²¹ The valley margin physiography is underlain by a deeply weathered stage of fluvial gravel of early Pleistocene age. The distinctive patterns on the Skylab imagery (Figure 21) result from sediment size variations that were controlled by the changing regimen of the Colorado River during the Quaternary.²²

In the Edwards Plateau broad flood plains have not developed along the resistant limestone bedrock stream channels.²³ Even the major rivers flow

through steep-sided, narrow canyons excavated from the Edwards Limestone and underlying Glen Rose Formation. Nevertheless, a distinct vegetation zonation²⁴ holds some promise as a recognition tool in flood hazard studies. To test the use of remote sensing imagery for botanic flood hazard zoning in this area, we employed N.A.S.A. - generated aerial infrared type 2443 imagery taken with the RC8 camera. In the Pedernales Falls area (Figure 22) the flood plain botanic association was clearly visible as a light pink response on the imagery. Pools of deep water along the discontinuous river course could also be easily mapped from their distinctive deep blue response. Areas of exposed bedrock in the channel bottom and bars of sand and gravel appeared bright white on the imagery. These frequently flooded zones presented a dramatic contrast to the dull green of adjacent grassy hillslopes and the maroon response of local clusters of juniper and live oak in the uplands. Field investigations near Pedernales Falls revealed that the principal trees giving the pink response were American sycamore, pecan, water hickory, and myrtle oak. The darker, maroon response of vegetation on the hillslopes and interfluvies resulted from eastern red cedar, juniper, and live oak.

Flooding in the smaller basins of the Edwards Plateau produces extensive channel scour and deposition. Freshly worked alluvium shows up on the imagery with a bright, strong response. Because of the high magnitude and infrequent character of the flood events, coarse, white limestone debris transported by a flood remains as a channel lag and is not appreciably modified by lower discharges. The response of this debris is clear enough to be recognized on orbital imagery (Figure 23).

A striking opportunity for the application of multi-date imagery to a flood event in a plateau basin was afforded by the flooding of May 11 - 12, 1972, near New Braunfels, Texas. The center of the flood producing storm dropped about 40 cm of rainfall. Reports from local residents indicated that the storm only lasted four hours and spread an average of perhaps 20 cm of precipitation over 780 square kilometers. Some of the most intense rain fell on the catchment of Blieders Creek, a tributary of the Comal River. The estimated peak flood discharge of 1370 m³/sec (48,400 cfs) for the 40-square-kilometer catchment area resulted in widespread devastation to the vegetation and soil cover and considerable property damage.

Comparison of pre-flood and post-flood imagery of Blieders Creek (Figure 24) indicates the morphologic response of the stream channel to an extreme hydrologic event. Prior to the flood, the valley floor was mostly covered by an organic soil and turf layer of 15 to 25 cm in thickness that had developed on coarse stream gravel marginal to the low-flow channel. Low brush, scrub oak, and large deciduous trees characterized the channelway (Figure 24A). The flood, through a combination of scour and coarse cobble and boulder deposition, created a bare valley bottom exposing white limestone bedrock and fresh alluvium (Figure 24B). Pre-flood and post-flood channel cross sections show that scour occurred in the deeper portions of the channel, probably at mean flow velocities of two - three meters per second. Boulders as large as 1.5 x 1.5 x 1 meters were transported for short distances. These effects show the great significance of high magnitude low frequency runoff events on the fluvial morphology of central Texas.²⁵

CONCLUSIONS

Central Texas is a region of highly variable flood responses that has not yielded to precise evaluation of flood potential by traditional hydrological methods.²⁶ This paper suggests that a rational model, emphasizing the permanent hydrogeomorphic controls on flood hydrographs, may be a practical alternative. The basis of the approach is the measurement of drainage basin, network, and channel characteristics from various kinds of remote sensing imagery. The most significant hydrogeomorphic controls were found to be drainage density, drainage area, Shreve magnitude, and ruggedness number.

Measures of network resolution such as drainage density and basin Shreve magnitude indicated that large-scale topographic maps (1:24,000) offered greater resolution than small-scale suborbital imagery (1:48,000 and 1:123,000) or orbital imagery. However detailed field surveys of high-relief drainage basins revealed that even networks developed from topographic maps failed to record some second order and many first order streams. This corroborates the results of other investigators.²⁷ The disparity in network resolution capabilities between orbital and suborbital imagery formats (including topographic maps) depends on factors such as imagery scale, rock type, vegetation, land use and valley morphology. For a given relief ratio, drainage network results from Skylab imagery appear to conform proportionately to the topographic map base data. Moreover, in the low relief basins of the inner Coastal Plain, such as Wilbarger Creek, orbital network definition is nearly as accurate as topographic map definition.

Remote sensing imagery was found to have a broad range of uses in a variety of flood plain mapping approaches. The Skylab S-190B sensor was found to be a useful tool for the rapid generation of geomorphic flood hazard zone maps. Studies of the Colorado River valley near Austin, Texas, easily distinguished the boundary between upland physiography and active flood plain. In addition, the recognition of paleochannel patterns associated with higher, less active portions of the flood plain allowed a distinction to be made between infrequent, intermediate, and frequent hazard zones. The significance of the hazard zones was confirmed by field profiles and detailed mapping using aerial infrared imagery and stereopairs of low altitude panchromatic aerial photography (1:22,000 scale).

N.A.S.A. - generated aerial infrared imagery, type 2443, at a scale of 1:48,000 was found to be useful for botanic and geomorphic flood hazard mapping both along the deeply entrenched bedrock streams of the Edwards Plateau and for the broad alluvial flood plain of the Colorado River east of the Balcones Fault Zone. These mapping techniques can provide rapid regional evaluation of flood hazards much more quickly than standard engineering-hydraulic approaches. Where a significant economic threat is identified in a local area, the regional remote sensing studies can be supplemented by the time-consuming, but more accurate engineering approaches.

ACKNOWLEDGEMENTS

This work was supported in part by the National Aeronautics and Space Administration under contract number NAS 9-13312. The Water Resources Research Center, Purdue University, made available computer programs for watershed analysis. S. D. Hulke and M. M. Penteadó contributed to various phases of the project. J. Boone and R. M. Looney assisted with the field mapping of drainage basins.

REFERENCES

- 1 Deussen, Alexander, 1924, Geology of the coastal plain of Texas west of the Brazos River: U. S. Geol. Survey Prof. Paper 126, 139 pp.
- 2 Baker, V. R., 1975, Flood hazards along the Balcones Escarpment in central Texas -- alternative approaches to their recognition, mapping and management: Univ. Texas, Bur. Econ. Geology Circular.
- 3 Orton, Robert, 1966, Characteristic meteorology of some large flood-producing storms in Texas: Texas Water Dev. Board Rept. 33, pp. 1-18.
- 4 Lott, G. A., 1952, Rainstorm of September 9-10, 1952: Monthly Weather Review, v. 80, pp. 161-163.
- 5 Hoyt, W. G., and Langbein, W. B., 1955, Floods: Princeton, Princeton Univ. Press, 469 pp.
- 6 Rodda, J. C. 1969, The flood hydrograph, in Chorley, R. J., ed., Water, earth, and man: London, Methuen and Company, pp. 405-418.
- 7 Baker, V. R., Holz, R. K., and Hulke, S. D., 1974, A hydrogeomorphic approach to evaluating flood potential in central Texas from orbital and suborbital remote sensing imagery: Proc. Ninth Int. Symp. on Remote Sensing of the Environment, Ann Arbor, Michigan, v. 1, pp. 629-646.
- 8 Gregory, K. J., and Walling, D. E., 1973, Drainage basin form and process, a geomorphological approach: London, Edward Arnold, 456 pp.
- 9 Horton, R. E., 1945, Erosional development of streams and their drainage basins: hydrophysical approach to quantitative morphology: Geol. Soc. American Bull., v. 56, pp. 275-370.
- 10 Morisawa, M. E., 1957, Accuracy of determination of stream lengths from topographic maps: Trans. Am. Geophys. Union, v. 33, pp. 86-88.
- 11 Strahler, A. N., 1957, Quantitative analysis of watershed geomorphology: Trans. Am. Geophys. Union, v. 38, pp. 913-920.
- 12 Shreve, R. L., 1966, Statistical law of stream numbers: Jour. Geology, v. 74, pp. 17-37.

- 13 Meiton, M. A., 1957, An analysis of the relations among elements of climate, surface properties, and geomorphology: Tech. Report No. 11, Office of Naval Research Project NR 389-042, Dept. of Geology, Columbia Univ., N. Y.
- 14 Wolman, M. G., 1971, Evaluating alternative techniques of flood plain mapping: Water Resources Research, v. 7, pp. 1383-1392.
- 15 Kilpatrick, F. A., and Barnes, H. H., 1964, Channel geometry of Piedmont streams as related to frequency of floods: U. S. Geol. Survey Prof. Paper 422-E, 10 pp.
- 16 Baker, V. R., 1974, Geomorphic effects of floods in central Texas and their application in recognizing flood hazards: Geol. Soc. America Abstracts with Programs, v. 6, no. 7, pp. 640-641.
- 17 Reckendorf, F. F., 1973, Techniques for identifying flood plains in Oregon: Oregon State Univ., Ph.D. dissertation (unpub.), 344 pp.
- 18 Leuder, D. R., 1959, Aerial photographic interpretations: New York, McGraw-Hill Book Co., 462 pp.
- 19 Baker, V. R., Garner, L. E., Turk, L. J. and Young, K. P. 1973, Urban flooding and slope stability, Austin, Texas: Austin Geological Society Field Trip Guidebook, 31 pp.
- 20 Hill, R. T., and Vaughan, T. W., 1897, Geology of the Edwards Plateau and Rio Grande Plain adjacent to Austin and San Antonio, Texas, with reference to the occurrence of underground waters: U. S. Geol. Survey Ann. Report No. 18, part 2, pp. 195-321.
- 21 Weber, G. E., 1968, Geology of the fluvial deposits of the Colorado River, central Texas: Univ. of Texas, M. A. thesis (unpub.), 119 pp.
- 22 Baker, V. R., and Pentead, M. M., 1975, River adjustment to late Quaternary hydrologic regimen changes in central Texas: Geol. Soc. America Abstracts with Programs, v. 7, no. 2, p. 144.
- 23 Tinkler, K. J., 1971, Active valley meanders in south-central Texas and their wider implications: Geol. Soc. America Bull., v. 82, pp. 1783-1800.
- 24 Wermund, E. G., and Waddell, C. T., 1974, Adapting biologic assemblage data for environmental needs, in Wermund, E. G., ed., Approaches to environmental geology: Univ. Texas, Bur. Econ. Geology Rept. Inv., pp. 236-246.
- 25 Patton, P. C., and Baker, V. R., 1975, Low frequency high magnitude floods and their relation to the morphology of streams in central Texas: Geol. Soc. America Abstracts with Programs, v. 7, no. 2, pp. 224-225.
- 26 Benson, M. A., 1964, Factors affecting the occurrence of floods in the southwest: U. S. Geol. Survey Water-Supply Paper 1580-D, 72 pp.
- 27 Coffman, D. M., 1970, Parameter measurement in fluvial morphology: Indiana Acad. Sci. Proc., v. 79, pp. 333-344.

TABLE 1.- CORRELATION MATRIX OF MORPHOMETRIC DATA AND RUNOFF DATA FOR CENTRAL TEXAS

	Drainage Area	Strahler Order	Shreve Magnitude	Total Stream Length	Drainage Density	Basin Length	Relief	Relief Ratio	Total No. Stream Segments	Main Stream Length	Ruggedness Number	Maximum Peak Discharge
Drainage Area ¹	1.000											
Strahler Order	.499	1.000										
Shreve Magnitude	.470	.842	1.000									
Total Stream Length	.715	.872	.905	1.000								
Drainage Density	-.390	.517	.570	.360	1.000							
Basin Length ¹	.896	.396	.323	.639	-.368	1.000						
Relief	.455	.737	.795	.808	.434	.385	1.000					
Relief Ratio	-.156	.423	.526	.333	.632	-.307	.737	1.000				
Total Number ¹ Stream Segments	.327	.875	.920	.882	.727	.295	.763	.523	1.000			
Main Stream Length	.911	.387	.371	.654	-.367	.941	.454	-.158	.318	1.000		
Ruggedness Number	177	.695	.847	.712	.686	.093	.918	.845	.813	.170	1.000	
Maximum Peak ¹ Discharge	.999	.500	.470	.714	-.389	.895	.453	-.157	.327	.910	.175	1.000

TABLE II.- CHARACTERISTICS OF THE SOURCES OF DRAINAGE NETWORK
INFORMATION USED IN THIS STUDY

Source	Scale	Date	Special Characteristics
A. Topographic Maps	1:24,000	Variable (1960's)	1:62,500 scale maps were used in 2 cases
B. Suborbital Imagery			
1. U.S.D.A. Air Photographs	1:20,000 and 1:13,000	1967	Standard B/W
2. U.S.A.F. Air Photographs	1:20,000	1968	Standard B/W
3. N.A.S.A. low altitude	1:48,000	Dec. 1, 1973	Color IR and multi- spectral
4. N.A.S.A. high altitude	1:116,000	Dec. 1, 1973	Color IR and multi- spectral
C. Orbital Imagery			
1. LANDSAT	1:500,000	Mar. 17, 1973	multispectral
2. Skylab S-190A	1:750,000	Jan. 29, 1974	multispectral
3. Skylab S-190B	1:500,000	Jan. 29, 1975	high-resolution color

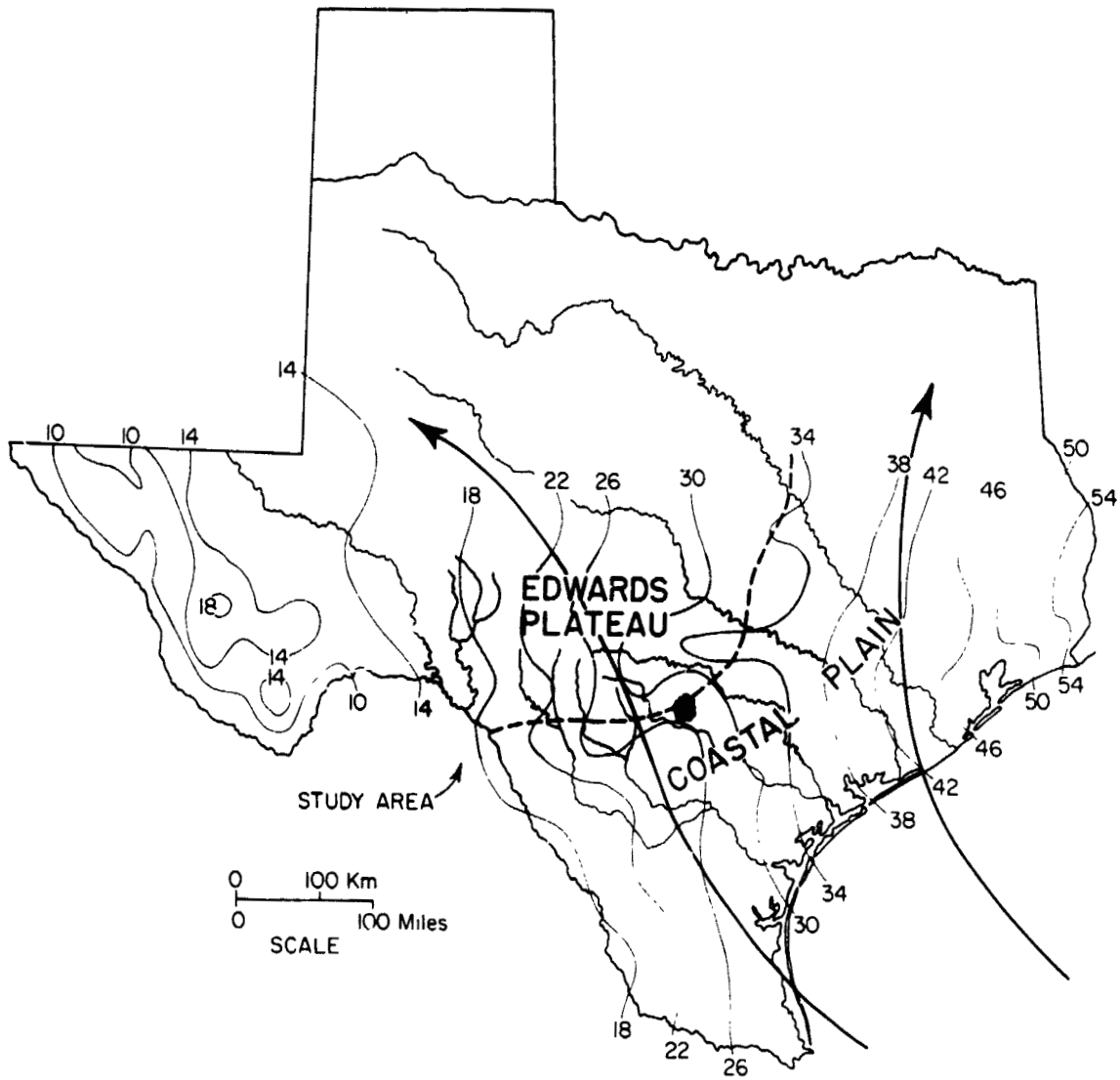


Figure 1.- Isohyets of mean annual precipitation for Texas. Large arrows show tropical major storm tracts from the Gulf of Mexico. The dashed line shows the general location of the Balcones Fault Zone.

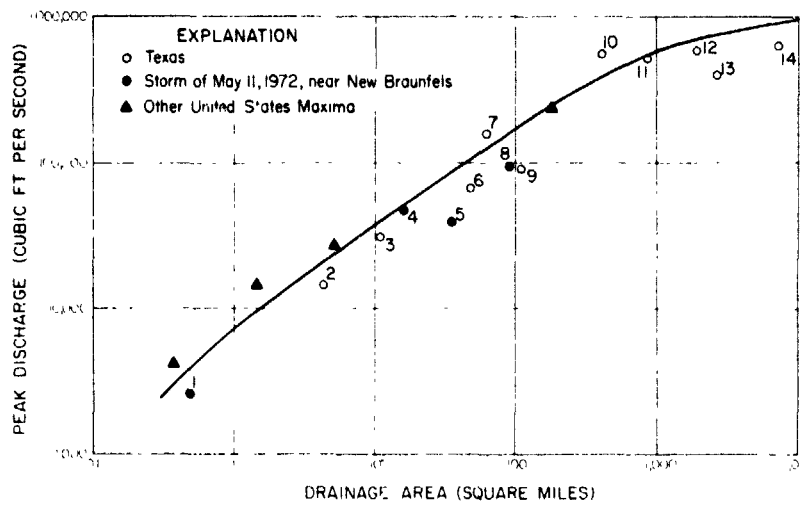


Figure 2.- Maximum flood discharges recorded in central Texas in relationship to contributing drainage area. The trend line represents the U. S. national maximum.

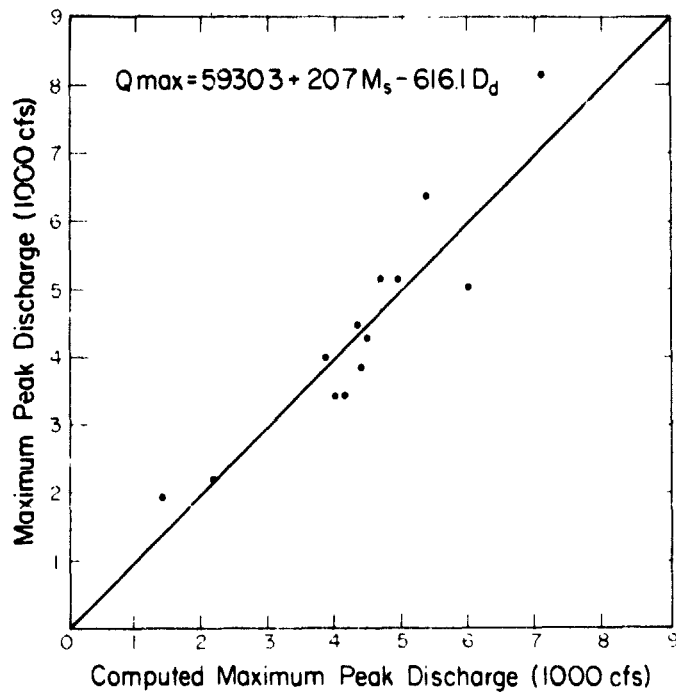


Figure 3.- Comparison of measured maximum peak discharge values versus maximum discharge computed from the equation $Q_{max} = 5930.3 + 20.7 M_s - 616.1 D_d$. The 45° line represents perfect agreement.

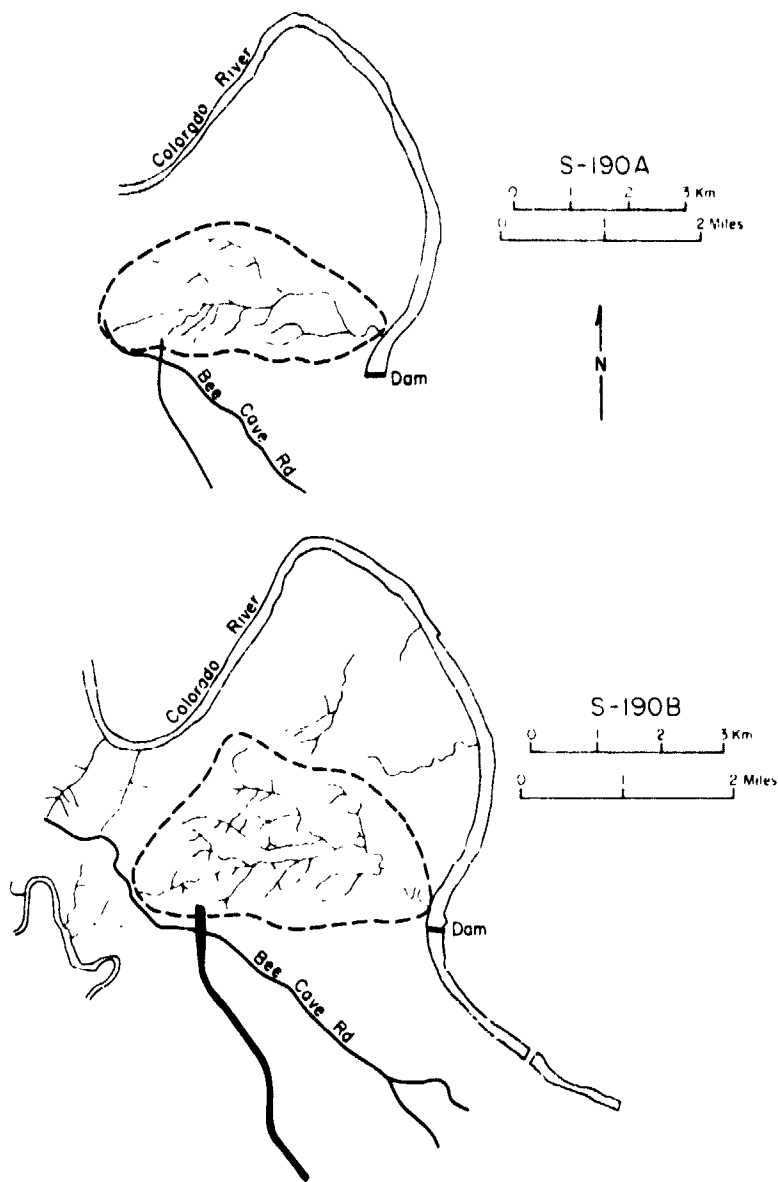


Figure 4.- Drainage maps of the Bec Creek basin: (A) Skylab S-190A, high resolution color film S0-356 with FF filter, enlarged to scale 1:56,000, (B) Skylab S-190B, roll 94, frame 123; the original 9 x 9" transparency was enlarged to 1:48,460 scale.

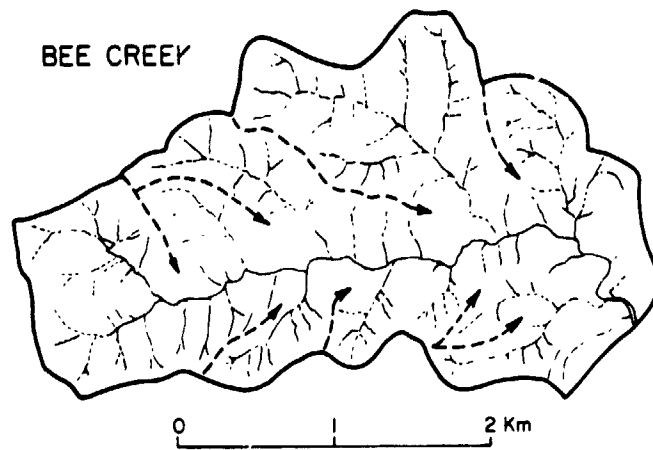


Figure 5.- Drainage map of Bee Creek constructed by the "method of V's"
using the Austin West 7.5' topographic quadrangle map (1:24,000).

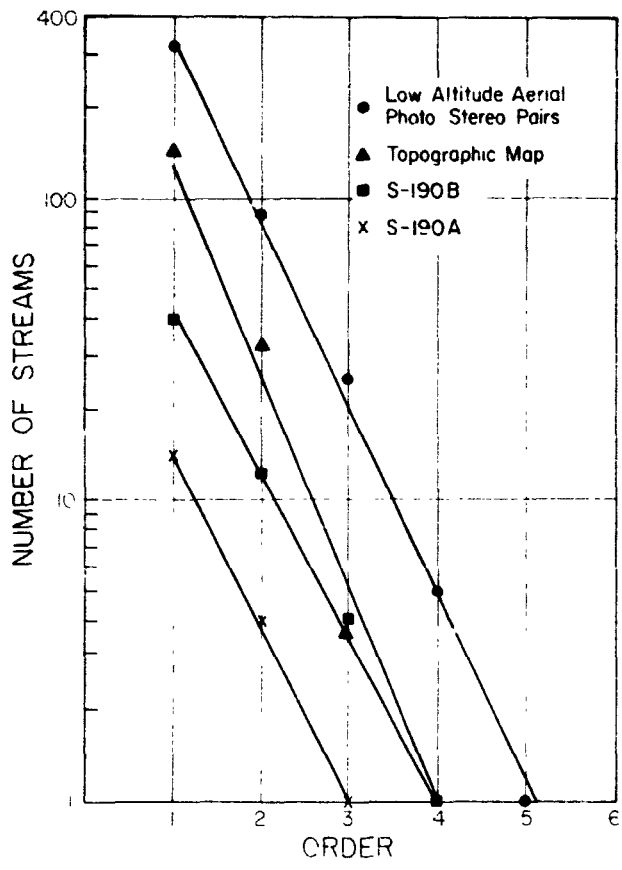


Figure 6.- Horton's law of stream numbers for Bee Creek networks mapped from various imagery sources.

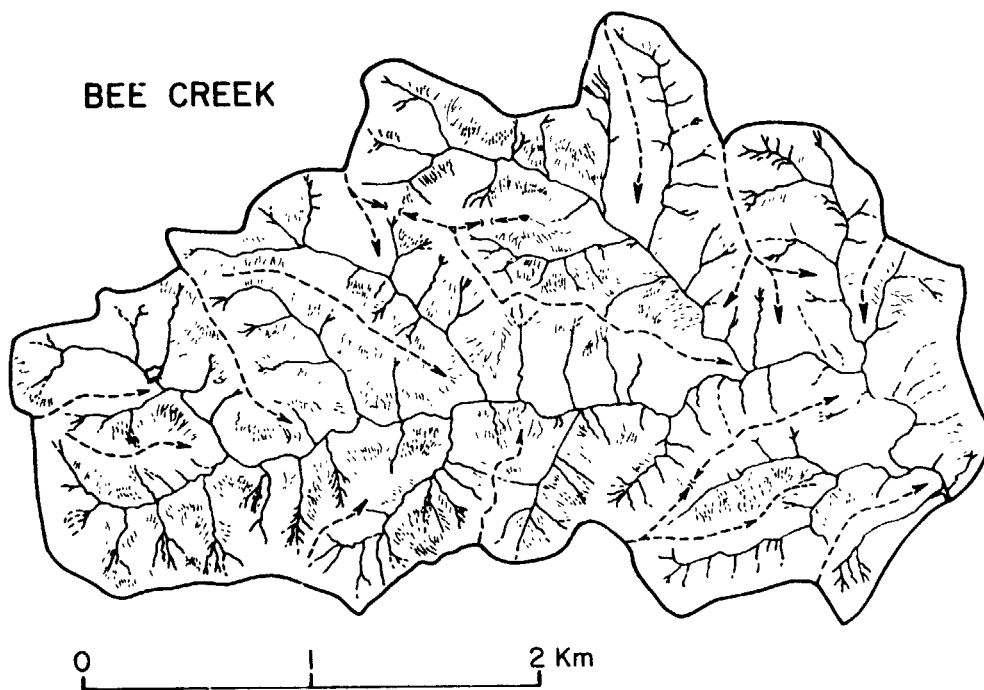


Figure 7.- Drainage map of Bee Creek constructed by detailed stereoscopic interpretation of a pair of low altitude black and white aerial photographs at 1:13,000 scale. Map was prepared by Dr. M. M. Pentado.

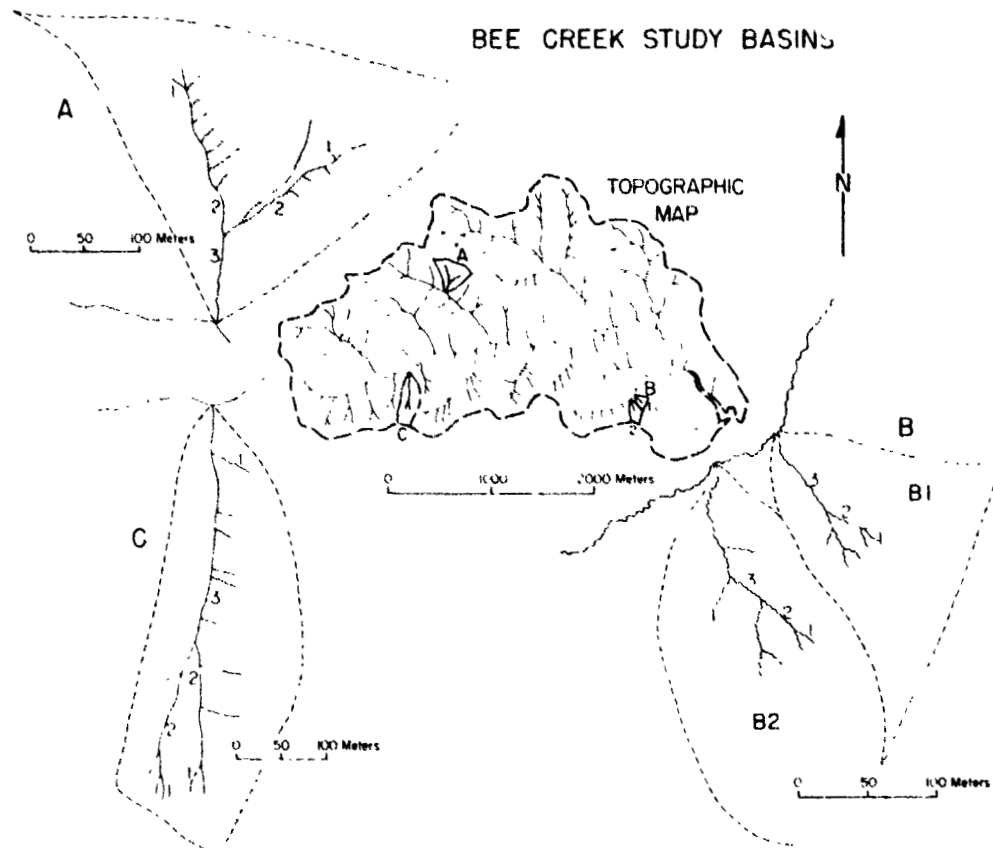


Figure 8.- Subbasins of Bee Creek analyzed by detailed field survey. Stream lengths were measured mostly by pacing and compass technique. Heavy vegetation made mapping by tape survey extremely tedious.

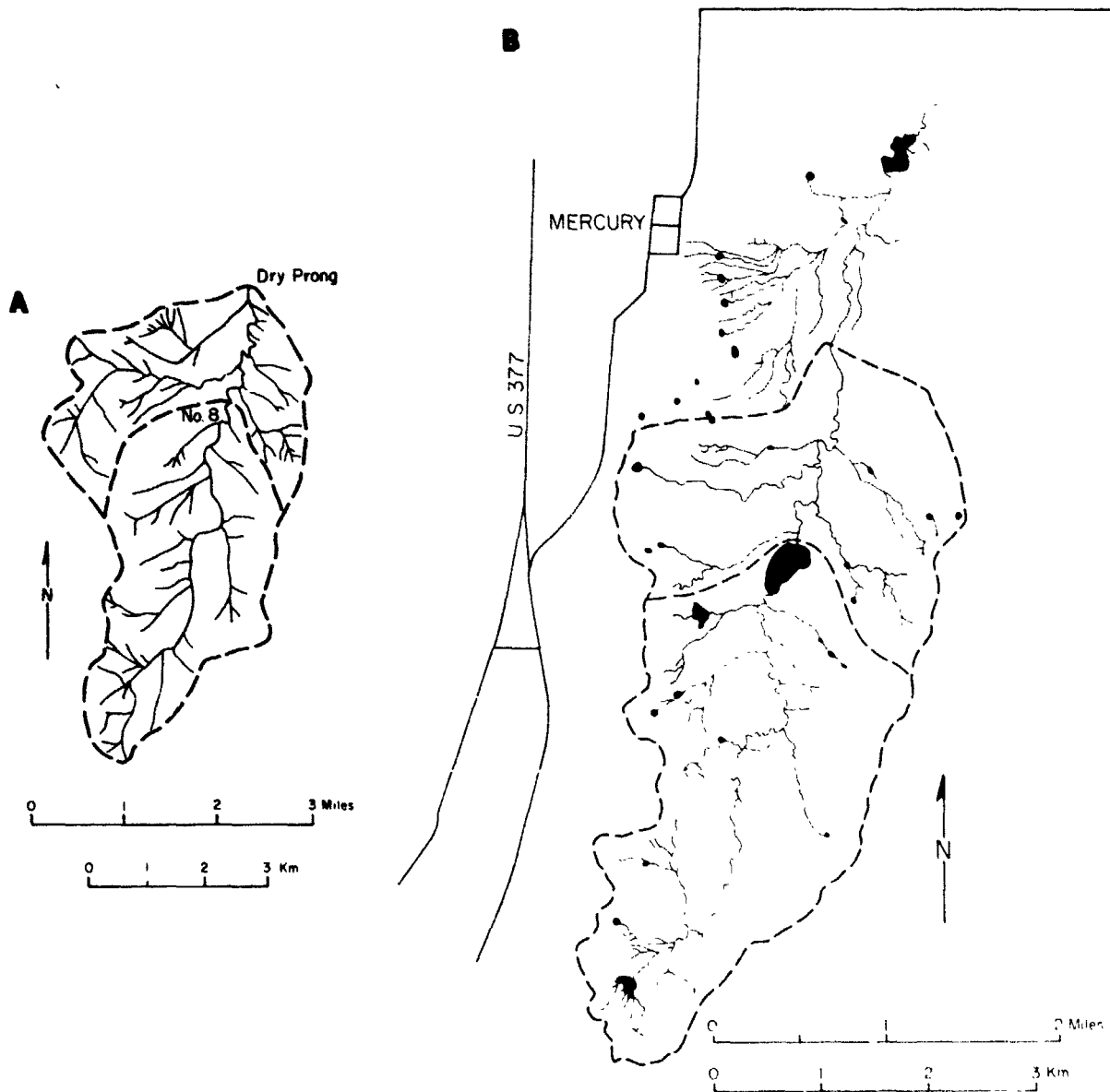


Figure 9A.- Drainage map of Dry Prong Deep Creek constructed by the 'method of V's' using a 1:62,500 scale topographic map.

9B.- Drainage map of Dry Prong Deep Creek constructed from a N.A.S.A. color infrared image in 9 x 9" format at 1:24,768 scale (Aircraft mission 261, image RL13-D017).

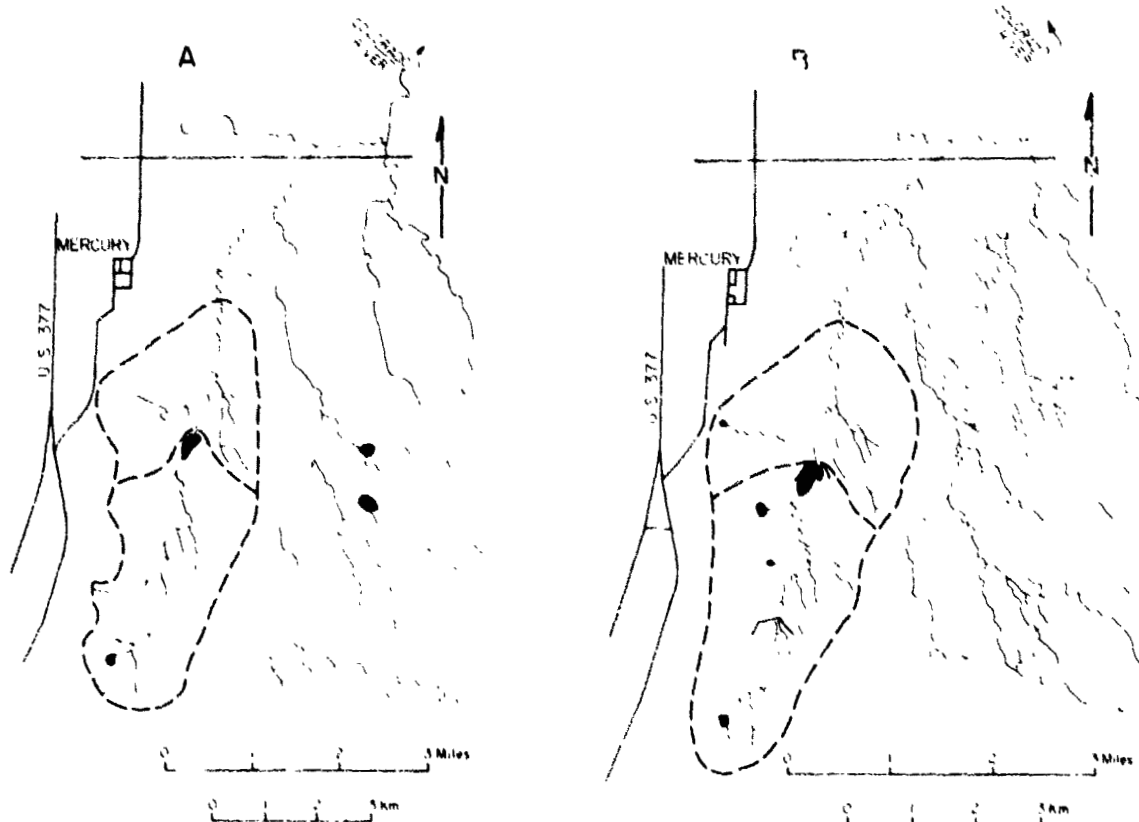


Figure 10.- Drainage maps of the Dry Prong Deep Creek basin constructed from the following imagery formats: (A) Skylab SL-4 S-190A enlarged to 1:53,879 scale (high resolution color film S0-356 with FF filter), (B) Skylab SL-4 S-190B, roll 94, frame 123; the original 9 x 9" transparency was enlarged to 1:45,625 scale.

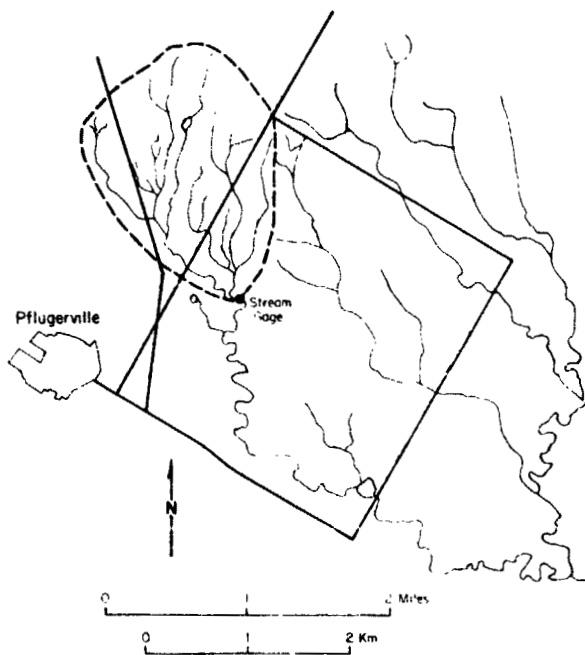


Figure 11.- Drainage map of Wilbarger Creek based on analysis of Skylab S-1908 imagery, roll 94, frame 123, 9 x 9" transparency enlarged to 1:48,480 scale.

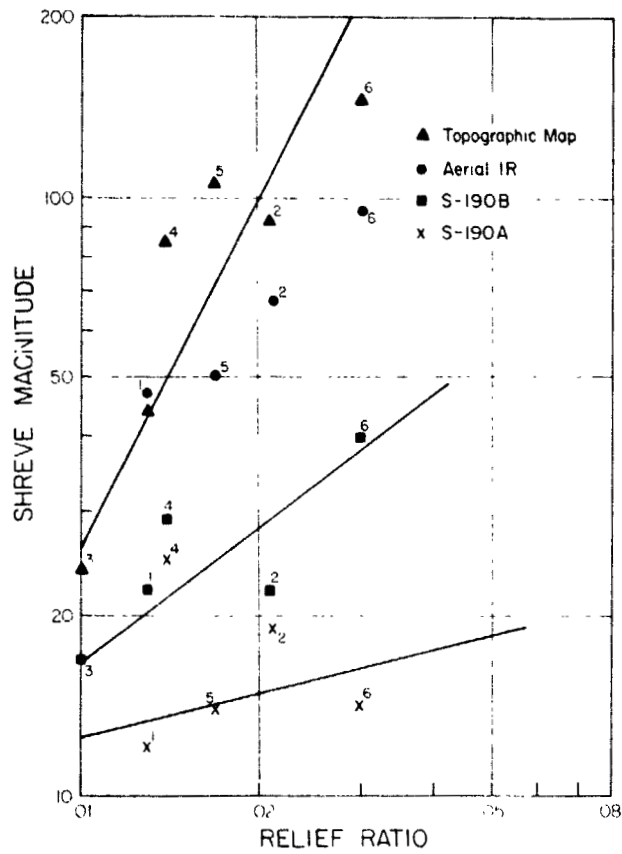


Figure 12.- Shreve magnitude versus relief ratio for similar-sized drainage basins with morphometric data supplied from differing imagery formats. Basins are indicated by number as follows: (1) Deep Creek no. 8, (2) Dry Prong Deep Creek, (3) Wilbarger Creek, (4) Dry Creek at Buescher Lake, (5) Upshaw Creek, (6) Bee Creek. Basin areas vary from 8 to 20 km².

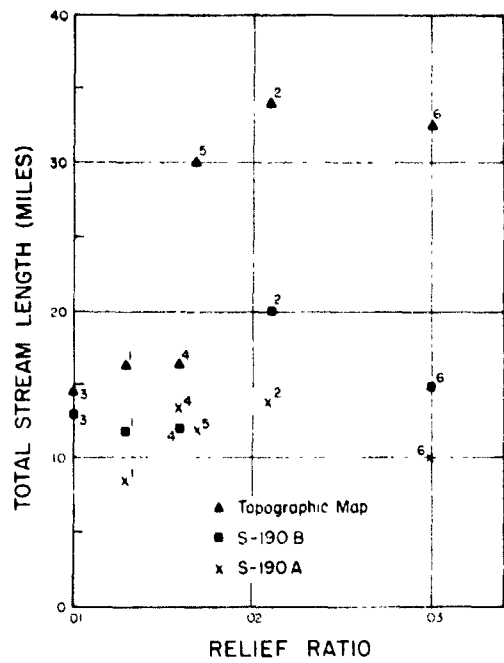


Figure 13.- Total stream length versus relief ratio for drainage basins interpreted from different imagery formats. Basins are indicated by number as in Figure 12.

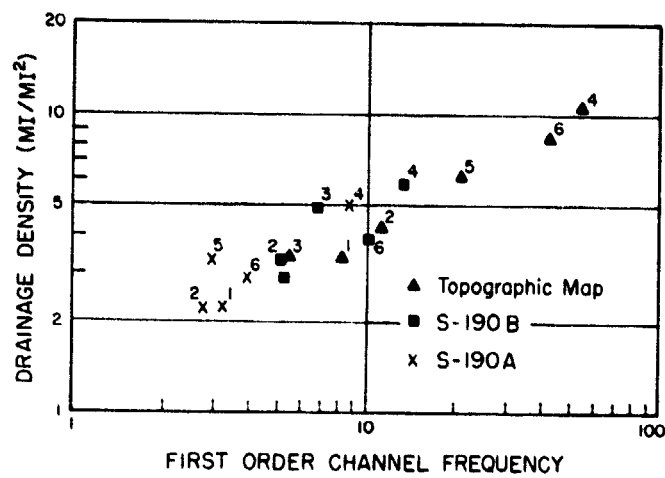


Figure 14.- First-order channel frequency versus drainage density for topographic map and Skylab data.

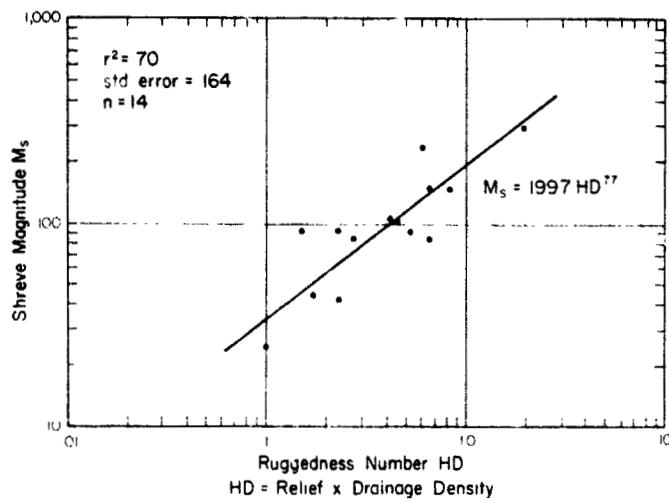


Figure 15.- Shreve magnitude versus ruggedness number (drainage density times relief).

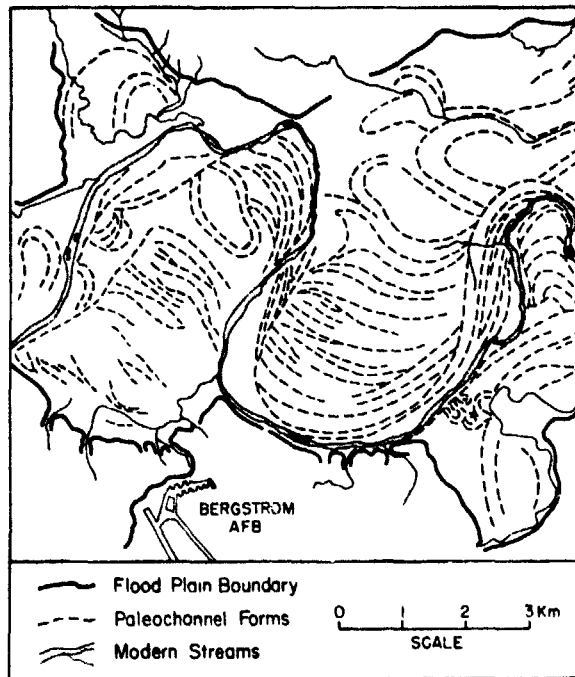


Figure 16.- Colorado River flood plain features near Austin, Texas, mapped from high altitude color aerial infrared imagery (Film Type S0-117). Mission was flown by the N.A.S.A. Colorado River-Brazos River Experiment on Dec. 11, 1969, using the RC8/4R sensor.

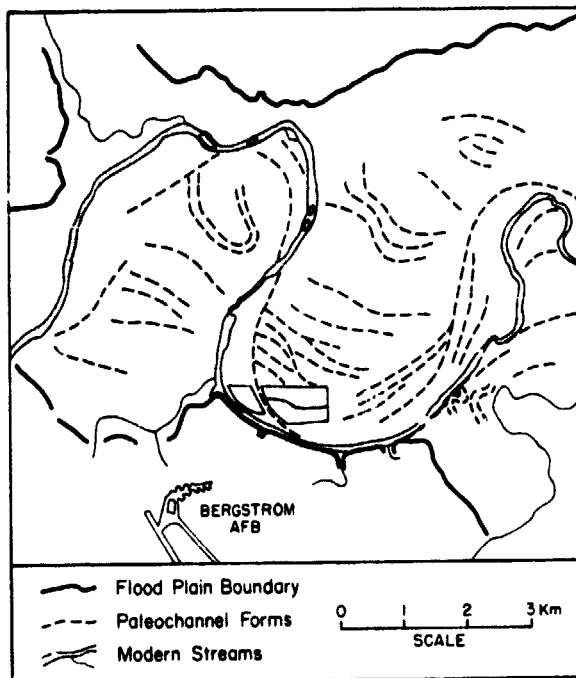


Figure 17.- Colorado River flood plain features near Austin, Texas, mapped from Skylab S-190B imagery.



0 1 2 3 Km
Scale

GEOMORPHIC FLOOD PLAIN FEATURES

- Younger Bars and Channels
- _____ Channels on Older Terraces
- ||||| Scarps Bordering Alluvial Valley

FLOOD HAZARD ZONES

- Intermediate Frequency
- ++++ 100 Year Flood
- 1935

Figure 18.- Comparison of geomorphic flood plain features of the Colorado River to regional flood lines from historic and hydrologic surveys.

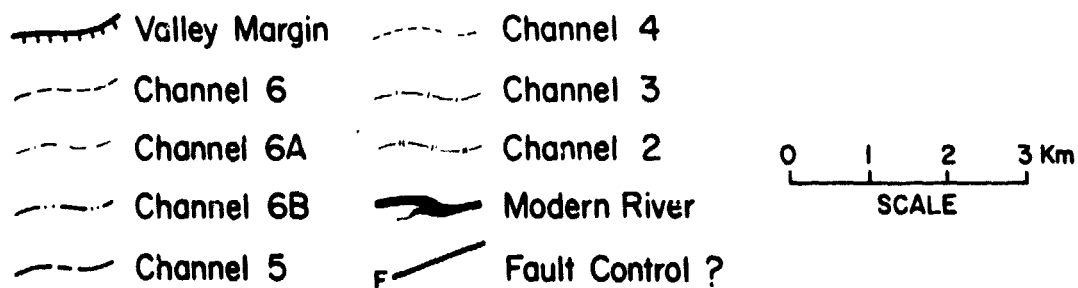
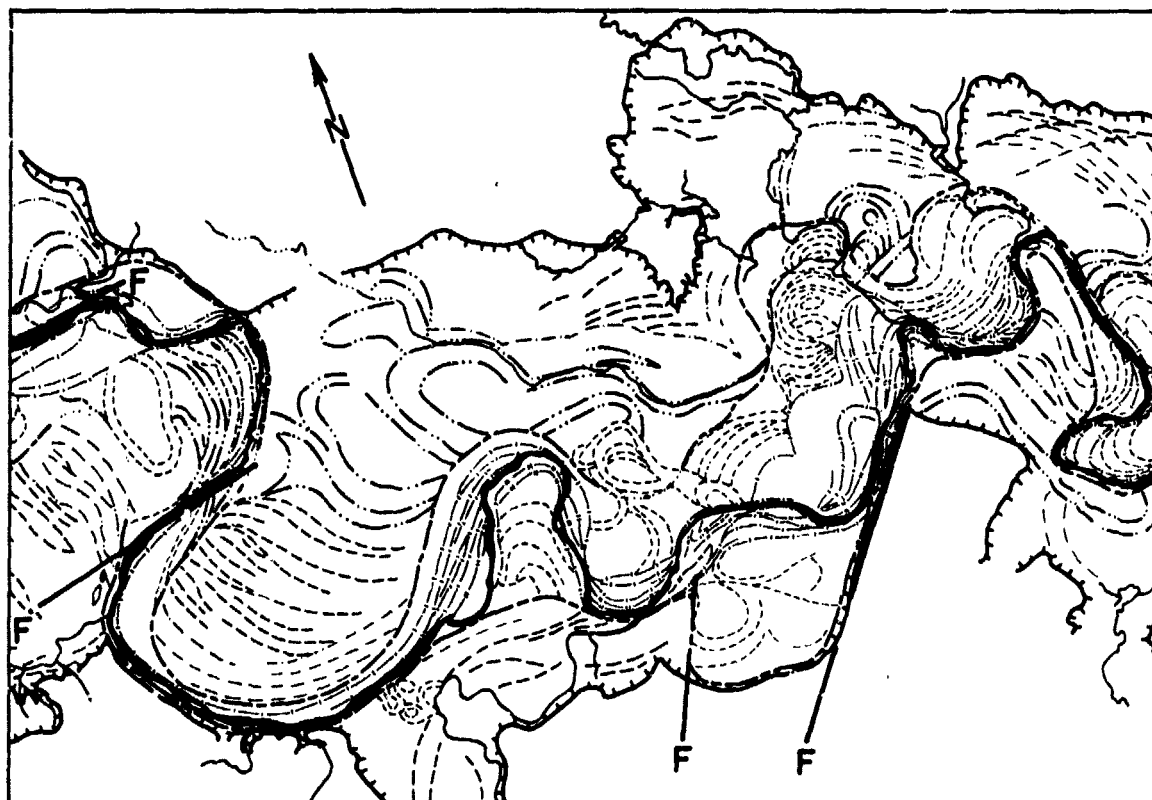


Figure 19.- Geomorphic map of Colorado River flood plain and channel morphology between Austin and Bastrop, Texas. Map was constructed by interpretation of stereo pairs of aerial panchromatic photography flown in April 1969 by the U. S. Air Force. Scale of original photography was approximately 1:22,000. Each channel pattern mapped is associated with specific sediment load characteristics that were established by field sampling.

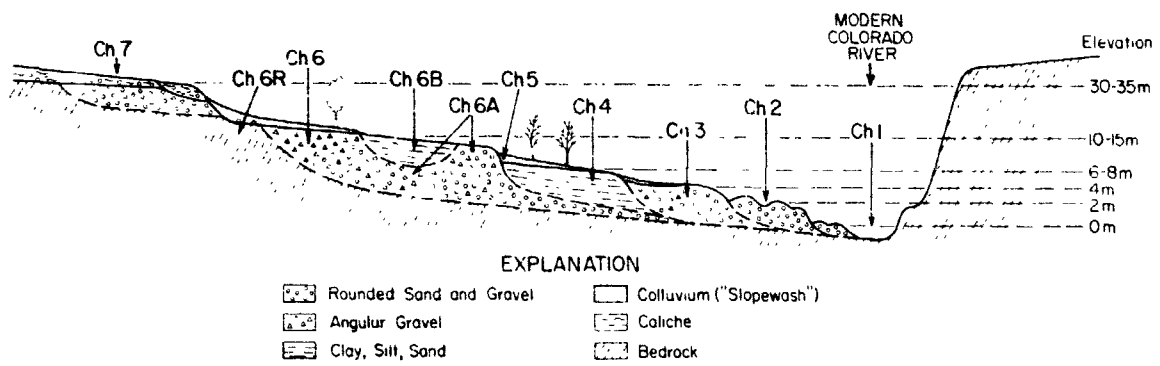


Figure 20.- Schematic cross section of the Colorado River near Austin, Texas, showing terrace levels associated with various channel forms.

REPRODUCIBILITY OF THE
ORIGINAL PAGE IS POOR



Figure 21.- Skylab S-190B image of the Colorado River near Austin, Texas.

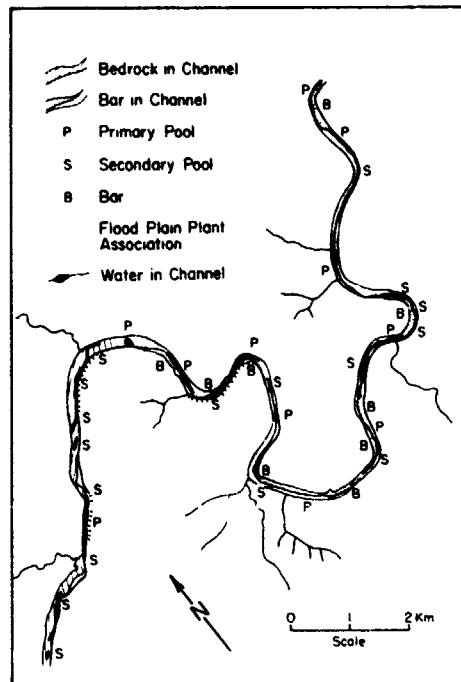


Figure 22.- Flood-related features in the Pedernales Falls area mapped from N.A.S.A. aerial infrared type 2443 imagery at 1:48,000 scale.

REPRODUCIBILITY OF THE
ORIGINAL PAGE IS POOR

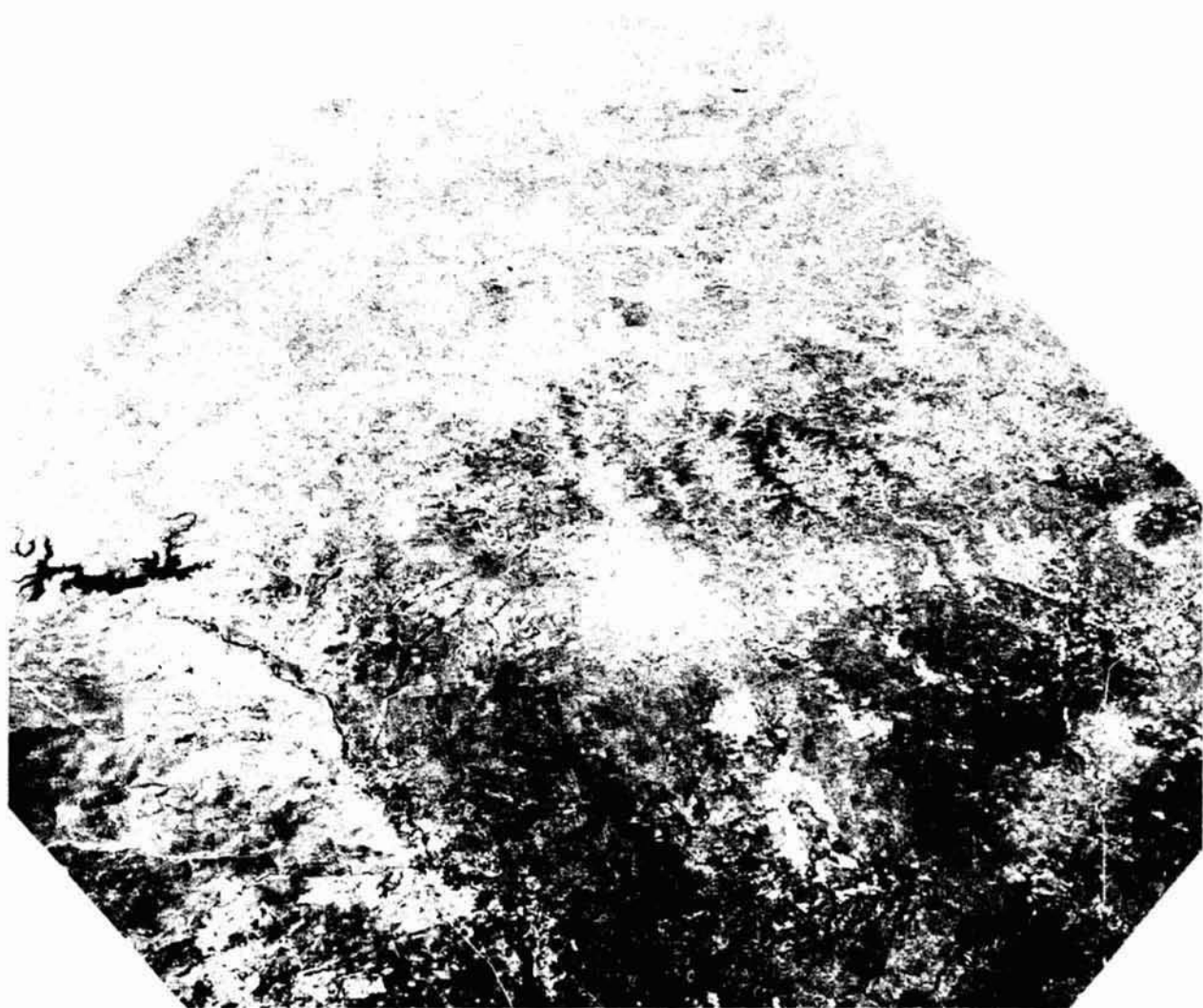


Figure 23.- Oblique S-190A photograph of the Balcones Escarpment from Del Rio (left) to San Antonio (right). Bright response of river channels on the Edwards Plateau clearly delineates effects of recent flooding.

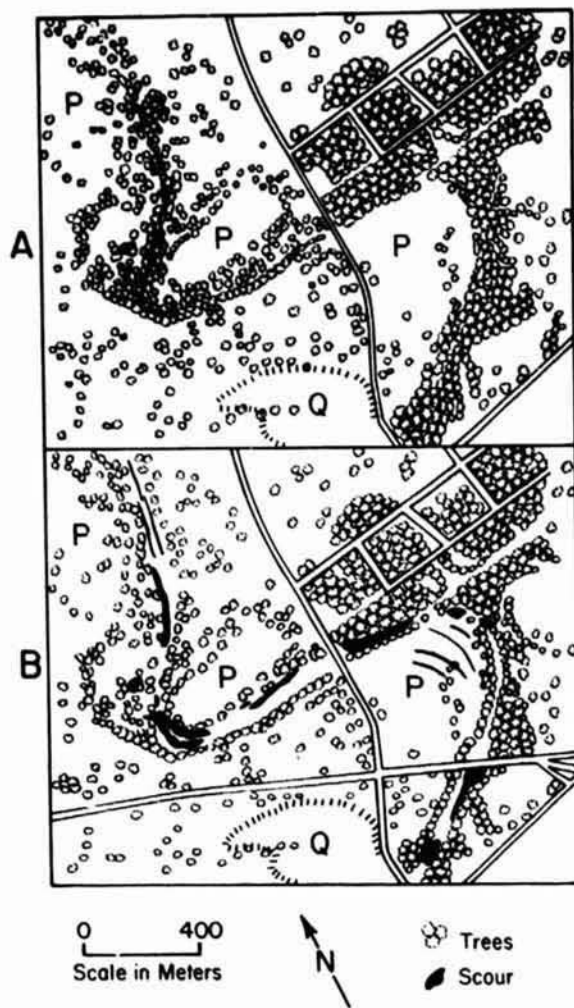


Figure 24.- Geomorphic effects of the 1972 flood along Blieders Creek. (A) as mapped from a vertical aerial photograph (U.S.D.A. BQu-2v-161) of Blieders Creek taken in February 1958. The active channel is somewhat obscured by grass and soil. Note the extensive brush and tree vegetation along the stream course. (B) as mapped from a high altitude infrared photograph taken by N.A.S.A. on December 1, 1973, nearly 7 months after the flood.

APPENDIX

COMPUTER-ASSISTED ANALYSIS OF DRAINAGE BASINS

Once a network pattern has been interpreted from a data source, the various stream junctions, sources, and link mid-points need to be reduced to morphometric parameters. To avoid the tedious nature of manual morphometric analysis from photographic or cartographic data sources, we have incorporated machine-assisted digitization of drainage networks and computer reduction of data into a systematic analytical procedure. We report here on preliminary testing of this procedure, as a first step in relating morphometric measurements from various remote sensing imagery to flood hydrology.

The W.A.T.E.R. System, a computer program for watershed analysis developed at Purdue University and the University of Toronto,² was used to calculate quantitative geomorphic parameters from digital input data. The transformation of spatial data (drainage maps) to digital data can be accomplished by selecting points within the drainage network which describe the branching pattern of the network (network topology) and assigning cartesian coordinates to these points to resolve their spatial position (Figure 1). Network topology can be described by a sequence of numeric codes which define the function of selected data points.

Besides recording data point function codes sequentially, it is necessary to record the spatial positions (cartesian coordinates) of the points in the same sequence. (X and Y coordinates of the end-of-data dummy point are ignored). These positions were automatically digitized with an accuracy of $\pm .005$ inches (.013 cm) using a d-mac pencil follower. Output from the pencil follower was recorded on 7-track magnetic tape. Input data to the W.A.T.E.R. System were the three sequential arrays of X and Y coordinates and associated function codes of the data points, and the scale of the digitized drainage network.

It is obvious that the method outlined above creates a schematic digital model of a drainage network. A more detailed model can be defined by inserting "midpoints" which break up curving segments of the network into several short straight segments rather than one long straight segment. Also, the W.A.T.E.R. System can perform three-dimensional analysis if the elevation is included as a Z coordinate in defining the spatial position of data points.

After the recording of coordinates for each data point on magnetic tape, a series of operations ensues to determine accuracy in the data array, to edit, and finally to interface the data with the W.A.T.E.R. System (Figure 2).³ The RCUHELP program was used to transfer data to punch cards or permanent file (disk). The KAREdit program was used to properly align data words as stored in the permanent file. The MIXER program was used to read word storage to transform data back to a graphical output for error detection. Errors were located on CALCOMP plots of network data at the same scale as the original spatial input (Figure 3). By overlaying the two spatial formats, data errors were quickly recognized.

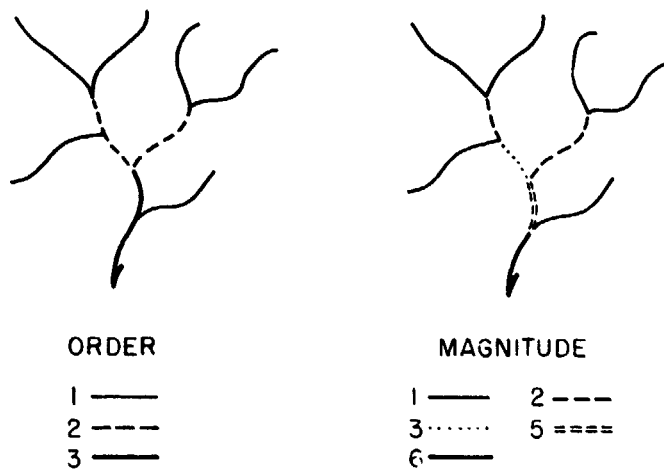
Errors were frequently encountered in the digitizing operation. We attribute this to the extremely monotonous and inflexible way in which the data must be collected. Minor errors are easily corrected, but major errors often

resulted in discarding the original data and starting again at the digitizing step. This concern with error is extremely important. Aberrant data points, incorrect X or Y coordinates, incorrect function codes, or mis-matching of position and function data will inevitably lead to errors in parameter calculation by the W.A.T.E.R. System. At best, this leads to prolonged computer number crunching on aberrant data which results in equally aberrant output and inflated time charges. At worst, data is simply incorrect, but the W.A.T.E.R. System output may seem plausible. Unfortunately this leads the user to assume that it is correct. The involved editing routine (Figure 2) was developed to overcome these difficulties.³

From the edited numeric data, the W.A.T.E.R. System assigns the Strahler orders to all segments of the drainage network, determines segment lengths, basin perimeter and area, and calculates basin statistics. Shreve magnitudes, link lengths, and basin statistics are likewise calculated. The output of the W.A.T.E.R. System characterizes a drainage network geometry as interpreted from a specific imagery source.

REFERENCES

- 1
Baker, V. R., Holz, R. K., and Hulke, S. D., 1974, A hydrogeomorphic approach to evaluating flood potential in central Texas from orbital and suborbital remote sensing imagery: Proc. Ninth Int. Symp. on Remote Sensing of the Environment, Ann Arbor, Michigan, v. 1, pp. 629-646.
- 2
Coffman, D. M., Turner, A. K., and Melhorn, W. N., 1971, The W.A.T.E.R. System: computer programs for stream network analysis: Purdue Univ. Water Resources Research Center Tech. Rept. 16, 138 pp.
- 3
Hulke, S. D., 1975, Quantitative geomorphic analysis and hydrology of some central Texas drainage basins: Univ. of Texas, M. A. thesis (unpub.).



ORDER

- 1 ———
- 2 - - - -
- 3 ———

MAGNITUDE

- 1 ———
- 2 - - - -
- 3 ······
- 5 =====
- 6 ———

Figure 1.- Assignment of Strahler orders and Shreve magnitudes.

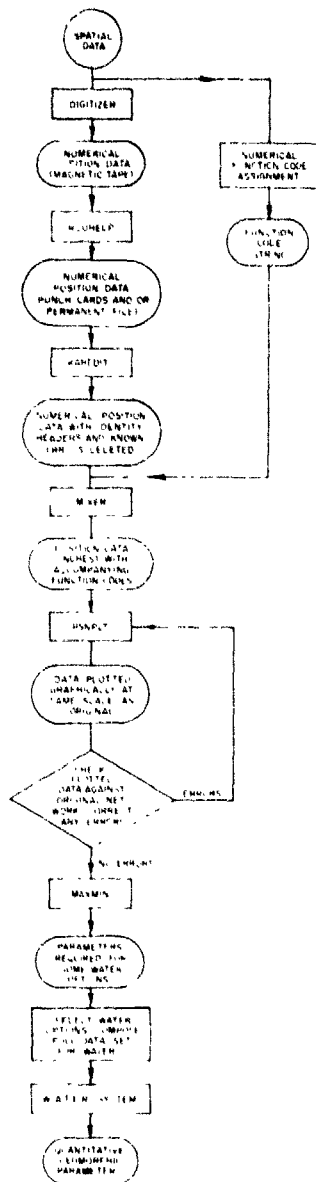


Figure 2.- Flow chart of operations to transform spatial drainage network data to quantitative geomorphic parameters using the W.A.T.E.R. System.

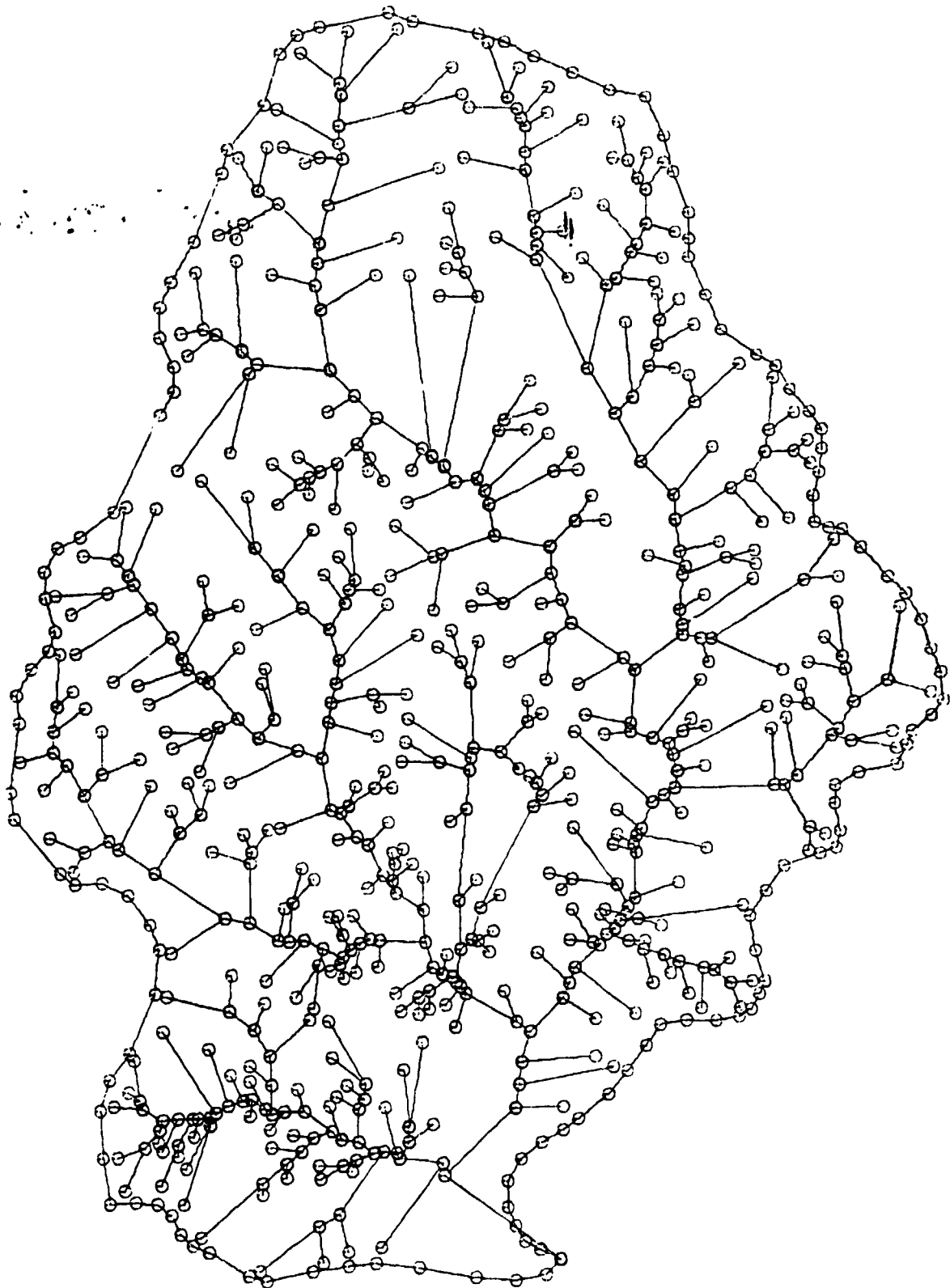


Figure 3.- CALCOMP plot of drainage network data used for detecting machine or operator errors encountered in the digitizing operation.

AN INUNDATION STUDY OF THE LOWER MAGDALENA-CAUCA RIVER BASIN

By Eduard van Es, Hernán Gómez, and Robert Soeters
 Centro Interamericano de Fotointerpretación (CIAF)
 Bogotá, Colombia

SUMMARY

N76-17596

Annual floodings affect about 35 000 km² of the Lower Magdalena-Cauca River Basin in the northern part of Colombia. Until recently, almost no information was available on the exact extension of the inundations nor on the complex of factors involved in the problem.

The Colombian Government is promoting an integrated survey of the entire river basin with the object of land reclamation in the lower part. The Centro Interamericano de Fotointerpretación (CIAF), Colombia's official international training center for photointerpretation, has been appointed to undertake the investigations of flooding, using a combination of modern remote-sensing techniques.

The objectives of this part of the project are to get good answers as to why, when, and where the floods really occur and to study within the complex of possible solutions (regulation dams, surface runoff control, construction of dikes, river-channel improvement) the possibility of using the river marginal lakes ("ciénagas") as reservoir basins during the high-water stages.

The material available for this study consisted of:

1. Two good coverages of five LANDSAT multispectral scanner (MSS) images each, taken on January 1, 2, and 3 and February 6, 7, and 8 of 1973
2. A 45 000-km² coverage of side-looking airborne radar (SLAR) images (Goodyear APS-102 X-band system) taken on November 14 and 15, 1973, during a high-water stage
3. Approximately 2000 km² of 1:10 000 aerial photography in individual strips of key areas taken almost simultaneously with the SLAR imagery
4. Several older and incomplete aerial photography coverages at different scales and of different water situations taken for other purposes

LANDSAT MSS IMAGES

Notwithstanding the fact that the LANDSAT-1 images of the first days of January 1973 were taken about 3 weeks after the beginning of the dry season, a high-water and inundation situation was imaged. The images of February, taken 36 days after the first ones and representing low water, showed considerable changes in the hydrological situation.

The two coverages formed the first pictorial representation of one particular hydrological situation of the whole inundation area and the changes in time occurring within this area.

Only open water bodies could be mapped (band 7), and the extensive areas covered with floating vegetation and reed could not be separated from the adjacent low-lying grasslands, thus giving a restricted impression of the land/water ratio (field data showed frequently over 2-m water depth in the reed fields). An interpretation of the sequential images enabled us to make a classification of the "ciénagas" according to their participation in tempering

the water wave and which of them might be used as a reservoir basin. This classification is as follows:

1. Lakes not participating; nearly without changes in time
2. Lakes actively participating; considerable changes in time
3. Areas drying up; extreme changes in time

The "ciénagas" of the first group offer great possibilities in improving the storage capacity if their drainage could be improved to obtain a smaller dephasing between high- and low-water stages in the river and the "ciénaga." The second group is apparently actively participating in the storage capacity. Interpretation of the images and comparison with field data and conventional photography showed that the third group consists principally of a complex of shallow inundated land and small "ciénagas." Criteria for this classification could only be obtained by sequential coverages of the LANDSAT images.

Furthermore, the interpretation of sedimentation patterns in the low-lying lands and in the "ciénagas" and interpretation of drainage conditions and land use (bands 5 and 7 principally) offered important information dealing with the surface hydrology, complementing in this way the SLAR interpretation.

SLAR IMAGES

The SLAR coverage was flown principally to get a complete instant coverage of a high-water stage at a reasonable scale (original strips 1:400 000; strips for interpretation and mosaics at 1:100 000) to prepare an inundation map. The acquisition of aerial photographs of such a situation is almost impossible within a reasonably short time due to bad weather conditions of the rainy season. The physiographical and hydrological interpretations of the radar were supported by the interpretation of the aerial photographs (scale 1:10 000) taken at the same time as the radar images and by previously existing aerial photography at different scales. LANDSAT images were used for hydrological information within the "ciénagas."

The principal mapping units that were later divided into physiographical subunits are as follows:

1. Permanent flooded areas
2. Complex of permanent flooded areas and inundable areas
3. Inundable areas
4. Noninundable areas (within the alluvial plain)
5. High-lying areas

THE AERIAL PHOTOGRAPHY AT 1:10 000

The aerial photography serves mainly for obtaining quantitative data on changes of the water volumes stored by the "ciénagas" by photogrammetric measurements. For this purpose, the same strips of photographs must be flown during a low-water stage (April 1975). Relative altimetric data related to changes in water level will be obtained from the large-scale photography, while changes in the surface of the "ciénagas" are known from LANDSAT data or by extrapolation of the photodata on the radar imagery.

Furthermore, the aerial photography supports the radar interpretation in preparing interpretational keys (i.e., differentiation between reed and grass fields).

CONCLUSIONS

Due to the sequential coverage, the LANDSAT images are actually the only ones that give a good idea of the dynamic aspects of the overall water situation in the Lower Magdalena-Guaviare River Basin. The interpretation of drainage conditions, sedimentation patterns, and land use also gives valuable information on the surface hydrology of the inundation area. LANDSAT images give quantitative data on surface changes of the "ciénagas," important in the computation of volume capacities in combination with height differences obtained from large-scale photography. However, a complete physiographical interpretation to obtain a relief map of the inundation area is not possible on LANDSAT images. Considering the weather conditions, radar is the only alternative and also provides good interpretability of physiographical features.

By J. F. Ruff, Colorado State University, Ft. Collins, Colorado,
M. M. Skinner, Colorado State University, Ft. Collins, Colorado,
B. R. Winkley, Corps of Engineers, Vicksburg, Mississippi,
D. B. Simons, Colorado State University, Ft. Collins, Colorado, and
D. E. Dorratcague, CH₂M Hill, Redding, California

ABSTRACT

N76-17597

The Corps of Engineers, Vicksburg District, initiated a data collection program to develop a workable knowledge of the principles relating to the transport of water and sediment to gain a better understanding of the Mississippi River characteristics. Aerial photographs and thermal infrared imagery were collected over two test reaches at low and high water stages. Qualitative interpretation of the data relates to the river characteristics such as flow patterns, relative velocities, sediment concentration distribution, water-depth effects, and effects of man made structures. Ground truth information is correlated with the remotely sensed data.

INTRODUCTION

Background.- Primary responsibility of the Vicksburg District, Corps of Engineers, is to provide flood control for the Lower Mississippi River, focused on the maintenance of levees and the stabilization of a channel which will safely pass flood flows. Secondary to the main effort is the requirement to maintain a channel which will provide the required depth and alignment for navigation of the river. River engineers have had to rely primarily on prior experience when trying to align and stabilize rivers. Such an approach has been necessary because of the dearth of adequate information collected on the entire river system at the same time. This is due in a large part to the inability to "see" a large reach of the river instantaneously or over a small time interval.

The Potamology Section of the Vicksburg District initiated a program directed toward developing a workable knowledge of the principles relating to the transport of water and sediment in an effort to gain a better understanding of the Mississippi River characteristics. In 1966 a comprehensive data collection program was begun on selected reaches of the river. In line with this effort a project was initiated to determine the feasibility of utilizing remotely sensed data obtained from an aerial platform to improve the data collection process when combined with conventional point sampling at the ground level. Colorado State University collected the remotely sensed data. The U. S. Army Corps of Engineers collected ground truth information. Interpretation and correlation of the data were carried out jointly.

Interpretation of visual observations by man are dependent upon the reflectance characteristics of the scene within the visible portion of the spectrum. Additional understanding of the behavior of a river can be obtained by looking at portions of the spectrum other than just the visible. Photography and imagery obtained in the visible and the infrared regions of the electromagnetic spectrum provide a record of the scene of interest. Qualitative information can be quickly extracted from the photography and imagery. The objective of this paper is to provide the techniques and analysis for extracting pertinent information from the remotely sensed data that can be used in the field office.

Scope of the Project.- The general scope of the project was to obtain photographs and thermal infrared imagery of selected reaches of the Mississippi River in the Vicksburg District and to interpret and extract useful information from such records. Qualitative interpretations of the remotely sensed data were based on color differences, specular reflection, and grey level differences. These interpretations were related to river

characteristics such as flow pattern, suspended sediment distribution, exposed sediment deposits, erosion patterns, water depths, bed forms, effects of man-made structures on the flow and sedimentation patterns, and the water surface temperature patterns.

Two flights were flown for the purposes of recording the variations and flow characteristics present in the river at low water stage and at high water stage. This paper deals primarily with the results from those two flights and presents photographs to show some of the comparisons between the low water and high water stages. Subsequent to these a third flight was made during the major flood of 1973 and photographic coverage of the Mississippi River from Cairo, Illinois, to the mouth of the Mississippi Above Head of Passes (AHP) was obtained. Only a small amount of these remotely sensed flood data have been analyzed at this time.

The Vicksburg District is responsible for approximately 300 miles (483 km) of the lower Mississippi River between river mile 615 AHP (Above Head of Passes) and mile 320 AHP. Within this reach of river the Potamology Section of the Vicksburg District selected two remote sensing test sites in the vicinity of Vicksburg as shown in Fig. 1. The North Site is near Lake Providence, Louisiana, and extends from approximately mile 476.0 AHP to mile 494.0 AHP. The South Site is near Point Pleasant, Louisiana, and extends from approximately mile 407.0 AHP to mile 417.0 AHP.

Data Collection

Considerable advanced planning was required to concentrate the boat survey crews and schedule the aircraft. A total time of five days was allocated for each flight. All data had to be collected during the time period if it was to be collected at all. Therefore, a concerted effort was made by the Survey Branch to collect the data simultaneously with the overflights of the study reach. This was not possible in every case because of inclement weather conditions at times, and because of an inadequate number of survey boats available for the study, and because of the rapid data acquisition facilitated by the aircraft. The ground truth task force consisted of five boats in each study reach. Survey crews collected data normally obtained during their regular potamology surveys.

...Each potamology survey of a reach provides the following data:
1) Hydrographic Survey; 2) bed form profiles; 3) surface current directions; 4) discharge and horizontal velocity distribution; 5) subsurface current directions; 6) bed material samples; and 7) water surface profiles. The data collection is done by a potamology task force consisting of a sounding party, a discharge party, and gage party....(2)

During the low water survey, data were collected with a precision mapping camera, equipped with a 6 in. lens that produces a 9 in. by 9 in. photograph, and a thermal infrared line scanner with an instantaneous field of view of 2.5 milliradians. The instruments were mounted side by side in the Colorado State University twin engine research aircraft. Color infrared photography was taken with the mapping camera. The thermal infrared line scanner was equipped with a mercury-cadmium-telluride detector sensitive in the spectral region from 8 μ m to 14 μ m and the imagery was recorded on 70mm film.

Prior to and during the low water survey, weather conditions were the result of a typical occluded frontal system which remained centered between Vicksburg and Greenville, Mississippi. It rained during every day of the survey. Extensive cloud cover, high humidity, and wind conditions existed over both the north and south test sites. The airborne data were collected during short periods of partly cloudy sky conditions. Fairly wet ground conditions prevailed over the entire area and in many cases standing water covered a large portion of the flood plain. Due to the weather conditions all overflights and ground truth measurements could not be accomplished simultaneously. Cloud shadows and

extensive overcast conditions seriously affected the quality of aerial photography and induced relatively uniform temperatures at the surface of the terrain.

During the high water survey, color infrared photography was the only airborne data recorded. Weather conditions were generally good. Scattered clouds were encountered occasionally, but in general, clear skies prevailed.

Data Analysis and Interpretation

Conventional manual interpretation procedures were used to study the various prints and transparencies of the photography and imagery. The color infrared film was processed to positive transparency and the thermal infrared imagery was processed to negative transparency. The film was viewed on a light table equipped with a magnifying glass and a zoom stereoscope. The following sections describe the general river characteristics observed, the interpretative keys used to identify them, a discussion of the ground truth and a general discussion of the observations. Photographs were taken at several altitudes, but the interpretation is based mostly on photographs with a scale of 1:20,000. All subsurface phenomena were deduced from the features observed at the water surface.

Mosaics of the test reaches provided planimetric characteristics of the channel that were used to determine the pool and crossing locations. Areas where the flow impinged against the bank or where excessively wide top bank exists were identified as potentially unstable locations. A wide top bank indicates a location of possible bar formation.

Flow Patterns and Velocities.- Higher velocity flows carry higher concentrations of suspended sediment. Changes of concentration of suspended material change the reflectance at the surface of the water which results in a change in color of the water. Color is the primary key to observing flow patterns. On the low water survey there appeared to be a definite relationship between water color indicated on the color infrared film and suspended sediment concentrations. Clear water normally was a dark blue or almost black color. With increased sediment concentrations the water color changed to a lighter blue or powder blue color. On the high water survey this relationship did not hold. The color was altered apparently by variations in the type of sediment caused by overbank and tributary inflows. These inflow areas changed the silt-clay content and the amount of organic matter in suspension and floating on the surface which in turn influenced the color. However, flow patterns could still be observed by changes in the water color. Whenever the high water inundated an island or overland flow entered the river a mottled pattern with a blue-green color could be traced on the water surface for some distance downstream. It was surmised that the mottled pattern was a result of decaying organic material floating on the surface of the water since this pattern was most noticeable downstream of flow entering from wooded areas.

Relative velocities are inferred from the flow pattern generated at the surface by observing foam lines, color differences due to suspended material concentration differences, or films on the water surface. Relative velocities of combining flow can be judged by the lines of vorticity developed along the shear zone. High velocity flow in deep sections is evidenced by a coarse pattern in the specular reflection at the surface. Wind shear can also cause specular reflection and prudent judgement must be used whenever using specular reflection as an interpretative key. Slow-moving water, such as in flooded bendways, can be identified by the relatively smooth water surface and by the foam and floating material with no distinct pattern.

Specular reflection indicated the portion of the river which has the most turbulence, the highest velocities and the highest sediment transport. Hydrographic survey data have shown that the portion of the cross section with the greatest water surface roughness is also the area carrying the highest percentage of the discharge. This portion of the flow often occupies only 10% to 40% of the total width, but in many cross sections it carries 70%

to 80% of the total discharge. This cell of high velocity flow has been observed at all river stages including the flood with 3m (10 ft) of stage over top bank. An example of this flow concentration cell (above the thalweg) is shown in Fig. 2 which is a 35mm photograph taken during the flood in April, 1973. This cell spreads out over 60% to 90% of the total river width wherever the river has poor alignment, i.e. long or irregular radius bends; relatively long straight reaches; or excessive top bank width. The velocities are reduced over the greater width thus reducing the sediment transport. Subsequently, deposition occurs and general deterioration of the river cross section results. Caving banks, irregular bank lines, and bars begin to appear. During high water stages, this cell also spreads out although a dike field is encountered. During high stages, the dikes seem to act as roughness elements instead of flow directors thus resulting in some removal of sediment from the dike field.

Water Depth Effects.- Water depth near sand bars can be inferred from the edge geometry of the sand bar. A serrated edge on a sand bar was found near shallow water with the bed having a small slope. Serrations are the result of ripples on the dunes and are random due to the deposition of sand and the movement of the ripples across the bar. Small isolated sediment deposits that were observable at the surface of the water were associated with shallow depths. The water temperature recorded by the thermal infrared line scanner were slightly warmer in these shallow regions in the latter part of the afternoon. Relatively deep water was observed near sand bars that had a smooth edge. In these areas the flow appeared to be attacking the bar causing some erosion of the toe of the slope of the bar in the vicinity of the smooth edge.

The relative depth of the water near an exposed sand bar could be inferred also from the interpretation of the thermal scanner imagery. If the bar has a relatively wide band of cooler temperature around the edge, the bar is relatively flat indicating that the water depth near the bar is relatively shallow. If the bar has a thin band of cooler temperature around the edge, the bar has a steeper bank indicating the water depth near the bar is relatively deep.

Scour Zones and Subsurface Features.- Potential scour zones can be identified by turbulence observed at the surface of the water, by shear zones in areas of combining flow or at the boundaries of high velocity flow enhanced by color differences, or by foam that emanates from the scour zone. Hydrographic survey maps showing river bed contours confirmed scour zones where large surface vortices developed, such as in the vicinity of control structures, along shear zones of combining flow, and along bank lines where clay-plugs existed.

Turbulence and circulation patterns observed at the water surface can be used to locate subsurface structures and large bed forms. The boundaries of submerged bars are enhanced by a distinct variation in the scale of the texture of the specular reflection. The pattern changed from small, closely spaced random reflections (for shallow water) to a larger "waffle type" appearance.

Vegetation.- Vegetation is one of the ideal parameters for detection on color infrared photography; most living vegetation produces some tone of red. Dead vegetation is recorded as a green or brown color on this film. The vegetative cover also can be identified on thermal infrared imagery; vegetation generally appears cool on the daytime imagery.

Species identification of certain trees is feasible using color infrared photography. The characteristics of color, texture, shape and association must be employed to facilitate the correct identification and to develop the interpretative keys needed for a given region. Tree species and maturity aid in identifying the direction of meander of the river.

Interpretation.- Photographs of one segment of each test reach are presented in this paper. These segments are in the vicinity of Range 486.4 in the North Site and Range 413.2

in the South Site. Other photographs of the study areas can be found in Refs. (1) and (2) along with an interpretation and discussion of the photographs and ground truth.

Range 486.4. - Range 486.4 at low water stage (July 3, 1971) is shown in Fig. 3. Flow is from left to right. Ben Lomond vane dikes are the straight white lines near the center of the river. The dark mottled pattern on this photograph is due to cloud shadow. Tones of blue of the water surface in this reach are deceiving because of the cloud cover at the time of exposure which masks any color differences which might normally be observed in the photograph. In addition, the wave action caused by wind produces excessive specular reflection and masks some of the color of the water surface. Even with these distractions, some information can be gleaned from the photograph.

Turbulence can be observed at the water surface near the upstream and downstream end of each of the dikes. The turbulence generated by the dikes assists in observing the flow pattern through this dike field. A large lateral flow component can be detected at about 45° from the down-channel direction through these guide vanes. This flow is most easily detected between the last two downstream dikes. Scour can be expected to occur in the vicinity of the observed turbulence. The scour is confirmed by the hydrographic surveys. The bed topography in the vicinity of this range is superimposed on the photograph of Fig. 3 and is presented in Fig. 4. The straight vertical line is the range line.

The direction of the flow and the condition of the dikes can be assessed from this photograph. Water is flowing over and through the upstream sections of the last three dikes indicating loss of dike material in these areas and potential failure zones.

The exposed sand bar in the left channel assists in determining the shoaling areas in this channel. The sand bar is the result of deposition behind a large transverse dike at Range 487.4. The transverse dike extends from the left bank of the river but cannot be seen in this photograph.

To the left of the shoaling region, near the left bank, turbulence at the surface is also evident. A constricted flow region can be observed near the left bank. Scour can be expected in the vicinity of this turbulence and is detected by the hydrographic survey.

Surface sediment concentrations and temperatures were obtained simultaneously with the exposure of this photograph. Near surface sediment and temperature samples were collected by dipping a bucket into the water and then sampling that grab sample on the deck of the survey boat. Accuracy of this sampling method is questionable. But this photograph was one of the few when samples could be collected at the time of the overflight. The samples obtained by the survey boats indicated relatively uniform sediment concentrations occurred. The maximum difference in suspended sediment concentrations was only 9 ppm. The blue-grey color observed in the channel to the right of the dikes is relatively uniform in the cloud-free section. Differences in color can be detected in the left channel, but interpretation is questionable because of the wind waves and cloud shadows.

The thermal infrared imagery for this area in the vicinity of Range 486.4 is shown on Fig. 5. The imagery shows a uniform grey level across Range 486.4. The temperatures measured by the boat crews agree with this observation indicating a maximum difference of 0.5°C. The imagery indicates relatively uniform temperatures throughout the reach with two noticeable exceptions: along the left bank upstream of the bar near the transverse dike, a cooler (darker) water area can be seen; a warmer (light grey) water area is identified along the left downstream portion of the bar. Water temperatures were not obtained at these locations and the magnitude of the temperature difference is not known. The warmer water area corresponds to a shallow water region. The cause of the cooler water area is unknown.

A photograph of the high water stage at Range 486.4 is shown in Fig. 6. A higher velocity zone exists in the right portion of the channel and is interpreted from the turbulence pattern enhanced by coarse textured specular reflection. The coarse specular reflection observed over the transverse dike on the photograph (not included) adjacent to Fig. 5 indicated that there is flow in the left portion of the channel. Thus, the flow cell is

spread out over a large portion of the channel. Very little color variation is evident across Range 486.4 which indicates a relatively uniform surface sediment concentration. However, based upon the interpreted velocity distribution, a high bed transport is expected in the higher velocity zone of the right channel. Analysis of the suspended sediment samples indicates concentrations near the surface were relatively uniform. Overall sand concentrations of over 200 ppm were found in the right section and less than 100 ppm in the left section of the channel.

The difference in the flow patterns at low water stage and high water stage can be observed by comparing Fig. 3 and Fig. 6. Distinct velocity components to the left at approximately 45° from the downstream direction were predominant in the vicinity of the guide vanes at low water stage (Fig. 3). This lateral flow results from spill through the guide vanes and is somewhat analogous to flow through a side channel spillway.

The guide vanes are completely submerged at the high water stage (Fig. 6). No lateral component of flow is evident. There is little evidence on the water surface to indicate the presence of the guide vanes. The flow appears to have spread out over a major portion of the channel width.

Range 413.2. - Range 413.2 is shown on Fig. 7. This particular photograph is one of the most interesting acquired during the study. The shear zone that exists along the boundary between the two recombining flows downstream from the bar formation is enhanced by the large clockwise circulations which initiate at the tip of the island and grow in size in a downstream direction. The growth of spacing and size of the individual circulations is quite uniform. The characteristic shape of the eddies observed in this shear zone is similar to those observed by Brown and Roshko (3) on a smaller scale in the mixing zone between two combining air flows of different velocities. It is intuitive that the eddies should extend to the bed of the channel and this is evident by looking at the contours of the bed shown on Fig. 8. The shear zone coincides with the deepest section of the channel in this range. The flow in the left channel is interpreted as being of a higher velocity than that in the right channel with the interpretation based upon the direction of the vortices in the shear zone. Velocities measured by the boat surveys confirm that the flow in the left channel is slightly faster than the flow in the right. The slightly lighter color of the left channel indicates a slightly higher suspended sediment concentration in that channel. Sediment samples show average concentrations of 283 ppm in the left channel and 146 ppm in the right channel at Range 413.2.

Examples of different vegetation can be seen on the color infrared photograph in Fig. 7. The regular pattern seen on the left bank is an area that has been cleared and replanted with a crop of trees. Drainage patterns are also observed within this cleared and reforested areas. The drainages are the approximately parallel lines detected throughout the field. The rip-rap along the right bank is delineated and those areas where vegetation is growing in the rip-rap can be identified readily by the red color.

The small embayment area at the downstream tip of the island appears to be an example of an embayment mouth filling with sediment. The small embayment shows a wide range of blue colors from a dark blue to a grey blue. The dark blue interpreted as relatively clear water and the grey blue as sediment laden water. Fingers of sediment laden water can be seen entering the embayment and mixing with the clear water. The sediment appears to settle out and deposit near the mouth of the embayment. There is a circulation set up with gradually decreasing sediment concentration moving in a clockwise direction within the embayment as indicated by the color change.

Examples of a serrated bar boundary and of a smooth bar boundary can be seen in the left chute channel above Range 413.2. The deepest section of the channel is interpreted as being near the right bank of the chute channel because of the smooth boundary. In addition some turbulence is evident immediately adjacent to the right bank which indicates high flow velocities and a potential scour zone. Shallower water exists near the downstream portion of the left bank as indicated by the serrated edge along the bar. The bed topography shown on Fig. 8 bears out this interpretation.

The high water stage at Range 413.2 is shown in Fig. 9. The shear zone between the recombining flows downstream from the bar is still evident at this stage. The turbulence patterns observed at the surface of the water approach the right bank as the flow continues downstream. Very little surface disturbance can be observed at other sections in this area. The convergence of the stream lines and the turbulence indicates higher velocities exists in the flow zone near the right bank downstream from Range 413.2. This velocity distribution is confirmed by ground truth measurements made in the constricted section of the channel near Range 412.2. The velocities measured at four points approximately equally spaced from left to right across the channel were 5, 6, 9, and 10 fps, respectively. The color of the water does not vary appreciably across this range, thus indicating a relatively uniform suspended sediment concentration. Sediment concentrations measured at the four velocity points are 240, 241, 264, and 230 ppm and confirm the interpretation.

A flow pattern can be distinguished in the left part of the channel downstream from Range 413.2. This pattern emanates from the downstream end of a large submerged bar which can be seen on the low water photograph of Fig. 7.

There is a similarity of flow patterns between the low water stage (Fig. 7) and the high water stage (Fig. 9). The chute flow has higher velocities and there is a convergence of the flow in the right portion of the channel downstream from the bar.

SUMMARY AND CONCLUSIONS

Aerial infrared photography and thermal infrared imagery for this study were obtained over two selected reaches of the Mississippi River. Interpretation of the photography and imagery were performed to identify river characteristics pertaining to the flow, sediment concentration and geometry.

Color infrared photography and thermal infrared imagery from an aircraft platform are effective for acquiring detailed spectral information of the water surface over extensive reaches of rivers at a very rapid rate. The remotely sensed data coupled with ground truth data can give an overview of large rivers that can be used for maintenance and design. Subsurface phenomena can be deduced from features observed at the water surface. Surface flow patterns are evident on all types of photography, but color infrared photography is most effective where suspended material concentration differences exist. Shear zones, mixing zones, regions of high velocity flow, slack water areas and localized flow patterns can be identified. The effect of man-made structures on the flow patterns is identifiable. Specular reflection indicates the portion of the river that has the most turbulence, the highest velocities and the highest sediment transport. When using specular reflection as an interpretative key, prudent judgement must be exercised.

A 1:20,000 scale provided sufficient detail for interpretation of flow patterns. A qualitative evaluation of the sediment transport and flow can be made at a given stage based upon flow patterns at the surface, the local boundary geometry, and the overall geometry. Mosaics of color infrared prints for reaches of the river are very useful for establishing the planimetric characteristics of the channel, evaluating the overall effect of structures, observing the pool-crossing-pool sequence, locating sources and sinks of sediment, and documenting and evaluating the general behavior of the river. As flow stage changes, the shifting of the thalweg can be identified.

The conditions observed in this study are for a single set of flow relationships for each flight and the overall picture changes with different sets of flow conditions. The goal is to extrapolate this and other information to a different set of flow conditions, to predict and identify changes in the navigation channel and to identify potential problem areas during floods. This study is an initial step toward interpretation of river characteristics and it should be recognized that there is a need to quantify some of the observed features as related to river characteristics.

During floods, the river should be flown at frequent intervals and the data used to extend minimal ground truth, thereby getting continual coverage of the entire river over the entire hydrograph. This would allow a trained observer to predict changing conditions and to anticipate problem areas faster than is possible with present techniques. This could minimize the need for ground data, indicate problem areas in which to concentrate surveys, release survey crews for work in other areas and save money.

REFERENCES

1. Skinner, M. M., Ruff, James F., and Barnes, A. H., The Use of Remote Sensing to Obtain Data for Describing the Large River. Prepared for the Corps of Engineers, Vicksburg, Mississippi District. November, 1972. CER72-73MMS-JFR-AHB20.
2. Skinner, M. M., Dorracague, Dennis E., Simons, D. B., and Ruff, J. F., The Use of Remote Sensing to Obtain Data for Describing the Large River. Prepared for Corps of Engineers, Vicksburg District, Vicksburg, Mississippi. July, 1973. CER73-74MMS-DED-DBS-JFR2.
3. Brown, Garry and Anatol Rochko, the Effect of Density Differences on the Turbulent Mixing Layer, Paper presented at AGARD Fluid Dynamics Panel Specialists' Meeting on "Turbulent Shear Flows", 13 - 15 September, 1971, London, England, Graduate Aeronautical Laboratories, California Institute of Technology, Pasadena, California, September, 1971.
4. Elliott, Charles, M., A. M. ASCE, Potamology Data Collection on Lower Mississippi River, Paper published in Journal of the Waterways, Harbors and Coastal Engineering Division, Proceedings of the American Society of Civil Engineers, August, 1970.

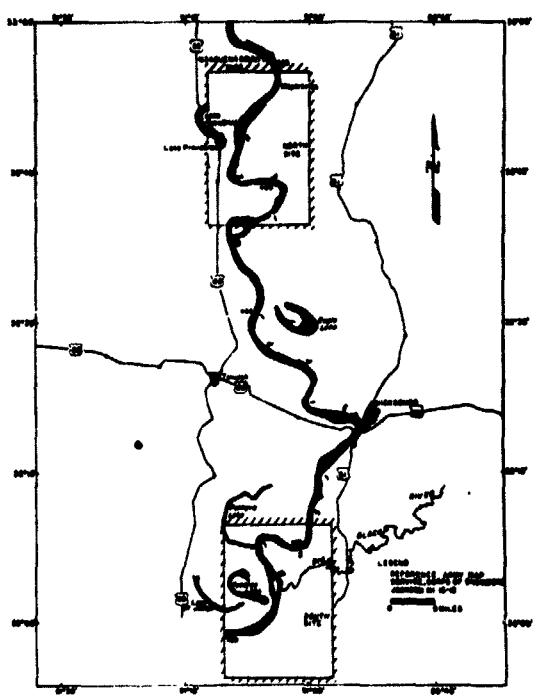


FIG. 1 GENERAL LOCATION MAP - "THE NORTH SITE" & "THE SOUTH SITE"



FIG. 2 FLOW CONCENTRATION CELL OBSERVED DURING 1975 FLOOD



FIG. 5 LOW WATER FLOW PATTERNS NEAR RANGE 486.1 (AMP)



FIG. 4 RIVER BED CONTOURS AT RANGE 486.4 (AHP)

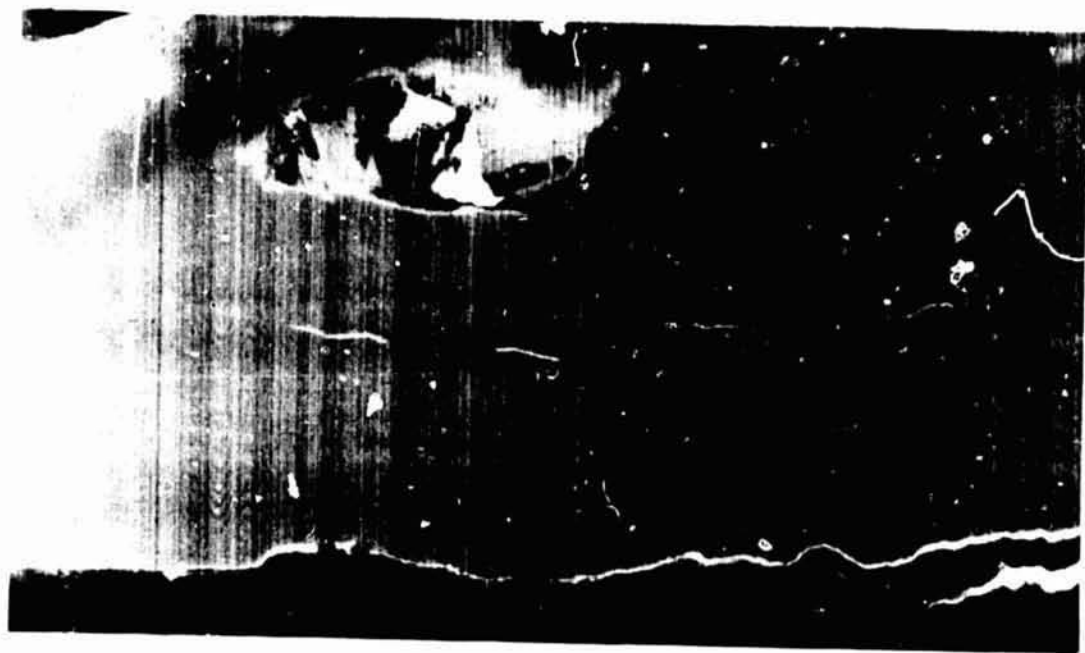


FIG. 5 THERMAL INFRARED IMAGERY NEAR RANGE 486.4 (AHP)



FIG. 6 HIGH WATER FLOW PATTERNS NEAR RANGE 486.4 (MIP)



FIG. 7 EDDY PATTERN AT LOW WATER STAGE NEAR RANGE 415.2 (MIP)

REPRODUCIBILITY OF THE
ORIGINAL PAGE IS POOR

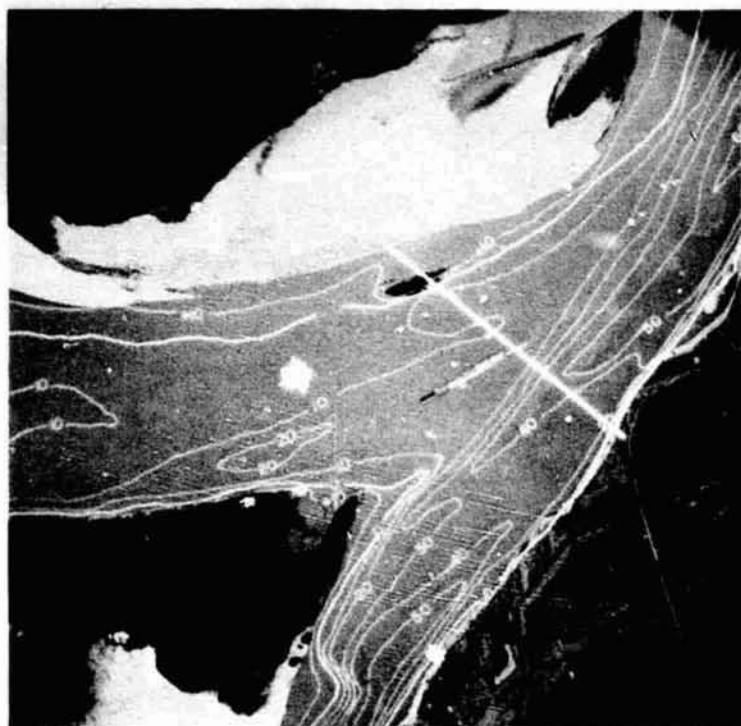


FIG. 8 RIVER BED CONTOURS AT RANGE 415.2 (AHP)

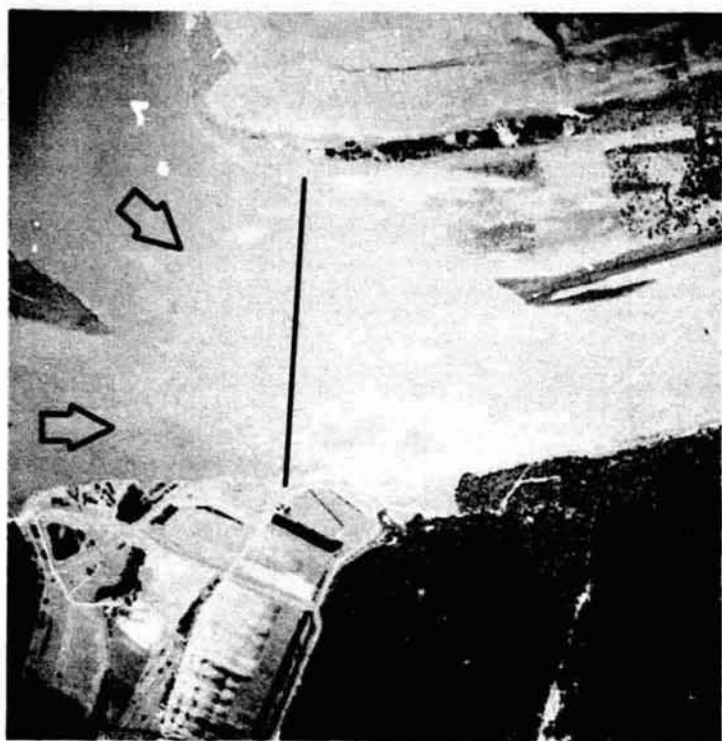


FIG. 9 HIGH WATER FLOW PATTERNS NEAR RANGE 413.2 (AHP)

By J. Wayland Eheart, University of Wisconsin, Madison, Wisconsin

ABSTRACT

N76-17598

Remote sensing has shown itself to be a valuable research tool in the study of transverse mixing in rivers. It is desirable, for a number of reasons, to study and predict the two-dimensional movement of pollutants in the region just downstream of a pollutant discharge point. While many of the more common pollutants do not exhibit a spectral signature, it was shown that the temperature difference between the pollutant and the receiving water could be successfully exploited by applying a mathematical model of mass transport processes to heat transport, and testing and calibrating it with thermal scanning data.

INTRODUCTION

When a pollutant is discharged from a bank outfall into a river, it frequently happens that complete cross-sectional mixing does not occur for a number of kilometers. Resultant zones of high local pollutant concentration, unaccounted for by existing one-dimensional prediction and management techniques, can have effects on the aquatic ecosystem above and beyond those resulting from the cross-sectional-average concentrations. In order to evaluate the effects of such regions of high local concentrations, it is necessary to know, either by accurate prediction or by measurement, the concentration distribution in two or three dimensions. For wide, shallow rivers of the sort usually found in densely populated areas, complete vertical mixing may usually be assumed to have occurred within the first few meters downstream of the outfall. In such cases a two-dimensional approach is often deemed adequate.

During the summer of 1974, a project was undertaken by the members of the Remote Sensing group at the University of Wisconsin, under the sponsorship of the National Aeronautics and Space Administration, to determine and predict the two-dimensional concentration distribution of BOD (Biochemical Oxygen Demand), resulting from the effluent discharge of the Sewage Treatment facility at Janesville, Wisconsin. The BOD problem was chosen because it is among the most ubiquitous faced by water resources planners. The dissolved oxygen problem associated with the BOD problem was not studied, due to the overpowering effects of algal oxygen production at the Janesville site.

A mathematical model was developed to simulate the movement of the BOD pollutant in the two horizontal dimensions. The model, presented in the Appendix, consisted of a series of mass balances on each of a two-dimensional array of small, contiguous, approximately trapezoidal elements, whose vertical dimension was the local depth of the river. It yielded values of time-averaged depth averaged BOD concentrations as a function of lateral and longitudinal distance from an arbitrary point, and required prior knowledge of the depth and velocity patterns of the river, as well as the concentration profile at an upstream boundary. Two assumptions upon which the model was based are of importance to remote sensing applications:

1. That full mixing occurred in the vertical direction.
2. That the system was at steady state.

The seeming contradiction between the latter of these assumptions and the preceding reference to the time-smoothed nature of the simulated concentration warrants explanation. Under normal circumstances, flow in a river is turbulent, resulting, at a fixed point in the river, in short, abrupt changes in the magnitude and direction of flow velocity, and thus in the concentration of any substance which is introduced into the channel. The model was developed to predict time-smoothed values of concentration, on the assumption that the concentration and velocity at a point fluctuated rapidly and randomly about a time-invariant mean. The period of time over which it was necessary to average instantaneous values in order to obtain

meaningful values for the means by time-averaging was estimated at about five minutes for the Janesville site.

The model was calibrated by taking water samples at various locations in the river from which BOD concentrations were determined, and adjusting the model parameters to obtain the best fit of predicted concentrations with experimental data. The problem facing the experimenter was one of taking individual samples and other measurements over a period of time sufficiently long to smooth out random fluctuations while at the same time taking all required data in a period of time sufficiently short to avoid the effects of long-term changes in river flow patterns and effluent discharge. It was felt that remote sensing might lend itself to the solution of this data-collection problem.

As is well known, BOD is a measure of the oxygen-demanding capacity of a frequently varying mixture of organic substances and has no spectral signature. It was proposed, therefore, to apply the mass transfer model to heat transfer, and to measure local temperatures by thermal scanning. The temperature of sewage effluents usually differs from that of the receiving water, being cooler in the summer and warmer in the winter. Assumption 1, above, meant that surface temperatures were representative of the temperature over the depth of the river at a given point. This assumption was confirmed by field measurements of temperature with a thermistor probe. The most significant obstacle to the use of airborne thermal scanning techniques was that they measure essentially instantaneous values of temperature, and thus do not perform the time-smoothing operation mentioned above. An attempt was made to overcome this problem by making several scanning passes and smoothing the resulting data.

EXPERIMENTAL PROCEDURE

Two field surveys are referred to in this paper. During the first, on 21 August 1974, BOD concentration data were taken by conventional sampling techniques. During the second, on 26 October 1974, temperature data were taken by thermal scanning. The thermal scanning system, shown in Fig. 1, consisted of an airplane operated by the Wisconsin Department of Natural Resources, equipped with a thermal scanner owned by the University of Wisconsin and operated by personnel of both institutions. The thermal scanning data were recorded on analog tape aboard the aircraft. The taped analog data were then converted to digital data at discrete points at equal increments of angular displacement on scan lines. These were stored on computer-compatible tapes, and were in turn converted to 36-level, single character digital data. These results were printed on standard 132-character computer paper in such a manner that five computer sheets were laid side by side to reconstruct the thermal "map", with the result that each scan line was represented by 660 characters. A small portion of such a map is presented in Fig. 2. It was not possible to locate ground points accurately by any commonly used rectilinearization technique. The effluent plume was confined to a band between 40 and 80 feet wide along the right bank of the river; the accuracy requirement was thus very great. There was an additional problem with aircraft crab and nonlinearity of flight line. The location of cross-sections where velocity and depth data were taken was thus determined by landmarks. The warming effects of the morning sun resulted in the very clear location of the right (west) bank and each of a row of houses along the left bank. Tangential distortion was corrected for, but was not of significance for most of the sampling locations, which were situated within 10° of the nadir line.

Points were picked off of these maps for each of the cross-sections where depth and velocity data were taken, and for each of the scanning passes. These data for the three passes were combined and converted into plots of temperature vs. distance from the right bank. This was assumed to represent a plot of a sufficient number of instantaneous data points to establish the time-averaged lateral temperature profiles by drawing a smooth curve through the band of data. The time-averaged data at the first cross-section were entered as boundary conditions for the model, the model was run for different parameter values, and the parameter value for which the predicted data best fit the observed data was chosen as optimal.

RESULTS

Table I contrasts the remote sensing method with the conventional method. The parameter K, which is a measure of the degree to which turbulent mixing occurs, was evaluated by the trial-and-error technique described above for data collected both ways. There is a statistical technique, outlined in reference 1, by which a confidence interval for the parameter may be estimated from data generated during the parameter search. The 90% confidence interval for the parameter evaluated from conventionally obtained data greatly exceeds that for the remote sensing data. The primary reason for this difference is the difference in the number of data points obtained. The confidence interval for K is to be construed as a lower bound of the true confidence interval, and does not reflect such errors as model bias, and errors in determining values of depth and velocity. It serves to illustrate, however, the advantages of bringing remote sensing to bear on problems involving a copious data requirement.

TABLE I.- COMPARISON OF CONVENTIONAL AND REMOTE SENSING SAMPLING TECHNIQUES

Method	Optimal K	90% Confidence Interval for K (approximate)	No. Points Observed
Conventional	0.06	greater than (0, .20)	37
Remote Sensing	0.11	(0.10, 0.15)	427

SIMPLER TECHNIQUES

The analysis of data described above was undertaken primarily for the purpose of model testing and parameter evaluation. However, in many cases, temperature may be used as a tracer for BOD and other pollutants by exploiting the relationship

$$\frac{T - T_b}{T_o - T_b} = \frac{C - C_b}{C_o - C_b}$$

where T refers to temperature at any point in the river, C refers to concentration at the same point, T_b and C_b refer to the background temperature and concentration, respectively, and T_o and C_o refer to the temperature and concentration of the outfall, respectively.

The use of this relationship requires simultaneous ground measurements of background and outfall concentration and temperature. It further requires that both constituents be assumed conservative, i.e. that neither heat nor mass are lost from the system. In the work referred to above, it was empirically determined that both constituents could be assumed conservative, due to relatively short length of the section of river studied.

When either heat or mass is lost (or gained), the above relationship does not hold. In such cases, a mathematical model like the one referred to above may be calibrated with temperature data, and then applied to a chemical constituent, as long as the decay or production behavior of each is known.

SUMMARY

Remote sensing may be effectively applied to the development of mathematical models for the two-dimensional movement of pollutants which do not exhibit a spectral signature. Such application may be construed as an indirect means of expediently measuring concentrations of such pollutants. Whether so construed or not, remote sensing has proven to be a valuable research tool in the development of such models.

UNIVERSITY OF WISCONSIN THERMAL SCANNING ANALYSIS SYSTEM

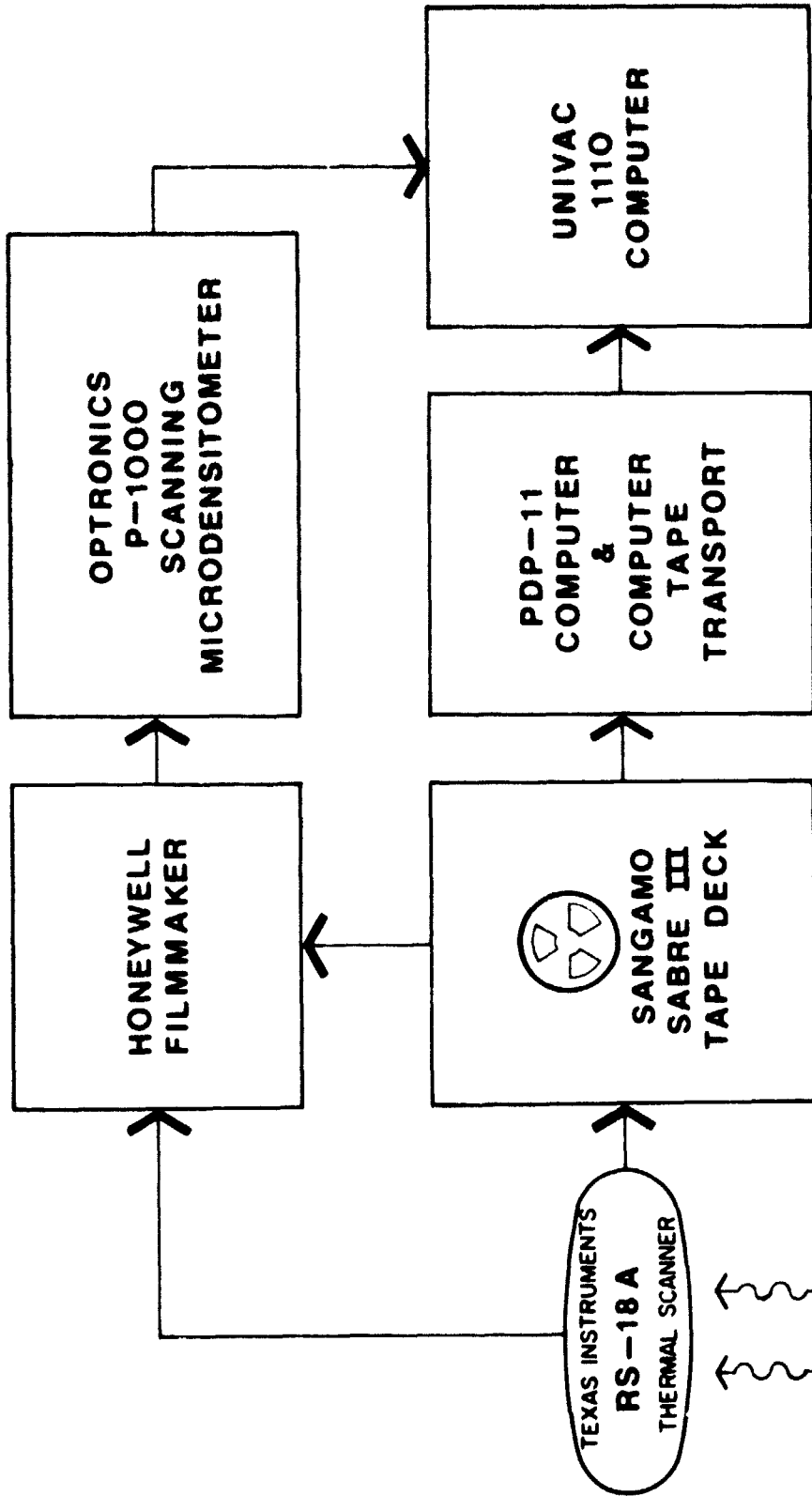


FIGURE 1.- UNIVERSITY OF WISCONSIN THERMAL SCANNING SYSTEM

APPENDIX

MATHEMATICAL MODEL FOR THE TWO-DIMENSIONAL MOVEMENT OF POLLUTANTS
IN A RIVER WHERE COMPLETE VERTICAL MIXING IS ASSUMED

The model is based on a mass balance on a trapezoidal prism, two of whose faces lie on streamlines, and two of whose faces are approximately perpendicular to these streamlines (see Fig. A.1). Mechanisms considered for the net accumulation of mass in the prism are advection, turbulent (eddy) diffusion, and source/sink activity.* Only turbulent diffusion is assumed to transport material across the prism faces lying along streamlines, and only advection is assumed to transport material across the perpendicular faces.

The mass balance may be written, with some rearranging of terms, as:

$$A_{1i,j}C_{i,j} + A_{3i,j}C_{i,j+1} + A_{4i,j}C_{i-1,j} + A_{5i,j}C_{i,j-1} + R_{ij} = 0$$

where $C_{i,j}$ refers to concentration or temperature at point i,j , and

$$A_{3i,j} = 2KU_{i,j+1}I_{i,j+1}^2DX_{i-1,j+1}/(DY_{i,j+1}+DY_{i,j})$$

$$A_{5i,j} = 2KU_{i,j}H_{i,j}^2DX_{i-1,j}/(DY_{i,j}+DY_{i,j-1})$$

$$A_{4i,j} = U_{i-1,j}H_{i-1,j}DY_{i-1,j}$$

$$A_{1i,j} = -U_{i,j}H_{i,j}DY_{i,j} - A_{3i,j} - A_{5i,j}$$

$$R_{i,j} = S DX_{i,j}DY_{i,j}H_{i,j}$$

The terms appearing in the above definitions of A_1 , A_3 , A_4 and A_5 are defined as follows:

$H_{i,j}$ is the depth at point i,j

$U_{i,j}$ is the depth-averaged velocity at point i,j

$DX_{i,j}$ is the length of the trapezoid face in the downstream direction at point i,j

$DY_{i,j}$ is the length of the trapezoid face in the direction from the right bank to the left bank at point i,j

K is the diffusion parameter, and is held constant for a given model run

S is the net addition per unit volume of heat or mass resulting from source/sink activity, and may be dimensioned or undimensioned. For all the work referred to in this paper, it was set equal to zero.

The subscript i takes on values 0 to m , and the subscript j takes on values 0 to n . The boundary conditions are defined as follows:

1. At $i=0$, $C_{0,j}$ is known for all j
2. At $j=0$, $C_{i,-1} = C_{i,0}$ for all i **
3. At $j=n-1$, $C_{i,n} = C_{i,n+1}$ for all i **

Boundary conditions 2 and 3 state that the normal flux of heat or mass at the banks is zero. These are superfluous if $H_{i,0}$ and $H_{i,n}$ are zero for all i .

*e.g. decay by chemical reaction, heat or mass transfer with air or bottom.

**In practice these conditions are accounted for in the model without identifying or creating values for $C_{i,n}$ or $C_{i,-1}$ by making appropriate changes in A_3 and A_5 , or A_5 and A_1 .

The $n-1$ values of C for $i=0$ are specified as a boundary condition. The $n-1$ equations for $i=1$ are solved simultaneously for all $C_{i,j}$ by gauss elimination, treating terms $A_{4i,j}C_{0,j}$ as constants. In a stepwise manner, the $n-1$ equations for each succeeding i are solved for $C_{i,j}$, treating the terms $A_{4i,j}C_{i-1,j}$ as constants.

REFERENCE

Marske, D. M. and Polkowski, L.B., "Evaluation of Methods for Estimating Biochemical Oxygen Demand Parameters," J. Water Pollution Control Federation, Vol. 44, No. 10, Oct. 1972, pp. 1987-2000.

SURVEYS IN THE CHOPTANK RIVER

By James M. Johnson, General Electric Company, Beltsville, Maryland, and
Dr. Philip Cressy, Earth Resources Branch NASA/GSFC, Greenbelt, Maryland,
and William C. Dallam, General Electric Company, Beltsville, Maryland

ABSTRACT

N76-17599

Computer processing of LANDSAT-1¹ multispectral digital data demonstrated the applicability of remotely sensed data to water quality survey in the Choptank River. Water classes derived by automated analysis correlate to river nuisance levels of chlorophyll a and sediment loading as defined by the Maryland Department of Water Resources and the U. S. Corps of Engineers. Results indicate that an increase in chlorophyll a concentration corresponds, relative to MSS 5, to decreases in 4 and increases in 6 relative to the trends with increasing sediment load. It appears that for the purpose of water quality analysis, under favorable atmospheric conditions, only MSS 4, 5 and 6 are necessary.

INTRODUCTION

It is generally recognized that new, economical water monitoring techniques must be developed to meet the needs of current and future environmental management. Existing data acquisition techniques have a major limitation in that they cannot provide time effective data for large ecosystems, such as large rivers or bays. The present monitoring of water quality with respect to physical, chemical, and biological parameters involves a variety of analysis procedures. Although the aquatic environment does not lend itself to simple analytical procedures, it appears that a certain number of monitoring functions are feasible with the use of satellite remote sensing.

The objective of this investigation was to evaluate the applicability of LANDSAT-1 multispectral (MSS) data for assessment of water quality parameters with respect to organic and inorganic pollution in the Choptank River.

Study Area

The Choptank is the largest river (194 sq. km) on Maryland's Eastern Shore, draining portions of Kent County in Delaware, and Talbot, Caroline, and Dorchester Counties in Maryland. The drainage area of the basin is 2000 sq. km and has a population of 55,000. The Choptank has a history of water quality problems related to discharge from insufficient overload wastewater treatment plants, sanitary code violations, agricultural runoff, erosion, and industrial discharges.

METHODOLOGY

Data Analysis

Data format.- Reflected energy values detected by LANDSAT-1 multispectral scanner (MSS)(altitude approximately 915 km) in four wavelengths between 0.5 and 1.1 micrometers are recorded as digital values on 9-track, 800 bpi computer compatible tapes (CCTs).

¹The LANDSAT program is managed by NASA/Goddard Space Flight Center. The prime contractor for the LANDSAT program is the General Electric Company, Valley Forge, Pennsylvania.

Spectral Band	Wavelength (um)
4	0.5 - 0.6
5	0.6 - 0.7
6	0.7 - 0.8
7	0.8 - 1.1

The area of each picture element (pixel) is approximately 1.1 acres. The information in Band 4, 5 and 6 is recorded on CCTs with a 7-bit resolution (128 gray levels), and in Band 7 with a 6-bit resolution (64 gray levels). Since the system gain was not optimized for data collection over water, the total information content for water areas was generally limited to a few gray levels in each band. The data used for this study was taken on two consecutive days, October 10 and October 11, 1972. Normally a particular site was covered by LANDSAT-1 only once every 18 days unless the particular area happened to be located in the overlap region of successive day satellite passes; the Choctank River test site is just such a case.

Data processing equipment.- The data analysis was accomplished on a computer assisted interactive multispectral image analysis system. The primary function of this system is to extract thematic information from multispectral imagery. This is accomplished via statistical measurement of the radiometric properties of the imagery in conjunction with the operator's visual and statistical interpretation of data presented. The system utilizes analog or digital data and outputs color CRT theme displays, map overlays and computer printouts.

Analysis techniques.- The computer analysis techniques involved the following procedures:

1. A single LANDSAT scene includes an area of approximately 34,225 sq. km. A working scene covering an approximate area of 28.8 km square and containing the test site was constructed. A working scene is referred to as a 1:1 display, i.e., for every LANDSAT pixel there is a display element.
2. After establishing the working scene, computer assisted analysis incorporates training and classification functions.
 - a. Training - the process of informing the system which object to analyze, and the system process of identifying the spectral properties of that object. (The term signature extraction is used interchangeably.)

As a result of training a multispectral signature is developed. This signature defines the characteristics of a given object as a function of its reflectance of electromagnetic radiation at a number of discrete wavelengths (visible or non-visible).

- b. Classification - after the spectral properties of the object are found, the system scans the total image, pixel-by-pixel (picture elements approximately 79 x 59 meters) and determines if the spectral properties of each pixel correlates with those of the object of interest.

The result of classification is thematic CRT display class type, binary map or bilevel map.

By repeating the training and classification procedures a one-dimension thematic display for what was discerned as total water was developed. (The one dimensional signature is a classification using only the upper and lower spectral limits in each channel.)

Note: Data analysis in this study was accomplished at two resolution levels, 128 gray levels, which is full resolution of LANDSAT data, and 64 gray levels.

To this total water theme a multidimensional signature acquisition technique was applied. This is a semiautomatic mode of operation, which classified the pixels within a particular cluster on the basis of 4-dimensional histograms. Based on these multidimensional signatures the pixels within the training area were grouped into several clusters. The clustering process is an automatic mode, but the number of clusters is determined by the operator.

The resulting clusters are then stored and retrieved individually, at which time they are subjected to one dimensional training, and the histograms and the CRT displays of the clusters are examined with respect to their significance. At this point, based on the operators judgment, a particular cluster can be further subdivided or a number of clusters may be combined and reclustered if so desired.

The computer analysis techniques also included supervised training/classification and clustering. The supervised procedure involved analyzing a specific site within the working scene for which specific ground truth data was available. The individual radiometric signatures of each pixel within these sub-sites (sewage treatment lagoon, tributaries, and embayments) were analyzed and then these signatures were extended over the entire surface water area in the test site. Also the technique of level slicing was applied to the multispectral (MSS) data. This involved supervised manipulation of the radiometric signature boundaries (upper and lower) of a particular cluster display with respect to the four MSS bands. All the results of the analysis work accomplished using the 10 October 1972 were stored on digital tape and were reapplied to the 11 October 1972 scene.

Ground Truth

The ground truth for this test site was based on historical data. The inorganic sediment data was acquired from results of a LANDSAT-1 investigation (1281A) which used the same area for analysis [1]. The organic water quality data was extracted from documentation provided by the Corps of Engineers [2] and the Maryland Department of Water Resources. It should be noted that the water quality data was not taken precisely at the time of imagery. The data used did indicate the type of water condition that could be expected to exist at this particular interval in time, in the Choptank. All water quality measurements were made in accordance with the procedure specified in the Standard Methods for the Examination of Water and Wastewater, 13th Edition, 1971.

Ground truth data also consisted of high altitude aerial color IR photography taken on 10 October 1972 and low altitude color photography taken at the time of this investigation.

All correlation of water classification, with respect to location, was accomplished using NOAA/NOS Coast and Geodetic Survey Charts (552 and 72266).

SPECTRAL ANALYSIS OF WATER

From a theoretical standpoint, the number of water quality parameters measurable through analysis of LANDSAT data is limited by the number of bands, the bandwidths, and gain a number of gray levels. Suspended solids and phytoplankton constitute two of the properties which can be considered potentially measurable in LANDSAT data.

Water, because it absorbs energy in the infrared region, reflects less energy than most other features on the surface of the earth in MSS 7 (0.8 - 1.1 μm). In a given scene, surface water is identified by the fact that the lowest reflectance values in Band 7 represent reflected energy over water feature pixels. Other than the delineation of surface water boundaries, MSS 7 has no significant application in water quality analysis. The water feature pixels are related to water quality on the basis of reflected energy in the three spectral bands measured by MSS 4, 5 and 6 (0.5-0.6, 0.6-0.7, and 0.7-0.8 μm).

Inorganic Suspended Solids

Both pure and polluted water absorb and scatter light. This phenomenon is caused by the water molecules and the suspended particulate materials in the water. The relative

importance of scattering and absorptions mechanisms of attenuation independent upon wavelength as illustrated in Figure 1. The attenuation wavelength relationship in typical surface water is illustrated in Figure 2.

Figure 3 illustrates the manner in which the reflectance spectrum is altered as a result of the introduction of particulates into a body of water. The curves represent a simple and ideal case, in which the receiving waters are clear, free of extraneous pollutants, and of sufficient depth so that bottom reflectance is not a factor. The important point extracted from the curves is that a significant change in the reflectance spectrum occurs in the 0.6 - 0.7 μm spectral band (MSS 5). The curves also illustrate that the reflectance levels in the 0.5 - 0.6 spectral band (MSS 4), also increase, but the utility of this band is dependent in part on the atmospheric condition at the time of the observation. The relationship shown is not linear and reflects both particle size and concentration. In general, the change in 4 is about 0.6 - 0.8 that in 5. Beyond 0.7 μm the curves for inorganic particulates drop off and the attenuation coefficient in the near infrared will increase rapidly, limiting observations essentially to the water surface. (Although within this restriction 6 & 7 reflectances also increase with sediment load.)

For this work, although no simple correlation exists between light transmittance and weight per unit volume of suspended matter, and because of the lack of need for detailed quantitative measurement, the reflectance values of MSS 5 were used to make gross classifications of water quality in relation to inorganic sediment load.

Phytoplankton

Figure 4 illustrates the expected response for a body of water which contains varying concentrations of phytoplankton. The response in the spectral band 0.6 - 0.7 (MSS 5) is caused by the fact that phytoplankton contains chlorophyll, carotenoids, and special accessory pigments, all of which absorb light. Thus, while MSS 5 reflectance does increase slightly with phytoplankton concentration, the change is much less than in 6 (or 4). Chlorophyll *a* is the predominant pigment in planktonic algae. In the near infrared band 0.7 - 0.8 (MSS 6), as the phytoplankton concentration increases there is a proportional increase in spectral reflectivity over band 5. This is the opposite of the expected response for inorganic particulates.

RESULTS

Results of this investigation indicate that the semiautomatic clustering and spectral band level slicing processes allow gross classification of the surface water in the Choptank on the basis of water depth and water quality (phytoplankton).

Water Quality

Figures 5 through 8 illustrate the results of this investigation, with respect to water quality at a resolution of 64 levels and 128 levels using all MSS bands. These clusters were derived utilizing both semisupervised and supervised clustering techniques. The association of the resulting clusters to water quality was based on the mean spectral signatures of a particular cluster in MSS band 5 (0.6 - 0.7 μm) and 6 (0.7 - 0.8 μm). Listed in Tables I and II are the mean signatures for MSS bands 4, 5, 6 and 7, for the clusters resulting from analysis at 64 and 128 gray levels respectively. Also included in these tables is a hierarchical classification of the clusters with respect to water quality (inorganic sediment and chlorophyll *a* concentration) and water depth.

Results at 64 Levels

Reflectances of 0-3 in MSS 7 were assumed to define water feature pixels. The clusters were developed by initially establishing four clusters. By examining the CRT display and histograms the original clusters were combined and/or further subdivided using the semiautomatic computer mode. This technique produced 10 distinct clusters. Six of the clusters characterized water predominantly in the lower Choptank, three characterized the water of the upper river, and one delineated the shoreline.

In Figure 5, the six clusters which characterized the lower river are identified as follows using C&GS charts and the sewage treatment lagoon at Easton, Maryland as references.

- Cluster 1 - water deeper than 1.5 m, lowest inorganic sediment 0-25 mg/l, lowest chlorophyll a <50 $\mu\text{g/l}$
- Cluster 2 - depth >1.5 m, inorganic sediment 0-25 mg/l, chlorophyll a <50 $\mu\text{g/l}$
- Cluster 3 - depth >1.5 m, inorganic 25-60 mg/l, chlorophyll a 50-100 $\mu\text{g/l}$
- Cluster 4 - depth >1.5 m, inorganic sediment 25-60 mg/l, chlorophyll a 50-100 $\mu\text{g/l}$
- Cluster 5 - depth <0.6 m, inorganic sediment 0-12 mg/l, chlorophyll a >100 $\mu\text{g/l}$
- Cluster 6 - depth 0.6-2.7 m, inorganic sediment 12-15 mg/l, chlorophyll a 50-100 $\mu\text{g/l}$

The three water classes which were predominantly in the upper Choptank, east and north of Cambridge, Figure 6, were characterized as follows:

- Cluster 7 - depth 0.9-2.4 m, inorganic sediment >60 mg/l, chlorophyll a >100 $\mu\text{g/l}$
- Cluster 8 - depth 0.9-2.4 m, inorganic sediment >60 mg/l, chlorophyll a 50-100 $\mu\text{g/l}$
- Cluster 9 - depth 0.9-2.4 m, inorganic sediment >60 mg/l, chlorophyll a >100 $\mu\text{g/l}$

A comparison of the mean signatures for these nine clusters as they relate to the water quality ground truth data is summarized in Table I. These results imply that a mean signature of 4.0 or less, 4.0-6.0, and 6.0 in MSS 5 are indicative of water with an inorganic sediment load of 15 mg/l or less, 15-25 mg/l and 25 mg/l, respectively. In MSS 6 a mean signature of 1.9 or less, 2.0-3.0, and 3.0 are characteristic of surface water which has chlorophyll a concentration of <50 $\mu\text{g/l}$, 50-100 $\mu\text{g/l}$ and >100 $\mu\text{g/l}$ respectively. Cluster 10, in Figure 6, delineates only areas which were determined to be a combination of land and water or shoreline.

Results at 128 Levels

Because LANDSAT-1 data is not optimized for water (only a few gray levels pertain to water data) and the raw data is composed of 128 gray levels it was thought that working at 64 level (in effect compressed data) may have severely reduced the amount of information obtainable from this type of analysis. The water quality classification derived as a result of analysis at 128 gray level is illustrated in Figures 7 and 8. The comparison of the mean signature of the resulting clusters the water quality ground truth is given in Table II.

A comparison of the results at 128 levels to the analysis results at 64 levels indicates that for the surface water in the Choptank, the results were very similar. Visually, the only difference appears to be that the data at 128 levels allowed more detailed classification of the water in relation to depth gradient in the lower river (Figure 8, Clusters 11 and 12). Possibly if the river bottom had less slope and/or the river water contained a larger variance in sediment load, both organic and inorganic, the increase in resolution would have been more significant. For statistical analysis of the data, the results at 128 levels show greater correlation.

The mean MSS 4 and 6 reflectances in Table II are plotted against mean MSS 5 values in Figure 9. The mean reflectances of 31 Easton lagoon pixels are denoted by X. The open circles are Clusters 6, 7, 8 and 10 of Table II. The first three are primarily found in the upper Choptank, typically high in chlorophyll a; Cluster 10 appears to include shoreline

mixed pixels. Because of their physical and spectral characteristics, the data for the lagoon and the four clusters were treated separately.

Data from the remaining eight clusters (solid points) were correlated by linear least squares regression analyses, with the resulting equations given in the figure. Standard deviations for the equations were calculated from the differences between observed and calculated MSS 4 (or 6) reflectances for the measured MSS 5 values. The R^2 values reflect the degree (on a scale of 0 to 1) to which the calculated equations account for the observed variations in the data; at $R^2 = 0.99$ and 0.91 the fits are excellent. In view of the correlation of some clusters with depth, it appears that depth effects cannot be distinguished from suspended sediment concentrations by MSS 4 - 6 reflectance patterns alone.

Cluster 10 falls about one standard deviation from the MSS 4 vs. 5 line, but has increased reflectance in MSS 6 (and in MSS 7, not shown), supporting the view that these pixels contain some shoreline vegetation.

The lagoon and Clusters 6, 7 and 8 fall conspicuously off the trend lines, and share the common characteristic of being associated with high typical chlorophyll a and/or surface algae contents. The displacements of these data points from the trend lines - $\Delta(\text{MSS } 4) / \Delta(\text{MSS } 5) < 0.74$ and $\Delta(\text{MSS } 6) / \Delta(\text{MSS } 5) > 0.58$ - are consistent with calculated reflectance changes for phytoplankton in water (Figure 4). The magnitudes of these displacements are 4 to 7 standard deviations for 4 vs. 5, and 0.5 to 4 for MSS 6 vs. 5. Although exact correlations with chlorophyll a content are not possible for this data, it appears that a relative decrease in MSS 4 reflectance is statistically more diagnostic of this phenomenon than is an increase in MSS 6.

Spectral Band Level Slicing

The results of level slicing MSS 5 and 6 are illustrated in Figures 10 and 11, respectively. The upper and lower bounds of MSS 5 and 6 in the water feature pixels were determined by application of a one-dimensional training process for the total water area. The level slicing of the individual channels was accomplished by holding the spectral limits of all other bands constant and manually adjusting the upper and lower bounds for the specific band being sliced. The results of this process reinforce results of the semisupervised clustering process. For MSS 5 and 6 the reflectance values were low near the mouth of the Choptank. The water feature pixels which were further up river and located in tributaries had higher reflectance due to increase inorganic sediment (MSS 5) and phytoplankton (MSS 6).

The Easton sewage treatment lagoon, in Figures 10 and 11, is characterized by low reflectance in MSS 5 and high reflectance in MSS 6. This occurrence is consistent with high organic load in the lagoon causing absorbance in MSS 5, while chlorophyll a content of the algae in the water increases the reflectance in MSS 6.

As indicated in the results at 64 levels, water pixels with reflectance values of < 2.0 , $2.0-3.0$, and > 3.0 were correlated with chlorophyll a concentration of < 50 μg , $50-100$ μg and > 100 μg , respectively.

Phytoplankton Detection

These results indicate that LANDSAT data has limited application for the detection of planktonic algae. The explanation of this is twofold. The bandwidth of MSS 6 ($0.7 - 0.8$ μm) is restrictive because the lower end of this band is well suited for chlorophyll detection, while the range approaching the upper end demonstrates a decreasing reflectance (see Figure 12).

The second reason is illustrated in Table III. The Corps of Engineers conducted a study of the nutrient - chlorophyll relationships in the Choptank River. Results of the survey indicate that nuisance algal blooms (measured as chlorophyll a concentrations) seem to be associated with total Kjeldahl nitrogen (TKN as N) concentrations above 0.9 mg/l and total phosphorus (TP as PO_4) concentrations above 0.3 mg/l . However, increases in nutrient

concentration do not produce proportional increases in algae growth. Nutrient availability as well as environmental factors such as water temperature, oxygen concentration, wind, and sunlight affect algal propagation.

Results of this study indicate that algal blooms can be detected and that the intensity of the reflectance of the water feature pixel in MSS 6 correlates to the chlorophyll a concentration. The detail in ground truth data for this study only allowed classification of the chlorophyll a concentration at three levels: <50 µg/l (below nuisance level), 50-100 µg/l (blooms occur) and >100 µg/l.

Inorganic Sediment

Results of this study indicate that there is no simple correlation between inorganic sediment content per unit volume of water and spectral reflectance in MSS 5. A comparison of sediment measurement and MSS signatures implies that over large test areas, ranges of sediment load are somewhat correlated. Ground truth in the Choptank allow the classification of water feature pixels in five ranges: 0-12 mg/l, 12-15 mg/l, 0-25 mg/l, 25-60 mg/l and greater than 60 mg/l.

The dynamic nature of a body of water such as the Choptank and the resolution of LANDSAT data (.44 hectares) contribute to the error in sediment correlations, because of the present sampling techniques. A point source sample in an acre area, or series of point samples in the area over a period of time could lead to serious errors in correlation to spectral reflectance. Acquiring a large number of samples over a given area, simultaneously with the satellite compass, would be more effective for determining sediment load correlation in dynamic waters.

Application of Signatures to 11 October Scene

Results of transferring the multidimensional signatures (64 level) from the 10 October 1972 scene to the 11 October 1972 scene are illustrated in Figures 13 and 14. The change in location of the clusters is due to a change depth (different tide level) and the incoming tide affecting the surface water circulation patterns.

As a result of observations of the clusters of the 11 October scene it was determined that possibly the change in water depth significantly affected the location of the cluster. Since water depth is not of a significant concern to water quality analysis it was speculated that a data processing technique which utilized only MSS 5 and MSS 6 would simplify problems of associating transferred signatures to water quality and significantly decrease the data processing.

Supervised Clustering

To develop a unique signature for water in the Easton sewage treatment lagoon a supervised classification technique was applied. The process involved the selection of a training site within the working scene and enlarging the display in order that the individual "water" pixels could be easily distinguished from shoreline.

After developing a total water theme, in which the lagoon was included, the lagoon water area pixels were classified using the multidimensional training mode. The results of applying this lagoon signature to the total water theme is illustrated in Figure 15. This cluster should distinguish water in the Choptank which is similar to lagoon water in sediment load, chlorophyll a content and depth. This cluster includes waters of the several small tributaries which according to ground truth were typified as having chlorophyll concentrations similar to that of the Easton lagoon.

Although a striping compensation technique was applied to the original data, the sensor calibration effect was not entirely eliminated. The similarity of the horizontal striation effect in the thematic display to a "banding" effect suggests that this cluster is an over-representation of river water which is similar to lagoon water.

CONCLUSIONS

Results of this investigation demonstrate that LANDSAT data can be utilized to survey water quality of a large water system on a timely and economical basis.

Although water quality does not lend itself to simple analysis, the four broad bandwidths between 0.5 - 1.1 μm allow limited water quality measurements which are essentially restricted to inorganic sediment concentrations and phytoplankton (chlorophyll a) detection.

Inorganic sediment concentration in the Choptank, although it does not represent a significant problem, was detectable in MSS 4 and 5. Also, it should be noted that bottom reflectance and sediment concentration are not distinguishable using MSS 4 and 5. Only in water having sufficiently large sediment load or of sufficient depth to eliminate bottom reflectance can correlation of MSS 4 and 5 to sediment load be determined.

The MSS 6 or the ratio of MSS 6/MSS 5 is applicable for the detection of high phytoplankton (chlorophyll a) concentrations. An increase in reflectance in MSS 6 relative to MSS 5 (and a decrease in MSS 4 relative to MSS 5), compared to the trend of data from sedimented water, is indicative of water which contains high chlorophyll concentration. Because inland water which has sufficient organic nutrient loads to support a phytoplankton bloom is, according to standards set by the Environmental Protection Agency, polluted, the capability of bloom detection alone would be useful for large scale water quality surveys of non-point pollution sources of nitrogen and phosphorous.

REFERENCES

1. Corps of Engineers. Chesapeake Bay Existing Conditions Report. December 1973.
2. Williamson, A. N. Movement of Suspended Particles and Solute Concentrations with Inflow and Tidal Action. Type III Final Report, LANDSAT-1 Investigation #1281A prepared for GSFC. May 1974.
3. Gazey, B. K. Visibility and Resolution in Turbid Waters. Underwater Science and Technology Journal, Vol. 2, No. 2; pp 105-115. June 1970.
4. Wezernak, C. T. Water Quality Monitoring Using ERTS-1 Data. Type III Final Report, LANDSAT-1 Investigation #1081A prepared for GSFC. March 1975.

TABLE I. TABULATION OF MEAN SIGNATURES VS. GROUND TRUTH

AT 64 LEVELS

CLUSTER	MSS 4	MSS 5	MSS 6	MSS 7	GROUND TRUTH DATA		
					Chloro. <u>a</u> ($\mu\text{g}/\text{l}$)	Inorg. Sed. (mg/l)	Water Depth (m)
1	9.1	4.0	1.9	0.6	<50	0-25	>1.5
2	9.4	5.1	1.9	0.6	<50	0-25	>1.5
3	9.8	5.8	2.5	0.9	50-100	25-60	>1.5
4	9.1	4.3	3.0	0.3	50-100	25-60	>1.5
5	12.0	7.8	4.1	1.1	>100	0-12 *	<0.6
6	11.2	6.2	2.4	0.6	50-100	12-15 *	0.6-2.7
7	9.0	6.1	3.4	0.8	>100	>60	0.9-2.4
8	10.0	6.1	3.0	0.4	>100	>60	0.9-2.4
9	10.3	6.3	4.1	0.9	>100	>60	0.9-2.4
10	11.1	6.4	3.0	0.7	*	**	**

* Interference due to bottom reflectance

** No measurement

TABLE II. TABULATION OF MEAN SIGNATURES AND GROUND TRUTH

AT 128 LEVELS

CLUSTER	MSS 4	MSS 5	MSS 6	MSS 7	GROUND TRUTH DATA		
					Chloro. a (ug/l)	Inorg. Sed. (mg/l)	Water Depth (m)
1	19.0	8.9	4.9	0.0	50-100	0-25	> 2.4
2	19.7	10.3	4.3	0.0	<50	0-25	> 2.4
3	19.4	9.9	5.3	2.0	50-100	25-60	> 1.5
4	19.6	9.8	5.8	4.0	50-100	25-60	> 1.5
5	20.9	11.7	5.0	0.9	50-100	0-25	> 2.4
6	19.7	12.3	8.5	4.2	> 100	> 60	1.5-2.7
7	20.2	12.3	6.8	1.9	> 100	> 60	1.5-2.1
8	18.5	11.9	7.8	1.5	> 100	> 60	1.5-2.1
9	22.7	13.2	6.9	2.2	50-100	0-12	1.5-2.7
10	22.4	14.3	9.9	4.6	**	**	**
11	24.8	16.1	8.4	2.2	> 100	0-12	0.9-1.5
12	26.5	19.5	11.0	3.8	*	*	< 0.6
Lagoon	18.1	5.9	7.4	1.9	> 100	*	> 2.4

* No measurement

** Shoreline

TABLE III. NUTRIENT - CHLOROPHYLL* RELATIONSHIPS

IN CHOPTANK RIVER [2]

Station	August 5, 1971			July 14, 1971		
	Chlorophyll <u>a</u> mg/l	TP mg/l	TKN mg/l	Chlorophyll <u>a</u> mg/l	TP mg/l	TKN mg/l
AFO 1	103	.510	1.49	150	.471	1.93
AFO 2	73	.519	1.68	171	.450	1.45
AFO 3	80	.373	1.33	121	.383	1.45
AFO 4	48	.361	.92	105	.27	1.54
AFO 5	28	.381	1.02	80	.3	1.58
AFO 5A	30	.410	.96	97	.313	1.13
AFO 6	28	.325	.76	73	.316	.95
AFO 7	22	.433	1.02	66	.333	1.34
AFO 8	33	.340	.56	35	.259	.87
AFO 9	14	.242	.40	17	.165	.66
AFO 10	38	.336	.94	15	.149	.52
AFO 11	17	.204	.41	48	.214	.66
AFO 12	10	.165	.75	30	.192	.92
AFO 13	13.5	.142	.33	16	.117	.54
AFO 14	11.3	.189	.52	13	.132	.92

* Chlorophyll a concentrations greater than 20 mg/l indicate high level algal blooms

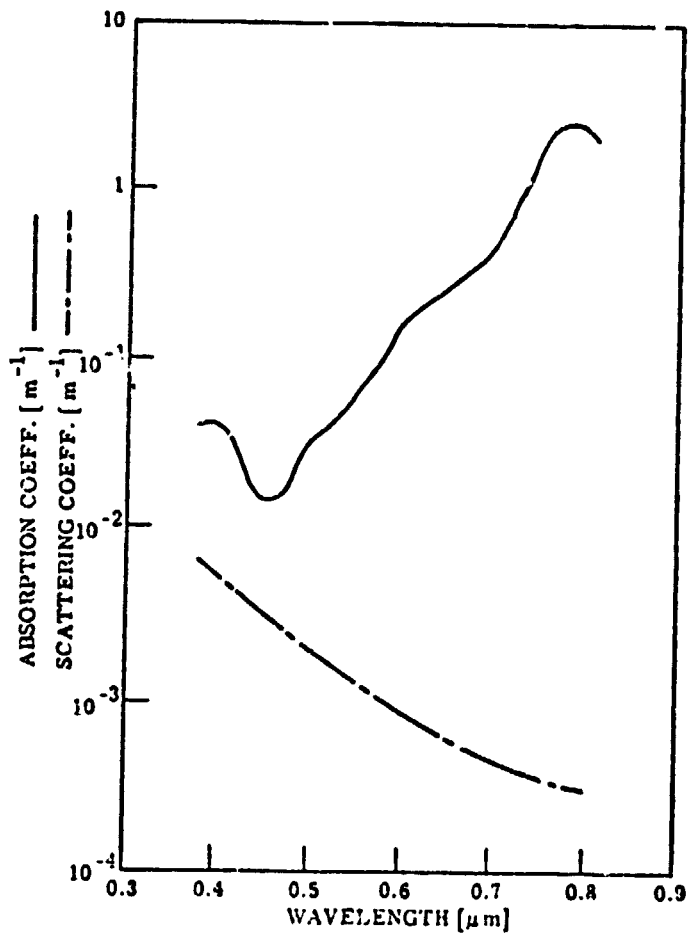


FIGURE 1. ABSORPTION AND SCATTERING COEFFICIENTS OF PURE WATER AS A FUNCTION OF WAVELENGTH [3]

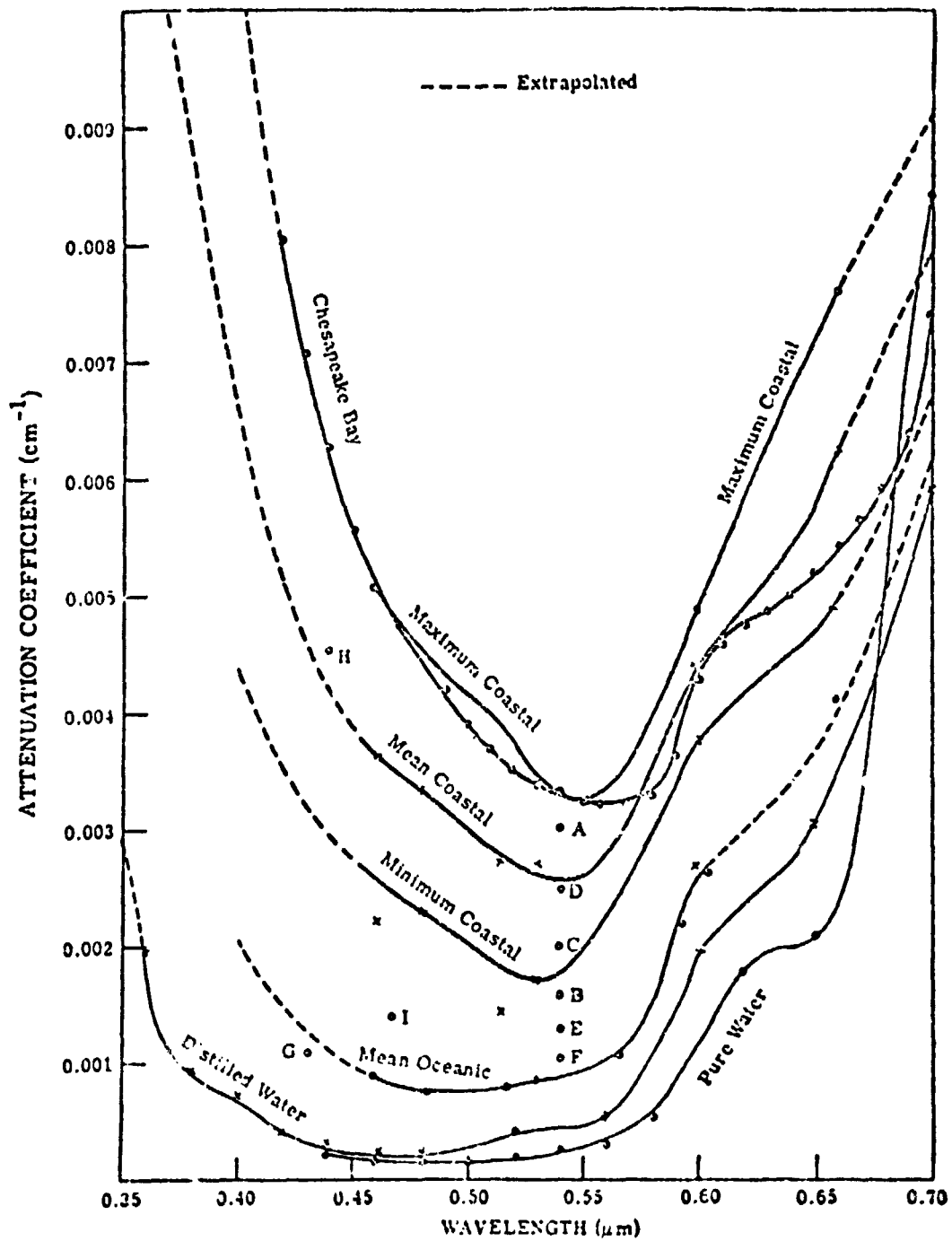


FIGURE 2. ATTENUATION - WAVELENGTH RELATIONSHIPS IN TYPICAL SURFACE WATERS [4]

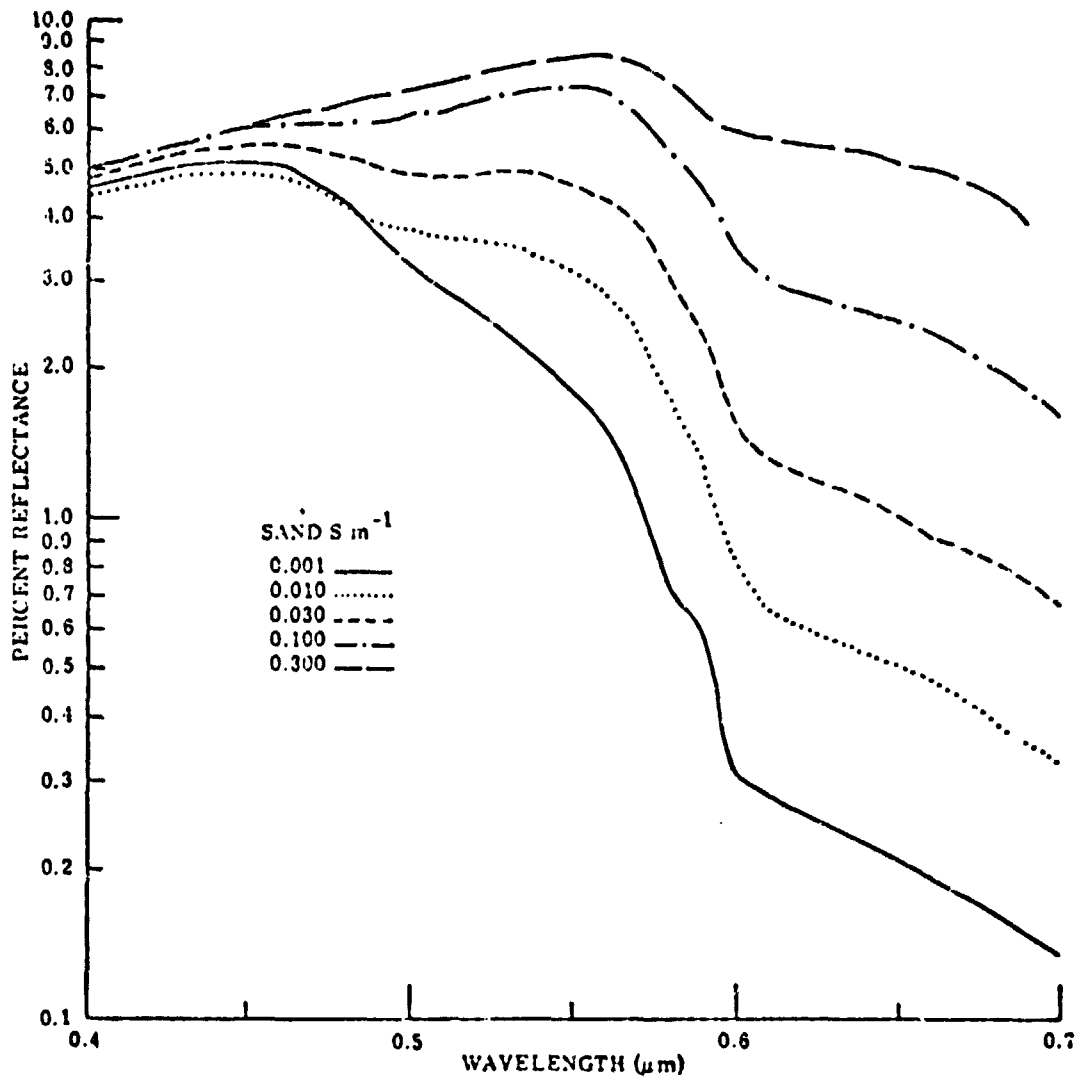


FIGURE 3. CALCULATED CHANGES IN REFLECTANCE OF WATER WITH INCREASING CONCENTRATION OF SUSPENDED SOLIDS [4]

2-3

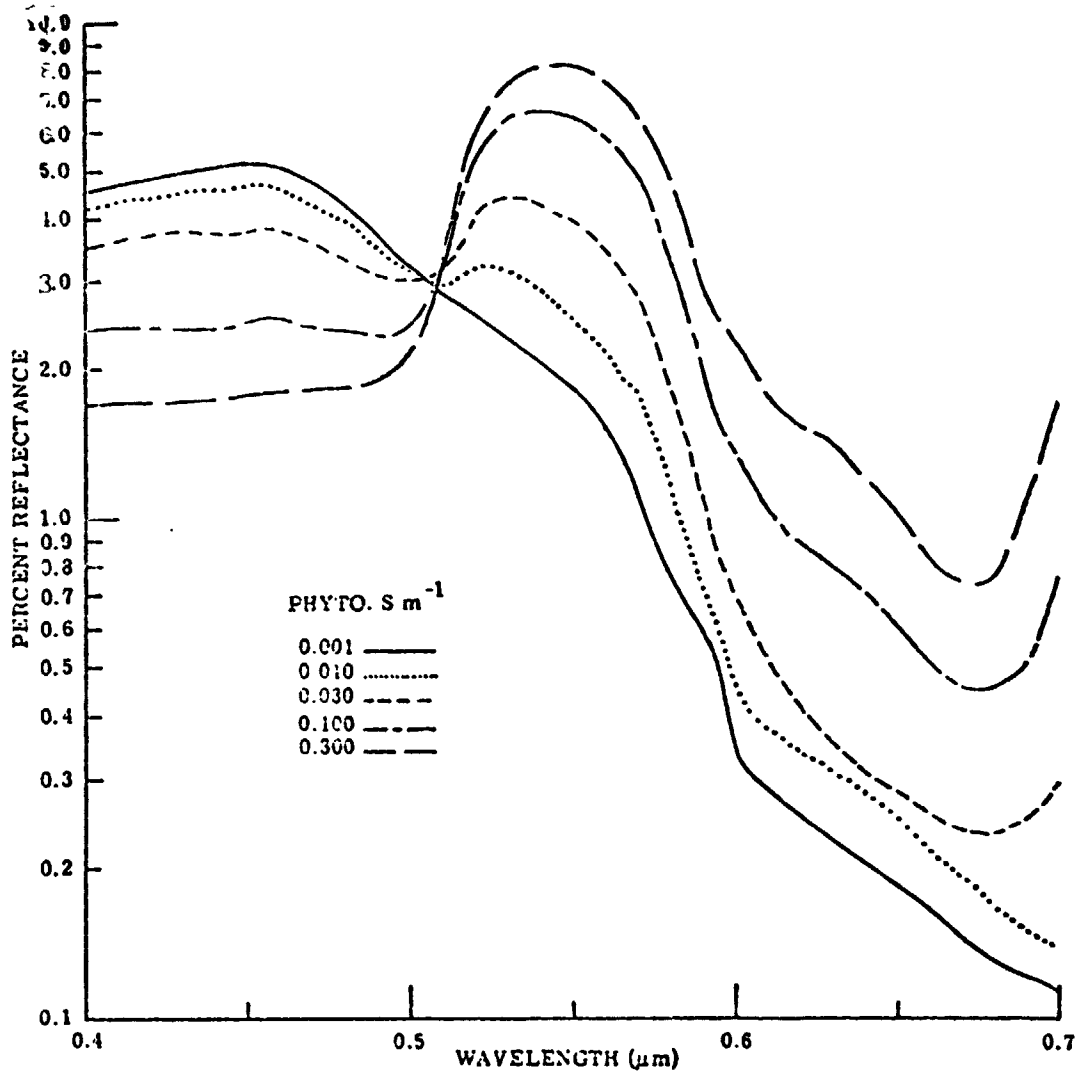
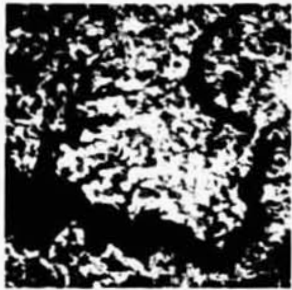
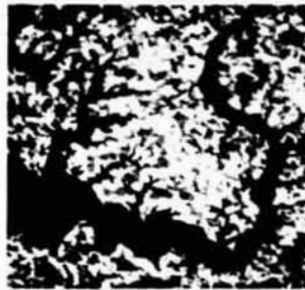


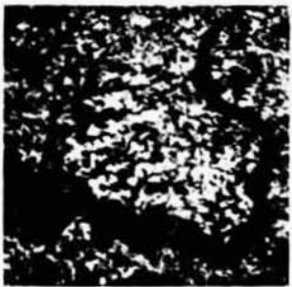
FIGURE 4. CALCULATED CHANGE IN REFLECTANCE OF WATER WITH INCREASING CONCENTRATION OF PHYTOPLANKTON [4]



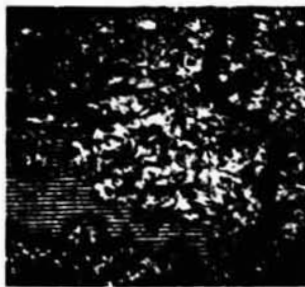
Cluster 1



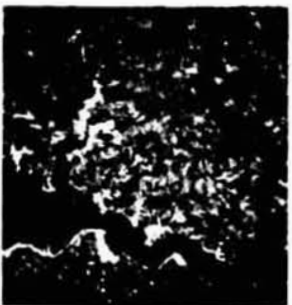
Cluster 2



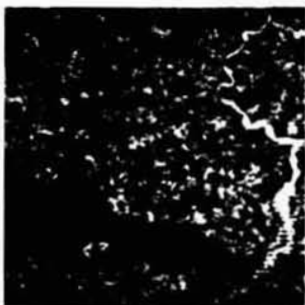
Cluster 3



Cluster 4

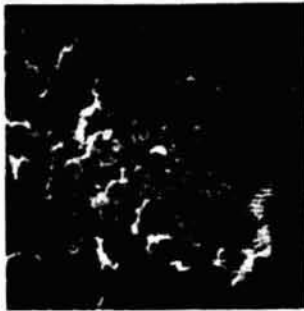


Cluster 5



Cluster 6

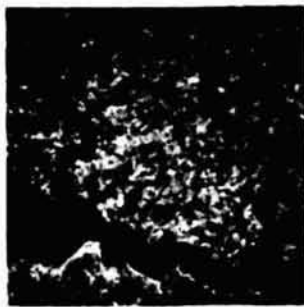
Figure 5. October Choptank River Clusters 1 - 6 at 64 Levels



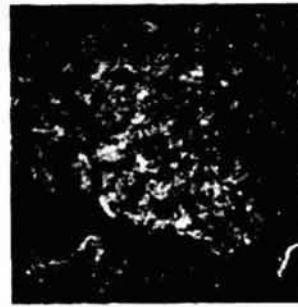
Cluster 7



Cluster 8

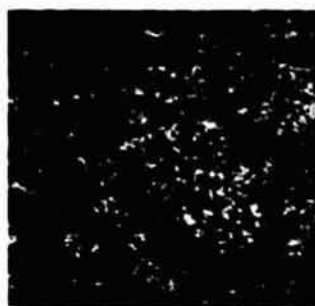


Cluster 9

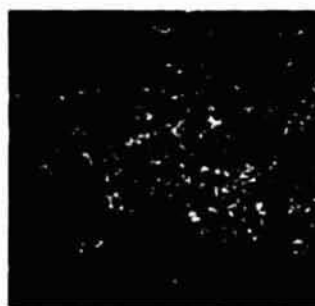


Cluster 10

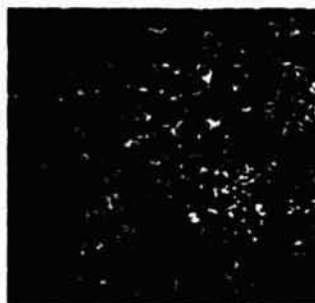
Figure 6. October 10 Choptank River Clusters 7 - 10 at 64 Levels



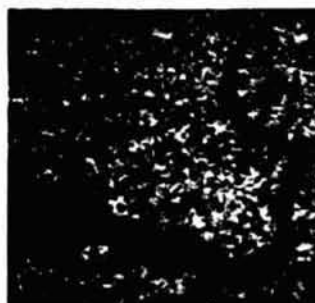
Cluster 1



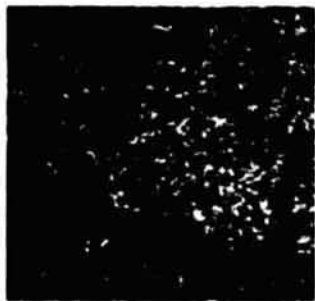
Cluster 2



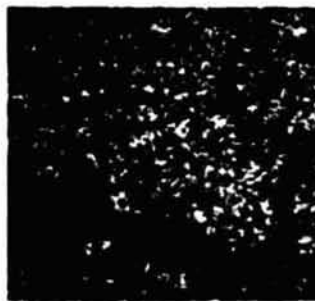
Cluster 3



Cluster 4

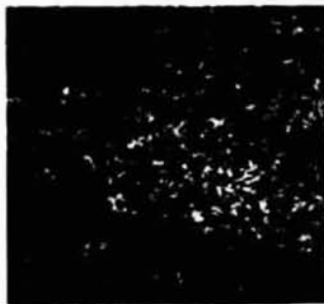


Cluster 5

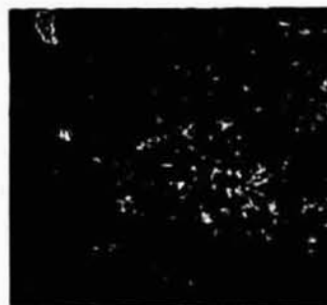


Cluster 6

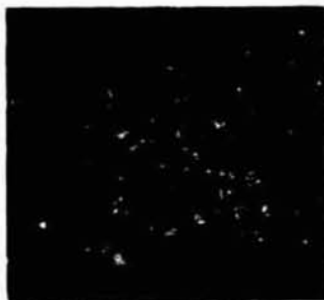
Figure 7. October 10 Choptank River Clusters 1 - 6 at 128 Levels



Cluster 7



Cluster 8



Cluster 9



Cluster 10



Cluster 11

Figure 8. October 10 Choctank River Clusters 7 - 11 at 128 Levels

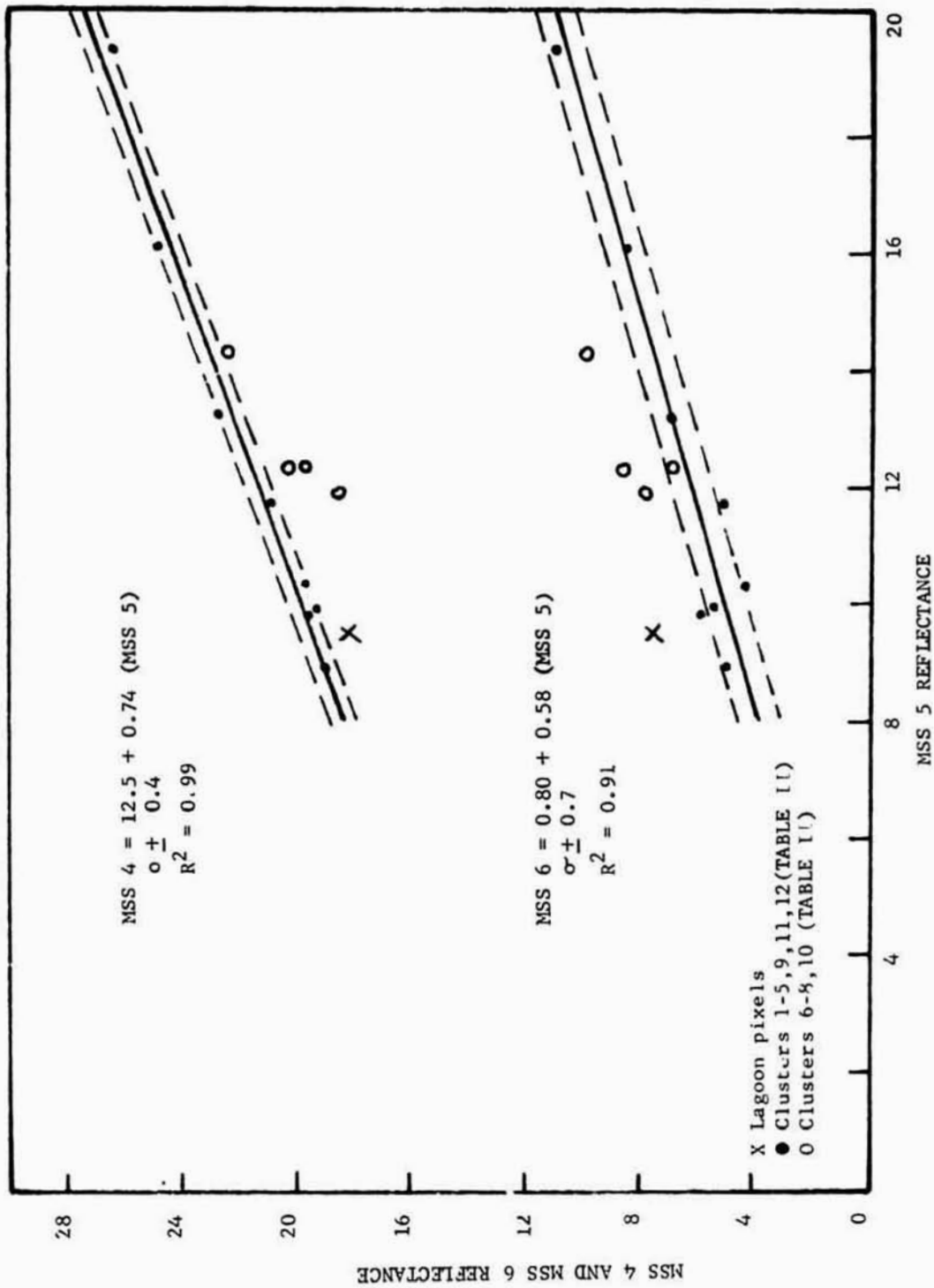


FIGURE 9. MEAN CHOPTANK RIVER CLUSTER SIGNATURES



MSS 5 = 4



MSS 5 = 5



MSS 5 = 6



MSS 5 = 7



MSS 5 = 8



MSS 5 = 9-11

Figure 10. Level Slicing MSS 5 at 64 Levels

REPRODUCIBILITY OF THE ORIGINAL PAGE IS POOR



MSS 6 = 1



MSS 6 = 2



MSS 6 = 3

Nuisance level
chlorophyll a

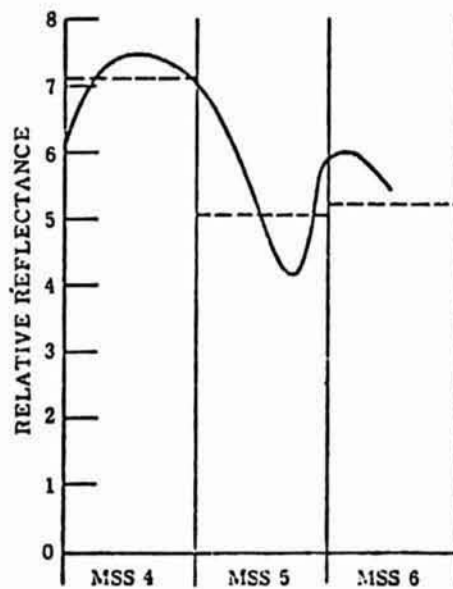


MSS 6 = 4



MSS 6 = 5-6

Figure 11. Level Slicing MSS 6 at 64 Levels

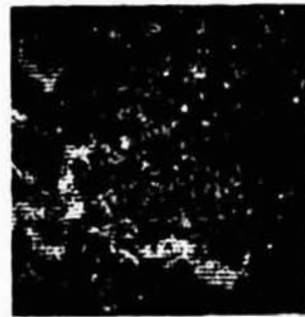


(a) Relative Reflectance of Algae in Surface Waters

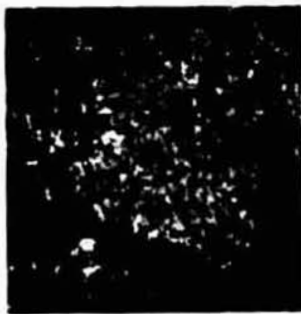
FIGURE 12. TYPICAL ALGAE REFLECTANCE CURVES IN AQUEOUS SUSPENSION [4]



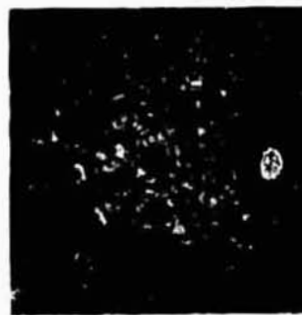
Cluster 1 + 2



Cluster 3 + 4



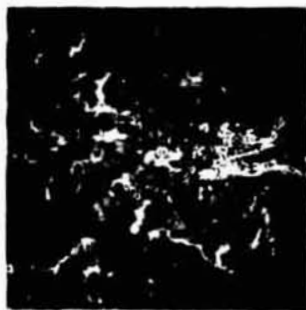
Cluster 5



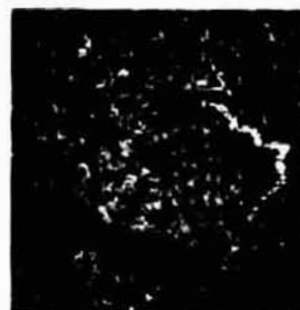
Cluster 6

Figure 13. October 10 River Clusters 1 - 6 Transferred to October 11 Scene at 64 Levels

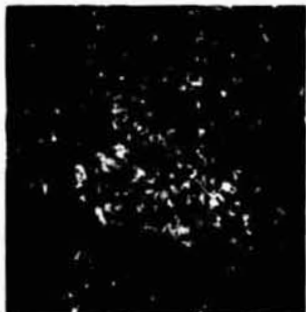
REPRODUCIBILITY OF THE
ORIGINAL PAGE IS POOR



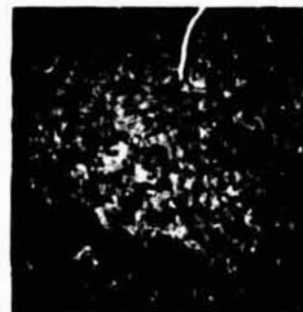
Cluster 7



Cluster 8



Cluster 9



Cluster 10

Figure 14. October 10 River Clusters 7 - 10 Transferred
to October 11 Scene at 64 Levels

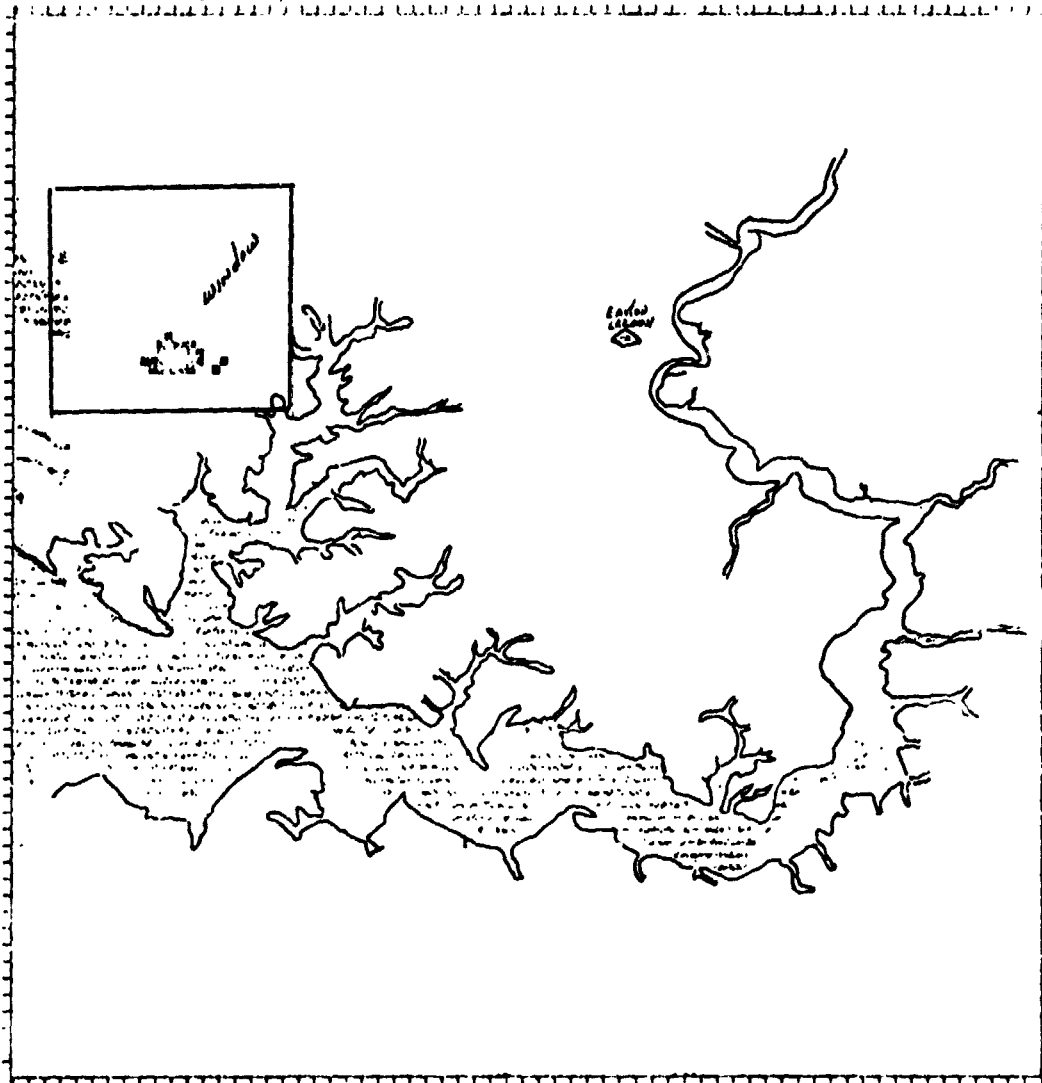


Figure 15. Results of Applying Multidimensional Easton Lagoon Water Signature to Total Choptank Surface Water Area

HYDROLOGIC LAND USE CLASSIFICATION OF THE PATUXENT RIVER WATERSHED USING
REMOELY SENSED DATA

W-13

By William C. Dallam, General Electric Company, Beltsville, Maryland,
Albert Rango, Hydrology and Oceanography Branch NASA/GSFC, Greenbelt, Maryland
and Lurie Shima, Earth Resources Branch NASA/GSFC, Greenbelt, Maryland

ABSTRACT

N76-17600

The Patuxent River Watershed is located in central Maryland between Baltimore and Washington, D.C. and is approximately 2330 km² in area and 175 km long. This region is now at a critical point because of major concerns such as water management and quality, flooding and land use within the watershed. Data from the NASA-directed LANDSAT and Earth Resources Aircraft Programs have been used to provide a new dimension in information collection and processing for the management of watersheds. Digital data from LANDSAT-1, ID number 1260-15201, were analyzed along with selected IR photography from U-2 flight number 74-060B taken 28 April 1974, which was digitized in three channels. Processing of the data was accomplished using a multispectral analysis system. Land use themes consisting of surface water, wetlands, forest, residential, cropland/pasture, urban, and extractive were developed and delineated through the watershed. Area measurements of watershed themes were obtained and will serve as a calibration input to a deterministic hydrologic model on a sub-watershed. Using the derived residential and urban theme areas from LANUSAT an estimated basin imperviousness was also calculated. Thematic maps were produced at 1:62,500 scale. The estimated cost of theme delineation was \$4.30/km². Floodprone areas were also classified and delineated at a scale of 1:24,000. Comparison with standard floodprone area maps at the same scale have indicated a few areas of discrepancy. Such information can be used for updating or checking floodprone area boundaries as well as monitoring changes in floodplain areas. This cooperative study has provided participating state and local agencies with remote sensing information as applied to hydrologic problems and has resulted in a technology exchange.

INTRODUCTION

The purpose of this study was to develop a series of objective hydrologic land use classifications of the Patuxent River watershed in Maryland primarily using LANDSAT (formerly ERTS) digital data to classify the basin area. This watershed survey should produce valuable statistical data to various state and local jurisdictions. Further, because the hydrologic land use themes are up to date and indicative of existing physical conditions, the data classifications are being used in the calibration of a numerical watershed model on the Western Branch watershed, a sub-basin of the Patuxent River. Such models are used to characterize the hydrologic behavior of a particular basin in planning or predictive purposes. The accuracy of theme classifications and area measurements were checked on the Western Branch watershed where LANDSAT data and high altitude U-2 color IR photography were available and ground truth surveys were conducted.

Associated with the hydrologic land use classification was an effort to delineate flood-prone areas adjacent to some of the major streams in the Patuxent River basin. In previous studies interpretation of LANDSAT imagery and high altitude photography has indicated that areas susceptible to flooding along river systems can be identified by the detection of various natural and artificial indicators on the floodplain (Ref. 1 and 2). Preliminary experience with LANDSAT digital data has indicated that the generation of floodprone area overlays at approximate scales of 1:62,500 and 1:24,000 is possible. Such products should be of value to local and state agencies for planning purposes. In order to physically explain the floodprone area

signatures that have been observed with remote sensing, known floodprone areas near Laurel, Maryland were selected for detailed study. An attempt was made to correlate the multispectral floodprone area classifications with vegetation, soils, and moisture data obtained by detailed ground surveys and low altitude photography. The possible extension of the floodprone area signatures thus derived were considered.

PATUXENT RIVER WATERSHED

The Patuxent is the largest intrastate river in Maryland (Ref. 3). It originates on Parrs Ridge at the junction of Howard, Montgomery, Frederick and Carroll counties and flows in a south-southeasterly direction for 175 kilometers (110 miles) to its confluence with the Chesapeake Bay (Figure 1). The main stream of the Patuxent River forms a boundary between Howard, Anne Arundel, and Calvert counties on the north and east, and Montgomery, Prince George's, Charles, and St. Marys counties on the south and west. The area of the Patuxent River watershed is approximately 2330 km² (900 mi²) and covers three distinct physiographic provinces.

The headwater region lies in the Piedmont Plateau within Howard and Montgomery counties and extends from the Frederick county line to the Fall Line at Laurel (Patuxent River) and Savage (Little Patuxent). The land in this region is primarily used for urban, residential, forest and agricultural purposes. Two reservoirs (Triadelphia and Rocky Gorge) are located in the region and provide for the water needs of approximately 1.2 million people. In this area stream valleys are relatively steep-sided with little if any floodplain. The floodplain that does exist is generally wooded.

The middle region of the watershed, starting from the Laurel/Savage area, is located in the Coastal Plain and extends approximately to the tidal zone at Wayson's Corner. The floodplain of the river and its tributaries in this region is characteristically broad, flat, low-lying and wet. The floodplain provides a continuous corridor of swamps and marshes, usually bordered by forested uplands. In this middle region of the watershed, land use is characterized by urban, residential and forested areas.

The lower part of the watershed drains into an estuary. In the vicinity of Wayson's Corner, the river enters an area of marshlands. The marshes are assumed to have been created by siltation from both natural causes and upstream agricultural and urban development. At Deep Landing, the Patuxent widens and deepens into a typical saline branch of Chesapeake Bay. The large marsh areas are replaced by bluffs, sometimes 20 feet high, with wide sandy beaches and rolling countryside.

In recent times, problems of flooding and water quality have become major problems within the watershed. At Laurel, the problems begin with Walker Branch draining the West Laurel area. This branch carries heavy sediment loads and suburban storm water during rainfall and discharges directly into the Patuxent. Laurel itself has developed on the floodplain of the river and suffers periodic flooding that has reached serious damage levels.

At the confluence of the main stem of the Patuxent with the Middle Patuxent, additional sedimentation is added to the river. Heavy silt loads, urban storm water and wastewater effluent carried by the Middle Patuxent from Howard and Anne Arundel counties joins the Patuxent. In this upper region of the watershed, the primary concern is the effect of urban development.

In terms of its future role as a unique natural resource in the Baltimore-Washington region, the Patuxent River has reached its most critical point. Basic commitments to protect the Patuxent have been accepted by the bordering counties. The State's concern for the river is indicative of the passage of "The Patuxent River Watershed Act and the Scenic Rivers Bill". To avoid future degradation of the river, cooperation and coordination is now needed between all agencies concerned.

It has been noted that more is known about the Patuxent watershed than any other estuary on the East Coast (Ref. 4) but more in-depth knowledge is needed before we can understand the way the watershed works as well as predict the probable effects of land use changes. It is through the use of watershed simulation models requiring inputs of physiography and land use that a better understanding of the runoff characteristics of the watershed may be achieved.

MULTISPECTRAL ANALYSIS

The digital processing for this study was performed using an interactive, multispectral image analysis system¹. This system is composed of the following principal components:

- input scanner unit
- image analyzer console
- image memory unit
- process controller (including peripherals)

A portion of a LANDSAT scene or digitized U-2 data were used to fill the system color display. Supervised training and classification were then performed on the four LANDSAT spectral bands or the three bands developed from digitizing the U-2 imagery.

Training sites were selected with an electronic cursor which is sized and positioned using a "joy-stick". The image analysis system's special purpose hardware identifies the spectral reflectance range of the training site in each specified band simultaneously. The minimum and maximum reflectance values in each band of the training area are used to define the limits of a 4-dimensional spectral parallelepiped. The picture elements of the displayed image are examined pixel-by-pixel. Pixels within the parallelepiped bounds are identified or "alarmed" on the color display. The user has the option of modifying the spectral signature through thresholding the parallelepiped boundaries. This procedure is known as single-parallelepiped training and classification.

PROCEDURES

Several LANDSAT-1 images were evaluated for use in the study. This evaluation considered the problem of cloud cover and the quality of the digital tapes. The scene selected, ID 1260-15201 (9 April 1973) depicted early spring in Maryland; foliage coverage is limited and surface moisture is abundant. The scene contained the total Patuxent River watershed. In addition to the LANDSAT-1 data, a NASA high altitude U-2 image dated 28 April 1974 was selected for the same area.

On a color composite of ID 1260-15201, study areas were outlined at full and half resolution. Full resolution is defined as sampling and displaying every LANDSAT-1 pixel for every display element (1:1). Each full resolution display (working scene) covers an area of approximately 839 km² (324 mi²). Half resolution is defined as displaying four equivalent display elements for each LANDSAT pixel. This covers approximately 216 km². Coordinates of these outlined areas were applied during machine processing to construct working scene files from the LANDSAT-1 CCTs.

Starting at the upper portion of the watershed, the first working scene "PAT1" was constructed (Figure 2). Consecutive working scenes were developed, each scene having an overlap area with the previous scene. This overlap was designed to eliminate the possible loss of data. Each working scene was corrected for earth rotation. All working scenes defining the total watershed were constructed at 1:1 resolution. Working scenes for the Western Branch drainage basin and for floodplain delineation studies, however, were constructed at half resolution. Working scenes using U-2 aircraft data were also constructed for Western Branch and the floodprone areas.

¹General Electric IMAGE 100 System

Theme development began with displaying a working scene containing particular training sites. A training site is a spatial area consisting of one object which is used as a data base for classification. The system cursor is located enclosing the known object and a multi-spectral signature is extracted. A multispectral signature is defined in four dimensions, that is, one for each LANDSAT-1 MSS channel. In each dimension, a lower and upper limit is defined resulting in a multidimensional parallelepiped. The classification of the working scene was performed after completion of signature acquisition.

Where modifications were required, two methods were used. The first method was the selection of a new training site. The signature extracted from the new site can be combined with the original or used separately. The second method was to arbitrarily adjust the limits of the histograms of the four MSS channels for the original multispectral signature.

Histograms and limits were recorded for all signatures after development and verification. Other working scenes were displayed, and the limits of the already developed signatures were inputted and modified where necessary. The transferring of signatures in this manner enabled themes to be mapped through seven working scenes covering the entire watershed.

The interactive system allows the masking of irregular shaped areas within a working scene. Therefore, boundaries of the watershed were defined using the system software capabilities. By the manipulation of the theme tracks of the interactive system, themes outside the watershed boundaries were masked. Area measurements of themes exclusively within the watershed boundaries were thus obtained.

RESULTS

The major concern of the study was to provide a precise inventory of land use to help determine the flow of runoff to the Patuxent River. The land use categories (themes) assumed to have significant impact on the hydrologic behavior of the watershed were:

- surface water
- wetlands
- total forest
- residential
- urban/commercial
- bare fields
- cropland/pasture
- extractive (e.g. gravel pits)

Additional subclassification of surface water and the separation of total forest into coniferous and deciduous forests was accomplished. The themes listed above correspond to the general categories of watershed land use as stated in Ref. 5, i.e., (1) non-vegetative, (2) non-herbaceous lowland vegetation and, (3) herbaceous upland vegetation. In the sub-division of the third class a difference is derived due to percent of cover of fields. The bare field theme is the same i.e., less than 10% cover. The cropland/pasture theme assumes the combination of cover from 10% to 100%.

Themes relative to the watershed boundaries were possible by digitizing boundary maps through the interactive system scanner. This was accomplished by superimposing the themes over the digitized maps. The digitized maps also served as guides in the development of a watershed theme. Area measurements of the land use themes for the Western Branch watershed were obtained using both LANDSAT and digitized U-2 data as shown in Figures 3 and 4.

In Table 1 a summary of the area measurements for Figures 3 and 4 are shown. In general, measurements using LANDSAT data have higher values than values derived from U-2 digitized data. Factors accounting for the deviations include the fact that because the U-2 data possess a higher resolution than the LANDSAT data, more specific land use classes can be delineated, and, as a result, the total area of each individual U-2 class will potentially be less than the corresponding LANDSAT class. Additionally, the U-2 data were acquired more than one year

later than the LANDSAT data and also about three weeks later in the month of April. As a consequence, seasonally changing land cover can logically be expected to vary. For example, LANDSAT bare fields and cropland/pasture themes total 18.1 and 15.5%, respectively, on 9 April 1973 and U-2 bare fields and cropland/pasture total 13.5 and 17.4%, respectively, on 28 April 1974. Even with these differences, the arithmetic average of the deviations of the theme area measurements derived from LANDSAT and U-2 data sources is only about 2% of the watershed area. Using LANDSAT data, over ninety percent (90%) of the Western Branch drainage basin was classified. This same percentage was applicable throughout the entire Patuxent watershed. In general, the remaining areas unclassified were agricultural or open areas possessing slightly different multispectral signatures than the eight basic themes. These remaining areas were not readily incorporated into the basic themes using the single parallelepiped classification system.

An important factor usually required by most hydrologic models is an estimate of the percent of imperviousness of a watershed. Using data and techniques from Ref. 6 and Ref. 7, respectively, an estimate of percent of imperviousness of 5.0% for the Western Branch drainage basin was obtained. The technique used the percentages of LANDSAT residential and urban themes (12% and .25%) and weighting factors of 40% for residential and 90% for urban. The percentage imperviousness was calculated by

$$(12.)(.4) + (.25)(.9) = 5.0\%$$

The corresponding imperviousness for the U-2 data for Western Branch was 4.7%.

Three training sites were selected to develop the multiband floodprone theme. Ground truth surveys in these sites have shown this theme to have the combined spectral reflectance of standing water or wet soils and dormant deciduous bottomland trees. This floodprone theme on both LANDSAT and U-2 data was referenced to a digitized standard USGS floodprone area boundary map as shown in Figure 5. Figure 6 shows the U-2 derived floodprone theme without the boundary map. When this theme was extended to another working scene and compared to the appropriate floodprone map in Figure 7, the visual correlation was good. Some major areas of discrepancy within the floodprone boundaries were field checked and estimated to be not floodprone on the basis that they did not flood during the greater than 100 year flood event produced by Hurricane Agnes in 1972. The particular areas checked were a golf course near Laurel, Maryland and open areas protected from flooding by elevated roads in the Patuxent Wildlife Center. Areas outside the floodplain having combinations of surface water, moist soils, and dormant vegetation similar to the floodprone areas will be detected as possessing the floodprone signature as can be seen in Figure 5 and must be considered separately.

CONCLUSIONS

Significant land use categories consisting of water, wetlands, forest, residential, urban, bare fields, cropland/pasture and extractive relative to the Patuxent River watershed were developed and classified into themes. Application of the themes throughout the watershed have resulted in over ninety percent (90%) area classification. Distribution of these themes has been illustrated photographically at a scale of 1:62,500. Assuming the watershed area to be 2330 km², the approximate cost of theme mapping the watershed using LANDSAT data was \$4.30/km² based on the rate of \$250/hour for the interactive system employed plus manpower and photographic processing costs.

Comparison of results using LANDSAT and digitized U-2 data for theme mapping the Western Branch sub-basin show an average theme area deviation of about 2%. In general, LANDSAT data yield larger theme areas than U-2 data because of differences in resolution and date of data acquisition. Using the derived residential and urban theme areas from LANDSAT an estimated basin imperviousness of 5% was obtained.

Delineation of a floodprone area theme using both LANDSAT and U-2 data has also been accomplished for the watershed. This theme was transferred to digitized USGS 1:24,000 scale floodprone boundary maps. On a regional basis this theme can be used for updating or checking floodprone areas as well as monitoring developmental changes.

Substantial savings in data collection and processing have been achieved using LANDSAT information and machine processing. State and local agencies have participated and are currently evaluating results. This satellite assisted land use classification is considered economical and provides current data for the operation of hydrologic models used for predicting watershed runoff response.

REFERENCES

1. Rango, A. and A. T. Anderson, Flood Hazard Studies in the Mississippi River Basin Using Remote Sensing, Water Resources Bulletin, Vol. 10, No. 5, pp 1060-1081, 1974.
2. Harker, G. R., The Delineation of Floodplains Using Automatically Processed Multispectral Data, Technical Report RSC-60, Texas A&M University, Remote Sensing Center, College Station, Texas, 227 pp, 1974.
3. Maryland Environment Service, The Patuxent River Basin Water Quality Management Plan, Vol. 1, State of Maryland, draft April 1974.
4. Marsh, L., The Patuxent: Our Forgotten River, Washington Star-News, p 12, August 19, 1973.
5. Wagner, T. and Rebel, D., An ERTS-1 Investigation for Lake Ontario and Its Basin, Final Report, NAS 5-21783, NASA, Goddard Space Flight Center, Greenbelt, Maryland 113 pp., April 1975.
6. Soil Conservation Service, U.S. Department of Agriculture, Urban Hydrology for Small Watersheds, Technical Release No. 55, p 2-5, January 1975.
7. Ealy, C. D., Ragan, R. M., and McCuen, R. H., Resource Identification Studies on Urban Watersheds Using Anacostia River Basin as An Example, Progress Report NSG5017, NASA, Goddard Space Flight Center, Greenbelt, Maryland, January 1975.

UPPER WESTERN BRANCH DRAINAGE BASIN												
THEMES	DATA SOURCE											
	LANDSAT					U-2 Imagery						
	Pixels ^a	Hectares	Mi ²	%*	Elements ^b	Hectares	Mi ²	%*	Elements ^b	Hectares	Mi ²	%*
Urban	39.7	18.3	.07	.25	6.3	.8	.003	.09	96.	7.8	.03	.13
Water	50.5	23.3	.09	.32	9469.	759.6	2.93	13.5	26867.	2151.4	8.3	38.4
Bare Fields	2848.4	1296.6	5.00	18.1	12184.	1177.9	4.5	17.4	7933.	648.0	2.5	11.4
Total Forest	7015.5	3193.6	12.3	44.5	56543.	5443.2	21.0	81.0	69886.	6713.3	25.9	
Cropland/Pasture	2452.3	1116.3	4.3	15.5								
Residential	1897.5	863.8	3.3	12.0								
Total Themes	14264.	6493.3	25.1	90.4								
Watershed	15784.	7185.2	27.7									

* % of watershed

LANDSAT Data: ID1260-15201 (9 April 1973)

U-2 Imagery: 28 April 1974

^c Effective pixel size 79.2m X 57.5m

^b Effective element size 34.7m X 34.7m

TABLE I

LANDSAT AND U-2 IMAGERY DATA AS SOURCES FOR UPPER WESTERN BRANCH DRAINAGE BASIN LAND-USE AREA MEASUREMENTS

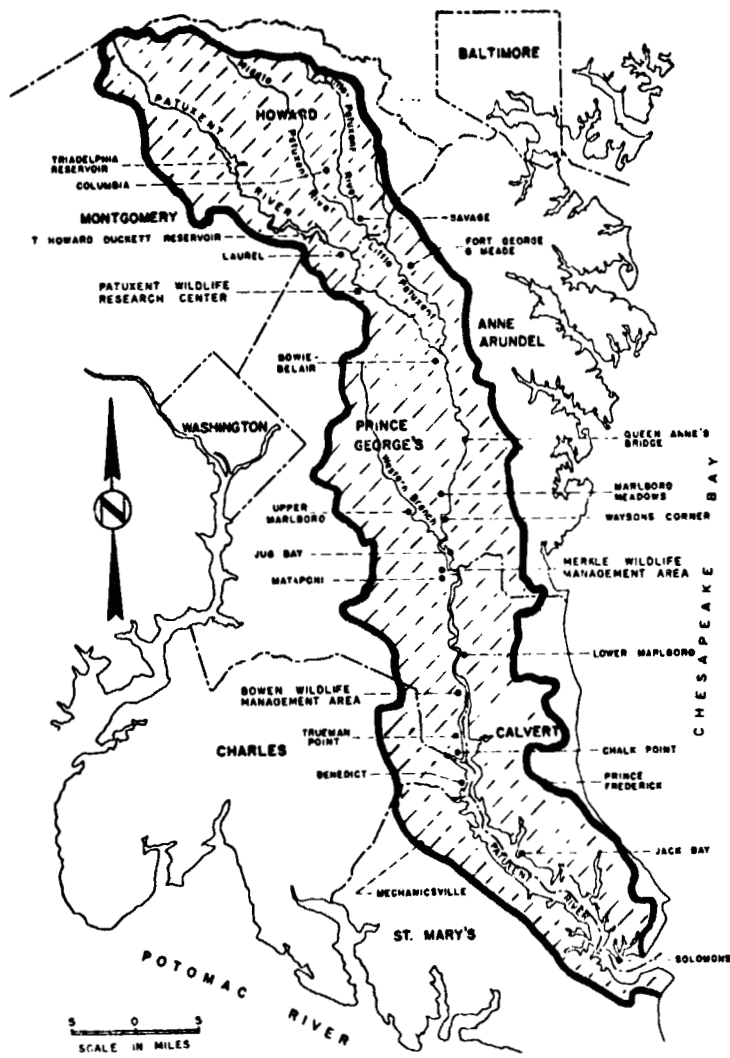


FIGURE 1
PATUXENT RIVER WATERSHED

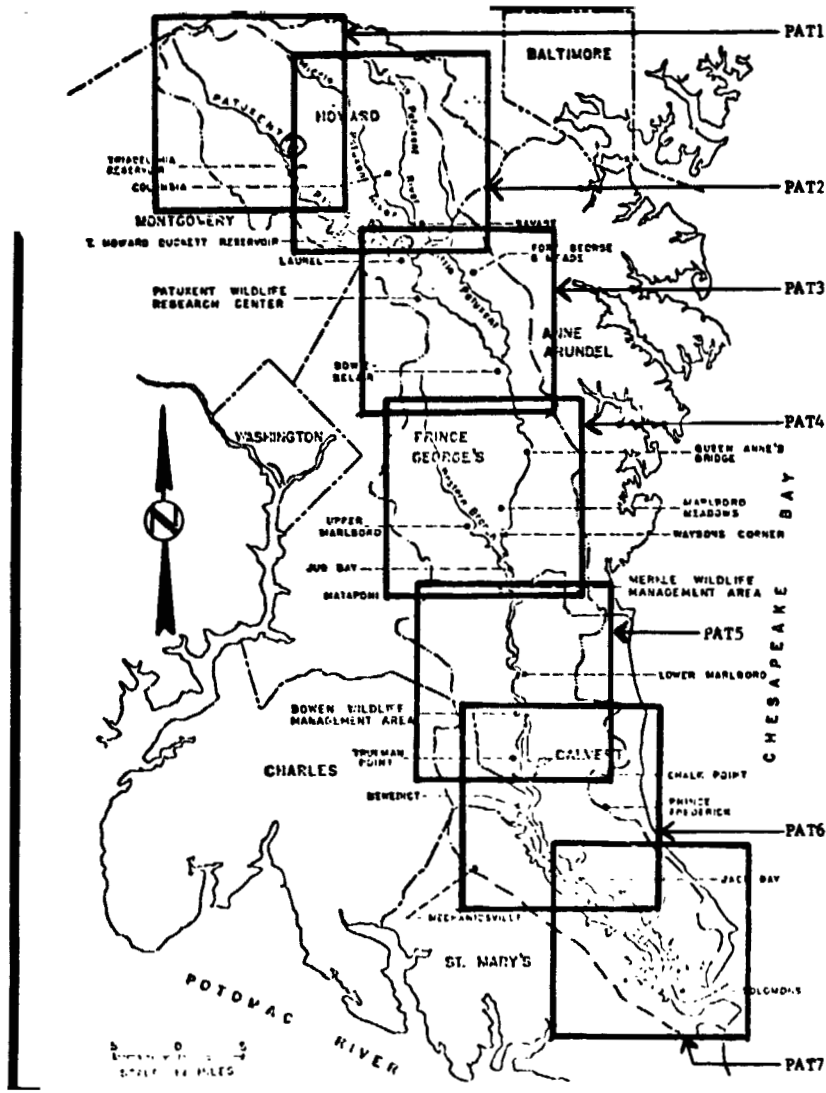


FIGURE 2
PATUXENT RIVER WATERSHED WORKING SCENES

R

REPRODUCIBILITY OF THE
ORIGINAL PAGE IS POOR



Figure 3.- LANDSAT Working Scene, Half Resolution, Upper Western Branch
Drainage Basin, Distribution of Land-Use

Yellow	: Forest
Dark Blue	: Bare Fields
Light Blue	: Residential
Pink	: Cropland/pasture
Gray	: Urban
Red	: Water

REPRODUCIBILITY OF THE
ORIGINAL PAGE IS FOUR

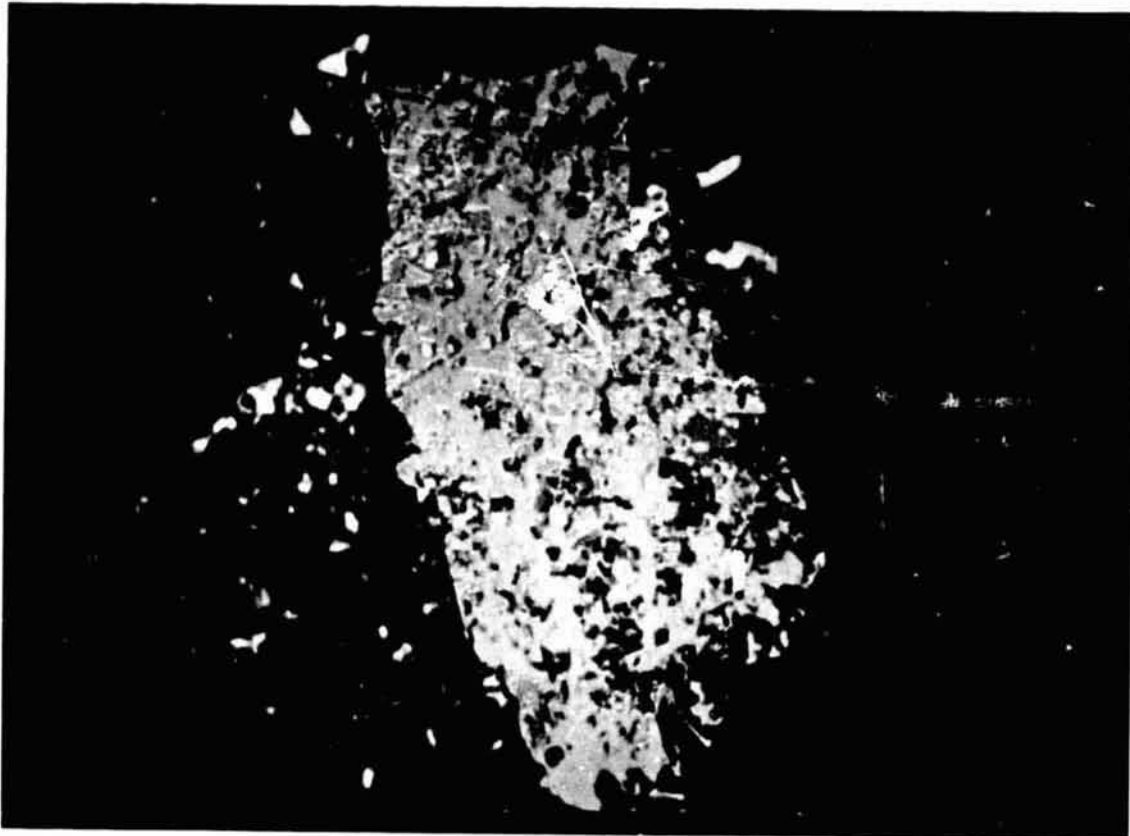


Figure 4.- U2 Digitized Data, Working Scene Upper Western Branch Drainage
Basin, Distribution of Land Use

Yellow	: Forest
Dark Blue	: Bare Fields
Pink	: Residential
Gray	: Urban
Purple	: Cropland/pasture

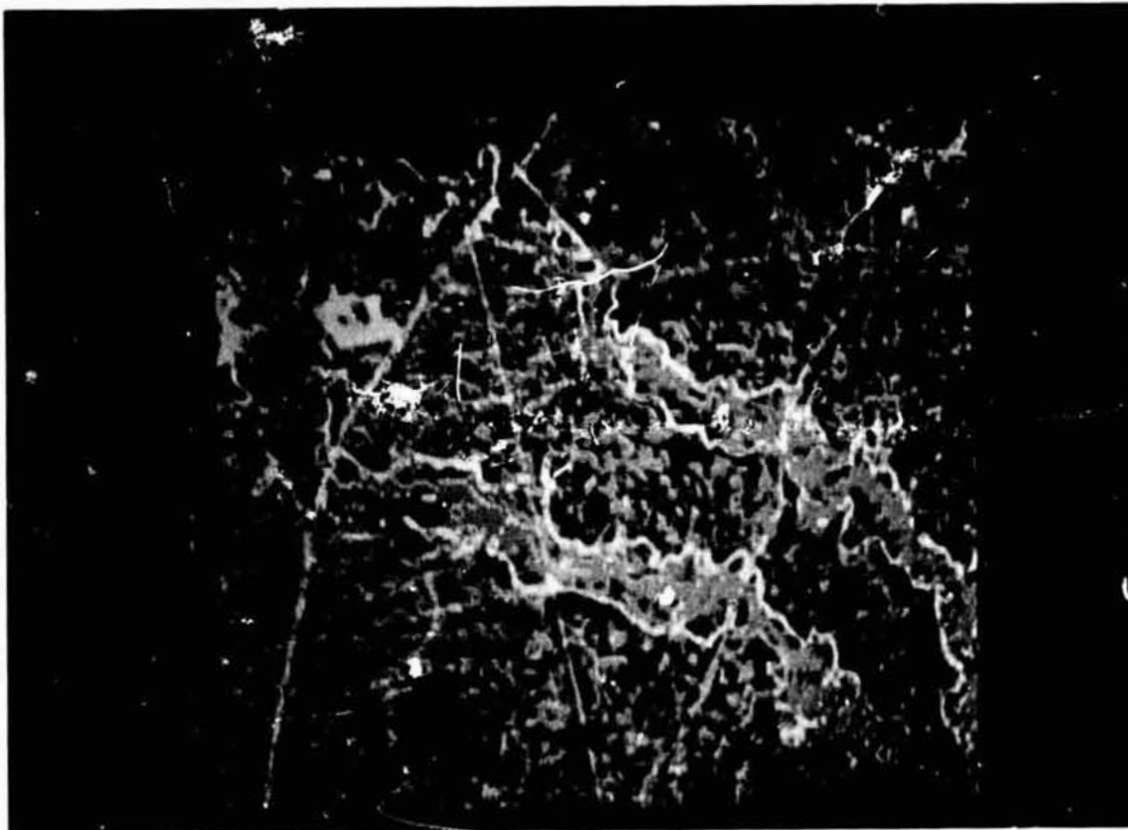


Figure 5.- LANDSAT Working Scene, Half Resolution, Flood-Prone Area Theme with Digitized Flood-Prone Boundary Map, Laurel Maryland

Yellow : Flood-prone theme

REPRODUCTION QUALITY OF THE
ORIGINAL PAGE IS POOR

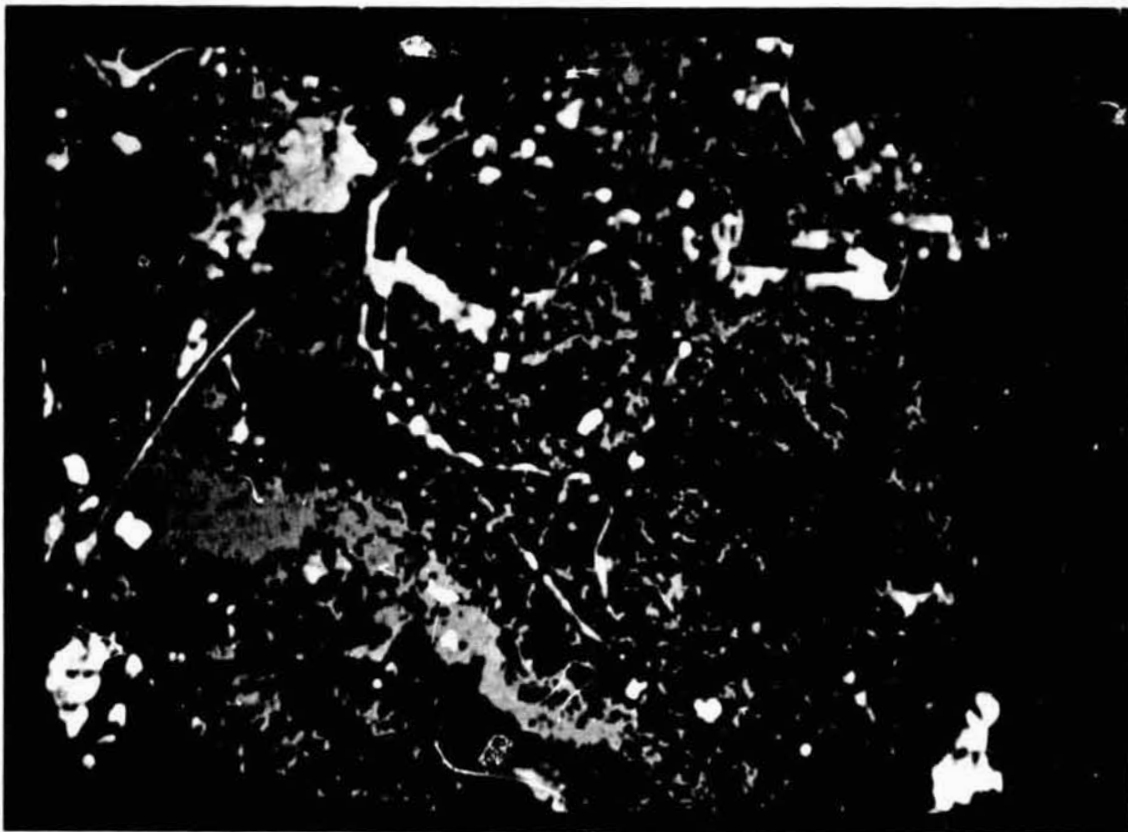


Figure 6.- U2 Digitized Data Working Scene, Flood-Prone Area Theme, Laurel Maryland

Yellow : Flood-prone theme

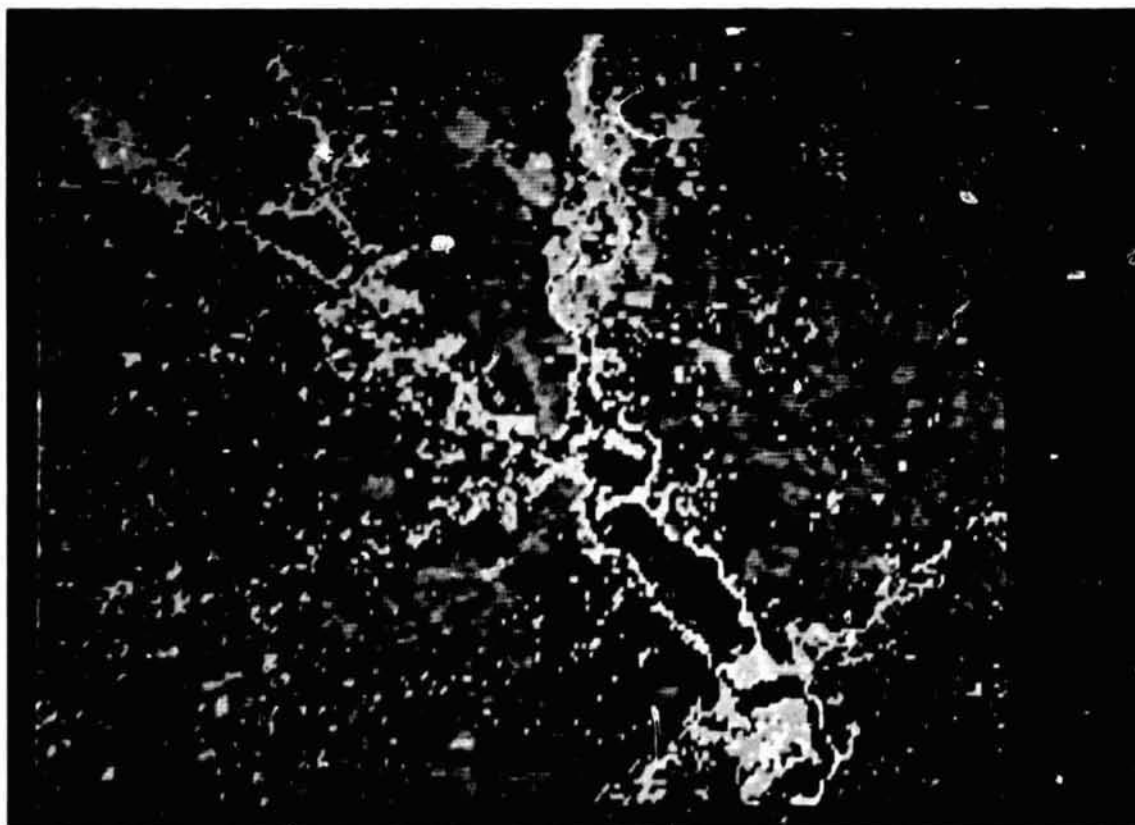


Figure 7.- LANDSAT Working Scene, Half Resolution, Flood-Prone Area Theme
Extended to Jug Bay Region

Yellow : Flood-prone theme
Dark Blue : Water
Red : Pine

LAND USE CLASSIFICATION FOR HYDROLOGIC MODELS USING INTERACTIVE
MACHINE CLASSIFICATION OF LANDSAT DATA

W-14

Thomas J. Jackson, Robert M. Ragan, Richard H. McCuen
Civil Engineering Department, University of Maryland
College Park, Maryland 20742

ABSTRACT

N76-17601

Models designed to simulate the hydrology of urban areas require input parameters describing the land use and degree of imperviousness of the watershed. Unfortunately, the magnitude and spatial distribution of these parameters are rather difficult to estimate when a large watershed is involved. Trade-offs between accuracy of the model parameters and the time or money available for their determination must be made. Because of the necessity of such trade-offs, a study was developed to investigate the use of computer aided analysis of LANDSAT multispectral data in estimating percent of imperviousness and associated land uses needed in urban hydrologic modeling. An interactive computer was used to delineate seven land use classifications in the 342 sq. km. Maryland portion of the Anacostia River Basin from LANDSAT data. These results compared favorably with those of an earlier study which obtained the same information through analysis of aerial photographs having a scale of 1:4800. Approximately 94 man days were required to complete the land use analysis using the aerial photographs while less than three man days were required to accomplish similar tasks using the LANDSAT data.

INTRODUCTION

Traditionally the planning and design of Urban Drainage Systems focused on the simple objectives of removing runoff from an area as quickly and as efficiently as possible. Today, socio-economic and water quality considerations require that planning and design be conducted within the framework of an overall stormwater management system. Consideration must be given to the protection of downstream land uses through such innovations as on-site detention storage, adjusting the timing of runoff through channel modification, and provisions for minimizing changes in water quality. These more sophisticated design and planning requirements have led to the development of a number of computer-based mathematical models intended to simulate both the quantity and quality of runoff from urban areas. These models vary in their structure and some are considered primarily as planning tools while others are much more detailed and intended for design purposes. Regardless of the particular structure of the model, all require land use information that is translated into hydrologic parameters needed as inputs.

Percent of imperviousness is perhaps the most important of these hydrologic parameters because it is an indication of the proportion of the drainage area from which surface runoff contributes directly to increased runoff rates in downstream areas. In an urban area, the percent of imperviousness reflects the fraction of the watershed that is covered by paving, roof tops, etc.

One common approach in estimating imperviousness is to delineate the various land uses from a map or aerial photograph and assign an average imperviousness to each based on surveys such as that conducted by Stankowski (1). Planimetry of the paved areas and roof tops from aerial photographs is perhaps the most accurate, but also the most time consuming and expensive approach to the problem. The accuracy of planimetry is not required when the relatively low accuracy of the other model inputs is considered.

Unfortunately, development of land use information and its translation into model parameters is a difficult and time consuming task, especially when a large watershed is involved. It is not uncommon for this phase of a study to require more man-hours than running the model and interpreting its results. Thus, trade-offs between accuracy of the model parameters and the time or money available for their estimation must be made. Because of the necessity of such trade-offs, a study was developed to investigate the problems associated with the use of satellite data in estimating percent of imperviousness and other information of importance in urban hydrologic modeling. Specifically, the use of computer aided analysis of data collected by the Multispectral Scanner sub-systems (MSS) on LANDSAT was studied. The distribution of imperviousness and associated land uses for the 342 sq. km. (132 sq. mile) Maryland portion of the Anacostia River Basin were estimated from the LANDSAT data. These results were then compared with those of an earlier study that obtained the same information through analysis of aerial photographs having a scale of 1:4800.

LARGE SCALE AERIAL PHOTOGRAPHIC STUDY OF ANACOSTIA RIVER BASIN

During the period July 1972 through August 1973, the Department of Civil Engineering of the University of Maryland conducted a resource identification study of the Anacostia River Basin for the Maryland Department of Natural Resources (2). The Anacostia joins the Potomac River in the southern part of Washington, D. C. A part of the Anacostia study was concerned with the identification of land use through interpretation of 1:4800 aerial photographs taken in 1971 and 1972. The approach was to lay out a rectangular grid on transparent mylar to represent an array of 610 meter (2000 ft.) square data cells. At this scale, each data cell was a 127 cm (5 in.) square and contained 100 sampling points at 1.3 cm (0.5 in) centers. Ten land use categories directly under each sampling point were identified. The ten categories were:

1. single family detached dwelling units
2. multi-family dwelling units
3. commercial or industrial structure
4. parking lot
5. street or highway
6. forested land
7. agricultural land
8. grass
9. contributing water body
10. non-contributing water body

The percentage of a data cell devoted to a given land use was determined from the number of sampling points covering that particular classification. Categories 1-5 contributed to the imperviousness of the watershed. The percent of imperviousness of a data cell was estimated from the number of sampling points it contained that were classified as categories 1-5. The average imperviousness of the watershed was found to be 23.5%.

Land use under the 92,400 sampling points in parts of 929 data cells was tabulated. This information was punched onto cards for computer aided statistical analysis and mapping using the SYMAP routine on a UNIVAC 1108. Column 2 of Table I shows the distribution of land uses in the Maryland portion of the 1:4800 Anacostia River Basin as estimated from the aerial photographs.

LAND USE DELINEATIONS FROM LANDSAT COMPUTER COMPATIBLE TAPES

A Multispectral Scanner senses a portion of the electromagnetic energy reflected or emitted by features on the earth's surface. The LANDSAT MSS separates the energy it receives into four spectral bands, green through near infrared. Energy detected in each band is converted to digital form and transmitted to ground receiving stations which

record the data on computer compatible tapes (CCT). The smallest area on which the energy is integrated and measured is termed a "pixel". In the LANDSAT System a pixel covers an area of approximately 1.13 acres.

Initial phases of the Study showed that use of photographic images of LANDSAT scenes could not provide the information needed for urban hydrologic models (3). Data on the CCT can be better utilized in the urban environment if the tape is loaded into a computer that has been programmed to accept and analyze LANDSAT MSS data. The computer is not only able to store all of the information available on the CCT, it is also programmed to aid the user in classifying features and land uses.

One approach in computer classification is directed toward automatic procedures that delineate, with minimal human intervention, areas having a particular land use. A second approach, the one used in the present study, is interactive. This latter approach centers on the user defining a training site on the scene displayed from the CCT on a color cathode ray tube (CRT). The training site encloses the pixels representing an area whose land use is known from ground observations or aerial photography. At least two alternate areas with the same and slightly different land uses are also located. The computer then assigns a false color to all pixels in the scene that have the same spectral characteristics as those enclosed in the training site. By examining alternate areas for which ground truth is available, the user is able to modify the pixel range to better define the areas of the scene that are devoted to the particular land use under investigation.

The interactive computer used in the study¹ was located in Beltsville, Maryland. The approach was to display a four band composite of the April 9, 1973 scene of the Washington, D.C. area on the color CRT at a scale of approximately 1:100,000. Training sites and alternate areas were determined by examination of a 1:24000 enlargement of a high altitude color infrared photograph taken with a NASA U-2 aircraft.

Two sessions with the interactive computer were used in the study. During the first, the entire scene shown as Figure 1 was classified. In two hours of computer time, seven land uses were delineated. These classifications were: 1) commercial-industrial-large parking lot; 2) recent residential; 3) old residential; 4) forested; 5) sand and gravel operation (extractive); 6) grass land; and 7) wetlands. Only the first three categories were considered to contribute to the imperviousness of the watershed.

The terms old and new residential are chosen for convenience. The old residential type is primarily single unit housing with weathered roofing and moderate foliage cover, it is referred to as old because the characteristics are typical of pre-1950's developments. The new residential is single and some multi-family housing with more reflective roofing and little foliage cover. The characteristics of the new residential class are typical of most recent housing projects.

Thirty-five mm color slides were made of the various classified land use distributions displayed on the computer CRT. These were then projected onto 1:100,000 base maps of the Anacostia River Basin so the land uses could be outlined. It was necessary to project onto small portions of the watershed map at a time because of distortions created by photographing the curved surface of the CRT.

Subsequent examination of the alphanumeric printout from the computer revealed that a significant number of the pixels in the scene had not been classified. This problem is attributed to the optics of the color CRT. The screen displays light colors that "bloom"

1. General Electric IMAGE 100

on a dark background to give an illusion of complete coverage.

A second session was then conducted on the interactive computer. During the interim between the two sessions, a screen projector had been added to the hardware of the computer. A transparent map of the Anacostia River Basin was loaded into the projector and overlaid onto the color CRT display of the LANDSAT scene. A cursor was then used to isolate the watershed from the rest of the scene. This second session, which required less than one hour, resulted in the classification of 93% of the pixels within the watershed. The resulting land use distribution was displayed on the CRT as shown in Figure 2.

By isolating the watershed from the rest of the scene, a listing of the pixel counts assigned to each class could be used to determine the percentages devoted to the various land uses. The distribution of the land use obtained from the pixel counts is shown as Column 3 of Table I.

The results of the second session agree quite well with those of the first. Recalling that the first session used the "blooming" to fill in unclassified pixels and that the second session result was close to 100% classified the close agreement is interesting.

Estimating the percent imperviousness from the LANDSAT data was based on the assignment of a representative imperviousness to the contributing classifications. Areas classed as commercial-industrial-parking lot were assumed to be 90% impervious. A 50% imperviousness was chosen to represent the recent residential land use. This value was selected after examining several data cells from the 1:4800 aerial photographs that included both single and multi-unit recent housing. The imperviousness of these cells varied between 45% and 50%. Similar cells encompassing old residential land use gave imperviousness between 35% and 47%. An imperviousness watershed of 40% was chosen to represent the old residential housing classification. The imperviousness based on the pixel counts assigned to the three contributing land use classes was 25.5%.

An areal distribution of the imperviousness within sub watersheds was developed from a grid delineating 610 m (200 ft.) squares laid out on transparent mylar and overlaid on a 1:100,000 map. The LANDSAT land use distributions had been drawn on the map. The portion of each cell occupied by the three land uses contributing to imperviousness was determined. This is a routine widely used by urban and regional planners to determine percentages devoted to various land uses. As an example, suppose a particular cell was occupied by 50% recent housing, 20% old residential, and 10% industrial-commercial land use. The remaining forty percent is distributed among classifications 4-7. The percent imperviousness in this particular grid square would be estimated on a weighting basis as

$$.3(50) + .2(40) + .1(90) = 32\%.$$

DISCUSSION OF RESULTS

The distribution of land uses from the two sources shown in Table I are in good agreement. Estimated imperviousnesses are 25.5% from LANDSAT and 23.5% from the large scale aerial photographs. Approximately 94 man days were required to complete the land use study using the 1:4800 aerial photographs. Less than three man days were required to accomplish similar tasks using the LANDSAT data. Although no records were kept concerning the computer time required to analyze and map the information obtained from the aerial photographs, it was several times greater than the interactive computer time needed for the LANDSAT approach.

The 342 sq. km. watershed land uses were defined by 92,400 sampling points on the 1:4800 aerial photographs and 68,885 pixels on the LANDSAT CCT. When dealing with such large sample sizes, it is not uncommon to be able to give a good estimate of the mean. In urban hydrology much smaller watersheds usually serve as the modeling elements. Because of

the need to model sub watersheds the distribution of the imperviousness within sub-areas of a watershed may be of more importance than the overall average. As a qualitative comparison, Figure 3 shows the distribution of percent imperviousness estimated from LANDSAT and the low level aerial photography. Each block represents the results obtained in the 610 m (2000 ft) square cell. The overall distribution appears to be good. Still, a cell by cell agreement can not be achieved because it was not possible, at the present time, to define the exact boundaries of the data cells from the aerial photograph sampling on the LANDSAT scene. Thus, a part of a land use included in one data cell in Figure 3a may be in one or more adjacent cells in Figure 3b.

In an effort to gain some insight into the effect of sub-watershed size on the agreement between the two approaches, a series of 25 paired data cell groups were selected from the numerical data which was used to prepare Figures 3a and 3b. First, 25 data cells, each representing 0.36 sq. km (0.14 sq mi), were randomly selected from the LANDSAT results. The corresponding 25 cells from the aerial photograph results were then located. Linear regression analysis of the 25 paired cells gave a correlation coefficient of 0.62. The process was repeated with sub-areas having 4, 9, 16 and 25 data cells each. These groupings of data cells corresponded to sub-areas of 1.48, 3.34, 5.93, and 9.30 sq. km. (0.57, 1.29, 2.29, and 3.59 sq. miles) respectively. The correlation coefficients and the standard error of estimates, as percent of imperviousness are presented in Table II.

Figures 4 and 5 are presented as a qualitative comparison between the LANDSAT results and those obtained by the U.S. Geological Survey (USGS) as part of the Census Cities Program. The USGS land use study involved aircraft as well as satellite sensors.

Figure 4 compares the industrial-commercial-large parking lot class of the LANDSAT study against the Livelihood Class of USGS. The USGS classification includes "Primarily Industry", "Extractive Industry", "Commercial" and "Services". There are several areas of disagreement. For example, the LANDSAT approach showed only the heavily impervious portions of a Commercial-Service area while the USGS might enclose a much larger area because they would include the grassed or wooded areas on the property. A particular case is the Naval Surface Weapons Laboratory. The LANDSAT approach showed only scattered pixel from the areas involving parking lots or buildings while the USGS enclosed the open space and a golf course on the property.

The LANDSAT approach also assigned highrise apartments and some dense town houses centering on large parking lots to the industrial-commercial-parking lot class. Such an assignment would be unacceptable in land use planning, but it is probably of little consequence in hydrology. The upper Northwest portion of the LANDSAT classifications on Figure 5 shows many pixels defined as residential. The USGS classed the Northwest portion above the dotted line in Figure 5b as "Agriculture with Residence". Thus, there is probably better agreement than one would initially suspect. The LANDSAT pixels classed residential were clusters of farm buildings, etc.

POTENTIAL USE IN URBAN HYDROLOGIC MODELING

Agreement between the results of the LANDSAT and 1:4800 aerial photographic studies on the Anacostia River Basin were good. It is believed that classification accuracy is sufficient for use in hydrologic planning models. As an example of what might be done, an examination of how LANDSAT data could be used in the recently developed Soil Conservation Services (SCS) Urban Hydrologic Model was undertaken.

Table III, reproduced from (4), is a matrix relating urban and non-urban land uses to a Curve Number, a form of runoff coefficient defined by the Soil Conservation Service. Present

techniques available for analysis of the LANDSAT CCT's are not able to differentiate among some of these SC's classifications. In an effort to substitute a classification scheme that would be consistent with LANDSAT capabilities, Table IV was developed. The curve numbers of Table IV were computed from those of the more extensive classification of Table III. "Grassed Open Space", for example, was considered to be an average of "Good Pasture", "Good Meadow", and "Good Condition Lawns, Parks, Golf Courses, etc.". Thus, for Soil Group A, the curve number was obtained as

$$(\text{Pasture (39)} + \text{Meadow (30)} + \text{Lawn-Parks (39)}) / 3 = 36.$$

Residential land use curve numbers were estimated by assuming the areas within this classification to be 40% impervious for the "Old" and 50% for the "New". These imperviousnesses are on the high side because of an inability to differentiate between single and multi-unit housing such as garden apartments. The "good" classifications of Table III were used to represent the pervious portions of each of the alternate classes of Table IV because it was assumed that urban land uses would generally be well managed.

The curve numbers obtained with Table IV agree quite well with all the examples included in (4). A comparison of the Table IV approach with the results of Example 2-3 that appears on pages 2-7 and 2-8 of (4) is presented as an Appendix.

CONCLUSION

Data collection expenditures should be reflective of the importance of the particular parameter in the urban hydrologic model. The Anacostia Study has shown that LANDSAT data interpreted on an interactive system is an effective method for determining the percent of impervious area and related land uses. Use of LANDSAT tapes to estimate percent of imperviousness for sub-watersheds at least as small as 1.5 sq. km (0.6 sq. mi) appears justified. A major advantage of the LANDSAT approach is the minimal man-hours required in comparison with an aerial photographic approach when working on large watersheds.

There are many instances where parameters are required as model inputs which LANDSAT may not be able to provide directly. In fact, it is doubtful that any single remote sensing platform can define all the input data needed for some models. In such cases prediction equations may be used to estimate those other parameter values.

REFERENCES

1. Stankowski, S. J., "Population Density as an Indirect Indicator of Urban and Suburban Land-Surface Modifications", U. S. Geological Survey, Prof. Paper 800-B, p 219-224, 1972.
2. Ragan, R. M., McCuen, R. H., Rebeck, H.C., and Otts, L. E., "Resource Identification Study of the Anacostia River Basin", Six Volume Final Report to Maryland Department of Natural Resources, Annapolis, Md., October, 1973.
3. Ealy, C. D., Ragan, R. M., and McCuen, R. H., "Resource Identification Studies on Urban Watersheds Using the Anacostia River Basin as an Example", Interim Report, NASA NSG 5017, January, 1975.
4. "Urban Hydrology for Small Watersheds", Tech Release No. 55, SCS-USDA, January, 1975.

TABLE I
PERCENT OF WATERSHED DEVOTED TO SPECIFIED LAND USE

1 Land Use	2 Large Scale Aerial Photo	3 LANDSAT
Forest	30.7	27.0
Industrial-Commercial-Parking Lot	4.9	6.5
Pasture-Gr s Park	8.5	10.4
Residential	44.9	43.5
Roadways	9.9	5.5
Extractive	N.C.	.4
Stream	1.0	N.C.
Pond or Pool	.1	N.C.
Unclassified Pixels	--	6.7

N.C. - Not Classified

TABLE II
AGREEMENT BETWEEN ESTIMATES OF
IMPERVIOUSNESS AS FUNCTION OF
SUB-AREA SIZE

Size of Sub-Area		Correlation Coefficient	Std. Error (% Imperviousness)
sq.mi.	sq.km.		
3.59	9.30	.93	5.29
2.29	5.93	.88	6.90
1.29	3.34	.88	7.20
.57	1.48	.83	8.33
.14	.36	.62	12.34

TABLE III - RUNOFF CURVE NUMBERS for SELECTED LAND USES

(Table 2-2, Pg. 2-5 of Ref. 4)

LAND USE DESCRIPTION	HYDROLOGIC SOIL GROUP			
	A	B	C	D
Cultivated land ^{1/} : without conservation treatment	72	81	88	91
: with conservation treatment	62	71	78	81
Pasture or range land: poor condition	68	79	86	89
good condition	39	61	74	80
Meadow: good condition	30	58	71	78
Wood or Forest land: thin stand, poor cover, no mulch	45	66	77	81
good cover ^{2/}	25	55	70	77
Open Spaces, lawns, parks, golf courses, cemeteries, etc.				
good condition: grass cover on 75% or more of the area	39	61	74	80
fair condition: grass cover on 50% to 75% of the area	49	69	79	84
Commercial and business areas (85% impervious)	89	92	94	95
Industrial districts (70% impervious)	81	83	91	93
Residential: ^{3/}				
Average lot size Average % Impervious ^{2/}				
1/8 acre or less 65	77	85	90	92
1/4 acre 38	61	75	83	87
1/3 acre 30	57	72	81	86
1/2 acre 25	54	70	80	85
1 acre 20	51	68	79	84
Paved parking lots, roofs, driveways, etc. ^{1/}	98	98	98	98
Streets and roads:				
paved with curbs and storm sewers ^{2/}	98	98	98	98
gravel	76	85	89	91
dirt	72	82	87	89

TABLE IV - RUNOFF CURVE NUMBERS FOR LANDSAT LAND USE DELINEATIONS

Land Use Description	Hydrologic Soil Group			
	A	B	C	D
Wood or Forest Land	25	55	70	77
Grassed Open Space	36	60	73	78
Commercial-Industrial-Parking Lot	90	93	94	95
New Residential	67	77	85	88
Old Residential	54	62	68	70

REPRODUCIBILITY OF THE
ORIGINAL PAGE IS POOR

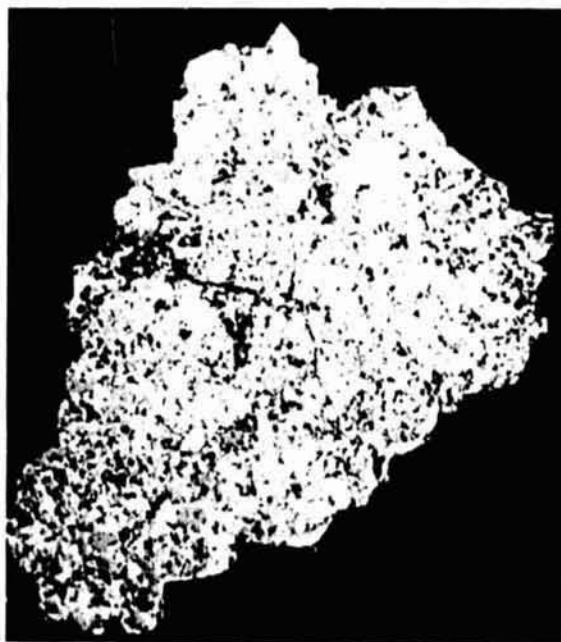


FIGURE 2
CRT DISPLAY OF ANACOSTIA RIVER
BASIN LAND USE CLASSIFICATIONS

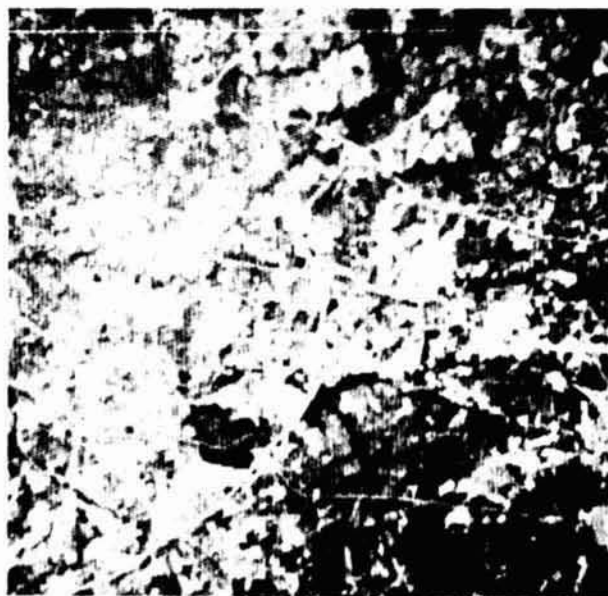


FIGURE 1
CRT DISPLAY OF APRIL 9, 1975
LANDSAT SCENE OF WASHINGTON, D. C. AREA

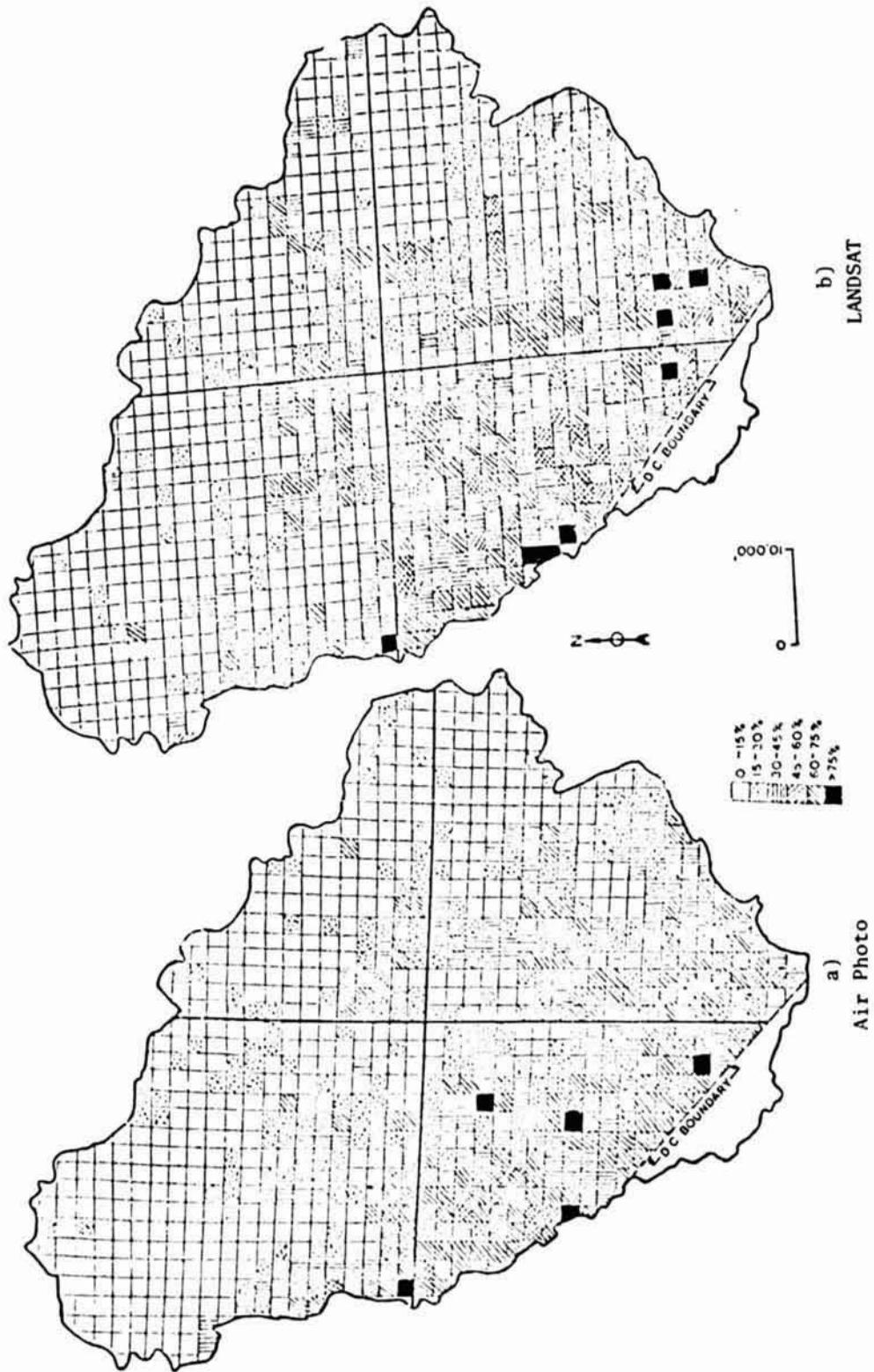


FIGURE 3
 DISTRIBUTION OF IMPERVIOUSNESS AS DETERMINED BY LANDSAT AND LARGE SCALE AERIAL PHOTOGRAPHS



a)
LANDSAT
Industrial - Commercial

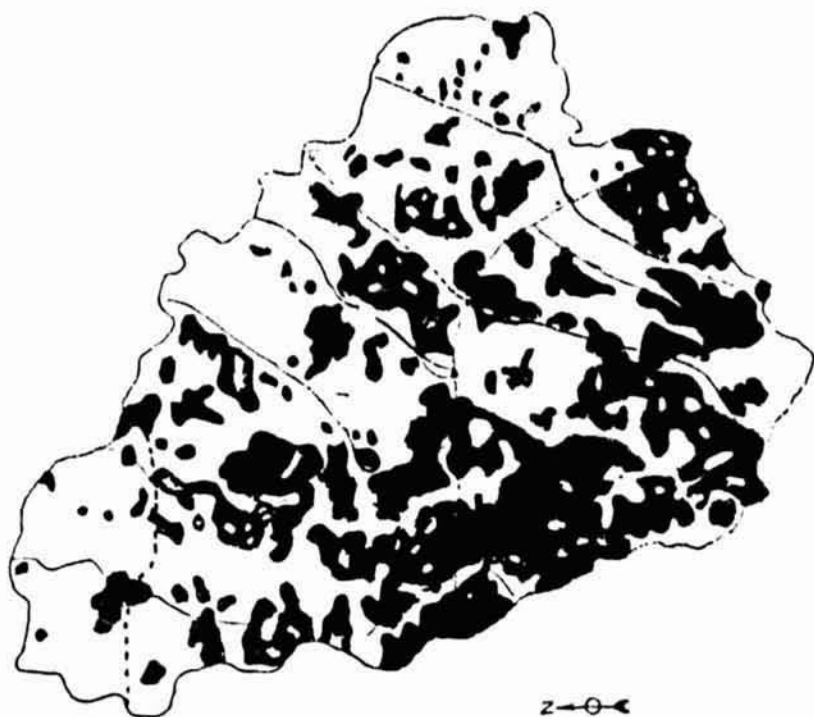


b)
USGS
Livelihood Classification

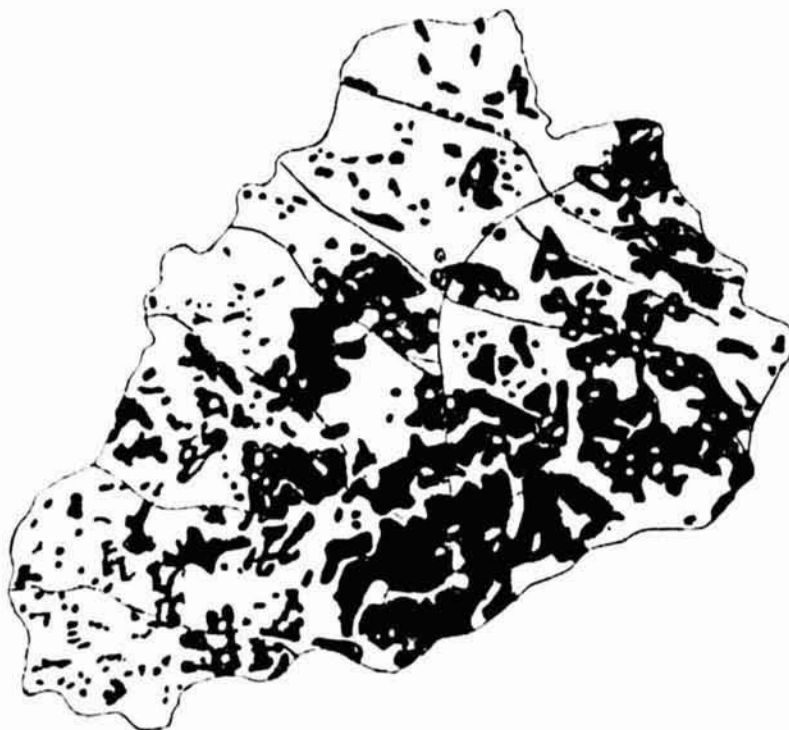


FIGURE 4

COMPARISON OF LANDSAT AND USGS CENSUS CITIES LAND USE DISTRIBUTIONS



a)
LANDSAT
Residential Classification



b)
USGS
Residential Classification



FIGURE 5
COMPARISON OF LANDSAT AND USGS CENSUS CITIES LAND USE DISTRIBUTIONS

APPENDIX

Comparison of Table III and IV Approaches to Curve Number Estimation

Example Problem 2-3, pages 2-7 and 2-8, SCS Tech Release Number 55 (4)

Compute the runoff curve number for a 1,000-acre watershed. The hydrologic soil group is 50 percent B and 50 percent C interspersed throughout the watershed. The land use is:

- a) 40 percent residential area that is 30 percent impervious
- b) 12 percent residential area that is 65 percent impervious
- c) 8 percent paved roads with open ditches
- d) 10 percent paved roads with curbs and storm sewers
- e) 16 percent open land with 50 percent fair cover and 50 percent good cover
- f) 14 percent parking lots, plazas, schools, etc. (all impervious)

Approach Using Table III

Land use	Hydrologic soil group					
	B			C		
	Pct.	CN	Product	Pct.	CN	Product
Residential (30 pct. impervious)	20	72	1,440	20	81	1,620
Residential (65 pct. impervious)	6	85	510	6	90	540
Roads with open ditches	4	89	356	4	92	368
Roads with curbs and sewers	5	98	490	5	98	490
Open land:						
Fair cover	4	69	276	4	79	316
Good cover	4	61	244	4	74	296
Parking lots, plazas, etc.	7	98	686	7	98	686
	50		4,002	50		4,316

Thus

$$\text{Weighted CN} = \frac{4,002 + 4,316}{100} = 83.18 \text{ (use 83)}$$

Approach Using Table IV

Categories a)-d) cover 70% of the watershed and would have all been classed as Residential: From Table IV $CN = (77 + 85)/2 = 81$

Category e) would be 16% Grassed Open Space

$$CN = (60 + 73)/2 = 67$$

Category f) would be Commercial-Industrial-Parking Lot

$$CN = 93$$

Weighted Curve Number

$$\begin{aligned} CN &= .7(81) + .16(67) + .14(93) = \\ &= 56.7 + 10.7 + 13 \\ &+ 80.4 \text{ (use 80)} \end{aligned}$$

REMOTE SENSING TECHNIQUES FOR PREDICT.
OF WATERSHED RUNOFF¹

W-15

Bruce J. Blanchard²
Texas A&M University
College Station, Texas

N76-17602

ABSTRACT

Hydrologic parameters of watersheds for use in mathematical models and as design criteria for flood detention structures are sometimes difficult to quantify using conventional measuring systems. The advent of new remote sensing devices developed in the past decade offers the possibility that watershed characteristics such as vegetative cover, soils, soil moisture, etc., may be quantified rapidly and economically.

Experiments with visible and near infrared data from the LANDSAT-1 multispectral scanner have indicated a simple technique for calibration of runoff equation coefficients is feasible. The technique was developed using data from a scene taken in a dry fall period. When tested on 10 watersheds in the Chickasha area, the technique using

¹Contribution from Texas A&M University, College Station, Texas, the Southern Region, Soil, Water and Air Sciences, Agricultural Research Service, USDA, in cooperation with the National Aeronautics and Space Administration; and the Oklahoma Agricultural Experiment Station, Stillwater, Oklahoma.

²Hydraulic Engineer, formerly of USDA-ARS, Chickasha, Oklahoma.

LANDSAT data produced more accurate runoff coefficients than conventional methods. The technique worked equally as well using a dry fall scene taken one year later over the same watersheds. The runoff equation coefficients were then predicted for 22 subwatersheds where flood detention structures had been built. Predicted values were again more accurate than the coefficients produced by conventional methods.

A similar approach has been used to relate passive microwave antenna temperatures to runoff equation coefficients by using data from the Passive Microwave Imaging System (PMIS) mounted in the NASA P3A aircraft. Eight highly instrumented watersheds in the Chickasha study area were used in this study. Results show runoff equation coefficients from these eight small watersheds were well related to average horizontal polarized microwave temperatures in the dormant season and also were related to differences in horizontal and vertical polarized temperatures in the growing season. Study of these data and the data systems indicate that passive microwave antenna temperatures may be more effective throughout the year for calibration of watershed runoff coefficients than systems using visible and near infrared light.

INTRODUCTION

Demands for water supply and protection against loss of life and property from floods have increased dramatically in recent years. Increased agricultural, urban, and industrial development projected for coming years indicates that the development of improved techniques for watershed management and flood control will be necessary in the next decade.

In order that natural rainfall can be used in a most beneficial way, it has become imperative that we control the water from the time it falls on the watershed surface until it leaves the drainage basin. To accomplish this, man has developed intricate computer programs for watershed management, applied improved techniques in agriculture, designed flood detention and flood control works, and implemented pollution-control programs. None of these can be effective without adequate prediction of runoff from watershed areas.

The improvement of present watershed management techniques is primarily dependent on improvement in watershed runoff prediction. There are two general types of watershed runoff prediction schemes. Empirical mathematical models have been used to predict flood flows from watersheds

since the early days of hydrology. Recently, due to the advent of large computers, more complex models to mathematically represent the entire hydrologic cycle over a period of time have been developed. Both the simple empirical storm runoff models and the more complex continuous models require, as input, one or more variables that are at present subjectively measured or simply estimated.

At our present state of the art in hydrology, both types of models are needed. When designing flood detention or flood control devices such as dikes or diversions, it may only be necessary to consider extreme hydrologic events. A simple empirical model for flood flow prediction may be all that is necessary to develop the design criteria and specify the size of structure needed. In other cases where watershed yield or water quality are of major importance, the added cost and difficulty of using a complex watershed model may be justified. Thus, both types of models are needed.

Simple models may require only one or two parameters to represent the state of the watershed surface, while the complex models may require as many as 20 parameters as input. Estimating these parameters from measurements on or near the watershed drainage area can be a major problem. Hydrologic measurements collected with conventional methods represent

a point in time at a point in or near a watershed. Extrapolating such measurements to a realistic measurement that is appropriate for part or all of the watershed drainage area is difficult and leads to errors in the prediction of runoff by either type model.

The simplest empirical storm runoff models require a measurement to represent the influence of soil cover complex over the surface of the drainage area and some measurement of the antecedent moisture conditions at the beginning of a storm. If a rainfall record is available for a point in or adjacent to the watershed, antecedent moisture conditions can be readily calculated by conventional techniques. To derive a measure of the soil cover complex, however, with conventional methods, the hydrologist must visit each field or area, identify the hydrologic classification of the soil, classify the crops on each soil, and index each soil crop area. A tabulated value for the runoff coefficient is then selected by the hydrologist to represent that area. After mapping and assigning runoff coefficients to each soil cover area, the coefficients are weighted by area to arrive at a weighted mean runoff coefficient that represents the entire drainage area. The method is tedious and subjective, however this system is widely used by practicing hydrologists for lack of a better system.

**REPRODUCTION OF THE
ORIGINAL PAGE IS POOR**

Complex watershed models may require the estimation of as many as 20 parameters. Many of these are estimated with schemes even more ambiguous than the system for estimating the measure of soil cover complex. The present capability in watershed modeling with computer systems limits the application of complex models to watersheds with quite complete records of hydrologic measurement for a period of 3 years or more. With development of advanced techniques for spatial measurement over the watershed surface of the more critical parameters, the complex models can conceivably become an extremely valuable hydrologic tool. In order to evaluate the transport of pollutants or to estimate safe yields for water supply from ungaged watersheds, continuous complex models will be necessary. At the present time, such models are not applicable to ungaged watersheds due to the fact that they establish the value of their parameters by fitting to an existing set of records. It is therefore imperative that the techniques be developed to provide the necessary input parameters for such models on ungaged areas.

Significant advances in remote sensing hardware and improved availability of remote sensing data offer promising opportunities to acquire spatial measurement of watershed surface characteristics never before available.

Color and color infrared photographs over watersheds having extreme differences in response to rainfall show that some of the surface characteristics that influence the rainfall-runoff relationship can be detected in a qualitative sense. Interest developed from such photographs led to the belief that a quantitative measurement of surface characteristics might be possible by use of digital spectral data from a multispectral scanner.

To predict runoff, we need a good estimate of measurement of the storage capacity of the near-surface soils over a watershed. A number of natural phenomena help us to infer permeability or storage capacity of soils from reflectance of visible or near-infrared light. Differences in soil type, and thus permeability, can many times be inferred by differences in color of bare soil. Differences in permeability also noticeably influenced the natural vegetation species that become dominant on different soils. A quantitative measure of the water storage capability on the watershed surface should therefore be possible by combining data that would not only infer the difference in soils but at the same time include a measure of vegetation.

A study of the early laboratory type passive microwave experiments indicates that the longer wavelengths

might be even more suitable for measuring watershed surfaces since they can penetrate unsaturated soils to some depth. These wavelengths are influenced by soil moisture, vegetation, roughness, and possibly, soil particle size. Increased passive microwave antenna temperatures are experienced for measurements over soils with low soil moisture, dense vegetation, increased roughness and high sand content. All of these characteristics tend to increase near surface storage and produce low runoff. Considering the response of passive microwave to these characteristics and the effective penetration of bare soil, average microwave temperatures should then be more sensitive to differences between watershed's than visible or near infrared sensors.

Experiments designed to test the ability of remote sensors to measure differences in the soil cover complex over watershed surfaces have been carried out using the LANDSAT I multispectral scanner and the X-band Passive Microwave Imaging System (PMIS). The PMIS is mounted on the NASA P3A aircraft operated by the Johnson Space Center. This report concerns the background, procedures, and results of these experiments.

PROCEDURES

A simple empirical storm runoff equation developed by the Soil Conservation Service was selected for this study.

$$Q = \frac{(P - .2S)^2}{P + .8S} \quad (1)$$

where $S = \frac{1,000}{CN} - 10$

Q = storm runoff (cm/2.54)

P = weighted storm rainfall (cm/2.54)

S = storage in the watershed surface (cm/2.54)

CN = Function of soil, cover, antecedent moisture (dimensionless)

This equation is extensively used by both government and private hydrologists to compute flood flows and thereby determine the required storage for flood detention structures. The equation also could conceivably be used as a submodel in the more complex continuous watershed models.

Equation 1 requires as input the weighted mean rainfall over the watershed and a parameter called "curve number" (CN) to represent the surface conditions of the watershed. For these studies, the average curve number derived from measured rainfall and runoff for all recorded significant events on each watershed was used as ground truth. A large majority of the storms and available records

occurred at times when antecedent rainfall was low, therefore the occasional storm with high antecedent rainfall was not included in the average.

Twenty watersheds located within an 1,130-square-mile reach of the Washita River basin in central Oklahoma were selected for the LANDSAT-1 study. Extensive hydrologic records on each of these watersheds had been collected and compiled by the Agricultural Research Service of USDA since 1961. After calculation of the average curve number for each watershed, the watersheds were divided into two groups of 10 watersheds each by ranking the curve numbers and selecting every other one for one group. A group of 10 was set aside for testing and the remaining group was used to derive a relationship between runoff curve numbers and the LANDSAT-1 data.

Digital data from the multispectral scanner on LANDSAT-1 was processed with a series of computer programs developed to excerpt the data within a watershed drainage area and copy it in the same format on another tape. The data could then be rapidly retrieved for quality analysis and computation of mean values for each spectral band. Mean values for the four bands were calculated for each of the 20 watersheds. In all, seven sets of data were processed from

scenes spread over approximately 1 year. The following is the antecedent precipitation index for scene dates.

Scene Number	Date	30-Day API (cm/2.54)
1058	09-19-72	.028
1094	10-25-72	2.27
1184	01-23-73	1.94
1256	04-05-73	1.19
1274	04-23-73	.928
1400	08-27-73	.0180
1508	12-13-73	1.063

Both discriminant analysis techniques and graphical techniques were used in attempts to find a reasonable relationship between these spectral data and the runoff curve numbers. The discriminant analysis program was first used with only the extremely high and low runoff watersheds to see if indeed the spectral data could separate the extremes. It was then applied to all 10 watersheds in the original set of data to find if a reasonable linear combination could be determined this way that would discriminate between all 10 watersheds. This procedure was not successful when more than two watersheds were used due to the makeup of the discriminant analysis program. Simple plots were then made comparing the spectral response to the watershed curve numbers for all seven scenes.

Eight small watersheds ranging in size from 1.46 to 16.45 km² were selected for the passive microwave measurements. Five watersheds in this group were also part of the LANDSAT-1 test watersheds. Curve numbers for the three additional watersheds used in the PMIS study were calculated in the same manner as those for the LANDSAT-1 study.

In the microwave study, the PMIS is mounted on an aircraft. Therefore, the size of the watersheds used in the study was limited to assure the width of the scan would encompass the entire drainage area. Also, no prior data from the PMIS had been collected over terrain where definite boundaries had to be defined, and at the time, there was no assurance that watershed boundaries could be located. The data requested was therefore confined to a small number of watersheds. Two flights were requested in an attempt to look at wet and dry conditions.

Three PMIS flights were ultimately made over the eight watersheds. The first flight was made in November of 1972 immediately after a saturating rainfall. The data from this flight was not useful as the location of watershed boundaries could not be determined with any measure of confidence. A second flight was made in April of 1973 when vegetation was relatively dormant and antecedent moisture

conditions were moderate. The third flight was in June of 1973 when vegetation was at its peak growth and antecedent moisture was again moderate. The watersheds were readily located in the later two flights.

Significant cross polarization effects were found in the outer beam positions of the PMIS data. A simple correction was applied to these data to remove this effect before attempting to locate the individual watershed boundaries. The data were then processed by first matching mosaics of color infrared photographs of watershed areas to overlay plots of the PMIS data. The extreme low microwave antenna temperatures experienced over open water surfaces served as excellent matching points. When the plot had been expanded or contracted to match photo scale, beam positions in the PMIS scan that fell within the watershed boundary were readily identified. Using data from the beam positions within the watershed boundary, the average vertically polarized temperature and the average horizontally polarized temperature for that watershed was calculated. The average temperatures were then graphically compared with the curve numbers for the watersheds.

RESULTS AND DISCUSSION

In the first attempt to compare the average digital response from the LANDSAT MSS, a discriminant analysis technique (Cooley & Lohnes) was used. Data from two watersheds having the highest and lowest runoff curve numbers in the first group of 10 watersheds was used as input. This technique indicated that a discriminant function using the two visible bands could be used to describe differences between the watersheds. The second best discriminant function resulted from use of all four bands of data while no combination of three bands seemed to produce satisfactory results.

Simple curve fitting techniques were then used to investigate the relations between the average runoff curve numbers and linear combinations of MSS data when all 10 watersheds in group 1 were considered. Linear combinations of the mean (μ) digital values for two bands (4 and 5) and all four bands were plotted versus the curve numbers. Two linear combinations of MSS data from scene 1058 were found to be reasonably well related to the curve numbers. (Figure 1). The lower curve based on all four bands of data from both visible and near infrared light is more sensitive and

could be expected to predict curve numbers for the watersheds in the test group better than predictions based on only visible light.

These relations do not appear in the following four scenes representing late fall, midwinter and early summer. However, in scene 1400 the relation between the MSS data and runoff curve numbers does exist. The final scene 1508, was typical of midwinter and again the relations did not exist. Plots of these data (Figure 2) show a similar relation to Figure 1. On the second figure only nine data points are shown since one watershed from the original group was obscured by a cumulous cloud. One data point included obviously falls far above the eight points used to describe the relation. The particular watershed represented by this data point was partially obscured under a high thin cirus cloud cover. The data point was left in the plot to illustrate that the value of the linear equation increases for both cases when the scene is partially obscured by thin clouds. Thus, prediction of curve numbers for ungaged watersheds in a region should be done with caution if the photographic image of the scene indicates thin cloud cover may be present over watersheds of interest.

The fact that the same linear equations of MSS data produce similar relations in two scenes indicates that

the technique is repeatable. The fact that the technique did not work on the remaining scenes also indicates there are some limitations to the application of the technique. Further examination of the data showed that the two scenes where the relation does exist both occurred when the watersheds were extremely dry. The 30 day antecedent precipitation index (API) (Linsley & Kohler) was .028 and .0180 for scenes 1058 and 1400 respectively. The API for the remaining scenes ranged from .928 to 2.27. The value 2.27 represents a virtually saturated condition.

The scenes used in this study represent a rather large range of green vegetation with the first scene almost barren after extended drought and two summer scenes at the peak of vegetative growth. Unfortunately no scenes were found during the study period where heavy vegetation and drought conditions existed together. Scenes used where vegetation was sparse or dormant (fall and winter scenes without snow cover) did represent both wet and dry antecedent conditions. It is apparent from these data that dry soils are necessary for the use of this technique during the dormant period of the year. The data however, are insufficient to show that dry conditions with heavy vegetation will allow use of the technique.

Figures 3 and 4 illustrate the prediction capability of the curves developed from four bands of spectral data on the first 10 watersheds. The lower curves in figures 1 and 2 are used to predict curve numbers on the test group. The average absolute deviation of predictions based on the curve developed from band 4 and band 5 data was 4.13 and 4.59 for scenes 1058 and 1400 respectively. Using all four bands of MSS data, predictions were 3.17 and 3.70 respectively for the same scenes. The average deviation of conventional curve numbers for the same test watersheds was 10.72 from the measured curve numbers. The technique based on predictions from MSS spectral data therefore shows considerable improvement over computation of curve numbers by the conventional method. After the prediction curve has been developed for calibration, prediction of curve numbers for any watershed within the scene can be accomplished with a minimum of computer time. It is also conceivable that by use of this technique a map of runoff capability could be developed for arid regions.

In the passive microwave experiment using the X-band PMIS data, average vertically polarized and average horizontally polarized temperatures were compared to the

measured curve numbers from 8 watersheds. The experiment had been predicated on the hypothesis that microwave measurements averaged over a watershed should be more sensitive to differences in the physical characteristics of the soil and therefore the storage capacity of the soil. It was presumed that the difference in temperature from a wet and dry condition might be necessary to describe this characteristic by essentially measuring differences in soil moisture and nullifying some of the roughness components and the unexplained anomalies in microwave measurement. In light of these considerations, measured curve numbers were plotted versus average temperatures, difference in vertically and horizontally polarized temperatures and difference in like polarized temperatures from April and June flights.

Average vertically polarized temperatures for the April flights decreased with increased curve numbers while in the June flight average vertically polarized temperature increased with increased curve numbers. In both flights the vertically polarized temperatures display a curvilinear relation and were insensitive to changes in curve numbers above 50. These data indicate there is little promise for use of vertically polarized temperatures alone as a measure of watershed runoff capability.

Average horizontally polarized temperatures

(Figure 5) from both flights can be related to the curve numbers with a straight line. The line representing the dormant season data from April would provide a sensitive prediction throughout the major range of curve numbers. The dense vegetation in the June time frame seems to make the horizontal polarization by itself insensitive to differences in the watershed. Even though the relation can be represented by a straight line it would not lead to a satisfactory prediction scheme. This response should be expected since the penetration of dense vegetation is considered unlikely with λ -band wavelengths at the PMIS look angle of 50° . This figure implies that if one can sense differences in the soil, a sensitive relation can be found between horizontally polarized microwave temperature and the runoff curve numbers of watersheds. The 30 day antecedent precipitation index averaged .558 for the April flight and .180 for the June flight. The prior studies with LANDSAT data would indicate that the moisture content of the soils at the time of these flights prohibit the use of visible and near infrared light to classify the runoff curve number. No reasonable relation was evident between the LANDSAT spectral data on April 23rd and the curve numbers.

However, only five days later the passive microwave measurement was very sensitive to differences between the watersheds.

In studies with truck mounted passive microwave equipment (Newton et al), there are indications that there is antenna response to soil moisture conditions under vegetative cover with the longer wavelength L-band systems. Thus, if longer wavelength sensors were available to effectively penetrate vegetation, sensitive relations could be developed when heavy vegetation was present in the summer months.

CONCLUSIONS

1. The LANDSAT-1 study demonstrated that when dry dormant surface conditions exist a linear combination of digital data for the visible light from some scenes can be related to measured watershed runoff curve numbers.
2. A linear combination incorporating the near infrared bands produces a more sensitive relation with measured watershed curve numbers than can be achieved using only visible bands.
3. The techniques using LANDSAT data appears to be limited to areas where extremely dry dormant conditions exist in conjunction with a clear atmosphere.
4. Average horizontally polarized passive microwave temperatures from the PMIS images with a wavelength of 2.8 cm can be related to watershed runoff curve numbers with a straight line that is equally sensitive throughout the normal range of curve numbers.
5. The relation between horizontally polarized passive microwave temperature and runoff curve numbers is not restricted to extremely dry conditions, but is restricted by interference from dense vegetation.

6. The prior conclusions along with results of L-band passive microwave measurements lead to the implication that a more universally applicable sensor for measurement of watershed surface characteristics can be developed by use of wavelengths in the L-band region.

REFERENCES

- Chow, V. T., et al. 1964. Handbook of Applied hydrology. McGraw-Hill Book Co., Inc., New York. Section 21, Hydrology of agricultural lands, pp. 21-1 to 21-95 by H. O. Ogrosky and V. Mockus.
- Cooley, W. W. and P. R. Lohnes. 1962. Multivariate procedures for the behavioral sciences, pp. 1-211. John Wiley, New York.
- Linsley, R. K., Jr., M. A. Kohler and J. L. H. Paulhus. 1949. Applied Hydrology. McGraw-Hill Book Company, Inc., New York.
- Mockus, V. 1971. National Engineering Handbook, Section 4, Hydrology. U. S. Government Printing Office, Washington, D. C., pp. 7.1-10.23.
- Newton, R. W., et al. 1974. "On the Feasibility of Remote Monitoring of Soil Moisture with Microwave Sensors," Proc. 9th International Sym. on Remote Sensing of Environment, University of Michigan, Ann Arbor.

REPRODUCIBILITY OF THIS
ORIGINAL PAGE IS POOR

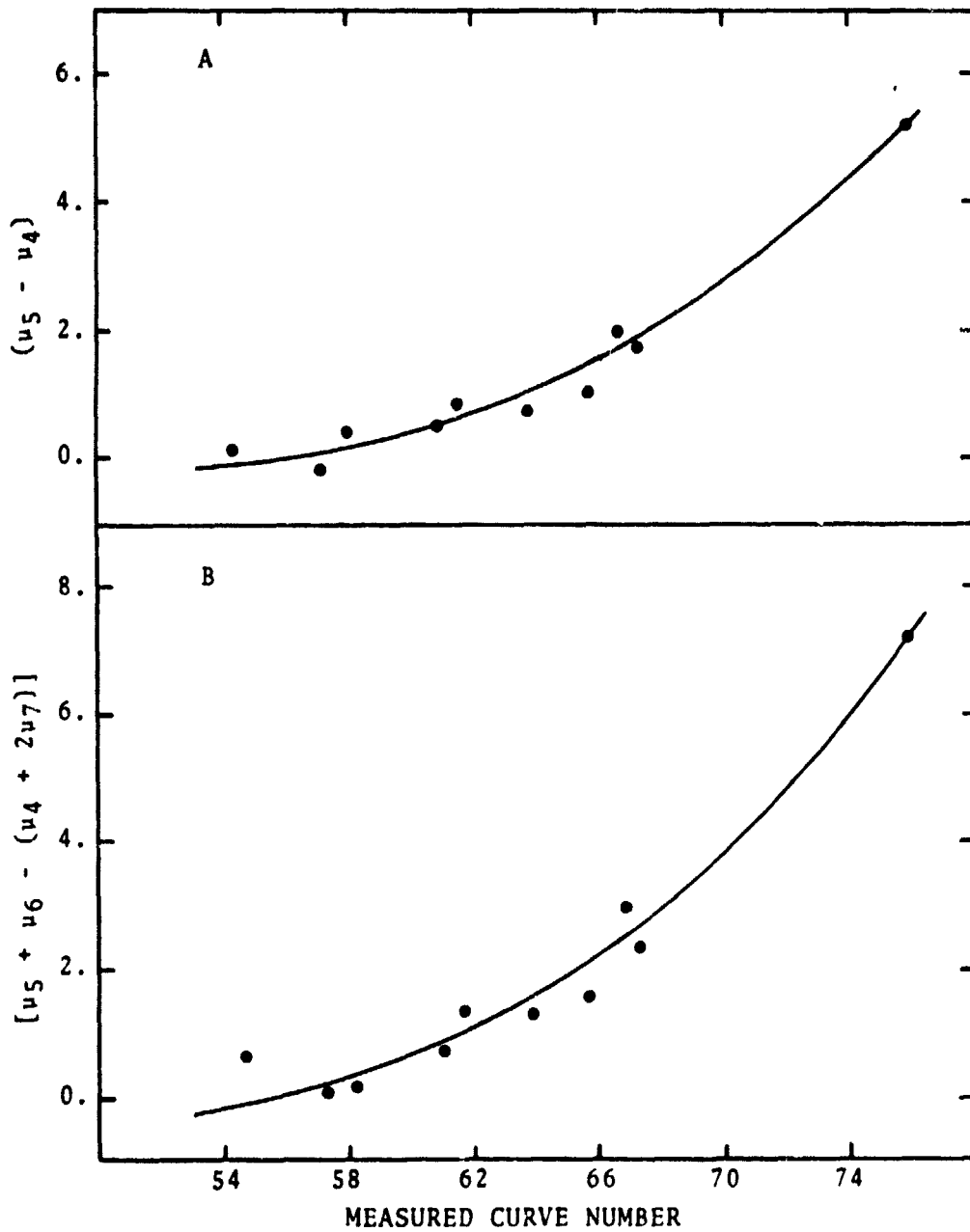


Figure 1. The relations of MSS data from Scene 1058 to measured watershed runoff curve numbers.

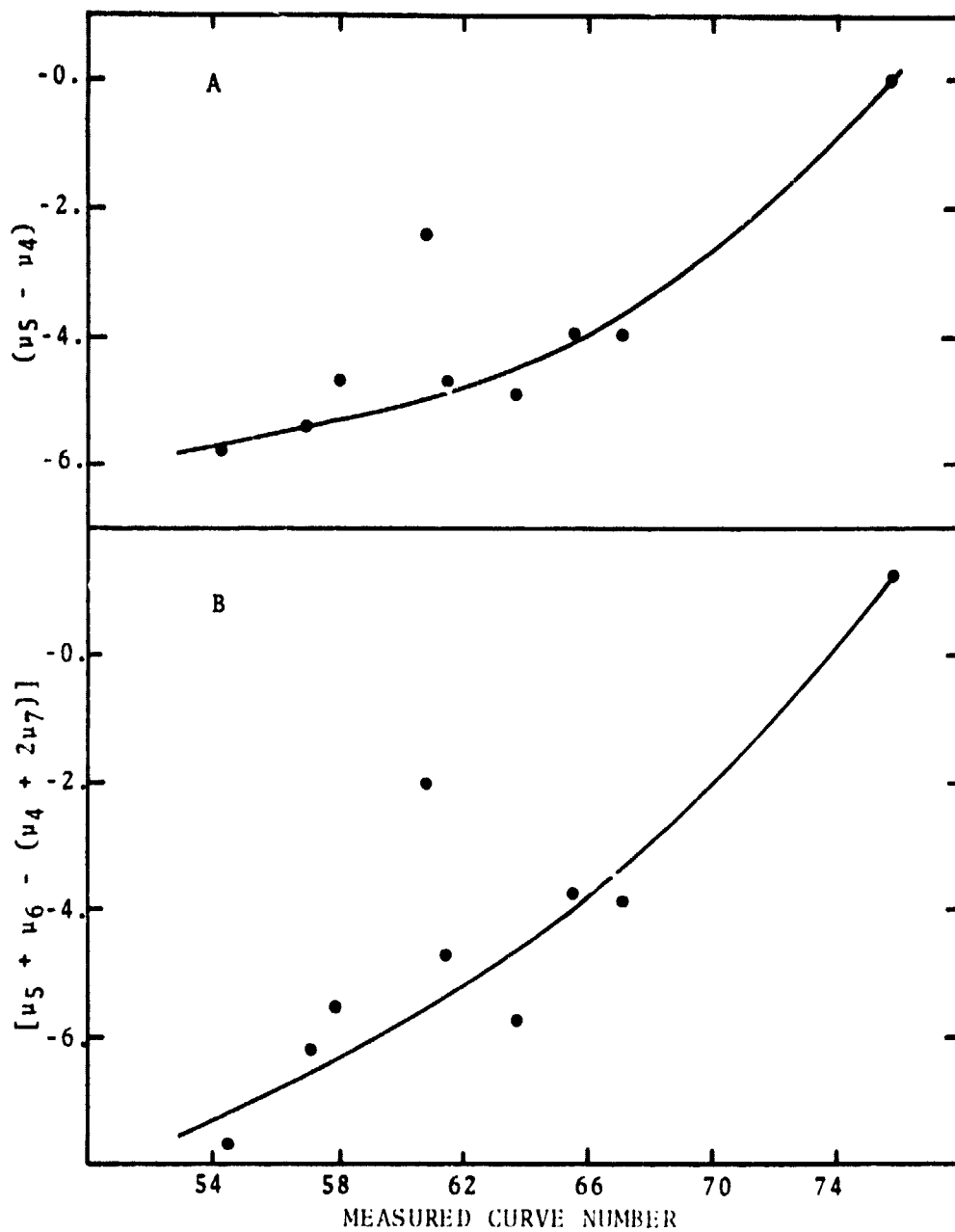


Figure 2. The relations of MSS data from Scene 1400 to measured watershed runoff curve numbers.

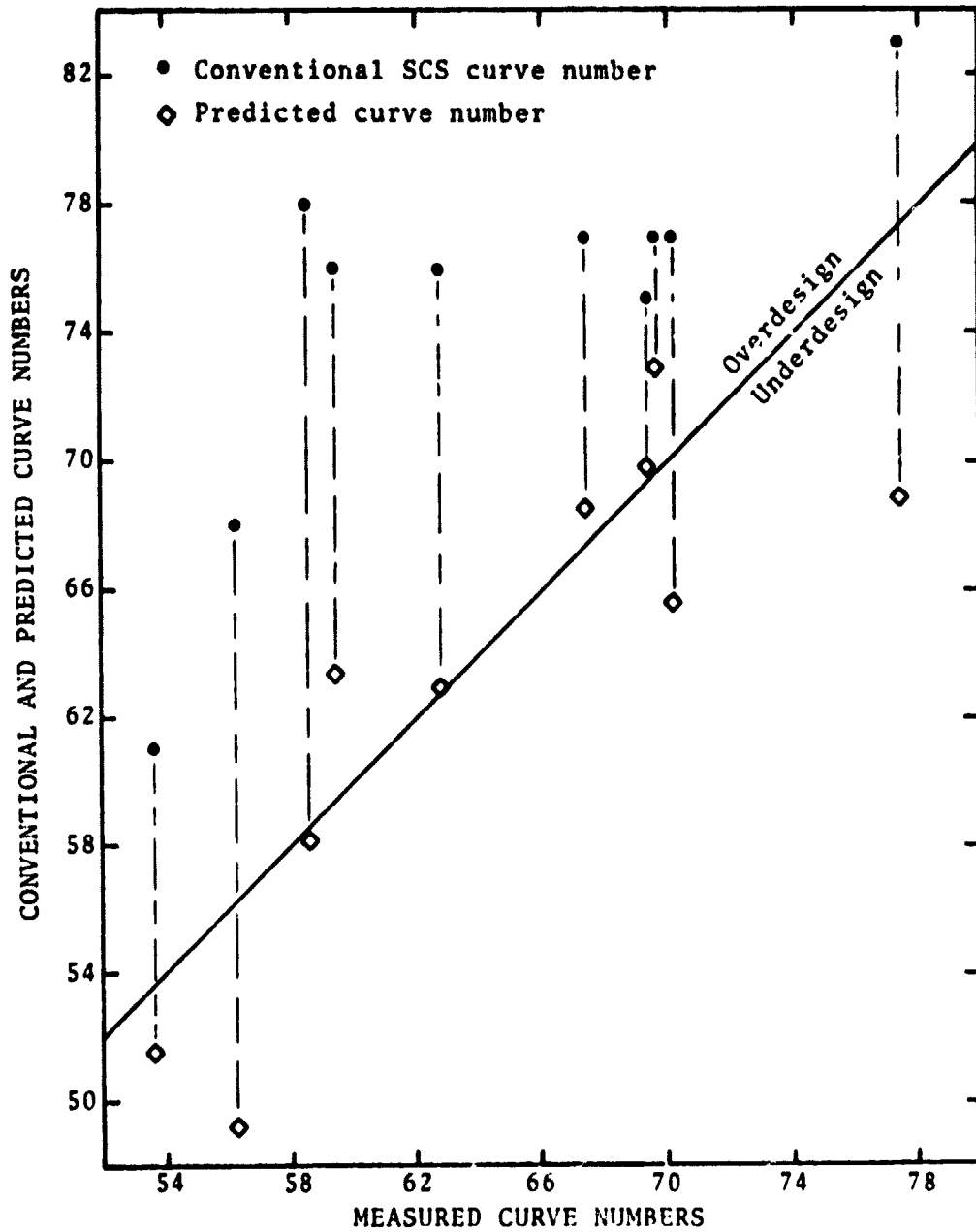


Figure 3. Comparison of conventional SCS curve numbers to curve numbers predicted with 4 bands of LANDSAT-MSS data (Scene 1058)

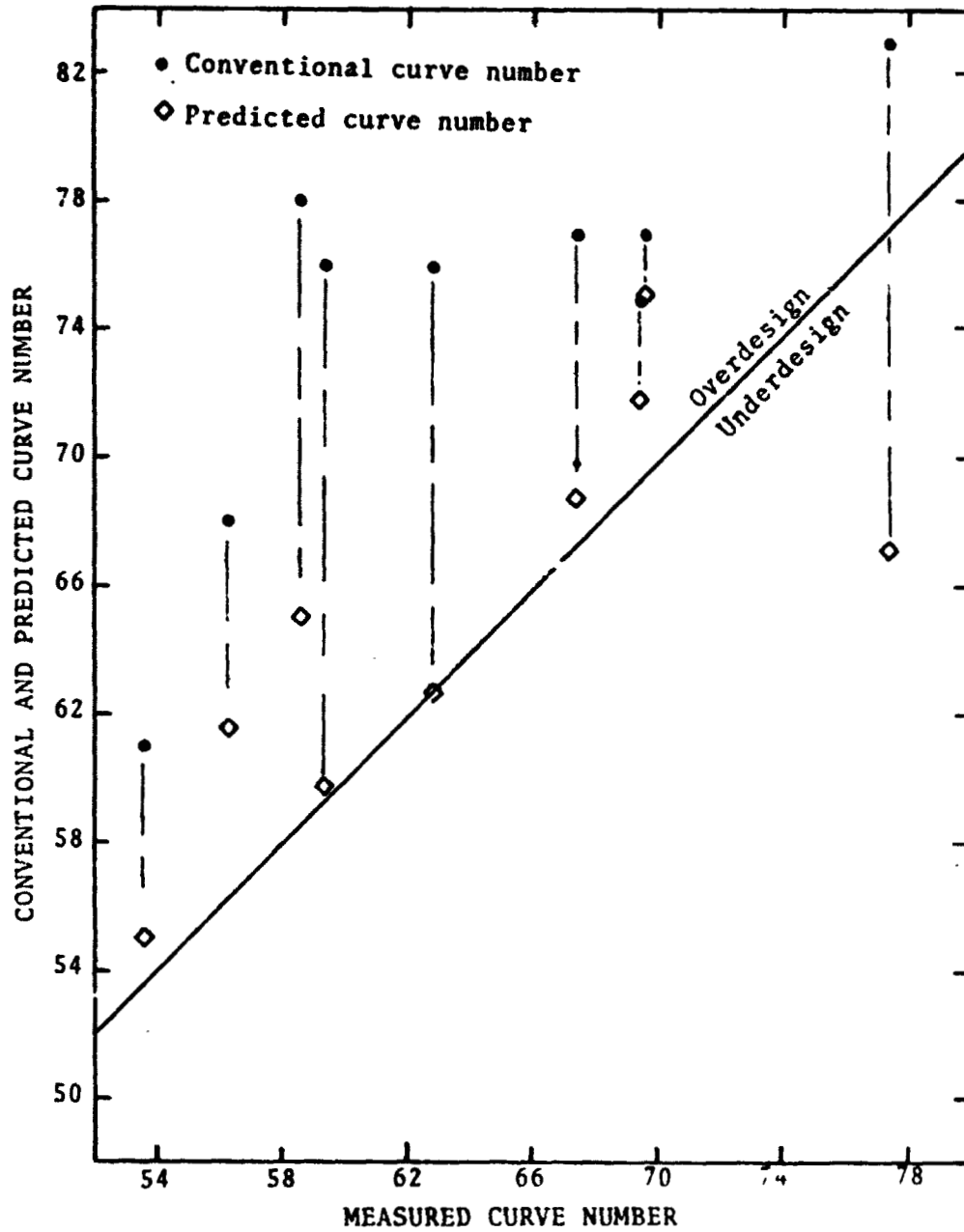


Figure 4. Comparison of conventional SCS curve number to curve numbers predicted with 4 bands of LANDSAT-MSS data (Scene 11-1).

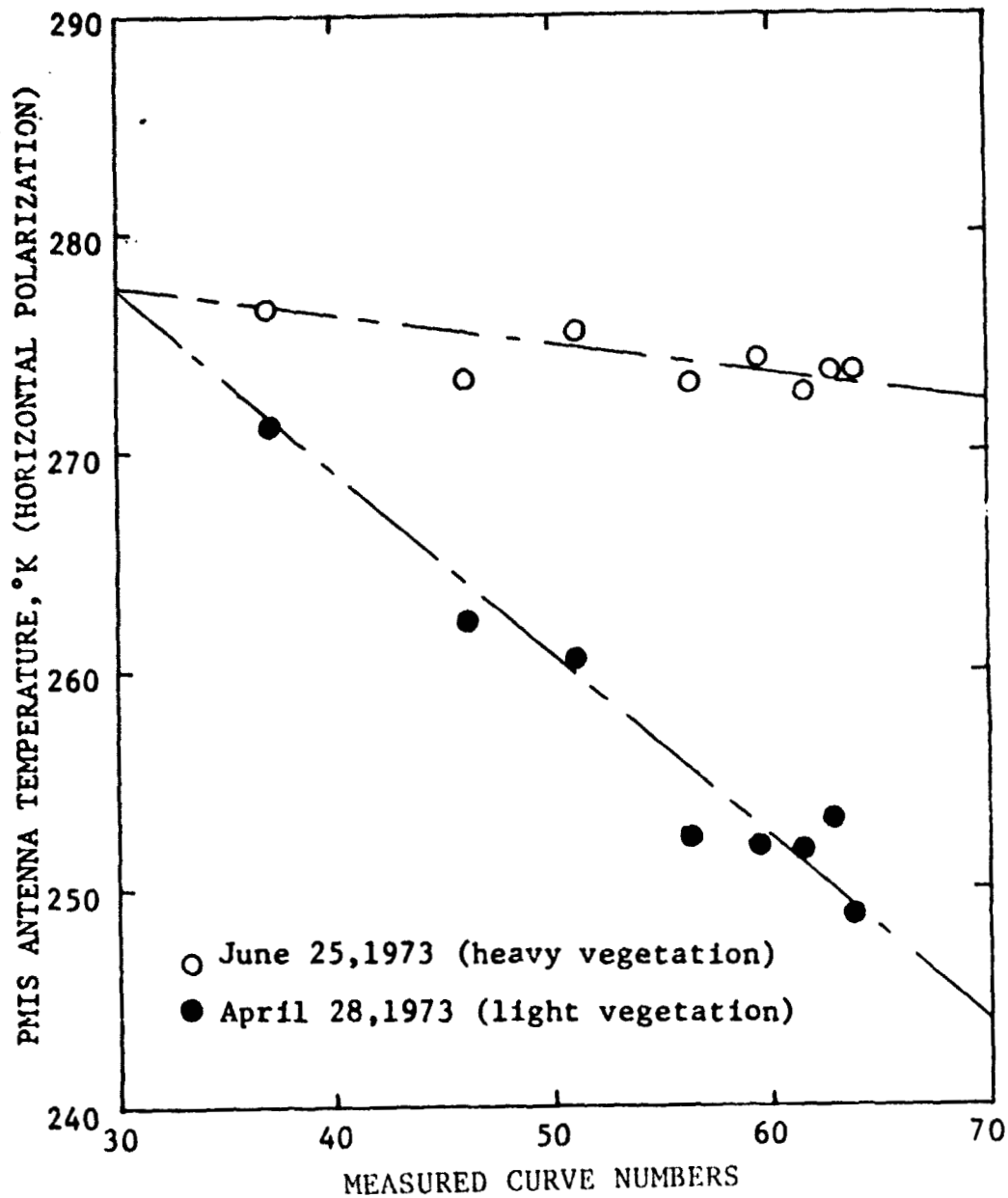


Figure 5. The relation between average horizontally polarized microwave temperature and storm runoff curve numbers. April 28th had moderate moisture conditions while June 25th was dry.

A. L. Higer**, E.H. Cordes**, A.E. Coker*, and R. H. Rogers ***

N76-17603

ABSTRACT

A prototype data acquisition and dissemination network, installed and operated by the U.S. Geological Survey, is a viable approach for providing the near real-time data needed to solve hydrologic problems confronting the nearly 2.5 million residents of southern Florida. Water-stage and rainfall data from ground stations are transmitted from the Everglades via LANDSAT, the NASA tracking stations, and the U.S. Geological Survey to the users in less than 2 hr, a significant improvement over conventional techniques requiring up to 2 months. LANDSAT imagery significantly enhances the utility of the ground station measurements. Water stage (depth) is correlated with water-surface areas from the imagery to obtain water stage-volume relations in near real-time for management decisions concerning the distribution of water to the people, fauna, and flora of southern Florida.

* U.S. Geological Survey; Water Resources Division; Tampa, Florida

** U.S. Geological Survey; Water Resources Division; Miami, Florida

*** Bendix Aerospace Systems Division; Ann Arbor, Michigan

NOMENCLATURE

Acoustic Coupler: Device used to link computers by telephone line.

Acre-foot: The quantity of water required to cover 1 acre to a depth of 1 foot equivalent to 43,560 cubic feet or about 375,821 gallons

Aquifer: Any part of the earth's crystal layer capable of storing water and yielding water for use on the earth's surface. The water in such formations is called ground water. The Biscayne aquifer is a shallow "water table" aquifer.

Carryover Storage: Reservoir storage capacity which will permit the retention of surface water surpluses for carryover to supply needs in subsequent periods of water deficiency.

Conservation Area: In this report, an area reserved for the purpose of conserving water.

Contents: The volume of water in a reservoir or lake. Unless otherwise indicated, volume is computed on the basis of a level pool and does not include bank storage.

Control: A feature downstream from the gage that determines the stage-discharge relation at the gage. This feature may be a natural constriction of the channel, an artificial structure, or a uniform cross-section over a long reach of the channel.

Control Structure: As used in this report, control structure is a structure on a stream or canal used to regulate the flow or stage of the stream or to prevent the intrusion of salt water.

DCP: Data Collection Platform; An electronic instrument which encodes, formats, and transmits data to the LANDSAT satellite.

DCS: Data Collection System; A system contrived and operated by NASA, using DCPs, the LANDSAT satellite, receiving stations, and a data processing facility.

Discharge, Mean: The arithmetic mean of individual daily mean discharges during a specific period.

Evapotranspiration: The process by which water is evaporated from moist plant surfaces and transpired to the atmosphere as water vapor.

ERTS: Earth Resources Technology Satellite. Renamed LANDSAT in 1975.

Gage Height (G. H.): The water-surface elevation referred to some arbitrary gage datum. Gage height is often used interchangeably with the more general term "stage", although gage height is more appropriate when used with a reading on a gage.

Gaging Station: A particular site on a stream, canal, lake, or reservoir where systematic observations of gage height or discharge are obtained. When used in connection with a discharge record, the term is applied only to those gaging stations for which a continuous record of discharge is computed.

NASA: National Aeronautics and Space Admistration.

NASA Progress Report: Periodical report required by NASA contract.

NDPF: NASA Data Processing Facility.

Nutrients: Although many chemical constituents are required for plant growth, nitrogen and phosphorous are considered to be the primary nutrients. Both occur in inorganic and organic forms. The inorganic forms of nitrogen found in solution in water bodies are nitrates, nitrites, and ammonia.

Partial-Record Station: A particular site where limited stream-flow data are collected systematically over a period of years for use in hydrologic analyses.

Programmable Calculator: Electronic calculator that has a programming mode.

Runoff in Inches (IN.): Runoff in inches shows the depth to which the drainage area would be covered if all the runoff for a given time period were uniformly distributed on it.

Seepage: A process by which water in surface storage is lost through levees and into ground water reservoirs.

Stage-Discharge Relation: The relation between gage height and the volume of water per unit of time, flowing in a channel.

Telecopier: Device used to copy and transmit by telephone to another telecopier, at a distant station, the print from a page.

Transpiration: A vital natural element of the hydrologic cycle; the return of water to the atmosphere in the form of water vapor as a result of the growth process of vegetation.

Water Budget: For any water system, an accounting over any fixed time span of where water comes from and where it goes.

INTRODUCTION

The water supply for southeastern Florida, with a population of more than 2.5 million, including the Everglades National Park, depends on the management of water within the Everglades basin (Figure 1). Decisions affecting the control of this supply are based on water budgets developed primarily from hydrologic data acquired and analyzed by the U. S. Geological Survey as part of their program of hydrologic investigations and data collection network.

The goal of this investigation is to evaluate the usefulness of LANDSAT in improving the overall effectiveness of this collection and dissemination network. Resulting network improvements in data timeliness and accuracy would have a direct beneficial impact on the water distribution to the people, fauna, and flora of southern Florida. To accomplish this goal, the Geological Survey used imagery from the LANDSAT Multispectral Scanner (MSS) and the LANDSAT Data Collection System (DCS) to evaluate their utility in supporting near real-time hydrologic data acquisition and dissemination. This paper reports on the work accomplished and results achieved in establishing and operating this prototype network.

Managing The Water System

The storage and flow of water in southeastern Florida is controlled by the Central and Southern Florida Flood Control District, which maintains and operates a system of levees, canals, control structures, pumping stations, and water storage areas. The control of this system (ref. 1) is based on water budgets developed from hydrologic data collected and disseminated primarily by the Geological Survey.

The levees retain water in four major impoundment areas (figure 2); (1) Lake Okeechobee, (2) Conservation Area 1, (3) Conservation Area 2, and (4) Conservation Area 3. Shark River Slough (figure 2), a water-course important to the environment of Everglades National Park, at the downstream end of these interconnected water bodies, also depends on overland flow from adjoining Conservation Area 3.

The four major impoundment areas impede the normal surface water flow from the Everglades and Lake Okeechobee through agricultural and urban areas during the rainy season, June through October. Pumping stations at the edges of the three conservation areas provide flood protection by pumping excess rainfall from the Everglades agricultural area and other flood-prone areas into Lake Okeechobee and the three conservation areas. Thus, the system not only provides flood protection, but also enhances water conservation. Water is transferred from the conservation areas into Everglades National Park or to coastal cities as needed through a network of surface canals.

Canals also drain the urbanized zone along the coast. They transfer water from Lake Okeechobee and the conservation areas to the Everglades agricultural area and to the east coast to replenish ground-water reservoirs near municipal well fields and to prevent seawater intrusion. Flow in the canals is regulated by coastal control structures which are normally open or partly open during the rainy season. The structures are generally closed during dry seasons to prevent inland movement of salt water and overdrainage of fresh water.

Scheduled releases from the conservation areas are made during the year to sustain plants and animals in Everglades National Park. Late in the dry season, water is also released from the conservation areas to the canals, as required, to maintain water levels near the coast and to replenish well fields. During much of the dry season, eastward flow in canals is maintained by water seeping under the levees of the water conservation areas, however, water in the canals is not discharged to the ocean; rather it infiltrates the Biscayne aquifer near the coast. During prolonged drought, some water can be transferred directly from Lake Okeechobee through the conservation areas to points of need along the coast. Usable storage in the lake is usually shared by municipalities, agricultural interests, and the Everglades National Park.

Water Budget

Management decisions as to where and when to store and release water from the impoundments are based on an accounting of the amount of water in surface storage. This accounting procedure (refs 2 and 3) relates basin water inputs and outputs as modeled in figure 3 and results in a water budget for the area.

Monthly water budgets for Lake Okeechobee and the three conservation areas are computed by the Central and Southern Florida Flood Control District and the U. S. Army Corps of Engineers. Two budgets are prepared; one for a condition of normal rainfall for the remainder of the dry season and the other for a condition of last year's rainfall for the same period.

The budget inputs (figure 3) include surface flow into the basin (inflow) and rainfall on the basin. The outputs are the combined losses: evaporation transpiration (water released to the atmosphere as part of the life process of vegetation), surface water seepage into ground water reservoirs, and the canal outflow for irrigation and municipal supply. Subtracting output from input, as shown in the model of figure 3, gives a surplus or a deficiency in the water storage for a specified storage area and time.

Several water budget studies for the conservation areas by Federal (U. S. Corps of Engineers) and State water-management agencies (Central and Southern Florida Flood Control District) are underway.

The major problem in developing a good water budget is to adequately measure the input and output quantities. Another task is to determine the water in storage in the conservation areas. This is difficult because of the large area extent and shallowness of water which makes representative stage recordings difficult to obtain. A good budget analysis requires large amounts of accurate and timely hydrologic data. It is this data need which the hydrologic data network is designed to satisfy.

Hydrologic Data Network

Hydrologic data used in developing water budgets are collected and disseminated (ref 4) in southeastern Florida by the U. S. Geological Survey, as part of the nationwide hydrologic data network. The network is operated by the Survey in cooperation with local, State, and other Federal agencies; the Survey gathers data on a wide variety of environmental parameters. In the Everglades alone, more than 100 gaging stations provide daily records of water surface elevation or flow. Nationwide, the Geological Survey has nearly 18,000 such stream-gaging stations, of which approximately 10,000 have digital water stage recorders. These small field instruments continuously monitor stream stage via linkage to a float in a stream-connected stilling well. Periodically, at 15-, 30-, or 60-minute intervals, the recorder punches the real-time stage value on a 16-channel paper tape, a machine-readable record.

Without the advantage of LANDSAT-DCS, data from a particular field instrument are retrieved by field engineers and technicians who visit the station about once a month, calibrate the instrument, perhaps take supplementary measurements and samples, and conduct general maintenance. The data, many of which are in machine-readable form, are returned to the office, checked for quality control, transferred onto punch cards or magnetic tape for entry into the computer system, analyzed, plotted, and disseminated to users. Time from data recording to dissemination to users is about 2 months after initial recording. These long delays reduce the utility of the data for current water budgets and, consequently, delay management decisions affecting the storage and flow of water. The need to reduce the time required to develop water budgets is becoming increasingly important in Florida, as in other areas of the Nation, where water managers are attempting to satisfy the water demands of an ever-increasing population while still retaining sufficient water in the system to meet the needs of the aquatic environments and upgrade and maintain the water quality in the water-storage areas, canals, and aquifers.

The Geological Survey, in addition to disseminating hydrologic data to users in southern Florida, also stores the data in the national water data storage and retrieval system (ref 5) in Washington, D. C. and Reston, Virginia. From this system the data are made available nationwide. Survey offices, such as the Miami office, are interlinked with the national water data storage and retrieval system by means of a national telecomputing system which provides general data processing support for the national water data storage and retrieval system. The national telecomputing network consists of the computer centers in Washington, D. C. and Reston, Virginia, and nearly 100 remote computer terminals in Survey offices across the Nation, one of which is in the Miami office. The Washington, D. C. computer center has an IBM 360/65 computer and the National Center at Reston, Virginia has an IBM 370/155 computer.

Thus, the major hydrologic activities of the Geological Survey, the collection, storage, retrieval, and analysis of hydrologic data are accomplished through the operation of three basic systems: the hydrologic data network, which provides data collection; the national water data storage and retrieval system, which processes and stores data generated by the hydrologic data network; and a national telecomputing system, which provides general data processing support for the national water data storage and retrieval system.

RESULTS AND DISCUSSION

To achieve the goals of the investigation, the Geological Survey analyzed both LANDSAT-MSS imagery and in situ monitoring by LANDSAT-DCS in order to evaluate their separate and combined capabilities in the Hydrologic Data Network. Paulson (refs 5 and 6), Schumann (ref 7), and Cooper (ref 8) applied similar techniques to operational systems with a DCS capability and Graybell (ref 9) and Deutsch (ref 10) used MSS to determine surface-water distribution. Anderson (ref 11) used the MSS imagery to identify and map vegetative communities within wetlands. Reeves (ref 12) used successive passes of LANDSAT imagery of playa lakes in the Texas high plains to demonstrate the dynamics of surface-water distribution within the lakes. However, the investigation described herein combines an operational LANDSAT data-collection system with the LANDSAT multispectral scanner data.

Twenty data collection platforms (DCP's) were established in southern Florida. Water-level and rainfall data collected and disseminated in near realtime (less than 2 hours) from these instruments, were also analyzed in conjunction with LANDSAT imagery enhanced by electronic processing. Results reported in this section show that the combined use of MSS and DCS data provides more benefits than the use of either technique alone.

LANDSAT - Data Collection System

The LANDSAT Data Collection System (DCS) is a communications system (ref 13) that consists of three elements: a small low-powered battery-operated radio transmitter called a data collection platform (DCP), a radio transponder aboard the LANDSAT satellite, and ground-receiving sites. The polar-orbiting LANDSAT makes about 14 orbits of the earth daily and can relay data from a DCP to a ground-receiving site whenever both are mutually visible from LANDSAT, this occurs during a brief period on each of several orbits. The DCP transmits a brief data message of 0.04 sec in duration once every 90 or 180 second and can communicate with the satellite during several mutually visible periods daily. The number of mutually visible periods is primarily a function of geographical position and local terrain interference. Two ground-receiving sites; one at the Goddard Space Flight Center in Greenbelt, Maryland; the other at Goldstone, California, provide good coverage for the contiguous 48 states. They receive data from continental American DCPs on 3 to 7 daily orbits during mutual visibility periods lasting 12 to 14 minutes per orbit.

Data Collection Platform. - Twenty DCPs were established in the Everglades (figs. 4, 5, 6, and 7) and Big Cypress Swamp to the west to transmit water level and rainfall. The flow of data from the area to the Geological Survey office in Miami starts with the water-level and rainfall gages at the DCP.

Housed at the DCP shown in Figure 6 are the DCP (ref 14), water-stage recorder, rainfall recorder, and timer and power supply for both recorders.

Before the DCP transmits the data to the satellite, it receives the data from a sensor (recorder) and then encodes and puts the data into a form for radio transmission. Although the DCP normally transmits a signal every 3 min, the DCP can be set to transmit every 90 seconds. When the LANDSAT satellite (figure 8) is in mutual line of sight of a DCP and a NASA receiving station, the data transmitted from the DCP is received by the satellite and transmitted to NASA receiving stations at Goddard or at Goldstone. In southern Florida, this mutual communication occurs from 3 to 6 times per day. Each time, 1 to 4 distinct messages can be transmitting every 3 minutes.

At the receiving station, the data are decoded and sent by NASA communication line to the Operations Control Center and then to the NASA Data Processing Facility at Goddard. At the processing facility, the data are verified and put in a form to be teletyped to Miami. The data are received by teletypewriter as perforated tape and printout. The total elapsed time from field measurement to printout in Miami is about 45 minutes.

From the teletypewriter, the data are fed into a programmable calculator, which analyzes the data and produces the finished product, which is telecopied to the water-management agencies on the same day.

On an average day, data are received in Miami 2 or 3 times each morning and 2 or 3 times each night. At future stations where parameters such as wind-speed are to be monitored, data will be required more frequently.

Handling of DCS Data. - After data are received in Miami by teletypewriter, the perforated tape from the teletypewriter is fed into the calculator through a tape reader. Equipment available in the Miami office include the programmable calculator, thermal printer, paper tape reader, x-y plotter, hopper card reader, cassette memory recorder, extended memory, and acoustic coupler.

The cassette memory recorder allows data and programs to be stored outside the programmable calculator. The extended memory is an attachment to the calculator which gives the calculator more capacity for memory storage. The acoustic coupler enables the calculator to be tied to computer by phone. The calculator first translates the teletypewriter data from its octal form into engineering units. At present, these units represent water stage, in feet, or cumulative rainfall, in feet. Second, the calculator sorts the data chronologically by station. Then it calculates daily rainfall, in inches, and prints the data in a format requested by the Corps of Engineers (table 1). The data are then scanned for errors. If the data appear correct, they are telecopied to the Corps of Engineers in Jacksonville and Clewiston, Florida. The time required for the transmission of data from the Everglades via the satellite, the NASA tracking stations, and the Geological Survey to the Corps of Engineers is less than 2 hours, a significant improvement over prior techniques requiring as much as 2 months. The National Park Service and the Fish and Wildlife Service receive a full table of data each Friday. The Central and Southern Florida Flood Control District at West Palm Beach receives data from the Corps of Engineers in Jacksonville.

After the data have been calculated, sorted, and sent to the users in the form shown in table 1, the data are stored on cassette tape. The data are condensed by eliminating all but daily readings and are stored in annual data files. After the data are loaded into the annual files, data from stations designated as key stations are fed into the plotter, which is on line to the programmable calculator. Figure 9 shows hydrographs compiled from data relayed from three DCPs in Conservation Area 1. Hydrographs are usually updated each month and mailed to the users. LANDSAT programs presently used on the calculator in Miami are:

- Reads teletypewriter tape and converts to gage heights or dial readings.
- Prints out weekly summary table of stage and rainfall.
- Stores midnight readings of stage and rainfall for each day.
- Prints daily calendar year plot.
- Prints daily water year plot of stage.

Additional programs for the programmable calculator are being written to analyze water-quality and additional meteorological data collected from LANDSAT-DCS stations now being installed.

LANDSAT Multispectral Scanner

LANDSAT imagery and DCS data acquired on Conservation Area 1 show a complementary application for these data.

Conservation Area 1. - Conservation Area 1 covers 221 square miles (572 square kilometers) and is contained within the Loxahatchee National Wildlife Refuge. As seen in the NASA image of figure 10, the area is pear-shaped and bounded by levees. Just inside the levees are ditches or canals formed by the removal of soil for the levees. The canals expedite the movement of water into or out of the refuge.

The vegetation of this area (ref 15) is shown in figure 11. This part of the Everglades (ref 16) consists of prairie-like flats that are covered with shallow water most of the year. Stands of sawgrass intersperse the flats. Shallow ponds and sloughs support white water-lilies and other aquatic plants that bloom throughout the year. The landscape is dotted with tree islands that vary in size from a fraction of an acre to several hundred acres. Wax myrtle, redbay, dahoon holly, and ferns on the islands retain their foliage throughout the year. Various air plants grow in profusion within its confines.

Fall and winter migrations result in spectacular bird concentrations. Flocks of herons, egrets, and ibises, often numbering in the thousands, congregate where receding water strands myriads of small fish and crayfish. The tree islands in winter are frequently alive with small birds, including several species that otherwise winter south of the United States. Among the more interesting resident species are limpkin, sandhill crane, wood duck, and mottled duck. Blue-winged teal and ring-necked ducks are the most abundant ducks during winter. Coots are year-round residents, but are abundant only in winter. The cattle egret, an emigrant from the Old World, is now common on the refuge and adjacent pasture lands.

A noticeable relation exists between water levels and the abundance of birds requiring an aquatic habitat. Thousands of colonial and water birds nest and roost on the refuge when sufficient water is available to provide the necessary environment.

LANDSAT Imagery. - Multispectral imagery of Florida is obtained every 18 days by LANDSAT from an altitude of approximately 560 miles (900 kilometers). These data are transmitted from the satellite to the NASA Goddard Space Flight Center or the Goldstone Tracking Station in digital format. The digital tapes are then mailed to the Miami office of the Geological Survey. Several systems were used to extract spectral information from these tapes in order to construct thematic maps. Electronic processing of the LANDSAT MSS data was accomplished using the computer facilities of the Bendix Aerospace Systems Division, NASA Kennedy Space Center Earth Resources Program Office, the General Electric Corporation, the Stanford Research Institute, and the IBM Corporation to produce different types of maps by computer.

Figure 12 shows radiance (or reflectance) maps of Conservation Area 1 derived from electronic processing of LANDSAT MSS band 7 data acquired on 14 February, 4 March, and 22 March of 1973.

For this illustration, the original LANDSAT radiance levels, which were enhanced and color-coded on film, are shown as gray-scale levels. The darker the gray-scale, the lower the radiance measurement, which infers water. The water depth in this area ranges from zero, as denoted by white, to about 2 feet (0.6 meter), denoted by black.

The change or loss in water stored in the area from February 14 to March 22 is readily observed by the changes in gray-scale of the enhanced images in figure 12. The water stored in the area for a given time is obtained as illustrated in figure 13, where the DCS (figure 14) is used to provide quantitative in situ data on the elevation of each water-depth category and MSS imagery is used to obtain the areal extent of each category. Surface area times elevation (depth) for each category yields directly the water volume retained by the area. Additionally, knowing the change in water storage and the surface inflow and outflow, it is possible to calculate the evapotranspiration and seepage, as illustrated in the model of figure 15.

Between February 14 and March 22 of 1973, three successive sets of LANDSAT-MSS data were combined with existing ground-truth data and the DCS data for Conservation Area 1. During this period, the water levels were declining, as noted previously in the hydrograph of figure 8, and the enhanced imagery, figure 12. For February 14 through March 22, the evapotranspiration and seepage, surface water distribution, and storage for Conservation Area 1 were computed as shown in figure 16. This trial run indicated that an operational water-management model for the Everglades is feasible.

SYSTEM DESCRIPTION

A system to satisfy the hydrologic data needs of water resources management is illustrated in figure 17. This system would be configured to achieve the benefits available from the combined use of LANDSAT MSS imagery and in situ monitoring by DCS.

The DCS part (figure 18) of the system is operational, however, the imagery part is not. One reason for this is the long delay (approximately 6 to 8 weeks after a LANDSAT pass) in obtaining LANDSAT imagery and computer tapes. The other reason is the difficulty of locating DCPs and other point sampling stations within the LANDSAT images and tapes. A computer technique (ref 17) has recently been developed that will permit the earth coordinates (latitude and longitude) of the sampling station to be called up and displayed on the LANDSAT scene (figure 19).

LANDSAT MSS images provide data on scene radiance, and changes in scene radiance corresponding to water "color" (reflectances) and changes that may be a result of parameters that include depth, turbidity, chlorophylls, algal population, particulate carbon among others. In situ measurements, by field teams or a DCP are essential to quantify the LANDSAT image response. LANDSAT imagery used as an adjunct to the point-sampling provides an economical basis for extrapolating water parameters from the point samples to unsampled areas, and provides a synoptic view of water mass boundaries that no amount of ground sampling or monitoring can provide.

The water budget example developed for Conservation Area 1 uses water stage from DCPs with water surface area from imagery to obtain water stage-volume relations. Figure 20 shows a color-enhanced image of southern Florida in LANDSAT band 7. As in the case of Conservation Area 1, water stage is associated with scene radiance as denoted by color but must be quantified by in situ measurements within each color category. The synoptic view by LANDSAT and computer processing (refs 17 and 18) rapidly provides surface area and volume relations.

In addition to using LANDSAT imagery to extrapolate from DCP measurements, LANDSAT imagery is also useful for optimizing the deployment of DCPs and field teams. As noted, LANDSAT responds to radiance and differences in scene radiance. Analysis of this imagery may show that two DCPs are occupying a water body of similar radiance. On the other hand, the imagery may show areas in which a significant change has occurred and in which a DCP should, perhaps, be positioned to quantify change. For

example, LANDSAT imagery may be used to monitor a basin wherein mining is occurring. A change in radiance of a water body in the area may be very significant. A field team may be deployed to point sample and to set up a DCP to quantify reasons for change.

The LANDSAT MSS data also provide an economical base for computerized mapping of land use about DCPs providing water quality indicators, i. e., dissolved oxygen, conductivity, turbidity, etc. Ready access of land use information about these DCPs will permit cause-effect studies which will result in a better understanding of factors causing changes in water quality.

SUMMARY

The usefulness of LANDSAT to improving the overall effectiveness of collecting and disseminating hydrologic data was evaluated. LANDSAT MSS imagery and in situ monitoring by LANDSAT-DCS were used to evaluate their separate and combined capabilities.

Twenty data collection platforms were established in southern Florida. Water level and rainfall measurements were collected and disseminated to users in less than 2 hours, a significant improvement over conventional techniques requiring up to 2 months. The improved network performance is having a significant and beneficial impact on the development of water budgets and the water distribution to the people, fauna, and flora of southern Florida.

LANDSAT imagery was found to significantly enhance the utility of ground measurements. Water stage is correlated with water surface areas from imagery in order to obtain water stage-volume relations. As an adjunct to the point sampling, the imagery provides an economical basis for extrapolating water parameters from the point samples to unsampled data and provides a synoptic view of water mass boundaries that no amount of ground sampling or monitoring could provide. Additional hardware and software developments are needed to fully achieve the benefits available in the combined use of DCS and MSS data.

The DCS system is now an operational element in the hydrologic data network in south Florida. Water-stage and rainfall from ground stations are transmitted from the Everglades via LANDSAT, the NASA tracking stations, and the Geological Survey, to the Corps of Engineers. Other users receiving water resource data from this network include Central and Southern Florida Flood Control District, the National Park Service, and the U.S. Fish and Wildlife Service.

The importance of the space-relayed data can also be shown by a comparison of the accuracy and frequency of data received through the Miami Geological Survey teletypewriter with data from the existing remote radio transmission systems in southern Florida. Even though these microwave systems transmit "line-of-sight" from tower to tower, the frequent meteorologic disturbances in south Florida prevent the reliable transmissions of accurate synoptic information on rainfall and water stage that is essential in managing water resources. LANDSAT on the other hand, has been providing the Geological Survey with five transmissions of these parameters per day and an opportunity to service faulty platform recorders within 24 hours. This enhances the opportunity for a constant flow of information and makes it possible for the U. S. Corps of Engineers and the Central and Southern Florida Flood Control District to make daily decisions in managing and controlling the water resources.

The DCS System also makes it possible to develop strategies for efficient field manpower deployment. For example, with DCS, manpower can be deployed to malfunctioning stations or to stations that are recording extraordinary hydrologic conditions where supplementary manual measurements are highly desirable. The emphasis can be shifted to sending personnel where they are most needed, instead of the routine station-servicing trips. This improves the manpower efficiency, decreases the down-time of hydrologic instruments and data loss, and frees manpower for new high-priority activities. Also, data from the network can be made available in near-real time to meet the growing data needs of water-resource management agencies.

ACKNOWLEDGMENTS

The authors wish to express their appreciation for the many contributions to this investigation supplied by:

- The NASA Kennedy Space Center Earth Application Office (for use of their digital-optical system for processing LANDSAT imagery).
- The Bendix Aerospace Systems Division; Larry E. Reed, N. J. Shah, and C. L. Wilson (for use of electronic data processing equipment and techniques).
- The U. S. Corps of Engineers, the U. S. Department of the Interior, Fish and Wildlife Service, and the U. S. National Park Service (for their support of the DCS Program).

REFERENCES

1. U. S. Dept. of Interior Geological Survey Investigation I-85 O; "Resources and Land Information"; South Dade County; 1973.
2. William V. Storch; "Budget Reflects State of Water Resources and Demands"; In-Depth Report Vol 1 No. 1; Central and Southern Florida Flood Control District; Jan 1972.
3. Aaron L. Higer Paper W6; "Water-Management Models in Florida from ERTS-1 Data"; Third Earth Resources Technology Satellite-1 Symposium; Vol I Sect B; Dec 1973.
4. U. S. Geological Survey, Water Resources Data for Florida, Part I Surface Water Records for 1973, U. S. Department of the Interior publication.
5. Richard W. Paulson; "An Evaluation of the ERTS Data Collection System as a Potential Operational Tool"; Cite Ref 3.
6. R. W. Paulson; An Evaluation of the ERTS Data Collection System as a Potential Operational Tool; Open-file, National Aeronautics Space Administration; ERTS-1 Third Symposium; 10 to 14 Dec 1973.
7. H.H. Schumann; Hydrologic Applications of ERTS-1 Data Systems in Central Arizona; National Aeronautics Space Administration; ERTS-1 Third Symposium; 10-14 Dec 1973.
8. Saul Cooper; A Real Time Data Acquisition System by Satellite Relay; National Aeronautics Space Administration; ERTS-1 Third Symposium; 10-14 Dec 1973.
9. Gary Graybell and Forrest Hull; ERTS-1 Data in Support of the National Program of Inventory and Inspection of Dams; National Aeronautics Space Administration; ERTS-1 Third Symposium; 10-14 Dec 1973.
10. Morris Deutsch and F.H. Ruggles, 1974; Optical Data Processing and Projected Applications of the ERTS-1 Imagery Covering the 1973 Mississippi River Valley Floods; National Aeronautics Space Administration; ERTS-1 Third Symposium; 10-14 Dec 1973.

11. R. R. Anderson, Virginia Carter, and G. C. McGinness; Applications of ERTS-1 Data to Coastal Wetland Ecology with Special Reference to Plant Communities, Mapping, and Typing and Impact of Man; National Aeronautics Space Administration; ERTS-1 Third Symposium; 10-14 Dec 1973.
12. C. C. Reeves, Jr.; Dynamics of Playa Lakes in the Texas High Plains; National Aeronautics and Space Administration; ERTS-1 Third Symposium 10-14 Dec 1973.
13. Earth Resources Technology Satellite Data Users Handbook; NASA Document 71DS4249; Goddard Space Flight Center, Greenbelt, Maryland; 1971.
14. General Electric Space Div; Earth Resources Technology Satellite Data Collection Platform Field Installation, Operation, and Maintenance Manual; Contract NAS S-21697; Valley Forge Space Center 7ZSD 4208; 27 March 1972.
15. W. Hagenbuck, R. Thompson, and D. Rogers; "A Preliminary Investigation of the Effects of Water Levels on Vegetative Communities of Loxahatchee National Wildlife Refuge, Florida"; Report DI-SFEP-74-20; US Dept. of Interior, Bureau of Sport Fisheries and Wildlife; Feb 1974.
16. US Dept of Interior, Fish and Wildlife Service, Bureau of Sport Fisheries and Wildlife; Paper RL-175-R-3; Birds of the Loxahatchee National Wildlife Refuge; Revised March 1967.
17. R. H. Rogers, L. Reed, N. J. Shah, and V. E. Smith; "Computer Mapping of Turbidity and Circulation Patterns in Saginaw Bay, Michigan (Lake Huron) from ERTS Data"; Proceedings of ASP-ACSM Convention at Washington, D. C.; March 1975.
18. R. H. Rogers, L. E. Reed, N. J. Shah; "Automatic Classification of Eutrophication of Inland Lakes from Spacecraft Data"; Proceedings of the Ninth International Symposium on Remote Sensing of Environment; Vol II, April 1974.

Table I

TYPICAL WATER LEVEL AND RAINFALL REPORT
TELECOPIED TO DATA USERS

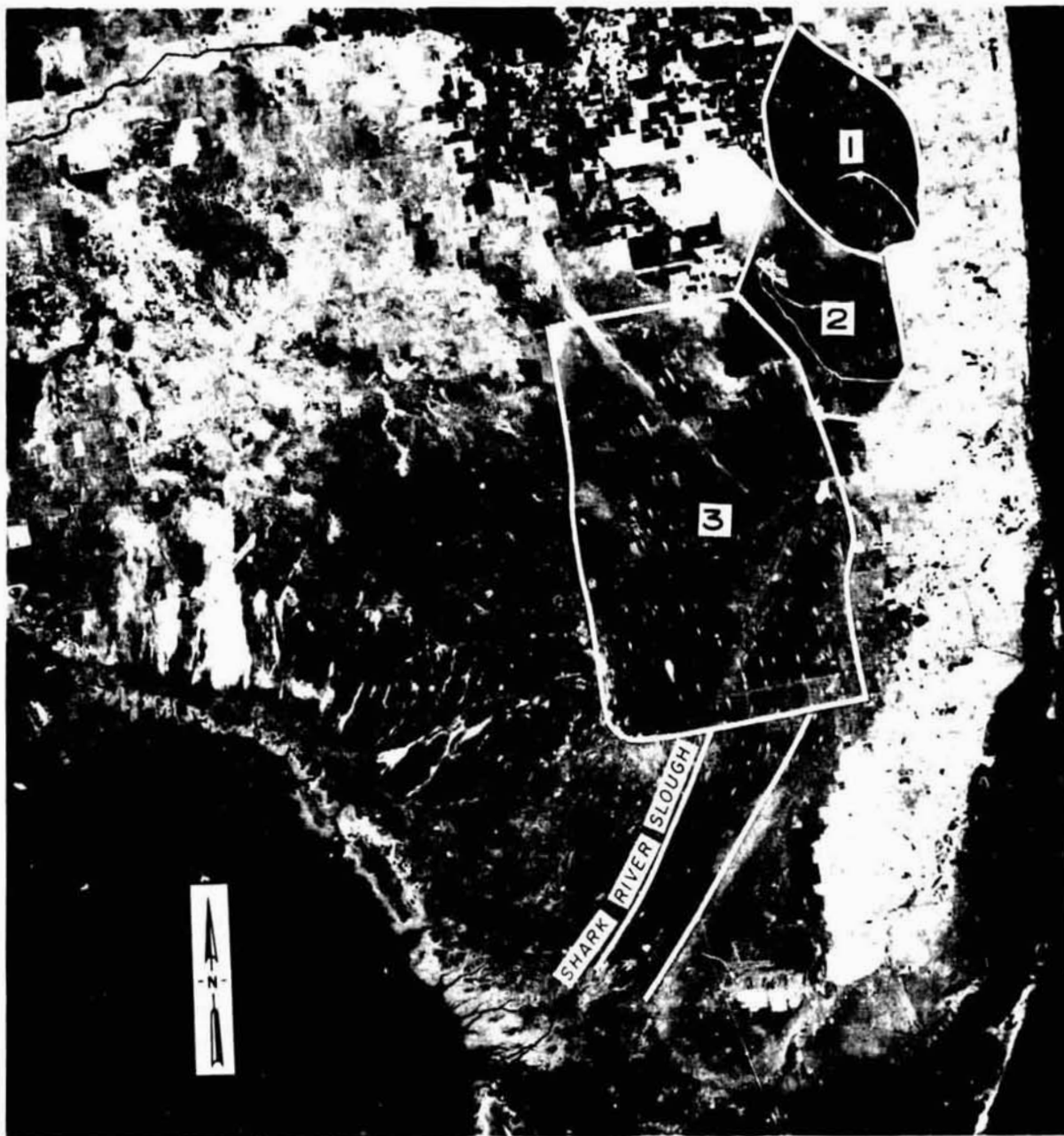
USGS MIAMI FLA. DATA FROM LANDSAT SATELLITE WATER SURFACE ELEVATION FT MEAN SEA LEVEL							
DATE DAY TIME	32 FRI 2343	33 SAT 2348	34 SUN 2354	35 MON 2359	36 TUE 2221	37 WED 2227	38 THUR 2355
128	16.62	16.61	16.61	16.59	16.56	16.53	16.52
141	16.48	16.47	16.49	16.46	16.44	16.43	16.42
142	16.44	16.42	16.42	16.41	16.39	16.37	16.35
111	12.36	12.34	12.33	12.30	12.27	12.26	12.23
112	12.10	12.07	12.05	12.02	12.00	11.98	11.97
62	9.42	9.38	9.38	9.36	9.31	9.26	9.21
63	8.67	8.64	8.64	8.61	8.58	8.56	8.54
64	8.47	8.46	8.46	8.44	8.43	8.42	8.41
65	8.41	8.40	8.39	8.38	8.37	8.36	8.35
5	5.67	5.66	5.65	6.64	5.62	5.62	5.61
15	2.77	2.76	2.75	2.74	2.73	2.72	2.71
105	6.71	6.67	6.65	6.61	6.57	6.54	6.50
RAINFALL IN INCHES							
128	0.00	0.00	0.00	0.00	0.00	0.00	0.00
141	0.00	0.00	0.25	0.00	0.00	0.00	0.00
142	0.00	0.00	0.00	0.06	0.00	0.00	0.00
111	0.00	0.00	0.19	0.00	0.00	0.00	0.00
112	0.00	0.00	0.06	0.00	0.00	0.00	0.00
62	0.00	0.00	0.06	0.00	0.00	0.00	0.00
63	0.00	0.00	0.00	0.00	0.00	0.00	0.00
64	0.00	0.00	0.00	0.00	0.00	0.00	0.00
65	0.00	0.00	0.00	0.00	0.00	0.00	0.00
5	0.00	0.00	0.00	0.00	0.00	0.00	0.00
15	0.00	0.00	0.00	0.00	0.00	0.00	0.00
105	0.00	0.00	0.00	0.00	0.00	0.00	0.00

Note: Readings will be revised as later data are received



12397A-1

Figure 1 Photo mosaic of Florida, compiled from 16 LANDSAT images between October 1972-April 1973 of band 7 of the multi-spectral scanner. The delineated area is the Everglades.



12397A-2

Figure 2 A LANDSAT Multispectral Image, Band 7, March 22, 1973, NASA, E-1242-15240, of South Florida. The areas outlined are: Conservation Areas 1, 2, and 3 and Shark River Slough. Lake Okeechobee can be seen at top of photo.

REPRODUCIBILITY OF THIS
ORIGINAL PAGE IS 100%

WATER BUDGET = $\text{INFLOW} + \text{RAINFALL}$
 $-\text{EVAPORATION} - \text{TRANSPIRATION} - \text{SEEPAGE} - \text{OUTFLOW}$

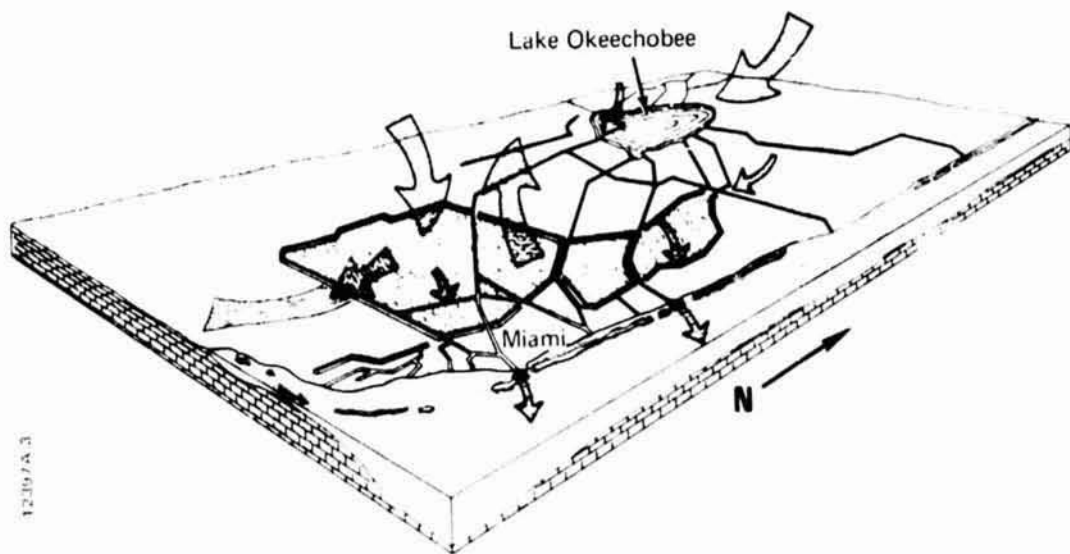


Figure 3. Schematic diagram of a water budget for the Everglades, southeast Florida

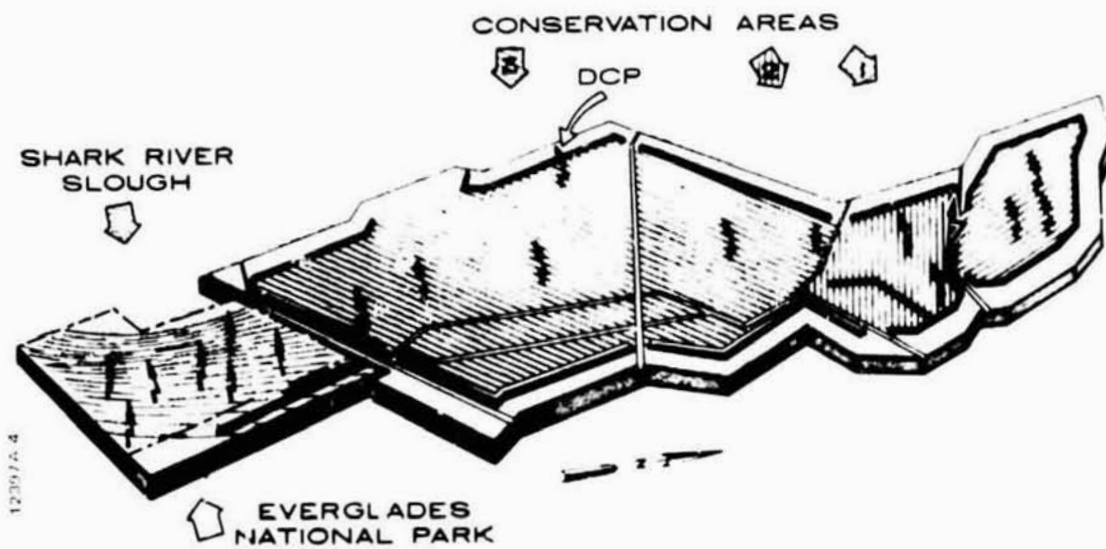


Figure 4 Schematic diagram of the Everglades basin, showing relative locations of the data collection platforms within the three conservation areas and the Shark River Slough.

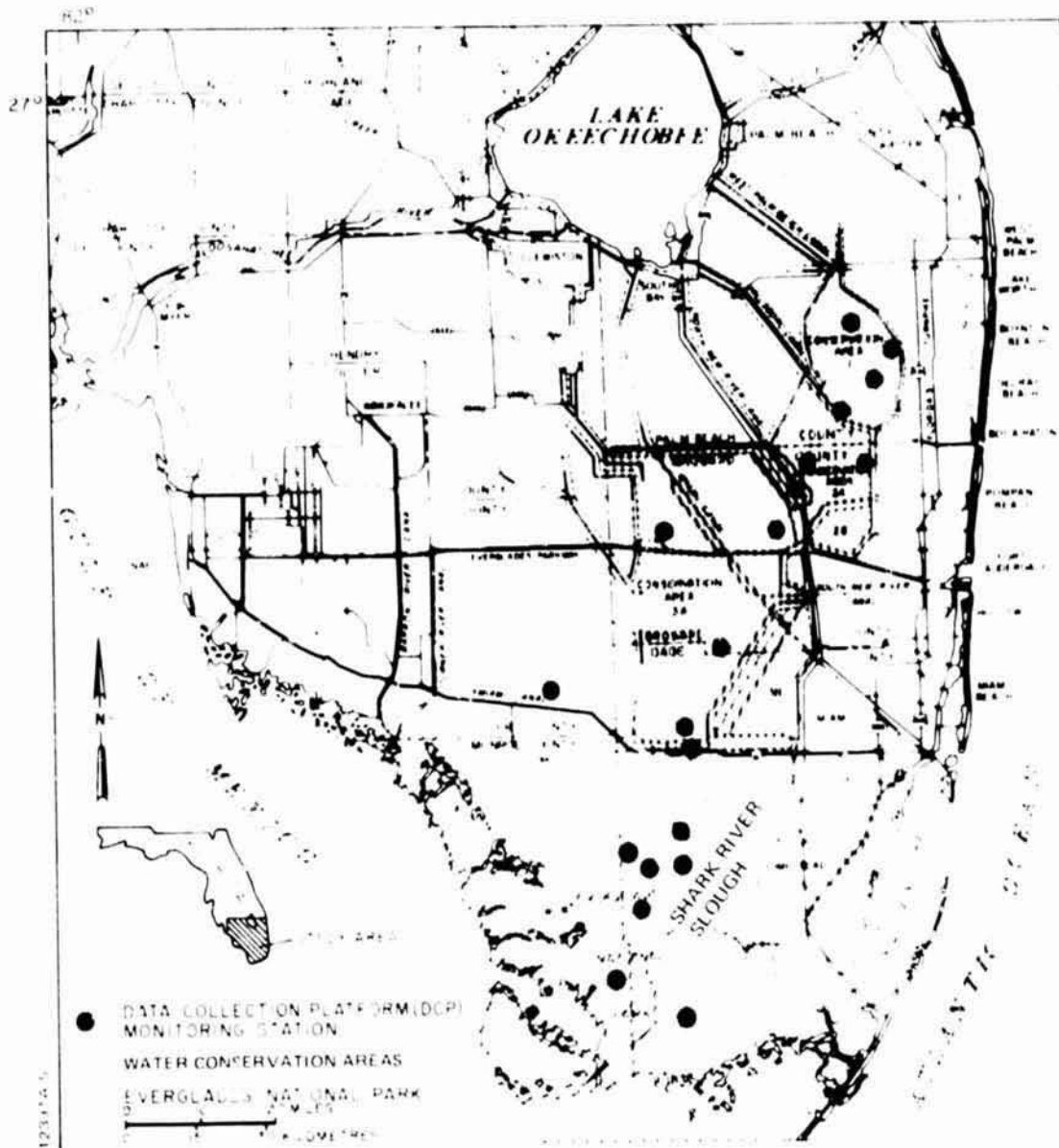


Figure 5 Locations of conservation areas and DCP monitoring stations.



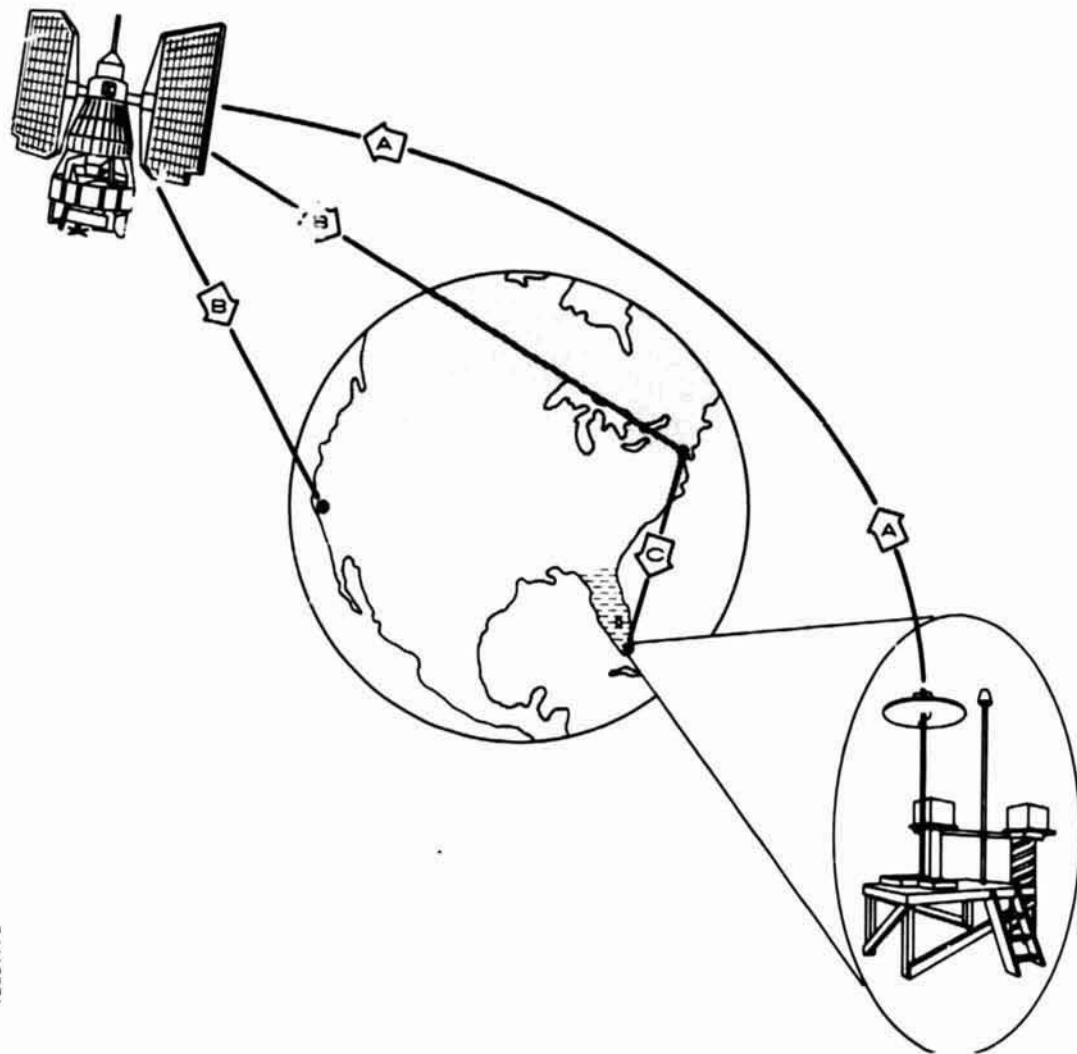
12397A-6

Figure 6 Data collection platform in Conservation Area 1. These stations collect and transmit water-level and rainfall data for relay by LANDSAT.



12397A-7

Figure 7 Team collecting ground truth data such as plant community identification and soil characteristics in Conservation Area 1.



12397A 8

Figure 8 Data are transmitted from the data collection platforms in the Everglades (A) via LANDSAT to NASA tracking stations at Goldstone, Calif., and GSFC, Greenbelt, Md. (B). The data are then transmitted, via NASA communications network, to the Geological Survey office in Miami.

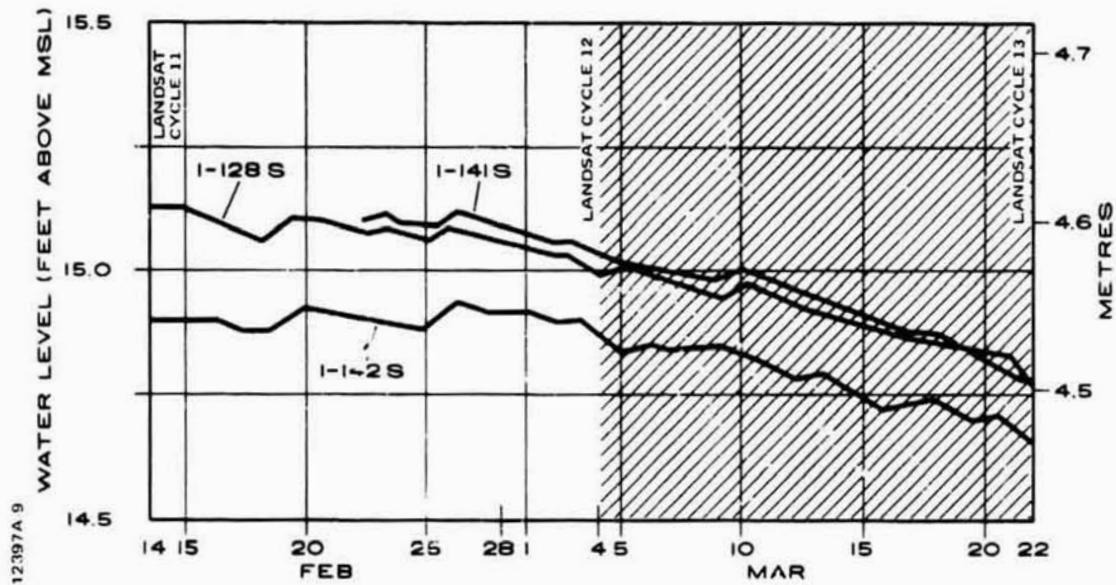
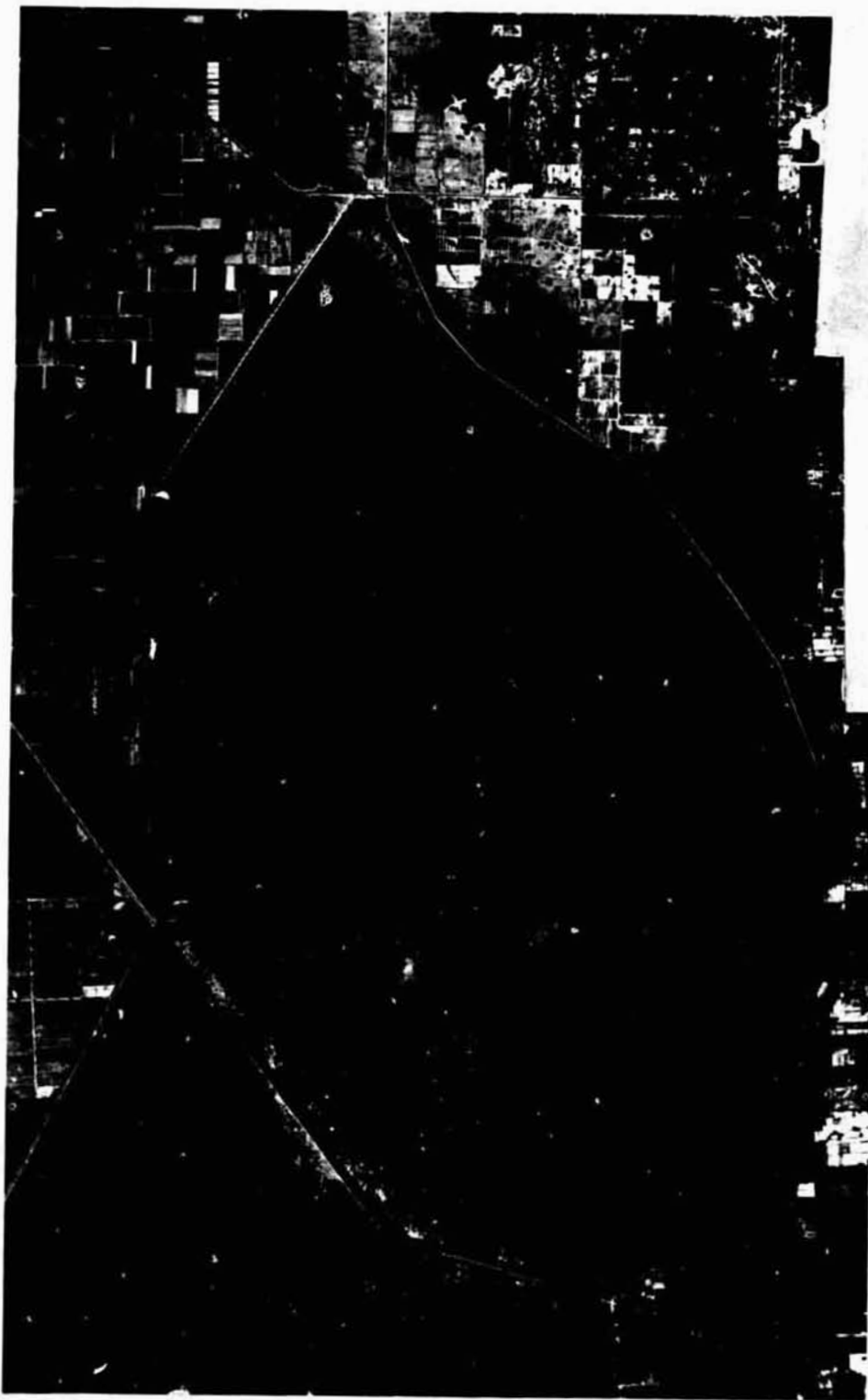


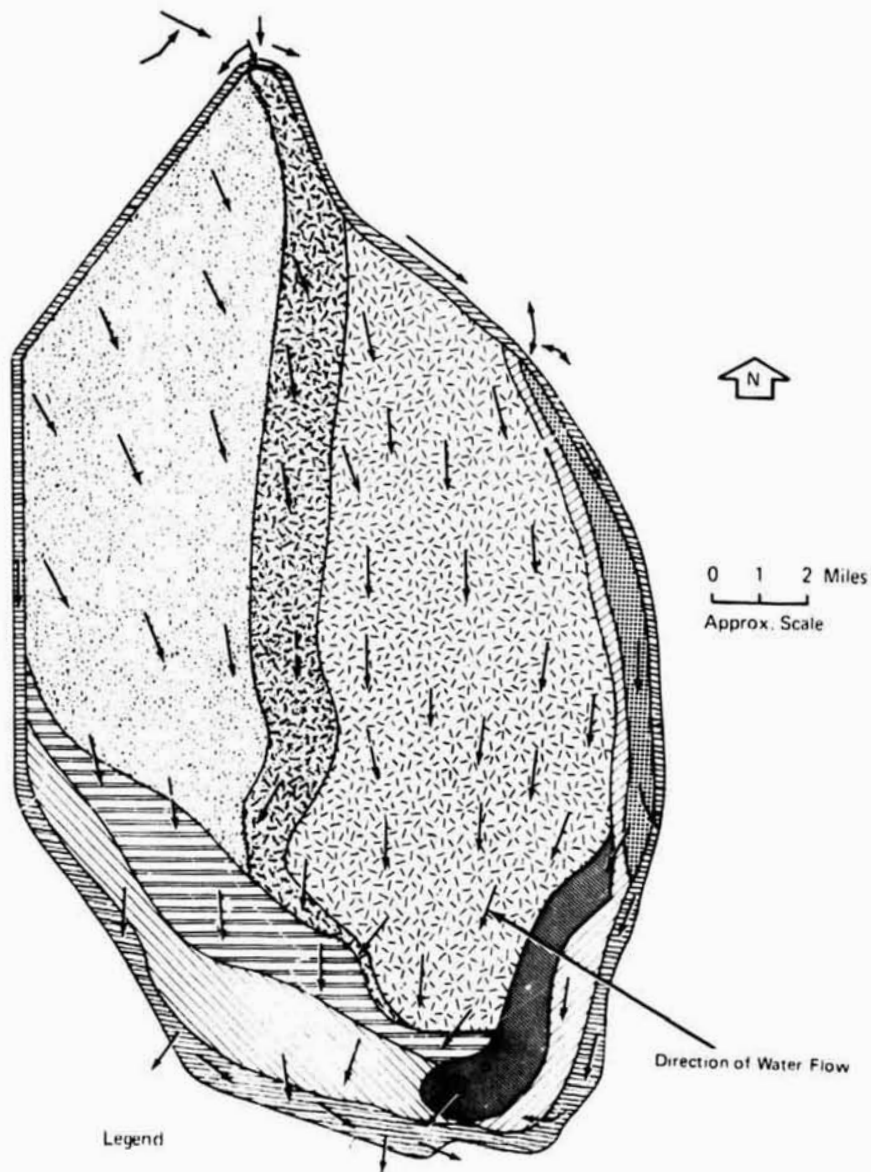
Figure 9 Hydrographs compiled from daily recordings from three DCPs in Conservation Area 1, February 14 - March 22, 1973. During this period LANDSAT MSS imagery was collected for the three LANDSAT overflights noted as cycles 11, 12, 13.



12397A-10

Figure 10 NASA U-2 Photomosaic of Conservation Area 1
January 1973

REPRODUCIBILITY OF
ORIGINAL PAGE IS 100%



Legend

- | | |
|--|---|
|  Sawgrass Mixed Grass
Myrtle Holly Heads |  Sawgrass Cattail |
|  Transition |  Aquatic |
|  Wet Prairie Tree Island
Aquatic Sloughs Lakes |  Sawgrass Pickerelweed Brush |
|  Ridge Sawgrass Myrtle |  Sawgrass Spikerush |
| |  Maidencane |

Figure 11 Vegetation zones of Conservation Area 1 as determined by US Department of Interior, Fish and Wildlife Service, Bureau of Sport Fisheries and Wildlife.

12397A 11



February 14, 1973

March 4, 1973

March 22, 1973

Figure 12 Radiance (reflectance) map, of the Loxahatchee Wildlife Refuge (Conservation Area 1) produced from enhanced LANDSAT band 7 imagery. Darker map tones correspond to lower radiance (reflectance) and deeper water. Black is deepest (0.6 Metre) and white is dry land.

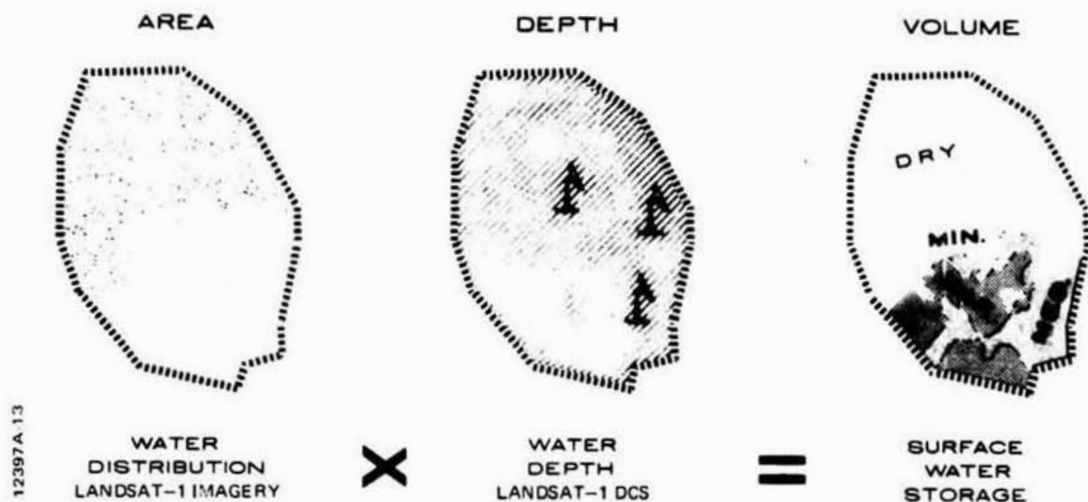


Figure 13 Schematic of use of space-relayed data to calculate surface-water storage. LANDSAT data of three successive passes on February 14, March 4, and March 23, 1973, of Conservation Area 1 were used to demonstrate feasibility of this method of determining surface-water storage.

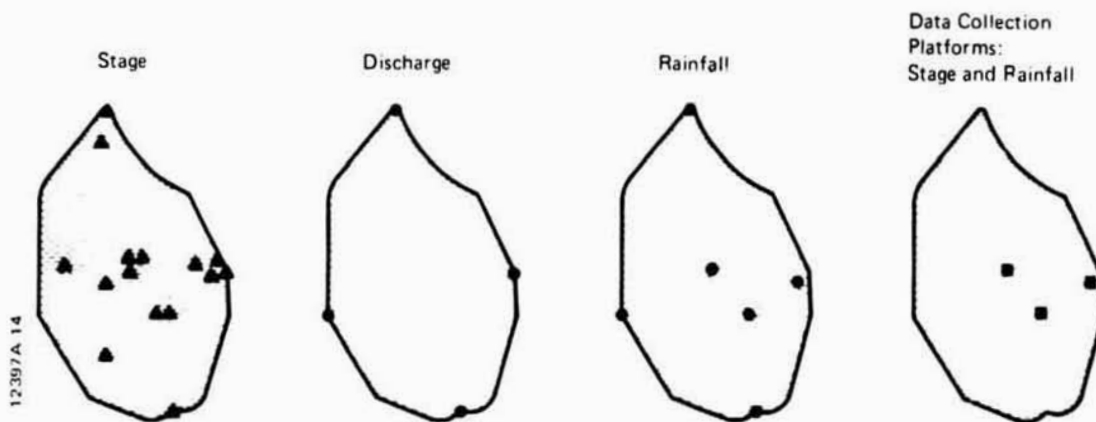


Figure 14 Location of ground truth station used in the evaluation of the February 14, March 4, and March 22, 1973, MSS data for Conservation Area 1.

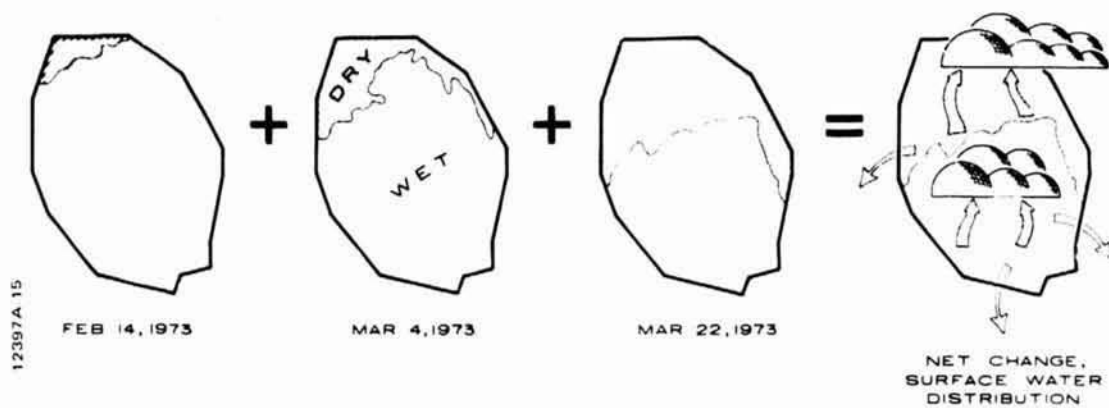


Figure 15 Schematic of use of space-related data to calculate evapotranspiration and seepage. LANDSAT data of three successive passes on February 14, March 4, and March 22, 1973, of Conservation Area 1 were used to demonstrate feasibility of determining evapotranspiration and seepage.

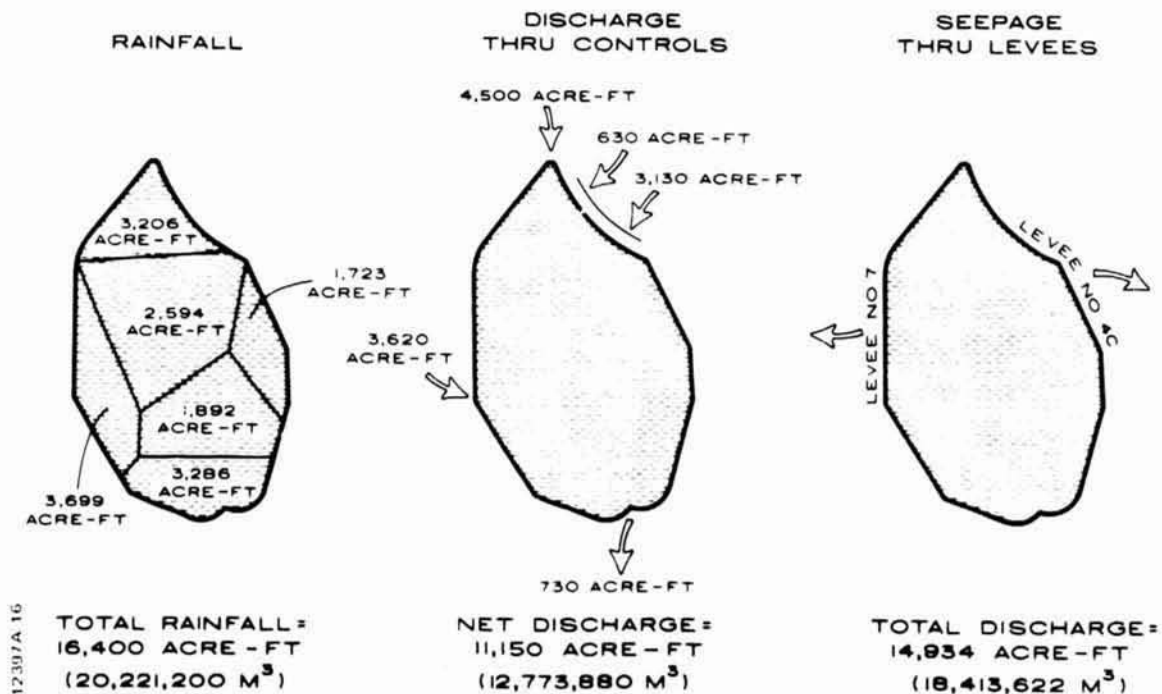


Figure 16 Hydrologic measurements compiled for interpreting MSS data for February 14, March 22, 1973 in Conservation Area 1. Source of Data: U.S. Corps of Engineers, oral communication.

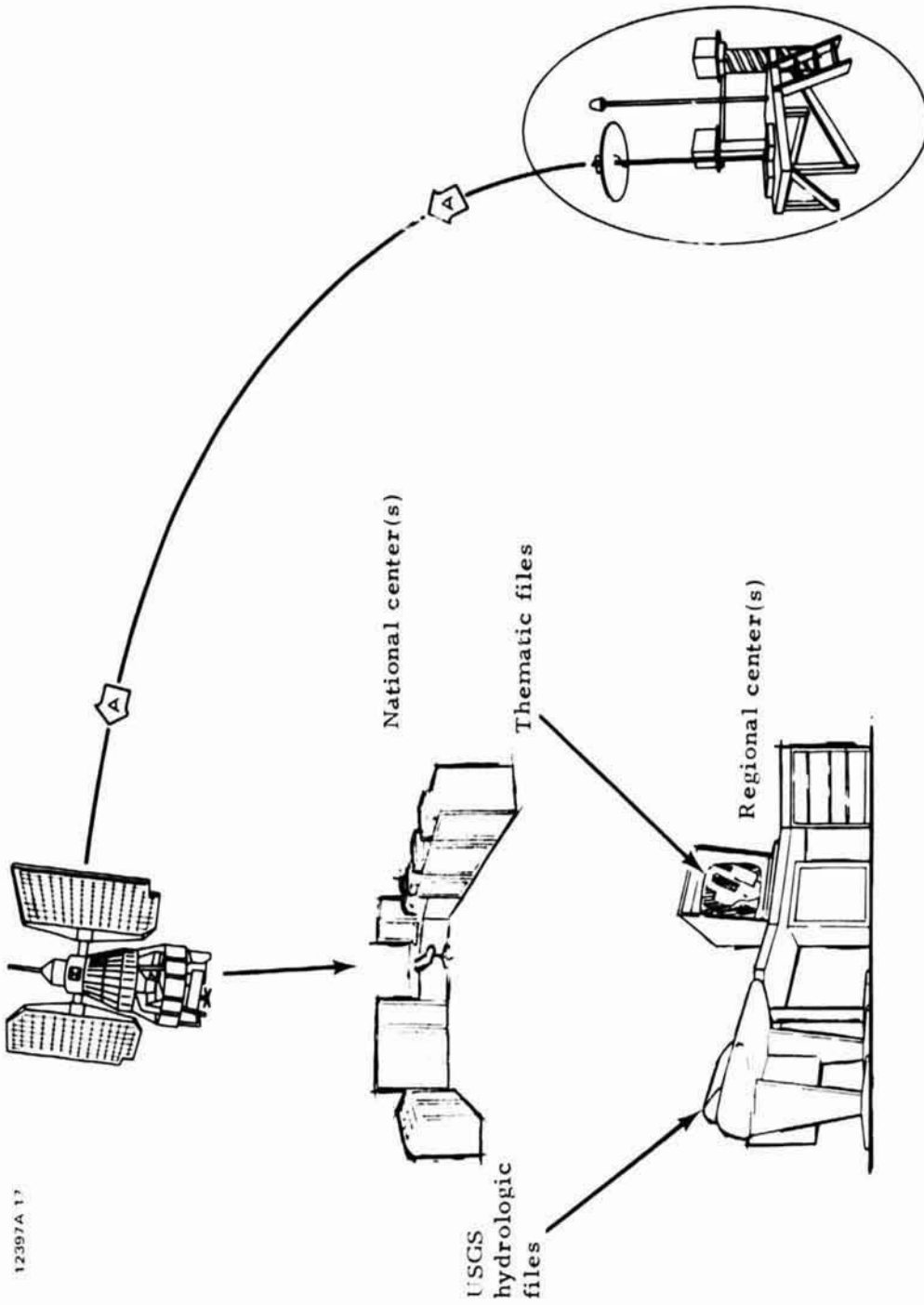
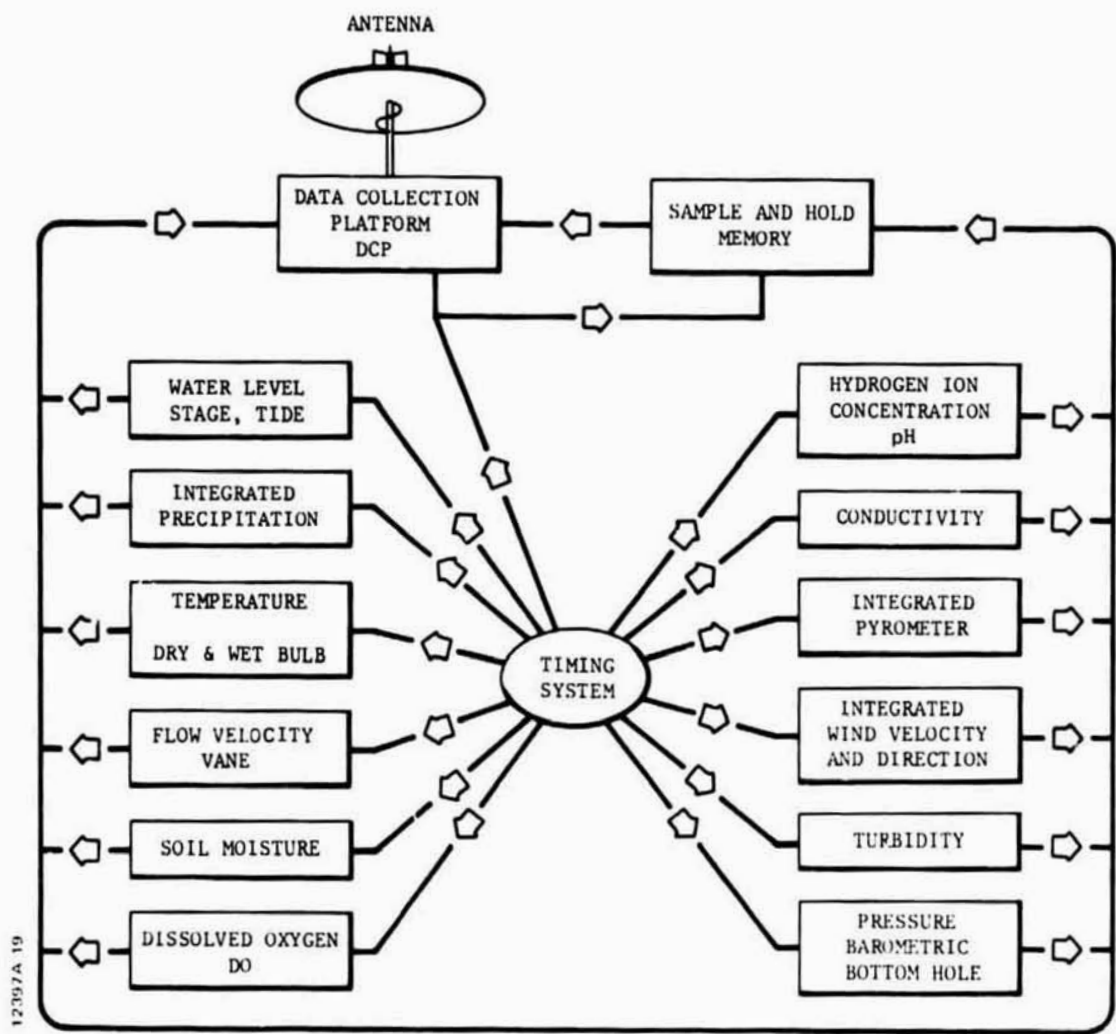


Figure 17 Concept of water management system operation.



12397A 19

Figure 18 Schematic of proposed system of parameters that are being connected to data collection platforms in water management areas in Florida. The sample and hold memory system developed by the Geological Survey will allow a daily collection of between 18 and 24 hours of data on the needed parameters to complete a water quality and quantity budget.

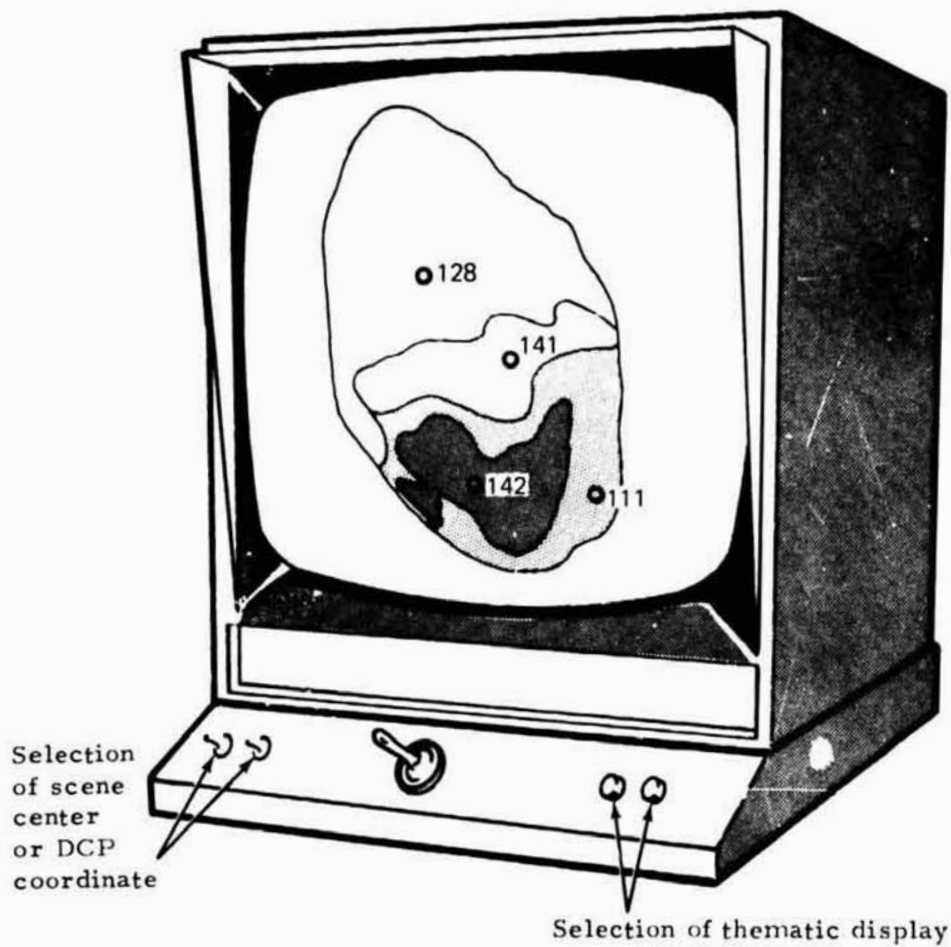


Figure 19

Simulated TV display of LANDSAT MSS data with annotated location map of DCF's. Display inputs include latitude and longitude of scene center and theme (land-water categories)

REPRODUCIBILITY OF
ORIGINAL PAGE IS 100%

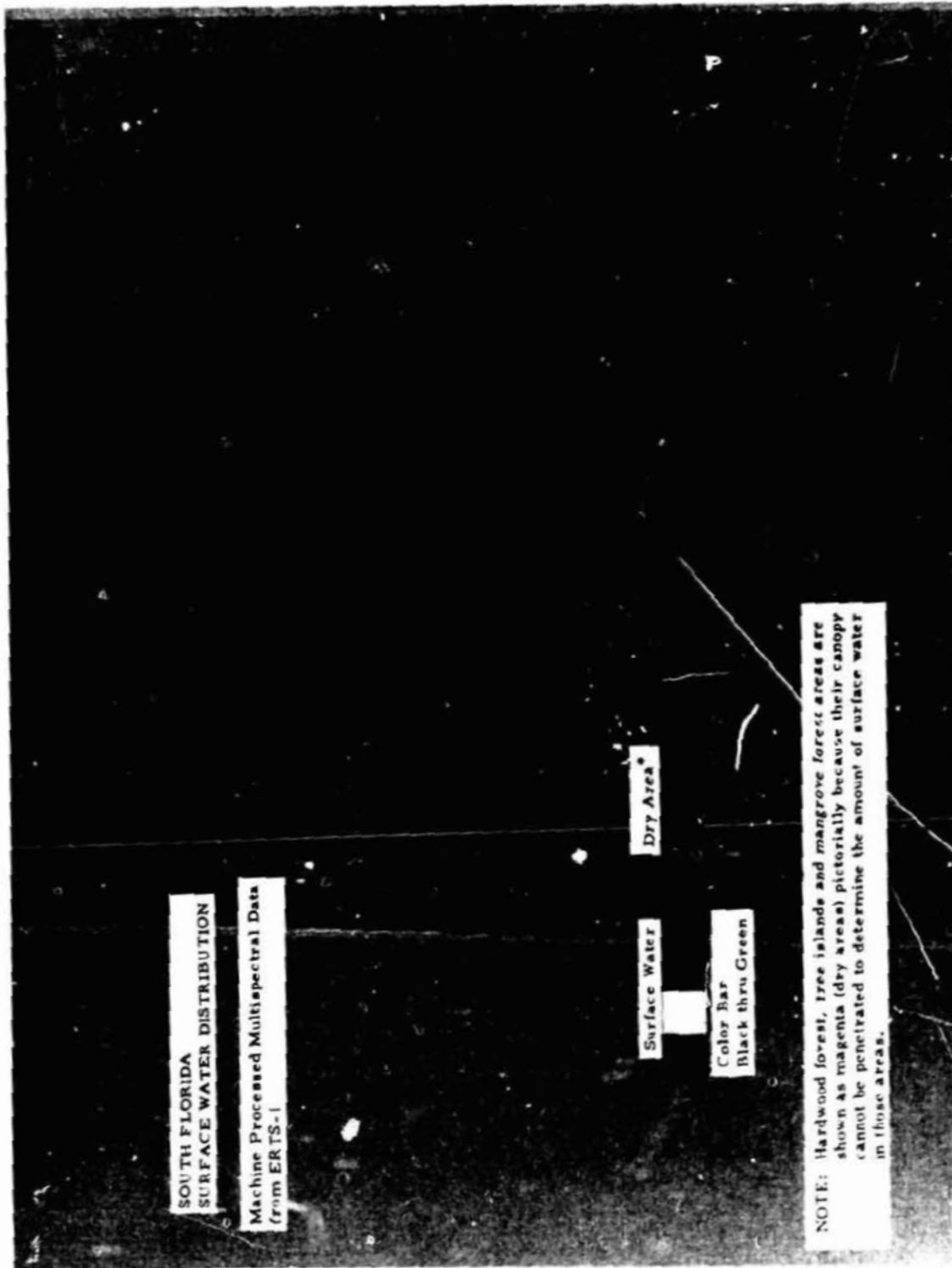


Figure 20 Color-enhanced LANDSAT image of south Florida. LANDSAT scene E-1242-15249, March 22, 1973. Yellow through black shades represent water of increasing depth, yellow indicating the shallowest water, black the deepest.

THE USE OF LANDSAT DCS AND IMAGERY IN
RESERVOIR MANAGEMENT AND OPERATION

W-17

Saul Cooper, New England Division, Corps of Engineers, Waltham, Massachusetts; Dr. Paul Bock, University of Connecticut, Storrs, Connecticut; Dr. Joseph Horowitz, New England Division, Corps of Engineers; and Dennis Foran, University of Connecticut

N76-17604

1.0 INTRODUCTION

The New England Division (NED), Corp. of Engineers has experimented with the LANDSAT-1 Data Collection and Imaging Systems for more than two years, following the launch of the satellite in July 1972. The purpose of this experiment has been to evaluate the future usefulness of data products received from satellites such as LANDSAT in the day-to-day operation of the NED water resources systems used to control floods.

2.0 BACKGROUND

The New England region, shown on figure 1, is comprised of a number of watersheds, draining hilly terrain. The NED area of responsibility covers all of Maine, New Hampshire and Vermont to the western limits of the Connecticut River basin, Massachusetts, Connecticut to the western edge of the Housatonic River basin and Rhode Island. Most of the population in New England lives in the southern and central regions. With the high degree of development that has taken place along the rivers and coastal locations have come the perennial problems of flood damage and flood protection. The Corps of Engineers has expended over \$300 million for a flood control system consisting of 35 reservoirs, 37 local protection projects and 4 hurricane barriers. The flood control plan in each river basin consists of upstream reservoirs and dikes and floodwalls at the principal damage centers. All reservoirs have storage allocated for flood control and many have storage for other uses such as recreation, water supply and conservation. NED reservoirs presently have no storage for power, irrigation or navigation.

The New England Division also is responsible for providing such flood prevention aids as engineering reports on streams, shores and flood plains, flood insurance studies and flood plain management services. National disaster recovery and restoration work is a continuing responsibility of the Corps. The Division also improves harbors and navigation channels and administers laws relating to the preservation of navigable waters as well as protection of water and overall environmental quality.

2.1 THE NATURE OF FLOODING IN NEW ENGLAND

The New England region is subject to floods every month of the year. The probability is greatest in the spring when snowmelt occurs and the rivers are flowing at or near bankfull capacity for several weeks. Most of the minor and moderate floods occur during the spring runoff period and can encompass the entire region rather than a single basin. During the hurricane season, various portions of the region may be exposed to both river and tidal flooding related to the path of a hurricane. Coastal storms in any season may produce similar although usually less severe conditions.

2.2 THE NEW ENGLAND DIVISION WATER CONTROL SYSTEM

Figure 2 shows locations of the Corps of Engineers flood control reservoirs in New England, most of which are in the following river basins:

<u>Basin</u>	<u>Square Miles</u>
Connecticut	11,300
Merrimack	5,000
Housatonic	1,900
Thames	1,500
Blackstone	500

The four hurricane barriers are on the southern New England coastline -- one in Massachusetts, one in Rhode Island, and two in Connecticut.

Of the 35 reservoirs, seven hold back floodwaters automatically, with releases controlled by small ungated conduits. These projects control runoff from drainage areas of 3 to 20 square miles. The remaining 28 reservoirs, with drainage areas of approximately 25 to 1,000 square miles are gated, staffed 24 hours a day, with all storages and releases under the direction of the New England Division, Reservoir Control Center (RCC) in Waltham, Massachusetts. Figure 3 shows North Hartland Lake, in Vermont, under normal conditions, while figure 4 shows the same reservoir using 50 percent of its storage capacity to hold

back floodwaters of early July 1973. Figure 5, the Quinebaug River at Putnam, Connecticut in 1955, shows the type of damage that can occur in the absence of any flood control measures.

Most of the NED reservoirs are regulated initially to reduce damaging stages on their respective tributaries. Further, in each of the five river basins the reservoirs are operated as part of a flood control plan to optimize flood stage reductions at main stem damage centers. Flows are regulated to desynchronize their contributions to main stem flooding. Following a flood the stored waters are released from each reservoir as quickly as downstream conditions permit in order to have storage space available for the next flood.

Two of the four hurricane barriers have navigation gate openings, and NED is responsible for directing the closure of these gates during severe coastal storms and hurricanes to prevent damage from tidal flooding. Figure 6 is a picture of the New Bedford hurricane barrier located in New Bedford, Massachusetts.

2.3 DATA COLLECTION FOR WATER RESOURCES REGULATION

2.3.1 Introduction

Regulation of a large flood control system to prevent potential damages requires the acquisition of important hydro-meteorological data on a reliable and timely basis. The types of data required and time constraints thereon have gradually increased, not only with the growing number of projects in New England, but also with the increasing complexities of functional requirements associated with the individual projects and systems. The following paragraphs will outline the manner in which the New England Division has responded to these needs to date.

2.3.2 Historical Perspective

Until the late 1950's NED did not have sufficient reservoirs in a single river basin to exert a large amount of control. Data collection was through field observation or telephone relay from instruments, with all information reaching the RCC via

telephone. Although this was time-consuming and subject to communication outages, telephone lines were considered adequate to meet regulation needs of that time.

With the growth of the flood control system over the past 15 years, NED can now effectively reduce flooding on the tributaries as well as control levels on main stems in the basins it regulates. In the 1960's a comprehensive voice radio data collection network was established in order to operate the NED flood control system. Each manned dam and hurricane barrier was equipped with a voice radio for relaying data, as well as for receiving instructions from the Reservoir Control Center. All project managers, residing at their respective dams, are responsible for obtaining and reporting data from a group of index stations, either from telephonically equipped river gages, cooperative observers or visual observations. This information usually consists of river stages and conditions at strategic locations, precipitation reports in the basin, climatologic and hydrologic data at the dams, and snow cover in the late winter and spring months.

2.3.2.1 The NED Automated Data Collection System for Real Time Management of Water Resources

Receiving reports, even by voice radio from approximately 30 projects is still time consuming; therefore, in January 1970, NED dedicated a new Automatic Hydrologic Radio Reporting Network (AHRRN). This system consists of 41 remote (unmanned) reporting stations which are situated at key index locations and report information such as river stage, reservoir level and precipitation directly to RCC in real time. Two stations provide data for the operation of hurricane barriers by reporting tide elevation, wind speed, wind direction and barometric pressure. Four ground-based relay stations transmit signals from different sections of New England to RCC. In order to bring strong, reliable radio signals from remote reporting stations to the relays, 12 repeater stations have also been established at various locations within the system. Figure 7 shows the location of the 41 remote unmanned reporting stations, 12 repeater and 4 relay stations. Table 1 lists the reporting stations and parameters.

The reporting stations and repeaters use batteries as primary sources of power. This eliminates many problems that

can arise during major floods and hurricanes when power and telephone lines are down and normal means of communication fail. Batteries are charged either by thermoelectric generators or AC power where available. When the outside source of power is out, the batteries have sufficient energy to operate for about three weeks without recharging. The relays are operated on commercial power and backed up by gasoline generators.

The Automatic Hydrologic Radio Reporting Network is interfaced at the RCC to a computer and can be interrogated in either a manual or automatic mode. Under computer programmed control, reporting stations can be interrogated singly or as a group at automatically selected or various time intervals. Normally an interrogation of all stations is made every 6 hours; however, during flood periods the system is interrogated every 2 or 3 hours. During hurricanes or severe coastal storms the two coastal stations report every 15 or 30 minutes. Response time is about 3 seconds for interrogation of any given station. A complete set of readings for all 41 stations is obtained and printed out in approximately 4 minutes (see figure 8). River stage data is converted to flow and all data received at the RCC are stored in the computer for further analysis.

Also, information received at RCC is retransmitted to five strategic manned reservoirs. In addition, each of these can interrogate certain stations in its own area without going through the RCC.

2.3.3 The Need for Further Advancements in Improved Water Information Systems

Technological advancements in data collection, transmission and analysis must continue to meet the growing demand of the public in multiple use water resources management and the parallel need for preservation of environmental quality. The RCC pursues studies in those areas which show promise of implementation either to improve functions or reduce costs.

3.0 THE NEW ENGLAND DIVISION LANDSAT EXPERIMENT - SCOPE AND OBJECTIVES

The purpose of this study is to determine and report on the extent hydrometeorologic information received from LANDSAT

can be utilized by the Reservoir Control Center in the performance of its regulation functions related to the operation of water control projects.

3.1 DATA COLLECTION SYSTEM STUDIES

LANDSAT-1 has been the first earth satellite available for demonstrating the potential of satellites to relay hydrometeorological data. NED's studies with the LANDSAT-1 Data Collection System have had the following goals:

a. Helping evaluate the potential future usefulness of earth satellites in the relay of real time hydrometeorological data in the day-to-day operation of NED water resource projects and including: (1) the development of statistics, based on the LANDSAT-1 experience, that demonstrate aspects of the relationship between satellite relay and the currently existing means of acquiring this data, and (2) a preliminary investigation into the desirability and feasibility of establishing and operating a satellite network on a Corps-wide basis.

b. Assisting in evolving procedures for the selection of the most economically feasible and technically useful combination of data collection points to provide all necessary information for the optimal regulation of our water control system.

3.2 IMAGERY AND IMAGERY/DATA COLLECTION SYSTEM INTERACTION STUDIES

The analysis of LANDSAT imagery at the New England Division has been focused on an evaluation of the ability of the LANDSAT imagery to provide useful and timely supplementary hydrologic information for reservoir regulation purposes. NED's studies with the LANDSAT-1 Imagery System have had the following goal:

a. Determining the extent to which LANDSAT-1 imagery can supplement or replace present data sources in assessing various operationally useful phenomena such as:

(1) Location and coverage of surface waters, especially during flood and low flow periods.

(2) Icing conditions on rivers, lakes, reservoirs

and around hurricane barriers.

(3) Turbidity and sedimentation in lakes and reservoirs.

(4) Location and extent of snow cover.

(5) Location and extent of excessive precipitation accumulation.

(6) Tidal levels and flooding at or near hurricane barriers.

(7) Soil moisture conditions.

b. Assessing the value of the LANDSAT Data Collection System for providing the ground truth necessary for correlation with information acquired from the images.

The imagery portion of the New England Division LANDSAT investigation has been accomplished under subcontract by the University of Connecticut at Storrs, under the supervision of Dr. Paul Bock, Co-Principal Investigator.

4.0 THE NEW ENGLAND DIVISION LANDSAT EXPERIMENT - PROCEDURES AND RESULTS

4.1 DATA COLLECTION SYSTEM STUDIES

4.1.1 The LANDSAT-1 Data Collection System

The New England Division, Corps of Engineers LANDSAT-1 Data Collection System is comprised of 26 remote reporting stations, better known as Data Collection Platforms or DCP's. The system relays hydrometeorological information such as river stage, precipitation, wind and water quality parameters from points located all over New England to the Reservoir Control Center in near real time.

Each installation contains a sensor or sensors, a 24-volt power supply, sensor to DCP interface equipment, a weather resistant shelter, the NASA supplied DCP consisting of logic to accept up to 64 bits of data in serial/parallel or analog form and

an antenna to transmit data to the satellite. Figure 9 shows the equipment necessary for operating a precipitation station, figure 10 shows a typical river gaging site, and figure 11 shows the locations of all the DCP's. Table 2 lists the DCP's with associated pertinent information for each.

Data are transmitted by the DCP's to LANDSAT-1, thence to NASA's ground receiving stations at Goddard Space Flight Center in Maryland or Goldstone in California, and finally through Goddard to RCC via a teletype link supplied by NASA for this experiment. The nominal time lag, from transmission at the remote site to RCC has been 45 minutes.

4.1.1.1 The Role of the Satellite

The satellite, in a near polar orbit about 547 miles above the earth, makes a complete circuit every 103 minutes with each successive orbit displaced westward by about 1,400 miles at our latitude (between 40° and 50° N). Each day there are 14 complete orbits and the succeeding day's orbits are displaced 65 miles westward from the previous day (see figure 12). This progression allows complete imagery coverage of the entire world once every 18 days. For data collection, information is obtained whenever the spacecraft is in mutual view of a LANDSAT DCP and one of the ground receiving stations. Readings can always be obtained from the orbital pass nearest to our area, and often from the orbital tracks immediately to the east and west of this (103 minutes earlier and later), dependent upon the distance between the satellite and the DCP. This series of two or three data collection opportunities occurs twice daily -- during the morning when the satellite is taking pictures over the Western Hemisphere and also at night, on the 'back-side' of what are the daylight, picture-taking tracks for the Eastern Hemisphere. During each data collection opportunity the satellite is in view for a few to as many as 13 minutes between the times it appears and recedes over the horizon. The exact duration of this period depends upon how far east or west of the DCP's the pass is occurring and upon the extent to which local obstructions interfere with the fields of view of the individual DCP's. In normal operation, each DCP is continuously transmitting data at 3-minute intervals. Thus, during each data collection opportunity period NED can obtain from one to five readings from each DCP.

4.1.1.2 DCS Data Products

In addition to near real time relay of data from Goddard via our teletype link, computer compatible punched cards and data printouts have been provided by NASA on a regular basis via mail. The cards form the basic input to our data analysis effort.

4.1.2 DCP Maintenance and Performance

As of 29 May 1974, 27 data collection platforms had experienced field service, two others were used intermittently by the U.S. Army Cold Regions Research and Engineering Laboratory (CRREL) and an additional DCP was excluded from the statistics because it was defective since delivery.

There have been 302 operational DCP months over the entire LANDSAT experimental period thus far, with one DCP month equivalent to one DCP operating for one month. Over this span nine installed DCP's have experienced component malfunctions, four more than once. There has been a total of 14 DCP component malfunctions, with an average of 4.0 months' operation before malfunction. Eight occurred in two months or less, many being due to improper installation. The remaining 18 DCP's that have never experienced component malfunction are enjoying long lifetimes, some approaching two years, thus leaving normal DCP life expectancy undetermined. Table 3 summarizes DCP component malfunction statistics.

Environment-related failures of the DCP's over the entire LANDSAT experimental period from 23 July 1972 through 29 May 1974 have been:

Vandalism = three instances (all to the DCP antenna)

DCP site struck by a truck = one instance (damaged the antenna)

Inundation by flood = one instance

Sensor performance has been good. River stage sensors have been maintained in good working order by the U.S. Geological Survey and precipitation sensors at dams by the National Weather Service. Some problems associated with ice jams have occurred and are described in section 4.1.6.2. The remaining precipitation, coastal wind velocity and water quality instruments have been maintained by NED personnel. Heavy buildup of solid wastes has caused failure of the water quality sensors several times, leading to the removal of two water quality monitors to cleaner waters.

The 24-volt Gel-Cell battery sets (each consisting of four 6-volt batteries connected in series) have performed well. However, it appears that if a set of batteries is allowed to discharge below 20⁺ volts its ability to hold a recharge is greatly reduced. Such recharged batteries discharge more rapidly under load and are more susceptible to failure during cold weather than new batteries. The new sets last at least six months, with an average life of 8.2 months before failure. However, as new batteries exceed a certain age, the number of transmissions from their sites decreases, i. e., on the average, the number of transmissions from a given site remains nearly constant for the first five months of battery life, but steadily declines thereafter until complete battery failure (see figure 13).

The overall Data Collection System performance is summarized as follows:

NASA-supplied DCP equipment that survived an initial 3 to 5 month operational period after installation had a low probability of failure of approximately one in seven. Installation related failures sharply reduced as proper installation techniques became better defined and understood. Consequently 19 of the last 21 system failures (no transmissions or erroneous transmissions from a site until DCP and/or battery replaced) have been due to battery failure. Figure 14 is a chronology of the Data Collection System performance characteristics.

Faulty sites have usually been easy to detect. Most often a site simply goes off the air; however, on occasion a DCP will transmit data despite a fault. In this case, invalid bit patterns are usually transmitted. When the readings arrive at a constant ratio of bad to good in the case of river stages or when they come in streaks of totally bad, then totally good for precipitation, the

R

problem probably lies with the interface between the sensor and the DCP. However, when the good and bad readings are randomly distributed, the DCP is almost always at fault.

Because of the experimental aspect of our mission, DCP site servicing has been given a low priority, and replacement has taken two weeks in some cases. However, in an operational mode replacement need not exceed one or two days for our remotest locations. Holding a 10 percent surplus of equipment has proved adequate for all our DCP maintenance. No regular servicing of the DCP's should be necessary in an operational mode except preventive maintenance and battery replacement every six months.

4.1.3 DCS Data Analysis

The following definitions are required:

- a. Signal - A radio signal sent every 3 minutes by a DCP containing station ID and sensor data
- b. Message - A signal relayed by LANDSAT-1 to NASA
- c. Report - All messages transmitted during a single pass of LANDSAT-1 from a particular DCP

Data were stored for computer processing from punched cards, with the data separated by DCP number and time of report, and then analyzed.

As of 20 September 1973, a significant change was made in the criteria for LANDSAT data transmitted from NASA to NED. Previously, only the highest confidence level (No. 7) data had been transmitted from NASA. However, meaningful operational statistics could only be derived if all data (confidence levels 0 through 7) were received at NED. So, commencing on this date, data were received from NASA regardless of confidence level. DCS reliability statistics in the following section apply only to this new data base.

4.1.3.1 DCS Reliability

In measuring the reliability of the DCS, consideration was given to comparing satellite relayed data with recorded sensor data.

However, in most instances, sensor data was recorded either every 15 minutes or every hour while DCP data was received at 3-minute intervals whenever the satellite was over the region. Visual comparisons were made of the two sets of data and it was concluded that within the time limitations they were basically the same. The DCS punched data cards contained the station identification, date and time, 64 data bits, confidence levels for the data, varying from a low of zero to a high of seven, and an error flag to denote errors in various portions of the message. DCS reliability was measured as a percentage of "Good Reports" divided by the total number of reports received. Good reports were defined as:

a. Those consisting of only one message -- a NASA confidence level of 7 and a valid bit pattern.

b. Those consisting of multiple messages at 3-minute intervals -- agreement between two consecutive messages within certain established limits and a valid bit pattern. Limits were:

River Stage -- 0.19' difference between readings
Precipitation -- 0.19" difference between readings
Water Quality -- no difference between readings

The 0.19 foot difference between river readings was selected as being the maximum that might be expected to occur during a moderate size flood and is equal to about 4 feet per hour. The same applies for the precipitation range which would be at a rate of 4 inches per hour. No difference was allowed for water quality since these values were sensed on the hour and held in storage for 1 hour. If successive values did not agree they were flagged by the computer and visually checked to see if the difference occurred at the sensing hour. For the period 20 September 1973 through 29 May 1974 results from 16 DCP sites showed 13,440 good reports versus 13,560 total reports received or a reliability percentage of 99.1. The remaining 10 sites were not included in the statistics because they did not report continuously during this period for various reasons. Technical problems with one of the three water quality monitors were not corrected until the spring of 1974. Four precipitation gauges and one water quality station were not completely installed, two river gauges and one coastal station reported intermittently during the period and one other site was abandoned.

4.1.3.2 DCS Data Availability

The availability of data from an operational DCP is a function of two parameters designated as follows:

a. Field of View - the openness of a site for unobstructed radio transmissions to the satellite.

b. Satellite Coincidence - LANDSAT-1 simultaneously within the field of view of a DCP and a ground receiving station.

DCP and battery failures and problems also influence data availability; however, replacement is so simple and can be so fast that any losses due to these need not be considered for the purposes of this discussion.

To obtain an approximation to field of view, regardless of the length of record, the following were exercised for each site location:

a. Separate the data into 18-day cycles.

b. Take the maximum number of reports received for each day with respect to the 18-day cycle (i. e., day 1 through 18) regardless of the cycle in which it occurs. For example, find the number of reports received for the sixth day of each cycle, take the maximum of these numbers and call that the number of reports possible for the sixth day of all cycles.

c. Sum the number of reports possible for each of the days as found in "b" above to find the total number of reports possible per 18-day cycle.

Based on the geographically varied locations of DCP's indications are that mountaintop sites have the best field of view (92 to 95 reports possible per 18 days); unobstructed coastal, damsite and wide-channeled river locations have good fields of view (86 to 92 reports); and obstructed locations generally have poor fields of view (78 to 84 reports). Trees represent the main obstruction in our cases, though buildings have also been a problem. A little tree trimming will generally improve field of view considerably. Field of view statistics together with descriptions of the site locations are summarized in table 4.

Concerning satellite coincidence, for each day and any one DCP, the total satellite coincidence consists of less than one hour. Every 12 hours LANDSAT-1 makes seven orbits. Of these, only two or three, 103 minutes apart, involve the relay of data from our DCP's to NASA. During the best of these, satellite coincidence lasts up to 12 or 13 minutes (maximum of five messages relayed). In the other or others satellite coincidence is considerably shorter. The total number of messages transmitted from a DCP in the course of a day is usually around 17 and rarely exceeds 20. In a situation where readings are needed every two or three hours (e.g., flood situation) the LANDSAT-1 DCS is inadequate.

4.1.4 Seasonal Variation

Seasonal weather variations, including extreme winter cold (to -30° Fahrenheit) and summer heat (to 100° Fahrenheit and higher) have had no noticeable effects on the life or performance of any of the components of the DCS nor on the availability or reliability of any of the DCS data.

4.1.5 Comparison of LANDSAT DCS and NED's Automatic Hydrologic Radio Reporting Network

To determine the feasibility of data collection by satellite we must compare all aspects of such a system with conventional data collection techniques. Specifically at the New England Division we can compare maintenance and performance characteristics, data reliability and availability, and cost of the LANDSAT DCS with our current Automatic Hydrologic Radio Reporting Network (AHRRN).

For the period 20 September 1973 through 29 May 1974 the AHRRN had 37 failures in 331 operational months for an average of one failure per 8.95 operational months (an operational month is equivalent to one station operating for one month). The LANDSAT DCS has experienced 34 failures in 302 operational months yielding one failure per 8.88 months. While these averages are not significantly different it is noted that the 34 DCS failures included 20 battery failures which probably would not have occurred in an operational situation with routine battery replacement every six months, and several installation related failures. In other words the comparison handicaps the LANDSAT DCS since the AHRRN is already debugged and operational.

Like the LANDSAT DCS, individual station component replacements constitute most of the repairs to the AHRRN so downtime for most sites is rarely more than one or two days. However, the AHRRN relies on the use of relay and repeater radio stations, so when one or more of these fails, data from entire sections of New England are lost.

On an overall system basis, all data on the AHRRN is ultimately passed to the Reservoir Control Center by the Wachusett Relay in Massachusetts. Failure of this would be roughly equivalent to satellite failure. However, satellite failure almost always requires complete and costly replacement.

Both the AHRRN and the LANDSAT DCS have system reliabilities over 99 percent which easily surpasses the requirements of the RCC.

The AHRRN is activated by command from the RCC and yields real time data, while the LANDSAT DCS yields near real time data, but only during satellite coincidence. This represents the biggest performance difference between the LANDSAT DCS and the AHRRN. For RCC data must be available in real time at 2- to 3-hour intervals. With a direct downlink (ground receiving station) at the New England Division, a geostationary satellite would satisfy these requirements -- two satellites in orthogonal, non-polar orbits might, but LANDSAT-1 alone is insufficient.

Two key advantages to data collection by satellite are the portability and flexibility of the data collection platforms. The DCP's can be placed in remote locations quickly, easily and without the almost prohibitive expense of setting up the additional repeater and relay radio stations necessary for comparable expansion of the AHRRN.

Preliminary cost analyses performed between a LANDSAT type system satisfying RCC's requirements and the New England Division AHRRN have shown that data collection by satellite would be more economical than conventional data relay methods if employed on a Corps-wide basis with a minimum of 2,000 platforms. The AHRRN had an initial cost per station in 1969-70 of \$20,000. This figure includes all equipment involved in the total system (i.e., transmitters, antennas, 4 relays, 12 repeaters and the central control facility with a computer for data readout and processing).

NED estimates the initial cost of an operational orbiting satellite data collection system to be between \$5,000 and \$10,000 per DCP station. This figure is based upon 2 operational satellites, 10 ground receiving stations and 2,000 DCP's nationwide. This cost per station could be decreased by adding more stations to the system.

4.1.6 DCS Operations During Flood Situations

During the New England Division LANDSAT-1 experiment several significant flood events occurred which proved to be of exceptional importance for the overall assessment of LANDSAT DCS for operational flood control purposes.

4.1.6.1 June- July 1973 Flooding in New England

A major flood occurred in Vermont and New Hampshire during the latter part of June and the first days of July 1973. Rainfall amounts for the 3-day period ending 8 a.m. on 1 July ranged up to 5 to 8 inches in the mountainous areas of the Merrimack and Connecticut River basins. This produced the largest July flood of record in the northern areas of the Merrimack, upstream of Franklin Falls Dam. The Vermont rivers which drain into the Connecticut River also experienced record levels for this time of year and caused the highest summer flood along the Connecticut River in New Hampshire and Vermont, with a lesser degree of flooding in Massachusetts and Connecticut. All flood control reservoirs in the Connecticut and Merrimack basins were closed during the flood period. Storage utilized ranged from a low of 6 percent to a high of 66 at both Franklin Falls Dam in the Merrimack and North Springfield Lake in the Connecticut, with a mean of 27 percent for the 19 reservoirs involved. Estimates are that the flood control system in the Connecticut River basin prevented \$27 million in damages and the Merrimack system \$3 million, for a total of \$30 million.

The LANDSAT-1 Data Collection System demonstrated the potential usefulness of real time data relay by satellite during the entire 6-day flood period. LANDSAT DCS showed that reliable data can be obtained with no adverse effect upon the system's performance from the stressful meteorologic and hydrologic conditions. However, the frequency of data relay from the present satellite configuration was inadequate for operational flood control purposes.

A reporting interval of 2 or 3 hours is essential for flood regulation in New England.

Nevertheless, data relayed by LANDSAT-1 proved useful in augmenting the information obtained through existing New England Division data collection methods. DCP's provided data from remote river gages in the State of Maine, from which real time data is not otherwise obtainable. The Androscoggin and Saco Rivers reached flood stages and LANDSAT monitoring followed the progress of these events.

This contribution proved useful in obtaining a more complete picture of the flood to help Corps emergency coordination activities in watersheds where there are no flood control projects. The information was also forwarded to the U.S. Geological Survey and the National Weather Service River Forecast Center for their use during the critical stages of this flood period.

LANDSAT-1 also provided data from several rivers in highly urbanized areas of southeastern New England to contribute to the overall flood picture.

4.1.6.2 Annual Spring Floods in Northern Maine

Rivers in northern Maine are subject to annual spring flooding as a result of melting snow. These floods are occasionally of considerable magnitude, especially when aggravated by unseasonably warm temperatures or heavy rains. Because of man-made developments along its banks, the Saint John River in northernmost Maine is particularly associated with damaging floods. Fort Kent is the first major town in the path of the floodwaters.

The DCP located at Fort Kent successfully monitored record flood conditions in May of 1973, once again proving the utility of satellites for real time relay of data from geographically remote areas. As a result of this experience and a meeting between officials from Canada and the United States, the DCP at Ninemile Bridge, in the headwaters of the Saint John, was established in July 1973. This key index station for flood forecasts of the river is inaccessible during the spring runoff period and has never been attainable for near real time data acquisition.

Beginning 1 April 1974, the New England Division began relaying information from the DCP's on the Saint John River in Maine on a daily basis to the New Brunswick Electric Power Commission to evaluate a new flood forecasting computer program. On 1 May, the flood of record occurred at Fort Kent, exceeding the previous year's stage by about 2 feet. Unfortunately, ice jams at both DCP locations caused serious problems for the river gages during this runoff period. At Ninemile Bridge, ice jamming near the gage first caused unnaturally high stages, rendering the data useless for forecasting purposes; later the ice damaged the gage itself causing the transmission of meaningless information. At Fort Kent, useful information was obtained up to the time of the flood peak, when a breaking ice jam destroyed the gage, and damaged all equipment beyond repair.

The 1974 experience re-emphasizes the utility of satellite relay of data from these remote areas, but at the same time makes all the more urgent some action concerning the effect of ice jams on river gaging activities.

4.1.7 Questionnaire to Determine Corps-Wide Need for Automated Data Collection

A questionnaire was sent to all Corps of Engineers offices in July of 1973 to obtain information on current Corps-wide data collection facilities and projected future needs. A total of 4,437 field locations was determined to be sufficient to adequately fulfill the Corps near real time data collection needs over the next five years, with 3,970 of these to be fully automated. A tabulation of the Interrogation Time Requirements for the various parameters appears in table 5.

The need, over the next five years, for nearly 4,000 fully automated data collection stations is far more than required for an economical Corps-wide operational orbiting satellite system as compared with ground-based methods (see section 4.1.5). In view of the potential orbiting satellite configurations, where continuous or hourly data is difficult to access, we intend to request all Corps offices which requested data on these bases. We expect that in most instances receipt of the data in a longer time frame would be acceptable. Two satellites in orthogonal orbit could provide data once every two hours. A geostationary satellite would satisfy all requirements; however, the economic feasibility of this has yet to be determined.

4.1.8 Conclusions and Recommendations

NED concludes that data collection by orbiting satellite relay is both reliable and feasible. Orbiting satellite systems can be designed that are more flexible, easily maintained and less expensive than conventional ground-based means.

The only drawback with the LANDSAT-1 DCS for NED operational purposes is the frequency of data reports (four to six times daily). However, it should be emphasized that the LANDSAT-1 DCS is an experiment to test the feasibility of data collection by orbiting satellite. An operational system could be designed involving more than one satellite, to increase the frequency of data reporting.

Based on its LANDSAT-1 experience, NED endorses the institution of a satellite data collection system on a Corps-wide basis or a nationwide system with other Federal and State agencies, whether it be of the orbiting type with which we have experimented, or the geostationary kind, for which evaluation is not yet available.

Since any operational satellite configuration should include ground receive stations at all major user locales to enable direct receipt of information from the satellite or satellites rather than acquisition from a national center, NED, with NASA support, is constructing an inexpensive semiautomatic and easily maintained ground receive station. This is expected to further demonstrate the utility of satellite data relay by testing a system in a quasi-operational mode.

4.2 IMAGERY AND IMAGERY/DATA COLLECTION SYSTEM INTERACTION STUDIES

The purpose of the LANDSAT-1 imagery investigation is to develop practical uses of the imagery in support of reservoir management and control operations within the New England Division.

The analysis of the LANDSAT imagery is directed toward development of operational benefits derived from improved NED operations rather than to "research" objectives per se. The thrust of the study is to integrate interpretations of the imagery analysis with DCS information, data from the Automatic Hydrologic Radio Reporting Network (AHRRN) and that from other conventional sources. The study is intended to explore the potential of LANDSAT imagery in contributing toward an improved information base for timely reservoir management decisions of the NED Reservoir Control Center.

4.2.1 The ERTS-1 Imaging System

The LANDSAT-1 imaging system consists of the orbiting satellite with its sensor payload, the ground receiving, telemetry, and tracking stations; and data processing facility. It is a passive remote sensing system which receives and processes reflected solar radiation from the earth's surface. The radiation is received from a given surface area of the earth in discrete segments of time (period of exposure measured in fractions of a second) with a relatively long recurrence interval of 18 days. The LANDSAT imagery produced by the processing of reflected solar radiation for a given surface area can be thought of as instantaneous slices in time out of the continuous and changing view one would have from the vantage point of the satellite's position in space over the given surface area for the period of the mission. These 'slices' are arranged so as to occur under the optimum (overall) viewing conditions over the desired surface area of coverage compatible with the systematic and repetitive orbiting of the satellite. Over the NED region this process of 'slicing' began on 26 July 1972 at approximately 10 a. m. (EST) as LANDSAT passed over eastern Maine for the first time and has been repeated every 18 days since.

The major controllable factor in providing optimum viewing conditions of the earth's surface is the diurnal occurrence of solar illumination. The regularity and period of this has enabled the satellite orbital motion to be synchronized so as to permit the instantaneous views or slices to be taken under the most favorable daily solar illumination conditions. Major disruptive factors for which no orbital compensation has been made are irregularly occurring, surface obscuring atmospheric conditions such as haze or cloud cover; also seasonal and geographic variation in solar elevation angle. Other factors which influence viewing conditions, occurring at or near the surface will be discussed later in this report.

The areas covered in individual LANDSAT image frames are approximately 100 nautical miles square. New England and its coastal waters are covered in 30 frames taken on five orbital passes corresponding to five successive days (see figure 15), the sequential cycle repeating itself every 18 days.

Some portions of successive days' orbital paths overlap to provide a glimpse of 24-hour repeated coverage. This is an incidental feature of the system which nevertheless has allowed the observation of interesting snowmelt and ice melt phenomena in the course of this investigation. These studies in the overlap regions have provided us with some experimental experience of the usefulness of 24-hour repeat coverage for NED purposes. The width of the corridor corresponding to the portion of overlap of two orbital paths is latitude dependent, being greater for higher latitudes than lower ones. In the New England region the range is between approximately 39 miles at 40° latitude and 52 miles at 50° latitude.

Repeated imagery coverage of a given area is not necessarily in perfect registration. Image centers may vary crosstrack within a nominal ground distance of 25 miles and in-track within a nominal distance of 20 miles. This investigation has shown very little crosstrack variation and a comparatively large in-track variation which sometimes exceeded the nominal range of variation.

4.2.1.1 Sensors

The following sections briefly describe the RBV and the MSS systems aboard LANDSAT-1. Due to early failure of the power

system of the RBV, nearly all products analyzed in this investigation are from the MSS.

4.2.1.1.1 Return Beam Vidicon Camera

The Return Beam Vidicon Camera (RBV) is essentially a high resolution TV system that contains three separate cameras operated in three spectral bands: blue-green .475 - .575 micrometers, green-yellow .580 - .680 micrometers, and red-IR .698 - .830 micrometers. The cameras view the same ground scene, 100 nautical miles on a side (see figure 16).

As the cameras are shuttered, images are stored on photo-sensitive surfaces on each vidicon tube. These are then scanned sequentially to produce video outputs which are transmitted directly to a ground receiving station if it is within range or stored temporarily on video tape to be transmitted when LANDSAT comes within the range of a ground station. To produce overlapping images on the ground along the direction of the LANDSAT motion, the cameras are shuttered every 25 seconds. At the ground the information received from the RBV is recorded on magnetic tape.

4.2.1.1.2 Multispectral Scanner

The Multispectral Scanner (MSS) is an optical-mechanical scanner consisting of an oscillating mirror which sweeps repeatedly across the nadir of the satellite orbital path reflecting image fragments onto photo detectors via an optical network (see figure 17). The width of the scanned strip is 100 nautical miles, identical to that for the RBV. Optical energy is sensed by the detectors simultaneously in four spectral bands: 0.5 - 0.6, 0.6 - 0.7, 0.7 - 0.8, 0.8 - 1.1 micrometers. During ground processing 100 x 100 nautical mile frames are constructed from the continuous strip. Figure 18 shows the same LANDSAT frame, taken over southwestern New England, in each of the four MSS spectral bands.

4.2.1.2 Imagery Products

LANDSAT imagery output consists of black-and-white and color products, and digital tapes. The black-and-white images come in 70 mm. and 9.5 x 9.5 inch sizes, the color in the 9.5 inch size only. Images are available as negative or positive transparencies or paper prints, but not necessarily all of these for each size or type. Digital output is available as either 7 track (556 bpi) or 9 track (800 bpi) computer compatible tapes (CCT's).

Two different types of processing can be applied to the LANDSAT output, for both the photographic and digital tape outputs. Bulk (or system corrected) processing refers to the "normal" imagery processing which contains the radiometric and initial spatial corrections introduced during the process of video tape to film conversion but not those corrections provided by the precision processing subsystem. Precision (or scene corrected) processing refers to all imagery that has received the extra radiometric and spatial corrections provided by the precision processing subsystem, including transformation into Universal Transverse Mercator coordinates.

In the NED investigation, the following five types of LANDSAT imagery products were used, all resulting from bulk (system corrected) processing: black-and-white 70 mm. negative and positive transparencies, 9.5 x 9.5 inch positive transparencies and paper prints and 9 track, 800 bpi computer compatible tapes.

4.2.1.2.1 The Diazo Process

The diazo process of producing contact acetate color composites of LANDSAT scenes from 9.5-inch system corrected black-and-white transparencies was used in this study. With proper registration composite images were obtained for combinations of two or more MSS bands, each band being assigned a different color, such as cyan, magenta, red, etc. Varying degrees of saturation of a particular color in a given band represented varying degrees of reflectivity received in that band. Thus the composite product allowed one image to represent the information that would otherwise have to be obtained from each of the constituent bands separately.

4.2.2 Imagery Studies - Photo Interpretation

4.2.2.1 Surface Waters - Location and Coverage, Especially During Flood and Low Flow Periods

Excluding such interfering factors as haze and cloud cover, and neglecting the effects of icing during cold weather, surface waters usually appear uniformly dark in the LANDSAT near IR bands (MSS 6 and 7), almost completely absorbing the incident radiation corresponding to these ranges of wavelength. There appears to be less response to the effects of bottom reflectance or suspended or dissolved materials in the water in these bands as compared with

bands MSS 4 and 5. For this reason, the best delineation of surface waters is generally afforded by the MSS bands 6 and 7.

Areas where vegetative ground cover has been stripped away are also highly absorptive of near IR radiation, and appear dark in MSS bands 6 and 7. This tends to mask the discrimination of surface waters located in such areas in these bands. This effect tends to be more pronounced in band MSS-7 than in MSS-6. In general water still appears dark in bands MSS-4 and MSS-5 compared with most other features while areas with stripped away ground cover appear to exhibit relatively high light densities. In such areas, the discrimination between water and land may be better in bands MSS-4 and 5 than in MSS 6 and 7. Because of this, the best overall visual discrimination between land and water may be in a color composite combining several bands.

Only the larger rivers in the New England region are clearly and distinctly displayed on LANDSAT imagery. These rivers include the Connecticut, Merrimack, Saint John, Androscoggin, Allagash, Aroostook, Kennebec, Penobscot, Housatonic, Thames River estuary and the Providence River estuary. In most cases the delineation of surface water boundaries can be made to within a single pixel in the near IR bands (MSS-6 and 7); however, there are some exceptions as in cases where boundaries are indistinct because water is adjacent to marsh or areas covered with aquatic vegetation. Thus, it was concluded that a river must be at least 2 pixels wide in order to be easily recognized.

Mapping of flooded areas using LANDSAT imagery is generally limited to those that are well displayed at scales down to 1:200,000 (enlargement of five times; which is the limit of enlarging LANDSAT photo imagery (using standard photo equipment) before significant blurring occurs. This tends to exclude all except the very largest flood plains in the NED region.

For most river basins under jurisdiction of the New England Division, peak flood conditions usually occur during periods of limited visibility and atmospheric interference by cloud cover. Lag times between peak precipitation and peak runoff tend to be relatively short for all but the largest river basins. The lower Connecticut River which may crest several days after the occurrence of peak flood conditions in the upper portion, provides the best opportunity for peak flood conditions to be recorded by satellite imagery in the NED region. Enough time is probably available

in most cases for cloud cover to clear off before the Connecticut River crests downstream. Until such time as atmospheric conditions can be compensated for, satellite imaging will continue to be severely limited for flood observations in New England. Also, while the 18-day cycle of LANDSAT coverage has allowed the observation of several serious floods during the course of this study, more frequent imaging would be essential for an operational system designed to provide information on all floods that occur, perhaps on the order of daily or even twice daily.

An interesting effect showing promise is the study of LANDSAT imagery over previously flooded areas. Locations which have been inundated seem to retain their absorptivity to near IR radiation for periods as much as several months after the floodwaters have receded. Figure 19 is a diazo color composite of a reach of the upper Connecticut River taken on 24 July 1973, three weeks after the flooding occurred. We believe the light blue areas along the river represent some type of residual effect upon the absorptivity as a result of the flooding. This may be due to either soil moisture or vegetative conditions.

4.2.2.2 Icing Conditions on Rivers, Lakes, Reservoirs and Around Hurricane Barriers

The icing of larger lakes, rivers and reservoirs is readily apparent on LANDSAT 9.5-inch images, scale 1:1,000,000. Ice conditions have been well displayed on major NED rivers - Connecticut, Merrimack, Saint John, Allagash, Aroostook, Penobscot, Kennebec and Androscoggin. However, in the case of smaller rivers, the same problem occurs with observation of ice as observation of rivers alone. The dimensions of resolution elements become large relative to those of the object being observed and a clear pattern cannot be formed. In general, rivers must be at least 2 pixels wide before ice can be reliably detected. Haze and cloud cover may also limit observations of ice.

Based on our experience to date for larger rivers, lakes and reservoirs, the study of LANDSAT imagery can verify icing conditions and specify the areal extent of ice cover. However, ice thickness or liquid water equivalency using LANDSAT imagery could not be specified. Reflectivity differences in the imagery over ice suggest that some correlation may be possible between varying

reflectivities and ice condition (i. e., well frozen or melting). Icing around the NED hurricane barriers was not studied in detail because of inadequate imagery spatial resolution.

From an operational viewpoint, repeated LANDSAT-type satellite coverage on a once-a-day basis could effectively monitor the icing conditions of large rivers. In the case of the Saint John River, Maine, shown in both winter and summer in figure 20, the spring thaw and breakup of ice has in the past caused serious problems of jamming, backing-up of water and then breaking and releasing floodwaters. The flood of late April 1974 at Fort Kent, Maine is a recent example. This particular river is large enough for such conditions to be detectable by LANDSAT if it were available on a once-a-day basis. The effective monitoring of these conditions which often occur in remote areas could provide valuable lead time in preparing for flood conditions and in possibly taking remedial action, such as breaking up of ice jams by means of explosives before they have a chance to impound excessive and potentially dangerous quantities of water.

A glimpse of the type of changes that could be detectable by daily coverage is shown in figure 21. This is a color composite picture of a portion of Lake Winnepesaukee, New Hampshire using the overlapping sections of imagery from two successive days in midwinter. The ice which melted considerably from one day to the next appears as the red colored region. Areas that had ice on both days appear as white in the picture, while those with open water on both days are black.

4.2.2.3 Turbidity and Sedimentation in Lakes and Reservoirs

Indications of surface water quality characteristics are recognizable in LANDSAT imagery. Figure 22 is a diazo print showing the sediment discharge plume of the Connecticut River into Long Island Sound after a flood. The imagery itself does not specify particular water quality parameters unless these are documented and correlate with ground-truth information. It can indicate possible differences in water quality among the various portions of a surface water body by the display of patterns formed by corresponding variations in spectral properties. In the case of figure 22 the pattern is large enough to be easily recognized. In the case of inland lakes, rivers, and reservoirs in New England, detection is more difficult due to limited spatial resolution. Detection of relative dif-

ferences in water quality are not possible for most rivers in New England because of their limited sizes and the limited spatial resolution capability of LANDSAT.

Even in well-mixed situations where the quality tends to be homogeneous in a given water body and differential surface patterns are not formed, some information can still be provided pertaining to water quality conditions. The spectral properties of known polluted or suspensoid-laden waters can be compared with those of other water bodies whereby differences can be detected. Silt and algae-laden waters tend to exhibit relatively high light densities in band MSS-4 and to a lesser extent in band MSS-5.

Differences in bottom reflectance caused by variation in light attenuation as a result of varying water depth and quality, and by varying spectral properties of the bottom sediments also manifest themselves in the imagery. The effects of water quality and bottom reflectance can be so intermingled that it is often difficult to distinguish them without supportive ground truth information.

The spectral aspects of surface waters can also be affected by interfering factors such as atmospheric haze and scatter, as well as glint from waves and ripples. The relatively wide-band spectral resolution and restricted spectral range of LANDSAT imagery is also a limiting factor in identification of water quality characteristics. More variations could probably be detected with narrower bands and an extended spectral range covering at least the blue visible and thermal IR portions. Although some impressive examples of water quality variations have been detected by LANDSAT, it should be noted that a number of instances of known differences have not been revealed on the imagery. Further study and relating of imagery to ground truth is required to establish the reason for these apparent anomalies.

The time intervals associated with changes in water quality characteristics vary according to the type of water body and the characteristic being considered. In the case of eutrophication in lakes and reservoirs, the changes are generally seasonal whereas the temporary silting of flooded streams and rivers may last only a day. Some pollution patterns may appear relatively unchanged over long periods of time, while others may change from day to day or even over shorter intervals. The 18-day cycle of coverage by LANDSAT is generally capable of detecting only longer term and seasonal

changes on a regular basis. The short term post flood sediment plume siltation shown in figure 22 was an opportune coverage, only fortuitously obtained within the 18-day cycle.

If LANDSAT-type imagery provided at least daily coverage, effective monitoring of post flood silting of larger rivers, reservoirs and lakes should be possible as well as many short term pollution episodes. Improved spatial resolution could extend the effective coverage to smaller bodies of surface water.

4.2.2.4 Location and Extent of Snow Cover

In general, NED winter snow cover patterns appear as high light density regions in LANDSAT imagery in comparison to the low density noncovered regions. It is necessary to view the entire snow pattern which in many cases may cover more than one image frame in the New England region, in order to view the scene with the proper perspective and contrast relative to a nonsnow covered background. Figure 23 is a diazo print of midwinter snow cover in western New England. The snow covered areas appear as the high light density regions dominating the upper portion of the picture. Even though there are many shadowed and dark regions within the overall snow pattern due to obscuration by vegetative cover and to low winter sun angle upon hills and mountains, the overall pattern separating snow covered from noncovered regions is recognizable. Viewing conditions are greatly improved in late winter and early spring due to better solar illumination and shadow reduction. Low sun elevation appears to be the more severe obscuring factor than that from the direct masking effects of vegetative cover. This has been verified by the fact that in the early spring the snow cover over heavily forested areas is highly visible in the LANDSAT imagery.

Superimposed on the imaged snow cover pattern in figure 23 are the snow isohyetal lines as determined from ground truth snow surveys. As can be easily seen, the imagery shows the snow/no snow line much more accurately than the snow survey data. The imagery, however, does not give any clue to snow depth or water content, the two parameters that are obtained in the surveys. For reservoir regulation purposes the water content of the snow-pack is the essential information to be obtained, especially for areas with a considerable accumulation. The exact demarcation of the snow/no snow line is of little or no use for reservoir regulation as the snow water content in these areas is negligible. Thus, the

potential of LANDSAT-type imagery with the present sensor package to provide snow information equivalent to that obtained from snow courses for reservoir regulation purposes is all but nonexistent. Finally, if LANDSAT could provide information on snow water content, the 18-day cycle of coverage would be too long for operational usefulness. Weekly coverage would be necessary.

4.2.2.4.1 Contoocook Basin Snowmelt Study

An intriguing opportunity to assess the potential of LANDSAT imagery for providing information concerning snowmelt was afforded to this investigation in the spring of 1973. A considerable amount of snowmelt occurred over the Contoocook River basin in New Hampshire between 6 and 7 April 1973. On both days the area was imaged by LANDSAT as it was located in the overlap region between two successive orbits. The images, shown in figure 24, were taken at approximately 10 a.m. on the respective days. The Contoocook River basin is outlined and labelled 'B'.

Based on detailed study of the images and corresponding hydrometeorological data from ground truth sources, the following information would have been provided by LANDSAT had daily repetitive coverage been available in an operational system:

a. The LANDSAT imagery added to the body of evidence tending to indicate that the high levels of runoff over the period 6 to 9 April 1973 were significantly contributed to by meltwater.

b. LANDSAT imagery provided confirmation that snow covered most of the basin on 6 April 1973 at 10 a.m. and fixed the time during which most of the snow cover disappeared as the 24-hour period from 10 a.m. 6 April to 10 a.m. 7 April 1973.

c. LANDSAT imagery provided information about snow cover distribution changes over areas too distant from regular daily measurement stations for meaningful extrapolation, especially at high elevations along the basin divide where accumulations appeared to remain on 7 April after melting had taken place at other locations.

In summary, based on the implications of the 6 and 7 April LANDSAT coverage of the Contoocook, it can be concluded that some useful information on snowmelt might be extractable for Reservoir Control Center purposes if data on a daily basis were available.

4.2.2.5 Location and Extent of Excessive Precipitation Accumulation

Although no specific instances were studied, it is likely that excessive precipitation accumulation on the ground could be detected by LANDSAT imagery in cases where pooling at a scale large enough to be resolvable by LANDSAT would occur. All of the same imagery attributes and limitations previously described for location and coverage of surface waters would likely apply here.

4.2.2.6 Tidal Levels and Flooding at or Near Hurricane Barriers

Only cursory looks at the LANDSAT imagery have been made of tidal levels and flooding at the NED hurricane barriers. This kind of information must be obtained in real time to be operationally useful to NED. Also data must be obtained during storm situations, at night, and at sufficient ground resolution to be operationally useful. None of these needs is satisfied by LANDSAT imagery.

4.2.2.7 Soil Moisture Conditions

Various investigators have reported on the discrimination of soil moisture using various spectral discrimination techniques. Our studies in this area are limited to the overall studies of flooding and post-flooding situations (see earlier discussion under "Surface Waters - Location and Coverage"). Using diazo color composites, it appears possible to delineate areas of inundation even months after inundation occurred. Further study is required.

4.2.3 Imagery Studies - Computer-Oriented

The LANDSAT Computer Compatible Tapes allow adaptation of the imagery data to computer processing and display techniques, thus increasing both the speed of analysis and the enlargement capabilities of the images.

Each LANDSAT MSS tape contains one-quarter of a LANDSAT scene in all four MSS bandwidths. Thus four tapes are required to depict one full scene in all four bands. A full scene in a given band comprises 2,340 scan lines with approximately 3,240 points (pixels or resolution elements) in each line, for a total 100 nautical mile square coverage. Each point represents the average reflectivity of an imaged area below the satellite of approximately 187 by 250 linear

feet. Reflectivity is expressed in terms of 128 different "grey level" values in MSS bands 4, 5 and 6, and 64 values in MSS-7, the grey levels ranging from white to black when presented in pictorial terms. These may be aggregated, for convenience, into broader gray level value sets of, say 16 or even 8 units.

4.2.3.1 Boundary Determination

In CCT imagery, feature boundaries are generally designated by a given cutoff level of grey scale intensity which separates one object or class of objects from others. A given location, represented by a pixel, for example, can be classified according to its spectral signature as represented by the following vector: (x_1, x_2, x_3, x_4) where x_i is a given level of intensity as represented by grey scale values ranging from 0 to 15 and i , in the case of MSS imagery, would designate one of the four spectral bands MSS-4, 5, 6 or 7. It may happen that two bands or even one particular band can, in some cases, designate a class of objects as well as if all four bands together were used. This appears to be true in many cases of the ability of band MSS-7 to designate surface waters. The occurrence of surface water is most frequent in the lowest radiance levels of band 7. The mean or most frequent level of the grey scale, or some other parameter, may then be used to designate the cutoff level. The problem is to determine what levels simultaneously are most inclusive of the given objects and exclusive of others. Surface waters appear to be most exclusively represented in the near IR bands (MSS 6 and 7) at the lowest levels of reflectance, but their occasional occurrence may extend to higher levels.

A criterion being used in this investigation to determine the extent to which the reflectance of an object or a particular class of objects in a particular band occurs within a specified range of reflectance levels is to compute the mean, mode, and standard deviation of the frequency of occurrence of the object or class of objects in an imagery sample for various levels of reflectance. The implication is that the smaller the standard deviation, the smaller the range of reflectance levels and the more exclusive the representation of the given class of objects by the specified range of values. If the mode differs with the mean by a significant amount, the implication is that the set of values is skewed or has more than one peak and that the objects very likely have not been correctly identified in the imagery samples or properly classified as a set with similar reflectance properties.

The objects that most interfere with the detection of water in band 7 by virtue of their proximity to water in having similar reflection characteristics in this band appear to be cloud shadows, those caused by mountainous or rugged terrain, and other features, urban and paved surfaces being the most predominant. This does not include the masking effect of clouds themselves or other direct interference but only that caused by objects with similar reflectance properties. The problem of overlap of occurrences between different classes of objects in a particular band may be solved by considering one or more other bands where the occurrences appear at more widely separated grey scale levels, thus providing contrasts of color as well as intensity. Urban pavement, for example, appears to occur most frequently at considerably higher levels of reflectance than water in bands MSS-4 and 5 than in MSS-7. For this problem, the operating variable might be considered to be the two-dimensional vector representing grey scale levels in MSS-5 and 7. For other problems the complete four-dimensional vector, (x_1, x_2, x_3, x_4) representing bands MSS-4, 5, 6 and 7 could be used to designate the optimum exclusive-inclusive vector space occupied by a given class of objects. Finally, a boundary may lie anywhere within the ground space covered by a resolution element, and perhaps within a choice of several elements depending on the separability of occurrence of classes of objects by virtue of their reflectance properties in a given spectral band or combination of spectral bands.

In this investigation the foregoing considerations were made when manually defining a land-water boundary from a set of alpha-numeric symbol clusters on a computer printout, with the ultimate goal being to be able to automate the boundary determination process and incorporate these considerations into computer software. In this investigation, a cutoff value such as grey level value is chosen for delineation of a given feature, such as water, depending on the particular image under investigation and on simple statistical tests and comparisons with ground truth or map information to designate the presence of water. All values of grey scale level beyond the chosen cutoff point are then assumed to represent the feature for the purpose of performing computer computations. This is in effect, a density slicing procedure which uses reflectance as the only criterion for boundary selection. More advanced pattern recognition techniques involving shape and other optical properties can also be applied along with density slicing to boundary or interface determination, but have not been applied in this investigation.

If full advantage could be taken of all information in an image to enable the determination of a boundary to within the dimension of one MSS resolution element, the maximum error in terms of ground distance would be about ± 90 feet. For the method of density slicing, referred to in the previous paragraph, without scene radiance corrections and without any attempt at more advanced pattern recognition techniques, the maximum possible error is greater. How much greater depends on factors such as atmospheric interference and interference by objects within the image with similar reflectance characteristics, as previously discussed.

4.2.3.2 Surface Water Identification

The identification of individual bodies of surface waters such as lakes, reservoirs, or rivers as well as other similar features is a fundamental part of image interpretation. This activity can be carried out visually and is dependent on the ability and background knowledge of an observer to recognize and associate image objects with correctly-identified ground objects. A human observer may perform these activities routinely and without being conscious or concerned over the details of the procedures of making associations. The bulk of the work of this investigation involved image interpretation of this type. These procedures must be considered in detail, however, if one desires to automate the interpretation process, using computer imagery.

In the identification, inventory and classification of surface waters using LANDSAT imagery, the proper utilization of CCT data can mean a savings of time and effort that would otherwise be required in manually observing, measuring and accounting for these image features. It can also lead to a more systematic and accurate procedure using the inherent advantages of the computer to sort, store, and perform operations on vast amounts of information in a short amount of time. An approach to doing this has been considered in this investigation and can be briefly summarized as follows: scan image data, identify surface waters, recognize and sort out individual water bodies and distinguish them from each other, perform operations over each image of a surface water body area on an individual basis, number and classify according to size or order of magnitude, and extract other pertinent information concerning these waters. This involves computer pattern recognition techniques, whereby the computer

"learns" from the human operator to identify and distinguish between various image patterns and progressively becomes less and less dependent on the operator.

4.2.3.3 Scale

The scale or dimension of ground objects in terms of dimensions of their imagery counterparts is a persistent problem in the case of LANDSAT imagery. The scale of any imagery or map product is rendered satisfactory or unsatisfactory depending on what the product is to be used for. Also, a usable scale generally depends on the size of objects being dealt with and the convenient working dimensions of the user which can in turn depend on such factors as good drafting or drawing size for making overlays or superimposing notations or boundaries, convenient sizes for filing, storage, reproduction, display, etc. Producing simple dimensional enlargements or contractions of images from one scale to another for various purposes has its limitations. The major one is image resolution which has already been discussed in some detail. In the case of photo products, enlargement will eventually produce blurring at the interface of an object and its background. We have judged that the practical limit of first-generation scale enlargement of LANDSAT photos is about 1:200,000. Other investigators on this project have indicated the capability of enlarging LANDSAT photos to greater scales.

The 1:24,000 scale used for U.S. Geological Survey quadrangle maps with 10-foot contour intervals is an adequate scale for a wide variety of water resources planning, investigation and engineering work. For detailed project or construction plans, still larger scales are generally necessary. Experience gained in using LANDSAT imagery in the NED region in the course of this investigation suggests that the capability of producing enlargements of selected portions of LANDSAT photos to scales in the order of 1:24,000, as used in USGS quadrangle maps would be most desirable. Because of the order of magnitude of size of most surface waters in the NED region, such a scale is convenient to work with and would facilitate direct comparisons between LANDSAT imagery and existing quadrangle map data. Also at this scale significant changes in such parameters as surface water area would be well displayed.

CCT processing provides a means of enlarging LANDSAT imagery to higher magnification. Besides providing a means of

quantifying scene radiance values over elemental areas, the CCT printout imagery composed of alpha numeric symbols spaced on a rectangular format provides better feature representation at a larger scale than would an enlargement of a photo to the same scale. In making overlay comparisons with map or ground truth data, the boundaries of surface water bodies, for example, have been properly delineated within the pattern of resolution elements making up the CCT-produced imagery. If the CCT images are to be printed on standard computer printout sheets, format distortions must be removed if these are to accurately represent the surface dimensions of ground objects in their true proportions. The corrections that must be applied are either approximately a 30 percent contraction in the in-track direction, or a 40 percent expansion in the cross-track direction on CCT printouts of MSS imagery.

The limitations on the uses of LANDSAT imagery due to scale to which the imagery can be enlarged are fundamentally related to the problem of limited resolution. This is in fact the basic limitation of the LANDSAT system for many purposes. For LANDSAT imagery there is, therefore, a minimum detectable object dimension. This limitation on the size of detectable dimension also limits the accuracy of measurement. In an absolute sense the error in determining, hence measuring a dimension is the same for all objects, large and small. In a relative sense, however, the same absolute magnitude of error is greater for small objects than for larger ones. The possible relative accuracy of measurement (percent accuracy) is least therefore for the minimum detectable object dimensions, and improves as the sizes of objects become larger.

The criteria used in this investigation for setting the minimum detectable object dimension are based on the automation of procedures for classifying objects according to radiation density and not on other pattern recognition criteria. The minimum size determined this way is conservative and is considered to be that size necessary to guarantee that at least one pixel projection onto the earth's surface will fall completely within the object's area. In the case of surface water, it would be the minimum size or dimension necessary to ensure that at least one pixel projection would be exclusively over water. For objects of smaller size than that of the projected pixel, the indicated intensity of reflectance will be due to radiation reflected in part from the object, e. g., water, and in part from its background, e. g., land. This presence of reflected background light interferes with the object's

detection as far as radiance density is concerned and therefore obscures it in relation to its background. Even though an object may still be recognizable, the true contrast or intensity level representative of the object will not manifest itself in the imagery then, unless a pixel projection lies completely within the area occupied by the object, e.g., completely over water. The minimum dimensions at which this can theoretically possibly occur are those of a single pixel. The probability that a pixel would fall exclusively over water on a body with the same dimensions as the pixel projection itself is however practically nil. On the other hand, an object of two pixel equivalents in linear dimension will always contain at least one full pixel projection exclusively over it in that dimension. If this criterion is used for determining the minimum sized LANDSAT detectable object, the following conclusions can be drawn:

Minimum possible width W of river that will always be detectable as water:

W = 2 pixel lengths = 374 feet (crosstrack),
500 feet (in-track)

Minimum possible areal size A of a water body (pond) that would always be detectable as water:

A = 374 x 500 (2 x 2 pixel block) = 187,000 feet² = 4.3 acres.

If objects are to be definable at the minimum sizes, the integrity of individual pixels must be maintained during image processing. This requires the processing of individual signal bits on CCT's in terms of the spatial representation of pixels, on a one-to-one basis. This type of work requires the computer processing of CCT's. For the study of large dimensional features however, as already discussed in the case of snow cover, over large or regional areas, where absolute accuracy need not be as great in order to obtain the same level of relative accuracy of measurement as for smaller features or objects such as inland surface waters, the processing of individual pixels does not have to be performed on a one-to-one basis with bits of signal data on CCT's in terms of spatial dimensions, thus allowing for considerable data reduction.

4.2.3.4 Surface Water Characteristics: Dunham Pond

A study was performed to determine how well the

digitized spectral density levels in CCT imagery correspond to both the location and depth of surface waters. Ground data for correlation with the LANDSAT imagery was taken at Dunham Pond, a 7-acre body of surface water in Connecticut with horizontal dimensions of approximately 1,100 x 600 feet. Figure 25 shows a reproduction of a CCT printout of the Dunham Pond area in MSS band 7 overlain with a surveyed map of the pond and its depth contours.

The symbols represent the density levels on a 16-step grey scale as 0, 1, 2, 3, 4, 5, 6, 7, 8, 9, A, B, C, D, E and F ranging from the highest to the lowest reflectance level. The scene shown is rather dark in band 7 and uses only the lowest five density levels. Correlation coefficient comparisons between reflectance and presence of surface water yielded $r = 0.974$ and between reflectance and water depth, $r = 0.949$.

It is likely that the relationship between reflectance and presence of surface water can be extended to all surface waters. That between reflectance and depth is certainly another question however, since detection of depth variations is dependent upon such factors as turbidity and other water quality parameters, as well as bottom reflectance, etc. The case of Dunham Pond provides hope that in certain waters, LANDSAT can detect differences in depth, however considerably more study is necessary to determine if and how this could be extended to the general case, perhaps using all the LANDSAT spectral bands, or other wave bands not available aboard LANDSAT.

4.2.3.5 Flood of July 1973 at Franklin Falls Dam, New Hampshire

A comparison was made of LANDSAT imagery of Franklin Falls reservoir area, New Hampshire, filled to approximately two-thirds capacity immediately after the flood of July 1973, with the post-flood unfilled condition of late August 1973 to delineate and compute surface areas of the flooded locations. Due to partial cloud cover immediately after the flood the entire surface area of the reservoir waters could not be accurately computed, so that the results as far as the original intent and purpose was concerned were inconclusive. An interesting phenomenon occurred, however, when the comparison between the two digital printouts of images taken immediately after the flood and again 8 weeks later was made. Even though the floodwaters had long since receded, much of the previously

inundated area still appeared at a low density level, not quite as low as that of the surface water in the adjacent pool, but lower than that of the surrounding forested terrain. The 29 August 1973 image indicated that the properties of the terrain which was flooded in early July had been altered by the July flood, possibly due to damage of vegetative cover. Areal computations were easily made by simply summing the elements forming the pattern representing the seemingly damaged area and multiplying by the ground area of a pixel. The total area of this pattern around the Franklin Falls reservoir area on 29 August 1973 computed in this manner was approximately 1,950 acres. More detailed studies are necessary to further explore this phenomenon in the LANDSAT imagery.

4.2.3.6 Man-Computer Interactive Approach

Work has been accomplished in the area of computational algorithms aimed at producing fast, efficient programs to display useful information relating to LANDSAT imagery analysis. This work was primarily supported by a National Science Foundation grant aimed at developing novel concepts and techniques for imagery data management. The work was carried out by Prof. Y. T. Chien, University of Connecticut, and his graduate students during the 2, 3 academic year 1973-74, in conjunction with the present project. The man-computer interaction approach to imagery analysis must pay special attention to the problem of putting various information in a form suitable for computer display and human observation. The information to be displayed usually involves several (more than two) channels such as the 4 spectral bands of the LANDSAT imagery. Thus, our problem is to transform data of high-dimensionality into two-dimensional space ready for display. This type of transformation must satisfy the following requirements:

- a. The intrinsic characteristics of the imagery must be preserved.
- b. It must be computationally fast to avoid any excessive idle time on the part of human observers while engaging in man-machine interactive analysis.

Several classes of display-oriented transformation methods have been studied in relation to the LANDSAT imagery. By combining several MSS bands of information we have examined the possibility of delineating various classes of hydrological features

(water, land, etc.) in an interactive environment. A limited experiment with a section of the Cape Cod Canal, Massachusetts and its adjacent land has been carried out to test the transformation methods developed. Results indicate that:

a. With the aid of a computer display, the human operator can play a direct and immediate role in selecting the MSS bands that will describe certain hydrological features in the most informative way.

b. Speedy display and user's interaction of information may be achieved by putting transformation algorithms in a recursive structure. This will allow the user to apply the algorithms to various sections of the image for analysis without introducing excessive calculations.

We have developed a number of computational techniques, operational programs, and utility subroutines that are designed to provide computer-oriented means for the interactive analysis of LANDSAT imagery. Due to the late arrival of tapes and extensive work in printing parts of scenes for human study, we did not progress very far in building a truly interactive pattern recognition system to facilitate the analysis of LANDSAT imagery. Given sufficient resources, a reliable, interactive system may be established which maintains as a data base information obtained from many MSS tapes, then uses this information to predict occurrences similar to those stored, upon input of image information on a real time basis in an operational situation. This development of a truly operational system would involve the relating of ground truth information about hydrologic events (i. e., snow conditions, flooding, rain data, etc.) to imagery entered into the computer, over a period of time to "train" the pattern recognition system to recognize and analyze future hydrologic events to be presented to it.

The specific objective of such a system would be for the identification and analysis of real time hydrologic events that are considered relevant to NED flood control operations, in an interactive environment, probably with a Cathode Ray Tube and light pen to allow the user to 'communicate' with the computer and outline the nature of the information desired in any given instance. There is no doubt that for many parameters a properly operating man-interactive system could save substantial amounts of time in the increasingly complex decision making processes involved with flood control reservoir regulation.

R

4.2.4 Imagery/DCS Interaction Studies

The present investigation has focused mainly on acquiring the practical experience in setting up and running the LANDSAT DCS experiment at NED and in interpreting the LANDSAT imagery within the context of a daily operational Reservoir Control Center. The DCS and imagery studies have been conducted as parallel but supportive studies at the outset. Our objective was to first acquire maximum "real-life" experience with each type of LANDSAT data. Having obtained a sampling of actual experience in real NED situations using DCS data and LANDSAT imagery, we are now better able to develop a strategy for overall coordination of all NED data sources.

Several general conclusions can be made at this time regarding the interreactions among the LANDSAT DCS, LANDSAT imagery and AHRRN for NED operational purposes.

a. Real time or near real time data acquisition and management systems are required for effective coordination of reservoir regulation activities. The longest time delay at present is in the LANDSAT imagery system (measured in weeks). LANDSAT DCS data are received in near real time (measured in hours). NED is dependent on real time data acquisition by the AHRRN (measured in minutes). To be most operationally useful in coordination with information obtained from the other sources, the time lag of LANDSAT imagery should be about comparable with that for the DCS and the AHRRN. The latter two would provide ground truth for better interpretation of the former. Real time imagery acquisition implies a capability similar to that of the NOAA APT system.

b. Management/hydrologic models that can input the DCS/imagery data are required. Generation of such models is a major undertaking. NED is moving in this direction with the development and upcoming testing of the flood forecasting and routing computer program in the Merrimack River basin in cooperation with the Corps of Engineers Hydrologic Engineering Center.

c. "Quasi-operational" or "demonstration" experience over a wide range of flood-and reservoir-management situations must be acquired before an overall system becomes operational.

d. Operational readiness of NED system components including management and operational personnel and hardware

and software is required. Management decisions are required at each step to move from the quasi-operational to the operational phase.

e. Studies and reevaluations must continue indefinitely, keeping pace with advancing technological and cost information to see that the system is composed of the most economically feasible and technically useful combination of modes of point data relay and imagery data acquisition as well as data processing techniques.

4.2.5 Conclusions and Recommendations

4.2.5.1 Imagery Studies - Photo Interpretation

Using standard photo equipment, experience in this investigation has indicated that LANDSAT photo imagery may be enlarged about five times, or to a scale of 1:200,000. This is sufficient for only rather large scale or gross feature patterns to be represented with the accuracy necessary for flood control reservoir regulation purposes.

Only the larger rivers in New England are clearly displayed on the imagery. Mapping of floods is restricted to gross overflow of waters from New England's rivers. However, since flooding may occur at any time, the LANDSAT 18-day cycle is insufficient for regular monitoring of New England floods. Daily or even twice daily coverage would likely be necessary. Even with this, clouds associated with flood producing storms often obscure flooding from the view of the satellite at those times when imagery acquisition would be most critically needed. An interesting effect worthy of further investigation is the apparent distinguishability on LANDSAT imagery of areas previously, but no longer flooded, for periods up to at least several months after flood recession.

Ice is readily detectable on LANDSAT imagery, as is the ice-open water interface. LANDSAT imagery could lead to early detection of ice jams on the larger New England rivers. Daily coverage during the cold months of the year could provide a useful supplement to other means of monitoring the development of ice jams, especially in remote areas.

Indications of varying water quality characteristics

R.

are recognizable in LANDSAT imagery. Again, information is normally obtainable only from larger water bodies. So many different parameters are involved in water quality, and in such varying degrees-often intermingled with each other, that much study still remains before LANDSAT imagery could relate specific imagery responses to specific ground truth information. Also, interference from atmospheric haze and scatter, glint from waves and ripples and bottom reflectance can be especially difficult to compensate for. Finally, LANDSAT imagery bands neglect some of the spectrally important wave lengths for water quality detection. Nevertheless, where ground truth can be confidently correlated to the imagery, some changing water quality patterns might be usefully displayed in repetitive imagery coverage. The 18-day cycle could effectively monitor these if changes were occurring over a similar or longer interval. Many water quality changes are of this nature. For shorter term episodes such as post-flood silting of rivers, daily coverage would likely be essential.

Winter snow cover patterns are readily obtainable with excellent accuracy from LANDSAT imagery; however, the imagery provides only snow location, not depth or water equivalent which is the operationally important parameter. If LANDSAT could provide information on snow water content, the 18-day cycle of coverage would be too long for operational usefulness. Weekly coverage would be necessary.

A look at 24-hour snowmelt as detected in the imagery over a region of overlap between two successive days' orbits showed some promise for the use of snow cover information for short term application. This would be especially useful if imagery on a daily basis were available, thus allowing a certain degree of educated extrapolation to be performed on the water equivalent measurements obtained by ground surveys on a weekly basis.

Excessive precipitation accumulation probably could be detected by LANDSAT imagery in instances where pooling at a scale large enough to be resolvable by LANDSAT would occur.

Tidal levels and flooding at or near hurricane barriers were briefly studied. This type of information must be obtained in real time. Also the data must be obtained during storm situations, at night and at sufficient ground resolution to be

operationally useful. None of these needs is satisfied by the present LANDSAT system.

The only specific look at possible moisture detection in the soil by LANDSAT imagery was made in association with flood and post flood conditions. As reported earlier in the Conclusions and Recommendations, LANDSAT imagery appears able to distinguish areas previously, but no longer flooded, for periods up to at least several months after flood recession. Whether this is a soil moisture or vegetation-related phenomenon is open to further study, however.

The diazo process of producing contact acetate color composites of LANDSAT scenes was frequently used in the Photo Interpretation portion of this LANDSAT investigation. It was found to be quite useful in that the composite product of several bands allowed one image to represent the information that would otherwise have to be obtained from each of the constituent bands separately.

4.2.5.2 Imagery Studies - Computer Oriented

The LANDSAT Computer Compatible Tapes (CCT's) provide data in digital form thus allowing high speed processing of the imagery information. This can be important since for most operational applications the mass of data in an ERTS image may tend to be too unwieldy for timely analysis by photo interpretive techniques. Computer processing provides the means of quantifying scene radiance values over elemental areas, and thus the CCT printout imagery, composed of alpha-numeric symbols spaced on a rectangular format, also allows for better feature representation at a larger scale than would an enlargement of a photo to the same scale. For computer imagery, it was decided that the minimum detectable object dimension was related to pixel dimensions and to be that size necessary to guarantee that at least one pixel projection onto the earth's surface will fall completely within the object's area. Thus, the minimum possible width of a river that will always be detectable as water = 2 pixel lengths = 374 feet (crosstrack) or 500 feet (in-track); the minimum possible areal size of a water body (pond) that would be always detectable as water = 187,000 feet² or 4.3 acres.

A study of surface water characteristics at a small pond (7 acres) in Connecticut yielded a correlation between imagery reflectance and presence of surface water of $r = 0.974$ and between

reflectance and water depth of $r = 0.949$. While the relationship between reflectance and presence of surface water can undoubtedly be extended to all surface waters, that between reflectance and depth probably cannot, since detection of depth variations is in turn dependent on such variable factors as turbidity and other water quality parameters, as well as bottom reflectance, etc. The particular case studied here nevertheless provides hope that in certain waters, LANDSAT can detect differences in depth, however considerably more study is necessary to determine if and how this could be extended to the general case, perhaps using all the LANDSAT spectral bands, or other wave bands not available aboard LANDSAT.

4.2.5.2.1 Man-Computer Interactive Approach

Work has been performed in the development of a man/computer interactive system, with a Cathode Ray Tube (CRT) and light pen, that could allow real time analysis and utilization of LANDSAT computer imagery for important water resource management decisions. A number of computational techniques, operational programs, and utility subroutines have been developed to provide computer oriented means for the interactive analysis of LANDSAT imagery. Due to the late arrival of tapes and extensive work required in printing parts of scenes for study, we did not progress very far in building a truly interactive pattern recognition system to facilitate the analysis of LANDSAT imagery. As part of our LANDSAT-2 follow-on investigation, we hope to continue development of a reliable interactive system which maintains as a data base information obtained from many MSS tapes, then uses this information to predict occurrences similar to those stored, upon input of image information on a real time basis in an operational situation.

4.2.5.3 Imagery/DCS Interaction Studies

The coordinated use of all data available to a real time operational Reservoir Control Center should include the interaction between real time imagery and point data sources such as the LANDSAT DCS for ground truth. Before this interaction situation can become a reality it would be necessary to provide some means of real time relay of LANDSAT imagery to an operational RCC. Even prior to such a situation, however, a useful interaction may take place as the management/hydrologic models that can input DCS/imagery data pass through various stages of development and testing.

4.2.5.4 General

4.2.5.4.1 Spatial Resolution

The LANDSAT-1 resolution is only marginally useful for NED purposes. Better spatial resolution approximating that of the SKYLAB S190B camera would significantly increase operational usefulness to the NED Reservoir Control Center, except perhaps for the monitoring of flood stages where ground truth data is practically a necessity.

4.2.5.4.2 Temporal Resolution

The 18-day LANDSAT-1 coverage is inadequate for the operational needs of the NED Reservoir Control Center. However, it is considered that an every day or every other day coverage would be significantly useful during high flood potential periods. If this were the case in order to conserve production costs and file space, it would be advantageous for NED to have the option as to how often the imaging cameras are "turned on" over its area of responsibility.

4.2.5.4.3 Spectral Resolution

The spectral resolution afforded by the LANDSAT 4-band MSS (0.5 to 1.1 micrometers) seems adequate for many operational concerns of NED. However, the experimental use of additional bandwidths, especially those in the ultraviolet and the thermal infrared might help solve some of the problems of quantifying certain feature characteristics on the imagery such as snow water content, water depth and water quality.

4.2.5.4.4 MSS Versus RBV Imagery

The 4-band MSS imagery was the major source of LANDSAT imagery available for study although a few early RBV frames were studied for comparison. For NED operational purposes, at this time, neither MSS nor RBV would have distinct relative advantages or disadvantages over the other. The RBV images have somewhat better geometric fidelity, a more convenient square format, intersections of latitude-longitude annotated on the image, and 3-bands ranging from 0.48 to 0.83 micrometers (which cuts off some of the near-IR). On the other hand, the MSS has better spectral fidelity, lesser geometric fidelity, a more inconvenient skewed

format, annotated marginal latitude-longitude tick marks, and a wider spectral range divided into 4 bands ranging from 0.5 to 1.1 micrometers in the near IR region.

4.2.5.4.5 100 x 100 Mile Format

The 100 x 100 nautical mile format of the LANDSAT imagery is satisfactory for NED purposes. Major tributary watersheds conveniently fit into one or two frames. However, the Connecticut River, with a length of 400 miles, would be best formatted using a long continuous strip produced by a single LANDSAT orbital pass from Canada to Long Island Sound. This long format would produce a true synoptic view of north/south trending rivers such as the Connecticut, rather than the pasted-together, butt-edged look of the present LANDSAT 100 x 100 mile format.

4.2.5.4.6 Side Overlap

The additional temporal information in the 39 to 52 mile side overlap in the New England latitudes produced by LANDSAT orbits 24 hours apart is not considered to be operationally useful for NED. These overlap strips produce the two views separated by 24 hours just once in every 18-day period -- and it is only fortuitous if the overlap strip occurs in a particular watershed of interest.

Overlapping pairs of imagery in the direction of LANDSAT flight produced by framing camera such as the RBV might be useful for producing stereo effects for improving interpretation of vertical dimensions.

4.2.5.4.7 Sun Angle

The constant sun angle inherent in the LANDSAT imagery is a distinct advantage in interpretation of scenes in the NED region. This advantage is particularly apparent when compared with aerial imagery taken at different sun angles of mountainous terrain typical of the New England region.

The 1000 hours LANDSAT overflights seem to be advantageous for viewing New England terrain. A much earlier morning LANDSAT passage and/or a late afternoon passage (especially in winter) would produce greater terrain relief shadows but less illumination

causing greater interpretational difficulties.

NED operations are not geared to a particular single time of the day; hence the particular time of LANDSAT imaging is otherwise not important from the NED viewpoint. However, one could speculate about the future usefulness of synchronizing LANDSAT imaging with the observational times of the meteorological observations of the National Weather Service and other hydrometeorological data collection networks. Such synchronization of LANDSAT with other weather and water observations could become quite important as computerized forecasting techniques using mathematical models become more and more relied upon.

4.2.5.4.8 Factors Which Degrade Resolution

Factors which degrade the spatial, temporal or spectral resolution of LANDSAT imagery are of extreme importance to NED operations. Any degradation of the interpreted product, for whatever reason can severely reduce the usefulness of the imagery for NED reservoir control purposes.

For example, in our studies, interpretation of LANDSAT imagery has been compromised by weather factors such as cloud cover, haze, and atmospheric attenuation caused by light scattering.

Seasonal variation of sun angle provides distinct differences in interpretation of LANDSAT imagery for NED purposes. In winter, the lower sun angle increases terrain shadows which enhances observability of terrain relief features; however, this advantage is reduced by the lower level of scene illumination. On the other hand, the high angle of the summer sun provides less noticeable terrain relief but greater scene illumination.

The increased summer vegetative cover obscures ground features. In winter with loss of vegetative cover, terrain features are more easily interpretable, and rivers and smaller tributaries are more distinct (especially after a light snowfall covers the ground, but not water surfaces).

In general, the early spring LANDSAT imagery (April) yields the best overall scene interpretability because of high sun angle, good illumination, and sparse vegetative cover.

4.2.5.4.9 Need for All-Weather, Day-Night Capability

For NED operational purposes, an all-weather, day-night capability would greatly enhance the usefulness of the LANDSAT imagery. Major decisions are made during flood situations which occur during inclement weather and many times at night. Restriction of imagery capabilities to clear weather daylight hours imposes severe difficulties for NED operational missions. The use of thermal infrared bands as well as radar should be considered in attempting an answer to these needs.

4.2.5.4.10 Timeliness of Receipt of Imagery

The day-to-day operational requirements of NED demand timeliness of hydrometeorological information. The usefulness of LANDSAT imagery is severely reduced as the time-lag of the data increases. For example, receipt of the LANDSAT imagery 1 to 5 months after the overflight occurs renders the imagery useless for operational purposes. Real time receipt at the NED Reservoir Control Center would be ideal. However, a 1 to 2 day delay of receipt of imagery could still be useful for certain operational purposes such as some water quality, ice, snow and soil moisture depictions. Longer delays would be acceptable for long range water quality, post flood and other similar studies.

4.2.5.4.11 Reliability of Regular Receipt of Unimpaired LANDSAT Imagery

NED must depend on reliable receipt of data for operational purposes. Failure to routinely receive unimpaired LANDSAT imagery for any reason (e.g., due to breakdown in data processing, excessive cloud cover, etc.) would: (a) jeopardize operational functions, (b) lower the reliance on the LANDSAT imagery on the part of operational personnel, and (c) in the absence of backup data for LANDSAT imagery, require special ad hoc operational procedures to be implemented (perhaps at greater cost and yielding reduced information to the Reservoir Control Center).

5.0 A LOOK INTO THE FUTURE

This investigation of the separate and coordinated uses of the LANDSAT-1 Data Collection and Imaging Systems has been

part of an overall Corps of Engineers R & D program to assess potential remote sensing capabilities for operational watershed management purposes. Since this study has indicated technological feasibility, albeit with the expectation of further advances in imaging systems and products, we feel that an immediate entry into the next stage of development is appropriate. This calls for pilot project test and evaluation demonstrations under quasi-operational conditions. At this stage, practical operational factors and economic feasibility will be tested. This is the express purpose of our LANDSAT-2 follow-on investigation which will heavily emphasize development of an interactive computer processing system for depicting hydrologic data from LANDSAT imagery. It is also the goal of our related construction of an inexpensive, semi-automatic and easily maintained ground receive station for direct real time acquisition of LANDSAT DCS data. If these demonstration projects are considered successful, steps leading toward full implementation of an operating system will be recommended.

In summary, we feel, that this opportunity to participate in the LANDSAT-1 experiment has significantly contributed to the ability of the Corps of Engineers to keep pace with the advancing technology applicable to watershed management. It is through the generosity and cooperation of agencies such as NASA that the operational arms of the Federal Government can seek new and improved means of meeting their increasingly complex goals.

REFERENCES

1. D. Foran. Potential Uses of ERTS-type Imagery in the Evaluation of Snow and Ice Cover and Effects of Melting Therefrom for NED Reservoir Control Operation and Management Purposes. Draft of Master's Thesis to be Submitted to University of Connecticut.
2. Y. T. Chien. Computational Algorithms for Interactive Pattern Recognition. University of Connecticut, School of Engineering Technical Report CS-73-12, 1973. 28 pp.
3. Y. T. Chien. Bibliography on Interactive Pattern Recognition and Related Topics. University of Connecticut, School of Engineering Technical Report CS-74-3, 1974. 29 pp.

TABLE 1

THE NEW ENGLAND DIVISION AUTOMATIC
HYDROLOGIC RADIO REPORTING NETWORK-REPORTING STATIONS AND PARAMETERS

STATION	LOCATION		REPORTING PARAMETERS			
	River	State	River Stage	Reser. Stage	Precip.	Tide Data*
PASSUMPSIC	Passumpsic	Vt.	X		X	
WELLS RIVER	Connecticut	Vt.	X			
WEST HARTFORD	White	Vt.	X			
WHITE R. JUNCT.	Connecticut	Vt.	X			
WOODSTOCK	Pemigewasset	N.H.	X		X	
RUMNEY	Baker	N.H.	X		X	
PLYMOUTH	Pemigewasset	N.H.	X			
PENACOOK	Contocook	N.H.	X			
SOUCOOK	Soucook	N.H.	X			
CONCORD	Merrimack	N.H.	X			
GOFFSTOWN	Piscataquog	N.H.	X			
GOFFS FALLS	Merrimack	N.H.	X			
N. WALPOLE	Connecticut	N.H.	X			
W. DEERFIELD	Deerfield	Mass.	X			
MONTAGUE CITY	Connecticut	Mass.	X			
CONANT BRK. DAM	Conant Brook	Mass.		X		
INDIAN ORCHARD	Chicopee	Mass.	X			
WESTFIELD	Westfield	Mass.	X			
SPRINGFIELD	Connecticut	Mass.	X			
WEBSTER	French	Mass.	X			
NORTHBRIDGE	Blackstone	Mass.	X			
LOWELL	Merrimack	Mass.	X			
MAD RIVER LAKE	Mad	Conn.		X		
COLLINSVILLE	Farmington	Conn.	X			
RAINBOW	Farmington	Conn.	X			
HARTFORD	Connecticut	Conn.	X			
HALL MEADOW DAM	Hall Meadow	Conn.		X		
EAST BRANCH DAM	Naugatuck	Conn.		X	X	
THOMASTON DAM	Naugatuck	Conn.		X		
NORTHFIELD BRK. LK.	Northfield Brk.	Conn.		X		
BLACK ROCK LAKE		Conn.		X		
HANCOCK BRK. LAKE	Hancock Brk.	Conn.		X		
HOP BRK. LAKE	Hop Brook	Conn.		X		
BEACON FALLS	Naugatuck	Conn.	X			
STEVENSON	Housatonic	Conn.	X			
WILLIMANTIC	Shetucket	Conn.	X			
NORWICH**	Shetucket	Conn.	X			
NATCHAUG	Quinebaug	Conn.			X	
OLD SAYBROOK		Conn.				X
BLOCK ISLAND		R.I.				X
WOONSOCKET	Blackstone	R.I.	X			
Total			29	9	5	2

* Includes Wind Dir., Wind Vel., Bar. Pres., Tide Elev.

** Includes both Headwater (Quinebaug R.) and Tailwater (Shetucket R.) stages.

TABLE 2

THE NEW ENGLAND DIVISION LANDSAT-1 DATA REPORTING
NETWORK - REPORTING STATIONS AND PARAMETERS

9 SEPTEMBER 1974

SITE ID NO.	TYPE*	STATION NAME	LA T	LONG
1	S	SAINT JOHN RIVER AT FORT KENT, MAINE	47 15	68 35
8	S	SAINT JOHN RIVER AT NINEMILE BRIDGE, MAINE	46 42	69 43
2	S	PENOBSCOT RIVER AT WEST ENFIELD, MAINE	45 14	68 39
3	S	CARABASSETT RIVER AT NORTH ANSON, MAINE	44 52	69 57
5	S	SACO RIVER AT CORNISH, MAINE	43 48	70 47
6	S	PEMIGEWASSET RIVER AT PLYMOUTH, N. H.	43 45	71 41
7	S	MERRIMACK RIVER AT GOFFS FALLS, N. H.	42 57	71 28
10	S	TOWN BROOK AT QUINCY, MASSACHUSETTS	42 15	71 00
41	S	NORTH NASHUA RIVER AT FITCHBURG, MASS.	42 34	71 47
11	S	PAWTUXET RIVER AT CRANSTON, R. I.	41 45	71 27
13	S	BRANCH RIVER AT FORESTDALE, R. I.	42 00	71 34
12	S	CONNECTICUT RIVER AT HARTFORD, CONN.	41 46	72 40
20	P	STINSON MOUNTAIN, NEW HAMPSHIRE	43 50	71 47
21	P	SOUTH MOUNTAIN, NEW HAMPSHIRE	42 59	71 35
22	P	FRANKLIN FALLS DAM, NEW HAMPSHIRE	43 28	71 40
23	P	BLACKWATER DAM, NEW HAMPSHIRE	43 19	71 44
24	P	MAC DOWELL DAM, NEW HAMPSHIRE	42 54	71 59
26	P	WACHUSETT MOUNTAIN, MASSACHUSETTS	42 29	71 53
25	P	MANSFIELD HOLLOW DAM, CONNECTICUT	41 46	72 11
30	C	STAMFORD BARRIER, STAMFORD, CONNECTICUT	41 02	73 32
42	Q	WESTFIELD R. AT WEST SPRINGFIELD, MASS.	42 06	72 38
43	Q	CHICOPEE RIVER AT CHICOPEE, MASS.	42 09	72 35
44	Q	FRENCH RIVER AT WEBSTER, MASSACHUSETTS	42 03	71 53
50	T	NED HEADQUARTERS, WALTHAM, MASS.	42 24	71 13
51	T	COLD REGIONS LABORATORY AT HANOVER, N. H.		VARIABLE
52	T	COLD REGIONS LABORATORY AT HANOVER, N. H.		VARIABLE
54	T	U.S. GEOLOGICAL SURVEY, BOSTON, MASS.		VARIABLE

* S - RIVER STAGE

P - PRECIPITATION

C - COASTAL (WIND DIRECTION, VELOCITY AND TIDE)

Q - WATER QUALITY (TEMPERATURE, CONDUCTIVITY, PH AND DISSOLVED OXYGEN)

T - TFST SET (SENSORS VARIABLE)

TABLE 3

DCP COMPONENT MALFUNCTION STATISTICS
 (For Entire LANDSAT Experimental Period From
 23 July 1972 Through 29 May 1974)

No Malfunction = 18 DCP's
 One Malfunction = 5 DCP's
 Two Malfunctions = 3 DCP's
 Three Malfunctions = 1 DCP

DCP No.	Life in Months Before First Component Malfunction	Life in Months Before Second Component Malfunction	Life in Months Before Third Component Malfunction
6201	1 (p, m)	-	-
6246	2 (p, m, f)	1 (f)	2 (f)
6271	2 (p)	2 (p)	-
6220	2 (p, m)	3 (p)	-
6106	5 (f)	2 (p)	-
6170	7 (p, m)	-	-
6021	8 (p)	-	-
6071	8 (t, m)	-	-
6242	11 (p)	-	-

Component Malfunction Type:

p = programmer board
 t = transmitter board
 m = parallel/digital multiplex board
 f = fuse

TABLE 4
DCP FIELD OF VIEW STATISTICS
(For Entire LANDSAT Experimental Period
From 23 July 1972 Through 29 May 1974)

Site ID No.	General Location	Location Description	Reports Possible/ 18 Days
1	River	Wide river channel, DCP in open field	88
2	River	Clear view on wide river channel	90
3	River	Narrow river channel, dense woods on bank side of DCP	82
4	River	Surrounded by large overhanging trees	78
5	River	High trees on bank side of DCP	83
6	River	DCP in shadow of large tree - many other trees around	81
7	River	Clear view on wide river channel	88
8	River	Clear view on wide river channel	92
9	River	Many trees over DCP	79
10	River	Two large trees near DCP limit view	84
11	River	Two-thirds open view, one-third in shadow of trees	84
12	River	Clear view on wide river channel	90
13	River	Surrounded by many overhanging trees	82
40	River	Narrow river channel, high trees on both banks	82
41	River	Clear view	87
42	River	Trees and buildings on one side of DCP	81
43	River	Clear view	88
20	Mountaintop	Clear view	94
21	Mountaintop	Clear view	92
26	Mountaintop	Clear view	95
22	Dan-site	Clear view	90
24	Dan-site	Clear view	86
30	Coastal	Clear view - DCP at hurricane barrier	90

* Exact locations may be found in Table 2 except for the following which were abandoned prior to 9 September 1974:

- No. 4 - Androscoggin River at Auburn, Maine
- No. 9 - Charles River at Charles River Village, Mass.
- No. 40 - Ashuelot River at Winchester, N. H.

Sites 23, 25 and 44 are not included in Field of View Statistics because either they were not in use during the period or not in normal operation enough to yield valid statistics.

TABLE 5

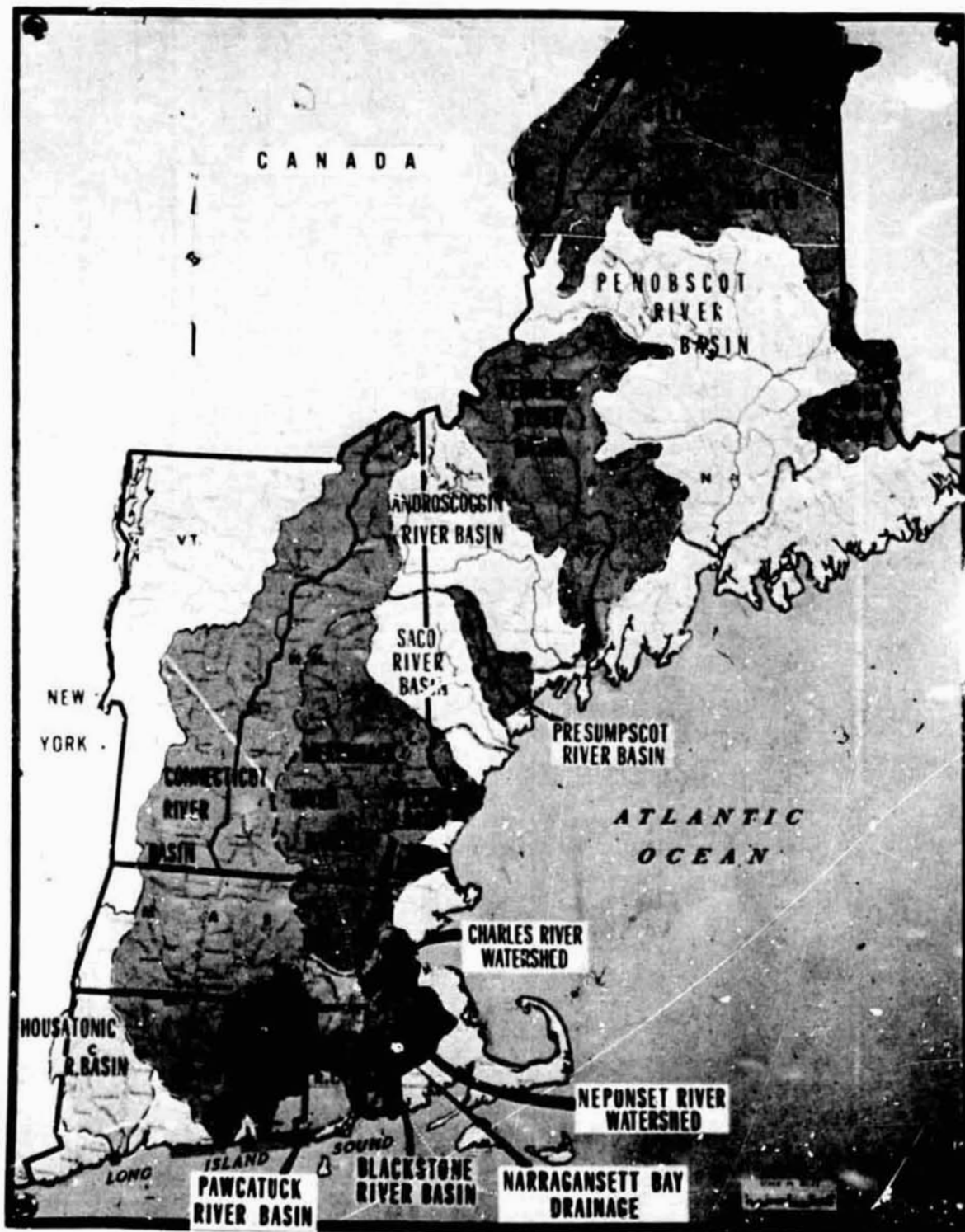
SUMMARY OF LANDSAT QUESTIONNAIRE

INTERROGATION TIME REQUIREMENTS

PARAMETERS	Number and Time of Parameters										Totals
	Continuous	1-Hour	2-Hour	3-Hour	6-Hour	8-Hour	12-Hour	24-Hour	Weekly	2-Week	
River Data (Stage, Tailwater, Current, Discharge)	732	480	60		227	325	23	106			1953
Precipitation	310	430	36	351	240	17	100	361			1845
Reservoir or Lake Stage	21	17	19		17						74
Snow Cover	84	10	7		319			75	68		563
Wind Speed and/or Direction	42	10				8		193			253
Barometric Pressure	10							16			26
Oceanographic Data (Tide Level, Current, etc.)	87							94			181
Air or Soil Temperature	10	55	3					190	20		278
Air or Soil Moisture		60						49			109
Water Quality Data	154	49		3				187	26	20	448
Evaporation					8			10			10
Spillway Gate Opening		15									15
Solar Radiation		5									5
Totals	1450	1131	125	354	811	350	124	1281	94	40	5760*

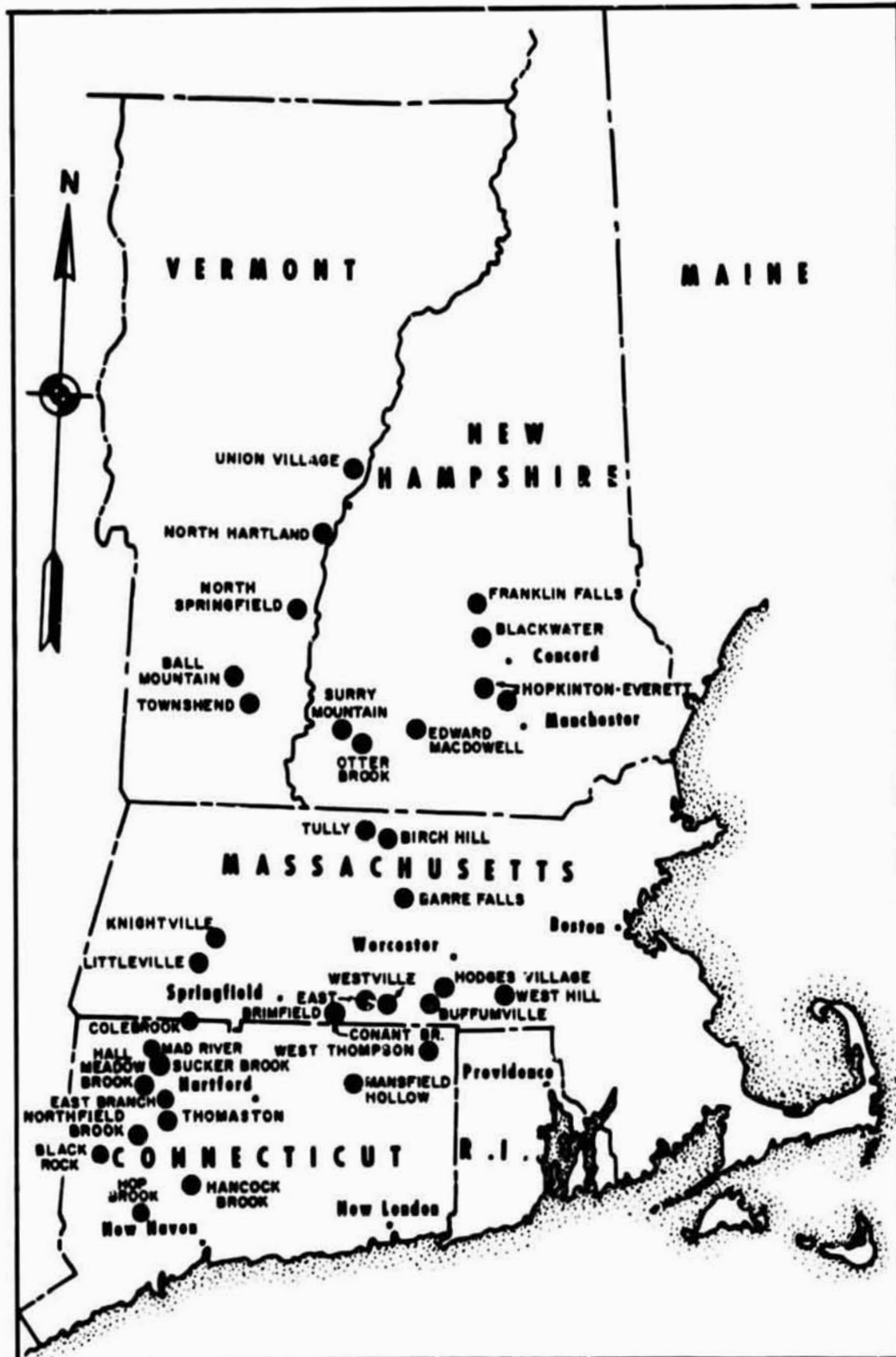
* Total number of sites = 4,437, thus indicating numerous multiparameter situations

REPRODUCIBILITY OF THE ORIGINAL PAGE IS POOR



NEW ENGLAND WATERSHEDS

FIG. 1



NEW ENGLAND DIVISION RESERVOIRS

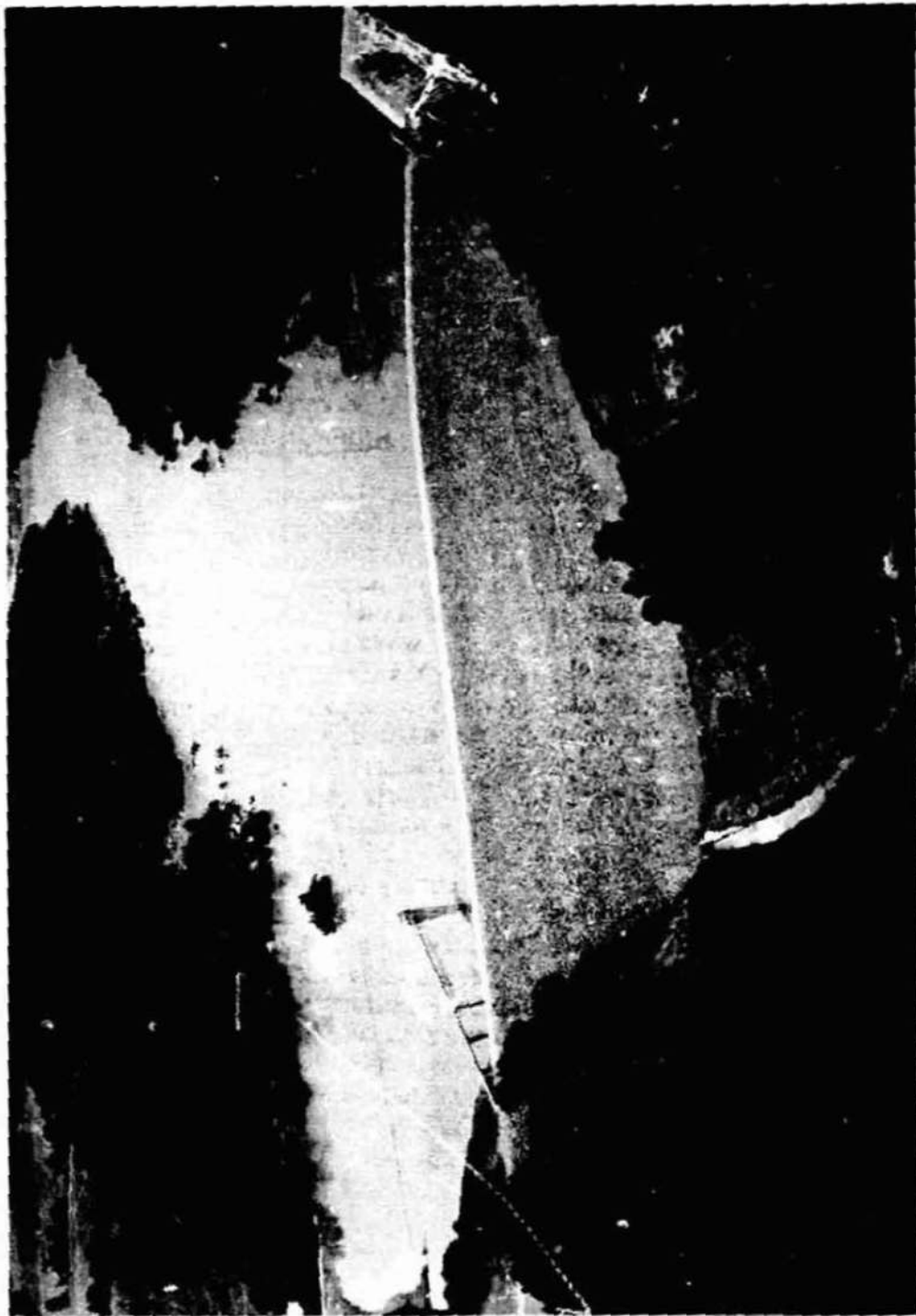
FIG. 2

REPRODUCIBILITY OF
ORIGINAL PAGE IS



FIG. 3

NORTH HARTLAND LAKE, VT. UNDER NORMAL CONDITIONS



NORTH HARTLAND LAKE, VT. 50 PERCENT FULL DURING JULY, 1973 FLOOD
FIG. 4



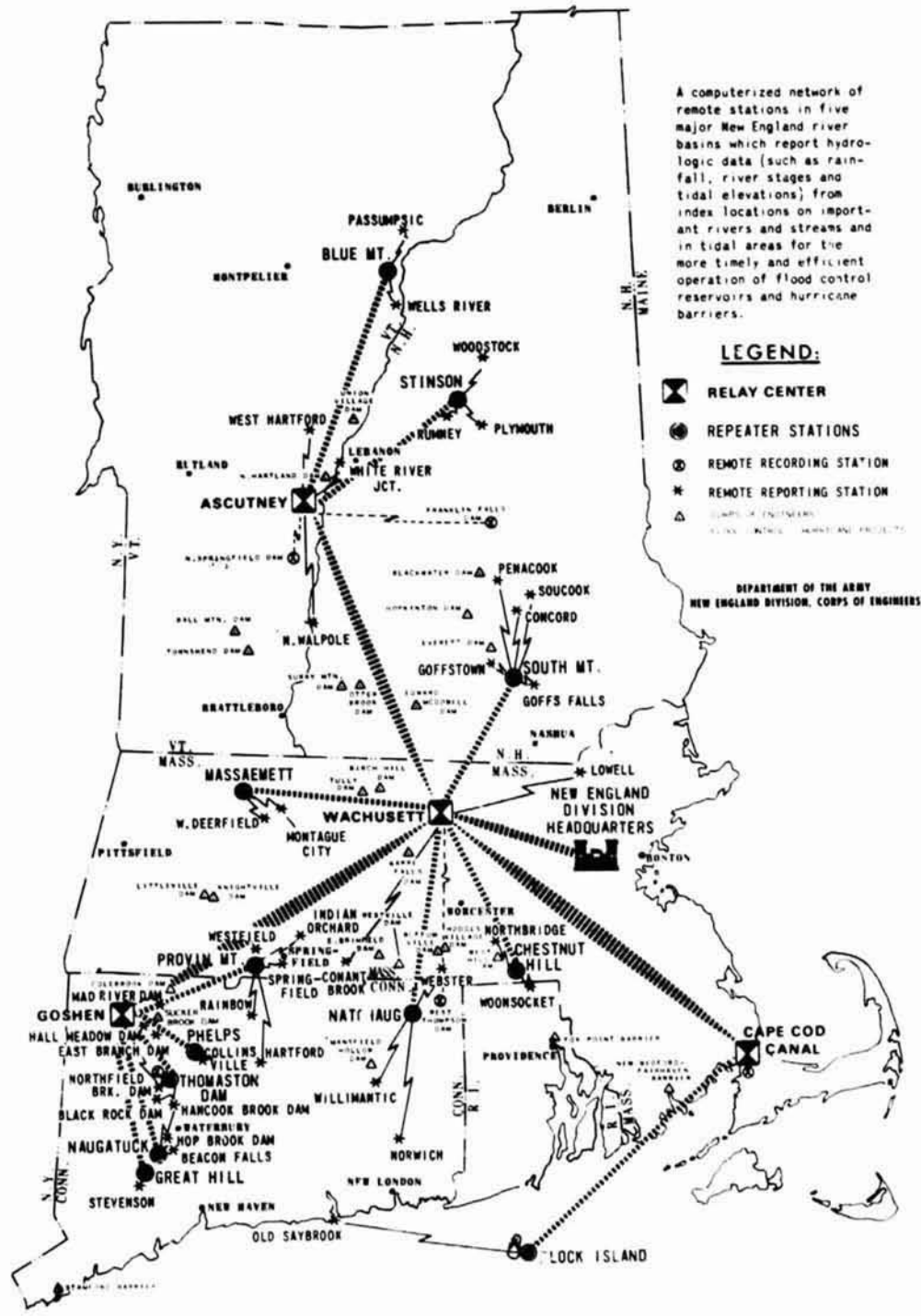
THE QUINEBAUG RIVER AT PUTNAM, CONN. DURING 1955 FLOOD

FIG. 5



NEW BEDFORD HURRICANE BARRIER, MASS.

FIG. 6



A computerized network of remote stations in five major New England river basins which report hydrologic data (such as rainfall, river stages and tidal elevations) from index locations on important rivers and streams and in tidal areas for the more timely and efficient operation of flood control reservoirs and hurricane barriers.

LEGEND:

- ☒ RELAY CENTER
- REPEATER STATIONS
- ⊕ REMOTE RECORDING STATION
- * REMOTE REPORTING STATION
- △ DAMS IN CONSTRUCTION
- △ DAMS UNDER MAINTENANCE PROJECTS

DEPARTMENT OF THE ARMY
NEW ENGLAND DIVISION, CORPS OF ENGINEERS

ATOMATIC HYDROLOGIC RADIO REPORTING NETWORK

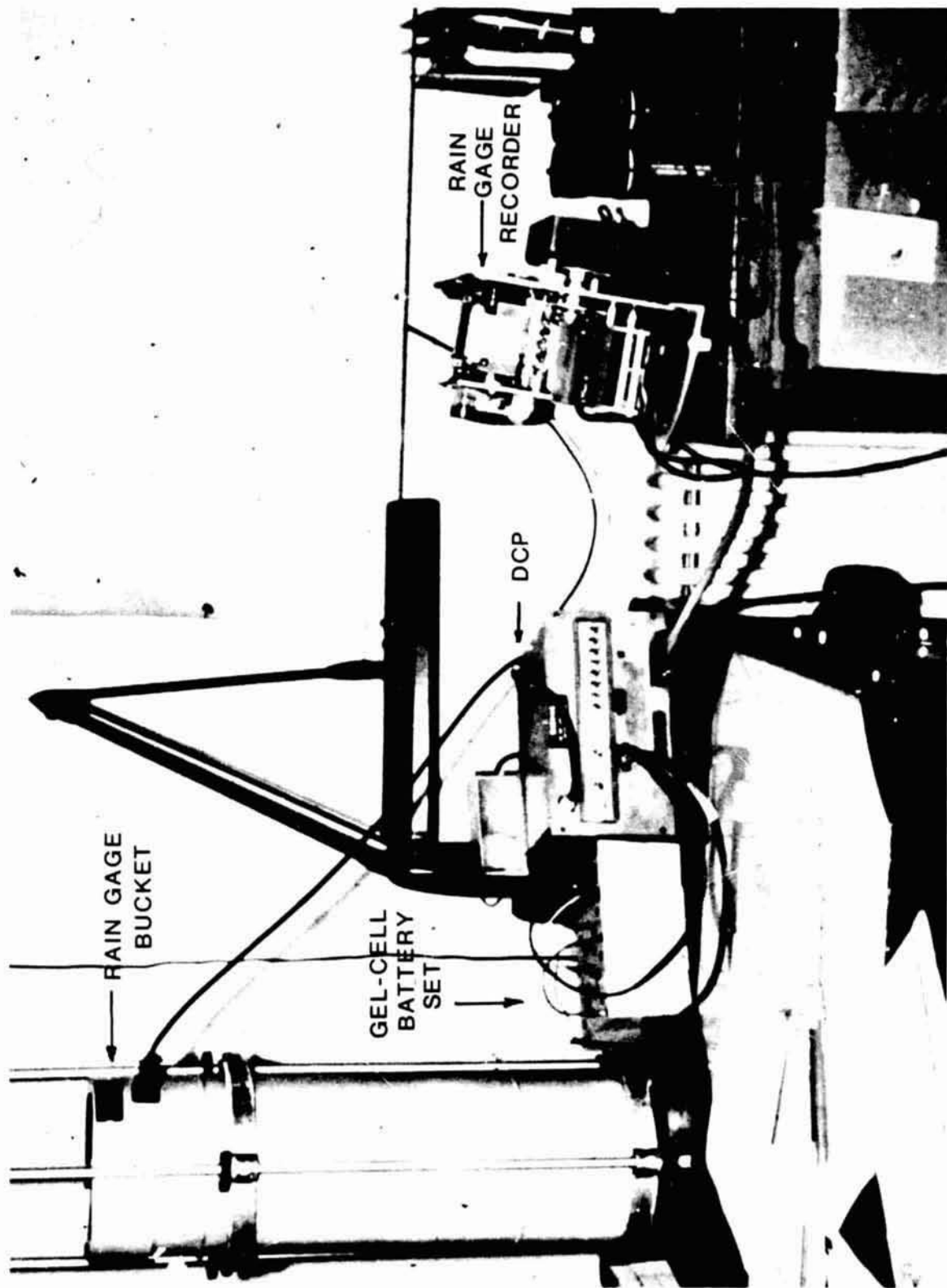
FIG. 7

ALL STATION SCAN		2 FEB. 1973		FILE NO.		DAY HR. MIN.		TIDE		BAROMETER		WIND VELOCITY		WIND DIRECTION	
STA. NO.	AND NAME	FILE NO.	DAY HR. MIN.	DISCH.	CFS	SM	STAGE	RAIN	INCR.	BAROMETER	WIND VELOCITY	WIND DIRECTION	BAROMETER	WIND VELOCITY	WIND DIRECTION
39	COASTAL STATION	54	33 2055		2.80	FT.	29.03	IN.	WARN	49	MPH	225	DEGR		
40	BLOCK ISLAND				2.50	FT.	29.12	IN.	WARN	39	MPH	149	DEGR		
41	COASTAL STATION	52	33 2055												
42	OLD SAYBROOK														
98	STA. NO. AND NAME	FILE NO.	DAY HR. MIN.	DISCH.	CFS	SM	STAGE	RAIN	INCR.	BAROMETER	WIND VELOCITY	WIND DIRECTION	BAROMETER	WIND VELOCITY	WIND DIRECTION
39	PASSUMPSIC	70	33 2055	1130.	2.6		4.00	FT.		29.03	IN.	WARN	29.03	IN.	WARN
38	WELLS RIVER	72	33 2055	7024.	2.7		4.60	FT.	0.17						
36	WEST HARTFORD	72	33 2056	840.	1.2		4.30	FT.							
35	WHITE RIVER JUNCTION	69	33 2056	11590.	2.8		8.70	FT.							
37	N WALPOLE	72	33 2056	14850.	2.7		10.90	FT.							
7	WEST DEERFIELD	73	33 2056	3234.	5.8		4.30	FT.							
6	MONTAGUE CITY	73	33 2056	21340.	2.7		14.10	FT.							
15	CONANT BROOK DAM	48	33 2056	1500.	2.2		6.10	FT.		NO REPORT					
17	INDIAN ORCHARD	72	33 2056	1824.	3.7		6.10	FT.							
18	SPRINGFIELD	72	33 2056	19600.	2.0		5.60	FT.							
16	MAD RIVER DAM	63	33 2057	9000.	25.4		12.20	FT.		NO REPORT					
24	COLLINSVILLE	72	33 2057	2210.	3.7		3.40	FT.		FSTG					
20	RAINBOW	70	33 2057	20600.	2.0		7.20	FT.							
19	HARTFORD														
34	RUMNEY	71	33 2057	387.	2.7		3.5	FT.							
33	WOODSTOCK	72	33 2057	3946.	20.4		6.70	FT.			15.67	IN.		0.36	WARN
32	PLYMOUTH	72	33 2057	3450.	5.5		3.00	FT.		CHRG	4.03	IN.		0.37	WARN
10	PENACOOK	73	33 2057	3520.	4.6		4.00	FT.							
13	SOUCCOCK	69	33 2057	214.	2.3		6.80	FT.							
11	CONCORD	73	33 2058	6190.	2.6		5.30	FT.							
8	GOFFSTOWN SOUTH BR.	72	33 2058	782.	1.5		5.70	FT.							
9	GOFFS FALLS	73	33 2058	6832.	2.2		5.60	FT.							
14	LOWELL	73	33 2058	27499.	5.9		48.20	FT.							
96	HALL MEADOW DAM	72	33 2058	132.	7.7		7.40	FT.							
30	EAST BRANCH DAM	71	33 2058	119.	13.0		17.30	FT.							
26	THOMASTON DAM	72	33 2058	996.	10.2		26.80	FT.			5.80	IN.		0.00	
31	NORTHFIELD BRK. LAKE	72	33 2058	89.	15.7		28.60	FT.							
25	BLACK ROCK LAKE	71	33 2058	345.	15.2		39.10	FT.							
23	HANCOCK BROOK LAKE	72	33 2058	190.	15.9		8.60	FT.							
29	HOP BROOK LAKE	2	33 2059	288.	17.6		27.80	FT.							
22	BEACON FALLS	73	33 2059	6832.	26.2		9.20	FT.		FSTG					
21	STEVENSON	72	33 2059	15400.	10.0		11.60	FT.		WARN					
99	WACHUSETT RELAY	0	33 2059	-0.	0.0		10.00	FT.		NO REPORT					
13	NORTHBRIDGE	3	33 2059	2658.	6.4		5.30	FT.		MVLDI					
12	WOONSOCKET	73	33 2059	574.	6.7		6.60	FT.		WARN					
1	WILLIMANTIC	73	33 2059	3602.	9.0		7.10	FT.		WARN					
4	NORWICH TAILWATER	73	33 2100	12200.	9.7		24.30	FT.		WARN					
5	NORWICH HW MATCHAUG P	73	33 2100	1821.	2.4		47.01	FT.							
39	STA. C.S.M.	34	2.2 HR PERIODS												
39	3.65	34	5.21 33 25.56	30	-1.00	5	6.46								

TYPICAL REPORT FROM THE AUTOMATIC HYDROLOGIC RADIO REPORTING NETWORK

FIG. 8

REPRODUCIBILITY (1971)
ORIGINAL PAGE IS



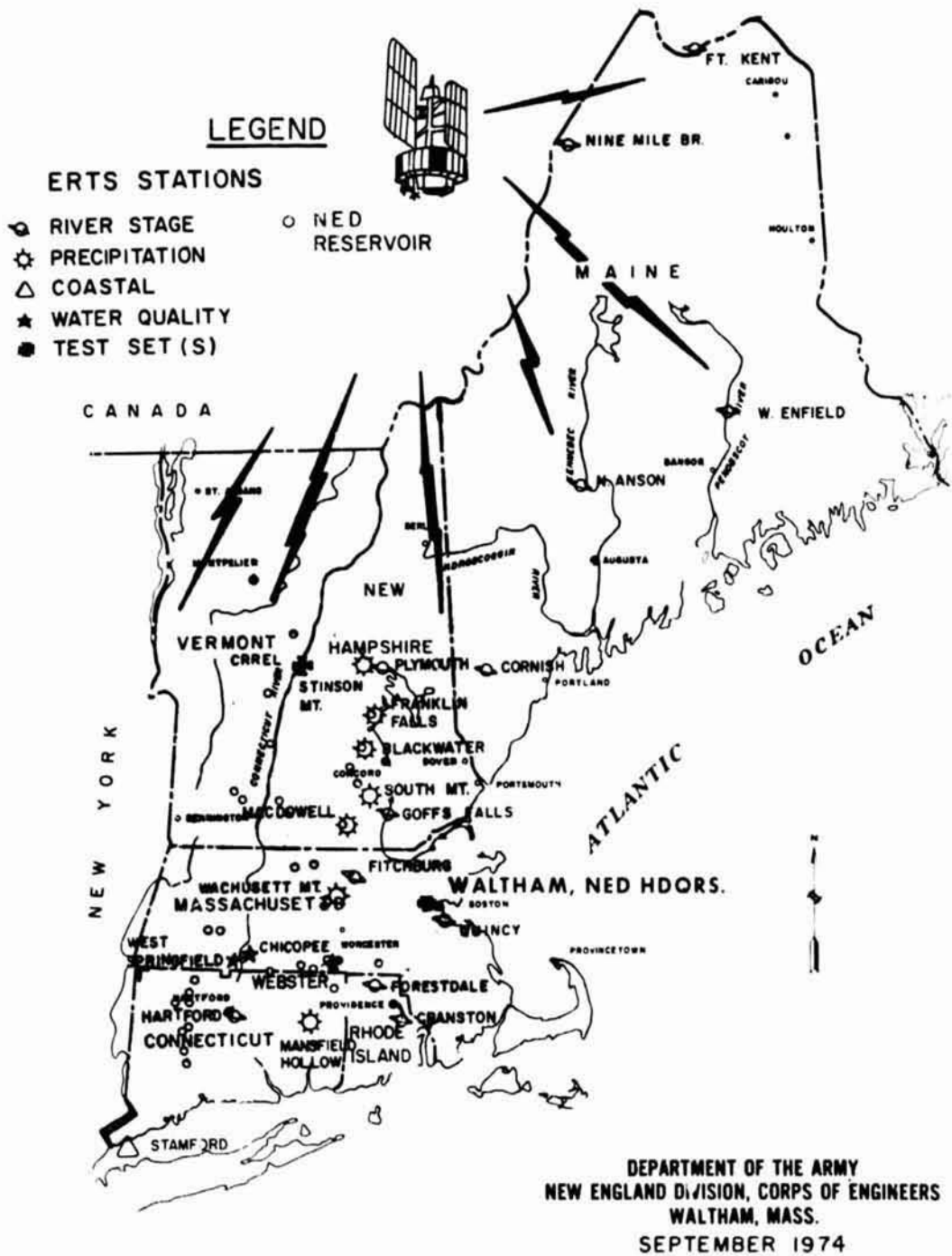
TYPICAL LANDSAT PRECIPITATION STATION EQUIPMENT

FIG 9



LANDSAT RIVER GAGING SITE
THE CARABASSETT RIVER AT NORTH ANSON, MAINE

FIG. 10



LANDSAT-1 DATA REPORTING STATIONS

FIG. 11

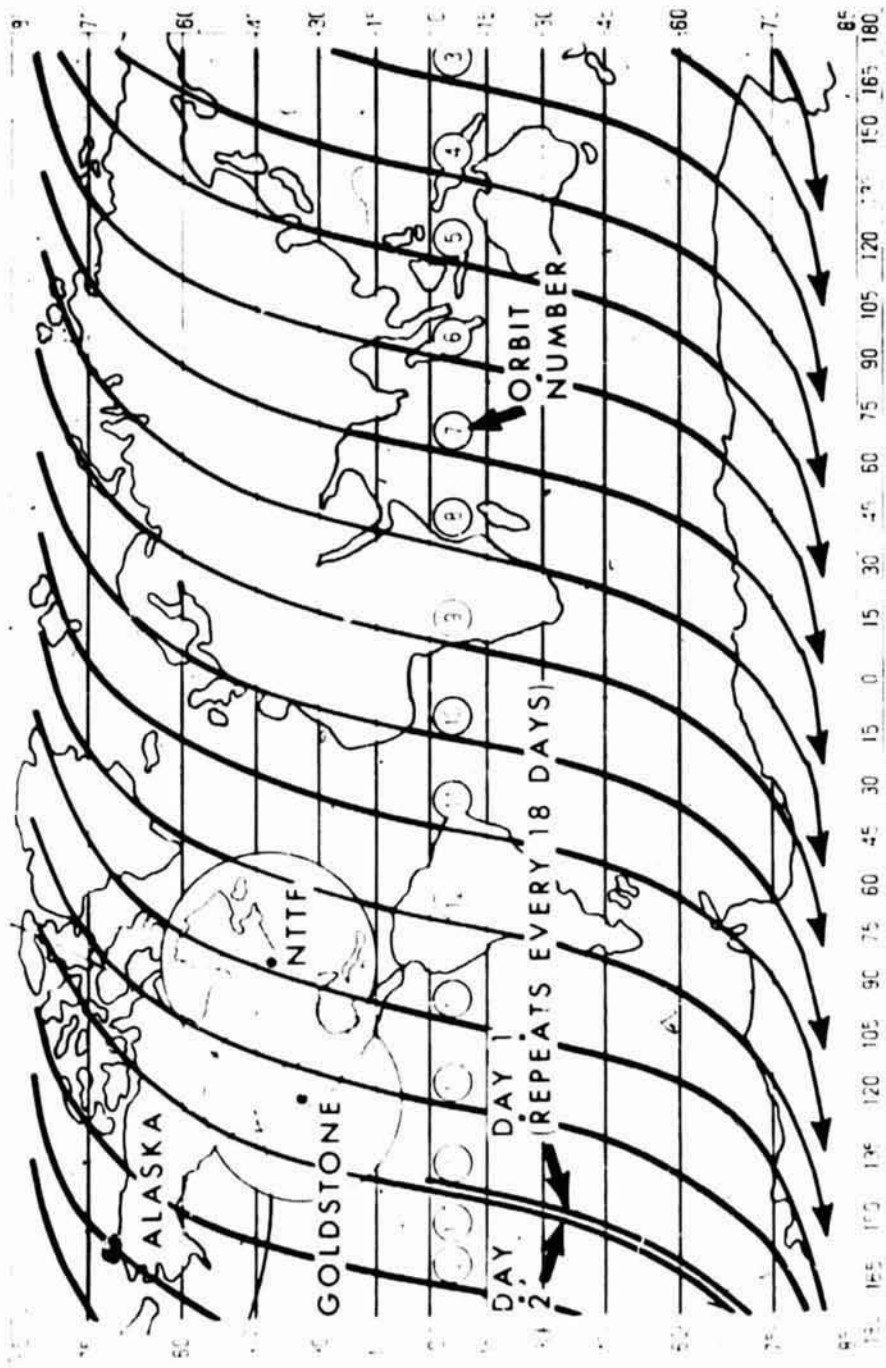
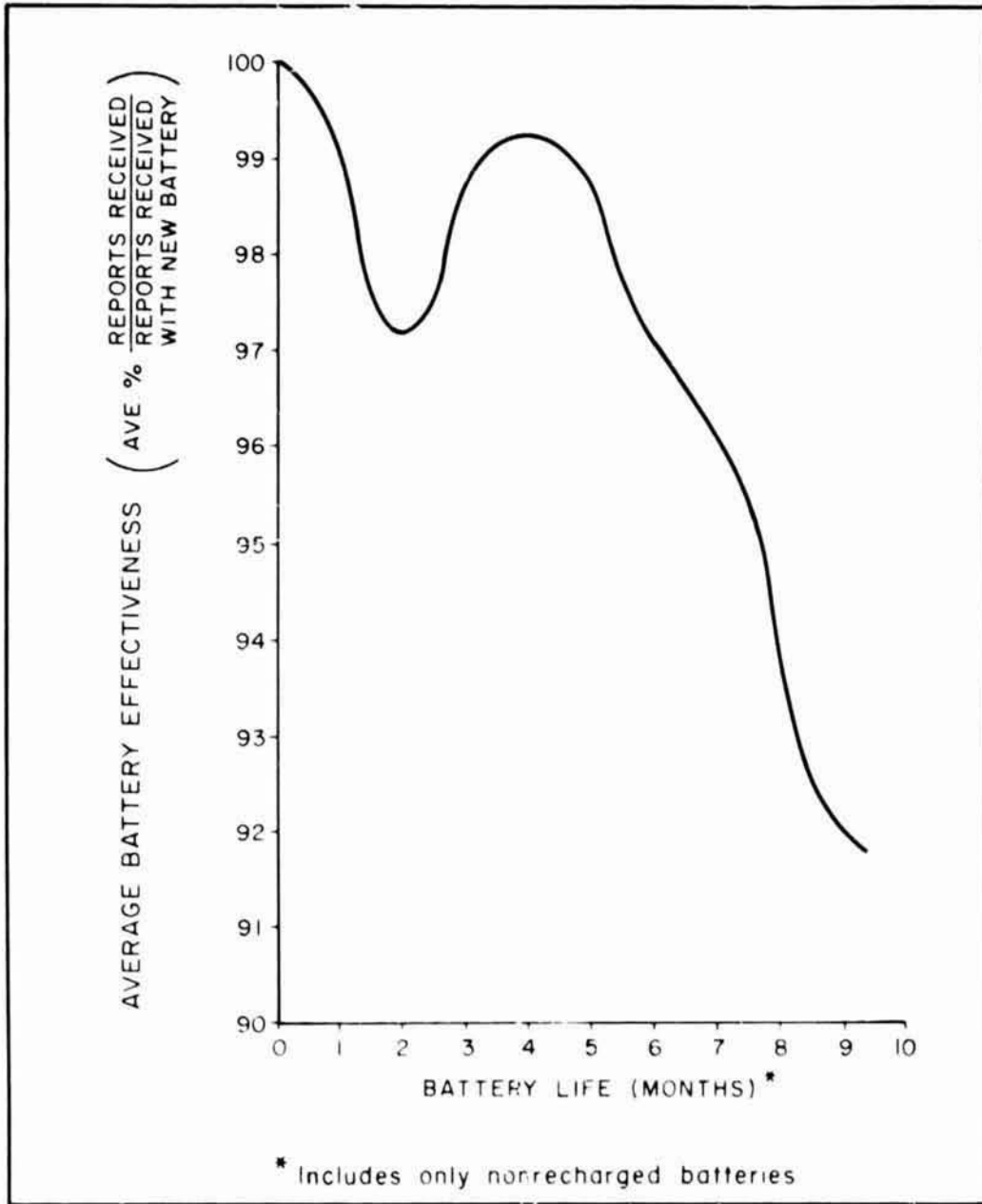
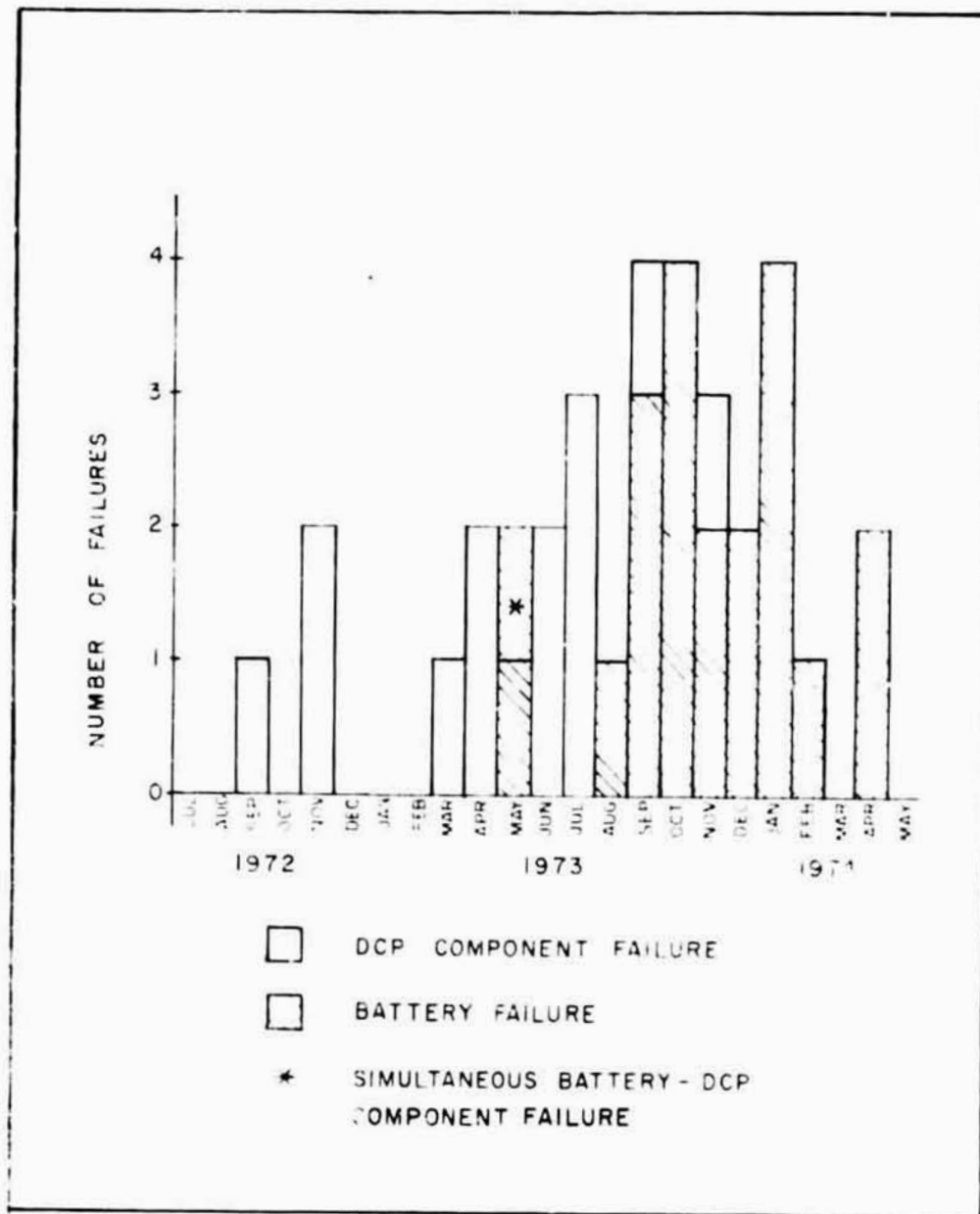


FIG. 12
TYPICAL LANDSAT DAILY GROUND TRACK



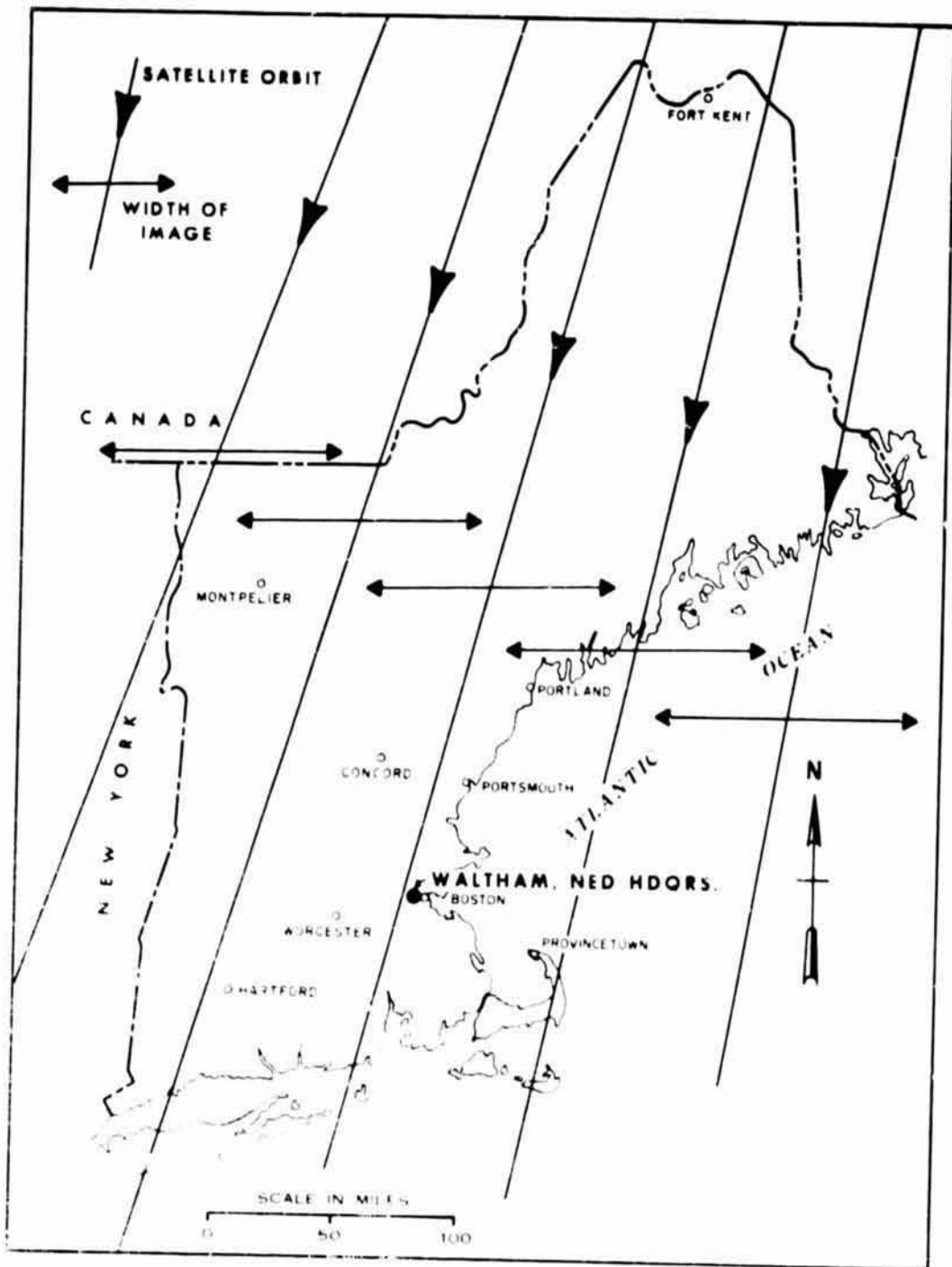
BATTERY AGE VERSUS BATTERY EFFECTIVENESS

FIG. 13



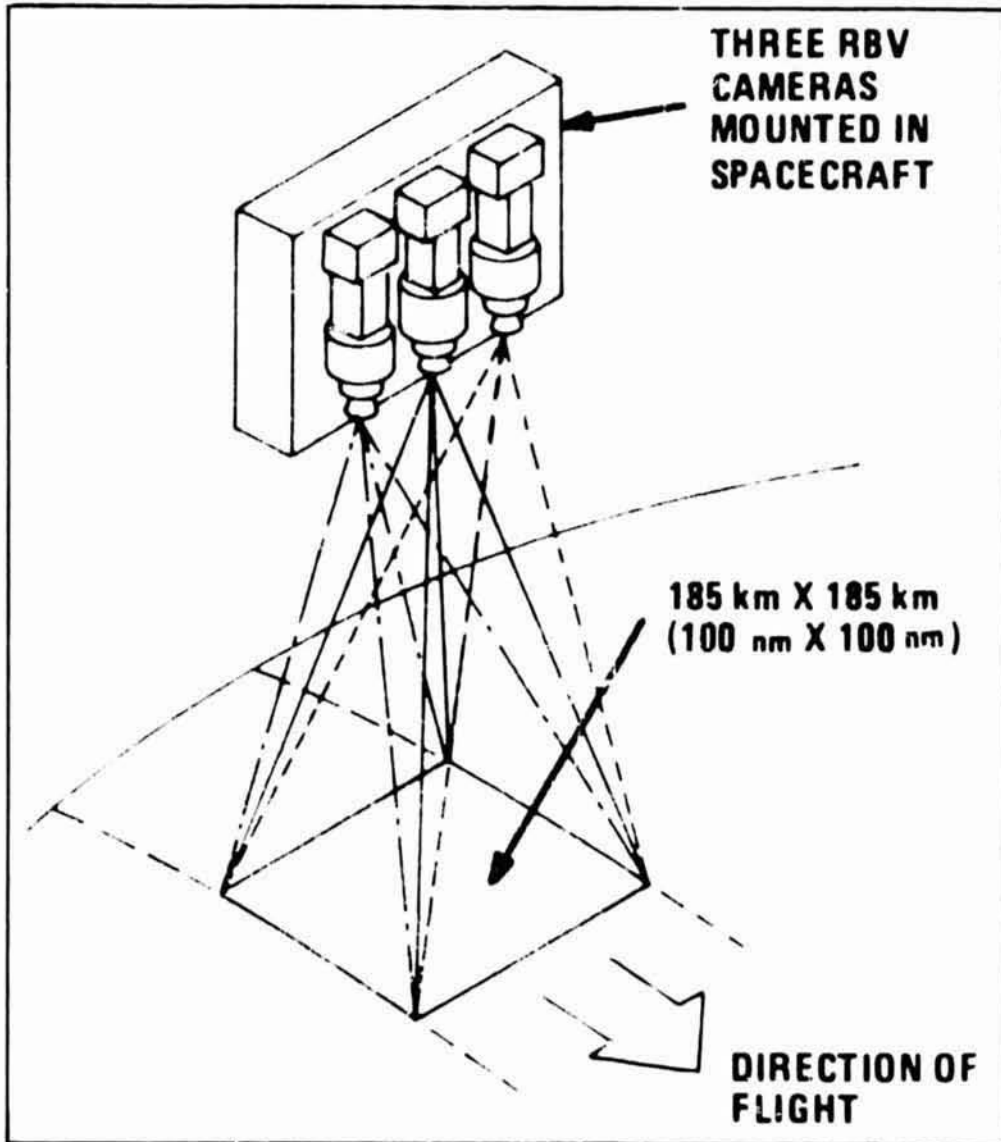
DATA COLLECTION SYSTEM PERFORMANCE VERSUS TIME

FIG. 14

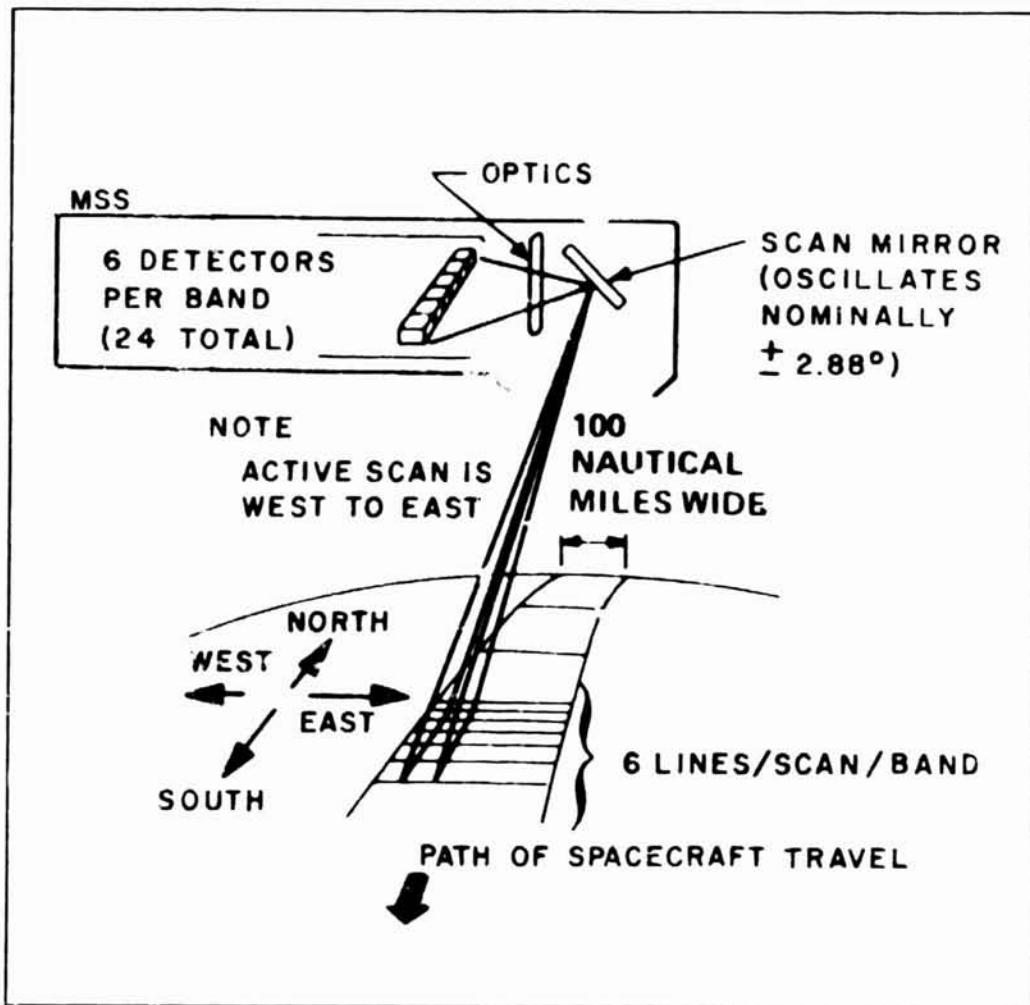


LANDSAT IMAGERY ORBITS OVER NEW ENGLAND

FIG. 15

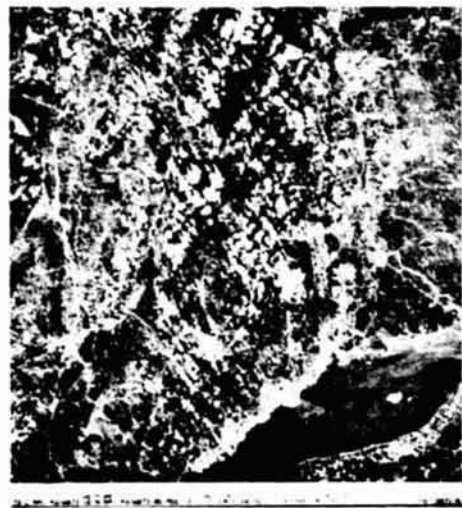
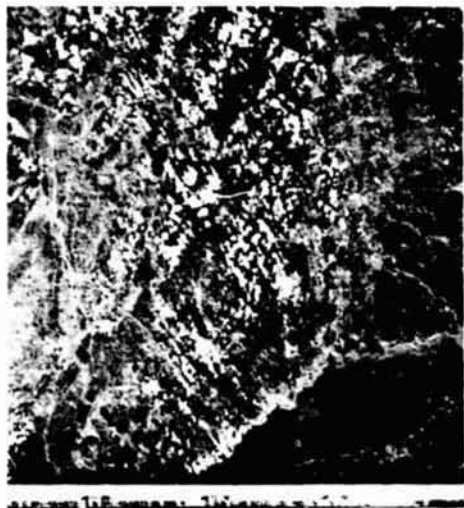


THE RETURN BEAM VIDICON CAMERA SYSTEM



THE MULTISPECTRAL SCANNER SYSTEM

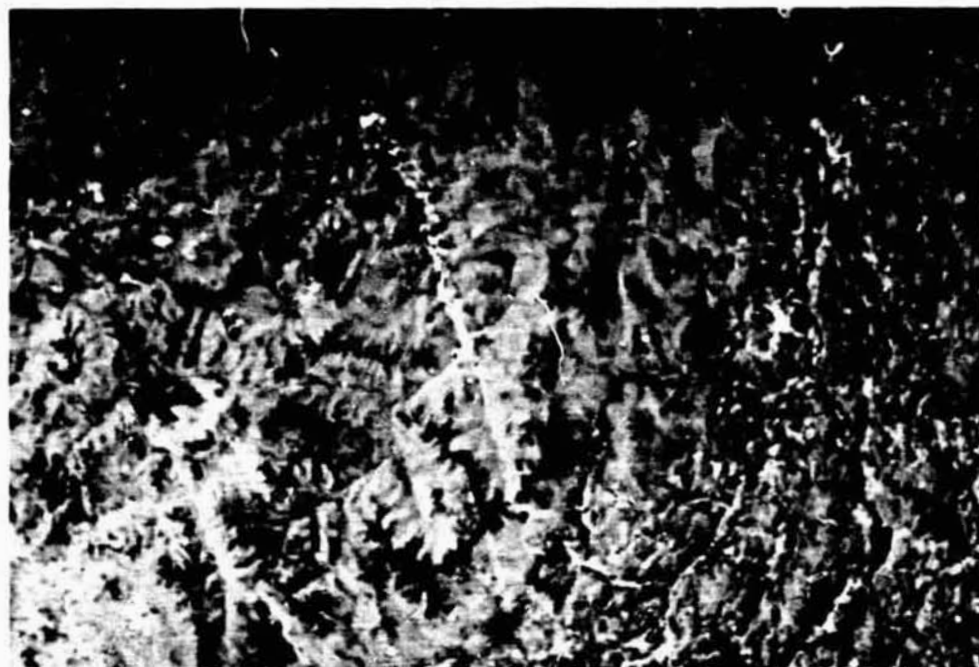
FIG. 17



LANDSAT MSS BANDS OF SOUTHWESTERN NEW ENGLAND

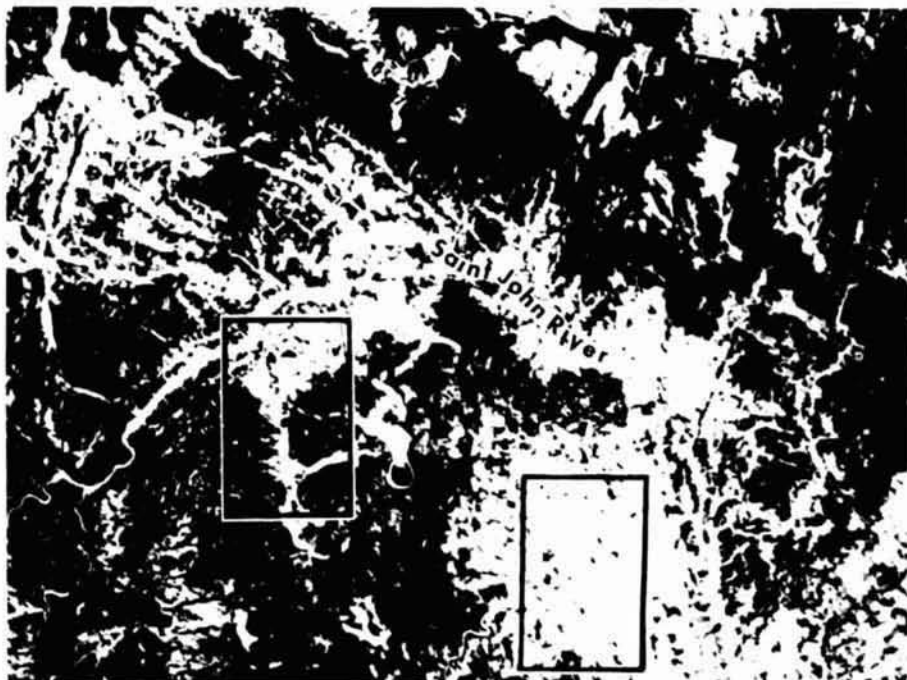
FIG. 18

REPRODUCIBILITY OF
ORIGINAL PAGE IS



LANDSAT COMPOSITE IMAGE OF CONNECTICUT RIVER THREE
WEEKS AFTER A FLOOD

FIG. 19



(a) WINTER



(b) SUMMER

LANDSAT COMPOSITE IMAGES OF SAINT JOHN RIVER, MAINE
(LEFT BOX - EAGLE LAKE AND THE FISH RIVER;
RIGHT BOX - AROOSTOOK RIVER)

REPRODUCIBILITY
ORIGINAL PAGE 1



LANDSAT COMPOSITE OF LAKE WINNIPESAUKEE, NEW
HAMPSHIRE, FROM OVERLAPPING SECTIONS OF TWO
SUCCESSIVE IMAGERY PASSES TO SHOW MELTING OF ICE

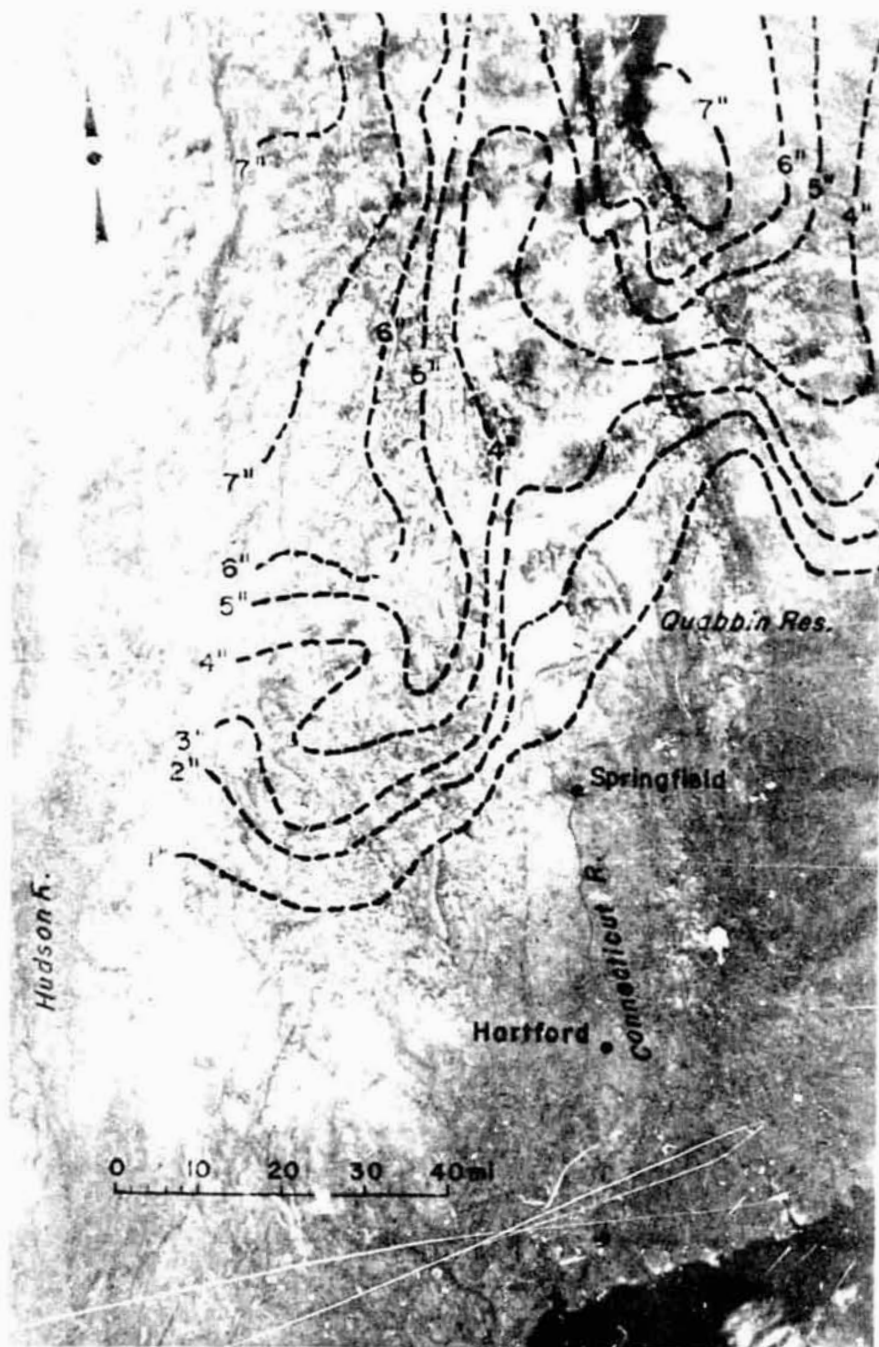
FIG. 21



LANDSAT COMPOSITE IMAGE OF SEDIMENT DISCHARGE PLUME
OF THE CONNECTICUT RIVER AFTER A FLOOD

FIG. 22

REPRODUCIBILITY OF THE
ORIGINAL PAGE IS POOR



LANDSAT COMPOSITE IMAGE OF MIDWINTER SNOW COVER
IN WESTERN NEW ENGLAND

FIG. 23

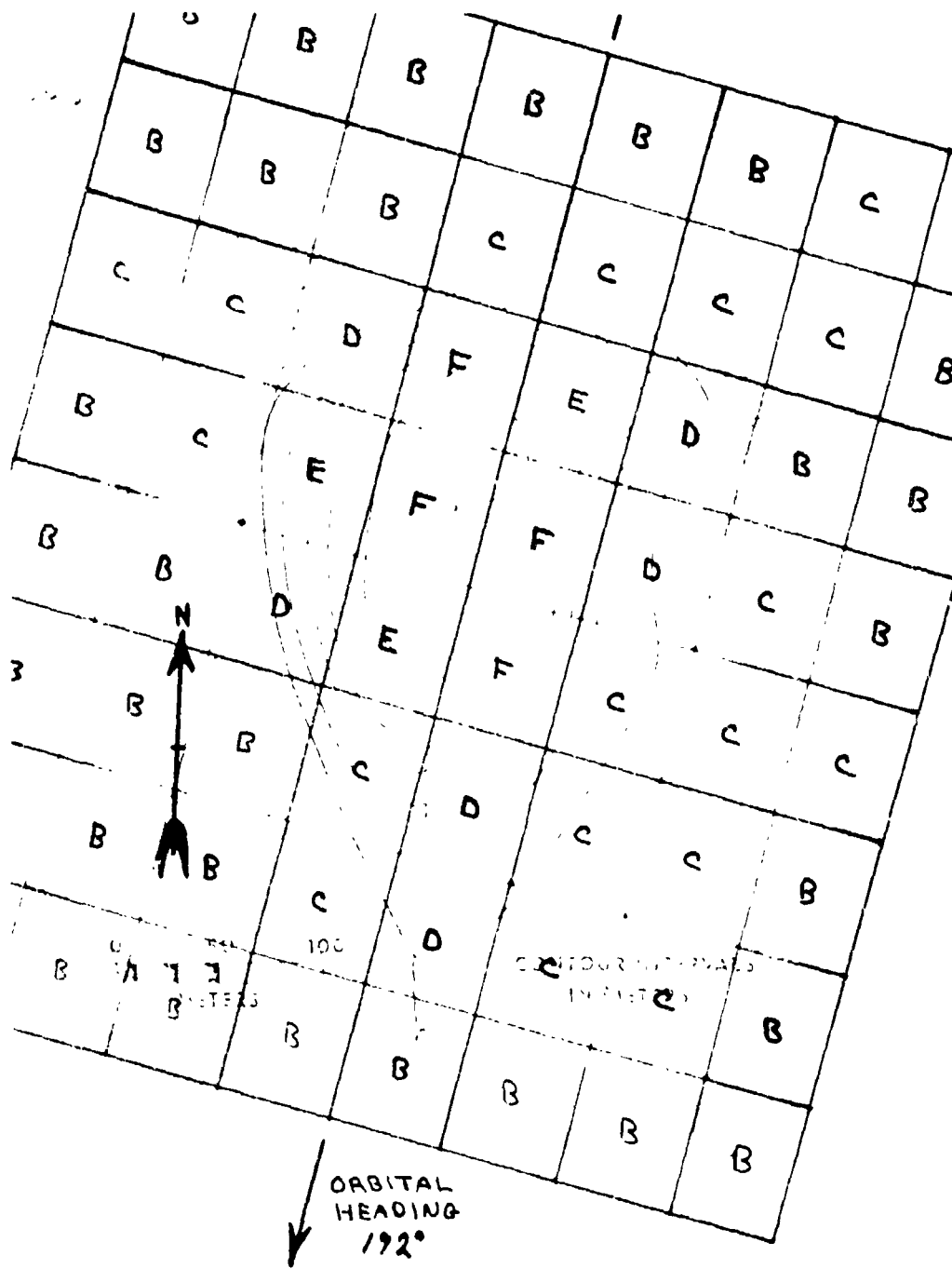


APRIL 7
10 A.M.

APRIL 6
10 A.M.

SUCCESSIVE LANDSAT COMPOSITE IMAGES SHOWING
DEPLETION OF SNOW COVER OVER THE CONTOOCCOOK
RIVER BASIN, N. H.

FIG. 24



SURVEYED MAP OF DUNHAM POND, CONN., COMPARED TO CCT
MSS BAND 7 PRINTOUT

FIG. 25

THE APPLICATION OF REMOTE SENSING TECHNOLOGY TO THE INVENTORY OF
PLAYA LAKES IN THE HIGH PLAINS OF TEXAS

W-18

By A. Wayne Wyatt, Michael L. Ellis, and Ann E. Bell, Texas Water Development Board, Austin
Texas

ABSTRACT

N76-17605

The Texas Water Development Board is planning a project to determine the feasibility of using LANDSAT digital data to inventory the playa lakes of the High Plains region of Texas. The project will use the Detection and Mapping (DAM) package developed at NASA-Johnson Space Center. The economy of the High Plains region is dependent on ground water for irrigation and the Ogallala aquifer is being depleted faster than it is being recharged. The playa lakes represent a potential source of artificial recharge for the aquifer and an inventory is the first step in that direction.

INTRODUCTION

The Texas Water Development Board (TWDB) has been closely associated with the development of an operational remote sensing technique for the detection and mapping of surface water bodies since June, 1973. The procedure was developed by NASA-Johnson Space Center (JSC) in support of the National Program of Inspection of Dams (established by Public Law 92-367). The procedure, which uses LANDSAT digital data, has been continuously refined, with input from the State of Texas on operational aspects, until it represents a significant step toward offering a functional agency a useful monitoring tool.

To further establish the actual utility of an operational remote sensing technique, the TWDB is currently designing a project, centered around the NASA/JSC procedure, to inventory the numerous playa (or shallow ephemeral) lakes of the Texas High Plains region. Prior to discussing the planned technical approach, some background on the Texas High Plains, and the need for an inventory of its playa lakes, is appropriate.

THE TEXAS HIGH PLAINS

The High Plains of Texas is the southernmost extension of the High Plains section of the Great Plains Physiographic Province of North America (Fenneman, 1931). The High Plains section extends from eastern New Mexico across western Texas, Oklahoma, Colorado, Kansas, Wyoming, and Nebraska into southern South Dakota. The High Plains within Texas covers an area of about 35,000 square miles, and is crossed by the Canadian, Red, Brazos, and Colorado Rivers. This broad area, which averages about 300 miles from north to south and about 120 miles from east to west, includes parts or all of 45 counties within the State.

Fertile land and a good climate make the Texas High Plains one of the leading agricultural production areas in the nation with a total farm income of over \$3 billion annually (Swann, 1974). Leading crops produced in the region are cotton, grain sorghum, wheat, soybeans, castor beans, corn, sugar beets, and vegetables. Numerous supporting agribusinesses also make significant contributions to the total income of the region.

Physical Features

The High Plains or "Llano Estacado," as named by the early Spanish explorers, exhibits very little relief. The surface is essentially flat, sloping eastward to a boundary which in most places, is sharply defined by a prominent caprock escarpment ranging upward to

several hundred feet high. The surface is characterized by thousands of small shallow depressions commonly referred to as playas or playa lakes, several large lakes, and small stream valleys. The average elevation of the High Plains is over 3,000 feet above sea level.

The climate of the High Plains is semi-arid. Average annual precipitation ranges from about 12 inches in the southwestern part of the High Plains to about 20 inches in the northwestern part of the High Plains to about 22 inches in the northeastern Panhandle. Much of the annual precipitation is local rather than regional in nature, and a large percentage of the annual total occurs within short periods of time, particularly during the growing season (April through September) when, on the average, about 70 percent of the annual precipitation falls. The average evaporation rate of about 80 inches per year and an average wind velocity of about 12 mph (miles per hour) is characteristic of this climate.

Water Resources of the Region

Ground water, produced from the Ogallala Formation, is extremely important to the economy of the High Plains inasmuch as most of the agricultural crops grown in the region are irrigated with the ground water to supplement the limited rainfall. More than 65 percent of the total irrigated acreage in Texas is located in the High Plains. Virtually all of the municipal, industrial, irrigation water supply is obtained from water stored in the Ogallala Formation.

Annual water-level measurements, made in hundreds of selected water wells throughout the High Plains show that the ground-water supply in the Ogallala Aquifer is being depleted. This aquifer is thought to have contained as much as 600 million acre-feet of water before large-scale irrigation began in the 1930's and 1940's. Today, the more than 70,000 irrigation wells which dot the region are believed to produce 5 to 6 million acre-feet of water annually. During the past three decades, the withdrawal of ground water has greatly exceeded the natural recharge to the aquifer.

Results of a recent computer evaluation and projection model developed by the Texas Water Development Board indicate that there are currently about 340 million acre-feet of recoverable ground water in storage in the area underlain by the Ogallala Formation. By the year 2020, this volume of ground water in storage may decrease to about 126 million acre-feet.

Saturated thickness contour plots produced by the model reveal that there is a very uneven distribution of this ground water resource in the 45 county study area. The uneven distribution is largely a result of the irregular configuration of the older beds on which the Ogallala was deposited. For this reason the formation is very thin in some areas (less than 100 feet) and very thick in others (more than 900 feet). Often these contrasts occur in relatively short distances.

The thin sections of the Ogallala provide limited storage capacity for water; therefore, intensive irrigation development and use of ground water from these limited resource areas have resulted in serious depletion of the aquifer in some localized areas. In contrast, other areas with very thick sections having large storage capacity, have been fully developed and have experienced high water use, yet still have adequate ground water resources to support irrigation for some decades to come. Use of the model revealed that the majority of the High Plains area falls between these two extremes. In addition to this important ground water resource, the playa lakes serve as the main surface water resource. In fact, if the playa lakes did not exist on the High Plains of Texas to serve as storage basins for rainfall runoff water, there probably would never have been large volumes of underground water stored in the water bearing formations of the area (Wyatt, 1966). Runoff water accumulated in these small undrained depressions is the main surface water supply available to the High Plains farmer for irrigation. These depressions, which influence the otherwise relatively smooth, flat contours of the Ogallala Formation, may range in size from very small (less than one acre) to more than 250 acres of surface area and may be from only a few inches deep to several feet in depth. Nine hundred to 1,000 depressions per county (an average of about 900 square miles) have been counted in previous studies (Reeves and Parry, 1967).

Most of the lakes contain water only when filled by surface runoff, and are normally dry many months of the year. The drainage area of the playa lakes may range from a few acres to more than 50 square miles. If water is allowed to remain in these lakes, evaporation accounts for great losses. During the summer when 75 percent of the rain falls, 85 percent of the total evaporation occurs. According to Jim Valliant (1975) of the Texas Agricultural Experiment Station, a 100-acre playa lake can lose an average of 600 gallons every minute during July. Therefore water in the shallow lakes could only be expected to remain for a few days. Some of the larger and deeper depressions may support lakes during a series of wet years, but dry up during a series of dry years. These larger playas are often called "alkali" or "saline lakes," because the water has a high mineral content as a result of the concentration of the salts by evaporation. The High Plains region may be divided into sub-areas on the basis of soil differences. The northern area, essentially that north of Bailey, Lamb, Lubbock, and Garza Counties, has primarily fine-textured soils. The southern area has primarily medium-textured soils with the southwestern portion having some coarse-textured soils. Generally the fine-textured soils area has a greater number of large lakes, and the lakes have larger volumes per unit surface size than lakes of the medium-textured soils area (Grubb and Parks, 1968). Lakes located in the fine-textured soils area, account for a large portion of the area's total storage capacity.

Geologic Origin of Playas

There are several theories as to the origin of the playa lakes formed on the Ogallala Formation, but the one that is generally accepted involves three factors. The Ogallala, derived from the erosion of the Rocky Mountains to the west, was deposited in the area during Pliocene time as a heterogeneous alluvial layer which resulted in differential settling. During the wet periods of the Pleistocene, water collected in low places and percolated downward, removing the soluble calcareous cement of the formation and causing slumping. During the succeeding dry periods, these depressions were eroded by the action of the wind to form the playas we see today. The remnants of transverse dunes which surround many of the larger playa lakes, and the vast amounts of sands and silts stretching as far as 5 to 6 miles from the playas serve to support this theory (Reeves, 1966).

The shapes of the present playa depressions indicate their origin and age (Reeves and Parry, 1967). Recent playas have a circular shape, but the older ones are subcircular to elliptical in shape because they have been altered by end-current erosion, during the short, intermittent wet periods following the arid intervals.

The Need for an Inventory

To the person flying over the High Plains, playas filled by runoff from recent rains, may be a beautiful sight to behold. The sunlight glistening off the surface of the many lakes dotting the landscape gives the appearance of jewels on the land. Perhaps they are jewels in disguise to the semi-arid High Plains agricultural enterprises, since runoff water is collected in the many playas and retained in the region rather than running off to another part of the State or Nation through well defined drainage channels (Bell and Sechrist, 1970).

In view of the fact that the economy of the region is based largely on irrigated agriculture supplied by water mined from the Ogallala, it would seem prudent to begin utilizing some of the surface water found in the playa lakes which have in the past been ill used.

In an effort to reduce the rate of evaporation, many farmers are attempting to modify the shape of these flat shallow lakes. By concentrating the storage of water in a small portion of the lake, an equal volume of water can be stored in a smaller area thereby allowing the remaining portion of the lake area to be farmed as well as reducing evaporation. This means more usable water with which to irrigate. The object of playa modification is to maintain the storage capacity of the playa while significantly reducing the surface area.

Very little is known regarding the quantity of water that annually collects in the playa lake basins though it is thought that possibly two to three million acre-feet may be a

reasonable estimate. Certainly, of the water that collects on the playas, some evaporates, some, infiltrates, and some is being utilized for irrigation.

Past studies show that 15 to 57 percent of the playa water percolates back underground (Valliant, 1975). Unfortunately, the 57 percent occurs only in about 1/3 of the area. This area is in the southern part where the coarse-textured soils exist and where there are small lakes. The 15 percent occurs in the northern two-thirds of the High Plains area where the lakes are larger and soils tighter.

Since a significant portion of the precipitation on the High Plains is collected in the playas, there is a potential to artificially recharge the Ogallala from these shallow depressions. To determine the feasibility of such a project, there is a need for a detailed inventory of the playas including such information as the total number, volume of water stored, and their spatial and temporal distribution.

DESIGN CRITERIA

An important point that must be emphasized before continuing is that the project described herein has not yet been fully implemented or evaluated, but will be in the near future. A second point is that it is not the purpose of this paper to present in detail the methodology of the DAM package, but to discuss an operational use of the system. For a technical discussion of the DAM package, the reader is referred to the numerous documents published by NASA/JSC on the subject which are listed in the references.

The overall goal of the Playa Lake Monitoring System (PLMS) is to demonstrate the feasibility of a functional state agency applying remote sensing technology toward the solution of a real-world problem. The specific goal is to provide, on a demand or repetitious basis, statistics on the number and sizes of the playa lakes in a six county test area¹, and to archive the geographical locations of these lakes for future comparisons.

As was noted in the introduction, this project will center around a procedure developed at NASA/JSC, known as the Detection and Mapping (DAM) package. This procedure offers numerous features which make it a viable technique to solve both the overall and specific goals of the proposed project. The following features of the package are desirable from a functional agency's viewpoint:

1. A documented, cook-book approach which can be executed by persons not familiar with either remote sensing or computers is provided.
2. The only physical requirements of the system are a general purpose digital computer and a set of easily obtainable maps and graphic tools - no expensive special purpose hardware.
3. The final product of the system (i.e., map overlays) is registered very accurately (currently +/- 300 meters or better) to the earth's surface. The map overlays may be at any scale and may be windowed to cover any selected area (even if it crosses CCT boundaries).
4. The procedure is very cost effective (approximately \$1,000-\$1,200 per 10,000 square miles of coverage²).

¹The six counties in the test area are Lubbock, Castor, Hale, Swisher, Lamb, and Hockley.

²This figure was developed by the Seattle District Corps of Engineers after extensive use of the package via the TWDB Computation Center.

Because of these features, the DAM package is ideally suited to assist the TWDB in monitoring the playa lakes on a continuing basis.

METHODOLOGY

The Playa Lake Monitoring System may be divided into a simple set of procedural steps which are discussed next. These steps will be initiated when it is determined that, because meteorological or other conditions warrant, it is time to take a 'look' at the playa lakes in the study region. Once at least two inventories (an inventory shall encompass a limited time frame) have been produced and archived as polygons in the TWDB's Geographic Information System (GIS)³, this information may be retrieved, combined, and analyzed at any time by existing software.

Data Acquisition

A standing order will be placed with the EROS Data Center in Sioux Falls, South Dakota for LANDSAT 9 x 9 positive transparencies in bands 5 and 7 for the study area (with a maximum cloud constraint of 10%). This imagery will be placed on file and be available to assist data selection when desired. When it is deemed appropriate to prepare an inventory, the imagery file can be checked for candidate coverage. The imagery will be indexed by geographic coverage, date, and cloud cover percent. The object, then, will be to select a set of LANDSAT scenes which (1) are virtually cloud free (in the Texas High Plains this is not a constraining factor); (2) completely cover the area of interest; and (3) are all taken reasonably soon after the period of interest⁴.

Once the desired scenes are determined, an order for the LANDSAT digital computer compatible tapes (CCT's) for these scenes will be sent to the EROS Data Center. At this point, one serious drawback occurs and that is the time that must elapse prior to the CCT's being received at the TWDB. This matter is complicated by the fact that there is a considerable delay from the image date until the standing orders are sent out also. These problems must be accepted for the time being, however, in hopes that projects such as this will help justify more timely dissemination of remotely sensed data in the future. The following steps assume the existence of the CCT's at the TWDB.

Control Point Establishment

To be able to produce output in a real-world coordinate system, the DAM package requires a set of at least six (6) control points per scene where the coordinates for each point are known in both the scanner-oriented system and the real-world system. The major effort in the control point establishment will have to be performed only for the first inventory. After that, very simple procedures can be followed to determine the new scanner-oriented coordinates (the real-world coordinates will remain the same as long as a control point is valid - the validity of control points will need to be checked occasionally). A computer program is run which computes the transformation coefficients between the two coordinate systems after removing scanner geometric distortions. Once the control networks for each scene in the set is established and adjusted via a computer terminal, this step is complete.

³The GIS is a set of computer tools to capture, refine, store, and analyze the informational and spatial content of map and map-related data.

⁴The period of interest may be a time of high or low rainfall depending on which aspect of the playas is being studied.

Classification

The next step is to run a computer program (all programs run on the TWDB's UNIVAC 1106 System) which accepts as input the transformation coefficients from the previous step and the digital CCT's for the scene and classifies each pixel (picture element) as water or non-water. The classification process is a very efficient two dimensional linear discriminate function which requires a small amount of CPU time, and almost no human intervention. The output files for each scene are saved for the next step.

Eliminate Overlapping Data

If the data set contains more than one scene, there will, in all likelihood, be some duplicate (and possibly triplicate) data points or pixels. This condition occurs because of the overlap between adjacent scenes, and must be eliminated prior to further processing.

To accomplish this, a computer program will be developed by the TWDB which will merge all of the scenes in the set into one spatially continuous file based on the real-world coordinates now inherent in all of the data. Since the individual scenes in the set will be from at least slightly differing times, the classification of the same area may be different between scenes (because of the dynamic nature of the target this may often be the case).

To provide flexibility in handling overlapping data, the program will perform either an AND or an OR on overlapping pixels to determine the resulting state. The AND option will cause the resulting pixel to be water only if all overlapping pixels are water. The OR option will cause the resulting pixel to be water if any of the overlapping pixels are water.

Boundary Extraction

The next and possibly the most difficult step is to extract a polygonal boundary for each detected water body. The reason for this approach is that there already exists a body of software at the TWDB to store, retrieve, and analyze data such as geographical polygons⁵. Therefore, once the boundaries of the playas are extracted from the DAM System files in the form of strings of geographic coordinates, existing software can be used to achieve the specific goals of the system (i.e., to produce certain statistics and to archive the data for future comparison).

Any boundary tracing algorithm is complicated by the border pixel problem (i.e., (1) the border pixels of any target are probably a combination of the target and its neighbor, or (2) the border pixels neighbor contains a small portion of the target, though not enough to cause it to classify as the target). To minimize the effect this problem has on surface acreage calculations, the boundary tracing algorithm employed must tend to average this effect out over a large number of cases. Because total surface acreage estimates for fairly large geographic areas are the desired product of this project, as opposed to individual playa sizes, this approach should be quite suitable.

A computer program will be developed to accept as input, the spatially continuous file created in the previous step and a percentage value for border pixel inclusion. The boundary will be traced around the perimeter of lakes represented by at least three (3) contiguous pixels⁶ and then shrunk by a factor which will tend to leave only the percentage of

⁵This refers to the Geographic Information System (GIS) previously mentioned.

⁶Three contiguous pixels represent a lake of approximately ten (10) surface acres and this is the smallest target that can be detected with suitable accuracy (Moore, 1973).

a border pixel as stated by the input parameter. The border pixel inclusion parameter can then be manipulated and the results compared with ground truth data until a relatively suitable value is obtained.

Final Products

With the locations of the playa lakes archived in GIS files (by date of inventory), the final step is to generate the required statistics and maps. The statistics of interest are the total number of the detected lakes, the total surface acreage, and the average surface acreage. Since the GIS already contains items such as county boundaries and aquifer recharge zones, the statistics will be computed for the entire study area and then by county and any other subdivision deemed important.

Maps can be generated at any scale and with any projection depicting the playa lakes and other features stored in the GIS (e.g., river traces, county boundaries, and soil type zones) on a pen plotter. Since the data from all previous inventories will also be archived, temporal changes can be detected either visually (by maps) or analytically (by mathematically combining the data).

CONCLUSIONS

The TWDB is planning to devote significant resources to ascertain the feasibility of using LANDSAT digital data in an operational and economically justifiable project. The successful completion of the project would be the first step in determining a valuable source of water for the High Plains region of Texas. The project will also determine the usefulness of archiving the results of remote sensing classifications by extracting field boundaries and storing them in an operational system. The detection and Mapping package is ideally suited to assist the project due to its many operational characteristics.

REFERENCES

- Anderson, A.C., 1973, Development of a Two-Channel Linear Discriminant Function for Detecting And Identifying Surface Water Using ERTS-1 Data: National Aeronautics and Space Administration, Lyndon B. Johnson Space Center, Houston, Texas.
- Bell, A.E., and Sechrist, A.W., 1970, Playas - Southern High Plains of Texas: Proc., Playa Lake Symposium, ICASALS, Texas Tech University, Lubbock, Oct. 1970, 6
- Cronin, J.G., 1969, Ground Water in the Ogallala Formation in the Southern High Plains of Texas and New Mexico: Hydrologic Investigations Atlas HA-330, U. S. Geological Survey, 9 p.
- Fenneman, N.M., 1931, Physiography of the Western United States: New York, McGraw-Hill Book Company., 534 p.
- Frye, J.C., 1970, The Ogallala Formation - a review: Proc., Ogallala Aquifer Symposium, Texas Tech Univ., Lubbock, 1970, p. 5-14.
- Grubb, H.W., and Parks, D.L., 1968, Multipurpose Benefits and Costs of Modifying Playa Lakes of the Texas High Plains: Texas Tech Univ., Dept. of Agric. Econ., ICASALS, Special Rept. 6, 66 p.
- Hauser, V.L., 1966, Hydrology, Conservation, and Management of Runoff Water in Playas on the Southern High Plains: Agricultural Research Serv., U. S. Dept. of Agriculture, Conserv. Res. Rept. 8, 26 p.
- Minter, T.C., 1973, Evaluation of Computer-Aided Procedure for Detecting Surface Water: National Aeronautics and Space Administration, Lyndon B. Johnson Space Center, Houston, Texas.
- Moore, B.H., 1973, Development of a Computer-Aided Procedure for the National Inspection of Dams: National Aeronautics and Space Administration, Lyndon B. Johnson Space Center, Houston, Texas.
- Reeves, C.C., Jr., 1966, Pluvial Lake Basins of West Texas: Journ. Geology, vol. 74, p. 269-291.
- Reeves, C.C., Jr., and Parry, W.T., 1967, Geology of Water Importation: The Cross Section High Plains Underground Water Conservation District No. 1, Lubbock, vol. 14, no. 3, August 1967.
- Schlosser, E. H., Moore, B. H., et.al., 1973, Procedures Manual for Detection and Location of Surface Water Using ERTS-1 Multispectral Scanner Data: National Aeronautics and Space Administration, Johnson Space Center, Houston, Texas.
- Schwiesow, W. F., 1965, Playa Lake Use and Modification in the High Plains: Texas Water Development Board Rept. 10, 17 p.
- Swann, T., 1974, Texas High Plains Facts: Lubbock, Water Inc., 10 p.
- Valliant, J., 1975, Opportunities for Artificial Recharge: Texas Water Resources, vol. 1, no. 5, p. 1-3.
- Wyatt, A. W., 1966, Thinking About Pumping Water From Your Playa Lake?: High Plains Underground Water Conservation District No. 1, Lubbock, 8 p.

REMOTE SENSING APPLICATIONS
IN WATER RESOURCES MANAGEMENT
BY THE CALIFORNIA DEPARTMENT OF
WATER RESOURCES

W-19

By Barry Brown, California Department of
Water Resources, Sacramento, California

ABSTRACT

N76-17606

For nearly 30 years the California Department of Water Resources has been using remote sensing techniques in all phases of planning, constructing and operating various features of the California Water Plan. Most of this experience has been with low altitude aerial photography. Recently the Department has initiated a program to evaluate possible applications of imagery from high altitude aircraft and satellite sensors. Results from seven applications studies comparing the costs of using high altitude imagery for various purposes to the costs of using conventional data sources, reveal the high altitude imagery to be more cost effective in six cases and equal to conventional data sources in one case. These results also reveal that the imagery provides a level of quality not generally achievable with uncorrected conventional imagery. Although satellite application studies are not yet complete, preliminary results indicate that some definite possibilities exist for employing satellite imagery on an operational basis within the next few years.

INTRODUCTION

The Department of Water Resources has long recognized the value of remote sensing for water resource development and management. For nearly 3 decades it has been using low altitude aircraft imagery of various types for inventorying and monitoring land features and water supply and use conditions over large areas of the state. Data obtained has been used in evaluating regional water use trends and in periodically reassessing the need for, location, size and uses of proposed water facilities.

While most of the conventional remote sensing applications that we have found are not new, what makes the Department's experience unique is the diversity of applications within a single agency. This diversity has come about, first, because of the magnitude of planning for statewide distribution of water brought about by the State's size and maldistribution of waters. Secondly, many remote sensing applications have resulted from special problems created by climate, topography and the fact that water resources management involves consideration of water resources underground, on the surface and in the atmosphere. A third factor that has involved the Department in a greater variety of remote sensing activities than most other agencies is the fact that this nearly 30-year period of involvement has encompassed planning, constructing, and operating phases of the California Water Plan.

In more recent times, a major factor that has influenced our remote sensing activities has been the need to protect and enhance our environment. Water and related land use planning is considered by many as the key to this type of function. Planning for water management is seen as particularly important because of (1) the direct impact which water development projects have upon the environment, and, (2) the indirect impact of such projects upon the social and economic well being of our society. The Department recognizes its responsibility to minimize adverse environmental impacts and is seeking new ways of evaluating environmental factors.

While conventional remote sensing and other data gathering techniques have proved adequate for most purposes, we have recognized for many years a number of shortcomings in the ability of the techniques to rapidly inventory or monitor land use and cover conditions over large areas. Because we believe that high altitude and satellite imagery in many cases will permit us to do this, we have undertaken a number of projects to explore their potential.

SCOPE

The remote sensing applications studies undertaken by the Department are summarized in Table 1. The table distinguishes between those applications that have been subjected to a qualitative evaluation and those that have received a quantitative assessment. In the eight cases involving the use of high altitude imagery exclusively, the quantitative evaluation has consisted of a cost effectiveness comparison with conventional imagery and a discussion of quality factors. Seven of the eight studies and the satellite studies are reported on in this paper.

The satellite studies have just been initiated and no significant results are yet available. The discussion in the text briefly describes test objectives and plans for implementing them.

APPLICATIONS STUDIES

In spite of the general recognition by Department investigators that high altitude and satellite imagery are potentially valuable planning aids, the process of getting them involved in evaluation studies has been a slow one. This hesitancy has been partly attributable to a basic reluctance to take on something new when the old techniques have worked well enough. However, probably a bigger factor has been the lack of special funding for application studies, making it necessary to carry out the studies in conjunction with budgeted work. Program managers felt that investigative and reporting requirements would be more demanding than their programs could support.

To overcome these problems, study personnel were asked to report only on the apparent advantages the imagery appeared to offer over conventional data gathering techniques. This approach placed few demands on the study participants and was successful in stimulating interest in the program.

The subjective evaluation comments by study personnel were useful in that they clearly revealed many potential applications and provided ample

justification for a second level of analysis--one aimed at comparing costs of data acquired from high altitude or satellite imagery to costs of data acquired from conventional data sources.

Some preliminary results of such cost effectiveness comparisons are discussed in the following sections. A third level of analysis (benefit-cost) may be attempted in the future for flood or flood related problems where imagery benefits can be clearly identified.

COST EFFECTIVENESS COMPARISONS

The cost effectiveness comparisons were carried out by a team of department economists who interviewed study participants. The informal subjective comments from the level one analysis were used as the starting point for these interviews. All data and important comments generated by the interviews were systematically recorded, evaluated, and where necessary corrected. The corrected data were then used to develop cost ratios. The ratios for the seven applications reported on are summarized in Table 2.

Cost data for each application are summarized in two tables, one for high altitude and associated data and one for conventional imagery and associated data. Nonquantifiable aspects of the applications are summarized in the text. Those costs associated with the use of high altitude imagery and conventional data sources are presented in Tables 3 and 4, respectively.

In making cost comparisons all costs were considered except flight costs of the high altitude aircraft. It was assumed that these costs would continue to be borne by federal agencies and that imagery obtained would continue to be available at current rates.

No costs were incurred in training study personnel; the various disciplines involved were adequately trained in the basics of imagery interpretation.

HIGH ALTITUDE IMAGERY APPLICATIONS

Detecting Possible Water Bearing Areas

Introduction.- This application compared the costs of using U-2 versus available conventional imagery in locating geologic indicators of possible water bearing areas (primarily lineaments) in a water deficit area of approximately 400 square miles surrounding the Sierra Nevada foothill community of Plymouth. The city requested the search to help decide if a study should be made of the feasibility of developing local ground water to alleviate a water shortage problem.

Both kinds of imagery revealed the presence of unmapped lineaments in the area which could be due to fractures or faults which might be water bearing areas. Although these results were sufficient to justify a feasibility study, the city decided not to conduct the study for other reasons.

Procedure.- For this study 9" x 9" 1:130,000 scale color infrared (CIR) positive transparencies obtained by U-2 aircraft were used. The conventional photos used were standard panchromatic 9" x 9" 1:20,000 scale contact photos. Because no funds were available for field work, the application study was carried out by imagery interpretation alone.

The focus of the study on lineaments as indicators of water bearing areas severely limited the usefulness of the low elevation black and white contact photos. The small coverage and great detail made it virtually impossible to detect lineaments on single photos. To overcome this problem, the contact prints were mosaicked together into two separate panels with each covering approximately the same area as a U-2 photo. The mosaics were then photographically reduced to U-2 scale, for the study.

Data processing was not included as a cost since it consisted only of marking unmapped lineaments on the photos and transferring to the base maps, a process that required but a few minutes.

Cost effectiveness comparison.- The detailed U-2 costs are presented in Table 3a and those associated with conventional imagery are found in Table 4a. These data are summarized below.

<u>Cost Comparison (dollars)</u>		
U-2 CIR	Conventional Panchromatic	
Acquiring Data Sources	44	873
-Data Collection/Interpretation	29	29
-Data Processing	--	--
Totals	73	903
Cost Ratio	12.3 : 1.0	

Discussion.- Unmapped lineaments could be detected on both photo formats but were interpreted with less confidence on the mosaics because of confusion created by photo match lines. The mosaic also was found to be less useful than the CIR U-2 photos in revealing vegetative anomalies associated with lineaments. This was partly due to the sharper ground-vegetation contrasts that existed on the CIR film. It also probably was partly due to the poorer resolution of the mosaic in going through two more reproduction steps than the U-2 imagery and in being on a poorer resolving medium (paper) than the CIR film.

The very large relative cost savings realized in using the U-2 photos resulted from not having to prepare photo mosaics.

Urban Boundary Delineation

Introduction.- The costs of mapping approximately 4,800 square miles of urban areas 10 acres in size or larger in the cities of Los Angeles, Dan Diego, Santa Barbara, and Ventura and in the Upper Santa

Area drainage using U-2 imagery were compared to the costs of doing the mapping with specially flown conventional imagery. The mapping of urban areas was done as a preliminary step in mapping prime agricultural lands adjacent to urban centers.

Procedure. - U-2 9" x 9" 1:130,000 scale CIR transparencies were used in the study. In the absence of complete or current available imagery, a decision was made to fly the area with 35 mm color film.

The U-2 transparencies were vertically projected onto 1:62,500 scale base maps and urban areas delineated on them. The 35 mm color slides were projected onto a screen and urban areas visually translated to the 1:62,500 base maps.

Processing of the data was not a cost factor since the maps showing the urban areas were all that the agency requesting the information wanted.

Cost effectiveness comparison. - Detailed costs are presented in Table 3b for the U-2 imagery and in Table 4b for the conventional imagery. These data are summarized below.

- Acquiring Data Sources
- Data Collection/Interpretation
- Data Processing

Totals

Cost Ratio

Cost Comparison (dollars)	
U-2 CIR	Conventional Color
1,472	5,816
3,335	3,640
..	..
4,807	9,456
2.0 : 1.0	

Discussion. - The two-fold greater cost associated with using 35mm color transparencies was due primarily to the fact that it took a week to fly the area and a week to index the slides. Total man-hours for photographer, navigator, and personnel to index the photos amounted to 128 hours alone. Rental costs for airplane and pilot were the equivalent of approximately 172 additional man hours.

In interpreting the photos it was observed that locating the boundary between contiguous urban and small agricultural areas was accomplished more easily on the U-2 CIR photos than on the color slides. This apparently was due to a greater contrast between the urban and agricultural areas than on 35mm color slides. On the other hand, 35mm photos generally were more useful for delineating urban areas from areas covered by native vegetation.

The comparison of the two film formats also revealed that the U-2 transparencies provided a more uniform scene rendition than the 35mm. The U-2 imagery was flown in less than an hour while the 35mm took a week to fly. As a result considerable variation in sun glare, atmospheric conditions, etc., were noted on the 35mm that were not apparent on the U-2 imagery.

A minor disadvantage noted in using the 35mm photos was the visual translation of urban area boundaries onto the base maps.

Land Use Updating - Coachella/Imperial Valleys

Introduction.- Costs of using U-2 imagery to update broad land use categories over approximately 500 square miles of the Imperial and Coachella Valleys were compared to costs of using available commercial panchromatic photos. The revised land use data were needed for a cooperative local-state-federal study of the Salton Sea and for a comprehensive water quality plan being prepared for the desert basins.

Procedure.- The U-2 imagery used was 1:130,000 scale 9" x 9" CIR positive transparencies. The transparencies were projected onto sepia prints at 1:24,000 scale containing an earlier land use pattern. Changes in urban irrigated and nonirrigated cropland and recreational boundaries were then interpreted and inked on the maps. The available panchromatic photography was 9" x 9" contact prints at a scale of 1:24,000. These photos were evaluated in the same manner as were the U-2 photos.

Both sets of maps were then taken to the field and delineations spot checked and missing data filled in. Sepia prints were obtained from these revised maps and land use acreage values derived by the cutting and weighing technique and the use of a computer.

Cost effectiveness comparison.- Detailed costs associated with using the U-2 and panchromatic photography are presented in Tables 3c and 4c respectively. These data are summarized below.

	Cost Comparison (dollars)	
	U-2 CIR	Conventional Panchromatic
-Acquiring Data Sources	296	262
-Data Collection/Interpretation	1,442	1,802
-Data Processing	721	721
Totals	2,459	2,785
Cost Ratio	1.1 : 1.0	

Discussion.- Both types of imagery were satisfactory for accomplishing the mapping task. The 13% higher cost of using the conventional panchromatic film was due primarily to the additional time required to handle 80 rather than 12 U-2 photos. This cost was partly offset by the higher cost of the CIR U-2 photos.

The mapping done using the small scale U-2 imagery, surprisingly, was as good as or better than that done using the large scale panchromatic photos. Although no attempt was made to quantify the accuracy of the interpreted data, the general observation was that irrigated cropland was more easily and more accurately mapped on the CIR imagery. Urban boundaries could be delineated equally well on both types of imagery.

Land Use Updating - Coastal Los Angeles County

Introduction.- This study was designed to compare costs of using U-2 versus conventional panchromatic photography in updating major land use types within the coastal Los Angeles region, an area of more than 1800 square miles. The information was needed to verify the adequacy of a land use survey by the Los Angeles City Planning Commission, to update their data where necessary, and to split out certain of their categories to bring them into conformance with the Department's classification system.

Procedure.- For this study 1:32,500 scale 9" x 18" CIR U-2 positive transparencies were compared against 1:24,000 scale commercial panchromatic 9" x 9" contact prints. Both sets of photography were projected onto sepia prints, interpreted and field checked in the same manner as described for the desert study (previous section).

Cost effectiveness comparison.- Detailed costs associated with using the U-2 and panchromatic photography are presented in Tables 3d and 4d respectively. These data are summarized below.

-Acquiring Data Sources
 -Data Collection/Interpretation
 -Data Processing

Totals

Cost Ratio

Cost Comparison (dollars)	
U-2 CIR	Conventional Panchromatic
2,433	513
12,164	14,272
10,215	10,215
24,812	25,000
1.0 : 1.0	

Discussion.- Both sets of photos adequately satisfied study mapping requirements. The parity reflected in the cost comparisons is surprising considering that the 1:32,500 scale U-2 photos cost almost five times that of the panchromatic photos. This cost was offset by the time saved in handling 62 percent fewer photographs. The cost ratio does not reflect the fact that the CIR U-2 imagery has greater utility for a variety of mapping purposes than the black and white imagery. As a result, it is expected to become relatively more cost effective with time as other uses are found for it.

Some of the minor disadvantages in using this imagery (which also slightly increase its cost) is in having to cut the roll film into the 9" x 18" images and protect with a clear plastic cover in order to use in an overhead projector. Also the 9" x 18" format created storage problems and resulted in rougher handling and consequently more photo damage than experienced with the contact panchromatic photos.

A mapping task which could not be accomplished as well on the CIR U-2 imagery as on the black and white was the separating of urban areas from areas of native vegetation. This same condition also was observed in the urban boundary study except that color imagery, rather than black and white imagery, provided the greater contrast.

Watershed Characterization

Introduction.- The costs of using U-2 imagery for extracting a variety of resource conditions in the Van Duzen River watershed in the north coastal area of California were compared to the costs of using conventional panchromatic photos for such mapping. The Department, in cooperation with the Planning Department of Humboldt County, undertook an environmental mapping study of over 430 square miles of the watershed as a preliminary step in developing a management plan for the river. Land features of interest were new roads, vegetative types, land uses, river characteristics, structures, etc.

Procedure.- The imagery used in the study was 1:32,500 scale 9" x 18" CIR U-2 transparencies and commercial 1:12,000 panchromatic 9" x 9" contact prints flown for Humboldt County. In addition, 35mm color slides of the upper 60% of the watershed were taken as an aid in interpreting data from both sets of imagery. The U-2 transparencies were projected onto 1:24,000 scale base maps and the various land features delineated on them. The 1:12,000 scale panchromatic photos were similarly projected onto the base maps. The 35 color imagery was projected onto a screen and used to develop signatures for various land features on both photo sets and to help make mapping decisions in complex areas. Approximately two hours of field checking the interpreted data was done for each base map (approximately 6 square miles).

Data processing consisted of preparing from the work maps a complete set of maps for publication.

Cost effectiveness comparison.- Costs associated with using the U-2 and panchromatic photos are detailed in Tables 3e and 4e respectively. These data are summarized below.

Cost Comparison (dollars)		
	U-2 CIR	Conventional Panchromatic
-Acquiring Data Sources	3,348	3,392
Data Collection/Interpretation	1,532	1,981
-Data Processing	290	695
Totals	5,170	6,068
Cost Ratio	1.0 : 1.0	

Discussion.- The 20 percent higher costs associated with the use of panchromatic photos was due almost entirely to the extra time involved in handling 550 photos compared to 30 U-2 photos. Most of this handling time consisted of projector adjustments to normalize photo scale to map scale. Because the study was carried out in an area with much contrasting relief, it was not uncommon to make several adjustments per photo. In using the U-2 photos, seldom was it necessary to make further adjustments after the initial photo-map match.

Also adding to the difficulty of using the contact prints was the considerable image fall-off around the photo edges which reduced the useable area of the photo and further increased handling (interpretation) time. This was not a problem with the U-2 photos where scale appeared uniform and free of distortion throughout.

Another, although minor, advantage of the U-2 imagery became apparent in areas with few landmarks to which the photos could be oriented. The greater areas covered by the U-2 photos provided more opportunities for locating landmarks and for reducing the handling time.

A major disadvantage of the U-2 imagery was the variability in quality. Images varied from washed out to overly saturated and many exhibited light fall-off around the edges. As a result, the 35mm color transparencies had to be used on occasion to help interpret land features.

Except for the 35mm use just discussed, the 35mm color slides generally were not of much value as a supplemental aid to either the U-2 or black and white photos. The severe relief and low altitude of exposure (5,000 feet above mean ground elevation) combined to provide so much image distortion as to make them virtually useless for accurately locating boundaries. Even at twice the altitude, the usefulness of the imagery for this purpose would be questionable. The exception would be the relatively flat areas along the river where such imagery could be used to good advantage.

Waterway Mapping

Introduction. The costs of using U-2 imagery for preparing a map of the Eel River delta in northern California were compared to the costs of using 35mm color photos. The new map was desired by fish and game specialists evaluating wildlife habitat in the area for the Department.

Procedure.- Two 1:32,500 scale 9" x 18" CIR U-2 transparencies were used for the study. In the absence of current conventional photography, 35mm color transparencies were obtained of the area from an elevation of approximately 7,000 feet. The U-2 transparencies were vertically projected onto a 1:24,000 scale USGS quadrangle and changes in the waterways posted to the map. The 35mm slides were horizontally projected onto a wall-mounted base map and changes posted. No field work was required for either technique. Data processing in each case consisted of drafting the corrected map onto a clean base, hand coloring and obtaining photographic reproductions.

Cost effectiveness comparison.- Tables 3f and 4f include the detailed costs of using the U-2 and 35mm imagery, respectively. These data are summarized below.

		Cost Comparison (dollars)	
		U-2 CIR	Conventional 35mm Color
-Acquiring Data Sources		89	890
-Data Collection/Interpretation		285	285
-Data Processing		--	-
	Totals	374	1,175
	Cost Ratio	3.1 : 1.0	

Discussion.- Both film formats proved satisfactory for accomplishing the study purpose. However, the much greater cost of acquiring the 35mm color slides probably would rule out this alternative in most cases.

One of the side benefits noticed in using the U-2 CIR film was its ability to more sharply depict the water-land interface than was possible with the color film. This advantage, while noticeable during the interpretation phase, had no appreciable effect on the accuracy of the finished maps.

Flood Damage Assessment

Introduction. - The costs of using U-2 imagery for mapping flood damage in Butte Basin in the center of the Sacramento Valley were compared to the costs using specially flown commercial panchromatic film. The data was needed in anticipation of flood damage litigation.

Procedure. - The U-2 imagery selected was a single 9" x 18" 1:22,500 scale CIR transparency. The conventional imagery was specially flown 1:24,000 scale panchromatic photos.

In order to delineate flooded or flood damaged areas on the U-2 photo, it was necessary to enlarge it. One half of the photo, which adequately covered the basin, was photographically enlarged to 1:24,000 scale. Delineations were accomplished right on the image without any field checking. The 9" x 9" 1:24,000 scale black and white photos were taken to the field by survey crews and used for locating damaged areas and for recording the damages. The data on the photos were then transferred to a set of 1:24,000 scale base maps.

Cost effectiveness comparison. - The detailed costs of using the U-2 photo are included in Table 3g; Table 4g includes the costs for using the panchromatic film. These data are summarized below.

Cost Comparisons (dollars)		
	U-2 CIR	Conventional Panchromatic
Acquiring Data Sources	143	937
-Data Collection/Interpretation	433	5,688
-Data Processing	--	288
Totals	576	6,913
Cost Ratio	12.0 : 1.0	

Discussion. - Because of the importance of precisely locating flood boundaries for litigation purposes and because timely conventional imagery is usually uncontrolled and not suitable for this purpose, the traditional technique has been to send survey crews out within a couple of days of a flood to survey the boundaries. As the cost figures demonstrate, this is an expensive procedure.

The comparison of field survey results with the results achieved by interpreting the enlarged U-2 image revealed essentially no difference in the boundaries. In fact, boundaries that could not be clearly located on the conventional photos or by the survey crews because of difficult access or other reasons often were visible on the U-2 photos. Some of this capability is due to the greater sensitivity of CIR film to subtle soil moisture and vegetative conditions. However, the greater uniformity and integrity of the U-2 image compared to the 1:24,000 scale photos also appeared to contribute to its greater usefulness.

Although no attempt was made to quantify the accuracy of the two mapping schemes, the results indicate that flood damage mapping on U-2 imagery of the flat Central Valley may be done with sufficient accuracy to eliminate much of the need for field survey data.

Another advantage noted in using the U-2 image was that it provided an instant view of the entire Butte Basin. By contrast, the collective view of the many panchromatic photos covers an elapsed time of about an hour, the time required to fly them. It was felt that this unique capability might prove useful in some rare instance in insuring against confusion as to the sequence of flood events that could result if a significant event were to occur at some unknown time during the photo flight mission. An instant view might not be as likely to raise such questions.

SATELLITE IMAGERY APPLICATIONS

In contrast to the high altitude imagery applications which the Department has been able to evaluate with existing equipment, materials and expertise under on-going programs, the satellite imagery applications of interest to the Department cannot be fully explored with existing resources. For this reason we are relying on the research community to assist us in such studies.

The nature of this research assistance is quite varied including a nonfunded student project, informal and formal cooperative agreements with a number of university researchers, a fully funded NASA project, and a partially funded NASA project involving a private research institute. Only the formal studies are reported here.

Some of the informal cooperative studies have been going on for over three years but the formal studies have just been initiated. The discussions below report on the status of the formal studies and the Department's experience in preparing a photo mosaic.

Irrigated Lands Study

This is a NASA-funded LANDSAT-2 (earth resources satellite) study with the University of California acting as the contractor. The experiment will investigate the feasibility of using LANDSAT-2 imagery for inventorying and monitoring irrigated lands in California. The Remote Sensing Research Program of the University of California, working through the University's Space Sciences Laboratory and in cooperation with the Department of Water Resources, will investigate the extent to which the desired data can be extracted from the LANDSAT-2 imagery, supplemented with supporting aircraft and ground information.

The primary object of the research is the development of an operationally feasible process whereby LANDSAT-2 satellite imagery can be used to provide periodic irrigated land acreage statistics for the whole state and for individual counties. In order to fulfill this objective, the investigation will necessarily involve the development of efficient techniques for: (1) interpreting sequential imagery covering an area of over 10 million acres, (2) sampling this area through the use of satellite

imagery, supporting aerial photography, and ground data, (3) converting the interpretation results into useable statistics, and (4) evaluating the end product in terms of the costs and/or resources required for its acquisition, and also in terms of its accuracy and timeliness.

The project is still in its formulative stage. Several meetings have been held with the research personnel to design the sampling network, develop processing techniques, assign ground data collection responsibilities, etc.

Snow Cover Observations

This is a fully funded NASA investigation with the Department acting as the contractor. It is a 5-year study designed to develop an operational program for incorporating satellite observations of snow cover into the hydrologic forecasting program of the Department.

Imagery from two satellite systems (LANDSAT and NOAA*) and U-2 overflights will be combined with ground data during the data reduction and analysis phases. This program also is in its early stages with no results yet to report.

Water Quality Study

This is an 18-month NASA study involving the Department, the State Water Resources Control Board and the Stanford Research Institute (SRI), a private corporation. The Department is the contractor.

The objective of this investigation is to determine, by systematic analysis, the choices of aerial observation systems and surveillance altitudes which are most likely to detect distinct classes of water quality problems. Water quality data and imagery obtained from LANDSAT and high altitude aircraft will be compared with new ground truth and existing data to determine the relative value of information collected by each mode of remotely sensed data. The investigation will involve two sites, the San Francisco Bay-Delta area and the Lake Tahoe area.

Most of the analysis work will be done by the Stanford Research Institute using a complex of electronic devices collectively termed an "Electronic Satellite Image Analysis Console". Department personnel will work closely with SRI personnel during the analysis phase. The Department and the State Water Resources Control Board will share equally in collecting the ground data needed by SRI.

*NOAA - A weather satellite used by the National Oceanic and Atmospheric Administration.

Color Infrared Photo Mosaic of California

Although not really a research effort, the preparation of a CIR photo mosaic of the State was our first real involvement in using satellite imagery. The Department prepared the mosaic for educational and display purposes. It has received wide distribution both inside and outside of the Department and has proved to be a very effective device for stimulating interest in remote sensing capabilities.

The technique used for enhancing the 32 LANDSAT-1 images that made up the mosaic was to triple-expose bands 4, 5, and 7 (one at a time with its appropriate colored filter) on a single frame of colored film. Positive 9.5" x 9.5" transparencies were selected for the project and photographed with an 8" x 10" copy camera on a 1:1 basis. Densitometer readings of the gray scale of each image were taken to set exposure.

This procedure produced color prints which could be mosaicked together without any additional adjustments. No problems were experienced in matching the prints to a 1:1,000,000 scale state base map.

The major problem encountered was an inability to produce a true gray scale on the color print. The gray scale was desired so that continuity of color hue could be maintained on images of a particular orbit. This problem was due to a number of factors but primarily to inexperience and will be resolved with time.

CONCLUSIONS

The California Department of Water Resources has been and plans to remain an active participant in the investigation of remote sensing capabilities. Our initial interest in the technology of "new remote sensing" naturally developed from an implied organizational dictum to continually seek new ways of acquiring more, as well as better data, preferably at no increase in cost and hopefully at less. This initial interest was heightened by the gradual realization on our part that high altitude and space imagery also might permit us to acquire certain kinds of data which we have had a long-time interest in but which, up to now, we have considered either impossible or impracticable to collect.

Our vicarious involvement in this new art-science has now given way to active involvement. With some experience now behind us in testing remote sensing capabilities and in reviewing the work of others, we are beginning to replace our uncertainty about this new planning tool with knowledge of some positive benefits.

One of these benefits, as shown by our U-2 cost effectiveness comparisons reported here, is the substantial savings that could be immediately realized in many of our programs if U-2 imagery were available on a timely, operational basis. Also, preliminary results of cost effectiveness studies by personnel of the Remote Sensing Laboratory, University of California, Berkeley comparing satellite to conventional data sources (one of the informal cooperative studies) are showing some dramatic savings in acquiring water supply information.

In the area of data quality improvement, our U-2 application studies revealed many possibilities for improving data quality without any sacrifice of data quantity or without increases in costs. In future studies we will be attempting to quantify quality aspects, particularly those relating to accuracy.

Because we recognize that demonstrated remote sensing applications cannot be implemented or sustained with experimental remote sensing platforms, we have no intention of abandoning the conventional remote sensing techniques that have worked so well for us in the past. However, where research results clearly indicate that cost-effective remote sensing applications exist which can achieve superior results or provide needed but previously unavailable data, we will continue to help achieve the technology transfer of such applications and to support the establishment of operational remote sensing platforms to make them operational realities.

TABLE 1 - CALIFORNIA DEPARTMENT OF WATER RESOURCES
REMOTE SENSING APPLICATIONS STUDIES

Application	imagery Evaluated				Nature of Evaluation	
	U-2	LANDSAT-1	LANDSAT-2	NOAA - 2	Qualitative	Quantitative ^a
<u>Water Resources Planning and Operations Applications</u>						
1. Geologic studies						
a. Regional geologic assessment	X				X	
b. Detecting possible water bearing areas	X				X	X
2. Urban boundary delineation	X				X	X
3. Land use updating (2 studies)	X				X	X
4. River studies						
a. Watershed characterization	X				X	X
b. Waterway mapping	X				X	X
c. Sand and gravel bar mapping	X				X	
5. Wildlife habitat inventorying	X				X	
6. Map substitute	X				X	
7. Snow cover assessment ^b	X	X		X		X
8. Irrigated lands mapping (2 studies) ^c	X		X			X
9. Algal detection and mapping	X				X	
10. Water quality monitoring ^d	X		X			X
11. Displays	X	X			X	
<u>Disaster Assessment Applications</u>						
1. Litigations	X				X	
2. Flood damage assessment	X				X	X

^a Cost effectiveness studies only

^b Contract with NASA through Goddard Space Flight Center

^c One of the studies is cooperative agreement with Space Sciences Laboratory, University of California, Berkeley

^d Contract with NASA through Goddard Space Flight Center

TABLE 2 - SUMMARY OF COST EFFECTIVENESS COMPARISONS

Application	Data Costs (dollars)		Cost Ratios
	From High Altitude Imagery	From Conventional Data Sources	
Detecting Possible Water Bearing Areas	73	903	12.3/1.0
Urban Boundary Delineation	4,807	9,456	2.0/1.0
Land Use Updating	2,459	2,785	1.1/1.0
Land Use Updating	24,812	25,000	1.0/1.0
Watershed Characterization	5,170	6,068	1.2/1.0
Irrigated Lands Mapping	9,101	12,380	1.4/1.0
Waterway Mapping	374	1,175	3.1/1.0
Flood Damage Assessment	576	6,913	12.0/1.0

TABLE 3a - COSTS ASSOCIATED WITH THE
USE OF HIGH ALTITUDE IMAGERY *

A. Acquiring High Altitude Imagery and Supporting Data Sources

	Quantity	Unit Cost <u>a</u>	Sub-Total	Total <u>b</u>
1. High altitude photos				
a. Purchase costs	2	18.53	37	37
b. Special processing costs				
2. Low altitude support photos - existing				
a. Purchase costs				
b. Special processing costs				
3. Low altitude support photos - specially flown				
a. Flight planning costs				
b. Contracted costs				
c. Film purchase and processing costs				
d. Flight observer costs				
e. Photographer costs				
t. Miscellaneous costs				
4. Maps				
a. Purchase costs	6	1.15	7	7
b. Map preparation costs				
B. Data Collection Interpretation - High Altitude Imagery				
1. Interpretation costs	4.5 hr	6.54	29	29
2. Field mapping checking costs				
3. Miscellaneous costs				
C. Data Processing				
1. Hand tabulating costs				
2. Preparing data for machine processing				
3. Machine processing costs				
4. Preparing data for publication, displays				
TOTALS				73

a Salaries include overhead cost of 70%

b Includes special charges

* DETECTING POSSIBLE WATER BEARING AREAS

**TABLE 3b - COSTS ASSOCIATED WITH THE
USE OF HIGH ALTITUDE IMAGERY ***

A. Acquiring High Altitude Imagery and Supporting Data Sources

	Quantity	Unit Cost <u>a</u>	Sub-Total	Total <u>b</u>
1. High altitude photos				
a. Purchase costs	70	14.05	984	984
b. Special processing costs				
2. Low altitude support photos - existing				
a. Purchase costs				
b. Special processing costs				
3. Low altitude support photos - specially flown				
a. Flight planning costs				
b. Contracted costs				
c. Film purchase and processing costs				
d. Flight observer costs				
e. Photographer costs				
f. Miscellaneous costs				
4. Maps				
a. Purchase costs	104	4.70	489	489
b. Map preparation costs				
B. Data Collection Interpretation - High Altitude Imagery				
1. Interpretation costs	185 hr	18.03	3,326	3,326
2. Field mapping checking costs				
3. Miscellaneous costs				
C. Data Processing				
1. Hand tabulating costs				
2. Preparing data for machine processing				
3. Machine processing costs				
4. Preparing data for publication, displays				
TOTALS				4,801

- a Salaries include overhead cost of 70%
- b Includes special charges

* URBAN BOUNDARY DELINEATION

TABLE 3c - COSTS ASSOCIATED WITH THE
USE OF HIGH ALTITUDE IMAGERY *

A. Acquiring High Altitude Imagery and Supporting Data Sources

	Quantity	Unit Cost a	Sub-Total	Total b
1. High altitude photos				
a. Purchase costs	12	23.34	280	280
b. Special processing costs				
2. Low altitude support photos - existing				
a. Purchase costs				
b. Special processing costs				
3. Low altitude support photos - specially flown				
a. Flight planning costs				
b. Contracted costs				
c. Film purchase and processing costs				
d. Flight observer costs				
e. Photographer costs				
f. Miscellaneous costs				
4. Maps				
a. Purchase costs	16	1.01	16	16
b. Map preparation costs				
B. Data Collection Interpretation - High Altitude Imagery				
1. Interpretation costs	64 hr	18.03	1,154	1,154
2. Field mapping checking costs	16 hr	18.03	288	288
3. Miscellaneous costs				
C. Data Processing				
1. Hand tabulating costs	40 hr	18.03	721	721
2. Preparing data for machine processing				
3. Machine processing costs				
4. Preparing data for publication, displays				
TOTALS				2,150

a Salaries include overhead cost of 70%

b Includes special charges

* LAND USE UPDATING-COACHELLA/IMPERIAL VALLEYS

TABLE 3d - COSTS ASSOCIATED WITH THE
USE OF HIGH ALTITUDE IMAGERY *

A. Acquiring High Altitude Imagery and Supporting Data Sources				
	Quantity	Unit Cost <u>a</u>	Sub-Total	Total <u>b</u>
1. High altitude photos				
a. Purchase costs	94	25.43	2,390	2,390
b. Special processing costs				
2. Low altitude support photos - existing				
a. Purchase costs				
b. Special processing costs				
3. Low altitude support photos - specially flown				
a. Flight planning costs				
b. Contracted costs				
c. Film purchase and processing costs				
d. Flight observer costs				
e. Photographer costs				
f. Miscellaneous costs				
4. Maps				
a. Purchase costs	56	.77	43	43
b. Map preparation costs				
B. Data Collection Interpretation - High Altitude Imagery				
1. Interpretation costs	651 hr	18.02	11,731	11,731
2. Field mapping checking costs	24 hr	18.02	433	433
3. Miscellaneous costs				
C. Data Processing				
1. Hand tabulating costs				
2. Preparing data for machine processing	850 hr	11.90	10,115	10,115
3. Machine processing costs	100	1.00	100	100
4. Preparing data for publication, displays				
TOTALS				24,810

a Salaries include overhead cost of 70%

b Includes special charges

* LAND USE UPDATING-COASTAL LOS ANGELES

**TABLE 3e - COSTS ASSOCIATED WITH THE
USE OF HIGH ALTITUDE IMAGERY ***

A. Acquiring High Altitude Imagery and Supporting Data Sources

	Quan- tity	Unit Cost <u>a</u>	Sub- Total	Total <u>b</u>
1. High altitude photos				
a. Purchase costs	30	26.40	792	792
b. Special processing costs				
2. Low altitude support photos - existing				
a. Purchase costs				
b. Special processing costs				
3. Low altitude support photos - specially flown				
a. Flight planning costs	4hr	18.03	72	72
b. Contracted costs	15hr	70.00	1,050	1,050
c. Film purchase and processing costs	140ft	1.26	170	170
d. Flight observer costs	15hr	18.03	270	340
e. Photographer costs	15hr	17.70	266	336
f. Miscellaneous costs	20hr	18.00	360	360
			+per 100 ft	
4. Maps				
a. Purchase costs	22	10.33	227	227
b. Map preparation costs				
B. Data Collection Interpretation - High Altitude Imagery				
1. Interpretation costs	25hr	18.00	451	451
2. Field mapping checking costs	60hr	18.00	1,081	1,081
3. Miscellaneous costs				
C. Data Processing				
1. Hand tabulating costs				
2. Preparing data for machine processing	16hr	11.90	190	190
3. Machine processing costs	1	1.00	100	100
4. Preparing data for publication, displays				
TOTALS				5,170

- a Salaries include overhead cost of 70%
- b Includes special charges

* WATERSHED CHARACTERIZATION

**TABLE 3^c - COSTS ASSOCIATED WITH THE
USE OF HIGH ALTITUDE IMAGERY ***

A. Acquiring High Altitude Imagery and Supporting Data Sources

	Quantity	Unit Cost <u>a</u>	Sub-Total	Total <u>b</u>
1. High altitude photos				
a. Purchase costs	2	42.03	84	84
b. Special processing costs				
2. Low altitude support photos - existing				
a. Purchase costs				
b. Special processing costs				
3. Low altitude support photos - specially flown				
a. Flight planning costs				
b. Contracted costs				
c. Film purchase and processing costs				
d. Flight observer costs				
e. Photographer costs				
f. Miscellaneous costs				
4. Maps				
a. Purchase costs	1	5.25	5	5
b. Map preparation costs				
B. Data Collection Interpretation - High Altitude Imagery				
1. Interpretation costs	46 hr	5.10	235	235
2. Field mapping checking costs				
3. Miscellaneous costs	5	10.00	50	50
C. Data Processing				
1. Hand tabulating costs				
2. Preparing data for machine processing				
3. Machine processing costs				
4. Preparing data for publication, displays				
TOTALS				374

a. Salaries include overhead cost of 70%
b. Includes special charges

* WATERWAY MAPPING

TABLE 38 - COSTS ASSOCIATED WITH THE
USE OF HIGH ALTITUDE IMAGERY *

A. Acquiring High Altitude Imagery and Supporting Data Sources

	Quantity	Unit Cost a	Sub-Total	Total b
1. High altitude photos				
a. Purchase costs	1	60.05	60	60
b. Special processing costs	2	51.00	51	56
2. Low altitude support photos - existing				
a. Purchase costs				
b. Special processing costs				
3. Low altitude support photos - specially flown				
a. Flight planning costs				
b. Contracted costs				
c. Film purchase and processing costs				
d. Flight observer costs				
e. Photographer costs				
f. Miscellaneous costs				
4. Maps				
a. Purchase costs	1 hr	18.00	18	18
b. Map preparation costs	12	.75	9	9
B. Data Collection Interpretation - High Altitude Imagery				
1. Interpretation costs	24 hr	18.00	432	432
2. Field mapping checking costs				
3. Miscellaneous costs				
C. Data Processing				
1. Hand tabulating costs				
2. Preparing data for machine processing				
3. Machine processing costs				
4. Preparing data for publication, displays				
TOTALS				575

a Salaries include overhead cost of 70%

b Includes special charges

TABLE 4a - COSTS ASSOCIATED WITH THE
USE OF CONVENTIONAL DATA SOURCES *

	Quan- tity	Unit Cost a	Sub- Total	Total b
A. Acquiring Conventional Data Sources				
1. Low altitude photos - existing				
a. Purchase costs	40	2.33	93	93
b. Special processing costs	?	38675	774	774
2. Low altitude photos - specially flown				
a. Flight planning costs				
b. Contracted costs				
c. Film purchase and processing costs				
d. Flight observer costs				
e. Photographer costs				
f. Miscellaneous costs				
3. Maps				
a. Purchase costs	6	1.15	7	7
b. Map preparation costs				
B. Data Collection Interpretation - Low Altitude Photos				
1. Interpretation costs	4.5hr	6.54	29	29
2. Field mapping checking costs				
3. Miscellaneous costs				
C. Data Collection Interpretation - Other Conventional Data Sources				
1. Field surveying costs				
2. Map interpretation costs				
3. Aerial visual reconnaissance costs				
D. Data Processing				
1. Hand tabulating costs				
2. Preparing data for machine processing				
3. Machine processing costs				
4. Preparing data for publication, display, etc.				
TOTALS				903

a Salaries include overhead cost of 70%

b Includes special charges

* DETECTING POSSIBLE WATER BEARING AREAS

TABLE 4b - COSTS ASSOCIATED WITH THE
USE OF CONVENTIONAL DATA SOURCES *

	Quan- tity	Unit Cost a	Sub- Total	Total b
A. Acquiring Conventional Data Sources				
1. Low altitude photos - existing				
a. Purchase costs				
b. Special processing costs				
2. Low altitude photos - specially flown				
a. Flight planning costs	8hr	18.00	144	144
b. Contracted costs	40hr	70.00	2,800	2,926
c. Film purchase and processing costs	230ft	1.20	280	280
d. Flight observer costs	40hr	17.99	720	720
e. Photographer costs	40hr	20.85	708	834
f. Miscellaneous costs	40hr	10.60	424	424
3. Maps				
+ per 100 ft				
a. Purchase costs	104	4.70	489	489
b. Map preparation costs				
B. Data Collection Interpretation - Low Altitude Photos				
1. Interpretation costs	200	18.20	3,640	3,640
2. Field mapping checking costs				
3. Miscellaneous costs				
C. Data Collection Interpretation - Other Conventional Data Sources				
1. Field surveying costs				
2. Map interpretation costs				
3. Aerial visual reconnaissance costs				
D. Data Processing				
1. Hand tabulating costs				
2. Preparing data for machine processing				
3. Machine processing costs				
4. Preparing data for publication, display, etc.				
TOTALS				9,457

a Salaries include overhead cost of 70%

b Includes special charges

* URBAN BOUNDARY DELINEATION

TABLE 4c - COSTS ASSOCIATED WITH THE
USE OF CONVENTIONAL DATA SOURCES *

	Quantity	Unit Cost a	Sub-Total	Total b
A. Acquiring Conventional Data Sources				
1. Low altitude photos - existing				
a. Purchase costs	80	3.00	240	240
b. Special processing costs	1	6.00	6	6
2. Low altitude photos - specially flown				
a. Flight planning costs				
b. Contracted costs				
c. Film purchase and processing costs				
d. Flight observer costs				
e. Photographer costs				
f. Miscellaneous costs				
3. Maps				
a. Purchase costs	16	1.01	16	16
b. Map preparation costs				
B. Data Collection Interpretation - Low Altitude Photos				
1. Interpretation costs	84 hr	18.00	1,512	1,512
2. Field mapping checking costs	16 hr	18.00	288	288
3. Miscellaneous costs				
C. Data Collection Interpretation - Other Conventional Data Sources				
1. Field surveying costs				
2. Map interpretation costs				
3. Aerial visual reconnaissance costs				
D. Data Processing				
1. Hand tabulation costs	40 hr	18.00	720	720
2. Preparing data for machine processing				
3. Machine processing costs				
4. Preparing data for publication, display, etc.				
TOTALS				2,700

a Salaries include overhead cost of 70%

b Includes special charges

* LAND USE UPDATING-COACHELLA/IMPERIAL VALLEYS

TABLE 4d - COSTS ASSOCIATED WITH THE
USE OF CONVENTIONAL DATA SOURCES *

	Quan- tity	Unit Cost a	Sub- Total	Total b
A. Acquiring Conventional Data Sources				
1. Low altitude photos - existing				
a. Purchase costs	248	1.87	464	464
b. Special processing costs	1	6.00	6	6
2. Low altitude photos - specially flown				
a. Flight planning costs				
b. Contracted costs				
c. Film purchase and processing costs				
d. Flight observer costs				
e. Photographer costs				
f. Miscellaneous costs				
3. Maps				
a. Purchase costs	56	.77	43	43
b. Map preparation costs				
B. Data Collection Interpretation - Low Altitude Photos				
1. Interpretation costs	768hr	18.02	13,837	13,837
2. Field mapping checking costs	24 hr	18.02	433	433
3. Miscellaneous costs				
C. Data Collection Interpretation - Other Conventional Data Sources				
1. Field surveying costs				
2. Map interpretation costs				
3. Aerial visual reconnaissance costs				
D. Data Processing				
1. Hand tabulating costs				
2. Preparing data for machine processing	850hr	11.90	10,115	10,115
3. Machine processing costs	100	1.00	100	100
4. Preparing data for publication, display, etc.				
TOTALS				25,000

a Salaries include overhead cost of 70%

b Includes special charges

* LAND USE UPDATING-COASTAL LOS ANGELES

TABLE 4e - COSTS ASSOCIATED WITH THE
USE OF CONVENTIONAL DATA SOURCES *

	Quantity	Unit Cost ^a	Sub-Total	Total ^b
A. Acquiring Conventional Data Sources				
1. Low altitude photos - existing				
a. Purchase costs	550	1.51	832	832
b. Special processing costs	1	4.00	4	4
2. Low altitude photos - specially flown				
a. Flight planning costs	4 hr	18.03	72	72
b. Contracted costs	15 hr	70.00	1,050	1,050
c. Film purchase and processing costs	140 ft	1.26	170	170
d. Flight observer costs	15 hr	18.03	270	340
e. Photographer costs	15 hr	17.70	266	336
f. Miscellaneous costs	20 hr	18.03	360	360
+ per 100 ft				
3. Maps				
a. Purchase costs	22	10.33	227	227
b. Map preparation costs				
B. Data Collection Interpretation - Low Altitude Photos				
1. Interpretation costs	50hr	18.03	901	901
2. Field mapping checking costs	60hr	18.03	1,081	1,081
3. Miscellaneous costs				
C. Data Collection Interpretation - Other Conventional Data Sources				
1. Field surveying costs				
2. Map interpretation costs				
3. Aerial visual reconnaissance costs				
D. Data Processing				
1. Hand tabulating costs				
2. Preparing data for machine processing	50hr	11.90	595	595
3. Machine processing costs	100	1.00	100	100
4. Preparing data for publication, display, etc				
TOTALS				6,063

^a Salaries include overhead cost of 70%

^b Includes special charges

* WATERSHED CHARACTERIZATION

TABLE 4f - COSTS ASSOCIATED WITH THE
USE OF CONVENTIONAL DATA SOURCES *

	Quantity	Unit Cost ^a	Sub-Total	Total ^b
A. Acquiring Conventional Data Sources				
1. Low altitude photos - existing				
a. Purchase costs				
b. Special processing costs				
2. Low altitude photos - specially flown				
a. Flight planning costs	1 hr	18.00	18	18
b. Contracted costs	8 hr	70.00	560	560
c. Film purchase and processing costs	3 ft	1.33	4	4
d. Flight observer costs	8 hr	18.00	144	144
e. Photographer costs	8 hr	17.70	142	142
f. Miscellaneous costs	1 hr	18.00	18	18
3. Maps				
a. Purchase costs	1	5.25	5	5
b. Map preparation costs				
B. Data Collection Interpretation - Low Altitude Photos				
1. Interpretation costs	46 hr	5.10	235	235
2. Field mapping checking costs				
3. Miscellaneous costs	5	10.00	50	50
C. Data Collection Interpretation - Other Conventional Data Sources				
1. Field surveying costs				
2. Map interpretation costs				
3. Aerial visual reconnaissance costs				
D. Data Processing				
1. Hand tabulating costs				
2. Preparing data for machine processing				
3. Machine processing costs				
4. Preparing data for publication, display, etc.				
TOTALS				1,176

^a Salaries include overhead cost of 70%

^b Includes special charges

* WATERWAY MAPPING

TABLE 4g - COSTS ASSOCIATED WITH THE
USE OF CONVENTIONAL DATA SOURCES *

	Quan- tity	Unit Cost a	Sub- Total	Total b
A. Acquiring Conventional Data Sources				
1. Low altitude photos - existing				
a. Purchase costs				
b. Special processing costs				
2. Low altitude photos - specially flown				
a. Flight planning costs	8 hr	18.02	144	144
b. Contracted costs		766	766	766
c. Film purchase and processing costs				
d. Flight observer costs				
e. Photographer costs				
f. Miscellaneous costs				
3. Maps				
a. Purchase costs	1 hr	18.02	18	18
b. Map preparation costs	12	.75	9	9
B. Data Collection Interpretation - Low Altitude Photos				
1. Interpretation costs				
2. Field mapping checking costs				
3. Miscellaneous costs				
C. Data Collection Interpretation - Other Conventional Data Sources				
1. Field surveying costs	344hr	13.60	4,678	5,688
2. Map interpretation costs				
3. Aerial visual reconnaissance costs				
D. Data Processing				
1. Hand tabulating costs	16hr	18.02	288	288
2. Preparing data for machine processing				
3. Machine processing costs				
4. Preparing data for publication, display, etc.				
TOTALS				6,018

a Salaries include overhead cost of 70%

b Includes special charges

* FLOOD DAMAGE ASSESSMENT

EVALUATION OF THERMAL X/5-DETECTOR SKYLAB S-192 DATA FOR
ESTIMATING EVAPOTRANSPIRATION AND THERMAL PROPERTIES
OF SOILS FOR IRRIGATION MANAGEMENT*

W-21

By D.G. Moore, Remote Sensing Institute; M.L. Horton, Water Resources Institute;
M.J. Russell, Remote Sensing Institute; and V.I. Myers, Remote Sensing Institute;
South Dakota State University, Brookings, South Dakota.

ABSTRACT

N76-17607

The energy budget of a volume element of the earth including the land surface is an expression of the relationship among factors affecting the gain, storage, and loss of heat. The surface of the earth varies in density, composition, water content, geometry, and other factors affecting the energy budget with consequent influence on the rate of heat exchange and the resultant temperature. Water is one of the major factors controlling the energy budget due to its mobility, large heat capacity, and large heat of vaporization. Therefore, application of energy budget concepts and models provides part of the information necessary to interpret remotely sensed thermal emittance as related to the occurrence and distribution of soil moisture.

An energy budget approach to evaluating the SKYLAB X/5-detector S-192 data for prediction of soil moisture and evapotranspiration rate was pursued. A test site which included both irrigated and dryland agriculture in Southern Texas was selected for the SL-4 SKYLAB mission. Both vegetated and fallow fields were included. Data for a multistage analysis including ground, NC-130B aircraft, RB-57F aircraft, and SKYLAB altitudes were collected. The ground data included such measurements as gravimetric soil moisture, percent of the ground covered by green vegetation, soil texture, net radiation, soil temperature gradients, surface emittance, soil heat flux, air temperature and humidity gradients, and cultural practices. Ground data were used to characterize energy budgets and to evaluate the utility of an energy budget approach for determining soil moisture differences among twelve specific agricultural fields.

The initial qualitative investigation for evaluating the various spectral bands of the S-192 data was accomplished by display of the digital data using the DAS system. The available spectral regions were viewed to determine those regions appropriate for mapping various landscape features associated with soil moisture differences. Wet versus dry fallow fields could be distinguished on the screening film from the NC-130B multispectral scanner and the SKYLAB DAS film products in the reflective region of the spectrum only in the longer wavelength, infrared channels (greater than 1.533 μm for NC-130B and greater than 1.55 μm for SKYLAB) and could be distinguished in all channels where emitted radiation was measured.

A boundary detection algorithm was developed to locate and map the high gradient boundaries within the matrix of digital S-192 data. Statistical means and variances of the data matrix surrounding ground sample points for each field were computed excluding data from the boundaries and other high gradient levels which were statistically separable for adjustment of classes in a variable quantizer. The means were statistically correlated with ground variables. Maps estimating evapotranspiration rates of the agricultural landscape were produced using the S-192 SKYLAB data as an input into the Jensen-Haise prediction model. Correlations of S-192 data and soil moisture at three different soil depths in a 0-30 cm profile and a composite moisture value in the 0-30 cm profile were all significant only for the thermal band of the S-192.

* SDSU-RSI-J-75-03. Supported in part by NASA Contract Number NAS 9-13337.

INTRODUCTION

The surface of the earth continually absorbs and emits energy. The balance achieved between energy inputs and energy outputs represents the energy budget. Many different models have been developed to simulate the complex interactions among energy budget components. Ground-based meteorological point-sample measurements have been used as inputs for verification of model accuracies. The use of these models with data supplied from aircraft and satellites equipped with sensors capable of measuring reflected and emitted energy offers a synoptic, yet detailed, approach for studying and using concepts from the energy budget models over a variety of landscape variables on a repetitive basis.

The temperature of a fallow soil or vegetated surface is an integrated response by that surface to environmental factors such as the level of incoming radiation, the air temperature and humidity, the wind speed, etc. Such surface characteristics as albedo, roughness, wetness, and other physical parameters alter the effect of the environmental factors on the energy budget and heat exchanges and consequently are expressed as temperature variations.

A major source or sink of heat energy in the soil-plant environment is water. Water plays a major role in determining the thermal properties of soils including the conduction and convection of heat to and from the soil surface. In addition, phase changes of water by vaporization and fusion absorb and release large quantities of heat. Fallow soil surfaces dissipate a portion of the incoming energy by evaporation. Dissipation of energy by evaporation from plants is termed transpiration. A land surface having a crop canopy dissipates the energy by evaporation from both the plant and the soil which is collectively termed evapotranspiration (ET). Since water has a considerable effect on the energy budget, estimates of surface temperatures using emittance measurements from remote sensors may provide the data necessary for estimating soil moisture contents. Point-time soil moisture and evapotranspiration estimates from remote sensors could provide a powerful management tool for irrigation scheduling, crop yield predictions, disease and insect infestations, flood forecasting, seed germination, land erosion potential, and numerous other applications.

A water budget estimate for a region is a widely accepted approach in determining the soil moisture status. The amount of rainfall and irrigation water entering the volume element is equated with the amount of water leaving. A portion of the water leaving is estimated by regional evapotranspiration rates. Predictive models using energy budget, mass transfer, or combination equations have been developed to estimate the potential evaporative flux. See Bartholic, Hamken, and Wiegand (1), McGuinness and Bordne (2), Stone and Horton (3), and Rosenberg, Hart, and Brown (4) for reviews and evaluations of the various models. The prediction normally estimates the potential ET in contrast to the actual ET. Morton (5) has stated that with adequate moisture supplied to the evaporating soil and vegetated surfaces, the actual ET is accurately estimated from the potential ET on a regional basis. However, this relationship is erroneous for surfaces which are not well watered. When conducting a water budget, terms other than evaporative flux are frequently neglected. For example, Black, Gardner, and Tanner (6) determined on a field water budget study that during the 60-day study period the total water loss from a field of snap beans was 35 cm with 17 cm lost to ET and 18 cm lost due to drainage from the 150-cm profile. Goltz et al. (7) found that for an onion crop, the drainage loss exceeded the ET loss. Therefore, the water budget approach is only applicable where a considerable knowledge of the landscape physical properties is known. If the crop canopy and fallow soil surfaces are an indicator of the surface and subsurface moisture at the time of measurement, the errors in the traditional water budget would not affect the estimation of soil moisture at a point in time. When the supply of water to the evaporating surface (primarily through conduction through the soil matrix to the fallow soil surface or

translocation through plant roots and tops to the leaves) is limited, the evaporation rate decreases with a subsequent increase in temperature of the evaporating surface. In early work, Tanner (8) used energy balance relationships to show that if the transpiration rate of plants decreases and if the radiation balance and wind structure remain the same, the decrease in latent heat exchange results in an increase in plant temperature. The incoming energy to the surface is utilized in heating the surface in contrast to being partitioned into latent energy with subsequent dissipation as latent heat flux. As moisture stress increases, with consequent decreases in ET rate and increases in surface temperature, the relative turgidity of the plant decreases. Wiegand and Namken (9) observed in cotton plants that a decrease in relative turgidity of plants from 83 to 59% resulted in a 3.6 C increase in leaf temperature. This magnitude of temperature effect is well within the resolution capabilities of modern remote-sensing systems. Moore, Horton, and Russell (10) have provided early indication by visual examination of S-192, X/5-detector thermal data from SKYLAB that soil moisture variations were evident in the space-altitude data.

The relationship of plant temperature and energy exchange has been further discussed by Gates (11, 12, 13). He suggested that if leaf temperatures and the radiant energy absorbed by the leaf are measured, the transpiration rate can be computed. The Jensen-Haise model for potential ET prediction (based on temperature and radiation) was developed and evaluated over large areas of the world (Jensen and Haise, 14). The model is extensively used for irrigation scheduling and has input parameters as:

$$ET_p = (0.025 T + 0.08) R_s$$

where ET_p = potential ET in mm min⁻¹.

T = air temperature in degrees C

R_s = equivalent depth of evaporation of incoming solar radiation in mm/min⁻¹.

Although air temperature is used, the temperature of the evaporating surface should be an improved parameter for relating to actual ET rates. The same would probably be true for R_s . If remote-sensing inputs into the model could supply T and R_s on a field-by-field basis, the ET on a field basis could be estimated using the model in its present form.

This paper contains preliminary results of an effort to evaluate the use of multispectral SKYLAB for assessing evapotranspiration and thermal properties of soils. The effort was pursued under NASA Contract NAS 9-13337.

METHODS

Aerial Data Acquisition

A test site which included both irrigated and dryland agriculture was established in Dimmit County, Texas, during the SL-4 mission of SKYLAB. The SKYLAB data were acquired at 20:12 GMT (14:12 CST) over ground track 20, orbit 94 on January 28, 1974. The thermal detector during the SL-4 overpass had been changed to the X/5 with a quoted ΔT of 1.1 C. Aircraft including the NC-130B at 7620-m above ground level (AGL), NASA mission 258, and the RB-57F at 18,300-m AGL, NASA mission 260, were direct underflights to the SKYLAB overpass. The sensors for all platforms included scanning radiometers and photography. This paper presents results from the scanner data of SKYLAB and NC-130B using a photographic image from the RB-57F as a base map.

Description of Test Site and Ground Data

The site near Carrizo Springs, Texas, (28°30'N, 99°50'W) was selected in accordance with the estimated coverage of the S-192 scanner and the availability of both irrigated and dryland agriculture. The soils were predominantly of the Uvalde-Montell-Atco Association which are nearly level to gently undulating, silty clay loams, clays, and clay loams that have moderately and very slowly permeable subsoils. The black and white print of color infrared aircraft photography in Fig. 1 includes coverage of the study area. The predominant land use was rangeland with some irrigated crops in the area including alfalfa, cabbage, onions, carrots, and pre-irrigated fallow. The dryland agriculture included fallow, improved range, and unimproved range. The thirteen test fields for which ground data were acquired and which were assumed to be representative of variations in land use and soil moisture are identified in Fig. 1. In addition, the letters A and B in Fig. 1 denote a seep area and center pivot irrigation systems, respectively, for which ground data were not acquired. A frost had occurred approximately one-month prior to the SKYLAB overpass; therefore, the dryland vegetation was essentially dormant.

Considerable energy budget data including thermocouple soil temperatures, soil heat flux, radiometry, air temperatures, surface emittance, etc., were collected for the test fields. Land use and soil moisture data were acquired for the twelve agricultural fields. The percent green vegetation was determined by placing a random dot grid containing 100 points on vertical hand-held photographic slides exposed at 1-m AGL. Each value reported was an average of four separate observations on each of three replicative slides. Soil moisture samples were collected in triplicate with each sample composed of two subsamples. The percent gravimetric soil moisture was determined by oven drying at 105 C for each of three depths: 0-2 cm, 2-10 cm, and 10-30 cm. A composite value for the 30-cm profile was computed by weighting and summing the averages for the depths represented. The means and field descriptions are presented in Table I.

Visual Evaluation of Scanner Imagery

The MC-130B multispectral scanner screening film products were evaluated visually in addition to the DAS products of the SKYLAB S-192 data. The preliminary visual comparisons were to evaluate the similar wave bands of both sensor systems for spectral discrimination of:

1. Dry versus wet fallow surfaces
2. Well- or medium-watered vegetation versus wet fallow
3. Well-watered versus dry alfalfa
4. Medium versus well-watered alfalfa
5. Recognition of extent of seep
6. Appropriateness for irrigation survey
7. Unique location of surface water.

Reduction and Analysis of Digital S-192 Data

Since the original scanner products of the S-192 data were in a conical form, recognition of field boundaries was difficult. Therefore, an algorithm was developed to locate boundaries between relatively homogeneous areas of the digital S-192 data. Assumptions incorporated in the algorithm include:

1. The rate of change of adjacent data values (gradient magnitude) within a homogeneous area is small

2. The gradient magnitude near a boundary is greater than within the homogeneous areas
3. The gradient vector direction at a boundary is perpendicular to the boundary
4. A boundary point is that point which has the maximum gradient value when compared to adjacent points in the gradient vector direction.

A flow diagram for boundary point selection is illustrated in Fig. 2. For example, a boundary point is at gradient point "b" in Fig. 2, only if the adjacent gradient magnitudes at points "a" and "c" are less than or equal to the gradient magnitude at "b". The complete algorithm with examples is documented in the Final Report to NASA Contract NAS 9-13337 (in preparation).

The boundary detection algorithm was applied to the digital S-192 thermal data. Figure 3 illustrates an output of the algorithm. Many field separations and other high gradient regions are easily apparent in Fig. 3.

Histograms of the entire test site (area approximately similar to that in Fig. 1) were generated for each of the spectral bands. Where apparent modes were present within the data, levels were chosen to generate gray-level overstrike maps using a variable quantizer. Using the boundary maps in reference with the overstrike maps, the thirteen test sites were located. Their extents were determined using the boundary and gray-level maps where possible. A region within each test site was chosen which represented the ground sampling points and did not include high gradient points at the boundaries and other areas as apparent in Fig. 3. Statistical means and variances were determined for each of the thirteen sites for each of the available S-192 spectral bands. Each mean represents at least 16 observations. The means representing each field were correlated with the ground variables for that field. The means within a spectral band were ranked and statistically compared. Classes of data were generated by combining similar means into grand means, where necessary. The data classes were statistically separable using the t-test at the 0.05 significance level. A flow diagram for this class grouping process is presented in Fig. 4 and class groupings for the thirteen test sites are shown in Table II. Values for separating classes around the means were chosen by equal percentage weighting of standard errors from each of the adjacent means. Gray-tone maps of the statistically separable classes were prepared by overstrikes on a line printer using a variable quantizer with the previously determined data values as class bounds.

Evapotranspiration Estimate

The Jensen-Haise model was used for an estimate of ET, where:

$$ET_p = (0.025 T + 0.09) R_s$$

where ET_p = potential ET in mm min⁻¹

T = air temperature in degrees C

R_s = equivalent depth of evaporation of incoming solar radiation in mm min⁻¹.

The incoming solar radiation at the SKYLAB overpass (20:12 GMT) was measured with an Eppley pyranometer as 1.020 cal cm⁻² min⁻¹ with the air temperature as 19.3 C. Therefore, the potential ET prediction is 10.0 x 10⁻³ mm min⁻¹. Assume that:

1) the actual ET is equal to the potential ET for the field having the coolest surface temperature, 2) the actual ET is zero for the field with the warmest temperature, and

3) assume the T in the Jensen-Haise model is linearly related to the fourth root of the steradianance as measured by the S-192 scanner. Assignment of ET values for the thermal data would, therefore, use the mean of fields #4, 11, 2, 7, and 10 (see Table II) as T minimum with ET computation of $10.0 \times 10^{-3} \text{ mm min}^{-1}$. The mean of fields #12 and 13 would correspond to T maximum with ET prediction as 0.0 mm min^{-1} . The remaining two classes weighted with the fourth root of steradianance would correspond to $8.4 \times 10^{-3} \text{ mm min}^{-1}$ and $5.4 \times 10^{-3} \text{ mm min}^{-1}$.

RESULTS AND DISCUSSION

Surface Temperature and Soil Moisture

The equivalent blackbody surface temperatures of fallow soils under wet and dry conditions are shown in Fig. 5 for one diurnal cycle. The wet and dry fields represented are #7 and 13, respectively -- refer to Fig. 1. The precision radiation thermometer (PRT) temperature differential between the wet and dry surfaces at 14:12 CST is approximately 6 C, well within the thermal resolution of the X/5 S-192 SKYLAB detector. Prior to 9:00 CST and after 18:00 CST, the two fields cannot be separated by surface emittance measurements which emphasizes the importance of data collection time in surface temperature observations.

If water is available for evaporation, a portion of the incoming radiation will be partitioned into energy dissipation by latent heat flux, thereby creating a cooling mechanism for the soil surface. In addition, the thermal conductivity of a wet soil is normally greater than for a dry soil. Heat is transferred from the surface into the body of the soil by conduction. The conduction rate is dependent upon the soil thermal conductivity and the temperature gradient from the surface. As soil moisture content increases soil thermal conductivity normally increases. Therefore, for a wet soil, the temperature gradient for an equal amount of heat transfer from the surface is less than for a dry soil. This provides an additional mechanism for lowering the surface temperature.

The combination of these two major effects is apparent in the data presented in Fig. 5. Note that during predawn hours, only a negligible temperature anomaly becomes greater. Daytime heating of fallow soil surfaces can serve to indicate a deficit in the supply of water to the evaporating surface. Cool evaporating surfaces in an otherwise moisture deficient area indicate high soil moisture regions.

Visual Interpretations from Photo Products

The man-machine interactive DAS system provides a rapid method of screening digital data. Photographic representations of five bands of S-192 SKYLAB data produced using the DAS system are presented in Figs. 6a-6e. A series of visual interpretations concerning specific landscape characteristics of interest to a water resources specialist were evaluated using these DAS products. Screening film from corresponding NC-130B multispectral scanner bands was also evaluated to provide additional data relating to the S-192 spectral analysis. Table III is a summary of the visual analyses.

Dry versus wet fallow soil surfaces could be separated in the longer reflective infrared bands (greater than $1.5 \mu\text{m}$) and the thermal infrared band. The alfalfa fields classified as "well watered, medium watered, and dry" (see Table I for quantitative data) were separable in only the 0.78-0.88 and 10.2-12.5 μm spectral bands of S-192 data. Identification of other water-related features including a seep and center pivot irrigation systems was accomplished using the thermal band. The thermal data did not separate land use from soil moisture as did the 0.78-0.88 μm band. Therefore, a survey of irrigated and other high soil moisture areas should be conducted using the thermal band. If both land use and soil moisture are to be determined using these five S-192 bands, the reflective 0.78-0.88 μm band must be included in the

analysis. If surface water is to be separated from the high soil moisture bands, a third band must be included which could be either 1.55-1.75 μm or 2.10-2.35 μm .

Statistical Tests of S-192 Data

Correlations among the ground variables for the twelve agricultural fields are presented in Table IV. Soil moisture in adjacent soil layers was significantly correlated. Except for the 0-2 cm layer, correlations of soil moisture with percent green vegetation were not significant. The 0-2 cm layer correlation to green vegetation could have been related to ground shading by vegetation and/or to irrigation scheduling.

Correlation coefficients of ground data to the S-192 data means are contained in Table V. Similar results as with the visual analyses presented in the previous section reveal that wavelengths shorter than 1.55 μm were not related to surface moisture. The wet and dry fallow fields (#7 and 13, respectively) were not statistically separable with the repeated t-test results, presented in Table II, for spectral wavelengths less than 1.55 μm .

The only spectral region to significantly correlate with soil moisture contents at all soil depths sampled was the thermal data from channels 15 and 16. The significant correlations for soil depths greater than 2 cm were encouraging in reference to crop canopy signatures of water deficits. Note for the thermal channel data-class separations in Table II, that the wet versus medium-watered versus dry alfalfa fields (fields 4, 5, and 3, respectively) were within separable classes. Upon further analyses of more of the fields for which ground data were acquired during the SKYLAB mission, emphasis on land use will be considered when relating the spectral data to subsurface soil moisture. The limited numbers of fields for this analysis did not allow those separations.

The statistically separable classes for the 12 agricultural fields and the water body are presented in Table II. If the 13 test fields were truly representative of the total test area, a total of five separable classes of data were present within the thermal band in contrast to the two classes displayed using the DAS system. The surface water was a separable class; however, this observation is considerably dependent on time within the diurnal cycle for measurement. Either of bands 1.55-1.75 μm or 2.10-2.35 μm should be used to uniquely separate surface water.

A significant correlation between percent green vegetation and S-192 spectral data was obtained for the 0.56-0.61 μm spectral band in contrast to the 0.78-0.88 μm band determined in the visual analysis. The 0.56-0.61 μm band was not available for visual analysis.

Prediction of Evapotranspiration

Figure 7 is an ET map produced from the four separable classes identified from statistical treatment of the data from the SKYLAB channels 15 and 16. The basis for the ET map is the temperature of the surface and its relationship to ET. Through use of the Jensen-Haise (14) ET Model equation, the surface was related to evapotranspiration. The fourth root of the calibrated steradianance from channels 15 and 16 was used to linearly relate the S-192 thermal detector responses to temperature differences according to the Stefan-Boltzmann Law. Use of satellite data as input into a similar type equation can lead to regional, yet detailed, ET estimates for use in irrigation scheduling, in watershed models, and in monitoring crop growth and yields.

CONCLUSIONS

1. Wavelengths greater than 1.5 μm were required to spectrally distinguish between wet and dry fallow surfaces.
2. The thermal data provided a better estimate of soil moisture than did the reflective bands.
3. Thermal data was dependent on soil moisture but not on the type of agricultural land use.
4. The emittance map, when used in conjunction with existing models, did provide an estimate of evapotranspiration rates.
5. Surveys of high soil moisture areas can be accomplished with space-altitude thermal data. If both soil moisture and land use are to be surveyed, at least one reflective channel must be included in the analysis.
6. Thermal data will provide a reliable input into irrigation scheduling.
7. The thermal and spatial resolution of the S-192 X/5 detector SKYLAB data is appropriate for monitoring soil moisture and for irrigation scheduling.
8. The time of data collection for soil moisture surveys should be close to midday.

REFERENCES

1. Bartholic, J.R., L.N. Namken, and C.L. Wiegand. 1970. Combination equations used to calculate evaporation and potential evaporation. ARS 41-170 USDA. 14 pp.
2. McGuinness, J.L. and E.F. Bordne. 1972. A comparison of lysimeter-derived potential evapotranspiration with computed values. ARS-USDA technical Bulletin No. 1452, U.S. Government Printing Office. 71 pp.
3. Stone, L.R. and M.L. Horton. 1974. Estimating evapotranspiration using canopy temperatures; field evaluation. Agronomy Journal 66:450-454.
4. Rosenberg, N.J., H.E. Hart, and K.W. Brown. 1968. Evapotranspiration: review of research. University of Nebraska MP20, Lincoln, Nebraska. 80 pp.
5. Morton, F.I. 1969. Potential evaporation as a manifestation of regional evaporation. Water Resources Research 5(6):1244-1255.
6. Black, T.A., W.R. Gardner, and C.B. Tanner. 1970. Water storage and drainage under a row crop on a sandy soil. Agronomy Journal 62:48-51.
7. Goltz, S.M., C.B. Tanner, A.A. Millar, and A.R.G. Lang. 1971. Water balance of seed onion field. Agronomy Journal 63:762-765.
8. Tanner, C.B. 1963. Plant temperatures. Agronomy Journal 55:210-211.
9. Wiegand, C.L. and L.N. Namken. 1966. Influences of plant moisture stress, solar radiation, and air temperature on cotton leaf temperature. Agronomy Journal 58:582-586.

10. Moore, D.G., M.L. Horton, and M.J. Russell. 1974. Preliminary evaluation of S-192 SKYLAB data for assessing energy exchange and land use in irrigated agriculture. Interim report to NASA Contract NAS 9-13337. Remote Sensing Institute Report Number RSI-SDSU-74-18, South Dakota State University, Brookings, South Dakota. 58 pp.
11. Gates, D.M. 1963. Leaf temperature and energy exchange. Archiv fur Meteorologie, Geophysik and Bioklimatologie. Series B: Allgemeine and biologische Klimatologie, Band 12, 2. Heft. 321-336.
12. Gates, D.M. 1964. Leaf temperature and transpiration. Agronomy Journal 56:273-277.
13. Gates, D.M. 1968. Characteristics of soil and vegetated surfaces to reflected and emitted radiation. In Proceedings Fifth Symp. Remote Sensing of Environment, Institute of Science and Technology, University of Michigan, Ann Arbor. pp. 573-600.
14. Jensen, M.E. and H.R. Haise. 1963. Estimating evapotranspiration from solar radiation. American Society of Civil Engineering Proceedings, Journal of Irrigation and Drainage Division. 89:15-41.

TABLE I. LAND USE AND SOIL MOISTURE OF FIELDS WITHIN TEST SITE.

<u>Field No.</u>	<u>Crop</u>	<u>% Green</u>	<u>Composite Gravimetric Soil Moisture in %</u>	<u>Wet or Dry Soil Surface</u>
1	range	1.2	15.1	dry
2	onions	28.0	18.2	wet
3	alfalfa	22.8	14.3	dry
4	alfalfa	86.8	24.4	wet
5	alfalfa	86.1	18.9	wet
6	fallow	0.0	22.5	dry
7	fallow	2.6	29.5	wet
8	fallow	0.0	19.2	dry
9	water			
10	fallow	6.0	25.6	wet
11	alfalfa	89.2	23.9	wet
12	alfalfa	10.3	15.9	dry
13	fallow	0.0	18.5	dry
A	seep			
B	center pivot irrigation			

TABLE II. STATISTICAL DIFFERENCES AMONG FIELDS FOR HIGH RATE CHANNELS OF S-192.^{1/}

Ch. 3-4 0.56±0.61 μm		Ch. 7-8 0.68±0.76 μm		Ch. 9-10 0.78±0.88 μm		Ch. 11-12 1.55±1.75 μm		Ch. 13-14 2.10±2.35 μm		Ch. 15-16 10.2±12.5 μm	
f.	\bar{x}	f.	\bar{x}	f.	\bar{x}	f.	\bar{x}	f.	\bar{x}	f.	\bar{x}
	$S\bar{x}$		$S\bar{x}$		$S\bar{x}$		$S\bar{x}$		$S\bar{x}$		$S\bar{x}$
13		4	102.5	3		13	122.2	13	128.1	13	128.1
12	47.3	8	23.4	8		12	88.8	12	103.7	12	103.7
7		1	89.5	7	41.3	8	13.0	1	84.9	8	120.4
8		3	20.0	2		3	82.1	8	24.3	3	120.4
2		7		11		6	71.2	5	67.8	5	114.9
10		11		10		5	8	3	18.1	6	114.9
11		12	70.9	4		7	64.2	5	54.1	4	103.5
5	34.5	5	26.0	5		11	12.7	11	23.3	11	103.5
11		2		12	33.3	7	9.7	11	11	2	14.7
3		13		13		10		10	7	7	
6		1		1		2	54.2	7	37.9	2	
4	98.4	6	53.4	9		4	8.0	10	13.6	10	
9	10.4	10	20.4	9		9	0.4	4	20.2	9	87.1
	11.8	9	3.7				1.7	4	12.9		3.7
								9	0.0	9	0.0
									0.0		0.0

^{1/} where breaks in groups were statistically different at 0.05 level using two-tailed t-test, f. is the field number, \bar{x} is the mean, and $S\bar{x}$ is the standard error of the mean.

TABLE III. RECOGNITION OF SELECTED LANDSCAPE FEATURES USING SKYLAB AND CORRESPONDING NC-130B DATA $\frac{1}{2}$.

Landscape Feature	SKYLAB Data - wave length in μm		Comparable IG-130B Data - wave length in μm						
	0.78-0.88	1.55-1.75	2.10-2.35	10.2-12.5					
Dry fallow vs. wet fallow (fields 6, 13 vs. 7, 10)	no	no	yes	no	no	yes	yes	yes	yes
"wet" or medium watered vegetation vs. "wet" fallow (fields 4, 5 vs. 7, 10)	no	yes	no	no	yes	no	yes	no	no
"wet" watered vs. "dry" alfalfa (field 4 vs. 3)	no	yes	yes	yes	yes	yes	yes	yes	yes
"medium-watered" vs. "wet" watered alfalfa (field 5 vs. 4)	no	yes	no	yes	no	no	no	no	yes
Recognition of extent of seep (area A)	no	yes	yes	yes	yes	yes	yes	yes	yes
Identification of center pivots (area B)	no	no	no	yes	NA $\frac{2}{2}$	NA	NA	NA	NA
Survey of irrigated land	no	no	no	yes	no	no	no	no	yes
Unique location of surface water	no	no	yes	no	yes	yes	yes	yes	no

$\frac{1}{2}$ The observations are based on visual analyses of the original color DAS products and should be verified using statistical analyses of the digital data.

$\frac{2}{2}$ Center pivots not imaged.

TABLE IV. CORRELATION OF GROUND VARIABLES.^{1/}

	soil moisture ^{2/}			percent green vegetation
	0+2 cm	2+10 cm	10+30 cm composite ^{3/}	
soil moisture				
0+2 cm	1.000			
2+10 cm	0.780**	1.000		
10+30 cm	0.584*	0.801**	1.000	
composite	0.482	0.909**	0.972**	1.000
percent green vegetation	0.615*	0.065	0.081	1.000

where * is 0.05 level and ** is 0.01 level.

^{1/} 10 df

^{2/} in percent over dry weight

^{3/} weighted combination of three depths

TABLE V. CORRELATION OF GROUND VARIABLES TO SKYLAB S-192 SPECTRAL DATA.^{1/}

	Wavelength of S-192 Channel in μm				T 4/	
	0.56+0.61	0.68+0.76	0.78+0.88	1.55+1.75		2.10+2.35
Soil Moisture ^{2/}						
0-2 cm	-0.438	0.151	0.173	-0.640*	-0.672*	-0.639*
2-10 cm	-0.126	-0.072	0.340	-0.486	-0.490	-0.595*
10-30 cm	-0.331	-0.234	0.297	-0.624	-0.543	-0.733**
composite ^{3/}	-0.323	-0.159	0.314	-0.641*	-0.590*	-0.744**
Percent Green Vegetation	-0.643*	0.216	0.088	-0.498	-0.498	-0.307
						-0.302

Where * is 0.05 level and ** is 0.01 level

^{1/} 10 df

^{2/} In percent oven dry weight

^{3/} Weighted combination of three depths

^{4/} Fourth root of digital count calibrated to steradian



Figure 1.- Black and white print of color infrared photography illustrating the intensive test site in Southern Texas. Data is from RB-57F NASA mission 260, Zeiss "12-inch" focal length camera at 18,300-m AGL. Refer to Table I for description of land use and soil moisture for fields 1 thru 13. Area "A" is a seep and areas "B" are apparent center pivot irrigation systems.

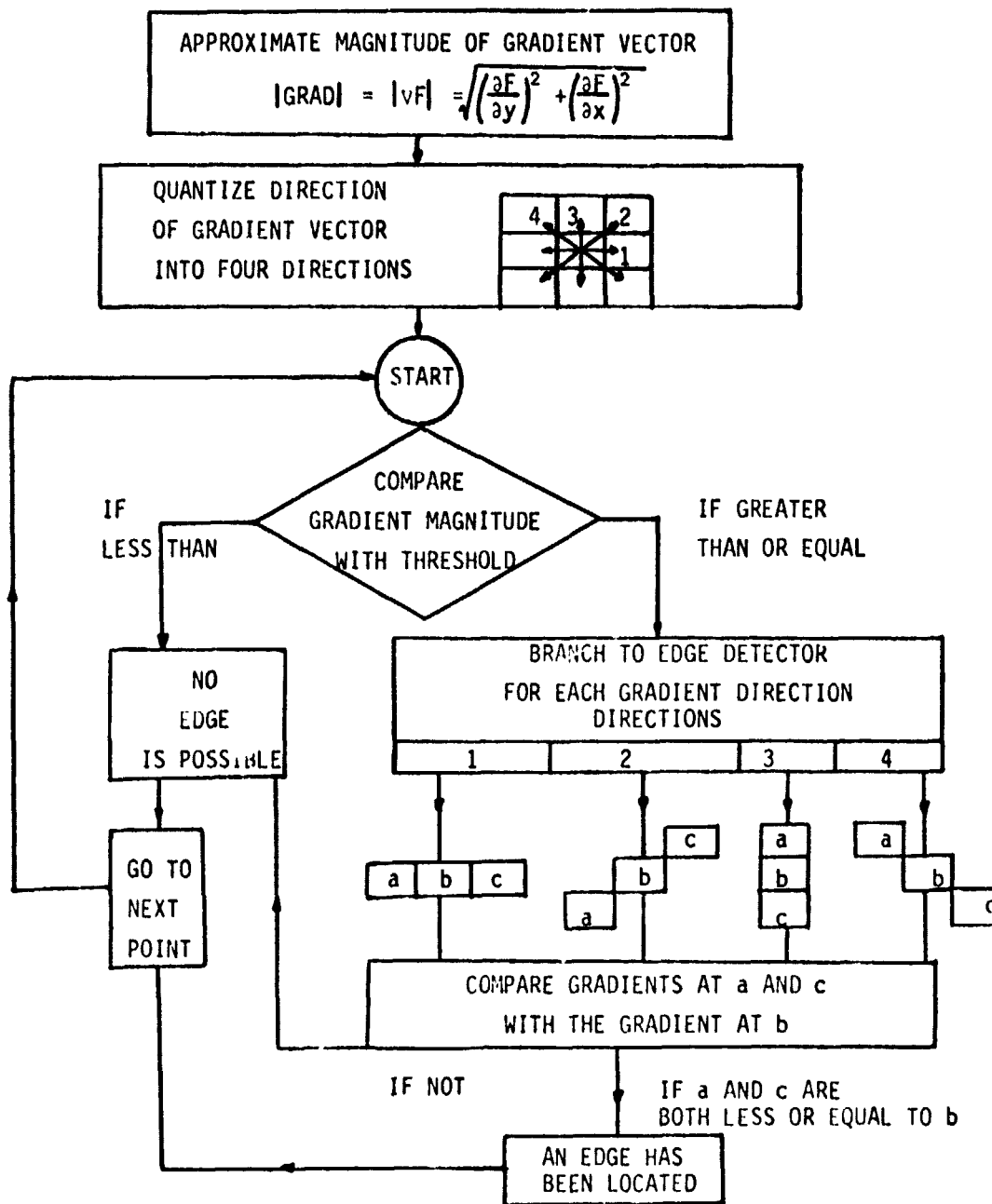


Figure 2.- Flow diagram of boundary detection procedure which was applied to digital S-192 scanner data.

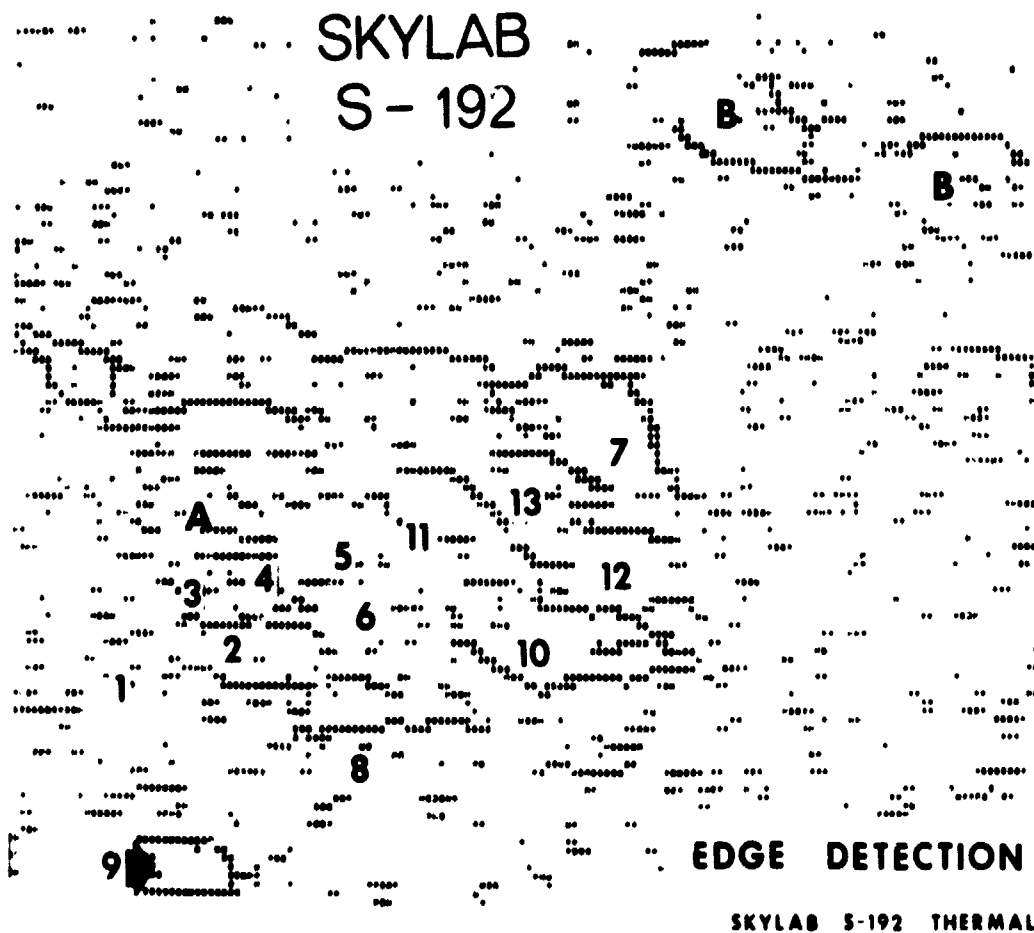


Figure 3.- Output of boundary detection procedure applied to channels 15-16 of S-192 SKYLAB thermal data. Approximate areal coverage similar to that in Fig. 1 with corresponding annotation of field test sites.

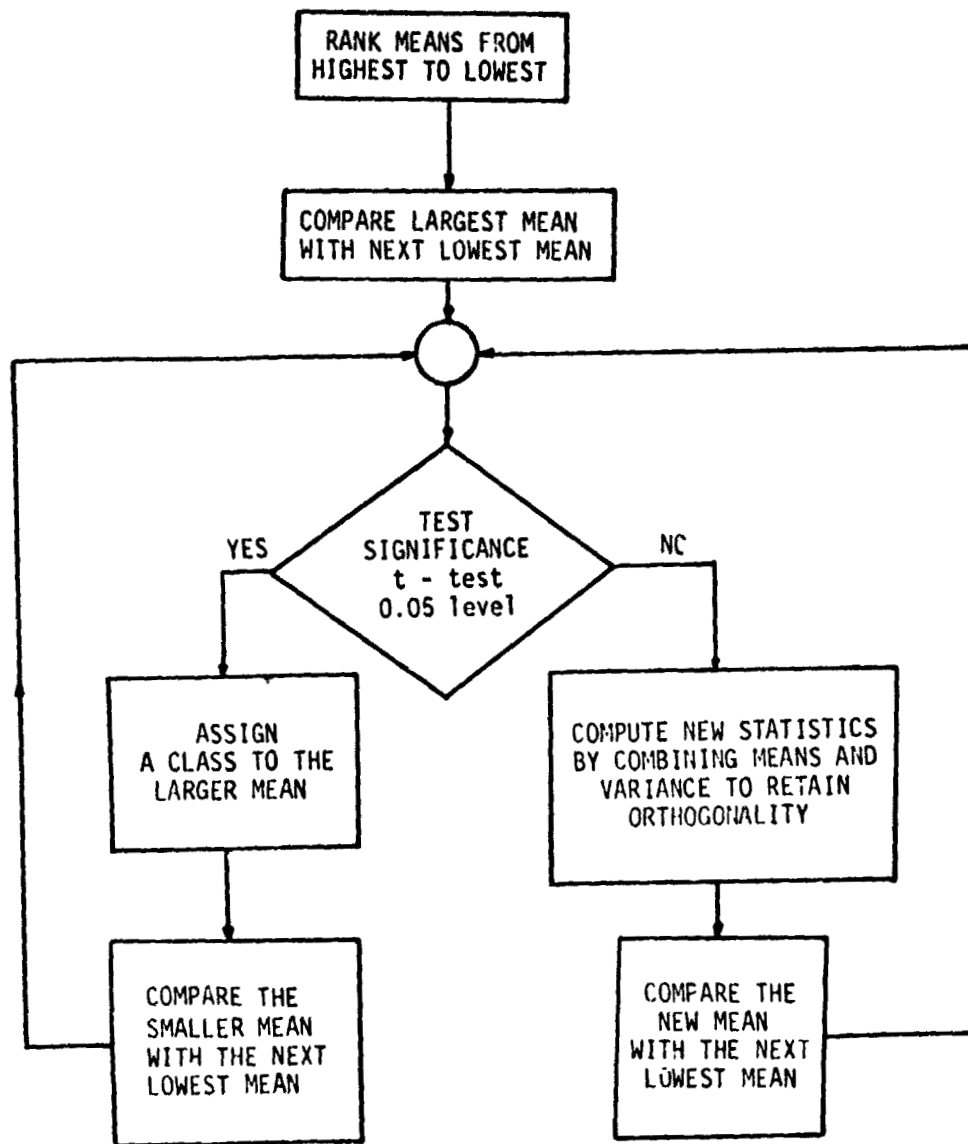


Figure 4.- Flow diagram of t-test procedure which was applied to the digital S-192 scanner data.

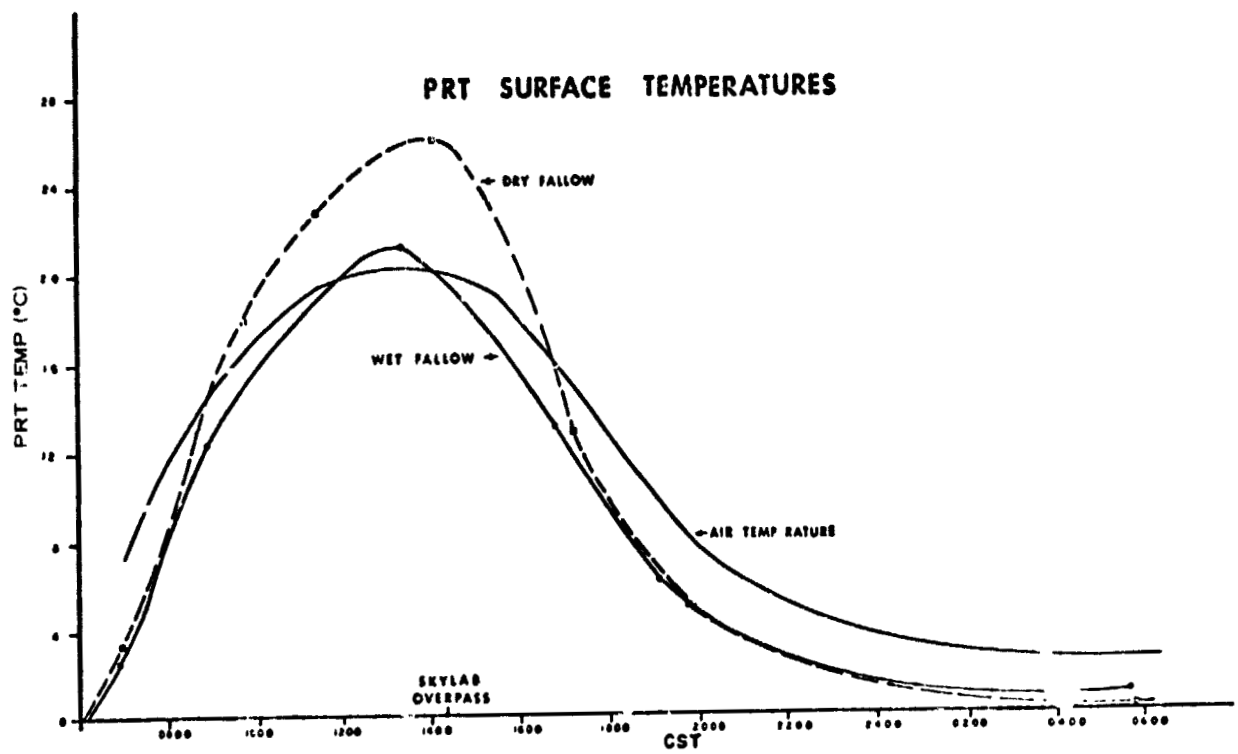
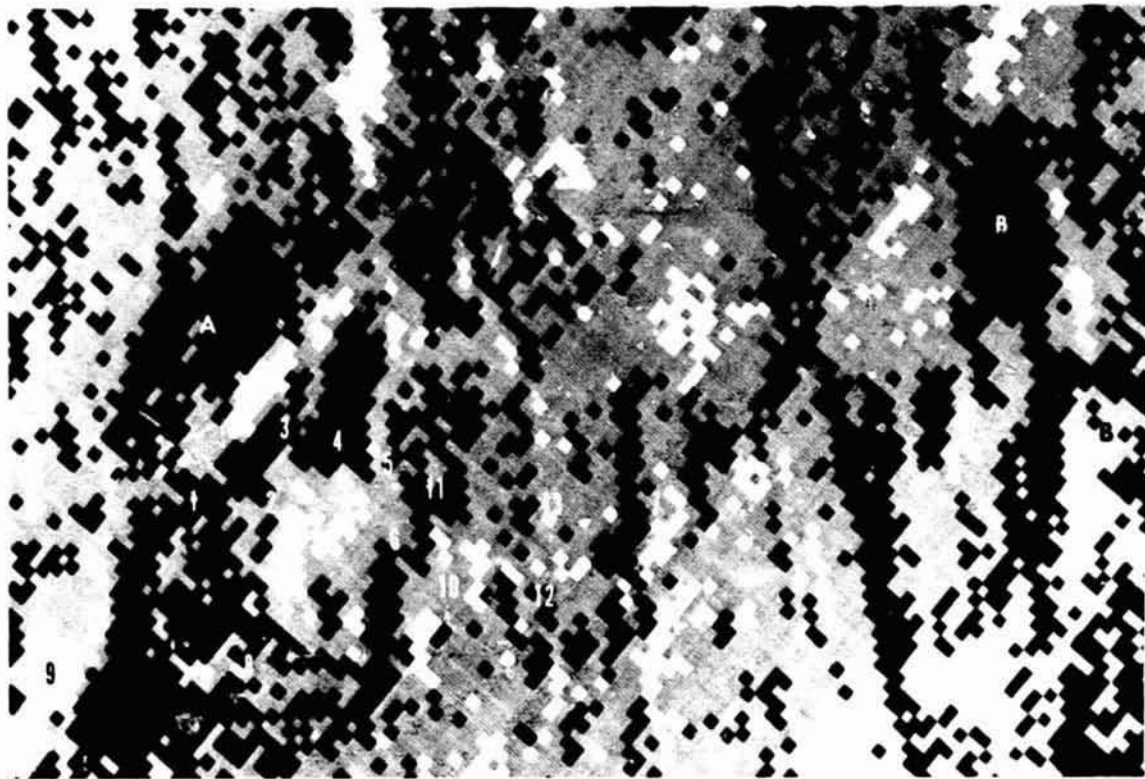


Figure 5.- Diurnal equivalent blackbody surface temperatures as measured with a quantitative hand-held radiation thermometer for wet and dry fallow fields.

REPRODUCIBILITY OF THIS
ORIGINAL PAGE IS POOR

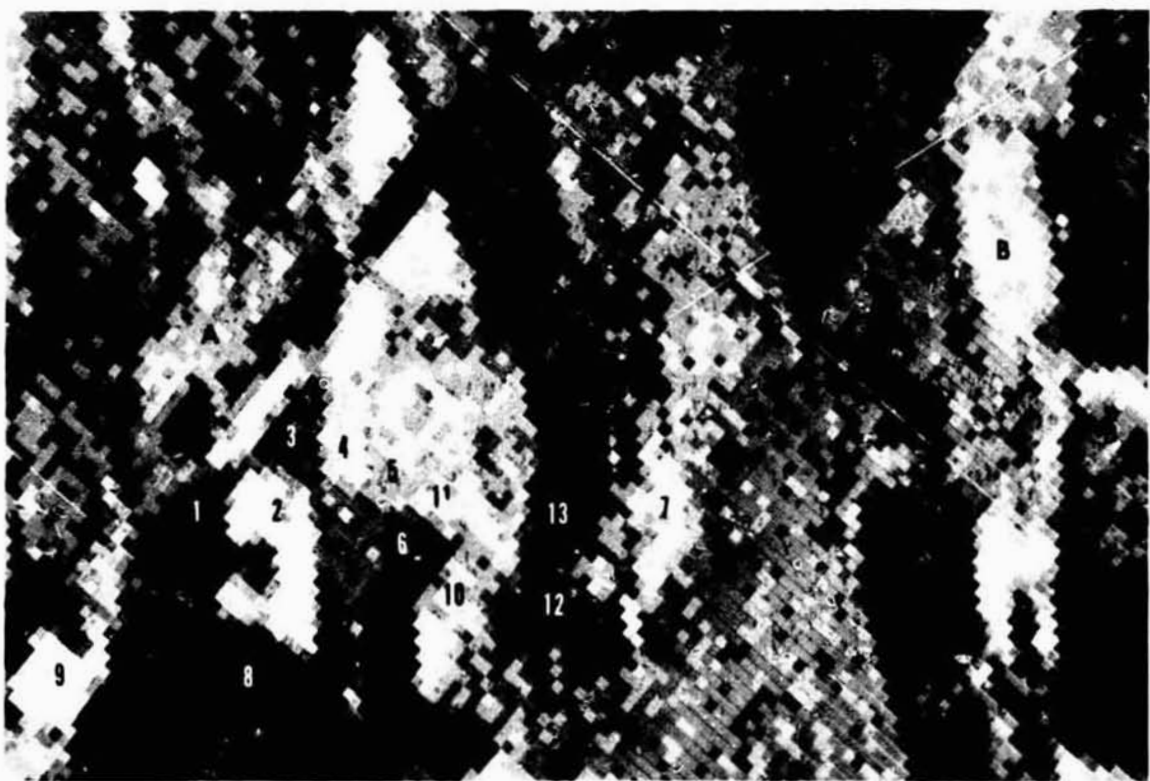


a. Channel 8, 0.68-0.76 μ m

Figure 6.- Black and white photographic representation of color products derived from the S-192 SKYLAB data using the DAS system. Approximate areal coverage similar to that in Figs. 1 and 3. Field numbers correspond to those presented in Figs. 1 and 2 and in Table I. Note the data from the conical scanner have not been rectified; therefore, the round pattern associated with the center pivots appears elliptical.



b. Channel 10, 0.78-0.88 μm

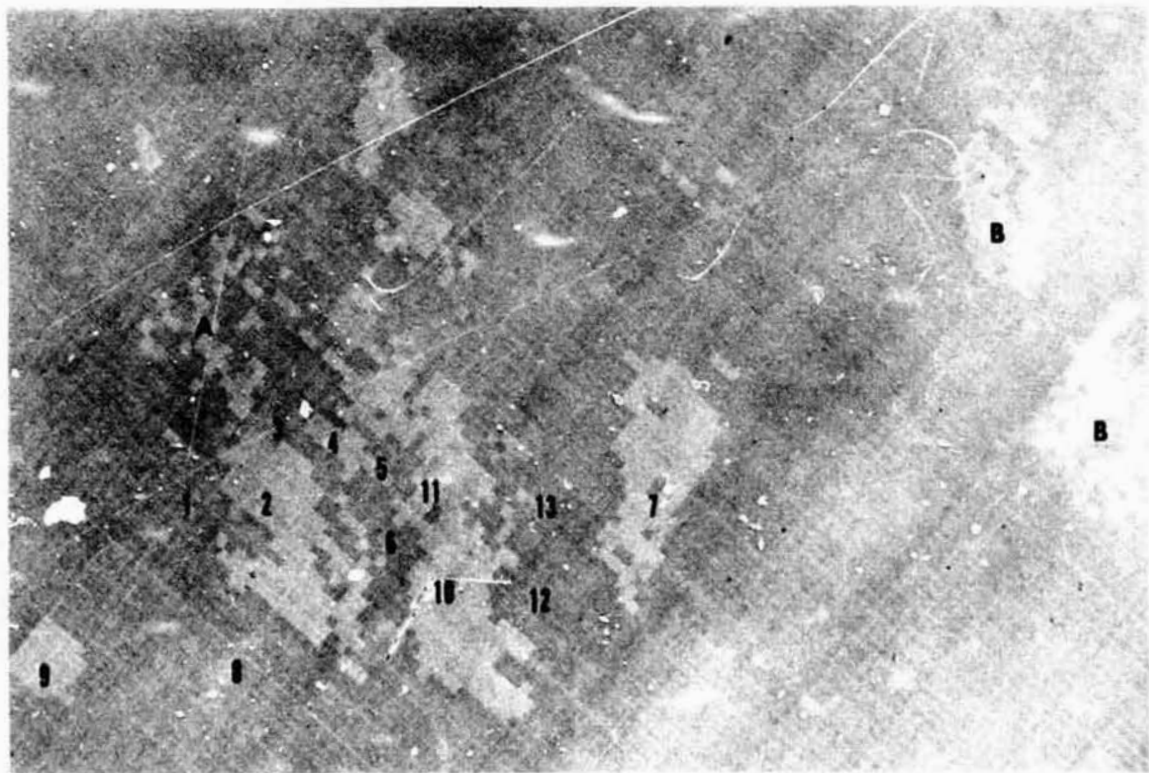


c. Channel 12, 1.55-1.75 μm

Figure 6.- (continued)



d. Channel 14, 2.10-2.35 μm



e. Channel 16, 10.2-12.5 μm

Figure 6.- (continued)

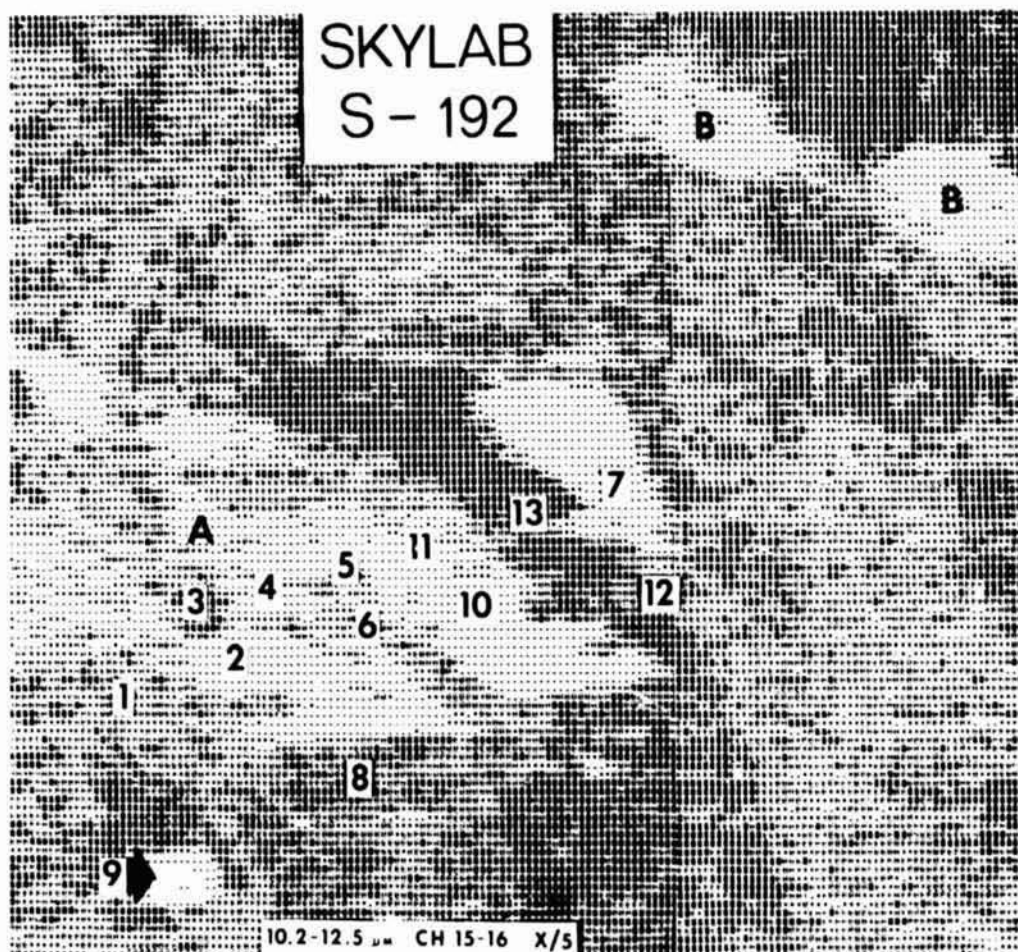


Figure 7.- Evapotranspiration map computed using emittance data from the S-192 SKYLAB thermal scanner as an input into the Jensen-Haise model. The ER levels times 10^3 include symbol sequences: \odot = 0.0 mm min^{-1} , \ominus = 5.4 mm min^{-1} , \oplus = 8.4 mm min^{-1} , \otimes = 10.0 mm min^{-1} , and blanks = surface water.

By John E. Estes, John R. Jensen, Larry R. Tinney, Geography Remote Sensing Unit, University of California, Santa Barbara, California, and Michael Rector, Kern County Water Agency, Bakersfield, California

ABSTRACT

N76-17608

Water resource managers require timely, accurate, and cost-effective data to model hydrologic dynamics in arid agricultural environments. In an attempt to determine the ability of remote sensing techniques to economically generate data required by water demand models, personnel of the Geography Remote Sensing Unit at the University of California, Santa Barbara, are presently involved in a cooperative research program with the Kern County Water Agency (KCWA), California. The KCWA model was developed, and is currently being refined, by the TEMPO Center for Advanced Studies, Santa Barbara. Based upon an analysis of the KCWA model, listings of all external quantities that serve as inputs to the model were compiled and analyzed in the following manner: 1) all data inputs were precisely defined; 2) related data inputs were grouped and categorized; 3) present sources of input data were identified; and, 4) preliminary determinations were made as to which inputs could possibly be generated more efficiently utilizing remote sensing technology.

As a result of this analysis it was determined that agricultural cropland inventories utilizing both high altitude photography and LANDSAT imagery can be conducted cost-effectively. In addition, by using average irrigation application rates in conjunction with cropland data, estimates of agricultural water demand can be generated. However, more accurate estimates are possible if crop type, acreage and crop specific application rates are employed.

An analysis of the effect of saline-alkali soils on water demand in the study area is also examined. KCWA must identify and assess the distribution of the saline-alkali environment if an effective water management program is to be implemented. GRSU has identified the dimension of the saline-alkali agricultural damage based on photo interpretation and extensive ground truth.

Finally, reference is made to other GRSU investigations in this area such as the detection and delineation of water tables that are "perched" near the surface by semi-permeable clay layers. Soil salinity prediction, automated crop identification on a by-field basis, and a potential input to the determination of zones of equal benefit taxation are briefly touched upon.

Techniques developed are considered economical, accurate, and timely in comparison to conventional methods. Particular emphasis in these investigations

* This research was performed as part of the ongoing NASA-funded project entitled "An Integrated Study of Earth Resources in the State of California Using Remote Sensing Techniques," NASA NGL 404-S5 Estes 4/75, undertaken as a multi-campus project by the University of California.

PRECEDING PAGE BLANK NOT FILMED

has been placed upon the development of techniques ultimately employable by user agency personnel.

INTRODUCTION

Hydrologic modeling in arid regions is an important step in maximizing the efficiency of water use. Efficient water management requires the ability to predict how a water basin will respond to various meteorological and operational conditions. The complexity of such a task, in terms of both conceptualization and data requirements, usually necessitates the use of mathematical models for the effective integration of ground and surface water supplies into an optimal management program. In an attempt to ascertain the ability of remote sensing systems to economically generate accurate and timely data as may be required by such models, personnel of the Geography Remote Sensing Unit (GRSU) at the University of California, Santa Barbara, are presently involved in a cooperative research program with the Kern County Water Agency (KCWA), California, to determine the extent to which remotely sensed data can provide input into a model of the Kern County groundwater reservoir. The model itself was developed and is currently being refined by the TEMPO Center for Advanced Studies, Santa Barbara, under contract to KCWA and the California Department of Water Resources.

Within Kern County, the geographical focus of this study, county-wide jurisdiction for water resource management lies with KCWA. KCWA (see Figure 1) is responsible for the forecasting of water supply and demand (on both a short and long-term basis) as well as the allocation and pricing of water to 15 cooperating water districts (2 municipal and 13 rural districts) within the county. In recent years Kern County has experienced an increase in agricultural acreage due to the input of new water supplies from the California Water Project. This input of new water, with its effect on agriculture, has made the need for methodologies to increase the effectiveness of water management decisions all the more important. One response of the KCWA has led to the development, previously mentioned, of a mathematical model of the water basin underlying the San Joaquin Valley portion of Kern County. This portion of Kern County contains the overwhelming proportion of the county's agricultural holdings and as such, information concerning this area is most important to the operation of the model. In addition to establishing a close working relationship with KCWA personnel, GRSU researchers also contacted a number of other local, state and federal agencies with responsibilities in the area of water supply and allocation. Principal among these agencies was the California Department of Water Resources (DWR). Both DWR and particularly KCWA, continue to play an important and interactive role in our research activities. They have done so by detailing their current water resource activities, suggesting potential remote sensing applications, providing "ground truth" data, and evaluating the potential utility of our methodologies to meet their present and projected data requirements.

In addition to these two major agencies other agencies and organizations concerned with water-related parameters, or having an expertise in crops, soils, hydrology modeling, etc., have also been contacted on an "as needed" basis. These contacts were made primarily to aid in the interpretation and definition of environmental parameters important in terms of hydrologic modeling. Notable among these contacts have been:

- | | |
|--|--|
| <ol style="list-style-type: none"> 1. University of California Agricultural Extension Service at Bakersfield 2. Lost Hills Water District 3. Semitropic Water District 4. Wheeler Ridge-Maricopa Water District 5. United States Salinity Laboratory at Riverside | <ol style="list-style-type: none"> 6. Kern County Water Association (at their request a slide discussion of GRSU activities in Kern County was presented to their Board of Directors) 7. United States Department of Agriculture's Soil Conservation Service 8. Kern County Agricultural Commission 9. TEMPO Center for Advanced Studies¹ |
|--|--|

KCWA Water Accounting Model

The computer model of Kern County is not a water demand model, per se, in that its major purpose is the total simulation of water transmission and storage throughout most of the Kern County water basin. Therefore, the model might be more appropriately referred to as a "water accounting model." As Kern County is mainly a "water-demanding" environment, that is, its arid climate and extensive agriculture requires extensive importations of water, it is appropriate to examine all model inputs for possible remote sensing applications.

The construction of the model utilized by KCWA is based upon the following assumptions: 1) that a real-world water basin consists of interbedded layers of sands, clay, silt and gravels which are saturated to some level with water and upon which a variety of land uses are superimposed; and, 2) that the mathematical modeling of such a complex, heterogeneous mass requires that the total complex be subdivided into more workable units of smaller size with greater homogeneity assumed, i.e., generalizations made.

Within the context of the model the subdivisions that have been made and the assumptions related to them include: 1) subdivision of the surface area of Kern County into 251 polygons or nodal areas (see Figure 2), most of which represent one quarter of a township or approximately 24 square kilometers; 2) the designation of a center point in each polygon which is termed its "node" (all events or circumstances occurring in the area corresponding to a given polygon are assumed to occur at the node); and, 3) the movement of water from one polygon to another is assumed to occur along the lines or "flow paths" connecting the nodes. The insert in Figure 2 illustrates how the system operates and depicts how the area of Kern County has been subdivided. It is on the basis of these subdivisions that data is collected as input to the model, that is to say, data is collected and generalized for each nodal region. The final model also takes into account complications resulting from the existence of multilayered aquifers, subsidence, perched water tables and other water-related phenomena.

¹ TEMPO received the original contract for the development of the KCWA ground-water-basin model and continues to be responsible for its operation.

Before remote sensing techniques could be used to generate meaningful inputs to this water demand model it was necessary to determine exactly what types of input were likely to be useful. Based upon an analysis of the KCWA model, listings of all external quantities that serve as inputs to the model were compiled (see Table I) with the aid of KCWA personnel and the following steps taken: 1) all data inputs were precisely defined; 2) related data inputs were grouped and categorized; 3) present sources of input data were identified; and, 4) preliminary determinations were made as to which inputs could possibly be generated more efficiently utilizing remote sensing technology. Based on this analysis, it was determined that remote sensing could provide immediate inputs into the model in several critical areas. These critical model inputs are listed in Table II. The remainder of this paper will discuss in detail two major research areas illustrative of the types of investigations being conducted by GRSU personnel to assess the ability of remote sensing to generate model input data. These areas are: 1) Croplands mapping including the need and rationale for both general and specific crop data and their impact on agricultural water demand prediction; and, 2) an investigation of the magnitude of the soil salinity problem in Kern County. Other research topics such as soil salinity prediction, the analysis of soil moisture and specifically perched water and methods of automating specific location of crop type on a by-field basis would carry this paper beyond practical page limitations. Information concerning these topics may be found in Estes, et al., 1975.

Croplands Mapping

The most dynamic element of water movement into and through the Kern County groundwater basin occurs as a result of the application of irrigation water on the agricultural lands. In comparison to an average Southern San Joaquin Valley precipitation rate of 7.6 cm (3 in.) to 12.7 cm (5 in.) per year, the average irrigation rate is 4196 m³ (3.38 acre-feet) per year or approximately 103 cm (40.6 in.). Irrigation water may be pumped from the groundwater basin itself or imported from other regions of the state. Presently, approximately 1,418,525,000 m³ (1,150,000 acre-feet) of water is imported yearly while future contractual agreements call for 2,035,275,000 m³ (1,650,000 acre-feet) by 1990.

An estimate of the "modelwide" water flow resulting from irrigation activities can be generated from knowledge of the total irrigated acreage and the average application rate. By subtracting the known amount of imported water, an estimate can also be obtained of the county's groundwater pumpage. If the KCWA model operated only at a general modelwide scale effective use could be made of multi-stage sampling techniques combining ground sampling and remote sensing to estimate total irrigated acreage. However, the model does not operate at such a general level and except for providing a method for monitoring general trends such information is of little value. In fact, it is a model requirement that the spatial dimension of cropland data be retained at least to the nodal level of aggregation, i.e., sampling has to be intensive enough to assure high spatial accuracies. Many sampling techniques are impractical under the restrictions imposed by the KCWA model, while mapping approaches such as those explored by the GRSU, have been found both accurate and cost-effective. In order to test the potential of remotely sensed data to provide information concerning croplands as model inputs research was directed towards a comparison of several methodologies which employed remotely sensed data, and conventional ground survey techniques. This research documented

both the relative and absolute accuracy as well as the cost-effectiveness of inventorying croplands by:

1. Conventional cropland inventory
2. Highlight 1:125,000 methodology
3. LANDSAT 1:1,000,000 methodology
 - a. Multiband/multidate optical enlargement
 - b. Multiband/multidate color composites, optically enlarged.

Ground truth information employed in the assessment of the interpretation accuracies associated with this portion of our research were compiled by the Lost Hills 31,036 hec (76,691 acres), Semitropic 90,649 hec (224,000 acres), and Wheeler Ridge-Maricopa 62,847 hec (155,300 acres) Water Storage Districts located in Kern County (see Figure 3 for district boundaries). The districts determined the August, 1974, condition of fields (cropland or non-cropland) by terrestrial examination. These data, although recognized as having their own variance, served as a control against which the remote sensing methodologies were tested for accuracy.

Individual water district costs associated with the acquisition of the terrestrial cropland data are summarized in Table III. The total estimated cost for conducting this 184,533 hec (456,000 acre) inventory for all three districts comes to \$3,000 and requires 6 weeks to implement. At this rate the cost for inventorying each 4,047 hec (10,000 acre) of cropland is approximately \$66.00.

The California Department of Water Resources (DWR) has estimated that a croplands survey of Kern County could be undertaken for approximately \$5,000. This would require the assessment of over 647,496 hec (1,600,000 acre) potentially irrigable acres of land to ascertain whether each acre is currently cropland or non-cropland (in the case of Kern County basically irrigated vs. non-irrigated). Thus, the DWR croplands inventory cost, utilizing oblique color aerial photography (35mm) and some ground truth, is estimated to be \$31.25 per 4,047 hec (10,000 acre). Therefore, the cost would be \$1424 for DWR to inventory the 456,000 acres in the three water districts under investigation.

Croplands Inventory Utilizing Highlight 1:125,000 Color Infrared Photography. To assure a uniform scale in the highlight cropland inventory maps generated for KCWA, mapped data is transferred to an acetate copy of a photogrammetrically controlled 1:125,000 basemap. These maps include all nodal and section boundaries in the valley portion of Kern County. As the 1:125,000 highlight image scale corresponds almost exactly with the 1:125,000 basemap the visual transfer of cropland detail can be accomplished with relative ease and without ancillary equipment. A majority of field boundaries and roads follow section lines. Whenever a variation between photo and map scale exists, such as that introduced by geometric distortions away from the nadir, the photograph (or map) can be adjusted on a section by section basis. Normally, realignment is necessary only every few townships if the major portion of the area under investigation is in the central portion of the photography.

As would be expected the primary object recognition feature for identifying croplands is the magenta signature expressed for healthy vegetation; however, hue may vary from dark to light in agricultural production areas depending upon the stage of the phenological cycle that a specific crop is in. The optimum date for utilizing highlight photography for croplands inventories in Kern County

has now been documented as being August, which is the height of the growing season. A minor problem which exists with respect to the application of single data high-flight photography has been that abandoned fields are often difficult to differentiate from fallow fields. In addition, uniform grasslands completely enclosed by croplands are at times misinterpreted as irrigated crops.

Table IV illustrates that for the 184,533 hec (456,000 acre) in the three Water Districts studied, the highflight croplands inventory had a mean relative and absolute error of 1.47% and 2.82% respectively. This means by utilizing high-flight photography to acquire cropland data on a spatial nodal basis, that out of 116,833 hec (288,701 acre) classified as being cropland greater than 97% of these lands were correctly inventoried.

The cost for acquiring croplands data by CIR highflight imagery is cost-effective when compared to terrestrial conventional methods. By referring to Table III it can be seen that for each 4047 hec (10,000 acre) inventoried the cost is approximately \$.87 per 4047 hec (10,000 acre). The \$40.00 it cost to acquire remotely sensed cropland data for the three districts represents only 1.3% of the \$3000 cost incurred by the water storage districts inventory. Time required for the GRSU to complete this three district analysis is minimal (only 8 hours). Each district requires a maximum of only three 9" X 9" transparencies which are at the same scale as the basemap. Despite the high accuracies and cost effectiveness of inventoring croplands with highflight imagery which we indicate here it must be kept in mind that this analysis does not take into consideration the cost of aircraft mobilization or image acquisition.

Croplands Inventory Utilizing LANDSAT 1:1,000,000 Multiband (Bands 5 and 7), Multidate Optical Enlargement Techniques. Several problems encountered with the highflight 1:125,000 technique are solved by using LANDSAT scale imagery, with no loss in accuracy. For example, the problem of acquiring multidate imagery of a specific study area is simplified because LANDSAT type imagery is currently available at 9-day intervals for all the earth's croplands. Atmospheric conditions permitting, user agencies can now acquire sufficient imagery throughout the year to conduct a cost-effective cropland inventory. The synoptic view and greater geographic coverage (109 X 109 nautical miles) per frame is a further benefit as a greater amount of land can be inventoried on a single frame resulting in a smaller expenditure for imagery. Of particular importance is the multiband (4, 5, 6, 7) capability of multispectral scanner data which allows the user to choose those bands best suited to detecting cropland in a particular environmental study area.

Copies of a 1:125,000 scale basemap of the three districts were produced and distributed to interpreters. By using an optical enlarging instrument each interpreter was instructed to inventory the croplands of the three districts separately. Each interpreter utilized the same 5 dates, which were previously determined as being optimum in terms of resolution, percent cloud cover, and date in the phenological cycle. By utilizing an optical enlarging instrument the interpreter can simultaneously view a single data (single band) of LANDSAT imagery and the 1:125,000 basemap. For each date of imagery a separate analysis of cropland acreage was recorded. A composite map of the 5 single overlays was then generated with the most recent data of imagery being used as the data base and all data discrepancies between this and earlier dates being carefully analyzed. In this manner a composite LANDSAT cropland map was generated by each interpreter

for each district and these maps were compared against the ground truth district maps to assess interpretation accuracy. The results in Table IV represent the mean cropland/non-cropland acreage estimates for interpreters involved in the inventory of each district.

The mean relative error for LANDSAT cropland inventories was found to be less than 1%, while the mean absolute error was less than 2%. This is significant because even though the scale has been decreased and resolution degraded when compared to highflight 1:125,000 imagery, the LANDSAT technique is capable of achieving better relative and absolute accuracies of 99% and 98% respectively. The interpreters involved in this research attribute this to the multidate capacity of LANDSAT to provide good resolution for many dates throughout the growing season. Also, band 5 (.6 - .7 μm) was judged the optimum spectral region for the analysis as it imaged plant agricultural fields as being dark against a lighter background, thus facilitating both the process of interpretation and transfer of detail.

By analyzing Table III it can be seen that the costs associated with inventorying the three districts via LANDSAT overlays is approximately \$82.50 or \$1.81 per 4047 hec (10,000 acre). The relatively higher cost per district for this type of inventory compared to highflight is due to the longer time required to compile the 15 separate overlay maps, with the mean time per date (single band) for creating an overlay being 1 hour. Certainly more dates (single band) could be interpreted to develop the composites but to acquire a 1% increase in accuracy would require a 50% increase in interpretation time and costs. The GRSU feels that a 5 band LANDSAT composite costing only \$1.81 per 10,000 acres at 98% absolute accuracy is sufficiently cost-effective for most cropland inventory user needs.

Croplands Inventory Utilizing Multidate, Multiband Color-Combined LANDSAT Imagery. After some initial experimentation it was found that when band 5 and 7 of a single or multiple date of LANDSAT imagery are color combined (band 5 filtered with a green filter and band 7 with a red filter) that a color combination takes place which facilitates the interpretation of croplands. In many situations band 5 and band 7 image the reciprocal signature of one another with respect to agriculture or other forms of vegetation. Agricultural cropland usually registers as dense (dark) on band 5 and transparent (approaching clear) on band 7. The following example will serve to explain the significance of this band 5 and 7 dichotomy as it relates to color combining. When color film is exposed through a green filter with band 5 back-lit by white light, the opacity of an agricultural field will allow very little green light to expose the negative. Conversely, when the same field in band 7 is registered in the exact location, back lighted, and exposed through a red filter, the transparency (less dense) of the field will allow the transmission of red light. This will expose the emulsion with red light and create a dark red image when the latent image is chemically processed. When the signature of a field is mid-gray in density on either band 5 or 7 then various hues of green-yellow-red are created. By carefully training with the known color combined signature of bare soil, fallow and cropped fields it is possible to identify these conditions with considerable accuracy. The image interpreters were also given a 3-color composite and trained to interpret signatures for bare soil, fallow and cropped lands.

Separate overlays were made for each color composite with a final cropland map for each district being a synthesis of the three maps. By examining Table IV it is apparent that the color-composite cropland relative and absolute accuracies

compare favorably with the highlight methodology while the non-cropland accuracies are the poorest of the methods tested. In effect, the 3.78% absolute error for non-croplands means that the interpreter assessed several fields as non-cropland while the district field crews identified them as cropland. GRSU believes that the reason for this misinterpretation may be due to two factors. First, the dates chosen may not be the optimum color combinations for inventorying croplands in this region. This may be the case even though the particular dates employed were chosen, initially, because of their high accuracy when used in the LANDSAT black and white analysis. Additional research may identify certain dates which when color composited yield a more optimum enhancement. Secondly, although interpreters were trained as to what each specific color should represent, there was some ambiguity at certain times as to what color the interpreter was actually viewing. This we believe led to errors at the cropland/natural vegetation interface where most of the interpretation errors associated with this test seemed to be concentrated (specifically, near the saline and perched water drainage areas). In several instances it was found that for the 2-color composites a greenish-red hue could systematically be misinterpreted by several interpreters when the value (tone) is very light.

In terms of cost, the color composite methodology lies midway between the highlight and LANDSAT black and white inventories. Table III illustrated that the color composite inventory was \$1.48 per 4047 hec (10,000 acre) or \$67.50 for the entire 184,533 hec (455,991 acre) of the three combined districts.

Croplands Inventory and a Summary. In terms of overall mean relative and absolute accuracy, the LANDSAT multidate, multiband black and white analysis yielded the best results, 98% accuracy. The highlight method is a serious alternative which can be very accurate if coverage is available for a specific study area. The LANDSAT color combined estimate fell somewhat short of GRSU's expectations in terms of absolute accuracy which may in reality be to some extent a function of the dates selected for this investigation. Nevertheless, when all three techniques are compared together at no point do the mean relative or absolute accuracies fall below 96% (Table IV).

The remote sensing croplands inventories documented are cost-effective (Table III). Compared to the \$31-66 cost per 4047 hec (10,000 acre) for the DWR and Water District cropland inventories, the highlight and LANDSAT inventories required only 2-4% of this amount; \$.87-1.81 per 4047 hec (10,000 acre). The mean time for the DWR and Water District inventories was 235 hours while the remote sensing inventories required only 12 hours. This represents a 95% reduction in time when croplands are inventoried using highlight or LANDSAT techniques.

AGRICULTURAL WATER DEMAND PREDICTION

The Kern County hydrologic system is complex and dynamic. The most dynamic element of this system is irrigation water applied to agricultural lands. This water may either be pumped from local groundwater basins, decreasing groundwater levels, or imported from other regions, thus increasing groundwater levels. At present, approximately 1,418,525,000 m³ (1,150,000 acre-feet) of water is imported yearly through state and federal projects. The exact amount of ground-water pumpage is not known, nor is the total amount of irrigation water applied to

the land. Estimates of these amounts are needed as inputs to periodically verify the KCWA hydrologic model.

As will be seen below, the most generalized method of estimating the total amount of irrigation water is to multiply the amount of irrigated cropland acreage by an empirically derived county-wide average application rate. A more specialized and more accurate procedure involves the utilization of the individual irrigation rates of different crops. In this method the amount of irrigated acreage for each crop is multiplied by each crop's specific irrigation rate (see Table V), which are derived empirically through the observation of test plots. This results in crop-specific water demand predictions. The water demand estimates of each of the crops are then totaled to produce the total water demand prediction. After estimating the total water demand the amount of ground basin pumpage can be calculated by subtracting the amount of imported water from the total demand.

A wide spectrum of techniques have been investigated to generate agricultural water demand predictions (see Figure 4). The procedures vary according to the generality of the data inputs. The most generalized method utilizes a county-wide average irrigation rate which is applied over several successive years to district-wide cropland acreage values. On the other end of the spectrum, the most specific procedure applies crop-specific irrigation rates to crop-type acreages, which have been measured annually on a nodal basis. The GRSU is investigating selected procedures from this range of possible techniques in order to determine and develop optimum procedures.

Water Demand Prediction Based on Cropland Data. This study was focused on the Lost Hills Water District in Kern County. This district is advantageous for study because it is dependent on imported water for its irrigation; i.e., no ground-water pumpage is known to occur. The total amount of irrigation water used can thus be determined by examining canal records. This allows the district to be used as a test area for methods of predicting total water demand.

As previously stated the most fundamental method being investigated by the GRSU entails the multiplication of the number of cropland acres by a county-wide average irrigation rate. This irrigation rate, 3.38 acre-feet/gross acre, has been derived from county-wide data on crop-type acreages and crop-specific average irrigation rates (based on 1969 data). The cropland acreage values used in this analysis have been obtained through the croplands mapping techniques discussed earlier in this paper. GRSU personnel have mapped and measured cropland acreages in each Lost Hills node for the years 1971, 1972, 1973, and 1974. These acreage values have been multiplied by average irrigation rates to yield water demand predictions for each node for the years 1971 through 1974 (see Table VI).

The district-wide mean error for all years examined is 38%, an unacceptable level to be of much use for the model. The predictions are consistently over-estimations, suggesting that a corrective estimator ratio could be calculated and applied to reduce the known bias. Such values have been obtained (Estes, et al., 1974) but as estimator ratios can only be calculated with knowledge of the total amount of applied water (such as that available for Lost Hills from canal records) such an approach would involve a great deal of field investigations to determine the amount of groundwater pumpage to be added to the amount of canal water applied. An alternative approach is discussed below.

Water Demand Prediction Based on Crop Type Data. The crop pattern in Lost Hills is continually changing, as is the average irrigation rate (Figure 5). Assuming that there is a trend in this change, a decrease in water demand prediction accuracy would be expected as the average irrigation rate being applied becomes increasingly outdated. Although an invariable trend in the change in crop pattern or average irrigation rates does not exist, Table VI does reveal a general decline in accuracy as the 1969 average irrigation rate becomes increasingly out-of-date. The use of crop type acreages presented in Figure 5 and their respective application rates results in refined water demand predictions, as shown in Table VII. The mean district-wide error of 8.6% for all years examined is considered tolerable for model input data, especially when the canal records against which the predictions are compared is known to have its own variance of up to $\pm 5\%$.

The preliminary results of GRSU research into water demand prediction procedures are encouraging. Accuracies of the district water demand predictions generally exceed 90%. However, some initial nodal results show large variations in accuracy. Although the crop breakdown and acreages in a node are probably the most important factor determining its water demand, there are many other factors which have to be considered. The GRSU is presently investigating the importance of agricultural practices such as land preparation, fallowing and dry-farming. These activities can be misinterpreted on highflight photography as irrigated agriculture, thus causing water demand estimations to be too large in the nodes where these activities occur. It is expected that mapping procedures using multi-date LANDSAT imagery will generally eliminate this problem. The GRSU is also investigating the possible occurrence of groundwater pumpage. If groundwater pumping is occurring in any of the Lost Hills nodes, this will directly affect our accuracy values for that node.

Inclusion of such factors which have varying effects on different nodes in a water demand prediction procedure is expected to produce nodal predictions which are more accurate and consistent than previously obtainable. GRSU research will continue to focus on consideration of these factors and on the refinement of prediction techniques to operate on a nodal scale in the Lost Hills and other Kern County Water Districts.

SALINITY

The Kern County area has salinity problems common to many arid environments. Under humid conditions soluble salts originally present in soil materials and those formed by the weathering of minerals are generally leached downward into the groundwater and ultimately transported by streams to oceans. Saline soils are therefore practically nonexistent in humid regions. Although weathering of primary minerals is the indirect source of nearly all soluble salts, there are few instances where sufficient salts have accumulated from this source alone to form a saline soil. Instead, saline soils generally occur in areas that receive salts from other locations with surface groundwater as the primary carrier. Large quantities of soluble salts may be added to irrigated soils over relatively short periods of time. In Kern County considerable expense has been taken to route irrigation water onto the lands; presently, however, only minimal consideration has been directed toward the removal of saline drainage water from the trough, lowland areas. In many arid regions, when bringing new lands under irrigation, farmers have frequently failed to recognize the need for establishing artificial drains to care for the additional water and soluble salts.

In any effective land management program in an arid region the salinity variable must be given significant attention, especially in regards to water resource management. For an effective management plan to be developed an accurate inventory of the areal distribution of saline soils is needed. However, the most recent county-wide soil survey for Kern County was conducted over 12 years ago by the Department of Water Resources and is in need of revision in terms of the locational expansion of saline-alkali soils.

A major responsibility of the KCWA is to inform its water users concerning preventative water management techniques. KCWA dispurses information to users concerning techniques such as tiling, leaching and drainage to improve soil productivity. In conjunction with these activities, KCWA requires data which will serve the following purposes:

1. Locate these agricultural areas that are, at present suffering the most severe salinity related stress. Such areas would be designated as priority areas in terms of the application of leaching and/or drainage water management measures.
2. Plot the distribution of salt damaged areas in relation to topographic relief, soils, geology, and proximity to natural drainage channels. Such data will enable KCWA to select the optimum locations for a series of lateral drains that will be designed in such a manner as to alleviate both the perched water and salinity problems for many years.
3. Provide soil salinity data on a nodal basis which will serve as input to the KCWA Hydrologic Model.
4. Finally, as additional information, KCWA and other agencies would like to locate those areas of natural vegetation that are not in cropland because of excessive concentrations of salts but which could be brought into production if proper leaching and drainage practices were implemented. In Kern County every acre of land brought into production generates, on the average, an income of approximately \$800 per year. (The crop value of a section of land would therefore be approximately \$500,000).

KCWA requested that the GRSU identify areas of salinity stress within our study area. Based upon this request a salinity damage map was produced. This information is being used by KCWA as justification for the reactivation of a Central Valley master drain proposal.

To compile the salinity damage map (Figure 6) trained image interpreters were assigned the task of identifying and mapping those agricultural areas of Kern County which were undergoing salinity stress. This interpretation was made from multirate CIR 1:125,000 scale photography with April, 1974 being the most recent date of imagery employed in the analysis. Interpreters identified, on a field-by-field basis, the percentage of each field that expressed salinity stress. This analysis included damage to croplands as well as areas of natural vegetation. It is acknowledged that the stress categorized as salinity damage may in reality be due to other factors, e.g., improper water application procedures, disease, etc.; however, salinity damage represents the major agent for yield decrement in Kern County and produces highly diagnostic stress signatures.

Interpreters used two major surrogates to aid in the identification of the salinity stressed fields: native vegetation and crop cover. Many areas of natural vegetation are covered by extensive caliche deposits. There is no question regarding the salinity of these areas which typically show up in the 50-100% category on the damage map. In several areas of natural vegetation, however, the presence of halophytic vegetation created an interpretation problem by masking the true salinity condition. It was found that this problem could be overcome by field checking and by exploiting the fact that in Kern County naturally vegetated areas tended to be nucleated in areal extent. GRSU personnel have done extensive field sampling in these areas of native vegetation/caliche and are confident of their interpretation.

The second and major method of identifying salinity stress was to examine the agricultural crop cover. Multirate imagery analysis techniques were used to assure the presence of crops in most fields. Hot-spot scalding, caliche deposits, and a mottled appearance of the crop cover represented the major image interpretation surrogates used to detect salinity damage. The ability of interpreters to identify and accurately classify those areas undergoing salinity stress was possible owing largely to the program of interpreter training based on extensive ground truthing undertaken by GRSU personnel. Five transects with the known crop type, soil type, and salinity data allowed the interpreters to use this regional information to train their manual classification procedure. It is significant to note that in many instances a field may be excessively saline but with a salt tolerant crop growing on it, e.g., cotton, the field may show only moderate damage. However, if a nontolerant crop, e.g., beans, were to be planted on the same field it should register more extensive damage. This characteristic will be considered in more detail in the salinity prediction discussion.

Probably the greatest handicap encountered in compiling the Kern County Soil Salinity Map was the interpretation of salinity damage for bare soil agricultural fields. As might be expected there are optimum time periods throughout the year when a maximum percentage of the fields in Kern County are being cultivated and have crop cover. For Kern County this has been determined to be the month of August. It has also been concluded that the best time for determining salinity stress was in the early stages of the phenological cycle. The relatively young fields do not possess a coalescing canopy of vegetation complete enough to

mask the effects of salinity.

At present the greatest problem encountered is the point sampling methodology used to gather ground truthed salinity values. In Figure 7 it is evident that the correlation between the damage class and the actual point salinity values is not consistent. Examination of the 50-100% damage class shows that actual field sampled salinity values as low as 0.2 (Ece) have been classified in this category. Although a general increasing trend exists from the lower to higher damage classes, the extreme overlap of the higher damage classes upon the lower classes (especially in the lower soil salinity values, where all damage classes include salinity values ≤ 1 mmhos/cm Ece) was not expected. Field sampling to date suggests that this is the result of the variable distribution of salinity.

As part of our continuing effort to evaluate the nature, extent, and variability of salinity distributions and their associated problems, GRSU has recently undertaken an intensive field sampling effort in a limited geographic region. To date, 13 fields, each approximately 65 hec (160 acres) in size, have been intensively sampled. Figure 8 depicts one of these intensively sampled fields and shows the wide variation of salinity values that can be found within a single field. In this particular example the mean salinity value for all samples taken is 7.2 mmhos Ece, while individual readings range from 0.6 to 47.0 mmhos. One purpose of this intensive sampling is to accurately document field salinity distributions in such a manner that a sampling methodology can be developed making optimum use of field investigation efforts. An even more important use of this data is its input into a remote sensing methodology that presently appears capable of predicting field average soil salinities within our study area by using crop damage as a surrogate.

Based on this investigation it has become clear that the point samples for ground control fields should be clearly identified and annotated on enlarged imagery prior or during the actual soil sampling. In this manner fields can be systematically sampled in both damaged and non-damaged regions to determine the best average salinity value to be used for the particular field to develop a correlation between damage, crop type, yield and salinity value.

The image interpreters did not use sample salinity values to determine damage classes. Each field was analyzed individually to determine the percent of visible damage present. Another method of assessing the accuracy of the percent damage map is to compare this areal analysis with some other areally dimensioned data, such as soil type. Soil type classifications are typically general in nature. Table VIII plots the four major soil types found along Highway 119 and the number of times a particular damage class was assigned to each soil type. Upon inspection 59% of the samples taken in Tx-PH (a typically high saline soil) were classified by the interpreter as being red (50-100% damage). Similarly, 21-47% of these samples taken within the Cd-TD (a low potential saline soil) region were found to exhibit green and blue (0-25%) damage. When one considers that almost 75% of the 25-100% damage occurs in Tx-PH soil, which has the highest potential for salinity, the interpreter is certainly approaching an acceptable standard of classification accuracy. Present research activities include the documentation of these accuracies.

CONCLUSIONS

Agricultural cropland inventories utilizing both high altitude photography and LANDSAT imagery can be conducted cost-effectively (less than \$1.50 per 4047 hec (10,000 acre)) with 98% accuracy. By using county-wide average irrigation application rates and the cropland data an estimate of agricultural water demand can be generated as input to the model. Such an estimate may have a large variance from the actual amount of applied water (Lost Hills district-wide mean error of 38%). However, a more accurate estimate (Lost Hills district-wide mean error 8.6%) of water demand is possible by determining crop type acreages and applying crop specific application rates.

The existence of saline-alkali soils in the study area affect crop yield and water demand. KCWA must identify and assess the distribution of the saline-alkali environment if an effective water management program is to be implemented. GRSU first identified the dimension of the saline-alkali agricultural damage based on photo interpretation and extensive ground truth. Recently, however, a quantitative procedure for assessing salinity damage based on field tonal (density) values has been developed which is highly correlated ($r=.76$) with field average electrical conductivity salinity values.

At this time, GRSU is also conducting research towards the detection and delineation of water tables that are "perched" near the surface by semi-permeable clay layers as another potential application of remote sensing input to the KCWA ground-basin model. Nearly 14,974 hec (37,000 acres) of this arid environment have perched water within 10 feet. The GRSU has investigated both high altitude color infrared photography and LANDSAT multispectral imagery to determine their utility for this task. The use of thermal infrared imagery for this problem is also being investigated. In the near future GRSU personnel will also begin to examine the potential of remote sensing to provide KCWA with information concerning areas of equal benefit for tax purposes. Recently, the KCWA hydrologic model has been adapted to delineate zones of equal benefits resulting from KCWA activities. This information is being developed to provide taxation schedules in an attempt to insure that those who benefit from water management policies will pay accordingly. The zones of equal benefit taxation schedules are based upon the following principles:

- * Not all farmers in the region managed by the KCWA are involved in or pay for KCWA activities. These activities include the importation of water, the transfer of water from one water district to another, and the recharging of groundwater.
- * By raising the groundwater level, these activities benefit non-participants as well as participants.
- * Accordingly, the fairest taxation schedule should incorporate these benefits and be applied to non-participants as well as participants.

As this type of taxation is new it is easy to appreciate that KCWA is hesitant to apply it until it has confidence that the model will withstand any legal challenge to its validity. This application again underscores the importance of accurate and timely model input data.

Finally, specific determinations as to the overall benefits that accrue by using remote sensing techniques are difficult to make principally because the KCWA model is still in an advanced developmental state. Therefore, a fixed set of input

data, with specific associated costs for all parameters, is not as yet available. However, it is hoped that in the near future it will become possible to operate the model in two modes, one with strictly conventionally gathered data and the other augmented by remote sensing data. This should allow some estimate to be made as to the sensitivity of the model to various accuracies of remotely sensed data and permit us to analyze the economic impact resulting from changes in the estimation of critical parameters.

Although our research in this area is, in essence, just beginning to reach a productive stage the magnitude of potential benefits is readily apparent. There are currently about 900,000 acres under irrigation in Kern County out of 1,600,000 potentially irrigable acres. The countywide crop value for a section of land³ (640 acres) is approximately \$500,000 (\$800 crop value/acre x 640 acres/section). Therefore, in principle, for each 1% of increased efficiency in the application of irrigation waters that results from the use of the hydrologic model, approximately 12.5 additional sections can be brought into production. An addition of this magnitude would represent a crop value of approximately \$6,250,000.

At the present time, Kern County is overdrafting its groundwater basin. Even with the maximum supplies of imported water contracted for in 1990 (the demand for which will be realized in 1980) Kern County will be overdrafting its basin if irrigated agricultural lands are expanded beyond their present areal extent. The situation is critical and the potential benefits which may occur as a result of increased efficiencies derived through the utilization of remote sensing techniques can be significant.

³ This is an estimate of the 1974 crop value per acre based on a projection from the 1973 crop value per acre rate of \$720.

REFERENCES

Estes, J. E., et al., 1973-1975, "Chapter 3: Water Demand, The Utilization of Remote Sensing Techniques for the Generation of Input Data for Water Demand Prediction," An Integrated Study of Earth Resources in the State of California Using Remote Sensing Techniques, University of California, Space Sciences Laboratory, December 30, 1973, NASA Grant NGL 404-S-3; April 30, 1974, NASA NGL 404-S5, December 30, 1974, NASA NGL 404-S5, April 30, 1975, NASA NGL 404-S5.

Kern County Agricultural Commissioner, "Agricultural Crop Report, County of Kern," 1973.

Tinney, Larry R., et al., "Operational Use of Satellite and High Altitude Remote Sensing for Generation of Input Data for Water Demand Models." Proceedings of the Ninth International Symposium on Remote Sensing of Environment, Ann Arbor, Michigan, April 1974.

U.S. Department of Agriculture, Diagnosis and Improvement of Saline and Alkali Soils, Agriculture Handbook No. 6, Washington D.C., 1969.

TABLE I

KERN COUNTY WATER AGENCY: WATER ACCOUNTING

External Quantities	Definition	Source(s)	Possible Application of Remote Sensing (Identify and/or Measure)
<u>Agriculture usage</u> gross irrigated acres	total amount of irrigated acreage	periodic air surveys, modified in districts	irrigated lands
unit agricultural consumptive use	acre-feet per acre irrigation requirement by individual crops for evapotranspiration	Department of Water Resources, experimentation with individual crops	crop type
irrigation efficiency	that percent of applied water that is evaporated or transpired	Iowa State University experimentation, by crops	agricultural lands and crop type
consumptive use by agriculture	water taken out of inventory by total evapotranspiration	summation of nodal consumptive use	
<u>Municipal & Industrial Usage</u>			
population x per capita factor (Unit cu)	population by node	cens. data, modified by planning projections	population estimation
percent of node in municipality	that percent of node within a municipality	computed from crop surveys	urban areas
Unit demand	acre-feet per person per year	Bakersfield and Kern County historical usage rates	
consumptive use	per cent of water considered consumed by municipal & industrial users	statistical analysis	

TABLE I - Continued

External Quantities	Definition	Source(s)	Possible Application of Remote Sensing (Identify and/or Measure)
<u>Municipal & Industrial Usage - Cont.</u> percent deep percolation	percent of municipal & industrially used water that becomes deep percolated	(varies from node to node - input from septic tanks, sewers, lawns, etc.)	
percent sewerage	percent of municipal & industrial water delivered to sewage treatment plants	sewage treatment plant records	
percent sewerage applied	sewage treatment plant effluent applied to crops	sewage treatment plant records	
oil field waste applied	oil field waste water applied to crops	oil company records or computed from crop survey	oil sumps
<u>Recreational Usage</u>	irrigated areas primarily devoted to recreation (duck clubs, etc.)	aerial photographs	recreational areas by types
unit recreational consumptive use	acre-feet used per acre	previous records of usage rates	
<u>Surface & Groundwater Movement</u>	water exported outside node (via pipeline or canal)	of record, water district and oil company records	
exports by source			

TABLE I - Continued

External Quantities	Definition	Source(s)	Possible Application of Remote Sensing (Identify and/or Measure)
<u>Surface & Groundwater Movement - Cont.</u>			
imports	water imported from out-side basin	of record, water district and oil company records	
conveyance loss, deep percolation, by source	losses via deep percolation of water moving in unlined canals	by observation and/or calculated (92 percent of total losses)	
total flow by source	total flow by source in streams and rivers, into modeled area	measured by flow gauges and/or calculated	
applied water by source	water put onto agricultural land	by inventory from Districts and Canal Company	
recharged water by source	water applied to a recharge basin to artificially recharge supply	by inventory from Districts and Canal Company	
unit effective precipitation	acre-feet of precipitation per acre that occurs during growing season (reduces required irrigation)	weather bureau records and crop calendar, modified by formula	areas covered by rain storms
volume of moisture	volume of unsaturated soil	calculated from field work (soil surveys)	soil moisture
percent of deep percolation to moisture deficient soil	percent of node overlying moisture deficient soil, nodal deep percolation	field investigation test holes, etc.	

TABLE I - Continued

External Quantities	Definition	Source(s)	Possible Application of Remote Sensing (Identify and/or Measure)
<u>Surface & Groundwater Movement - Cont.</u> percent to perched water table	percent of node overlying perched water table x nodal deep percolation	field investigations	perched water table area
evaporation by source	evaporation of spread or ponded water	prior experience; 5 percent of spread water lost (8% of total losses) 5'/yr. of ponded water	ponded water area
subsurface inflow from outside basin	underground input to balance nodes in verified period	trial and error with some mathematical control	
clay flow (in clay, castings, gravel and total)	estimated flow from upper aquifer to lower aquifer through well bore and gravel pack and through continuing clay layer	analysis of demand-applied with irrigation efficiencies	
agricultural pumpage	residual (demand-applied correction for irrigation efficiency)	municipal records	
municipal extractions	percent of a total municipal extraction from a particular node	soil surveys (in forebay area, no separation between upper and lower layer exists.)	
presence of lower layer	presence or absence of a separation between upper and lower soil layers		

TABLE I - Continued

External Quantities	Definition	Source(s)	Possible Application of Remote Sensing (Identify and/or Measure)
<p><u>Surface & Groundwater Movement - Cont.</u> percent pumped in lower layer</p>	<p>percent of pumpage (agricultural mainly) from lower layer</p>	<p>computed from well examinations</p>	
<p>lower layer extractions for export</p>	<p>total export from lower layer</p>	<p>examination of well data</p>	
<p>percent export pumped in lower layer</p>	<p>percent of nodal extraction from lower layer for export</p>	<p>export records and well examinations</p>	
<p>subsidence</p>	<p>amount of soil subsidences usually the result of water, oil, or gas extraction</p>	<p>measured in field, projected in time by rate</p>	<p>possibly by long-term repetitive low-flight imagery (comparative topography)</p>

TABLE II
 KERN COUNTY WATER AGENCY: CRITICAL WATER ACCOUNTING MODEL INPUTS AMENABLE
 TO REMOTE SENSING TECHNIQUES

EXTERNAL QUANTITIES	DEFINITION	SOURCE(S)	REMOTE SENSING CAPABILITIES (IDENTIFY - MEASURE)
<u>Agriculture Usage</u> gross irrigated acres	total amount of irrigated acreage	periodic air surveys, modified in districts	irrigated croplands
unit agricultural consumptive use	acre-feet per acre irrigation requirement by <u>individual crops</u>	Department of Water Resources, experimentation with individual crops	crop identification
<u>Surface & Groundwater Movement</u> volume of moisture deficient soil % to perched water table	volume of unsaturated soil % of node overlying perched water table x nodal deep percolation	calculated from field work (soil surveys) field investigations	soil moisture perched water table areas
<u>External Quantity not yet Incorporated into Model</u> soil salinity	salinity of soil as measured by electrical conductivity (Ece)	field investigations	salinity damage assessment, soil salinity prediction

TABLE III
THE COST-EFFECTIVENESS OF TERRESTRIAL VERSUS REMOTE SENSING TECHNIQUES FOR CROPLAND INVENTORIES

Cropland Mapping Agency (Technique)	Cost for Inventorying all 3 Districts	Total Hectares (Acres) in all 3 Districts Cost for each 4047 hec (10,000 acres)	Total Cropland Hectares (Acres) Inventoryed	Time Required to Inventory all 3 Districts
Department of Water Resources (DMR) (Lowflight & Terrestrial)	\$1,424 ^a	184,533 (455,991) \$31.25	116,833 (288,701) \$49.32	230 hrs. @ \$6.20 per hr.
GRSU - 3 Districts U-2 1:125,000 (Highflight Inventory)	\$40.00 ^a	184,533 (455,991) \$.87	118,067 (291,750) \$1.37	8 hrs. @ \$5.00 per hr. to compile basemap

^a Does not include aircraft mobilization or the cost of photography

TABLE III - Continued

Cropland Mapping Agency (Technique)	Cost for Inventorying all 3 Districts	Total Hectares (Acres) in all 3 Districts	Total Cropland Hectares (Acres) Inventoryed	Time Required to Inventory all 3 Districts
		Cost for each 4047 hec (10,000 acres)		
GRSU 3 Districts LANDSAT 1:1,000,000 (Multidate, Band 5 or 7)	\$82.50 ^a	184,533 (455,991) \$1.81	116,833 (288,701) \$2.85	16.5 hrs. @ \$5.00 ^b per hr.
GRSU - 3 Districts Color Composite LANDSAT 1:1,000,000 (Multidate, Multiband Color Composite Inventory)	\$67.50 ^a	184,533 (455,991) \$1.48	116,883 (288,701) \$2.35	13.5 hrs. @ \$5.00 ^c per hr.

a Does not include aircraft mobilization or the cost of photography

b Each district was inventoried by making 5 single date, single band (5 or 7) overlays and compositing these to form the cropland map. The dates examined required a mean interpretation time of 1 hour. Therefore, the three districts required a total of 15 separate LANDSAT maps @ 1 hour each totaling 16.5 hours.

c Each district was inventoried by making 3 cropland overlays from 3 different LANDSAT color composites. The color composites were produced by registering and photographically combining multiband and multiband images into a 2 or 3-color composite. The district map represented a composite of these 3 interpreted color composites. Therefore, the 3 districts required a total of 9 separate LANDSAT maps @ 1.5 hrs. each totaling 13.5 hours.

TABLE IV
 RELATIVE AND ABSOLUTE ACCURACY OF CROPLAND ACREAGE ESTIMATES AS DERIVED FROM HIGHFLIGHT
 PHOTOGRAPHY, MULTIDATE, MULTIBAND LANDSAT AND COLOR-COMBINED LANDSAT IMAGERY

Water District (Total Acres)	Water District Field Check		Highflight 1:125,000		(Band 5 and 7)		(Color Composite)	
	Cropland Hectares	Non-Cropland Hectares	Cropland Hectares	Non-Cropland Hectares	Cropland Hectares	Non-Cropland Hectares	Cropland Hectares	Non-Cropland Hectares
Lost Hills 31,036 hec (76,691 acres)	20438 (50504)	10597 (26187)	20611 (50930)	1042 (2576)	20288 (50134)	10747 (26557)	20681 (51105)	10354 (25586)
			.84% 995 (2360) 4.67%	1.63% 583 (1440) 5.5%	.74% 605 (1495) 2.96%	1.41% 92 (227) .86%	1.19% 809 (2000) 3.96%	2.29% 607 (1500) 5.72%
Semitropic 90,649 hec (224,000 acres)	50339 (124390)	40311 (99610)	50033 (123635)	40616 (100365)	49566 (122480)	41084 (101520)	49161 (121480)	41488 (102520)
			.61% 615 (1520) 1.22%	.75% 1714 (4235) 4.25%	1.54% 656 (1620) 1.3%	1.91% 1416 (3500) 3.51%	2.34% 935 (2310) 1.85%	2.92% 1549 (3827) 3.84%
Wheeler Ridge- Maricopa 62,847 hec (155,300 acres)	46056 (113807)	16792 (41493)	47423 (117185)	15425 (38115)	46290 (114385)	16558 (40915)	46547 (115020)	16301 (40280)
			2.96% 1192 (2945) 2.58%	.91% 170 (420) 1.01%	.51% 791 (1955) 1.71%	1.4% 263 (650) 1.56%	1.06% 1230 (3040) 2.67%	2.97% 299 (740) 1.78%
Total	116,833 (288,701)	67,700 (167,290)						
	\bar{X} relative error		1.47%	1.09%	.93%	1.57%	1.53%	2.72%
	\bar{X} absolute error		2.82%	3.58%	1.99%	1.97%	2.82%	3.78%

TABLE V - YEARLY CROP IRRIGATION REQUIREMENTS FOR KERN COUNTY
(AGRICULTURAL CROP REPORT, 1973, COUNTY OF KERN)

Crop	Yearly Requirement	Percent Total County Irrigated Acreage
Barley	1727 m ³ (1.4 acre-foot)	7%
Cotton	3207 m ³ (2.6 acre-foot)	32%
Alfalfa	4934 m ³ (4.0 acre-foot)	15%

TABLE VI - LOST HILLS WATER DISTRICT: WATER DEMAND PREDICTION USING THE KERN COUNTY AVERAGE IRRIGATION RATE AND CROPLAND ACREAGES.

	% Error			
	1971	1972	1973	1974
Node 2	+6%	+32%	+55%	+3%
Node 29	+24%	+8%	+11%	+36%
Node 30	+35%	+1%	+70%	+78%
District-Wide	+24%	+34%	+59%	+33%
Mean Error for All Years			+38%	

TABLE VII

ACCURACY OF WATER DEMAND ESTIMATIONS DERIVED USING ANNUAL

LOST HILLS DISTRICT CROP DATA Cu. M. (Acre-Feet)

	1969	1970	1971	1972	1973	1974
Predicted Water Demand	36,997,053 (29,994)	37,929,565 (30,750)	82,501,065 (66,892)	95,631,844 (77,530)	108,500,760 (87,963)	138,907,319 (112,614)
Actual Water Demand	36,511,061 (29,600)	39,630,537 (32,129)	91,271,485 (73,995)	106,956,440 (86,711)	126,308,536 (102,400)	155,698,181 (127,848)
Error	485,992 (394)	1,700,971 (1,379)	8,761,421 (7,103)	11,324,596 (9,181)	17,807,777 (14,437)	18,790,862 (15,234)
% Error	+1.3%	-4.3%	-9.6%	-10.6%	-14.1%	-11.9%
Mean Error for all Years	8.6%					

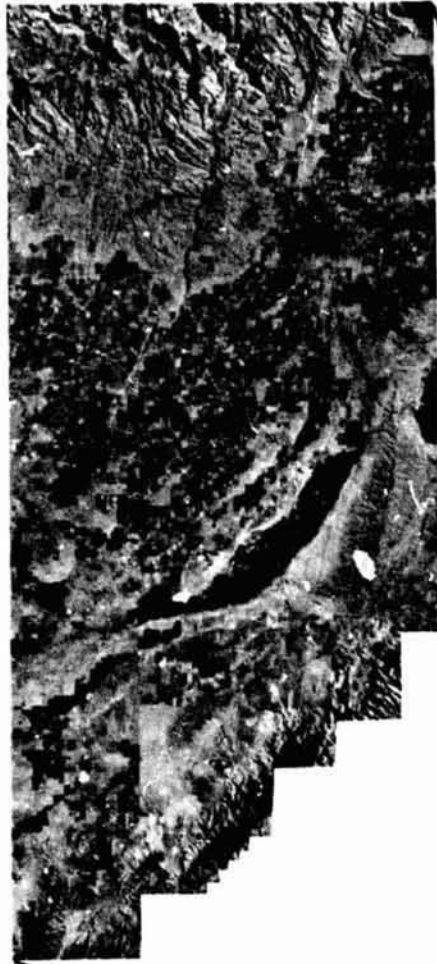
TABLE VIII

SOIL TYPES AND DAMAGE CLASSES FOR SALINITY SAMPLES ALONG
TRANSECT HIGHWAY 119

		SOIL TYPE			
		<u>High Salinity Potential</u>		<u>Low Salinity Potential</u>	
		Tx-PH	Gw-HL	HL-HD	Cd-Td
% SALINITY DAMAGE	RED 51-100%	(10) [*] <u>59%</u> ---	(12) <u>29%</u> ---	(7) <u>26%</u> ---	(2) 11%
	ORANGE 26-50%	(4) <u>24%</u> ---	(10) <u>24%</u> ---	(7) <u>26%</u> ---	(4) <u>21%</u> ---
	BLUE 6-25%	(2) 12%	(15) <u>36%</u> ---	(11) <u>41%</u> ---	(9) <u>47%</u> ---
	GREEN 0-5%	(1) 6%	(5) 12%	(2) 7%	(4) <u>21%</u> ---

* (10) = number of fields

UNIVERSITY OF CALIFORNIA AT SANTA BARBARA
WATER DEMAND STUDY AREA
IN KERN COUNTY, CALIFORNIA



WEST KERN COUNTY
LANDSAT-1, 2 JANUARY 73, BAND 6

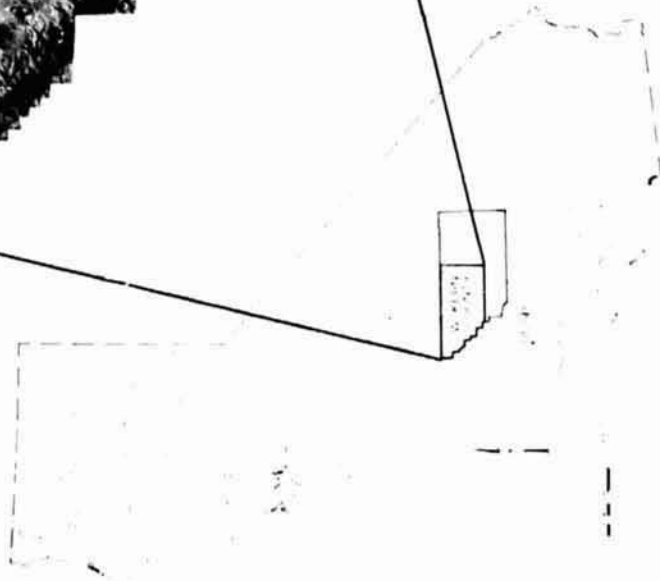


Figure 1. Locational map showing the University of California at Santa Barbara's water demand study area in Kern County, California. The insert depicts the major portion of cropland over which Kern County Water Agency (KCWA) has direct jurisdiction.

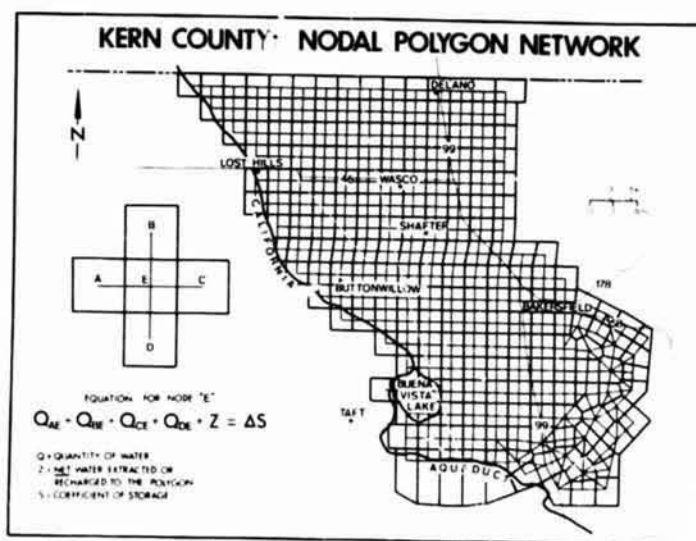


Figure 2. The nodal polygon network of the KCWA water accounting model.

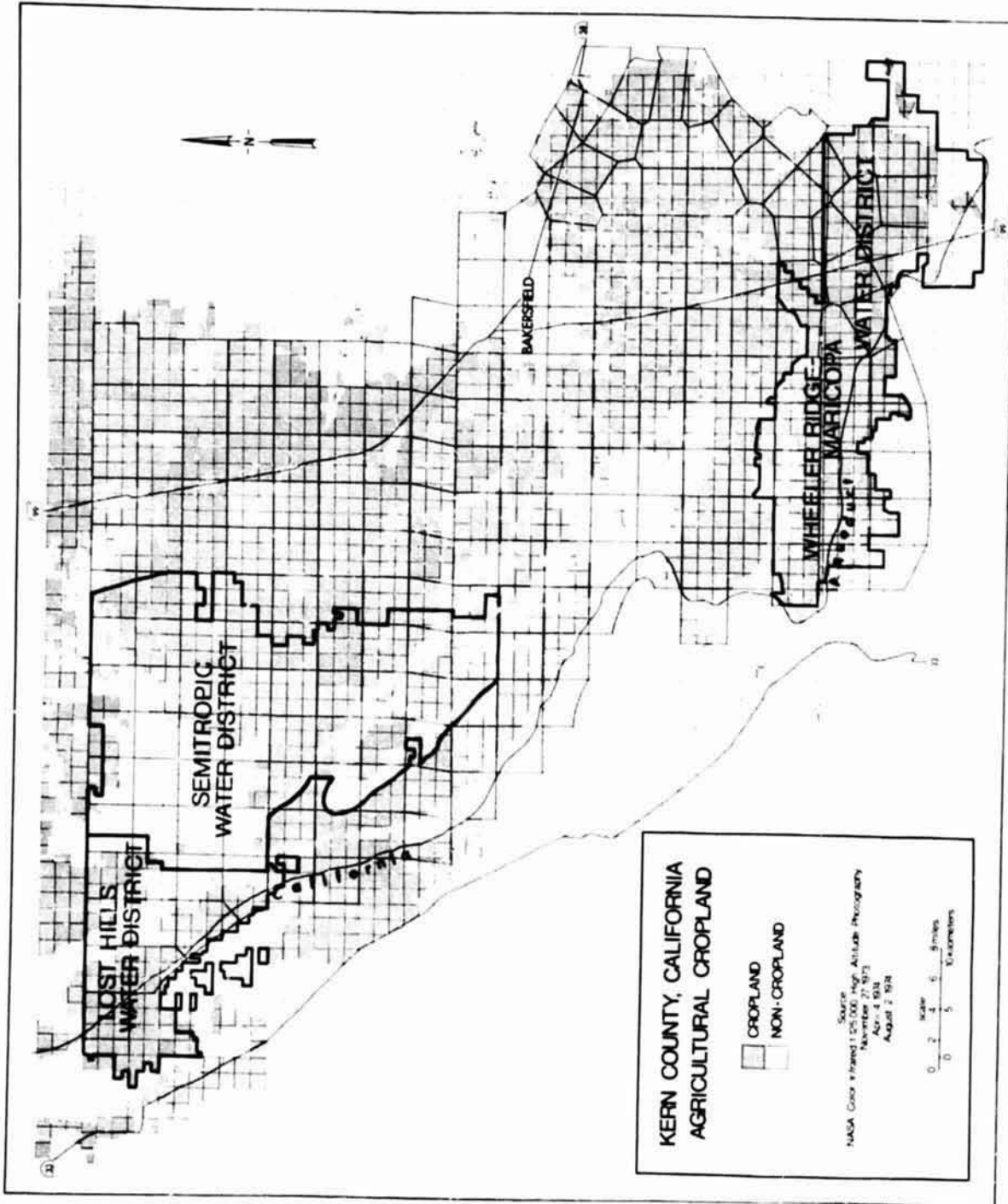


Figure 3. District boundaries for three Kern County water districts studied for cropland mapping.

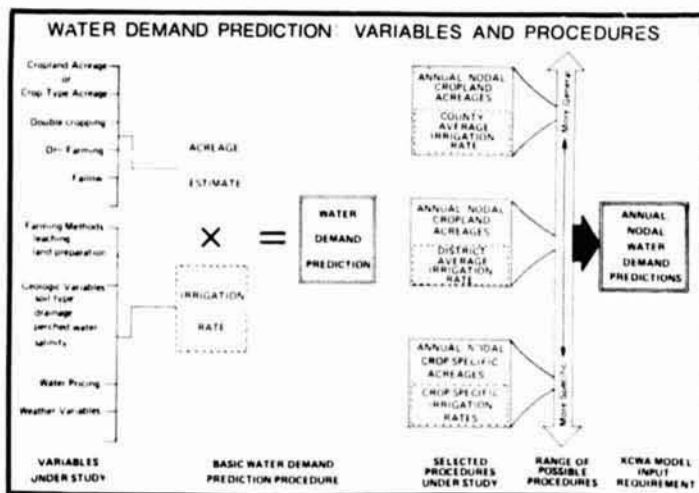
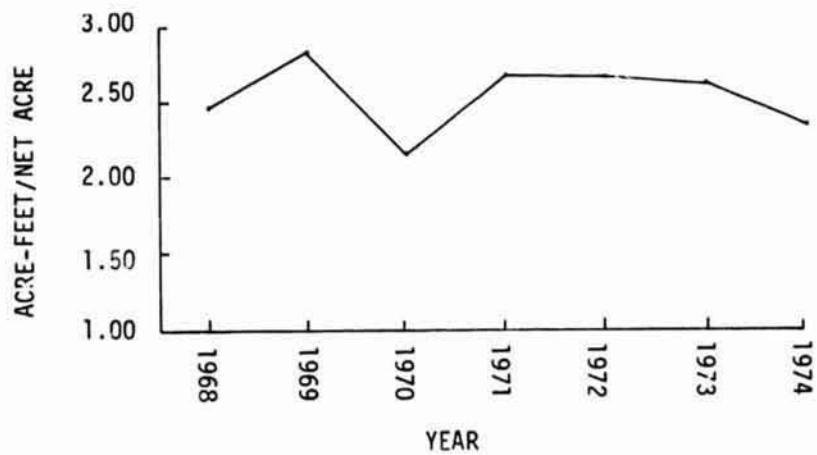


Figure 4. Water Demand Prediction. On the left is the basic water demand prediction procedure including listings of specific variables and the basic elements of the procedure. On the right is a range of possible prediction procedures (from general to specific) and the procedures selected by GRSU personnel to generate water demand predictions as required by the KCWA model.

LOST HILLS WATER DISTRICT
 AVERAGE IRRIGATION RATE 1968 - 1974



LOST HILLS WATER DISTRICT CROP BREAKDOWN 1968 - 1974
 (% of total cropland acreage)

CROP	1968	1969	1970	1971	1972	1973	1974
Alfalfa Hay	-	-	2%	2	4	4	5
Alfalfa Seed	1	29	22	7	-	-	-
Almonds	-	T	T	-	-	1	2
Barley	4	3	4	2	1	2	23
Beets	-	T	-	-	-	-	-
Black-eyes	5	-	T	-	-	T	-
Carrots	-	1	T	-	-	T	-
Cotton	30	27	33	45	61	65	48
Figs	1	2	2	1	1	1	1
Lettuce	-	T	-	-	-	T	1
Melons	-	3	1	-	-	-	-
Milo	40	18	-	-	T	-	T
Okra Seed	-	T	-	-	-	-	-
Olives	-*	1	14	17	16	14	9
Peppers	T	-	-	-	-	-	-
Pistachios	-	-	1	2	9	8	7
Potatoes	-	1	T	-	-	-	-
Safflower	-	4	-	-	-	-	-
Sugar Beets	5	6	19	22	4	-	-
Tomatoes	3	1	-	-	-	-	2
Vines	-	-	-	1	4	3	-
Watermelons	-	T	-	-	-	-	-
Wheat	-	3	2	1	-	T	2
Test Crops	-	T	-	-	-	-	-
Onions	-	-	-	-	-	-	T

* T = trace

Figure 5. Change in crop pattern and average irrigation rate for Lost Hills Water District, 1968 - 1974.

UNPRODUCTIVITY OF LAND
 GENERAL FERTILITY IS POOR

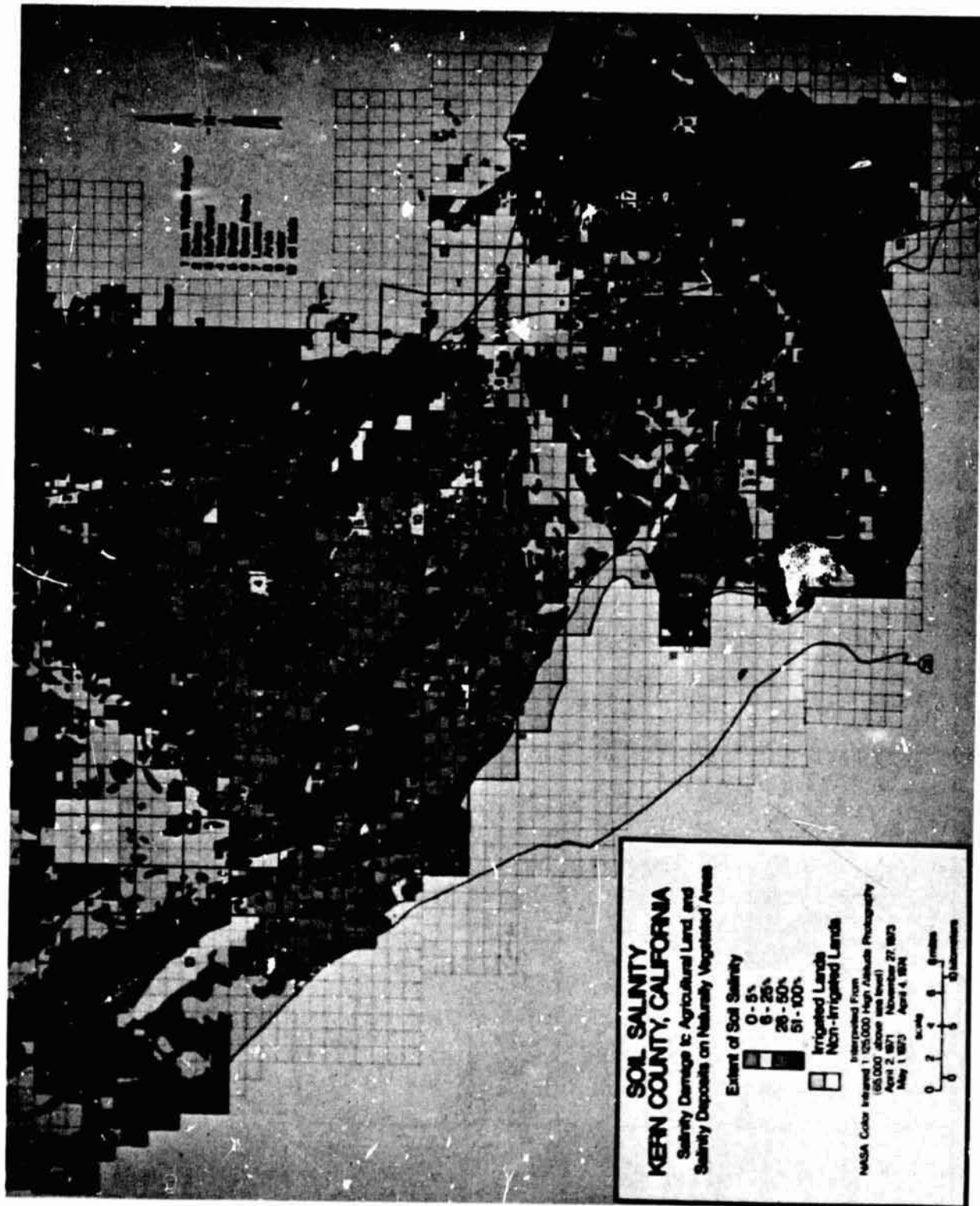


Figure 6. Salinity Damage Map of Kern County.

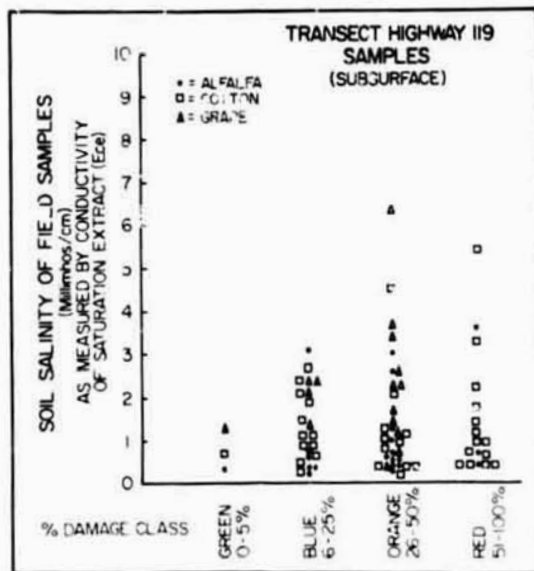


Figure 7. Subsurface soil salinity samples taken along transect Highway 119 and the corresponding damage classification.

REPRODUCIBILITY OF THE
ORIGINAL PAGE IS POOR

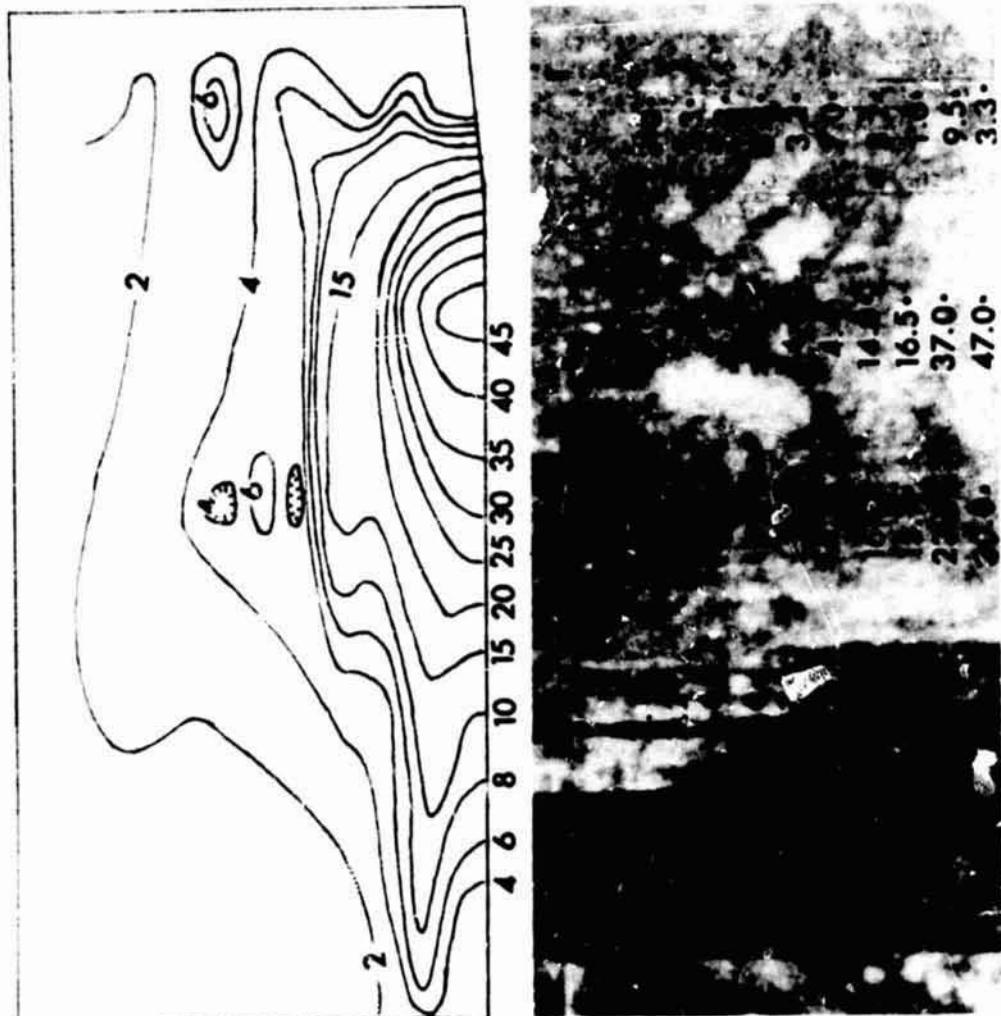


Figure 8. Salinity (Ece) contour map compiled from intensive point sampling of a cotton field in the Goose Lake area of Kern County.

AREAL EXTENT OF SNOW ESTIMATION IN THE NORTHERN SIERRA NEVADA
MOUNTAINS USING LANDSAT-1 IMAGERY

W-23

By Edwin F. Katibah, Remote Sensing Research Program,
University of California, Berkeley, California

ABSTRACT

N76-17609

Quantification of the surface area of snow covering watersheds is believed to be a useful parameter in estimating snow water content for inclusion in water runoff prediction equations. This paper documents an operational manual interpretation technique which allows fast and accurate estimates to be made of the areal extent of snow parameter using LANDSAT-1 imagery. The analysis procedures, the statistical results, and the associated costs of this research are presented.

INTRODUCTION

One of the most easily detected of all resources from Earth orbiting satellites is snow. Investigators have proposed that relationships could be developed between snow-cover depletion and water runoff (Leaf, 1969) and in more specific terms, between snow-cover depletion and snow water content. It is also deemed possible and cost-effective to relate areal extent of snow in specific vegetation, elevation and aspect relationships to the actual snow water equivalent for a given area using snow survey data collection systems similar to those in use in many areas (Thomas, 1974; Thomas and Sharp, 1974). Since it is highly probable that relationships such as the ones described above could be developed using areal extent of snow to provide the major portion of the information to be used in water runoff equations, techniques had to be developed which would provide fast, economical, and accurate estimation of this parameter. The following research deals with the development of techniques for estimation of snow areal extent.

Using conventional aerial photography as the data base for obtaining snow areal extent information would obviously prove extremely costly if this necessitated covering entire watersheds on a sequential basis. Satellite imagery, more specifically LANDSAT-1 satellite imagery, could provide the data base, relatively inexpensively and on a repetitive basis. In order to quantify areal extent of snow, techniques were developed which analyzed the imagery for areal extent of snow based on reflectance and such parameters as elevation, vegetation and aspect. The technique describes research using a relatively simple procedure which none-the-less provides some very solid quantitative results. In conjunction with this technique, a description of a method to substantially lower costs for such a survey has been included under the title of "library of snow cover conditions".

PROCEDURE

The estimation procedure described in the following pages is based upon analyses of imagery defined by artificial units (grids). This technique differs substantially from the snow mapping approach reported in the literature (Barnes and Bowley, 1969; Rango and Foster, 1975; Rango Salomonson, and Foster, 1975, Wiesnet, 1974), where the snowpack boundary is delineated directly. The procedures developed allow the image analyst to make decisions in discrete units of the imagery as to the areal extent of snow based upon such factors as density and type of vegetative cover, elevation, aspect, actual reflectance of the snowpack, and by inference (i.e. by the presence of directly observable snowpack). These techniques also provide for the direct application of appropriate statistical methods for the estimation of the true areal extent of snow, as well as providing a means of determining the precision of that estimate.

LANDSAT-1 imagery in the form of simulated color infrared enhancements of bands 4, 5, and 7 was used for the interpretation procedures. These enhancements were made from individual 9-1/2 inch LANDSAT-1 black-and-white positive transparencies and combined using a technique developed at the Remote Sensing Research Program (Katibah, 1973). Consequently, enhanced imagery of just that portion of the LANDSAT-1 frame desired could be produced with excellent quality. Use of this technique also provided original enhancements directly on negative color film so that high quality reflection prints could be produced for interpretation purposes.

Snow Areal Extent Inventory

During the spring of 1973, the LANDSAT-1 satellite provided essentially cloud-free coverage of the Feather River Watershed on April 4, May 10, and May 28. On these days (or at the most, two days thereafter) random transects were flown across the watershed using a 35 mm camera to acquire large scale aerial photography that could be used as an aid in determining the actual snow condition on the ground (i.e. "ground truth").

To estimate the areal extent of snow, the LANDSAT-1 images were gridded with image sample units (ISU's), each equaling 400 hectares (Figures 1, 2, 3, and 4). These image sample units were then transferred to the large scale photography where applicable. The image sample units on the large scale photography were coded as follows:

<u>Code</u>	<u>Snow Cover Class</u>	<u>Midpoints</u>
1	No snow present within the ISU	0
2	0-20% of ISU covered by snow	.10
3	20-50% of ISU covered by snow	.35

<u>Code</u>	<u>Snow Cover Class</u>	<u>Midpoints</u>
4	50-98% of ISU covered by snow	.74
5	98-100% of ISU covered by snow	.99

The gridded LANDSAT-1 images were then interpreted, sample unit-by-sample unit, and coded using the following method to account for vegetative cover and density and to some degree, aspect, elevation and slope as they impact snow cover.

Scale matched simulated color infrared enhancements of LANDSAT-1 imagery were produced for April 4, 1973; May 10, 1973; May 28, 1973 and also for August 31, 1972 in reflection print form. The April and May dates represent the snowpack and were gridded, while the August 1972 date, representing a cloud free summer image, was not gridded. The purpose of the August date was to provide a clear aerial view of actual ground relationships of vegetation/terrain features. The August date was superimposed with each of the snowpack dates using a mirror stereoscope. By blinking first one eye and then the other the image analyst could observe what conditions actually occurred on the ground in the image sample unit he was interpreting for snowpack. Obviously this technique capitalizes on the human image analyst's ability to synthesize large amounts of pertinent data and quickly arrive at a decision.

The image analyst, using this technique, spent three hours training himself to interpret the LANDSAT-1 imagery. The April 4th date comprising 2218 image sample units was subsequently interpreted in nine hours, the May 10th date (2050 image sample units) in six hours, and the May 28th date (2013 image sample units) in three hours. The decrease in interpretation time can undoubtedly be related to the increasing experience of the analyst and the decreasing snowpack.

The costs associated with this research were determined for the April 4th date (Table I). The total cost for estimating the areal extent of snow over 897,642 hectares in Feather River Watershed on this date was \$715.75 or approximately 33¢ per ISU. While this figure may appear to be fairly large it must be remembered that it includes such things as start up costs, interpreter training, and interpreter experience all of which could be, but were not amortized. Use of a technique such as that described under the section entitled "Library of Snow Cover Conditions" would also virtually eliminate the \$500 cost of the resource photography on each date inventoried.

The LANDSAT-1 interpretation results were compared to the coded large scale photography where applicable. Tables II, III, and IV summarize the interpretation test results. The sample unit-by-sample unit interpretation of the LANDSAT-1 image was then used to find the estimate for the areal extent of snow in the watershed. Totals for each of the individual snow cover classes were found and multiplied by 400 hectares, the area of each image sample unit on the ground. This gave the hectares for each class; these values were then multiplied by the appropriate snow cover class midpoints to give the total

hectares of snow in each class. Finally, these totals were added to give the estimated areal extent of snow. See Table V.

The areal extent of snow thus calculated was based solely upon the LANDSAT-1 interpretation results. To correct this estimate, the image sample units where snow areal extent "ground truth" was obtained (from large scale aerial photographs) were compared with the same image sample units on the LANDSAT-1 imagery. The relationship between the snow areal extent values on these corresponding LANDSAT-1 and "ground truth" sample units is the basis for the application of the ratio estimator statistical technique (Cochran, 1959). This technique not only provides a correction for the original interpretation estimate, but also allows for an estimate of the precision of this technique through the application of confidence intervals. The confidence intervals around the areal extent of snow estimates were calculated for four different levels of confidence 99%, 95%, 90%, and 80% for comparative purposes. The confidence intervals are expressed as hectares and in the form of allowable error (Table VI). The ratio estimator statistics as well as the manner in which the confidence intervals and allowable errors were calculated are shown in Appendix I.

It is desirable to check and see if the values in the snow cover class from the LANDSAT-1 image data come from the same statistical probability distribution as the values in the snow cover classes from the large scale photography data. If they come from the same distribution it may be expected that our estimation procedure will provide good results. If there were also a way to lump snow cover classes to improve the indications that the two sets of values came from the same distribution, this would give some idea on how to improve the estimation procedure in the future. To perform such probability distribution likeness tests, a Chi-square statistic, $\chi^2 = \sum_{i=1}^k \frac{(O_i - E_i)^2}{E_i}$, was

used. The values in the snow cover classes from the large scale photo data were designated as the expected values (E_i), since they were assumed to be "ground truth". The values in the snow cover classes from the LANDSAT-1 image data were designated as the observed values (O_i). For each date a Chi-square test was run, using the data as recorded versus the data with snow cover classes 4 and 5 combined, to see if an improvement in class widths could be realized.

Results of the Snow Areal Extent Inventory

The results of this inventory are summarized in the following tables of interpretation results, statistical computations (including areal extent of snow estimates, variance of areal extent of snow estimate, population ratio estimator, etc.), confidence intervals and allowable errors, and Chi-square tests results are found in the following pages. Tables II, III, and IV deal with April 4, May 10, and May 28 interpretation data respectively. Table V deals with the results of the ratio estimator statistic on all three dates. Table VI deals with the confidence intervals and allowable errors associated with the areal extent of snow estimates on all three dates. Tables VII, VIII, and IX deal with the results of the Chi-square tests on April 4, May 10, and

May 28 respectively.

Conclusion of Snow Areal Extent Inventory

Improvement in the snow areal extent inventory, as it is currently done is possible by increasing the sample size and by optimizing the image sample unit size.

The Student's-t statistic reaches its smallest value when the degrees of freedom (sample size minus one) are approximately 120. In subsequent inventories using this approach, each date for which large scale aerial photography is flown should have approximately this number of image sample units definable.

One of the items that should be investigated is the optimum size of the image sample unit. Several approaches are possible as well as a combination of all of them. For instance, image sample unit size may be plotted against interpretation time, variance, or variance times cost to determine the optimum image sample unit shape and size under those constraints.

The one improvement that by itself can substantially decrease the width of the confidence intervals (and consequently the allowable errors) is that of decreasing the sample variance. As already shown, the April 4 data had the smallest variance, the May 10 data had the next smallest and the May 28 data had the largest. The reason for this progressive increase in sample variance most likely can be attributed to the decrease in the snow pack over the three dates. The image analyst's ability to classify seems to be related to the proportion of snow cover; however the majority of the variance may not be due to the analyst, but rather to a natural state of greater snow areal extent variability among sample units over an area defined as a watershed.

The Chi-square test indicated that on all dates the experimental set-up was adequate except for May 10. Substantial improvements in matching the corresponding value distributions of the large scale photography data and the LANDSAT-1 image data were realized by lumping snow cover classes 4 and 5. This indicates that the analyst had difficulty in separating snow areal extent class 4 areas from class 5 areas. If the snow cover classes were to be redistributed (0-20%, 20-40%, 40-60%, 60-80%, 80-100% for example) the analyst might realize an improvement in his ability to classify snow cover conditions. Provided the analyst's ability to classify snow cover conditions did improve, then it would be expected that the sample variance for each set of interpretation results would go down, and consequently, the width of the confidence interval would decrease (as well as the allowable error, AE) given constant sample sizes and confidence levels.

Library of Snow Cover Conditions

One of the possible avenues for lowering the expense of estimating snow areal extent is to develop a library of snow cover conditions, in which the appearance of the snow pack is compared between low altitude photography and satellite LANDSAT imagery, along with other relevant data on an image sample

unit (ISU) basis. This approach could virtually eliminate the yearly low altitude photography requirement once the library is complete.

Parameters which represent relevant snow cover related data that might be included in such a library are: (1) the general time period (by month) in which a particular image sample unit took on a specific appearance with regard to snow cover, (2) data dealing with the magnitude (based on average precipitation), temperature (freezing or thawing), and date of the previous winter storm which affected the appearance of the image sample unit, (3) the environmental units (based on unique combinations of vegetation/terrain, aspect, and elevation) which compose a given landscape and thus affect the way in which snow cover is imaged, and (4) the snow water content of key ground station points associated with the image sample units. Information in this form provides an input, based on snow depletion rates, for use in a remote sensing-aided prediction of basin-wide snow water content estimation (Thomas, 1974).

Of all the parameters previously described that could be useful in such a library, probably the most difficult to incorporate is that of the environmental unit. Preliminary studies using the Spanish Creek Watershed (a sub-watershed of the Feather River Watershed) as a representative example have yielded 115 different combinations based on 18 vegetation/terrain classes (adapted from Krumpke, 1973), 7 aspect classes, and 5 elevation classes. All of the environmental units defined can be produced in transparent acetate from corrected to overlay directly on LANDSAT images thus aiding the image analyst in his appraisal of the snow conditions within a given image sample unit.

For training purposes, the specific image sample units (as imaged on LANDSAT) that were chosen for inclusion in the snow cover condition library would have associated overlays. These overlays would define the relationships between the environmental units and snowpack appearance in specific ISU's. Additionally the environmental units could also be related to the ISU's on the cloud free summer date. Consequently, the image analyst would be able to judge not only the appearance of snow in specific environmental units but also the appearance of the snow-free summer landscape. The combination of the two landscapes allows the image analyst to make better decisions on areal extent of snow using the stereoscope technique described previously.

The true benefit of compiling a library of snow cover conditions lies in the fact that upon completion, training and testing of the image analyst could be conducted from the data contained from within the library. Relatively frequent acquisition of a sample of supporting aerial photography is therefore unnecessary. Such a library would allow the analyst to choose a date from a previous year which most closely matches the appearance and other criteria of the current snowpack condition being analyzed for snow areal extent.

Determination of whether one year's conditions match another's is based upon the fact that the snowpack builds up and depletes in a unique fashion (Garstka, Love, Goodell, and Bertle, 1958). By comparing the visual appearance the date, and the previous winter storm data between specific ISU's, in the library and of the current date of imagery being analyzed, the individuals conducting the investigation can make the decision of which date of previous imagery contained in the library best approximates the current snowpack situation.

Once a date of imagery which satisfies all the specified conditions is found, the image analyst may be trained. The training procedure essentially allows the analyst to look at a representative set of ISU's which cover a wide variety of snowpack and environmental conditions and establish the snow cover classes determined previously. By reviewing the information contained in the library for these ISU's the analyst can also form some ideas on why the snowpack appears as it does. This procedure will help him form more confident and accurate opinions of snowpack cover class during the actual interpretation of the imagery. The testing procedure, discussed in an earlier section, would derive its "ground truth" from the evaluation of the snowcover class of specific ISU's as contained in the library. These values would be compared to the analyst's interpretation values and the appropriate statistical tests could then be applied.

Conclusions and Recommendations

Although the nature of the data required by the LANDSAT-1 satellite lends itself directly to automatic computer analysis for areal extent of snow estimation, research in manual techniques can be justified by comparing the two methods of operation to one another on a cost-effective basis. Research is currently being carried out on both phases of snow areal extent estimation procedures and analyses will be conducted testing both automatic, manual and a combination of automatic and manual on a cost-effective basis.

Besides being justifiable on this basis, continued research utilizing manual techniques can provide analyses in certain circumstances where computer classification has not been sufficiently refined. Scattered cloud cover over snowpack may present some difficulty to present computer analysis; however the human has little difficulty distinguishing the two as they appear on LANDSAT-1 imagery.

The inventory methods for areal extent of snow estimation described in this paper show great promise for providing fast, economical, and accurate inventories of snowpack extent. As it is refined, such as by optimizing image sample unit sizes and snow cover class width, estimates as to the true areal extent of snow should become more precise and should be made with greater confidence, all other factors being equal.

ACKNOWLEDGEMENTS

The research reported on in this paper was sponsored by NASA Grant NGL 05-003-404.

REFERENCES

- Barnes, J.C. and C.J. Bowley, 1969. Satellite Photography for Snow Surveillance in Western Mountains. In Proceedings of the 37th Annual Meeting of the Western Snow Conference. pp 34. Salt Lake City, Utah.
- Garstka, W.V., L.D. Love, B.C. Goodell, and F.A. Bertle, 1958. Factors Affecting Snowmelt and Streamflow. A Report on the 1946-53 Cooperative Snow Investigations At Fraser Experimental Forest, Fraser, Colorado. U.S. Government Printing Office.
- Katibah, E.F., 1973. A Simple Photographic Technique for Producing Color Composites from Black-and-White Multiband Imagery with Special Reference to ERTS-I. Information Note, Remote Sensing Research Program, Berkeley, California.
- Krumpe, P.F., 1973. A Regional Approach to Wildland Resource Distributional Analysis Utilizing High Altitude and Earth Orbital Imagery. In proceedings of the 39th Annual Meeting of the American Society of Photogrammetry. pp 336. Washington, D. C.
- Leaf, C.F., 1969. Aerial Photographs for Operational Streamflow Forecasting in the Colorado Rockies. In Proceedings of the 37th Annual Meeting of the Western Snow Conference. pp. 19. Salt Lake City, Utah.
- Rango, A., V.V. Salomonson, and J. L. Foster, 1975. Seasonal Streamflow Estimation Employing Satellite Snowcover Observations. Document X-913-75-26. pp. 34. Goddard Space Flight Center, Greenbelt, Maryland.
- Rango, A., and J.L. Foster, 1975. A Method For Improving the Location of the Snowline in Forested Areas Using Satellite Imagery. Document X-910-75-41. pp 8. Goddard Space Flight Center, Greenbelt, Maryland.
- Thomas, R.W., 1974. Approach to Remote Sensing-Aided Water Yield Estimation; Chapter 2(b), Section 2.100b; In An Integrated Study of Earth Resources in the State of California Using Remote Sensing Techniques; R.N. Colwell, Principal Investigator, Semi-annual Progress Report, NASA Grant NGL 05-003-404, December 1974, Space Sciences Laboratory Series 16, Issue 2, University of California, Berkeley.
- Thomas, R.W. and J.M. Sharp, 1974. A Comparative Cost-Effectiveness Analysis of Existing and LANDSAT-Aided Snow Water Content Estimation Systems; Chapter 6; In An Integrated Study of Earth Resources in the State of California Using Remote Sensing Techniques; R.N. Colwell, Principal Investigator, Semi-annual Progress Report, NASA Grant NGL 05-003-404, December 1974, Space Sciences Laboratory, Series 16, Issue 2, University of California, Berkeley.
- Wiesnet, D.R., 1974. The Role of Satellites in Snow and Ice Measurements. In Advanced Concepts and Techniques in the Study of Snow and Ice Resources. pp 447. National Academy of Sciences. Monterey, California.

TABLE I

COST OF AREAL EXTENT OF SNOW ESTIMATION RESEARCH

Image Acquisition		
1 LANDSAT Date, 3 bands @\$3/band		\$ 9.00
Resource Photography		
Medium scale aerial photography for image analyst environmental type training		500.00
Image Sample Units		
Gridded LANDSAT color composite print generation; film, processing, and printing @11/date		11.00
Labor		
.5 hours per date @\$13.50/hour		6.75
Interpreter Training		
3 hours @\$13.50/hour		40.50
Image Interpretation		
9 hours @\$13.50/hour		121.50
Analysis of Image Analyst Results		
2 hours @\$13.50/hour		27.00
	TOTAL	<u>\$715.75</u>
	Per ISU	\$.33

TABLE II

APRIL 4, 1973 LANDSAT-1 AREAL EXTENT OF SNOW INTERPRETATION RESULTS (ALSO LISTING OF x_i 's AND y_i 's)

		Large Scale Photo Data				
		Snow Cover Classes				
		1	2	3	4	5
LANDSAT-1 Image Data	Snow Cover Classes	1	0	40		
		0	6	1		
	2		40		296	1
	3		40	10	40	
	4		140	2	140	2
	5			140	296	12
					396	6
					396	33

x_i = sample LANDSAT-1 estimate of the number of hectares of snow per cell by snow cover class = (snow cover class midpoint)(400 hectares).

y_i = sample large scale photo estimate of the number of hectares of snow per cell by snow cover class = (snow cover class midpoint)(400 hectares).

f = interpretation frequencies

y_i	x_i
	f

TABLE IV

MAY 28, 1973 LANDSAT-1 AREAL EXTENT OF SNOW INTERPRETATION RESULTS (ALSO LISTING OF x_i 's AND y_i 's)

		Large Scale Photo Data					
		Snow Cover Classes					
		1	2	3	4	5	
LANDSAT-1 Image Data	Snow Cover Classes	1	0	40			
			3	0	4		
		2	40	1	40	16	40
						140	1
		3		140	2	140	2
				40		296	
4					296	2	296
							296
5							396
							296
							4

x_i = sample LANDSAT-1 estimate of the number of hectares of snow per cell by snow cover class = (snow cover class midpoint)(400 hectares).

y_i = sample large scale photo estimate of the number of hectares of snow per cell by snow cover class = (snow cover class midpoint)(400 hectares).

f = interpretation frequencies

x_i	y_i
	f

TABLE V
 SUMMARY OF RESULTS
 AERIAL EXTENT OF SNOW ESTIMATION

	April 4, 1973	May 10, 1973	May 28, 1973
LANDSAT-1 estimate of the areal extent of snow	x	511,378	205,768
Estimate of the true areal extent of snow	\hat{Y}_R	501,355	195,644
Standard deviation of the areal extent of snow estimate	$\sqrt{V(Y_R)}$	12,776	14,526
Population ratio estimator	\hat{R}	.9804	.9509
Total number of acres inventories		879,642	813,014
Total number of image sample units inventories	N	2,218	2,050
Total number of image sample units sampled	n	80	52
			49

TABLE VI

CONFIDENCE INTERVAL AND ALLOWABLE ERROR STATEMENTS

AREAL EXTENT OF SNOW ESTIMATION

Level of confidence	April 4, 1973		May 10, 1973		May 28, 1973	
	Confidence Level	AE	Confidence Interval	AE	Confidence Level	AE
99%	$477,649 \leq Y_R \leq 545,107$	6.13%	$166,897 \leq Y_R \leq 244,638$	19.87%	$14,566 \leq Y_R \leq 106,466$	79.43%
95%	$485,940 \leq Y_R \leq 536,816$	5.07%	$176,601 \leq Y_R \leq 234,935$	14.91%	$26,075 \leq Y_R \leq 94,958$	59.54%
90%	$530,575 \leq Y_R \leq 532,651$	4.24%	$181,423 \leq Y_R \leq 230,112$	12.44%	$31,778 \leq Y_R \leq 89,242$	49.68%
80%	$494,858 \leq Y_R \leq 527,898$	3.30%	$186,899 \leq Y_R \leq 22,463$	9.64%	$38,252 \leq Y_R \leq 82,781$	38.49%

TABLE VII

CHI-SQUARE TEST FOR APRIL 4, 1973 DATA

Null Hypothesis: Ho: The observed values (O_i) come from the same distribution as the expected values (E_i)
Alternative Hypothesis: H₁: The observed values do not come from the same distribution as the expected values
Significance Level: 5%

Test Statistic Under The Null Hypothesis: $\sum_{i=1}^k \left[\frac{(O_i - E_i)^2}{E_i} \right] \sim \chi^2_{k-1}$; where k-1 = the degrees of freedom

Full Class Data Summary

Class	O _i	E _i	$\frac{(O_i - E_i)^2}{E_i}$
1	7	6	.1667
2	11	13	.3077
3	10	7	1.2857
4	13	21	3.0476
5	39	33	1.0909

$$\sum_{i=1}^k = 5.8992$$

Table Value = $\chi^2_{5-1, .05} = \chi^2_{4, .05} = 9.49$

Conclusion: The null hypothesis is accepted since the calculated value of 5.8992 is less than the table value of 9.49.

Lumped Class Data Summary:

Class	O _i	E _i	$\frac{(O_i - E_i)^2}{E_i}$
1	7	6	.1667
2	11	13	.3077
3	10	7	1.2857
4	52	54	.0741

$$\sum_{i=1}^k = 1.8342$$

Table Value = $\chi^2_{4-1, .05} = \chi^2_{3, .05} = 7.81$

Conclusion: The null hypothesis is accepted since the calculated value of 1.8342 is less than the table value of 7.81.

TABLE VIII - CHI-SQUARE TEST FOR MAY 10, 1973 DATA

Test at 5% significance level

Null Hypothesis: Ho: The observed values (O_i) come from the same distribution as the expected values (E_i)

Alternative Hypothesis: H₁: The observed values (O_i) do not come from the same distribution as the expected values (E_i)

Test statistic under the null hypothesis: $\sum_{i=1}^k \left[\frac{(O_i - E_i)^2}{E_i} \right] \sim \chi^2_{k-1}$; where k-1 - the degrees of freedom

Class	O _i	E _i	$\frac{(O_i - E_i)^2}{E_i}$
1	8	4	4.000
2	15	18	.5000
3	11	13	.3077
4	5	9	1.7777
5	13	8	3.1250

$$\sum_{i=1}^5 = 9.7104 = \text{calculated value}$$

$\chi^2_{5-1}, .05 = \chi^2_4, .05 = 9.49 = \text{table value}$

∴ Since the calculated value (9.7104) is more than the table value (9.49) the null hypothesis is rejected.

Class	O _i	E _i	$\frac{(O_i - E_i)^2}{E_i}$
1	7	4	2.25
2	18	22	.7272
3	14	12	.3333
4	10	11	.0909

$$\sum_{i=1}^4 = 3.4014 = \text{calculated value}$$

$\chi^2_{4-1}, .05 = \chi^2_3, .05 = 7.81 = \text{table value}$

∴ Since the calculated value (3.4014) is less than the table value (7.81), the null hypothesis is accepted.

TABLE IX - CHI-SQUARE TEST FOR MAY 28, 1973 DATA

Test at 5% significance level

Null Hypothesis: Ho: The observed values (O_i) come from the same distribution as the expected values (E_i).

Alternative Hypothesis: H₁: The observed values (O_i) do not come from the same distribution as the expected values (E_i)

Test statistic under the null hypothesis: $\sum_{i=1}^k \frac{(O_i - E_i)^2}{E_i} \chi_{k-1}^2$; where k-1 = the degrees of freedom

Class	O _i	E _i	$\frac{(O_i - E_i)^2}{E_i}$
1	7	4	2.500
2	18	22	2.7272
3	14	12	.3333
4	6	11	2.2727
5	4	0	0.0000
			$\sum_{i=1}^5 = 5.5832$

= calculated value

$\chi_{5-1}^2, .05 = \chi_4^2, .05 = 9.49 = \text{table value}$

∴ Since the calculated value (5.5832) is less than the table value (9.49), the null hypothesis is accepted.

Class	O _i	E _i	$\frac{(O_i - E_i)^2}{E_i}$
1	8	4	4.0000
2	15	18	.5000
3	11	13	.3077
4	18	17	.0588
			$\sum_{i=1}^4 = 4.8665$

= calculated value

$\chi_{4-1}^2, .05 = \chi_3^2, .05 = 7.81 = \text{table value}$

∴ Since the calculated value (4.8665) is less than the table value (7.81), the null hypothesis is accepted

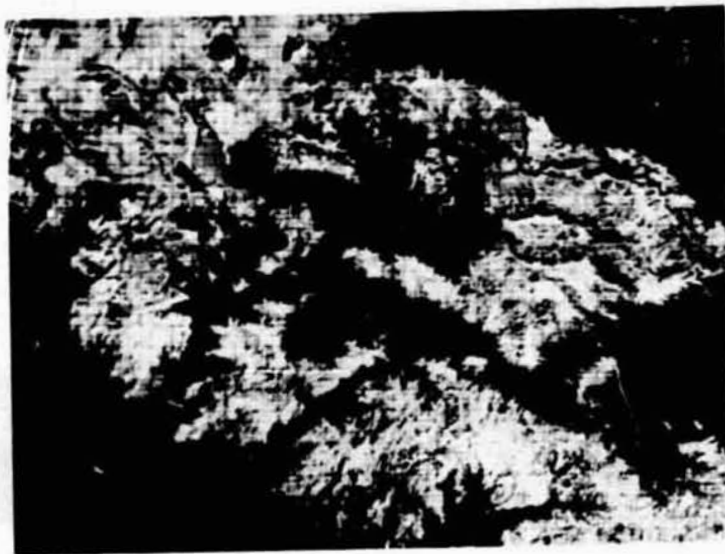


Figure 1. April 4, 1973 LANDSAT-1 simulated color infrared enhancement.
Image sample units (grids) = 400 hectares each

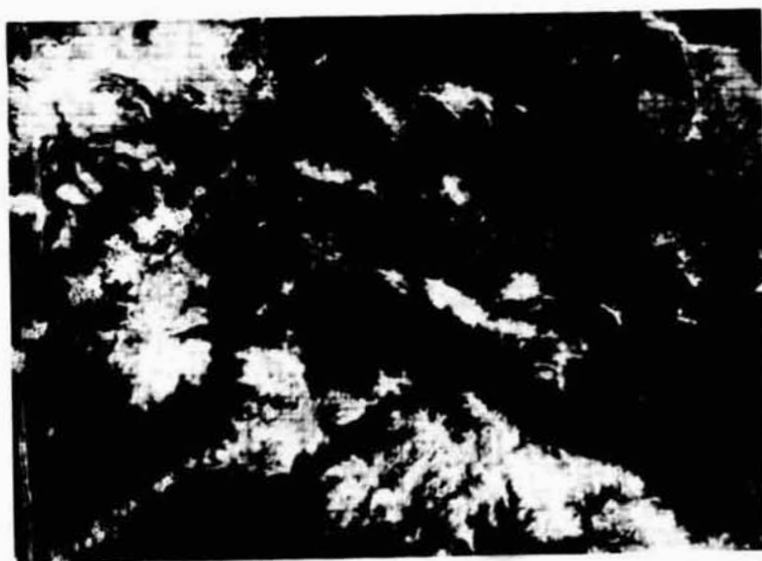


Figure 2. May 10, 1973 LANDSAT-1 simulated color infrared enhancement.
Image sample units (grids) = 400 hectares each.

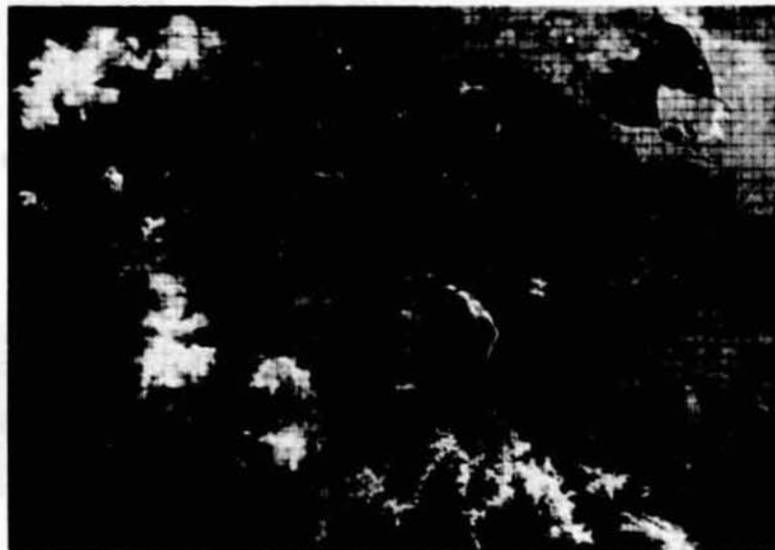


Figure 3. May 28, 1973 LANDSAT-1 simulated color infrared enhancements.
Image sample units (grids) = 980 acres each.

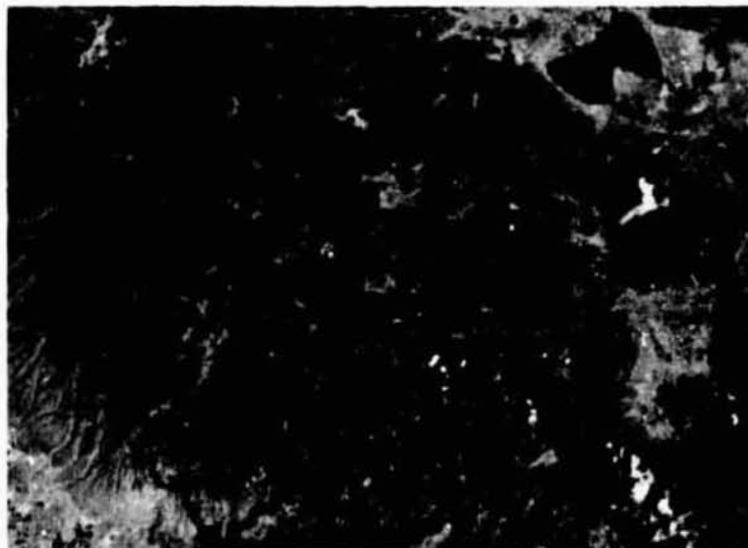


Figure 4. August 31, 1972 LANDSAT-1 simulated color infrared enhancement.
Cloud-free summer image.

APPENDIX I

Ratio Estimator Statistic

Y_R = The true areal extent of snow

\hat{Y}_R = The estimate of the true areal extent of snow

$$= X\hat{R}$$

where: $X = \sum_{j=1}^N X_j$

Given that: X_j = LANDSAT-1 interpretation estimate of the
number of acres of snow by snow cover class

$$= (\text{Snow cover class midpoint})(400 \text{ hectares})$$

j = Index for all LANDSAT-1 image sample units

N = Maximum LANDSAT-1 image sample unit index
number

Where: $\hat{R} = \frac{\bar{Y}}{X}$ = The population ratio estimator

Given that: $Y = \sum_{i=1}^n y_i$

$$X = \sum_{i=1}^n x_i$$

n = Total number of ERTS-1 image sample units
sampled with large scale aerial photography

i = Sample index

y_i = Large scale photo estimates of the acres of
snow for sample LANDSAT-1 image sample unit i

$$= (\text{Snow cover class midpoint})(400 \text{ hectares})$$

x = LANDSAT-1 interpreter estimate of the number of
acres of snow for sample image sample unit i

$$= (\text{Snow cover class midpoint})(400 \text{ hectares})$$

$$V(\hat{Y}_R) = \text{Sample variance} = \frac{N(N-n)}{n(n-1)} \left[\sum_{i=1}^n y_i^2 + \hat{R}^2 \sum_{i=1}^n x_i^2 - 2\hat{R} \sum_{i=1}^n x_i y_i \right]$$

Confidence interval around Y_R : Example for 95% level of confidence

As expressed in acreage limits:

$$\text{Probability} \left[\hat{Y}_R - t_{n-1} \cdot .025 \sqrt{V(\hat{Y}_R)} \leq Y_R \leq \hat{Y}_R + t_{n-1} \cdot .025 \sqrt{V(\hat{Y}_R)} \right] = .95$$

As expressed as allowable error (AE):

$$AE = \frac{t_{n-1} \cdot .025 \sqrt{V(\hat{Y}_R)}}{\hat{Y}_R}$$

REFERENCES

Cochran, W. G., 1959, Sampling Techniques. John Wiley & Sons, Inc., New York.

SNOW SURVEY FROM SPACE, WITH EMPHASIS ON THE RESULTS OF THE
ANALYSIS OF SKYLAB EREP S192 MULTISPECTRAL SCANNER DATA

W-24

By James C. Barnes and Michael D. Smallwood, Environmental
Research & Technology, Inc., Concord, Massachusetts 01742

ABSTRACT

N76-17610

The Skylab EREP S192 Multispectral Scanner data have provided for the first time an opportunity to examine the reflectance characteristics of snowcover in several spectral bands extending from the visible into the near-infrared spectral region to about 2 μm . The analysis of the S192 imagery and digital tape data from five EREP passes, two from the SL-2 mission and three from the SL-4 mission, indicates a sharp drop in reflectance of snow in the near-infrared, with snow becoming essentially non-reflective in Bands 11 (1.55-1.75 μm) and 12 (2.10-2.35 μm). The results are in good agreement with the results of laboratory experiments. Two potential applications to snow mapping of measurements in the near-infrared spectral region are possible: (1) the use of a near-infrared band in conjunction with a visible band to distinguish automatically between snow and water droplet clouds; and (2) the use of one or more near-infrared bands to detect areas of melting snow.

INTRODUCTION

Snow has an enormous effect on the large-scale geophysical environment of the Earth. Seasonal changes in snowcover produce significant variations in the albedo of the land areas. These albedo variations strongly influence the radiation balance at the surface, which, in turn, influences both short- and long-term weather conditions. In many regions, such as the western United States, snow also has a direct economic impact. The snowmelt runoff is used for irrigation, industrial production, power generation, municipal water systems, and recreation. However, too much runoff may produce destructive flooding.

Snow was one of the first terrestrial water resources to be observed from space. Approximately 15 years ago, snow in eastern Canada was detected in images from TIROS-1, the first weather satellite launched by the United States. Since then, as improved satellite systems have been developed, an increasing use has been made of remote sensing from space to monitor snowcover. Quasi-operational use in snow hydrology is currently being made of the NOAA satellite Very High Resolution Radiometer imagery, and the data from the LANDSAT (formerly ERTS) satellite has been shown to have substantial practical application for snow mapping. A summary report on the status of satellite snow survey was prepared by an international committee for the World Meteorological Organization in 1973 (1); recently, a handbook of techniques for satellite snow mapping has been prepared (2) to assist NASA Goddard Space Flight Center in the planning of a practical demonstration project of the application of satellite data to snow hydrology.

Two snow mapping experiments were conducted as part of the Skylab mission, one an EREP (Earth Resources Experiment Package) experiment and the other an experiment in the Skylab-4 Visual Observations Project. The purpose of the EREP investigation was to analyze data from the various sensors in conjunction with the photographic data to determine how much additional information on snowcover can be derived from measurements made in other than the visible portion of the spectrum. The purpose of the Visual Observations Project experiment was for the crewmen to select specific test areas and to make observations of snowcover at various viewing angles in order to detect features not readily apparent in vertical-view photographs.

In this paper the results of the Skylab EREP investigation, in particular the analysis of snow reflectance characteristics using EREP S192 Multispectral Scanner data, are described. The results of the Visual Observations Project snow-mapping experiment are described in the Project Report (3).

SPECTRAL REFLECTANCE OF SNOW COVER

The initial spacecraft measurements in the near-infrared portion of the spectrum were those of the 0.7-1.3 μm band of the Nimbus-3 HRIR (High Resolution Infrared Radiometer). In studies using the HRIR data (4), it was first noticed that snowcover could not be distinguished in the near-infrared spectral band. In a subsequent, more thorough investigation of the HRIR near-infrared data (5), the observed low reflectance of snow and ice was attributed to the existence of melt water on the snow or ice surface; the investigators pointed out that with even a thin layer of water on the snow or ice, the surface would appear highly reflective in the visible portion of the spectrum but essentially non-reflective in the near-infrared.

In an investigation of LANDSAT-1 imagery (6,7), the contrast between snow and bare ground was found to be considerably lower in the MSS-7 near-infrared band (0.8-1.1 μm) than in the MSS-5 visible band. Moreover, in some late spring cases, the areas appearing very bright in MSS-7 were found to be significantly smaller than those appearing bright in MSS-5. It was concluded that the snow visible in the near-infrared image may be the high-elevation dry snow, whereas both the dry and lower elevation wet snow surfaces are detectable in the visible image. In another study of several river basins in the Wind River Range in Wyoming (8), the LANDSAT MSS-7 imagery consistently indicated less snowcover than did the MSS-5; the difference was attributed to the reduced near-infrared reflectance associated with melting or refrozen previously melting snow.

Recent laboratory experiments (9) have also been conducted to determine the effects of various natural conditions, especially melting and refreezing, on the spectral reflectance of a snowcover in the red and near-infrared regions. The results of these experiments indicate that toward the red end of the visible spectrum, the reflectance declines somewhat and falls off rapidly in the near-infrared region. As fresh snow ages without melting, there is a small decrease in reflection, but temperatures near-melting (but no melting) do not produce a great reduction in reflectance; melting to the point of producing wet snow on the surface, on the other hand, produces a significant reduction in reflectance.

S192 MULTISPECTRAL SCANNER DATA

The EREP S192 Multispectral Scanner provided for the first time an opportunity to examine the spectral characteristics of snow from space over the spectral range extending from the visible to well into the near-infrared. The S192 is a 13-band radiometer with 12 of the bands being in the visible or near-infrared portion of the spectrum extending to about 2 μm (the thirteenth band is in the thermal infrared). The spectral range for each band is as follows:

TABLE I.-S192 MULTISPECTRAL SCANNER SPECTRAL BANDS

Band Number	Description	Spectral Range (μm)
1	Violet	0.41-0.46
2	Violet-Blue	0.46-0.51
3	Blue-Green	0.52-0.56
4	Green-Yellow	0.56-0.61
5	Orange-Red	0.62-0.67
6	Red	0.68-0.76
7	Infrared	0.78-0.88
8	Infrared	0.98-1.08
9	Infrared	1.09-1.19
10	Infrared	1.20-1.30
11	Infrared	1.55-1.75
12	Infrared	2.10-2.35
13	Thermal Infrared	10.2-12.5

The conical scan pattern of the S192 covers a swath of the earth's surface that is approximately 72.4 km wide; the instantaneous field-of-view (IFOV) is 79.25 meters (260 feet). A detailed description of the Multispectral Scanner is given in the Skylab Earth Resources Data Catalog (10). Both the S192 imagery and Computer Compatible Tapes (CCT) were used in the data analysis.

S192 data for use in this study were acquired for four test site areas: the Sierra Nevada-White Mountains area in California; the Wasatch Range in Utah; the central Arizona mountains; and a portion of the Upper Mississippi-Missouri River Basin area in the north-central part of the country. As indicated below, Table 2, data from five EREP passes were analyzed:

TABLE II.- S192 MULTISPECTRAL SCANNER DATA SAMPLE

Case Number	Test Site	EREP Pass	Date	Approximate Time of Observation (Local Time)
1	Sierra Nevada-White Mountains	3	3 Jun 73	1130
2	Wasatch Range	5	5 Jun 73	1100
3	Central Arizona Mountains	83	14 Jan 74	1000
4	Upper Mississippi-Missouri River Basins	89	24 Jan 74	1200
5	Sierra Nevada-White Mountains	98	1 Feb 74	0900

Since two of the EREP passes were from the SL-2 mission in June 1973 and three from the SL-4 mission in January-February 1974, it was possible to investigate the reflectance characteristics of snow in late spring situations, representative of presumably melting snow, and in mid-winter situations, representative of presumably dryer, colder snow. Digitized data were available for only one of the two SL-2 passes, however; CCT's were not processed for EREP Pass 3 because the sensor was not aligned correctly (film products were available).

Since the design of this experiment was to examine EREP data collected over relatively large areas, it was not feasible to collect detailed information on the snow conditions at a particular test site. The overall snow conditions can be estimated, however, through routinely collected snow reports and the meteorological conditions prior to and at the time of the Skylab pass. In each case, the limits of the snowcover were mapped using the S190A and S190B photography.

In summary, meteorological data indicate the snowcover in the test site areas observed in June 1973 was quite probably in a melting condition, except perhaps at the highest elevations. In each of the test site areas observed in mid-winter, some melting could have been taking place at lower and middle elevations, or the snowpack could have been refrozen from melting that had occurred during the preceding few days. However, the snow conditions were more stable than in the two springtime cases. No S192 data were collected over a test site area immediately following a fresh snowfall or during a very cold period.

ANALYSIS OF S192 IMAGERY

The S192 imagery displays a marked drop in the reflectance of snow in the near-infrared bands. This effect is readily apparent in the imagery from the two SL-2 EREP Passes, over the Sierra Nevada-White Mountain area and the Wasatch area. For the Wasatch area the S192 Band 2 and Band 11 imagery is shown in Figures 1a and 1b. Similarly, the S192 Band 3 and Band 11 imagery for the White Mountains is shown in Figures 2a and 2b. In both cases, snowcover has a high reflectance in the visible band, but appears essentially black in the near-infrared.

In the Pass 3 imagery (Figures 2a and 2b), not only is the difference in the reflectance of the snow between the visible and near-infrared bands dramatic, but also the distinct nature of the clouds in the near-infrared spectral region. The S190A photograph indicates that cellular-type clouds, a pattern representative of cumulus (water clouds) cells, cover much of the area. Over the mountains, it is difficult to distinguish between the clouds and the snow. The same is true in the visible band S192 imagery, where the clouds and snow have essentially the same reflectance. In the Band 11 imagery, however, the clouds still appear white whereas the snow appears essentially black; therefore, each cumulus cell is distinct, even those cells directly over the snowcovered mountains.

In the initial interpretation of the S192 imagery for Pass 3, it was also noticed that in Band 9 some snow can be detected, but the extent of the snow appears to be less than in the visible band. The complete spectral coverage of the line-straightened imagery permitted a more thorough investigation of the snow reflectance in the intermediate bands between the visible and Band 11. In Figures 3a through 3f, the images for Bands 3, 7, 8, 9, 10, and 11 from Pass 5 are shown; the area covered includes the Mt. Nebo Range and San Pitch Mountains in the Wasatch Range. In the visible band, the entire snowpack has a high reflectance. In Band 7, however, a slight decrease in the apparent snow extent in the Mt. Nebo Range is observed; in Bands 8, 9, and 10, the apparent snowcover successively decreases until in Band 10 the only bright area is along the highest ridge of the range; in Band 11, no snow can be detected. In the San Pitch Mountains, which are at a lower elevation, the less extensive snowcover can barely be detected in Band 7 and cannot be detected in Bands 8 through 11.

The results of the analysis of S192 imagery for the wintertime cases are essentially the same as those for the SL-2 data discussed above. In each case, snow has a high reflectance in the visible, except in areas that are forested, whereas in the Band 11 imagery, the entire snowcovered area is non-reflective. In the intermediate spectral bands, a gradual lowering of the reflectance is observed beginning with about Band 8 or 9; however, the decrease in reflectance is uniform across the snowcover, and no gradual decrease in the apparent snow extent is observed, as was the case in the data from each of the SL-2 passes.

ANALYSIS OF S192 COMPUTER COMPATIBLE TAPES

Data Processing Procedures

The high data rate of the S192 instrument presented some problems in working with the Computer Compatible Tapes (CCT's). Even for the rather limited time segments for which CCT's were provided, it was not feasible to perform digital count to radiance conversions for the entire data segment. The principal problem, therefore, was to devise a technique for the selection of specific data segments of only a few scanlines corresponding to the locations of known ground features.

The technique devised to accomplish this task was a pre-selection procedure based on the analysis of raw channel counts. Knowing from the information on the S192 data supplied by NASA/JSC that snowcover would likely be saturated in the visible bands, a channel (SDO) corresponding to one of the visible bands was selected. The CCT's were then manipulated such that each pixel in that channel that was saturated (raw data count = 255) would be printed out as a black dot and each pixel that was not saturated (raw data count < 255) would be left blank. The result produced an image-like printout where all snowcovered (non-forested) areas appear black, and, therefore, specific features could be located.

Following selection of the specific numbers of scanlines and pixels from the printout, the calibrated radiances for each required channel were computed using the appropriate conversion equation supplied with the tapes. This processing technique was found to be extremely efficient and greatly facilitated the handling of the S192 Computer Compatible Tapes.

Results of Digital Data Processing

The radiance values obtained from the processing of the CCT's were analyzed for each of the four cases (no CCT's were available for Case 1, EREP Pass 3). A single pixel determined to be located within a uniform snowpack was selected for each of the four test site areas. The radiance value for the pixel was averaged with the five pixels before and after it to acquire a true representation of the snow response. This process was repeated for each band, and the averaged values were then graphed. The resulting graphs of the radiance values for each spectral band are shown in Figures 4, 5, 6, and 7 for the Wasatch, Arizona, Mid-west, and California test site areas, respectively.

For each of the test sites, the graphs indicate saturation or near saturation values (triangles indicate saturation levels) throughout the visible portion of the spectrum followed by a significant decrease in reflectance in the near-infrared. In the interpretation of the graphs it is necessary to consider not only the curve itself, but also the curve in relation to saturation levels; in this way, a saturated value is not misinterpreted as a decrease in reflectance (such as Band 4).

DISCUSSION OF RESULTS OF S192 DATA ANALYSIS

Comparison of SL-2 and SL-4 Data

For the five cases for which S192 data were analyzed, the overall results of the analysis of the imagery and the digital radiance values are consistent. In each case, snowcover exhibits a marked drop in reflectance in the near-infrared portion of the spectrum. Moreover, no significant difference in the reflectance characteristics of snow is apparent in the five cases examined, even though two of the cases were from the late spring and the other three from mid-winter. One difference that was observed, however, is that in both of the late spring cases the apparent extent of the snowcover gradually decreases from Band 7 through Band 11; in the winter cases, a uniform decrease in reflectance is observed with no apparent change in the detectable snow extent.

As was pointed out in the earlier discussion of the data sample, even in the winter cases no data were collected immediately following a fresh snowfall. Thus, the two spring cases were at times when the snowpack was in a general melting condition, whereas the three wintertime cases were at times when the snowpack was more stable but still consisting of somewhat aged snow that might be undergoing slight melting or had undergone melting and become refrozen.

It must also be remembered that the problem of measuring radiance values from a spacecraft platform is extremely complex. Many factors, such as the slope of the reflecting surface and especially the solar elevation angle, can influence the measurements. The solar elevation angle must be considered when attempting to compare measurements taken over different areas at different times of the year. Atmospheric attenuation must also be taken into account; however, the preliminary results of another Skylab investigation being conducted at ERT indicate that the error in determining surface reflectance for snow would be less than five percent for all spectral bands (11).

Comparison With Laboratory Experiments

The results of the analysis of the Skylab data are in general agreement with the results of laboratory experiments of the red and near-infrared spectral reflectance of snow (9). The S192 digital data results indicate a decrease in snow reflectance beginning in Band 3 (0.98-1.08 μm); the laboratory experiments indicate a high reflectance in the red, with a

tendency for the reflectance to begin to decline at about 1.03 μm . Secondly, the S192 results show a slight leveling off of the drop in snow reflectance in Band 10 (1.20-1.30 μm); the laboratory experiments show that the reflectance decreases rapidly from 1.1 to 1.5 μm with the exception that at about 1.25-1.35 μm it levels off and even makes a slight recovery. Finally, the S192 results show the lowest reflectance values to be in Bands 11 (1.55-1.75 μm) and 12 (2.10-2.35 μm); the laboratory experiments show low reflectance values at about 1.5-1.6 μm and an even stronger depression at 1.95-2.05 μm with a very slight rise at about 2.25 μm .

In the laboratory experiments, natural aging of the snow influences both the degree and rate of change of the reflectance. In general, melting lowers the reflectance, with some recovery if the snow is refrozen. A significant difference in the reflectance curves for dry and melting snow occurs at about 1.2-1.4 μm . The snowcover observed in the Skylab experiment had in each case aged to a certain extent.

The more advanced state of melting in the two late spring cases could account for the decrease in the apparent snow extent observed in the S192 imagery. In each case, it is probable that the lower elevations were undergoing more rapid snowmelt than the higher elevations at the time of the EREP Pass. Therefore, the shorter wavelength spectral bands (Bands 8, 9, and 10) will show a low reflectance where the snow is the wettest, but still a relatively high reflectance where the snow is drier, at the higher elevations. In the longer wavelengths (Bands 11 and 12), even the drier snow has a low reflectance. It is difficult to account for the progressive decrease in apparent snow extent in Bands 7 through 11, unless it is that snow wetness has a stronger influence in the shorter wavelengths than it does the longer wavelengths.

Snow Reflectance vs. Cloud Reflectance

A result of the analysis of the S192 data that has a significant potential application is the observed differences in the reflectance of snow and water droplet clouds. Whereas snow has a very low reflectance in the near-infrared, the water clouds remain at a high reflectance throughout the visible and near-infrared spectral regions. In a recent report discussing possible reasons for this observed difference (12), it is pointed out that a water droplet cloud displays two strong absorption bands centered at 1.41 and 1.92 μm . The spectrum of such a cloud observed from satellite altitudes will be distorted by atmospheric absorption, primarily by water vapor. The presence of these vapor bands in the radiation received at satellite altitude will tend to distort a water cloud spectrum toward shorter wavelengths. Snow also displays the two strong molecular vibration bands seen in spectra of liquid water and water vapor, but shifted to considerably longer wavelength. These bands lie at a sufficiently long wavelength so that they are relatively little distorted by atmospheric water vapor absorption bands.

POTENTIAL APPLICATIONS OF RESULTS OF S192 DATA ANALYSIS

Based on the results of the analysis of S192 data, two potential applications to snow mapping of measurements in the near-infrared spectral region are possible: (1) the use of a near-infrared band in conjunction with a visible band to distinguish automatically between snow and clouds; and (2) the use of one or more near-infrared bands to detect melting snow.

The nearly complete reversal in snow reflectance between the visible bands and Bands 11 and 12 observed in each case indicates that in this portion of the near-infrared, snow surfaces are essentially non-reflective regardless of the condition of the snow. In contrast, the reflectance of clouds (water droplet) is essentially the same in each of the S192 bands, displaying no drop in the near-infrared. As a result, a technique combining two spectral bands, one in the visible and one in the near-infrared at the position of Band 11 or 12

(1.55-1.75 μm or 2.10-2.35 μm), can be used to distinguish between snow, clouds, and non-snowcovered ground. A feature having a high reflectance in the visible and a low reflectance in the near-infrared would be classified as snow; a feature having a high reflectance in both bands would be classified as cloud; and a feature having a low reflectance in the visible and a medium reflectance in the near-infrared would be classified as non-snowcovered ground. An automatic technique for distinguishing snow from clouds is of particular significance, since this has been recognized as a serious problem with regard to the eventual machine processing of satellite data for snowcover mapping.

The second potential application, that of detecting melting snow, is based on the observed behavior of snow in the intermediate bands from about Band 7 (0.78-0.88 μm) through Band 10 (1.20-1.30 μm). Although the data sample was not optimum in that no data were collected over fresh, cold snow surfaces, the S192 film products for the spring cases (June 1973) display snow reflectance characteristics not observed in the winter cases (January-February 1974). In the two spring cases, the apparent snow extent decreases gradually from a maximum in the visible (Band 6) to a minimum in Band 11. This gradual decrease in the area of high reflectance is difficult to account for unless it is because the snow at the lower elevations is melting, and therefore exhibits a more rapid drop in reflectance, whereas the snow at the highest elevations is dryer or refrozen, and therefore does not exhibit a significant drop in reflectance until Band 11 (1.55-1.75 μm). In the winter cases, the snowpack is more uniform at all elevations, so does not display the gradual reduction in reflectance. It is concluded, therefore, that bands in the spectral range from about 0.8 μm to about 1.30 μm should provide the most information on the condition of the snow surface with regard to the snow being melting (wet surface) or being not melting or refrozen (dry surface).

The results of the analysis of the Skylab EREP S192 data have potential cost-saving application to snow mapping, although it is realized that further study of snow reflectance characteristics is needed. The available data sample did not include a situation where snow and ice clouds are present, where the technique to distinguish between snow and water droplet clouds could be tested to determine its application to ice clouds; also, measurements over fresh, dry snow as well as additional measurements over areas of known melting snow are needed before the relationships between reflectance and snow condition are completely understood.

Nevertheless, the results of the analysis of Skylab EREP data are believed to be sufficiently conclusive to warrant careful consideration for including one or more near-infrared spectral bands on radiometers to be flown on future operational satellite systems. Measurements in the near-infrared spectral region, in combination with visible and thermal infrared measurements, have the potential for providing greatly improved information with regard to snow hydrology and thus have the potential for providing eventual significant cost savings to snow survey programs.

ACKNOWLEDGEMENTS

The investigation described in this paper was supported by NASA Johnson Space Center under Contract No. NAS 9-13305. The authors are grateful for the assistance provided throughout the study by the Technical Monitor, Mr. Larry B. York, of the Principal Investigations Management Office.

REFERENCES

1. McClain, E.P., 1975: Snow Survey from Earth Satellites, World Meteorological Organization, WMO Pub. No. 353, Geneva, 42 pp.

2. Barnes, J.C., and C.J. Bowley, 1974: Handbook of Techniques for Satellite Snow Mapping, Report prepared under Contract NAS 5-21803, Environmental Research & Technology, Inc., Concord, MA, 95 pp.
3. Barnes, J.C., C.J. Bowley, J.T. Parr, and M.D. Smallwood, 1975: Skylab-4 Visual Observations Project: Snow Mapping Experiment, Final Report, Contract No. NAS 9-13974, Environmental Research & Technology, Inc., Concord, MA, (in publication).
4. Barnes, J.C., and C.J. Bowley, 1970: The Use of Environmental Satellite Data for Mapping Annual Snow-Extent Decrease in the Western United States, Final Report, Contract No. E-252-69(N), Allied Research Associates, Inc., Concord, MA, 116 pp.
5. Strong, A.E., E.P. McClain, and D.F. McGinnis, 1971: "Detection of Thawing Snow and Ice Packs through the Combined Use of Visible and Near-Infrared Measurements from Earth Satellites", Monthly Weather Review 99(11), pp. 828-830.
6. Barnes, J.C., C.J. Bowley, and D.A. Simmes, 1974: The Application of ERTS Imagery to Mapping Snowcover in the Western United States, Final Report under Contract NAS 5-21803, Environmental Research & Technology, Inc., Concord, MA, 77 pp.
7. Bowley, C.J., and J.C. Barnes, 1975: The Application of ERTS Imagery to Mapping Snowcover in the Western United States, Supplemental Report under Contract NAS 5-21803, Environmental Research & Technology, Inc., Concord, MA, 43 pp.
8. Rango, A., V.V. Salomonson, and J.L. Foster, 1975: Seasonal Streamflow Estimation Employing Satellite Snowcover Observations, Preprint X-913-75-26, NASA/Goddard Space Flight Center, 34 pp.
9. O'Brien, H.W., and R.H. Munis, 1975: Red and Near-Infrared Spectral Reflectance of Snow, Research Report 332, 18 pp., U.S. Army Cold Regions Research and Engineering Laboratory, Hanover, N.H.
10. NASA, 1974: Skylab Earth Resources Data Catalog, Doc. No. JSC-09016, NASA/Johnson Space Center, Houston, Texas 359 pp.
11. Chang, D.T. and R.G. Isaacs, 1975: "Evaluation of Atmospheric Effects on Radiometric Measurements Using the EREP of Skylab", paper presented at Annual Meeting of AGU, Washington, D.C., June 1975.
12. Hunt, G.R., J.W. Salisbury, and J.T. Bunting, 1974: Distinction Between Snow and Cloud in DMSP Satellite Imagery: A Preliminary Report, unpublished report, Terrestrial Sciences Laboratory, Air Force Cambridge Research Laboratory, Hanscom AFB, MA, 15 pp.

REPRODUCIBILITY
ORIGINAL PAGE IS



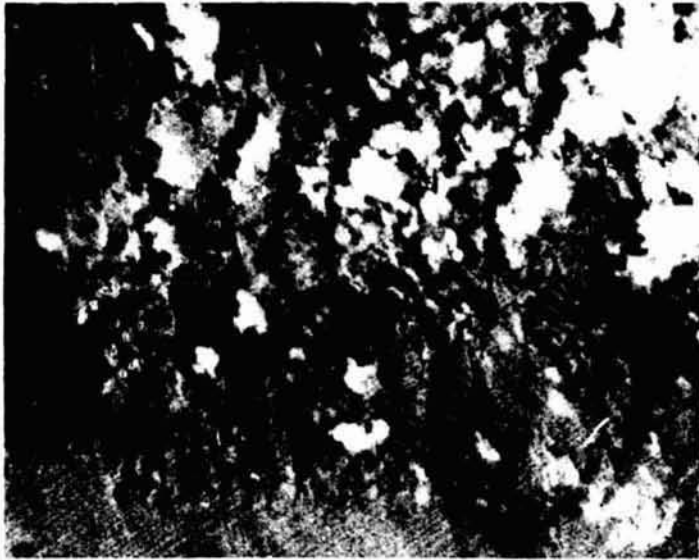
(a) Band 2



(b) Band 11

Figure 1 S192 imagery from EREP Pass 5, 5 June 1973; (a) Band 2 (0.46 - 0.51 μm), (b) Band 11 (1.55 - 1.75 μm). Area covered is the Wasatch Range in Utah. Note decreased reflectance of snow in Band 11 as compared to the Band 2 imagery.

REPRODUCIBILITY OF
ORIGINAL PAGE IS



(b) Band 11



(a) Band 3

Figure 2 S192 imagery from EREP Pass 3, 3 June 1973; (a) Band 3 (0.56 μm), (b) Band 11 (1.55 - 1.75 μm). Area covered is the White Mountains. Because of the decreased reflectance of the snow, clouds that cannot be detected in Band 3 are distinct in Band 11.



(a) Band 3

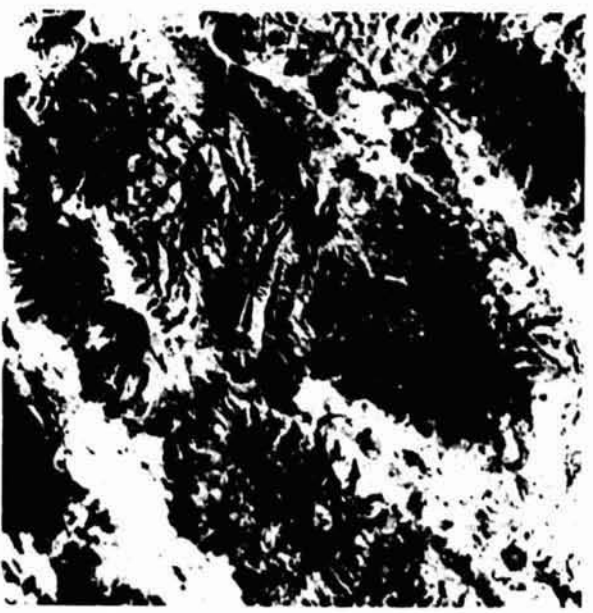


(b) Band 7

Figure 3 S192 imagery from EREP Pass 5, 5 June 1975; area covered includes Mt. Nebo Range and San Pitch Mountains in Utah. (a) Band 3 (0.52 - 0.56 μm), (b) Band 7 (0.78 - 0.88 μm), (c) Band 8 (0.98 - 1.08 μm), (d) Band 9 (1.09 - 1.19 μm), (e) Band 10 (1.20 - 1.30 μm), and (f) Band 11 (1.55 - 1.75 μm). Note the gradual decrease in the extent of snowcover that maintains a high reflectance from Bands 3 through 11.



(c) Band 8



(d) Band 9

Figure 3 continued



(e) Band 10



(f) Band 11

Figure 3 continued

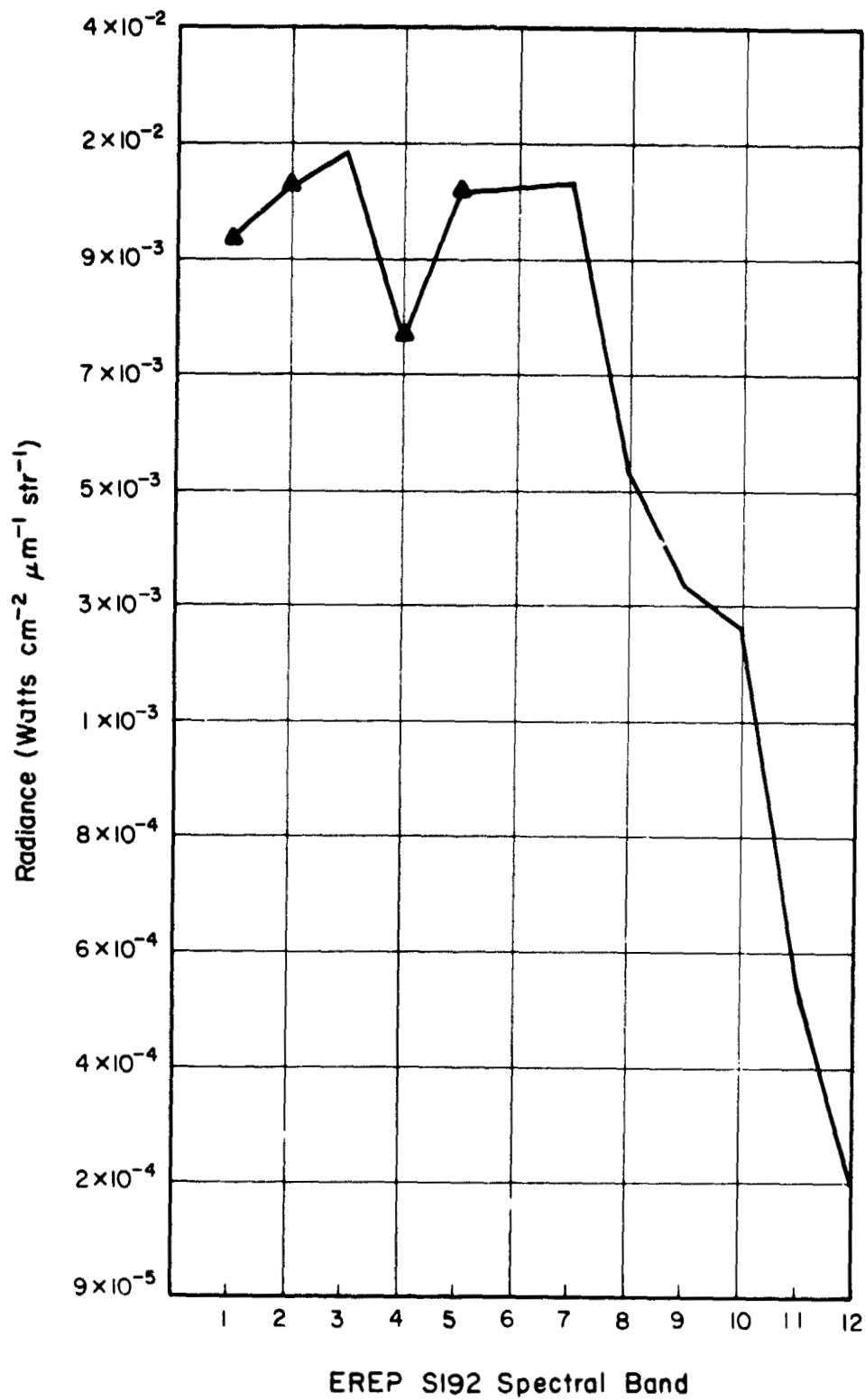


Figure 4 Graph showing S192 measured radiance vs. spectral band for snowcover in the Wasatch test site. Triangles indicate saturated values.

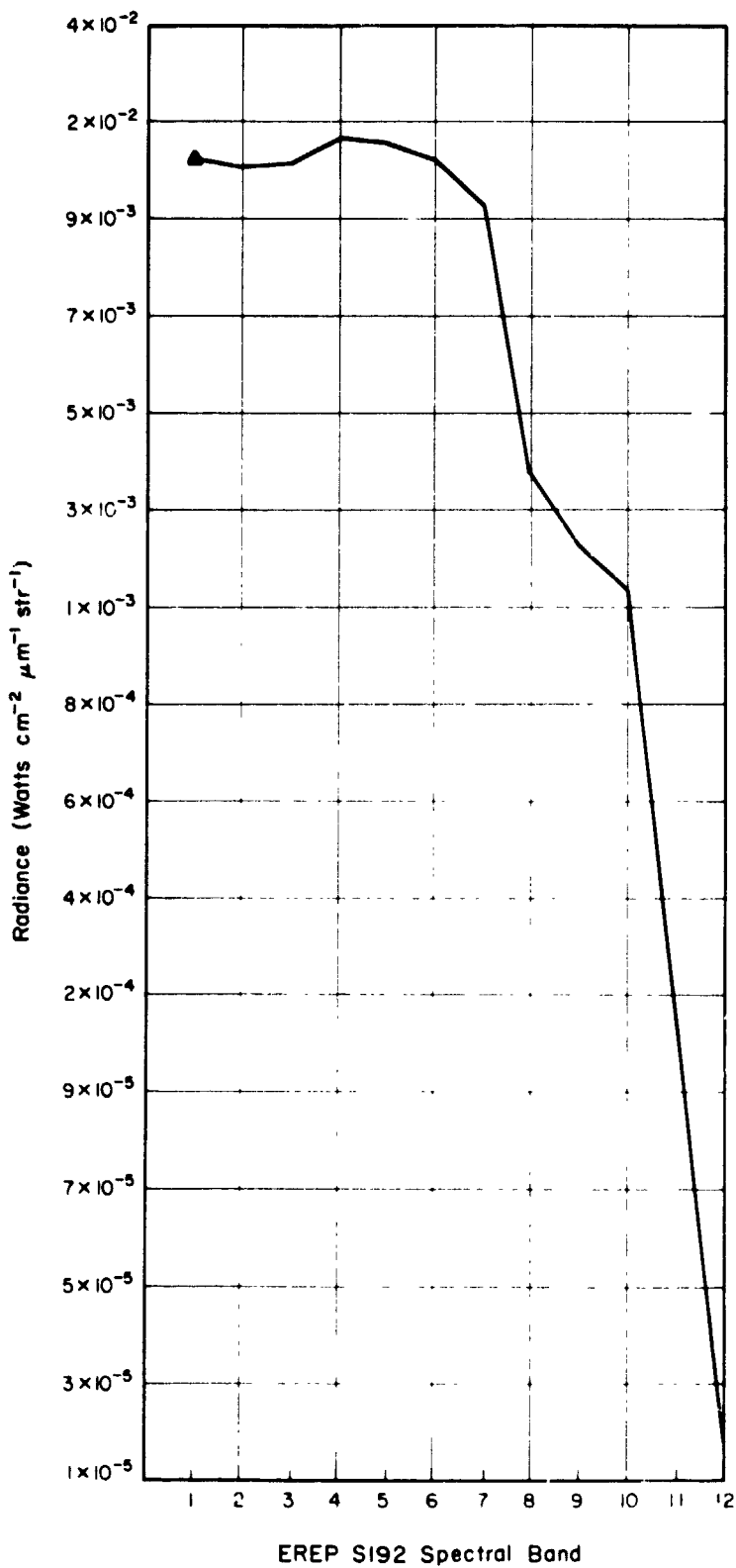


Figure 5

Graph showing S192 measured radiance vs. spectral band for snowcover in the central Arizona test site. Triangles indicate saturated values.

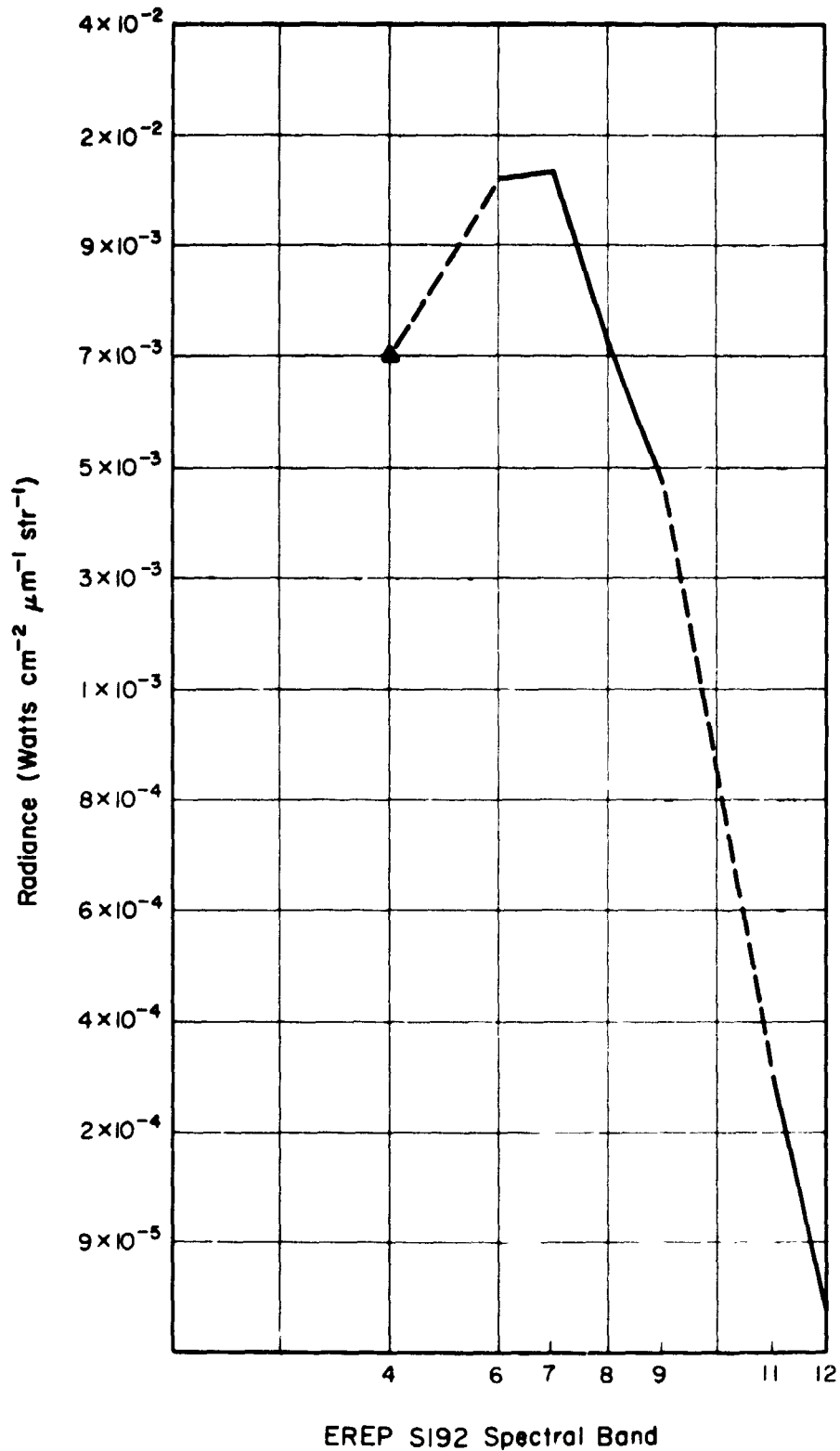


Figure 6 Graph showing S192 measured radiance vs. spectral band for snowcover in the Midwest test site (dashed lines indicate spectral bands for which no data were available). Triangles indicate saturated values.

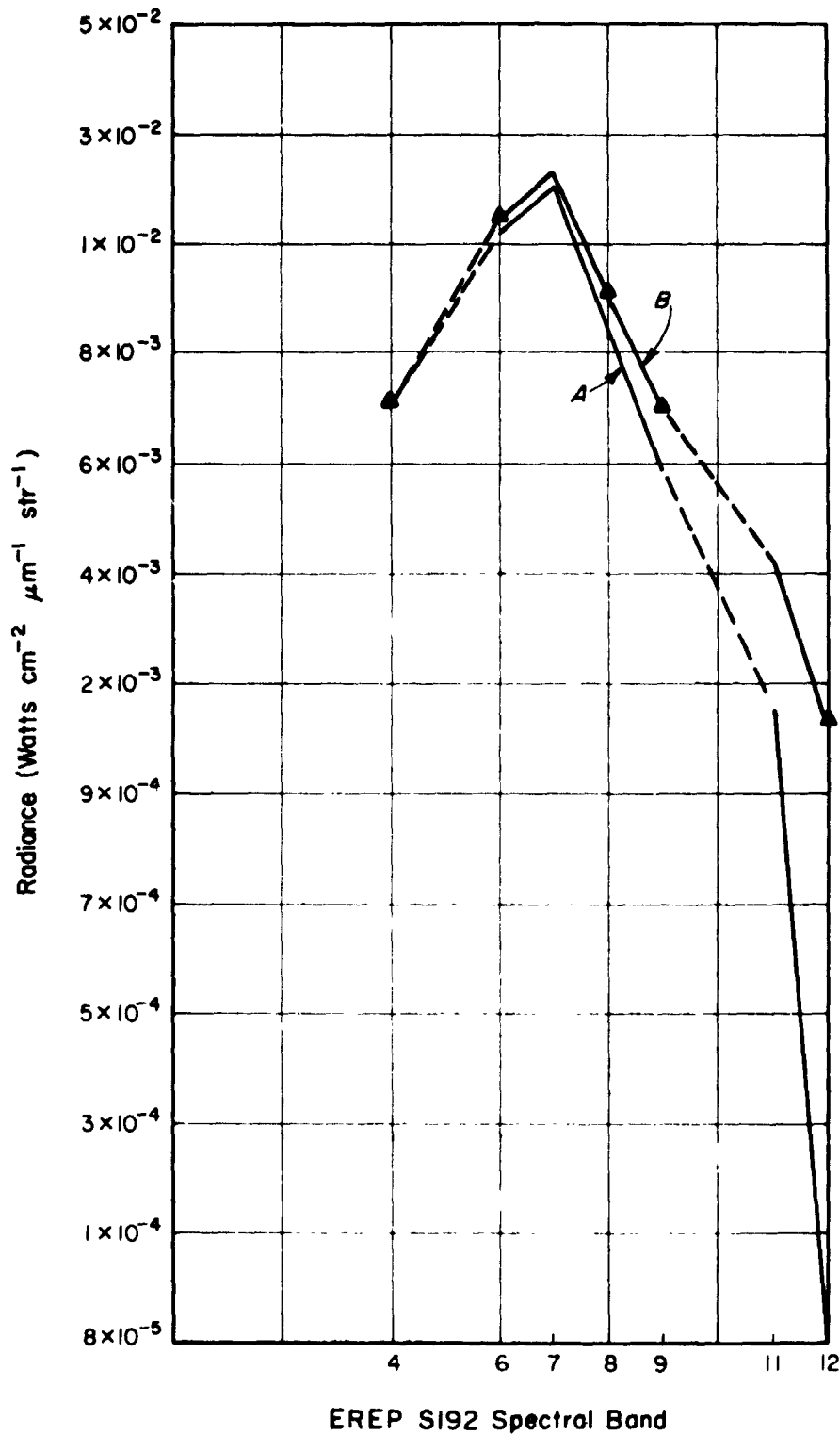


Figure 7 Graph showing S192 measured radiance vs. spectral band for (A) snowcover and (B) clouds in Sierra Nevada-Walker Lake test site (dashed lines indicate spectral bands for which no data were available). Triangles indicate saturated values.

By David F. McGinnis, Jr., Michael C. McMillan and Donald R. Wiesnet
National Environmental Satellite Service, NOAA, Suitland, Maryland

ABSTRACT

N76-17611

LANDSAT imagery has been used to map snow extent with great accuracy. Present orbit and sensor characteristics, however, restrict LANDSAT as a snow monitoring satellite. A better understanding of the complexities affecting the radiation reflected by a snowpack will enhance the usefulness of remote sensing of snow from aircraft and satellites. Problems of aspects and slopes may hinder thematic mapping of snow but can be resolved with available solar tables. Detection of snow in forested areas via satellite is a problem still under study.

INTRODUCTION

LANDSAT-1 (formerly ERTS-1) has drawn praise as a means of studying snow: "Snowline altitudes were also determined by combining ERTS images with maps with an accuracy of about 60 meters under favorable conditions" (Meier, 1973); "...Remote sensing from earth-orbiting satellites offer promise for the development of a more cost-effective means for monitoring snow cover." (Barnes and Bowley, 1973); "ERTS-1 MSS has no peer as a snow mapping instrument." (Wiesnet, et al., 1975). Salomonson (1974) presents a detailed summary of the ERTS snow experiments.

A decade of research in snow studies from earlier National Aeronautics and Space Administration (NASA) and National Oceanic and Atmospheric Administration (NOAA) satellites had permitted evaluations of satellite capability in determining areal extent of snow and snowline in mountainous areas (McClain et al., 1973, and Barnes and Bowley, 1969). Snow "brightness" was related to snow depth (Barnes and Bowley, 1968) and near-infrared (also called "reflected-IR") reflectance decrease was related to "melting" snow and ice surfaces (Strong et al., 1971). Snow runoff relations in the Himalayas (Salomonson and MacCleod, 1972) were also under scrutiny. Prior to the launch of LANDSAT-1 in July 1972, scientists in seven countries had been experimenting with satellite snow studies (McClain, et al., 1973).

After more than a decade of viewing satellite images it seems appropriate to pause and reflect on where we are, how we got there and where we ought to be heading in reference to snow studies via satellite and aircraft remote sensors. Our goal in NOAA is better understanding and better applications of remote measurements of snow reflectance, because it is through understanding that better measurements, sensors, and forecasts will ultimately be made.

Measurements of the spectral reflectance of snow are not common in the literature. Mantis (1951), and O'Brien and Munis (1975) are several contributors. A number of measurements of reflectance and albedo exist, especially in the Soviet literature, but these are seldom accompanied by details of the type of snow or its physical properties. Laboratory studies of the spectral reflectance of snow, and how it is affected by the physical properties of the snow, are needed. Sun angle, sensor angle, time of day, temperature, density, degree of metamorphism, grain size, etc. affect reflectance as viewed by the satellite sensor. Field studies of these parameters are needed to determine the effect of vertically protruding vegetation, shadow effects, reflectance effects of underlying soils, rock types, etc. Aircraft studies such as the ERAP U-2 and P-3 data collections are necessary for improving not only photo interpretation techniques but for

identifying "noise" in the system and for measuring attenuation effects of the atmosphere. Satellite studies using satellites--Nimbus, NOAA, and LANDSAT-1--in conjunction with one another can often improve interpretation. (Wiesnet and McGinnis, 1974; Salomonson, 1974).

Remote sensing of snow via satellite has given a new perspective on snow assessment. However, the effects of spacecraft orbit and sensors, radiative properties of snow, solar irradiance and forest cover need to be considered. The purpose of this paper is to discuss the significance of these factors on the application of LANDSAT data for snow evaluation.

IMPROVEMENTS FOR LANDSAT

The 80-meter ground resolution of the MSS on LANDSAT produces detailed images of excellent cartographic fidelity for snow studies, surpassed only by Skylab data. Data from this sensor has enabled snow hydrologists to obtain synoptic data in unprecedented volumes. However, the dynamic nature, as well as the radiative properties, of a snowpack do impose several constraints in using the current LANDSAT satellite system for snow evaluation.

Images from the MSS data, which cover an area of about 34,000 km², are most effectively used for snow extent mapping in small or moderately-sized (250-30,000 km²) river basins, for example, the American River basin in the Sierra Nevada. Larger basins, the Lake Ontario drainage basin for example, have proven virtually impossible to map because of the necessity of cloud-free conditions during adjacent orbits on successive days (Wiesnet, McGinnis and McMillan, 1975).

An 18-day revisit cycle is insufficient for adequate assessment of changes in areal extent of a snowpack, particularly during the melt season. Changing the sensor swath width from 185 km to 280 km and using two spacecraft would provide a 5-day repeat cycle at a slightly degraded resolution (King, 1971). Such a combination could be sufficient to properly monitor many of the mountainous as well as non-mountainous snow areas. The following table presents various combinations of spacecraft and the resulting repeat cycles (from McGinnis and Rango, 1975).

Repeat Period	Satellite Modification
18 day	1 ERTS
10 day	1 ERTS, swath width increased to 279 km
9 day	2 ERTS
6 day	3 ERTS
5 day	2 ERTS, swath width increased to 279 km
3 day	6 ERTS

Operational hydrologic assessment is further limited by the time delay necessary for processing and shipping the data. Establishment of "quick look" facilities such as the Canadians have developed would greatly improve the value of LANDSAT data for the operational community.

Most critical for the evaluation of physical changes within a snowpack are the optical

properties of a snowpack. O'Brien and Munis, 1975, published a report on snow spectral reflectance from 0.6 to 2.5 μ m. The results of this study, however, cannot be immediately applied to LANDSAT data, owing to the low saturation limits of the MSS. This saturation limit hinders studies over bright snowfields (Wiesnet, McGinnis and McMillan, 1975, Chap. 3).

The energy range of the Very High Resolution Radiometer (VHRR) on board NOAA environmental spacecraft is such that saturation has been detected only in cases of intense sunlight. On a scale of 1 to 256, a function of the voltage received by the VHRR, snow surfaces have produced values from 40 to 120--far below the saturation limit of 256. This sensor, however, has a spatial resolution of but 900 meters.

Studies by Barnes et al. (1974) using Skylab imagery indicated a unique phenomenon in the reflective-IR between 1.55-1.75 μ m. In this spectral region snow is highly absorbent appearing almost black, while clouds appear white. Hence, it is very easy to distinguish clouds from snow. The reflective-IR limit using the MSS is 1.1 μ m (band 7), and in this portion of the spectrum clouds and snow have the same order of reflectance. An additional band or restructuring of the existing near-IR band of future MSS's to include the 1.55-1.75 μ m region would appear advantageous.

RADIATIVE PROPERTIES OF SNOW

The amount of radiation absorbed and reflected by a snow pack depends largely on its physical properties. Many of these physical properties change significantly as the snow undergoes metamorphism. Variables responsible for the physical characteristics of the snow--such as crystal size, density, temperature profiles, and homogeneity--are inter-related in their effect on the spectral radiation reflected by snow. It has been hypothesized in recent articles (Strong, et al., 1971; McGinnis, 1972; Wiesnet, 1973) that "melting" snow conditions can be detected from space with near-IR detectors. This work was largely based on simple photo-interpretation techniques combined with knowledge of concurrent meteorological conditions. Since water is highly absorbent at near-IR wavelengths, these authors inferred by using a heuristic approach that snow which appeared less reflective there than in the visible band must have had water present at its surface, i.e. it was "melting." This is not necessarily always the case. More fundamentally, the physical changes within a snowpack must also be considered. Whether melting snow can be identified unambiguously has not been definitely established.

Recent laboratory work by O'Brien and Munis (1975) has examined changes in the spectral reflectance of snow, simulating conditions often occurring in nature during the metamorphism of snow. Figure 1 shows a typical example of the spectral reflectance of snow observed under sub-freezing temperatures. The high reflectance, relatively independent in the red portion (0.6-0.7 μ m) of the spectrum declines greatly in the near-IR.

The changes in snow reflectance for natural aging samples from one mid-winter snowfall are presented in Figure 2. Curve A represents a sample collected fourteen hours following cessation of the snowfall. A second sample (curve B) was collected thirty hours later. This naturally aged snow had a slightly higher density than the original sample (0.104 g/cm³ compared with 0.097 g/cm³) although clear, sub-freezing conditions existed throughout the intervening period. Reflectance values over the entire spectral range were lower than those from the first sample. During a period when afternoon temperatures rose to 7°C, a third sample was taken after almost three days of natural aging. The density of the snow had increased to 0.34 g/cm³. A further and much larger drop in reflectance had occurred and is shown in curve C.

O'Brien and Munis (1975) state that spectral reflectance of snow in the red and near-infrared portions of the spectrum exhibits rather predictable changes as snow ages naturally. The meteorological conditions during aging, however, do influence the degree

and rate of change of the reflectance.

The decrease in snow reflectance due to natural aging is likely to be the result of changes in the physical characteristics of the snow such as density and microstructure. Blowing and drifting of the snow causes densification by settling and wind compaction. Melting of the snow not only increases the effective mean grain size and density by melting the smaller particles first but it also produces free water in the snow.

Most processes related to the aging of snow result in an effective increase in ice particle size. In calculating the theoretical spectral reflectance of a snow cover for varying particle sizes, Dunkle and Bevans (1956) indicated, "as snow ages and the snow crystals grow, the albedo should tend to decrease from the initial high values." A reduction in spectral reflectance is thus anticipated from the combination of densification and increased particle size associated with aging.

Radiation reflected from a snowpack is affected by the snowpack depth as well as internal characteristics. Some radiation penetrating the snowpack may be absorbed by underlying vegetation and soil. The amount of incoming radiation reaching the ground surface beneath the snow, and thus the amount available for possible absorption is related to the depth of the snow (Giddings and LaChapelle, 1961), as is shown in Figure 3 for snow with an underlying black surface. Barnes and Bowley (1969) and McGinnis et al. (1975) have used this relationship to estimate snow depth from ESSA and NOAA satellite data. LANDSAT data could be used in similar studies if the aforementioned low threshold of detector saturation were raised sufficiently.

OTHER FACTORS AFFECTING THE REFLECTANCE OF SNOW COVER

Variations in snowpack reflectance, when integrated over areas of 0.64 ha. (LANDSAT pixel size) and from spacecraft altitudes, are also due to differences in solar angles, area topography and forest areas. These variations can significantly disguise the snowpack's signal, hindering both photo-interpretation of images and computer-assisted thematic mapping of the digital data.

Solar Geometry

Solar geometry configurations of primary effect are the declination and hour angles. For temporal studies at one location, however, variations in solar hour angle become insignificant due to the LANDSAT orbit. The spacecraft is programmed to cross a given latitude at nearly the same local solar time each day. Images at that location would all be sensed with nearly the same solar hour angle.

The range of solar declination (the angular distance north or south of the celestial equator) is large (47°) and the effect on snowpack irradiation is profound, especially at higher latitudes (Lee, 1963). Declination is predictable, though, and tables of values for specific years are available (for example: U.S. Naval Observatory, 1974a and b).

Area Topography

Snowpack irradiation can vary greatly due to the area topography. These variations are largely due to differences of slope and aspect. Solar radiation is not transmitted vertically to most snowpack surfaces in mountainous areas. The slope, therefore, may either increase or decrease the amount of energy received per unit area. Similarly, snowpack aspect may affect the amount of incident radiation. In the Northern Hemisphere, south-oriented slopes receive more radiation than northern slopes. Since LANDSAT crosses the equator before solar noon, east facing slopes are receiving more energy than western slopes when sensed. Tables of potential solar beam irradiation for various slopes, aspects and dates are available (Frank and Lee, 1966).

Forest Cover

Heavy vegetative cover, such as coniferous forests, can also significantly alter the amount of solar radiation reaching a spacecraft from snowfields. LANDSAT's current sensors integrate over an area approximately 0.64 ha; an area often containing considerable forest cover. This cover masks the snowpack directly through its mass and indirectly through its shadows. The distribution of snow is also altered by the trees, clearings generally accumulating more snow (Hoover, 1971). Although up to one-third of falling snow is caught in conifer crowns (Satterlund and Haupt, 1970) the albedo remains low. Leonard and Eschner, 1968, report the albedo of snow-covered coniferous forests is very low, 0.14 to 0.20.

Several methods have been used to offset the effect of forest cover in LANDSAT data. Foster and Rango, 1975, reported success by slightly over-exposing diazo esochrome film to increase the contrast between forest with and without snow. Lauer and Draeger, 1974, developed a technique of alternately viewing summer and winter scenes. This allows the interpreter to integrate the appearance of the snow with information regarding the type, density and distribution of the vegetation and terrain. Itten (1974, personal communication) has reported limited success in a multispectral signature approach to distinguishing snow in forested areas. Evans, 1974 (p. 44), reported computer assisted multispectral analysis of LANDSAT data as the "most promising approach to reducing the subjectivity of snow area measurements."

CONCLUDING REMARKS

The satellite signal received from a snowpack results from a complex interrelation of various internal physical properties of the snow. Various snow field aspects and slopes may hinder thematic mapping, but normalization problems can be resolved with available tables. Detection of snow in forested areas presents problems; however, several promising approaches are already being explored to achieve a solution.

LANDSAT-1 and -2 have revealed the potential for multispectral studies of snow. With minor modifications of sensor and orbit, future spacecraft could become "SNOWSAT's." Raising the detector saturation threshold and extending the upper spectral limit of the MSS will not only improve mapping of snow extent, but provide the likelihood of monitoring some aspects of the physical condition of the snowpack.

REFERENCES

1. Meier, M.F., 1973, Evaluation of ERTS Imagery for Mapping and Detection of Changes of Snowcover on Land and on Glaciers, Sympos. on Significant Results obtained from ERTS-1, v. 1, pp. 755-760.
2. Barnes, J.C., and C.J. Bowley, 1973, The Use of ERTS Data for Mapping Snow Cover in the Western United States, Sympos. on Significant Results obtained from ERTS-1, v. 1, pp. 855-862.
3. Wiesnet, D.R., D.F. McGinnis, and M.C. McMillan, 1975, Evaluation of ERTS-1 Data for Certain Hydrological Uses, Final Rept. Contract No. S-70246-AG, NASA/GSFC, Greenbelt, Md., 113 pp.
4. Salomonson, V.V., 1974, **Water Resources**, Proc. Third Earth Resources Technology Symposium, Washington, D.C., NASA SP-357, v. 3, pp. 52-80.
5. McClain, E.P., A. Piaget, and K. Itten, 1973, Snow Survey from Earth Satellites--A Technical Review of Methods, WMO/IHD Rept. No. 19, WMO No. 353, World Meteorological Organization, Geneva, Switzerland, 42 pp.

6. Barnes, J.C., and C.J. Bowley, 1969, Satellite Surveillance of Mountain Snow in the Western United States, Final Rept. Contract No. E-196-68, Allied Research Assoc., Concord, Mass., 78 pp.
7. Barnes, J.C., and C.J. Bowley, 1968, Operational Guide for Mapping Snow Cover from Satellite Photography, Allied Research Assoc., Inc., Concord, Mass., 116 pp.
8. Strong, A.E., E.P. McClain, and D.F. McGinnis, 1971, Detection of Thawing Snow and Ice Packs through the Combined Use of Visible and Near-Infrared Measurements from Earth Satellites, Monthly Weather Review, v. 99, no. 11, pp. 828-830.
9. Salomonson, V.V., and N.H. MacCleod, 1972, Nimbus Hydrological Observations over the Watersheds of the Niger and Indus Rivers, Proc. Fourth Ann. Earth Resources Program Review, Jan. 1972, pp. 5-1 to 5-11, Houston, Tex.
10. Mantis, H.T., 1951, ed., Review of the Properties of Snow and Ice, U.S. Army Corps Eng., Final Report Contract No. W-21-018-eng-676, Env. Exp. Sta., U. of Minnesota.
11. O'Brien, H.W., and R.H. Munis, 1975, Red and Near-Infrared Spectral Reflectance of Snow, Cold Regions Research and Engineering Laboratory Research Rept. 322, 18 pp.
12. Wiesnet, D.R., and D.F. McGinnis, 1974, Snow Extent Mapping and Lake Ice Studies using ERTS-1 MSS together with NOAA-2 VHRR, 3d ERTS-1 Sympos., v. 1, Sec. B, NASA-SP-351, pp. 995-1009.
13. King, J.C., 1971, Swathing Patterns of Earth-Sensing Satellites and their Control by Orbit Selection and Modification, Paper No. 71-353, AAS/AIAA Astroynamics Specialists Conference, Fort Lauderdale, Fla., 36 pp.
14. McGinnis, D.F., and A. Rango, 1975, Earth Resources Satellite Systems for Flood Monitoring, Geophysical Research Letters, AGU, Vol. 2, No. 4, pp. 132-135.
15. Barnes, J.C., C.J. Bowley, and M.D. Smallwood, 1974, A Study to Develop Improved Spacecraft Snow Survey Methods Using Skylab/EREP Data, Interim Report under Contract NAS-9-13305, Environmental Research and Technology, Inc., Concord, Mass., 51 pp.
16. McGinnis, D.F., 1972, Detecting Melting Snow and Ice by Visible and Near-infrared Measurements from Satellites, Intern. Sympos. on Role of Snow and Ice in Hydrology, Vol. 2, pp. 751-761.
17. Wiesnet, D.R., 1973, Detection of Snow Conditions in Mountainous Terrain, Proc. ERTS-1 Symposium, Sept. 1972, Greenbelt, Md., pp. 131-132.
18. Dunkle, R.V. and J.T. Bevans, 1956, An Approximate Analysis of the Solar Reflectance and Transmittance of a Snow Cover, Journal of Meteorology, Vol. 13, No. 2, pp. 212-216.
19. Giddings, J.C., and E. LaChapelle, 1961, Diffusion Theory Applied to Radiant Energy Distribution and Albedo of Snow, Journal of Geophysical Research, Vol. 66, No. 1, pp. 181-189.
20. McGinnis, D.F., J.A. Pritchard, and D.R. Wiesnet, 1975, Snow Depth and Snow Extent using VHRR Data from the NOAA-2 Satellite, NOAA Technical Memorandum NESS 63, Wash., D.C., 10 pp.
21. Lee, R., 1963, Evaluation of Solar Beam Irradiation as a Climatic Parameter of Mountain Watersheds, Hydrology Paper No. 2, Colorado State University, Fort Collins, Colo., 50 pp.
22. U.S. Naval Observatory, 1974a, The American Ephemeris and Nautical Almanac, U.S. Government Printing Office, Wash., D.C., 520 pp.

23. U.S. Naval Observatory, 1974b, The Air Almanac, May-August, U.S. Government Printing Office, Wash., D.C., 490 pp.
24. Frank, E.C., and R. Lee, 1966, Potential Solar Beam Irradiation on Slopes, U.S. Forest Service, Rocky Mountain Forest and Range Experiment Station, Fort Collins, Colo., 66 pp.
25. Hoover, M.D., 1971, Snow Interception and Redistribution in the Forest, in Biological Effects In the Hydrologic Cycle, Purdue University, West Lafayette, Ind., pp. 114-122.
26. Satterlund, D.R. and H.F. Haupt, 1970, The Disposition of Snow Caught by Conifer Crowns, Water Resources Research, Vol. 6, No. 2, pp. 649-652.
27. Leonard, R.E., and A.R. Eschner, 1968, Albedo of Intercepted Snow, Water Resources Research, Vol. 4, No. 5, pp. 931-935.
28. Foster, J.L., and A. Rango, 1975, A Method for Improving the Location of the Snowline in Forested Areas using Satellite Imagery, NASA Doc. X-910-75-41, Goddard Space Flight Center, Greenbelt, Md., 8 pp.
29. Lauer, T., and W.C. Draeger, 1974, Techniques for Determining Areal Extent of Snow in the Sierra Nevada Mountains using High Altitude Aircraft and Spacecraft Imagery, in Advanced Concepts and Techniques in the Study of Snow and Ice Resources, National Academy of Sciences, Wash., D.C., pp. 532-540.
30. Itten, K., 1974, personal communication, Dept. of Geography, University of Zurich, Switzerland.
31. Evans, W.E., 1974, Progress in Measuring Snow Cover from ERTS Imagery, Proceedings of the 42nd Annual Western Snow Conference, Colorado State University, Fort Collins, Colo., pp. 37-45.

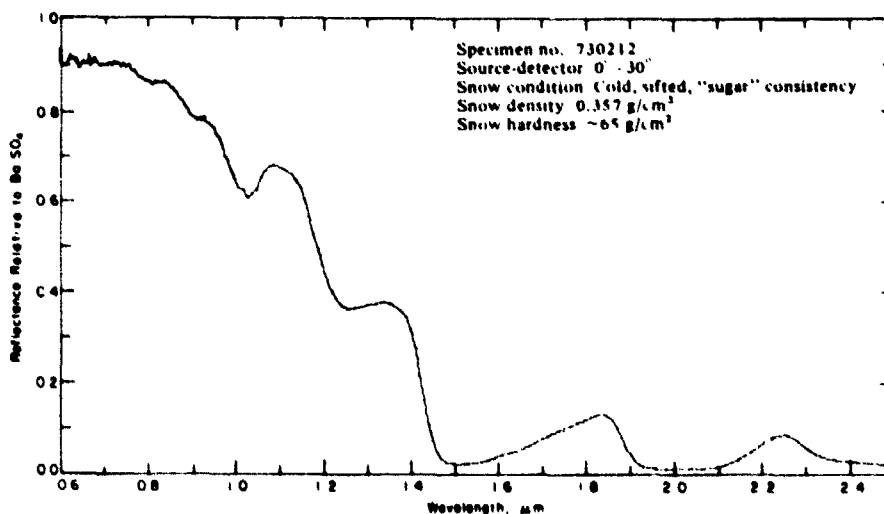


Figure 1. - Typical spectral reflectance curve for snow (O'Brien and Munis, 1975).

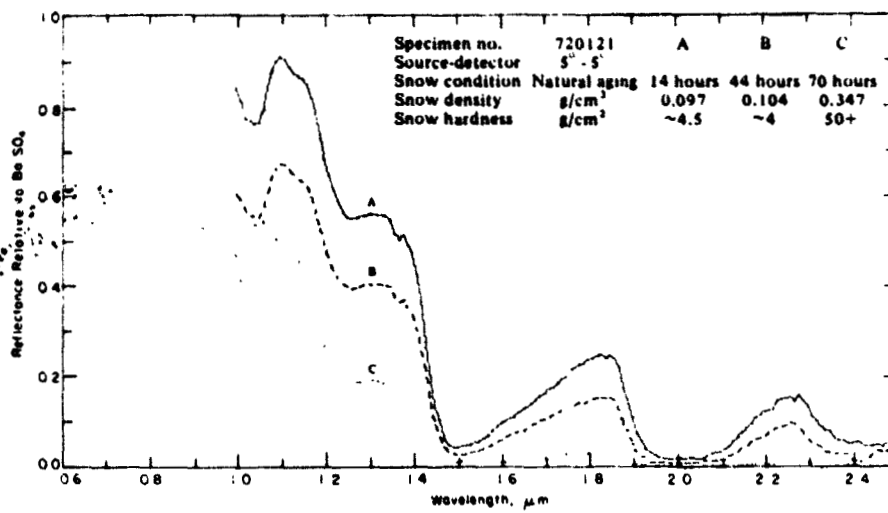


Figure 2. - Changes in snow reflectance with natural aging (O'Brien and Munis, 1975).

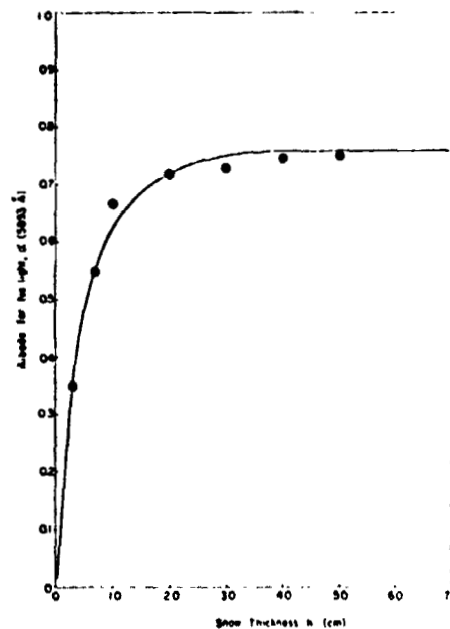


Figure 3. - Variation of albedo with snow thickness (Giddings and LaChapelle, 1961).

OPERATIONAL WATER MANAGEMENT APPLICATIONS OF
SNOWCOVERED AREA OBSERVATIONS

W-26

By Albert Rango and Vincent V. Salomonson, NASA Goddard Space Flight Center,
Greenbelt, Maryland, and James L. Foster, University of Maryland, College Park, Maryland.

ABSTRACT

N76-17612

Timely and accurate prediction of snowmelt runoff has great value in the Western United States for organizations or individuals involved in power generation, irrigation, flood control, management of domestic and industrial water supplies, and recreation. An effort has been made to evaluate the utility of satellite snowcover observations for seasonal streamflow prediction. On a representative, large watershed (10^5 to 10^6 km²) it was found, based on six years of data, that meteorological satellite observations of snowcover early in the snowmelt season exhibit a relationship to seasonal runoff having a statistically significant coefficient of determination of 0.92. Analyses of LANDSAT-1 snowcover observations over the Wind River Mountains of Wyoming reveals that for areas with infrequent cloud cover the extent of snowcover and its change with time can be monitored on watersheds as small as 10 km² in areal extent. The change in the snowcover with time as observed from LANDSAT-1 is found to reflect major differences in seasonal runoff from high altitude (mean altitude >3 km) and low altitude (<3 km) watersheds. There are quantitative indications that LANDSAT observations over small watersheds could be used in a manner similar to that employed for meteorological satellite observations to relate the percent of a basin snowcovered on a given date to seasonal runoff.

As an outgrowth of the results derived in the study referred to above, as well as others in the LANDSAT Program, an Applications Systems Verification Test (ASVT) has been initiated in four areas of the Western United States. Six federal agencies and three states agencies are participating. Results and experience derived from the analysis of three years of LANDSAT snowcover observations during the 1973, 1974, and 1975 snowmelt periods are being compiled in preparation for a Workshop to be held in August, 1975.

INTRODUCTION

The melting of the snowpack in the Spring is the source of greater than 50 percent of streamflow in most areas of the Western United States (Committee on Polar Research, 1970 and Rooney, 1969). The early prediction of the amount of runoff to be derived from the snowpack allows more efficient utilization of the limited water resource for power generation, irrigation, flood control, domestic and industrial water supplies, and recreation. For the Western United States, error in seasonal runoff forecasts prepared on 1 April ranges from 7 to 40 percent, with an average of approximately 18 percent (U.S. Department of Interior, 1974). These discrepancies are due to errors inherent in the procedures used and to errors resulting from variations in the weather after 1 April. The procedural errors tend to remain constant throughout the runoff season, whereas the errors due to uncertainties in the weather decrease markedly as snowmelt progresses. The errors in predicted runoff tend to be largest in years of unusually heavy or light snowpack accumulation.

Observation of the areal extent of the snowpack has long been recognized as an important (but difficult to obtain) hydrologic parameter related to both the average snowpack water equivalent and the snowmelt-derived runoff. The rate at which the snowcover depletes is an index which is inversely related to the snow water equivalent and the generated snowmelt runoff. As the snow leaves the low elevations of the watershed, the hydrograph begins to rise and continues to do so until the snowpack area reaches a critical value where meteorological snowmelt conditions cannot produce ever increasing amounts of runoff. The hydrograph then begins to recede until the remaining snowpack disappears and the runoff is maintained by baseflow. The slower the snowline retreats up the watershed to the elevation where the hydrograph starts a downward trend, the greater the resulting runoff volume and, usually, peak flow.

The purpose of this study was to examine the possibilities of seasonal streamflow estimation employing satellite snowcover observations, both from existing long term, low resolution meteorological satellite data and from the newly available high resolution multispectral satellite information. There are various reasons why satellite snowcover data, if proved effective, would be desired by water resources agencies in preference to aircraft or ground derived data. Fatal accidents have occurred during both ground-based and aerial snow surveys, and, as a result, the safety factor would optimally increase with unmanned space surveys. Wiesnet and McGinnis (1974) have shown that snow extent mapping is both six times faster from LANDSAT-1 imagery than from high altitude aerial photographic surveys, and that the cost of snow maps produced from LANDSAT-1 is about one-two hundredth the cost of the simplest maps made from aircraft surveys. In addition, the procedures for mapping snowcover from space and its excellent comparison with conventionally derived snowcover maps have been documented by many investigators. Such techniques and results have been compiled in handbook form by Barnes and Bowley (1974). Ground-based snow observations are gradually being restricted in mountainous areas as a result of marked increases in wilderness areas developed under the 1964 Wilderness Act. Because these areas are continually increasing and accessibility to high alpine snowpack areas is continually decreasing, satellite observations may be the way to serve both the environmentalist's and the snow surveyor's objectives. Even in nonrestricted areas snow data are difficult to obtain from remote regions and often too few and perhaps unrepresentative samples are available. Remote sensing provides a reasonable way to monitor snow in these remote regions, and the data may even eventually be used to extrapolate conventional point data more effectively over entire watersheds. Finally, some numerical watershed models are beginning to require the input of the observed snowcovered area. Satellite derived snowcover seems to be a logical source for satisfying such requirements in the future.

Even though it has been shown that snow extent can be accurately measured from LANDSAT-1 imagery (Barnes, Bowley, and Simmes, 1974), there has been some question about usefulness in terms of predicting snowpack yield or seasonal runoff in view of the fact that only the area covered by snow, and not snow depth or water equivalent, is observed. This is true of all visible, near infrared, or thermal infrared sensors, no matter what their resolutions. Only two years of snowcover versus runoff information exist for LANDSAT-1 (or NOAA-2), and this is generally not a sufficient number of observations to indicate the validity of any empirical statistical relationship that might appear to exist between snowcovered area and runoff. As a result, longer duration data than presently exists for LANDSAT-1 had to be obtained.

Using the Image Dissector Camera System on Nimbus 3 and 4, Salomonson and MacLeod (1972) mapped the areal extent of snowcover over the Indus River Basin in the Western Himalayas. The areal extent of snowcover for 1969 and 1970 was plotted so as to relate a decrease in the snowcover to an increase in the mean monthly runoff. The results by Salomonson and MacLeod (1972) indicated that some success might be achieved in predicting the seasonal runoff volume or the level of peak discharge if the snow areal extent in late winter or early spring were monitored by satellite. Because several years of meteorological satellite data now exist, this research has been extended to cover six years of snowcover versus runoff and to test whether an empirical relationship of statistical significance was evident. Additionally, LANDSAT-1 data have been used over seven watersheds in the Wind River Mountains of Wyoming to determine if any of the relations prevalent on the Indus River might similarly exist on relatively small watersheds.

STUDY AREAS AND DATA SOURCES

The Indus River Basin above Attock, Pakistan covers approximately 260,000 km² with elevations ranging from 305 m at the streamgage (IHD Station HD-23) to over 8,500 m in the Hindu Kush, Karakoram, and Himalayan Mountains. At the time of the study, no major diversions for water resources projects occurred above the streamgage thus making the recorded flow indicative of the snowmelt runoff. Watersheds this large without significant flow diversions do not exist in the United States.

Streamflow data were received from the Pakistan Water and Power Development Authority for 1967-1972. The 4km resolution Advanced Vidicon System on various ESSA satellites provided coverage for the years 1967-1972, and similar resolution Scanning Radiometer data from NOAA satellites are available for 1973 and 1974.

The Wind River Mountains are located in west central Wyoming and range in elevation from 2000 to 5000 m. Two major rivers rise out of the Wind River Range, namely, the Green and Wind Rivers, and flow diversions for irrigation are numerous; only in the extreme headwaters or on small tributary streams do relatively unimpaired records exist. Seven such small watersheds were selected ranging in the area from 200 km² to 1200 km². Preliminary streamflow records for 1973 and 1974 were supplied by the U.S. Geological Survey for the seven streamgages. Eighty meter resolution LANDSAT-1 multispectral scanner data in the 0.5-0.6, 0.6-0.7, 0.7-0.8, and 0.8-1.1 μ m wavelength bands were available from July 1972 to the present.

METHODS

Images over the Indus River Basin from April through July were selected from 35 mm microfilm rolls of available ESSA and NOAA satellite data. The data were scanned on a daily basis and approximately one clear image per week over the Indus Basin was selected and made into a 35 mm positive slide. The 35 mm slides were projected onto a 1:2,000,000 scale aeronautical chart of the basin and the scale of the image adjusted using a zoom lens to fit the chart. The amount of snowcover was then mapped from the chart onto a transparent overlay and the percent of snowcovered area calculated with a planimeter. Due to a lack of detail on maps of this scale and the large size of the basin, the snowline altitude was not calculated for the Indus Basin.

In order to simulate a prediction situation, percent snowcover area from satellite images between 1-15 April of each year were averaged and plotted against the seasonal runoff occurring from 1 April to 30 June. A regression equation for the years 1967-1971 was developed initially. When the 1972 snowcover data were obtained, the regression equation was used to predict the seasonal streamflow. Subsequently, the 1972 snowcover and runoff data were incorporated into the regression relation.

LANDSAT-1 imagery was obtained for each pass over the Wind River Mountains watersheds for 1973 and 1974 in the standard photographic, single-band 1:1,000,000 scale positive transparency format. Generally, only the 0.6-0.7 μ m black and white transparencies were used for snowcover area extraction. The snow was mapped using the LANDSAT-1 transparencies, U.S. Geological Survey 1:250,000 scale topographic maps, and a zoom transfer scope. The zoom transfer scope with its mirrors, lenses, and scale adjustments allowed the 1:1,000,000 scale image to be superimposed optically onto the map so that drainage areas could be delineated and snowlines mapped at a scale of 1:250,000. Once the snowline was located, the percent and area of snowcover within a given watershed was calculated with the aid of a planimeter. LANDSAT-1 snow mapping was facilitated by examining false color composites employing 0.5-0.6, 0.6-0.7, and 0.8-1.1 μ m data taken during the summer so that forested and bare rock areas could be located and positioned.

The percent snowcovered area on 15 May in 1973 and 1974 for each watershed was plotted versus the 15 May-31 July seasonal runoff for the high elevation watersheds (6 data points) and the low elevation watersheds (8 data points). A regression analysis was performed on these two data sets assuming that the watersheds within each elevation group were very similar in all respects. Factors that could contribute to the total regression variance, however, were recognized as differences in watershed shape, percentage of forest cover, and mesoscale meteorology and climatology. In order to account for variations in watershed size and subsequent runoff, the streamflow data were converted to discharge per unit area values.

RESULTS AND DISCUSSION

Figure 1 presents an example of the annual variation in snowcover at the beginning of April over the Indus River Basin as observed from ESSA 9. Early April was chosen as the beginning of significant snowmelt and the index time for predicting the April-June seasonal runoff. Figure 1 shows that on 4 April 1969 the snowcover was heavy and covered 60 percent of the basin. Resulting seasonal runoff was about 29.6 million acre-feet ($3.65 \times 10^{10} \text{m}^3$). On 3 April 1971, however, the snowcovered area was 44 percent and the subsequent seasonal runoff totalled approximately 25 million acre-feet ($3.08 \times 10^{10} \text{m}^3$). The scenes in Figure 1 were indicative of the 2-3 scenes that were averaged between 1-15 April of 1967-1971, and the snowcover area mapping was easily accomplished.

The 1967-1971 average percent basin snowcover for 1-15 April was then plotted against the 1 April - 30 June corresponding measured runoff in acre-feet (m^3) and a straight line relationship was evident. A significant linear regression equation was derived using these points which took the form $R = (.288S + 11.98) \times 10^6$ where R is the April to June yield in acre-feet and S is the percent basin snowcovered. The coefficient of determination, r^2 , for this equation is 0.91 (significant at the one percent level) and the standard error was 5 percent of the mean seasonal yield. When the 1972 satellite snowcover data became available, the above regression equation was used to predict the April-June 1972 seasonal runoff. The satellite-measured 1-15 April average snowcover was 67.3 percent and the predicted April-June yield was 31.5 million acre-feet ($3.88 \times 10^{10} \text{m}^3$). When the 1972 stream-gage records were obtained, the actual April-June yield was determined to be 32.3 million acre-feet ($3.98 \times 10^{10} \text{m}^3$). The difference between predicted and actual yield was only 0.86 million acre-feet ($1.06 \times 10^9 \text{m}^3$) or within three percent of the actual seasonal yield. Figure 2 shows the 1967-1972 snowcover versus seasonal yield data plotted and a new regression line obtained by incorporating the 1972 data into the relation. The new equation is $R = (.300S + 11.52) \times 10^6$ with r^2 being 0.92 (significant at the one percent level) and the standard error again equalling 5 percent of the mean seasonal yield.

These results indicate that even though snow depth or water equivalent are not directly measured, it appears that areal snow extent is a useful index parameter for aiding in the prediction of seasonal runoff on a large data-sparse watershed. Because watersheds of this size and relatively undisturbed nature are not commonly found in areas such as the United States, the same kind of test was applied to several very small watersheds in Wyoming using the high resolution LANDSAT-1 data.

Figure 3 is a 0.6-0.7 μm view of the Wind River Mountains taken in August 1972 which delineates the seven watersheds selected for analysis. The Green, Pine, East Fork, and Big Sandy watersheds are in the Colorado River Basin, whereas Bull Lake, Dinwoody, and Wind are in the Missouri River Basin. More importantly, for this analysis, Wind River, Green River, East Fork River, and Big Sandy River were grouped as low watersheds with mean elevations less than 3050 m. Bull Lake Creek, Dinwoody Creek, and Pine Creek all had mean elevations in excess of 3050 m and were grouped as high watersheds. The smallest watershed under study was Pine Creek (200 km^2) and the largest was Green River (1200 km^2).

As an example of the kind of snowcover changes observed during the course of a year with LANDSAT-1, Figure 4 presents four 0.6-0.7 μm views of the Wind River Mountains during the 1972-1973 snow season. The 6 August scene shows bare rock, late-lying alpine snow, and glaciers above the tree line during minimum snowcover. The 10 December scene illustrates total snowcover over the entire area with the darker tones indicating areas of forest cover over the snowpack. The 21 May and 8 June scenes are taken during the active snowmelt season and display the kind of changes detectable from one LANDSAT-1 pass to the next. To illustrate, in the 21 May scene Bull Lake Creek and Green River are 86 and 55 percent snowcovered, respectively. Because of persistent snowmelt during the 18 day interval between satellite passes, 8 June snowcover has decreased to 58 percent for Bull Lake Creek and 27 percent for Green River. Such clear imagery was common during the melt season, and only in a few instances was a particular watershed obscured by clouds during a LANDSAT-1 overpass in 1973 and 1974.

In an attempt to produce a quantitative snowcover-runoff relationship, i.e., a regression equation similar to that derived for the Indus River, the available data were treated as two different data sets based on elevation. In Figure 5 the percent snowcover on 15 May (S) is plotted against the seasonal runoff from 15 May-31 July (R) in cfs/mi²(m³/sec/km²) for the three high elevation watersheds for both 1973 and 1974. In order to increase the data base for a regression analysis, the three high elevation watersheds, although possessing some differences, were assumed to be alike enough to be treated as a single watershed. Six data points were thus available for the two years and the resulting regression was $R = 30S - 2198$ with a r^2 of 0.89 significant at the one percent level and a standard error equal to 13 percent of the mean seasonal yield (15 May-31 July). For the lower elevation watersheds, the same similarity assumption was made and the data plotted in Figure 6. The equation was $R = 5.8S - 156$ with a r^2 of 0.85 significant at the one percent level and a standard error equal to 14 percent of the mean seasonal yield. Although a crude estimate of seasonal runoff could be made for nearby watersheds using these equations based on only two years of data, the real importance of such relations rests in the fact that the changes in areal snow extent as observed from space are quantitatively related to snowmelt runoff and, as a result, indirectly to the volume of water on a watershed. With an adequate number of years of snowcover versus runoff observations on single watersheds, seasonal runoff predictions could possibly be made from space. More importantly, however, these data, if combined with conventionally gathered data used for streamflow forecasting, should be useful for reducing the errors associated with current prediction techniques. Because streamflow predictions are needed before the time of snowcover breakup - about 1 May in the Wind River Mountains - the satellite data could be used later in the snowmelt season to update and refine the earlier conventional predictions. The U.S. Department of Interior (1974) sponsored study has shown that such late season refinements may be worth considerable amounts of money for power generation alone.

OPERATIONAL APPLICATIONS

The capability of the LANDSAT and NOAA satellites to accurately measure snowcovered area on various size watersheds has been demonstrated in several research projects sponsored by NASA, NOAA, and other agencies. Additionally, the research previously mentioned in this paper has provided an indication that satellite-derived snowcovered area can be employed as an additional parameter in the prediction of snowmelt-derived runoff. Because of the positive results in these two areas, the decision was made to operationally test the use of remotely sensed snowcovered area for improving snowmelt runoff forecasts in an Applications Systems Verification Test (ASVT) Program where quasi-operational evaluations of total technical capability are performed. The objective of a NASA ASVT project is to provide all of the information necessary for a potential user to make effective decisions concerning the implementation of the technology in an operational applications system. Mandatory products from an ASVT are a documented methodology suitable for widespread use, a comprehensive user evaluation of the systems accuracy and reliability, and a complete cost-benefit relationship study.

The Operational Applications of Satellite Snowcover Observations (OASSO) project became part of the NASA ASVT Program in July 1974. Being conducted in cooperation with nine operational water management agencies in the Western U.S., the OASSO project is scheduled for completion in 1978. The general objectives of OASSO are:

1. Map snowlines, areal snowcover, and associated changes in snowcover using satellite data for the 1973 and 1974 snow seasons in four separate Western U.S. study areas in order to evaluate the usefulness of the data had they been available in near real-time.
2. Map snowcover changes through FY 78 in each of the study areas in a near real-time mode (data to user \leq 72 hours) so that the data base can be extended to a total of at least five years.

3. Compare and evaluate satellite-derived snow mapping products with reference to products from conventionally-derived snow data.
4. Develop or modify methods in an operational framework over the study period that will allow incorporation of satellite derived snowpack observations into the prediction of snowmelt-derived streamflow for specific areas.
5. Produce a documented methodology and cost/benefit analysis sufficient for user organizations to make Go/No Go decisions concerning the use of this satellite-assisted snowmelt runoff methodology in their operational responsibilities.

Each of the four study areas in the West have operational agency personnel working in cooperation with remote sensing specialists to adapt the existing technology to water supply forecasting needs. Tables I through IV present the study area organization, watersheds under investigation, and the applications of the data for Arizona, California, Colorado, and the Northwest, respectively. NOAA's National Environmental Satellite Service (NESS) is also participating in the OASSA project by supplying operational NOAA satellite data and supporting research as shown in Table V.

The agencies participating in the project are interested in substituting satellite snowcover measurements for many of the conventional low altitude aircraft surveys, and at the same time using the satellite information to identify critical snowmelt situations where it would be advantageous to fly an aircraft mission. Moreover they would like to use satellite snowcover data to obtain additional snowpack knowledge from restricted access wilderness areas and other remote regions. One of the principal goals for all study areas is to use satellite information to reduce existing streamflow forecast errors, primarily by updating forecasts after April 1 through the end of the snowmelt season. Procedural forecast errors would thus be treated rather than the early season, weather-variability errors.

In an attempt to reduce forecast errors, historical records are being analysed and correlated to conventional watershed and snowpack measurements. It is hoped that with five years of satellite data as a base, meaningful snowcovered area indices could be used in normal regression approaches to streamflow forecasting. Additionally, various numerical watershed models are being employed with the snowcovered area estimates in the study areas to attempt to improve shorter duration runoff forecasts. The Streamflow Simulation and Reservoir Regulation (SSARR) model used by the Columbia River Forecasting Service, as an example, requires the input of snowcovered area for generating daily streamflows. Satellite snowcover data will be input to the SSARR model for studying possible improvements in streamflow forecasts for past years as well as for current years. The utility of the remotely sensed data for the various models being tested will be assessed and documented.

In order to capitalize on the approaches being used and experience being gained in each of the study areas, a workshop on the Operational Applications of Satellite Snowcover Observations will be held August 18-20, 1975 at South Lake Tahoe, California sponsored by NASA and the University of Nevada. The major objective is to discuss solutions to various snow mapping problems and gain new insights as to how the satellite derived information can be used for improving streamflow forecasts. Additionally the workshop will attempt to promote an exchange of information between operational water management interests and remote sensing specialists through presentations concerning the ongoing operational test of satellite information, recent progress in remote sensing of the snowpack, and pertinent snow survey and snow hydrology studies.

At the end of the OASSO project the user agencies will evaluate the utility of the satellite data in light of their own unique requirements and comment upon possible continuing application of the data. Recommendations will also be made for changes and improvements necessary to make the data more applicable to operational functions. The required cost-benefit study will produce results regarding the worth of using satellite snowcover data for operational purposes based upon the results obtained

in each of the four study centers. Documentation and dissemination of the results from the OASSA project for informational purposes will include widespread distribution of handbooks, workshop proceedings volumes, final reports, and scientific papers.

SUMMARY AND CONCLUSIONS

The efforts involving the analyses of satellite data and its relationship to seasonal runoff provide several conclusions listed in the following paragraphs.

1. On large watersheds (10^5 to 10^6 km²) where the flow is relatively unimpaired by reservoirs or water withdrawals, meteorological satellite snowcover observations apparently can be used in lieu of other snowpack parameters, such as depth or volume, to estimate seasonal runoff if enough years of information exist.
2. On watersheds as small as 10 km² in areas with infrequent cloud cover during the snowmelt season, LANDSAT-1 data can be used to accurately measure the extent of snowcover and monitor its change with time. It seems to be possible to quantitatively relate the percent of the basin snowcovered on a given date to a measure of seasonal runoff on the small watersheds similar in nature to that performed on the large Indus River Basin. In the United States it is necessary to develop such relations on small watersheds in order to effectively predict streamflow at points above significant water diversions.
3. Because of the quantitative relations developed here it appears that satellite observed snowcovered area could be usefully employed as an additional seasonal runoff index parameter or as an input into certain hydrologic models. The advantage of such information is that they are non hazardous, easy to obtain data requiring no access to restricted wilderness or remote areas. In the Western United States, because of the significance of water stored in the form of snow for hydroelectric power generation, irrigated agriculture, and reservoir regulation, the importance and value of more accurate runoff information provided by satellite observations is very promising.

As a result of the promising results derived in this study and others, an Application Systems Verification Test (ASVT) has been initiated in the Western United States to evaluate under operational conditions the overall utility of satellite snowcover observations for streamflow forecasts. A total of six federal agencies and three state agencies are cooperating in four regions centered in Arizona, California, Colorado, and Oregon. All cooperators in the project will be comparing results and experience acquired to date in a workshop to be held in August 1975. At the conclusion of the ASVT, handbooks, workshop proceedings, final reports, and scientific papers produced in conjunction with this project will be disseminated so that all interested parties may evaluate the overall results and assessments of the application of satellite snowcover observations.

ACKNOWLEDGEMENTS

We would like to thank Mr. M. Umar and Mr. K. Jawed of the Pakistan Water and Power Development Authority; Mr. D. J. O'Connell and Mr. J. F. Wilson of U.S. Geological Survey, Water Resources Division, Wyoming; and Mr. G. W. Peak and Mr. G. P. Claggett of the U.S. Soil Conservation Service, Casper, Wyoming for supplying streamflow and ground snow survey data necessary for conducting this study. The snow mapping and runoff correlation part of this study was partially funded by NOAA/NESS under Contract No. NA-776-74.

REFERENCES

- Barnes, J. C., and C. J. Bowley, Handbook of techniques for satellite snow mapping, Final Report, NAS5-21803, 95 pp., National Aeronautics and Space Administration, Goddard Space Flight Center, Greenbelt, Maryland, 1974.
- Barnes, J. C., C. J. Bowley, and D. A. Simmes, Mapping snow extent in the Salt-Verde watershed and the southern Sierra Nevada using ERTS imagery, in Proceedings of the Third ERTS-1 Symposium, NASA SP-351, vol. 1, pp. 977-993, U.S. Government Printing Office, Washington, D.C., 1974.
- Committee on Polar Research, Polar Research, a survey, 204 pp., National Research Council, National Academy of Sciences, Washington, D.C., 1970.
- Rooney, J., The economic and social implications of snow and ice, in Water, Earth, and Man, pp. 389-401, edited by R. J. Chorley, Methuen and Company, Ltd., London, 1969.
- Salomonson, V. V., and N. H. MacLeod, Nimbus hydrological observations over the watersheds of the Niger and Indus Rivers in 4th Annual Proceedings, Earth Resources Review, vol 1, pp. 5-1 to 5-11, NASA Document MSC 05937, Manned Spacecraft Center, Houston, 1972.
- U.S. Department of Interior, Snow mapping and runoff forecasting: Examination of ERTS-1 capabilities and potential benefits from an operational ERS system, Interim Report, Contract No. 14-08-001-13519, Office of Economic Analysis, Washington, D.C., 1974.
- Wiesnet, D. R., and D. F. McGinnis, Snow-extent mapping and lake ice studies using ERTS-1 MSS together with NOAA-2 VHR, in Proceedings of the Third ERTS-1 Symposium, NASA SP-351, Vol. 1, pp. 995-1009, U.S. Government Printing Office, Washington, D.C., 1974.

TABLE I. - ARIZONA SNOW ASVT ORGANIZATION AND RESPONSIBILITIES

A. Project Coordinator	Mr. Herbert H. Schumann USGS, WRD Phoenix, Arizona
B. Operational Agency Cooperators	Mr. William Warskow, Watershed Specialist, Watershed Division Mr. Ted Wilson, Lead Engineer, Water Resource Operations Salt River Project Phoenix, Arizona
C. Remote Sensing Specialist	Mr. Herbert H. Schumann
D. Study Watersheds	Salt River Verde River
E. Applications of Data	Reservoir Regulation (for power, irrigation, water supply, and flood control in order of priority) Short Duration Runoff Forecasting

TABLE II. - CALIFORNIA SNOW ASVT ORGANIZATION AND RESPONSIBILITIES

A. Project Coordinator	Mr. A. J. Brown, Chief Snow Surveys and Water Supply Forecasting Section California Department of Water Resources Sacramento, California
B. Operational Agency Cooperators	Snow Surveys and Water Supply Forecasting Section, California Dept. of Water Resources Sacramento, California
C. Remote Sensing Specialist	Mr. Barry Brown, California Department of Water Resources
D. Study Watersheds	Feather River Upper Sacramento River San Joaquin River Kings River Kern River Kaweah River Tule River
E. Applications of Data	Supply various California Snow Surveys Cooperators with Seasonal Runoff Forecasts. Irrigation Power Generation Flood Control

TABLE III. - COLORADO SNOW ASVT ORGANIZATION AND RESPONSIBILITIES

A. Project Coordinator	Mr. Jack Washichek Snow Survey Supervisor Soil Conservation Service Denver, Colorado
B. Operational Agency Cooperators	Mr. Jack Washichek Soil Conservation Service Dr. Jerry Danielson, Deputy - State Engineer Colorado Division of Water Resources Mr. Bob Hansen Bureau of Reclamation
C. Remote Sensing Specialist	Mr. Bob Hansen, USBR
D. Study Watersheds	Rio Grande River Above Del Norte Conejos River Above Mogote Culebra River Above San Luis San Juan River Above Carracus Arkansas River Above Salida
E. Applications of Data	Better Flow Forecasts on the Rio Grande River so that the State of Colorado can Better Regulate Reservoir Releases of Water to the State of New Mexico as Required by Law. Reservoir Regulation for Irrigation and Power Requirements.

TABLE IV. - NORTHWEST SNOW ASVT ORGANIZATION AND RESPONSIBILITIES

A. Project Coordinator	Mr. Fred A. Limpert, Head Hydrology Section Bonneville Power Administrator Portland, Oregon
B. Operational Agency Cooperators	Columbia River Forecasting Service. (CRFS) Portland, Oregon CRFS is composed of: 1) Bonneville Power Administration Mr. Fred A. Limpert, Head Hydrology Section 2) U.S. Army Corps of Engineers Mr. Morris Larson, Chief Hydrologic Engineering Section 3) NOAA/National Weather Service
C. Remote Sensing Specialist	Dr. Mark Meier, USGS
D. Study Watersheds	Boise River Above Lucky Peak Reservoir North Santiam River Above Big Cliff Reservoir Snake River Above Heise
E. Applications of Data	Power Generation Flood Control

TABLE V. - NOAA/NESS SNOW ASVT SUPPORT STUDY

<p>A. Study Coordinator</p>	<p>Mr. Russ Koffler, Chief Environmental Products Group NOAA/NESS Washington, D.C.</p>
<p>B. Operational Agency Cooperator</p>	<p>Mr. Jack Bottoms, Manager NOAA/NESS Satellite Field Services Station Redwood City, California</p>
<p>C. Remote Sensing Specialists</p>	<p>Mr. Don Weisnet Dr. David McGinnis NOAA/NESS Environmental Sciences Group Mr. Stan Schneider NOAA/NESS Environmental Products Groups</p>
<p>D. Operational Services</p>	<p>Support in the Form of Imagery for Each of the ASVT Study Watersheds from the Satellite Field Services Station and Supplemental Snowcover Analyses for Several other Rivers in the West. Snowcover Values are sent by Teletype to NWS River Forecast Centers.</p>
<p>E. Research Study</p>	<p>Investigate Effect of Vegetation, Tree Lines, and Mountainous Terrain on Snow Mapping. Digital Enhancements of Snow/Terrain Interfaces. Examination of Sources of Snow Mapping Errors.</p>

REPRODUCIBILITY OF THE ORIGINAL PAGE IS POOR

4 APRIL 1969



SNOWCOVERED AREA = 60%
APRIL—JUNE RUNOFF =
29,590,000 ACRE—FEET

3 APRIL 1971



SNOWCOVERED AREA = 44%
APRIL—JUNE RUNOFF =
24,990,000 ACRE—FEET

Figure 1. - ESSA 9 observations of the annual variation in snowcovered area at the beginning of snowmelt in the Indus River Basin above Attock, Pakistan.

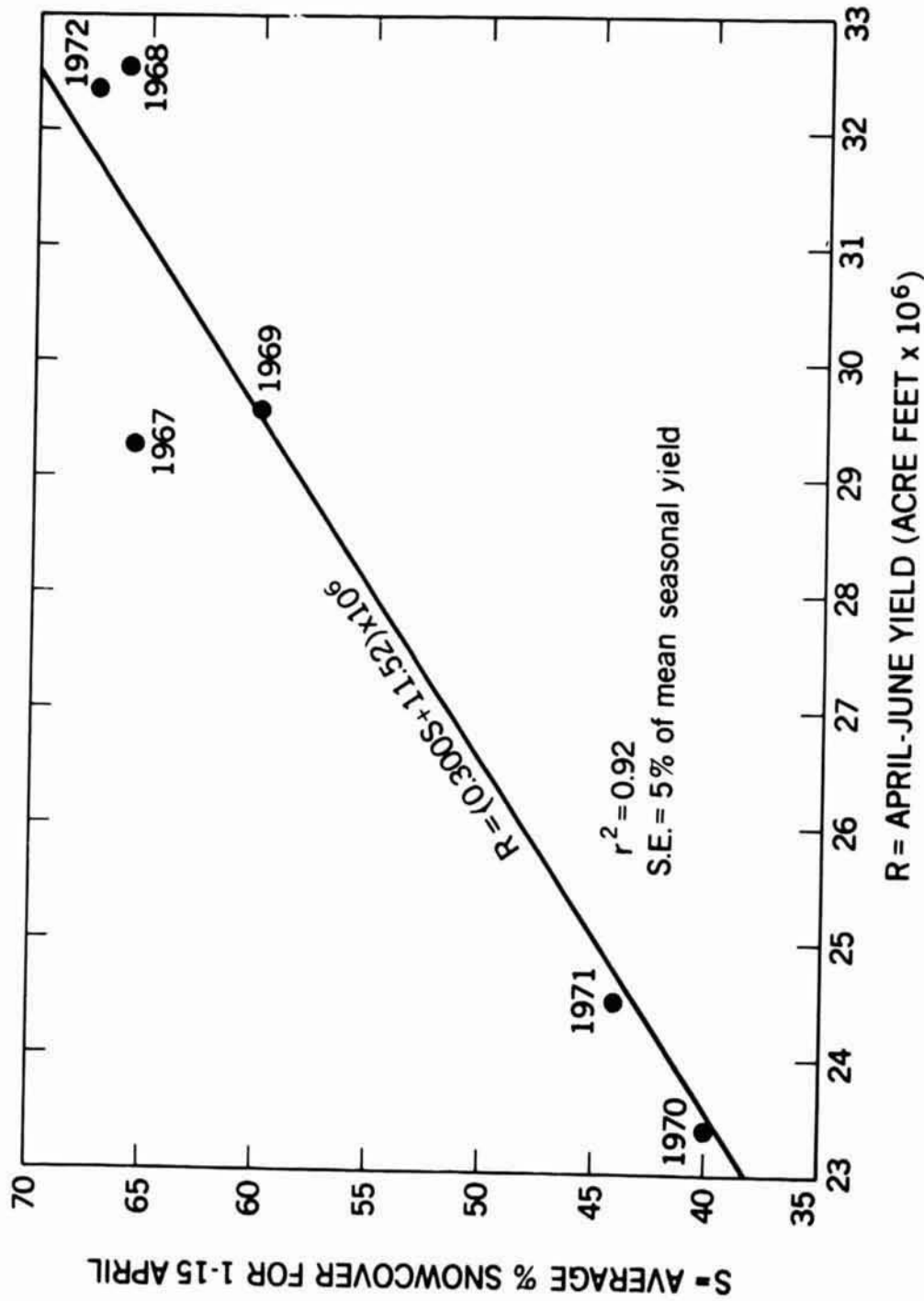


Figure 2. - Satellite-derived snowcover estimates versus measured runoff for the Indus River, 1967-1972.

REPRODUCIBILITY OF THE
ORIGINAL PAGE IS POOR

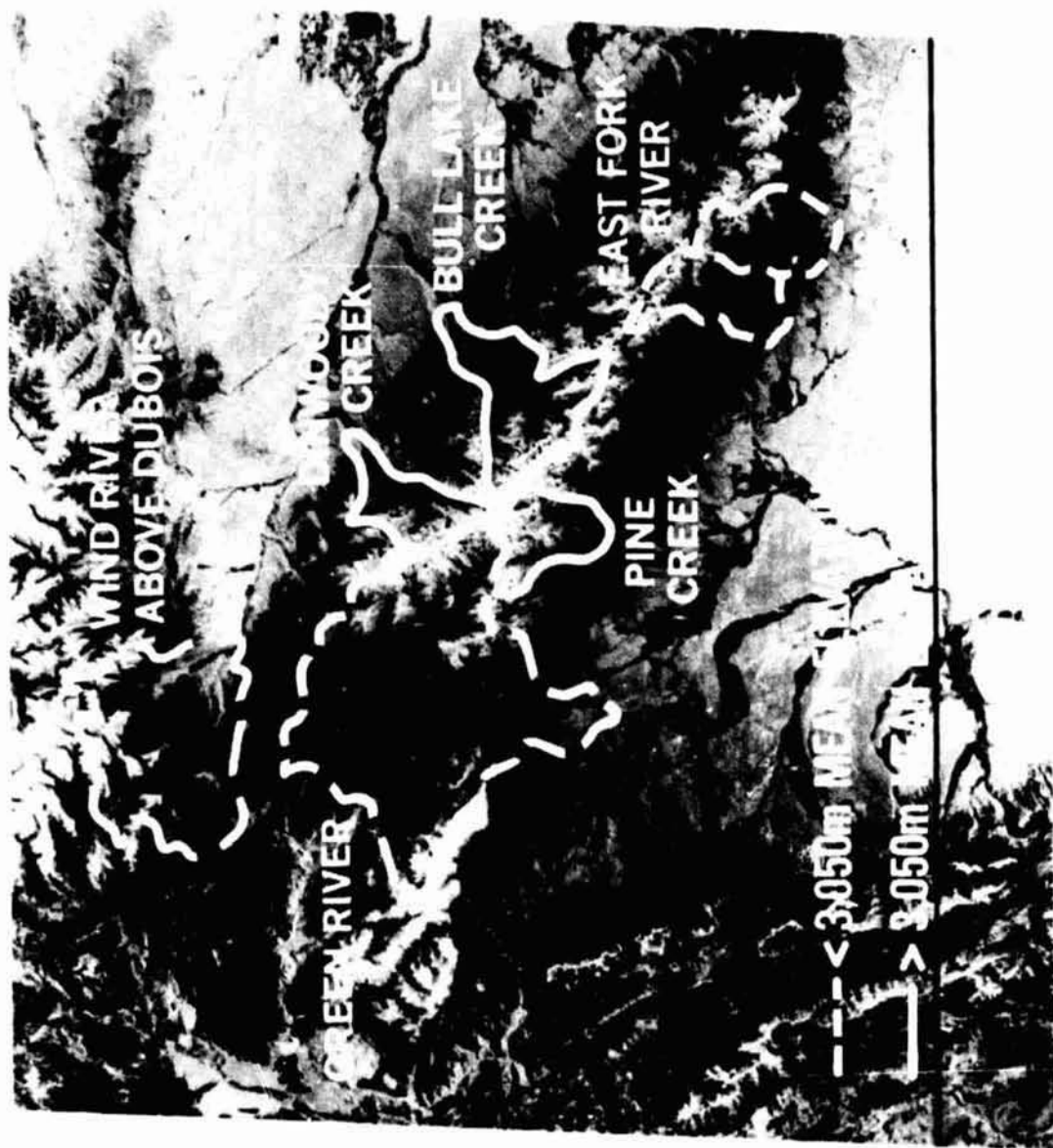


Figure 3. - LANDSAT-1 0.6 - 0.7 μ m view of the Wind River Mountains of Wyoming, 6 August 1972. The boundaries of the seven watersheds used in the LANDSAT-1 snowcover depletion-runoff analysis are indicated.

REPRODUCIBILITY
ORIGINAL PAGE IS P. 2683



10 DECEMBER 1972



8 JUNE 1973



6 AUGUST 1972



21 MAY 1973

Figure 4. - Snowcover changes in northwestern Wyoming, 1972-1973.

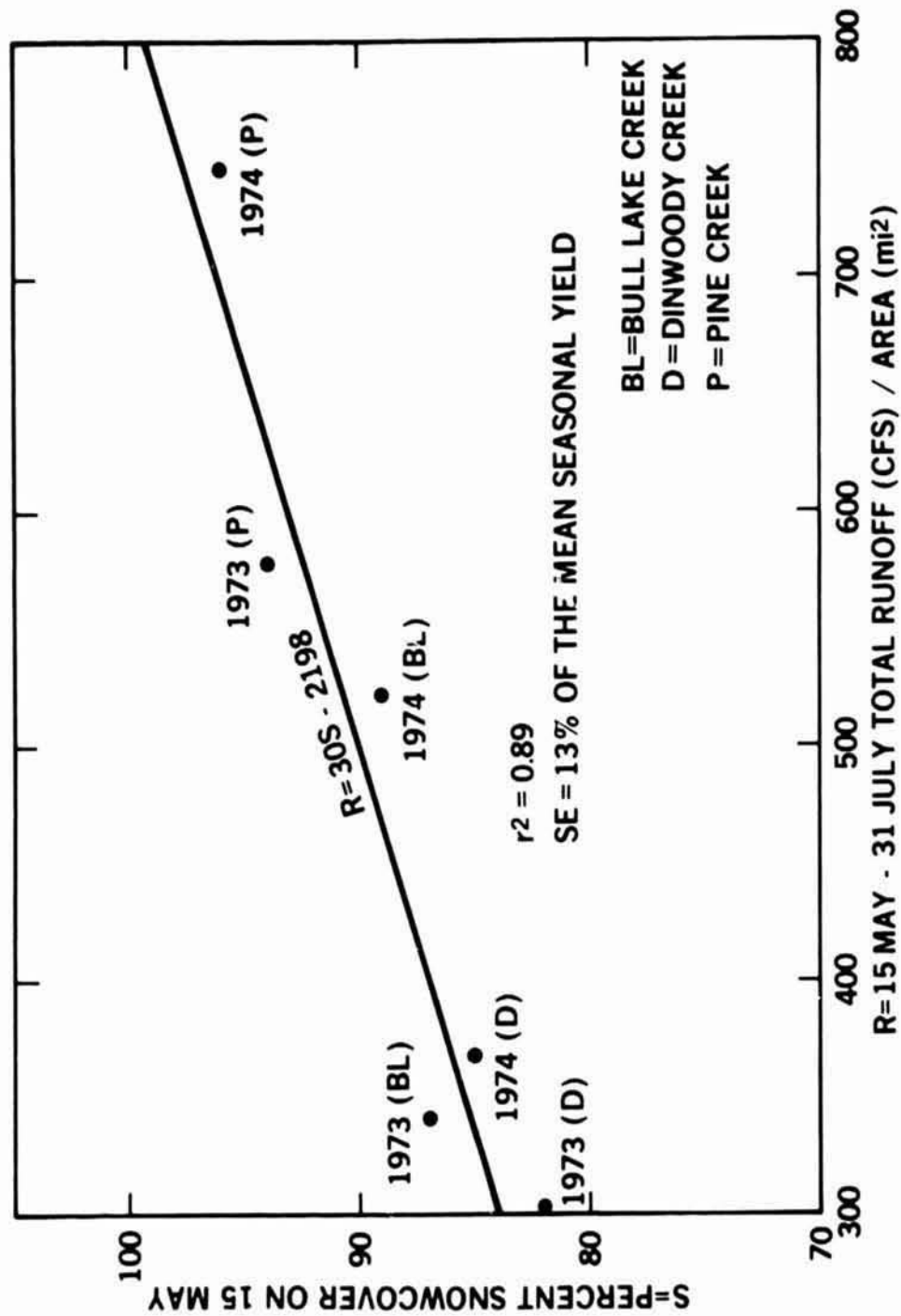


Figure 5. - LANDSAT-1 derived snowcover estimates versus measured runoff (1973 and 1974) for three watersheds greater than 3,050 m mean elevation in the Wind River Mountains, Wyoming.

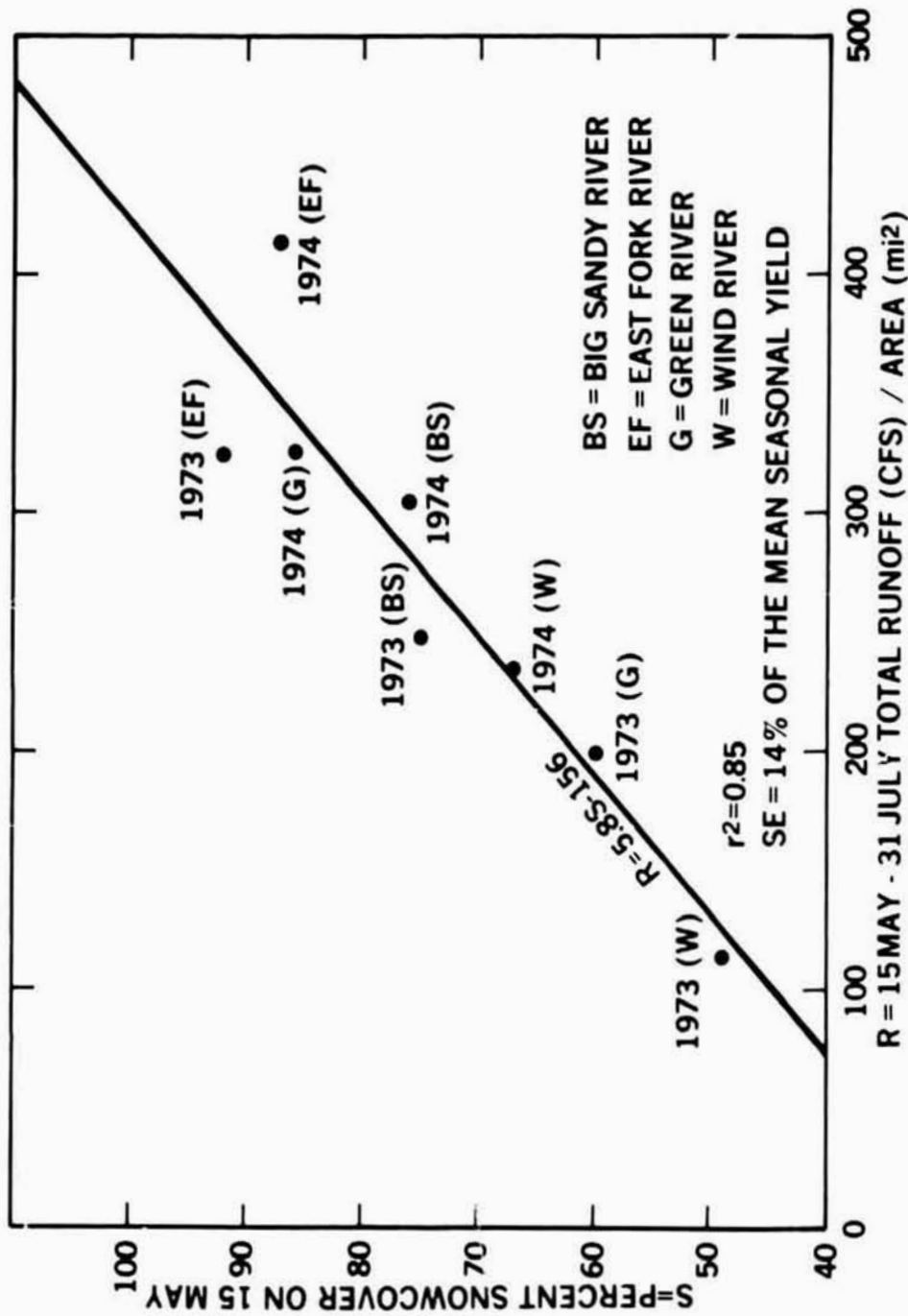


Figure 6. - LANDSAT-1 derived snowcover estimates versus measured runoff (1973 and 1974) for four watersheds less than 3,050 m mean elevation in the Wind River Mountains, Wyoming.